GEOLOGICAL SURVEY OF FINLAND

Special Paper 44

2007

Gold in the Central Lapland Greenstone Belt

Edited by V. Juhani Ojala

GTK

Front cover: Detail of the Au-mineralised deformation zone in the Suurikuusikko deposit (photo Reijo Lampela).

Geological Survey of Finland, Special Paper 44

Gold in the Central Lapland Greenstone Belt

V. Juhani Ojala (ed.)

Geological Survey of Finland
Espoo 2007

Ojala, V. Juhani (ed.) 2007. Gold in the Central Lapland Greenstone Belt. *Geological Survey of Finland. Special Paper 44. 267 pages, 143 figures, 27 tables and 6 appendices.*

The publication presents 12 papers on the gold exploration and gold related research conducted by the Geological Survey of Finland in northern Finland since 1980's. The first paper gives a general description of the regional deformation and metamorphic history of the Central Lapland Greenstone Belt and its adjoining areas. This is followed by an overview of the characteristics gold deposits in the northern Finland and synthesis of their genetic aspects. The structural controls on the orogenic gold mineralization in the Central Lapland Greenstone Belt are examined in the third paper which is followed by case studies on the Suurikuusikko, Hirvilavanmaa, Kaareselkä and Levijärvi-Loukinen gold mineralizations. Further papers review the use of aerogeophysical data, and ground geophysical characteristics of gold occurrences. Last papers include the palaeostress modelling of the Central Lapland Greenstone Belt and the prospectivity analysis using the geophysical and geochemical data. The results from the last papers demonstrate the increasing power of GIS methods as tools to integrate and quantify the spatial association of different datasets for the production of an integrated prospectivity map, which includes all conventional geological, structural, geophysical and geochemical targeting parameters.

Key words (GeoRef Thesaurus AGI): gold ores, greenstone belts, Central Lapland Greenstone belt, structural geology, mineral exploration, geophysical methods, geochemical methods, Paleoproterozoic, Kittilä, Sodankylä, Lapland Province, Finland.

Ojala, V. Juhani
Geological Survey of Finland, P.O. Box 77, FI-96101 Rovaniemi, Finland
E-mail: juhani.ojala@gtk.fi

ISBN 978-952-217-020-0 (PDF)
ISBN 978-951-690-980-9 (paperpack)
ISSN 0782-8535

Vammalan Kirjapaino Oy 2007

CONTENTS

Gold in the Central Lapland Greenstone Belt, Editor's Preface by *V. Juhani Ojala* 5

Paleoproterozoic metamorphism and deformation in Central Lapland, Finland by *Pentti Hölttä, Markku Väisänen, Jukka Väänänen & Tuomo Manninen* 7

Characteristics of gold mineralisation in the greenstone belts of Northern Finland by *Pasi Eilu, Heikki Pankka, Veikko Keinänen, Vesa Kortelainen, Tero Niiranen & Eelis Pulkkinen* 57

Structural controls on gold mineralisation in the Central Lapland Greenstone Belt by *Nicole L. Patison* 107

The Suurikuusikko Gold Deposit: Project development summary of Northern Europe's largest gold deposit by *Nicole. L Patison, George Salamis & Vesa J. Kortelainen* 125

The alteration and fluid Inclusion characteristics of the Hirvilavanmaa gold deposit, Central Lapland Greenstone Belt, Finland by *Helena Hulkki & Veikko Keinänen* 137

Exploration history of the Kaaresselkä gold-copper occurrence, Central Lapland by *Helena Hulkki and Eelis Pulkkinen* 155

The Levijärvi-Loukinen gold occurrence: An example of orogenic gold mineralisation with atypical metal association by *Marko J. Holma & Veikko J. Keinänen* 165

Application of aerogeophysical data for gold exploration: implications for the Central Lapland Greenstone Belt by *Meri-Liisa Airo* 187

Ground geophysical characteristics of gold targets in the Central Lapland Greenstone Belt by *Heikki Salmirinne & Pertti Turunen* 209

Palaeo-Stress modelling of the Central Lapland Greenstone Belt: implications for gold exploration by *V. Juhani Ojala, & Vesa Nykänen* 225

Prospectivity analysis of gold using regional geophysical and geochemical data from the Central Lapland Greenstone Belt, Finland by *Vesa Nykänen & Heikki Salmirinne* 251

Gold in the Central Lapland Greenstone Belt, Finland
Ojala, V.J. (ed.)
Geological Survey of Finland, Special Paper 44

EDITOR'S PREFACE

The purpose of this special paper is to summarise the gold research and exploration in the Central Lapland Greenstone Belt (and its surrounding area) in northern Finland conducted by the Geological Survey of Finland (GTK). Gold exploration in northern Finland has a long history and the first signs of gold were found in early 1800's in the Kemi area, in southern Lapland. Even though these did not lead to any discoveries, interest in the gold prospecting was seeded. After many years of prospecting along the major rivers in Lapland small placer deposits were discovered in 1868 in the Ivalojoki area in northeastern Lapland. Recorded gold production till 2006 is about 1300 kg. Individual prospects contain typically few hundreds of grams to few tens of kilograms of pannable gold, and hobby mining and small-scale panning operations have continued more or less continuously since 1870's. Many small vein-style gold occurrences were located in the panning areas in early 1900's. Several exploration shafts were sunk and although reported gold grades were several grams per tonne in places, the veins were narrow and no economic deposits were found. These vein style occurrences were explored again in 1950's, but no significant discoveries were made. Geologically these are located within the Lapland Granulite Belt, which is mainly composed of psammitic and pelitic sedimentary rocks with minor volcanic rocks and intrusives metamorphosed at granulite facies metamorphic conditions.

Although the early exploration was not successful locating gold deposits, it was the foundation for further geological mapping and research in northern Finland. Greenstone belts were recognized and their ore potential was noticed and a small gold mine operated (production 3 kg of Au) in near the Sirkka village in the Central Lapland Greenstone Belt in 1955–1956. GTK's mapping and exploration in northern Finland was boosted in 1970's when the regional office was opened in Rovaniemi. In late 1970's high gold price increased the interest for gold. Exploration for gold with improved geochemical and geophysical methods lead to discoveries three gold mines: Saattopora (mined 1988-1995), Pahtavaara (opened 1996–), and Suurikuusikko (under construction, published resource 2.4 Moz in 2006). Saattopora was discovered by Outokumpu company, and Pahtavaara and Suurikuusikko were discovered by GTK. In addition, over 30 drilling indicated occurrences have been located in the Central Lapland Greenstone Belt. Research into the formation of gold deposit, and especially on the orogenic gold deposits has been particularly important for the recent exploration success.

Rovaniemi, October 10, 2007

V. Juhani Ojala

Gold in the Central Lapland Greenstone Belt, Finland
V. Juhani Ojala (ed.)
Geological Survey of Finland, Special Paper 44, 7–56, 2007.

PALEOPROTEROZOIC METAMORPHISM AND DEFORMATION IN CENTRAL LAPLAND, FINLAND

by
Pentti Hölttä[1], Markku Väisänen[1,2], Jukka Väänänen[3], Tuomo Manninen[4]

Hölttä, P., **Väisänen, M., Väänänen, J. & Manninen, T. 2007**. Paleoproterozoic metamorphism and deformation in Central Lapland, Finland. *Geological Survey of Finland, Special Paper 44,* 7–56, 23 figures 2 tables and 2 appendices.

Three main ductile deformations, D1-D3, and contemporaneous and later shear zones account for most structures in Central Lapland. The oldest tectono-metamorphic feature is the bedding-parallel, mostly microscopic S1, overprinted by the main foliation S2, which is the most prominent structural feature seen in almost all rock types throughout the study area. Subhorizontal S2 is an axial plane foliation to tight or isoclinal, inclined to recumbent F2 folds. Kinematic indicators in the central and southern parts of the study area indicate a northward transport direction, but close to the S and SW border the Lapland Granulite Belt it may be of opposite direction. F3 folds deform the D2 structures. F3 folding show an extreme variety regarding the fold vergence with N-vergent folds in south, SW-W-vergent folds in north and E-vergent folds in west close to the Kolari shear system. Apparently, the F3 folding seems to be associated with complex tectonic movement directions, from S to N direction in the south, from NE to SW in the north and northeast part, and from W to E in the western part of the study area.

Several metamorphic zones have been mapped in the area. These are I) granulite facies migmatitic amphibolites south of the granulite complex (including the so called Tanaelv belt next to the granulites); II) high pressure mid-amphibolite facies rocks south of Zone I, characterised by garnet-kyanite-biotite-muscovite assemblages with local migmatisation in metapelites, garnet-hornblende-plagioclase assemblages in mafic rocks, local cordierite-orthoamphibole rocks intercalated with mafic volcanics; III) low-pressure mid-amphibolite facies rocks south of Zone II, garnet-andalusite-staurolite-chlorite-muscovite assemblages with retrograde chloritoid and kyanite in metapelites, hornblende-plagioclase-quartz±garnet in metabasites; IV) greenschist facies rocks of the Central Lapland Greenstone Belt, fine-grained white mica-chlorite-biotite-albite-quartz in metapelites, actinolite-albite-chlorite-epidote-carbonate in metabasites; V) prograde metamorphism south of Zone IV from lower amphibolite facies (andalusite-kyanite-staurolite-muscovite-chlorite±chloritoid schists, V.1–2) to mid-amphibolite facies (kyanite-andalusite-staurolite-biotite-muscovite gneisses,V.3) and upper amphibolite facies garnet-sillimanite-biotite gneisses (V.5); VI) amphibolite facies pluton-derived metamorphism related with heat flow from central and western Lapland granitoids, where Zone VI.2 represents both andalusite and sillimanite-present, and Zone VI.3 only sillimanite-present, andalusite absent gneisses. Pelitic rocks exhibit decompressional PT paths where andalusite grade metamorphism was preceded by higher pressure. Metamorphism was partly related with tectonic thickening during overthrusting of the Lapland Granulite Belt to the south, but the present metamorphic structure may record later, postmetamorphic faulting and folding events.

Key words (GeoRef Thesaurus AGI): metamorphic rocks, metapelite, metabasite, mineral assemblages, P-T conditions, Central Lapland Greenstone Belt, Paleoproterozoic, Finland.

[1] *Geological Survey of Finland, P.O. BOX 96, FI-02151 Espoo, Finland*

[2] *present address: Department of Geology, FI-20014 University of Turku, Finland*

[3,4] *Geological Survey of Finland, P.O. Box 77, FI-96101 Rovaniemi, Finland*

email: [1] pentti.holtta@gtk.fi [2] markku.vaisanen@utu.fi [3] jukka.vaananen@gtk.fi [4] tuomo.manninen@gtk.fi

INTRODUCTION

The Central Lapland Greenstone Belt and adjacent areas bordering the classical Lapland Granulite Belt in the south and south-west, have recorded six hundred million years of Paleoproterozoic depositional evolution from c. 2.5 Ga to 1.88 Ga (Lehtonen et al. 1998, Hanski et al. 2001). The structural and metamorphic history of the Lapland Granulite Belt has been constrained in many papers (e.g. Eskola 1952, Hörmann et al. 1980, Raith et al. 1982, Marker 1988, Barbey & Raith 1990, Korja et al. 1996, Perchuk et al., 2000), but systematic large-scale regional metamorphic and structural mapping has not been accomplished in the adjacent lower grade Proterozoic areas, although many special studies have dealt with the tectonometamorphic evolution of these regions (Gaál et al. 1978, Kärkkäinen 1982, Gaál et al. 1989, Ward et al. 1989, Rastas and Kilpeläinen 1991, Sorjonen-Ward et al. 1997, Lehtonen et al. 1998, Tuisku & Makkonen 1999, Hölttä & Väisänen 2000, Perchuk et al., 2000, Evins & Laajoki, 2002). However, the structural and metamorphic history of these areas is in a key position in tectonic modelling of the Proterozoic orogeny in the northern Fennoscandian Shield.

The purpose of this work is (i) to map the regional metamorphic zones in Central Lapland (Fig. 1) by describing the distribution of metamorphic mineral assemblages in metapelites and metabasites and by using geothermometry and geobarometry, (ii) describe the petrography and mineral chemistry of metapelites and metabasites, (iii) outline the main deformation phases and their relationship to metamorphism. This paper is mainly descriptive, trying to give a general framework for further development of both tectonic models and detailed structural and metamorphic analysis of metamorphogenic ore genesis.

GEOLOGICAL SETTING

The Proterozoic evolution of the Central Lapland area started with rifting of the Archean crust, producing andesitic lava flows and dacitic to rhyolitic ash-flow tuffs and ignimbrites of *the Salla Group* at the Archaean-Proterozoic boundary. These subaereally erupted volcanics are followed by crustally contaminated komatiites, siliceous high-Mg basalts and mafic volcanic rocks of *the Onkamo Group.* The 2.4 Ga old Koitelainen layered intrusion cuts the volcanic rocks of the Salla Group but not those of the Onkamo Group. This initial rifting-related volcanism was followed by the sedimentation of arkosic quartzites, carbonate rocks and mica schists of *the Sodankylä Group,* probably before 2.2 Ga that is the age of the mafic/ultramafic sills of the gabbro-wehrlite association (Hanski 1996) that have intruded these metasediments. Investigations of sedimentary facies of these metasediments suggest a continental margin setting. Deepening of the sedimentary basin caused accumulation of fine-grained sediments like phyllites and black schists of the *Matarakoski Formation, the Savukoski Group*. These pelitic metasediments are conformably overlain by basaltic and peridotitic komatiites and picrites of *the Sattasvaara Formation.* Emplacement of the 2.05 Ga old Keivitsa layered intrusion gives a minimum age for the Savukoski Group. The sedimentary-volcanic associations described above are in tectonic contact with *the Kittilä Group,* interpreted as an allochtonous oceanic unit comprising various MORB- (mid-ocean ridge basalts), OIB- (ocean-island basalt) and IAT-type (island arc tholeiitic) volcanic rocks, ophiolitic mantle rocks of Nuttio, and chemical sediments (Hanski 1997). The allochtonous nature of this group is, however, questioned by Sorjonen-Ward et al. (1997), who regard it as an ensialic, autochtonous unit. Younger quartzites and conglomerates of *the Lainio* and *the Kumpu Groups* cap all the previous rocks with unconformity. These molasse-type sediments contain pebbles of ca 1.88 Ga magmatic rocks, providing the maximum age of sedimentation (Hanski et al. 2000). Detailed descriptions of the above mentioned stratigraphic successions are provided by

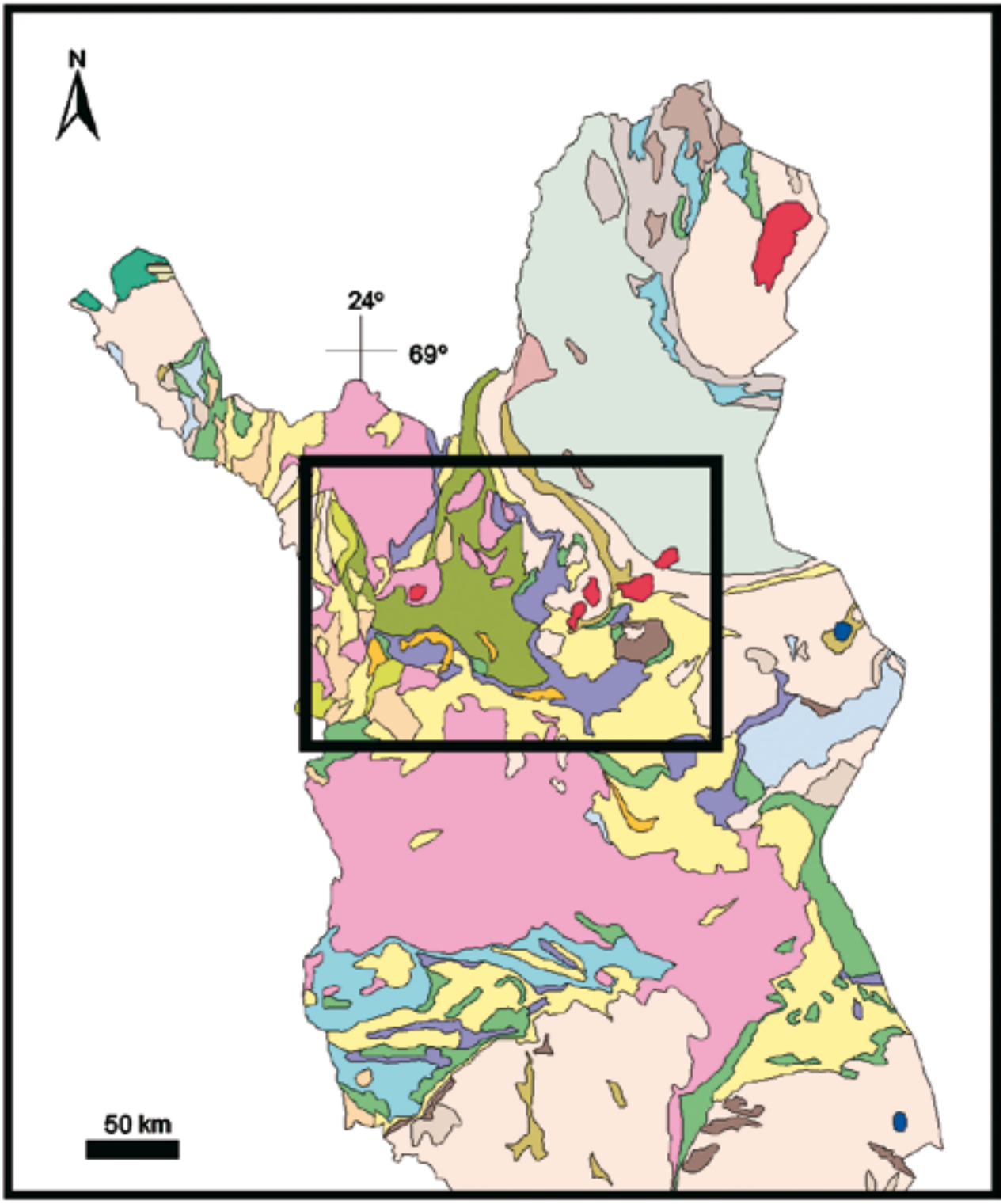

Fig. 1. The location of the study area as indicated by the box on the geological map of Finland after Korsman et al., 1997.

Lehtonen et al. (1998) and Hanski (2001) and Hanski et al. (2001).

The oldest dated Proterozoic intrusion is the Nilipää granite in the northern side of the Central Lapland Granitoid Complex. Th U-Pb age on zircon in this granite is 2.1 Ga, but also younger granitoids, dated at c. 1.84 Ga, occur in the complex (Huhma, 1986). Rocks of the so called Haaparanta Suite occur in the western part of Central Lapland and comprise c. 1.88–1.89 Ga deformed (foliated) tonalites, granodiorites and monzonites (Lehtonen et al. 1998), but granitoids of this age have been found also in the Sodankylä area in eastern Lapland (Räsänen & Huhma 2001). They probably represent the magmatism associated with the main

Svecofennian accretional tectonics. So called Hetta granites in the northern part of the Kittilä greenstone area are fine- to medium-grained, variously foliated, granodioritic to tonalitic intrusive rocks. Some of them are dated at c. 1.80 Ga, while some contain an older inherited component (Huhma 1986), suggesting the origin of deeper source by crustal anatexis. Youngest granitoids in the area are post-orogenic, 1.77 Ga old Nattanen-type granites (Huhma 1986; Haapala et al. 1987; Wennerstöm and Airo 1998).

Rastas and Kilpeläinen (1991) and Lehtonen et al. (1998) made structural analyses on selected key areas in Central Lapland. They reported a polyphase folding from various directions with at least two late folding phases, of which E-W folding is younger than N-S folding. Gaál et al. (1978), however, had an opposite opinion. Ward et al. (1989) and Sorjonen-Ward et al. (1997) on the other hand, provided a kinematic approach. They suggested a plate motion from two directions: the Svecofennian movement from south to north and a more or less simultaneous transport of the Lapland Granulite Belt from north to south or southwest. This created folds of opposing vergences in north and south, respectively. Dextral rotation caused some of the interference patterns seen on geophysical maps. The overall structural style of the area resembles that of a fold and thrust belt (Ward et al. 1989).

Deformation

We describe here those ductile deformation events which are closely related with the evolution of the regional metamorphism (D1–D3). Apart from these there is later postmetamorphic deformation that e.g. accounts for the evolution of late shear zones (Lehtonen et al. 1998; Väisänen, 2002).

Structural correlation across such a large area is problematic without detailed geochronological data of different tectonic episodes, recalling the possibility that even a single deformation can locally produce superimposed structures (e.g. Burg 1999). Since the now exposed orogen probably was formed by plate motions from different directions, at different times, and at varying intensities, the resulting tectonic mosaic is extremely heterogeneous. Therefore, the grouping of structures under labels D1–D3 below is only descriptive and is based on the overprinting criteria within smaller subareas. There are many different kinds of tectonic and metamorphic blocks exposed in the area and therefore, we do not believe that different structures (e.g. D3 structures) in different places were formed simultaneously. Therefore in a strict sense, the structures can not be correlated. The geometrical structure analysis has its limitations in Central Lapland.

Volcanic and sedimentary depositional structures (bedding) are quite common in Central Lapland, helping to identify rock types and the paleoenvironment. Unambiguous younging criteria were, however, observed very rarely during mapping, the observations were mostly made on quartzites. This hampered the identification of possible overturning of the strata. According to Ward et al. (1989) and Evins & Laajoki (2002), however, in spite of recumbent folding, there are sufficient younging data to preclude the existence of large-scale fold nappes in Central Lapland.

D1 deformation

The oldest tectono-metamorphic feature in Central Lapland is the bedding-parallel foliation, S1. It can be seen in mica rich sedimentary rocks within F2 fold hinges, perpendicular to S2 axial plane foliation, but rarely observed macroscopically. S1 is also preserved as inclusion trails within andalusite, garnet and staurolite porphyroblasts. Hölttä and Väisänen (2000) called it as S1a foliation (predating D1), because the origin of the foliation was ambiguous and it was not a mappable unit. However, the S1 foliation appears to be locally even stronger than S2. Therefore, we believe that it is of tectonic origin, older than S2 and deserves a separate D1 term, in accordance with terminology in Lehtonen et al. (1998). However, we did not detect any folds associated with S1 that would have been clearly overprinted by D2 deformation.

D2 deformation

The most prominent structural feature seen in most rock types throughout the study area is the main foliation, S2. In most cases it is subparallel to bedding, but in some competent rock types such as quartzites and sandstones, the foliation can be in larger angle to bedding. Minerals defining the foliation are protolith and metamorphic grade dependent: in lowest grade rocks foliation in pelitic rocks comprises chlorite and muscovite, whereas in higher grade rocks chlorite is replaced by biotite. When associated with F2 folds, S2 is an axial plane foliation to commonly tight or isoclinal folds deforming bedding, S0, and the bedding-parallel, microscopic S1. The orientation of the main foliation and the early folds vary, but in most places S2 is gently dipping to flat-lying, and the folds

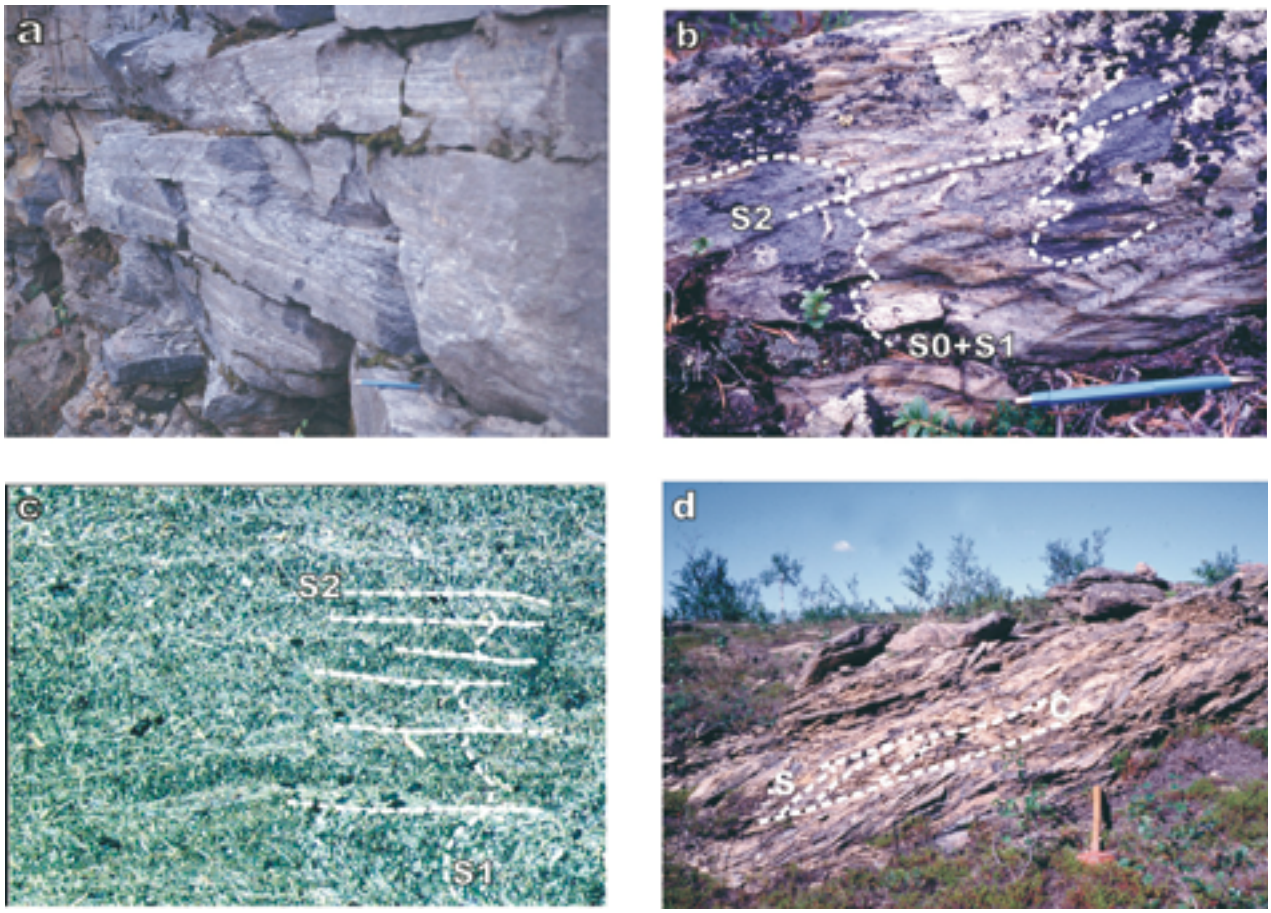

Fig. 2. (a) Recumbent folds on a vertical wall of an abandoned marble quarry in Äkäsjokisuu. Pen in the lower right corner points north. N 7490585, E 3355993. (b) Recumbent N-vergent folds in chlorite-muscovite schist in Rajala. Pen points north. N 7502895, E 3460515. (c) Photomicrograph of the rock in Fig. 2b displaying a vertical S1 and horizontal S2. Field of view is 5 mm. (d) Sheared ultramafic rock in Tarpomapää displaying a metre scale NNE-vergent S-C structure. The hammer shaft points north. N 7527806, E 3453228. Locations of the photograph sites are presented in Fig. 7.

are either recumbent or reclined (Figs 2a and 2b). Vertical axial planes with steep fold axes also exist. The field observations suggest that this early deformation was caused by horizontal movements related to thrust tectonics. However, it is not sure if S2 was originally horizontal throughout Central Lapland (see also Ward et al. 1989 and Evins & Laajoki 2002).

In the study area, the gently dipping to horizontal foliations are still preserved in many places, with an approximately NNE-SSW elongation lineation on the foliation plane. In Figs 2b, 2d, 3a and 3b, four independent observations from different parts of the study area are presented to argue that the movement direction was from SSW to NNE. The measurements of the main lineations are plotted on Fig. 4 and F2 folds on Fig. 5. Some of the S2 form lines, main thrusts, shear zones and tectonic transport directions are presented in Fig. 7.

In Fig. 2b, the fold vergence in recumbent F2 folds indicate a northward transport direction in an outcrop situated close to the Sirkka shear zone (Fig. 7). Fig. 2d displays a vertical section of an ultramafic rock, partly altered to serpentinite. This belongs to the same rock series as the Nuttio serpentinite that, according to Hanski (1997), is a piece of mantle part of an ophiolite. The outcrop displays a well-developed S-C structures that occurs both in millimetre and metre scales, indicating top-to-the NNE movement direction. Fig. 3a shows a spectacular example of a sigmoidal garnet, where shear sense is top-to-the N. The example in Fig. 3b shows a thin section photomicrograph of a strongly deformed quartzite with a well-developed quartz rod lineation on a subhorizontal foliation plane. Small-scale shear bands show top-to-the NNE movement direction.

The examples above indicate northward transport during D2. It is possible, however, that the structures described above were reactivated during D3 and some of them display a composite D2+D3 structure (see below). Kinematic information from this tectonic stage is lacking in this work from the S and SW border the Lapland Granulite Belt. Korja et al. (1996),

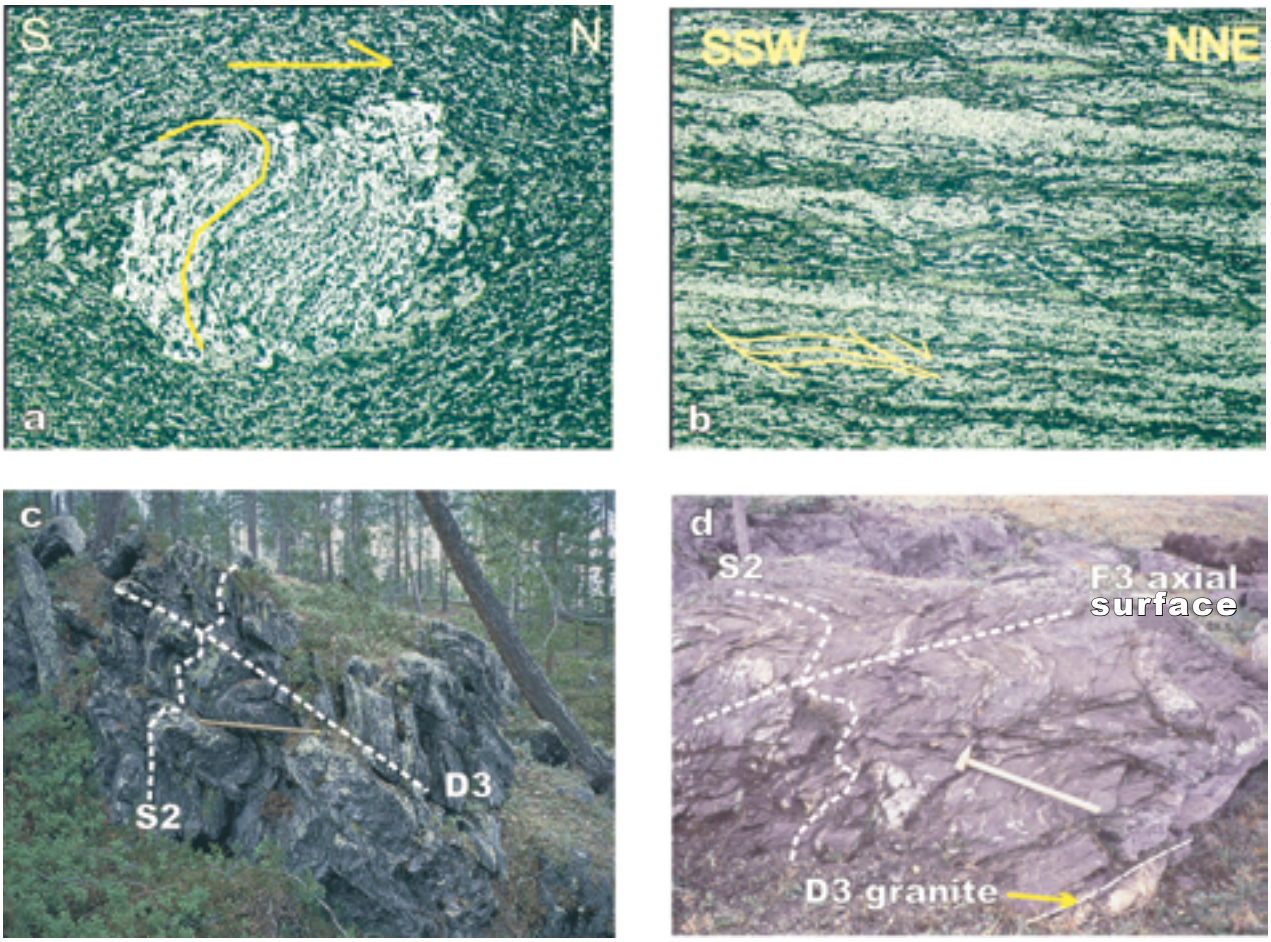

Fig. 3. (a) Sigmoidal garnet in mica schist, north is to the right. Field of view is 10 mm. Nuttion Tuorelaki. N 7515889, E 3457831. **(b) Dextral shear** bands in quartzite. Field of view is 10 mm. Petkula. N 7510986, E 3490942. **(c) Subvertical S2 is folded by E-W late folds with gently S-dipping** axial surfaces. Hammer shaft points north. Petäjävaara. N 7476509, E 3495903. **(d) Mica schist folded by inclined N-vergent late folds. Pink granite** is folded and intrudes along axial surfaces (lower right corner). The hammer shaft points north. Pikku-Venevaara. N 7482989, E 3516295. Location of the photograph sites are presented in Fig. 7

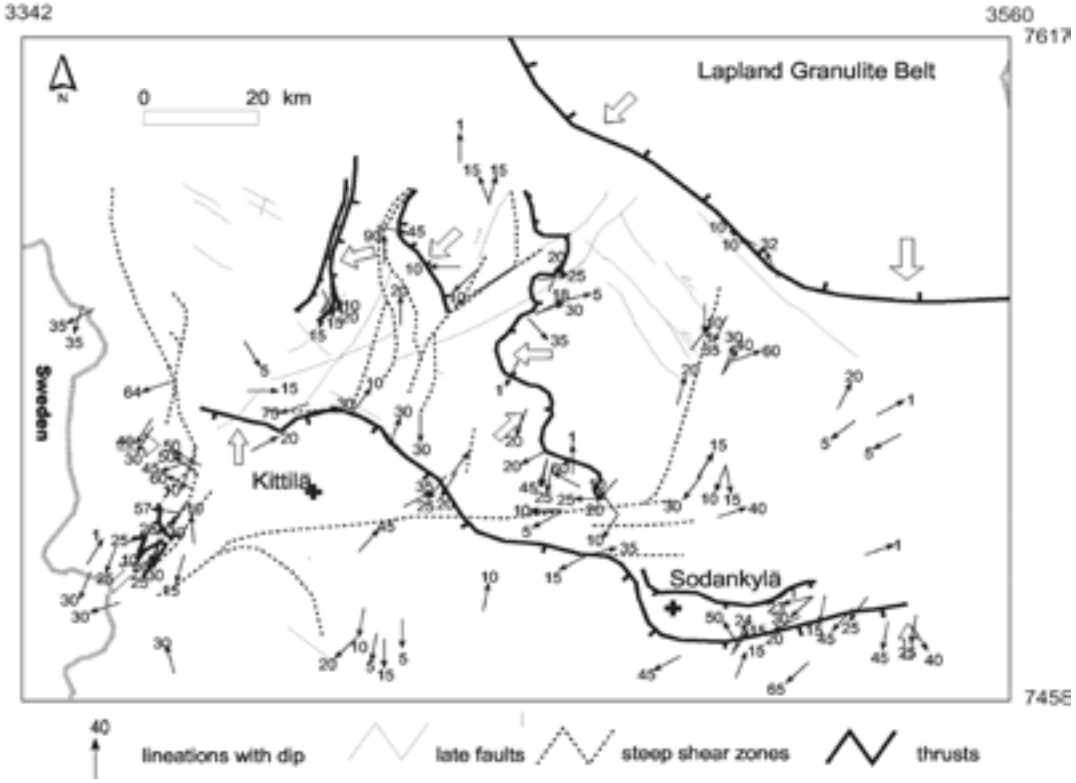

Fig. 4. Measurements of lineations. Broad arrows show the interpreted tectonic transport directions.

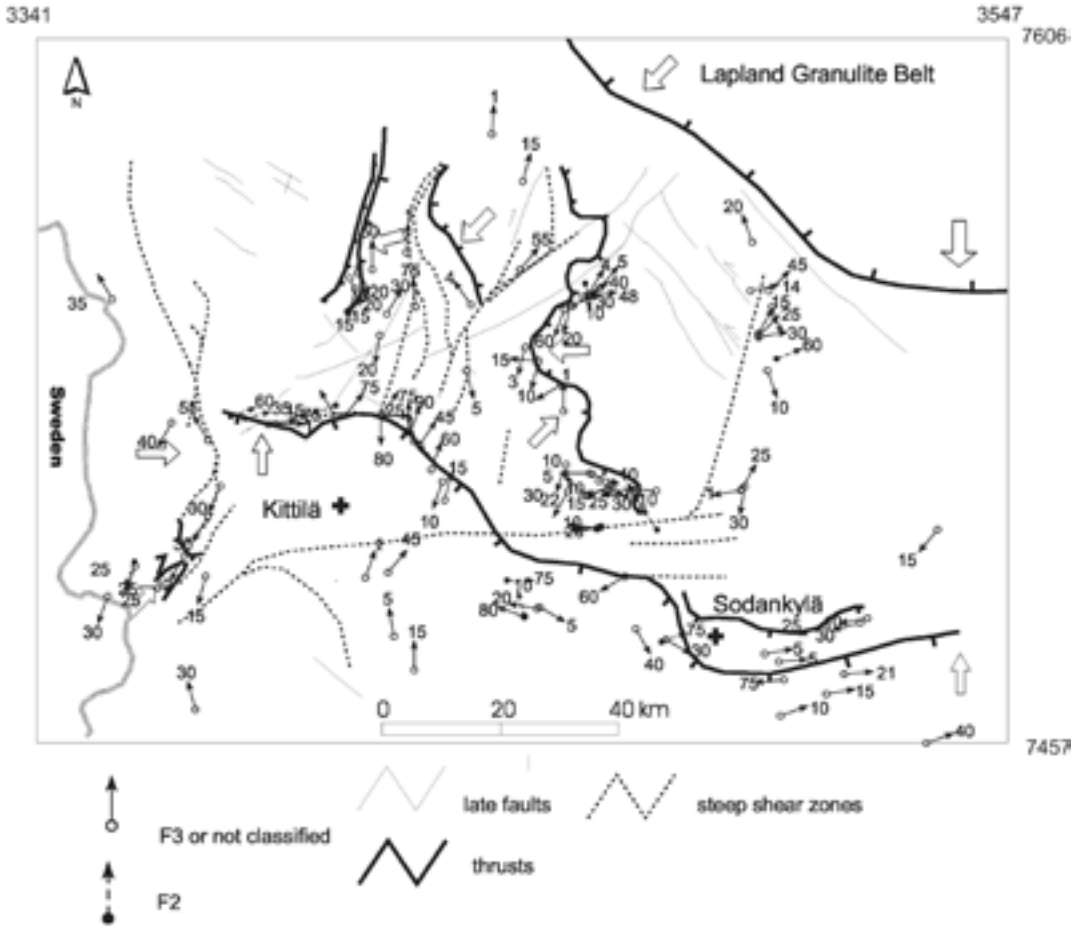

Fig. 5. Measurements of the F2 and F3 folds. Boad arrows show the interpreted tectonic transport directions.

however, describe SE verging recumbent folding, but the correlation to structures described above and below is unclear.

D3 deformation

The geological structures described above are overprinted by a set or sets of late folds (here collectively called F3 folds) and late shear zones of various orientation and attitudes (Väisänen 2002). Folds with E-W, N-S, NE-SW and NNW-SSE axial traces are all observed and measured, but the E-W and N-S orientations dominate. The dips of the axial surfaces of F3 folds also vary from horizontal through moderately dipping to vertical. These observations closely resemble that of a polyphase folding previously described as F3 and F4 by Rastas and Kilpeläinen (1991) and Lehtonen et al. (1998).

We did not find any unambiguous systematic and repetitive overprinting relationships of late folds of different orientations in this work. On the contrary, some observations suggest that they could have been formed approximately simultaneously or in the course of the same progressive deformation, possibly accompanied by rotation. These include e.g. (i) the similar fold geometry, (ii) the similar metamorphic grade using mineral growth as criteria, (iii) same relationship to vein material (carbonate veins, quartz veins, iron carbonate veins), (iv) fold axes of different orientation and attitude were found occasionally within same outcrops without any obvious overprinting relationships.

In general, in the southern and south-eastern part of the study area (Sodankylä area), late folds, plotted as F3 in Fig. 5, are E-W trending, their axial surfaces range from vertical to moderately dipping, locally even

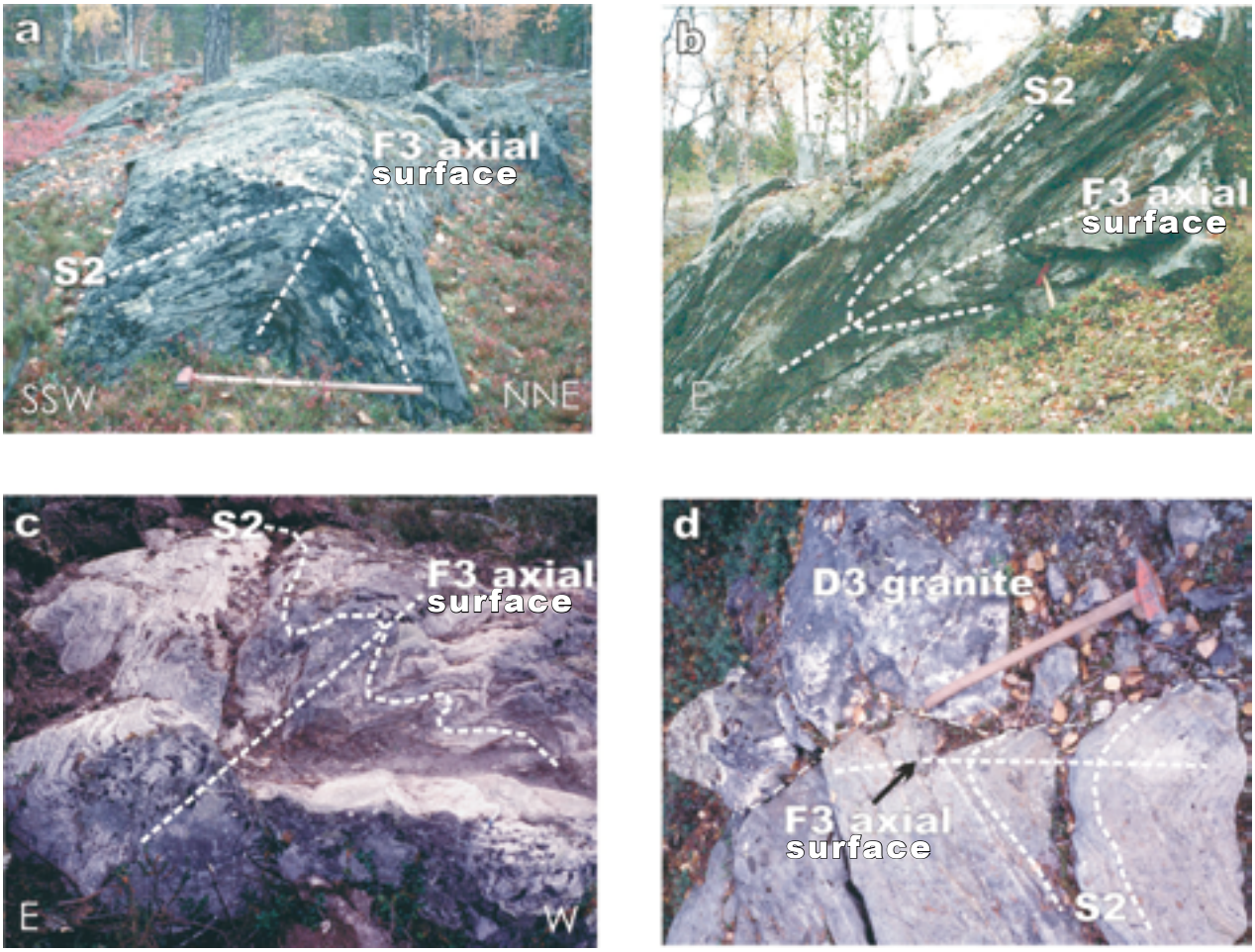

Fig. 6. (a) Asymmetric NNE-vergent late fold with a steep northern fold limb and a gently dipping southern limb. Rovalaki. N 7511749, E 3463811. (b) Inclined W-vergent late fold, view looking south. Haapanalehto. N 7555046, E 3458000. (c) W-vergent inclined fold, view looking south. Lompolo, N 7557161, E 3409693. (d) Granite dike intrudes along the N-S axial surface of a late fold, the hammer shaft pointing north. Vuomilehto. N 7553309, E 3496939. The thin dot-dash line shows the contact of granite with the folded felsic gneiss. Locations of the photograph sites are presented in Fig. 7.

subhorizontal with N-vergent fold asymmetry (Fig. 3c). Occasionally, pink granite dikes, folded and injected along axial surfaces, suggest at least some syn- to late tectonic granitoid magmatism (Figs 3d and 6d). Late folds are upright to steeply inclined, displaying a northward vergence in the central part of the area (Fig. 6a), but eastward vergent in SW and W part of the area close to the Kolari Shear system (Sorjonen-Ward et. al. 1997). W-vergent folds have been observed in N and NE part of the area, close to shear zones (Figs 6b and 6c), and late folds appear to be upright in the north-central part of the area. Kinematically, the late folding seems to be associated with a complex tectonic movement directions with S to N direction in the south, from NE to SW or ENE to WSW in the northern and northeastern parts, and from W to E in the western part of the study area (see Fig. 7).

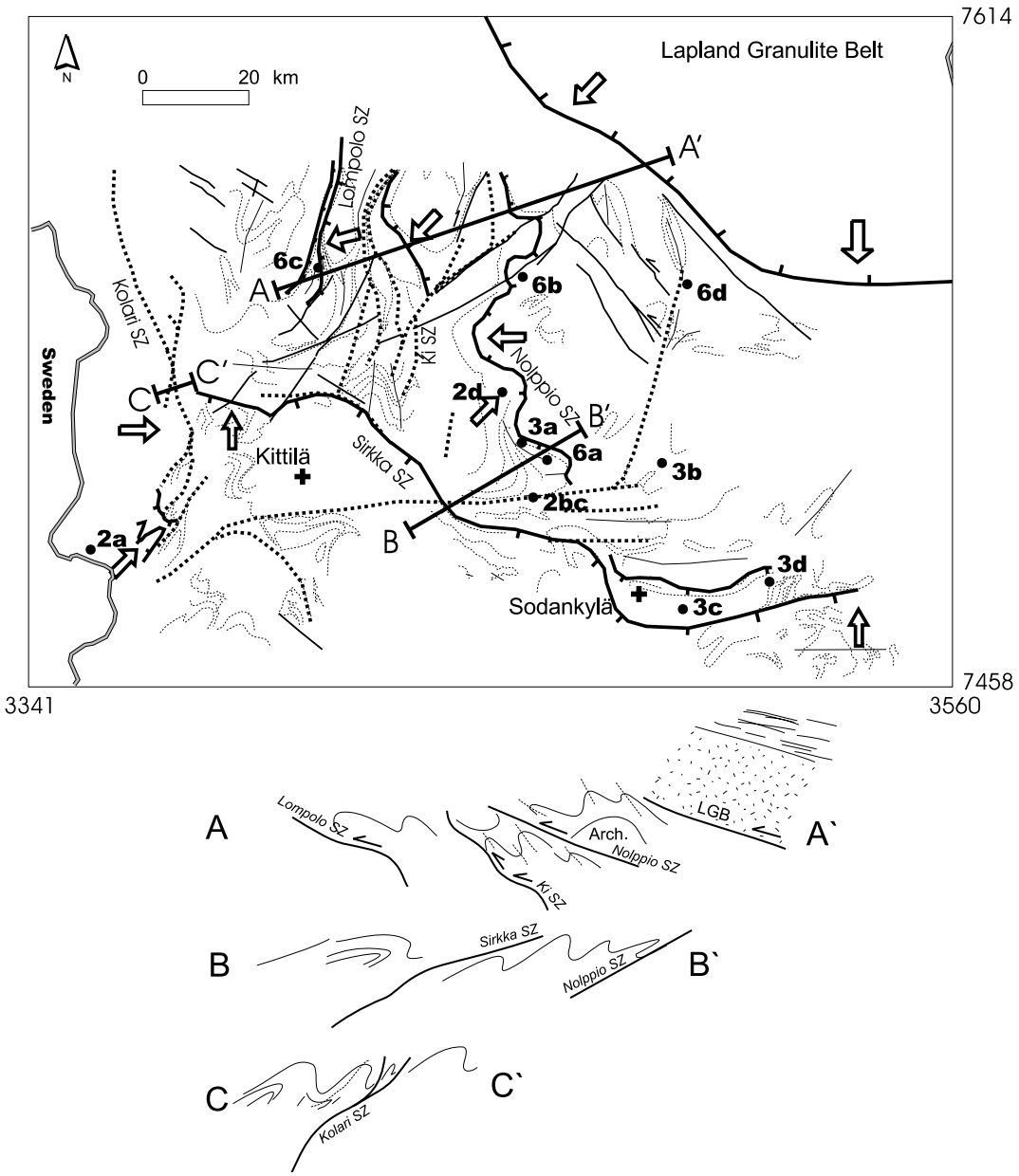

Fig. 7. Tectonic map of the Central Lapland Granitoid Complex. Arrows show the interpreted tectonic transport directions. Thick solid lines with ticks are thrusts, dashed thick lines are steep shear zones, solid medium lines are late faults, dashed medium lines are S2 form lines, thin solid lines are S3 axial surfaces. Ki SZ = Kiistala Shear Zone, SZ = Shear Zone, LGB = Lapland Granulite Belt. Below the map, schematic vertical sections along lines A-A', B-B' and C-C'. Numbers with letters show the locations of the photographs presented in Figs 2, 3 and 6.

Metamorphism

Based on the observed mineral assemblages in mafic and pelitic rocks, the following metamorphic zones have been observed in the study area (Fig. 8). Mineral assemblages in each zone are listed in Table 1. Mineral abbreviations are after Kretz (1983).

I Granulite facies migmatitic mafic rocks with grt-hbl-pl-qtz±cpx±opx assemblages, rare peraluminous migmatites with grt-bt-sil-pl-qtz. Assemblage grt-hbl-cpx-pl-qtz was observed only in this zone in the study area.

II Mid-amphibolite facies high pressure rocks, grt-ky-st-bt-ms-pl-qtz assemblages in pelites, local minor migmatisation, grt-hbl-pl-qtz in mafic rocks, locally cordierite-orthoamphibole.

III Mid-amphibolite facies low-pressure rocks, grt-and-st-chl-ms-pl-qtz±bt assemblages with retrograde chloritoid and kyanite, hbl-pl-qtz±grt in metabasites, typically a strong retrograde metamorphism with extensive chloritisation.

IV Greenschist facies rocks, fine-grained ms-chl-bt-ab-qtz in metapelites, act-chl-ep-ab-crb-qtz in mafic rocks.

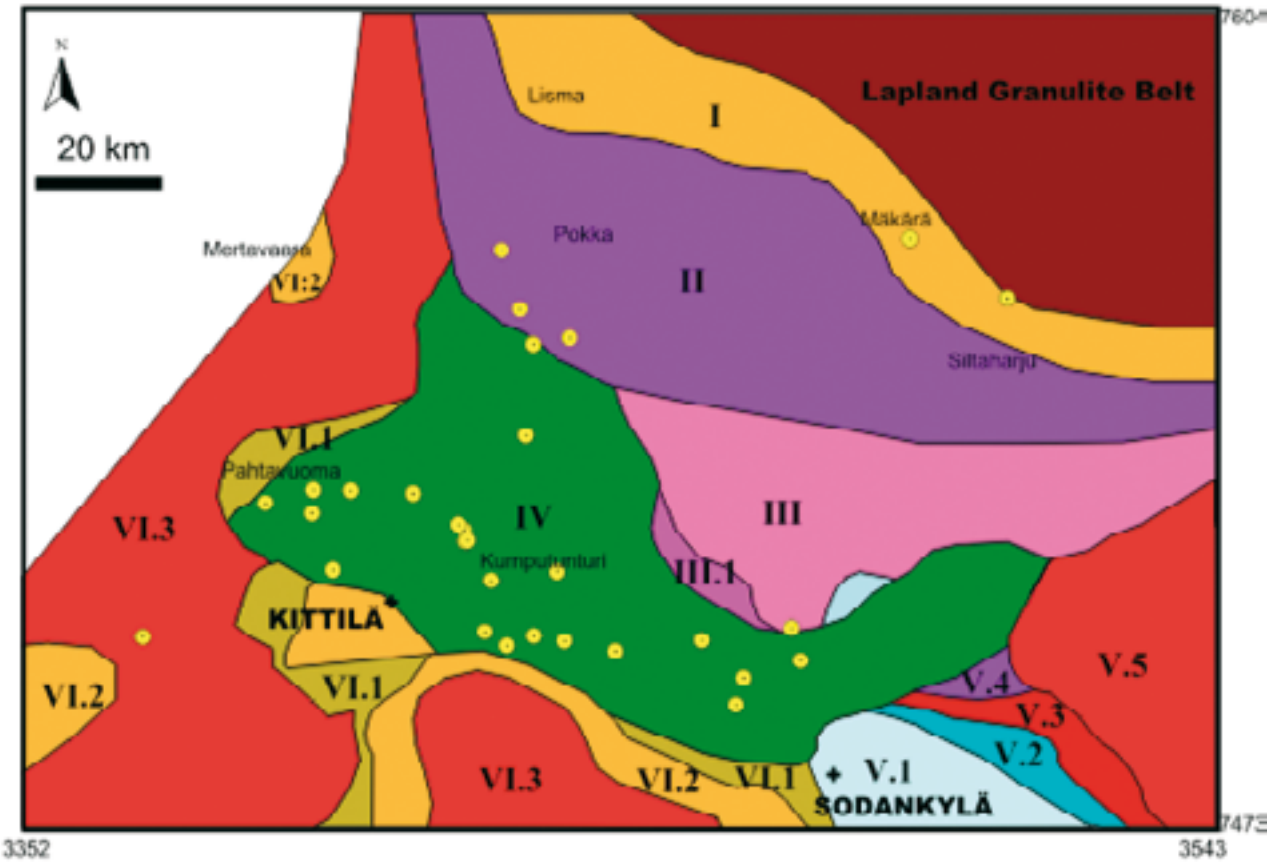

Fig. 8. Metamorphic map of the study area. See Tabel 1 and text for explanation of the zones, indicated by the Roman numerals. Yellow spots indicate the known gold desosits after Eilu (1999).

Table 1. Observed silicate mineral assemblages in metapelites and metabasites.

Zone	Assemblages	Retrograde minerals
I	– grt-bt-sil-ms-chl-pl-qtz±kfs – *grt-hbl-pl-qtz±cpx±bt±cum±ep±chl±ttn* – *hbl-pl-qtz±bt±ep±chl* – *grt-hbl-opx-cpx-cum-pl-qtz*	ms, ep, chl, cum, grt, partly hbl
II	– grt-bt-ms-qtz±ky±st±pl – ky-bt-pl-qtz – grt-bt-qtz±pl±cc – *hbl-pl-qtz±grt±ep±chl* – *tre-chl±ol±crb* – *tre-spl-pl-chl* – *tre-cor-pl-ch* – *oam-crd-pl-qtz±bt* – *oam-pl-qtz-chl±bt* – *grt-bt-chl-pl-qtz±oam±crd* – *grt-oam-chl-pl-qtz*	chl, ep
III	– grt-st-ms-chl-qtz ±ctd±and±ky±pl – ms-chl-qtz±tur – *hbl-pl-qtz±grt±ep±chl* – *grt-cum-qtz*	ctd, ky, partly ms, chl, st
III.1	– grt-ms-bt-chl-st-pl-qtz±ctd – bt-ms-qtz±tur±chl±pl	ctd, chl, partly ms, chl

Continue next page.

Zone	Assemblages	Retrograde minerals
IV	– chl-ms-qtz±pl±bt±tur±mnz – bt-chl-qtz±crb – *chl-act-pl-qtz±ep±crb ±ttn* – *chl-pl-qtz±crb±rt±ep* – *act-pl-ep-qtz-±rt* – *act-chl±cum* – *chl-crb-ep-pl±qtz* – *bt-chl-qtz-±ms* – *bt-ms-pl-qtz-mnz* – *bt-cum-qtz±pl* – *ol-crb-srp-op* – *srp-op* – *ol-tre-op±opx*	
V.1	– and-chl-ms-qtz±cld±ky±pl – st-cld-chl-pl-qtz±ky – ky-chl-ms-qtz±pl±and – and-bt-ms-pl-qtz±chl – ms-bt-ky-qtz±grt±chl	partly cld, chl
V.2	– st-ms-chl-pl-qtz±ky±tur – and-ms-chl-pl-qtz±st±ky – ky-st-ms-chl-pl-qtz	chl (?)
V.3	– st-ky-ms-chl-bt-pl-qtz±sil – st-ky-and-sil-ms-chl-bt-pl-qtz – st-bt-ms-pl-qtz±chl – ky-st-bt-ms-pl-qtz±grt – ky-bt-ms-pl-qtz±and	chl, partly ms
V.4	– ky-st-bt-ms-pl-qtz±grt±st – bt-ms-pl-qtz	
V.5	– st-sil-bt-ms-pl-qtz±grt±ky – sil-bt-ms-pl-qtz±chl±grt	chl, partly ms
VI.1	– bt-ms-qtz-tur±chl±pl±crd ±and±grt – bt-scp-crb-qtz – bt-cum-chl-qtz – chl-ms-qtz±bt±pl – bt-ms-kfs-pl-qtz – bt-ms-ep-pl-qtz – *grt-bt-crb-tlc±cum* – *grt-bt-crb-cum* – *grt-bt-Fets-crb±cum±qtz* – *grt-Fets-bt-chl-qtz* – *hbl-chl-ep-qtz-crb* – *hbl-pl-qtz-ep-ttn* – *hbl-pl-bt* – *hbl-ep-pl* – *bt-chl-ep-qtz* – *cpx-tr-scp-bt-qtz* – *cpx-tr-bt-kfs-qtz±scp* – *cpx-hbl-kfs-pl-qtz-ttn± bt*	
VI.2	– bt-ms-pl-qtz±and±chl±tur – ms-chl-pl-qtz±grt – grt-st-bt-ms-pl-qtz – and-crd-bt-ms-qtz±grt±chl±st – and-st-bt-ms-pl-qtz±sil ±grt±chl – grt-st-bt-pl-qtz±sil±and ±chl – bt-ms-ky-crd-qtz±and±sil ±chl – ky-and-sil-ms-crd-qtz – and-bt-ms-qtz-pl±crd±sil – *hbl-pl-qtz±grt*	chl, partly ms, partly st
VI.3	– bt-ms-pl-kfs-qtz±sil±pl±chl – st-sil-bt-ms-pl-qtz±grt – bt-ms-sil-pl-qtz±chl – bt-ms-crd-qtz±sil±pl – grt-bt-ms-pl-qtz±st±chl – grt-bt-sil-pl-qtz – grt-bt-ms-ep-pl-qtz – grt-bt-ms-sil-kfs-qtz – grt-bt-cum-chl-crd-pl-qtz – *hbl-pl-qtz±ep±chl±cpx*	chl, ep, partly ms, partly crd, partly st

V Prograde metamorphism from lower amphibolite facies (and-ky-st-ms-chl-cld-pl-qtz schists = V.1) to mid-amphibolite facies (ky-and-st-ms-pl-qtz gneisses =V.2, st-als-bt-ms-pl-qtz gneisses = V.3, ky-st-bt-ms-pl-qtz-grt gneisses = V.4 and upper amphibolite facies grt-sil-bt bearing gneisses = V.5), hbl-pl-qtz in metabasites.

VI Amphibolite facies, pluton-derived metamorphism-related with Central and Western Lapland granitoids, grt-and-ky-sil-crd-bt-ms assemblages, grade increasing from ms-bt-chl schists (VI.1) to and-sil-st-bt-ms gneisses (VI.2), and to grt-bt-ms-sil (VI.3) gneisses towards the granitoid contacts, locally migmatites, hbl-pl-qtz±grt and hbl-pl-qtz±cpx in metabasites.

Petrography

Zone I

In Zone I, mafic rocks are mostly migmatitic, the proportion of tonalitic leucosome varying from few per cents to >50 % of the rock volume. Garnet-bearing migmatites have the assemblage grt-hbl-pl-qtz±cpx, indicating that migmatites were at least partly produced in a melting reaction

(1) hbl + pl + qtz = grt + cpx + liq.

This reaction is considered as a transition reaction from amphibolite to granulite facies in high pressures, although in some compositions it may take place also in amphibolite facies (Pattison, 2003). High degree of melting and thermobarometric results indicate in this case granulite facies conditions. Metatexites and schlieren-type migmatites are common, epidote, chlorite and cummingtonite being retrograde phases after amphibole and pyroxene. Primary brownish green hornblende has commonly been altered into bluish amphibole. Orthopyroxene is rare but it occurs locally in the grt-hbl-opx-cpx-cum-pl-qtz assemblage, where cummingtonite is a retrograde phase. The texture of the mafic rocks is granoblastic, and main minerals are mostly in textural equilibrium forming dihedral angles. Leucosomes have a typical magmatic texture, where interstitial quartz is surrounding idiomorphic and subidiomorphic plagioclase crystals. In the Mäkärä area, close to the Lapland Granulite Belt contact zone, garnet occurs both as big grains and narrow coronas between hornblende and plagioclase (Fig. 9a) in clinopyroxene-absent rocks, indicating, instead of reaction (1), a continuous reaction

(2) hbl + pl = grt + qtz + H_2O.

In the Mäkärä area, there are metavolcanic rocks with primary volcanic textures like amygdules, and randomly oriented, euhedral plagioclase phenocrysts in a fine-grained matrix. These rocks have the high-grade assemblage with grt-amph-pl-qtz±cpx but annealing has not destroyed the primary magmatic texture, although these rocks have metatexite interlayers. Garnet forms coronas around plagioclase in these rocks, too. In the Lisma area, there are metadolerites in which clinopyroxene is altered from crystal rims into brownish green hornblende, indicating a reaction that took place during cooling,

(3) cpx + pl + H_2O = hbl

and garnet coronas are formed between clinopyroxene and plagioclase (Fig. 9b) in a reaction

(4) cpx + pl = grt + qtz.

Melting reaction (1) has a steep dP/dT slope so that melting is favoured by increasing temperature (Pattison, 2003). Reactions (2) and (4) have shallow positive dP/dT slopes that indicate either near-isobaric cooling or pressure increase during cooling or heating.

Zone II

The rocks in the zone II represent lower grade metamorphic conditions than in the zone I. Mafic rocks are not migmatized but metapelites have leucosomes in small abundances in the northern part of the zone II. Migmatization of the metapelitic gneisses is schlieren-type. Leucosomes form 5–20 mm wide veins and they are compositionally tonalitic, indicating melting in water-saturated conditions (Whitney & Irving 1994, Mouri & Korsman 1999). Bt-st-grt-ms-ky-pl-qtz assemblages are common (Figs 9e, 14a, 14c.). Rims of staurolite and kyanite crystals have often altered respectively, into sericite, and garnet into chlorite and biotite, some kyanites are intergrown with muscovite, biotite and staurolite inclusions occur in muscovite, garnets are crystallized on staurolite rims, and garnet has sometimes staurolite inclusions, indicating that peak metamorphic conditions were probably close to the univariant KFMASH reaction boundary (Fig. 23a)

(5) bt + st + qtz = grt + ms + als + H_2O.

The PT conditions of the reaction (5) are close to the univariant melting reaction

(6) bt + ms + st + pl + qtz = grt + ky + liq

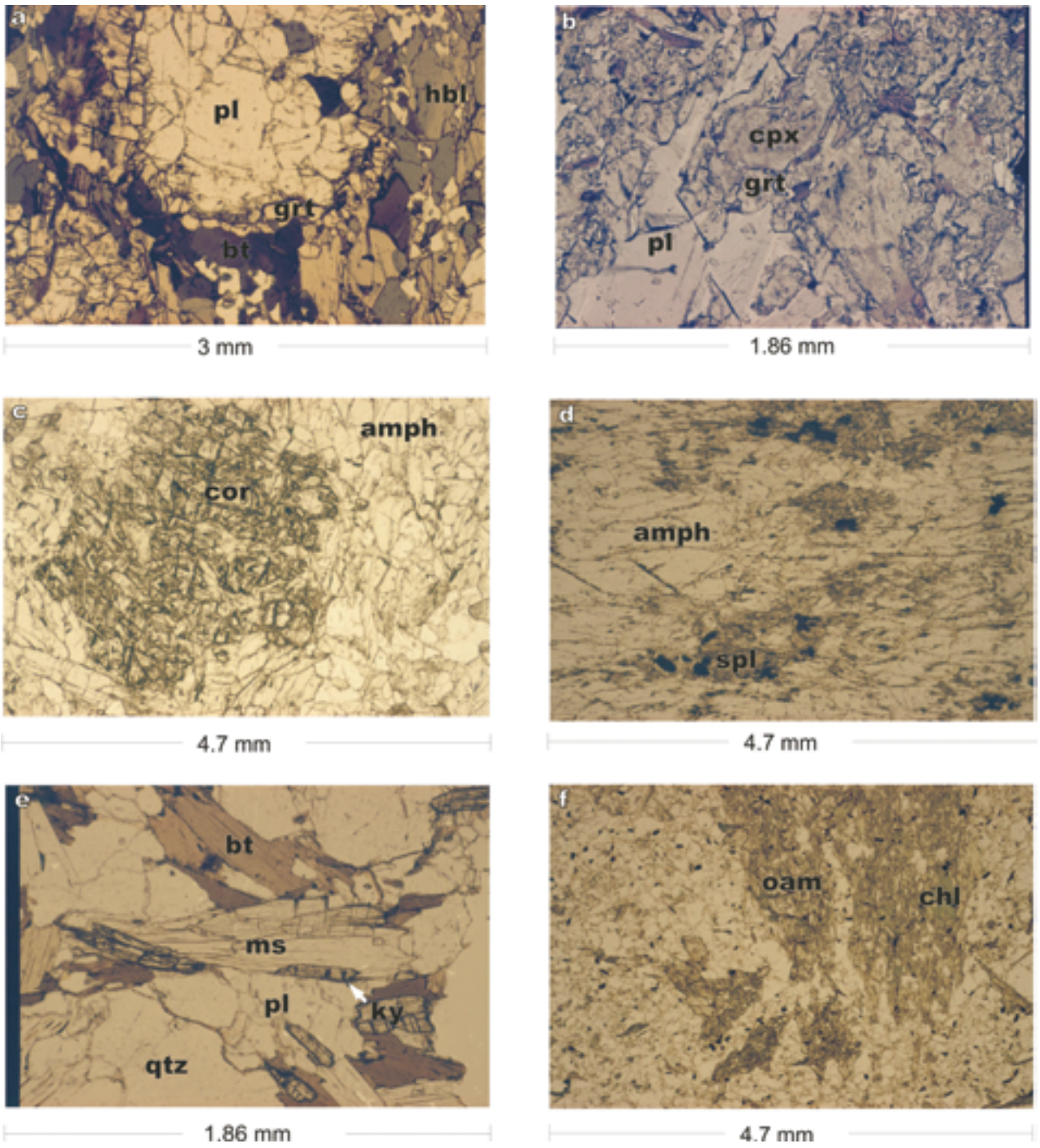

Fig. 9. Metamorphic textures and reactions in Zones I–III. a) garnet corona between hornblende and plagioclase. Zone I, sample PSH-97-20.2, N 7572940, E 3494520, b) garnet corona between clinopyroxene and plagioclase in metadolerite. Zone I, sample PSH-00-42.1 N7590218, E 3440182, c) corundum in a mafic rock. Zone II, sample PSH-99-100.3, N 7579148, E 3437489, d) spinel inclusions in tremolitic amphibole. Zone II, sample PSH-99-101.2, N 7578910, E 2561370, e) kyanite replacing muscovite. Zone II, sample JTV-98-49.1, N 7576663, E 3445005, f) chlorite, quartz and biotite replacing orthoamphibole, sample PSH-97-2.1, N 7544660, E 3494130.

in the system CNKFMASH (Fig. 23b). Because metapelites are migmatitic in the zone II, it is evident that the reaction (6) or the divariant melting reactions emanating from this univariant caused most migmatisation in staurolite and kyanite bearing rocks.

In the Pokka area, there are boninitic mafic rocks whose mineral assemblage is colourless-pale green tremolite and anorthitic plagioclase. These rocks locally contain corundum, which is texturally in equilibrium with amphibole and plagioclase (Fig. 9c). Also spinel inclusions occur in amphibole (Fig. 9d). In the same area, migmatitic pelitic gneisses have the assemblage grt-ky-bt-ms-pl-qtz.

In a few localities, there are schists that have the assemblage grt-bt-qtz±pl±cc. In places, garnets in carbonate-bearing schist (sample PSH-00–62.1) have

inclusion-free domains that have preserved the crystal shape of the reactant garnet-producing mineral, probably epidote (Fig. 11a). Epidote and chlorite are common retrograde phases after amphibole in mafic rocks of Zone II. Amphibole is often green to bluish green hornblende. In the Siltaharju area, there are hyrdo thermally altered cordierite-orthoamphibole rocks, which are intercalated with mafic metavolcanic rocks. Typically, in these rocks coarse-grained, orthoamphibole-bearing layers alternate with quartz and plagioclase-bearing layers, giving the rock a spectacular centimetre-scale banded structure. Orthoamphiboles garnets of the area may be up to centimetre in size, the latter containing many quartz inclusions. There are some exposures where the peak metamorphic mineral assemblage is not retrograded, but in most cases amphiboles and biotites are strongly altered into chlorite which occurs only as a retrograde phase. Orthoamphiboles typically occur as pseudomorphs that are totally replaced by chlorite, quartz and biotite (Fig. 9f). Unaltered orthoamphiboles are mostly brownish gedrites having, crystals sometimes almost colourless anthophyllite rims.

Zone III

Metapelites in Zone III are strongly schistose, although the primary bedding structures are still observable in many places. Grt-st-ms-chl-qtz±cld±and±ky±pl and ms-chl-qtz±tur are typical mineral assemblages. Chloritoid was observed only in the southern parts of Zone III. Biotite is rare in rocks that have grt-st-Al_2SiO_5-ms assemblages, and when present it is only an accessory or a retrograde phase. Instead, biotite is common in mica gneisses which have less aluminium or more calcium than the Al-rich pelitic gneisses of the zone, having bt-ms-qtz±tur±chl±pl or grt-bt-qtz±pl±ep±crb assemblages. Biotite-bearing gneisses occur sporadically throughout the area so that any biotite-in isograd cannot be defined. Garnet-staurolite-andalusite-chlorite assemblages are common, and staurolite tends to form pseudomorphs after garnet, together with chlorite (Fig. 10a). This indicates the divariant FMASH cooling reaction

(7) grt+H_2O=st+chl+qtz.

Garnet has sometimes chloritoid inclusions, which may indicate that some garnet was formed in the univariant FMASH reaction

(8) cld + qtz = chl + grt + st + H_2O.

Kyanite occurs as small crystals that overgrow andalusite and muscovite and in coronitic aggregates on staurolite and muscovite, often together with chlorite (Figs 10b–10c). The latter texture indicates that much of the kyanite was formed in a divariant FMASH cooling reaction

(9) st + qtz + H_2O = chl + als.

Kyanite occurs also as inclusions in andalusite and may therefore also be an earlier phase than andalusite. However, inclusions in andalusite are similarly randomly oriented as kyanites in the matrix (Fig. 10b), reflecting more likely that kyanite overgrows andalusite that occurs as big helisitic grains which may be centimetre-sized. The reaction relationship of andalusite with staurolite is not clear, but sometimes andalusite has staurolite inclusions, indicating that andalusite was at least partly produced in the reaction (9).

In garnet-absent rocks chloritoid occurs in chlorite and muscovite-filled pseudomorphs after staurolite, often together with kyanite (Fig. 10d) indicating that chloritoid was formed in a cooling reaction

(10) chl + st + qtz + H_2O = cld + als.

Chloritoid also occurs in pseudomorphs after garnet that are filled with chlorite, chloritoid, muscovite, quartz and sometimes andalusite (Fig. 10f), but biotite not being present in the thin section. These pseudomorphs have many relic garnet inclusions. It is possible that garnet first decomposed into chlorite and staurolite in the reaction (7) and then staurolite was consumed and chloritoid was formed in the cooling reaction (10).

Zone III.1

In the southwestern side of Zone III, there is a narrow zone belt honzon where, unlike in Zone III, biotite occurs in peraluminous rocks. Sedimentary rocks in this zone are more coarse-grained and gneissose compared with the schists in Zone III. Therefore this zone is considered a separate metamorphic Zone III.1. Some peraluminous rocks contain garnet, staurolite and retrograde chloritoid, but Al_2SiO_5 polymorphs where not observed in this zone. Biotite is mostly randomly oriented and occurs in muscovite and chlorite-filled pseudomorphs, where biotite overgrows muscovite and chlorite and replaces also garnet from the rim. Pseudomorphs are sometimes elongated, having the crystal form of staurolite. Small randomly oriented staurolite crystals are sometimes present in these pseudomorphs. These textures indicate that the reaction

(11) chl + ms (± grt) = bt + st + qtz + H_2O

proceeded into both directions during cooling and reheating (Fig. 23c), staurolite having been decomposed

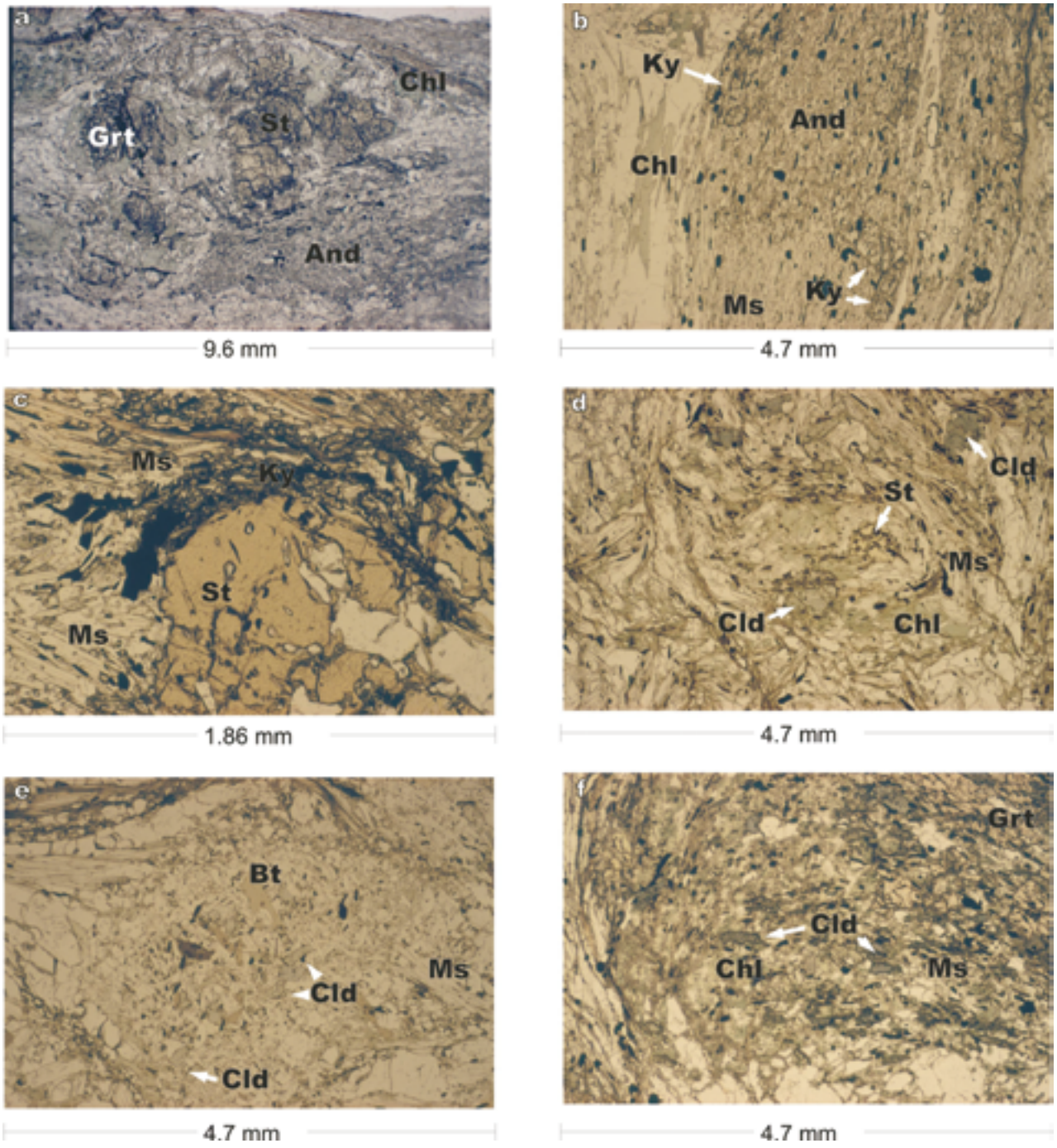

Fig. 10. Metamorphic textures and reactions in the zone III. a) Staurolite and chlorite replacing garnet, a big andalusite in the lower right corner of the figure. Sample PSH-98-60, N 7518130, E 3481410, b) Small kyanite crystals overgrowing andalusite and muscovite. Sample PSH-97-11.1, N 7517280, E 3478240, c) Small kyanite grains intergrown with muscovite on staurolite rims. Sample PSH-01-14.2, N 7521952, E 3519947, d) Chloritoid, chlorite and muscovite filled pseudomorph after staurolite, sample PSH-97-7.3, N 7528450, E 3485900, e) Biotite, chloritoid and muscovite filled pseudomorph. Sample PSH-98-41.2, N 7517980, E 3457930, f) Chlorite, chloritoid, muscovite and quartz filled pseudomorph after garnet. Sample PSH-97-7.4, N 7528450, E 3485900.

into chlorite and muscovite and then recrystallized with biotite again. Chloritoid occurs only in these pseudomorphs (Fig. 10e, PSH-98–41), having obviously been crystallized in the reaction

(12) st + chl + H_2O = cld + qtz

during cooling (Fig. 23c).

Zone IV

Zone IV represents the lowest grade metamorphic zone in the study area. The rocks sampled for this study are ultramafic, mafic and intermediate metavolcanic rocks and pelitic schists, although the latter are rare in Zone IV. Mafic and ultramafic metavolcanic rocks,

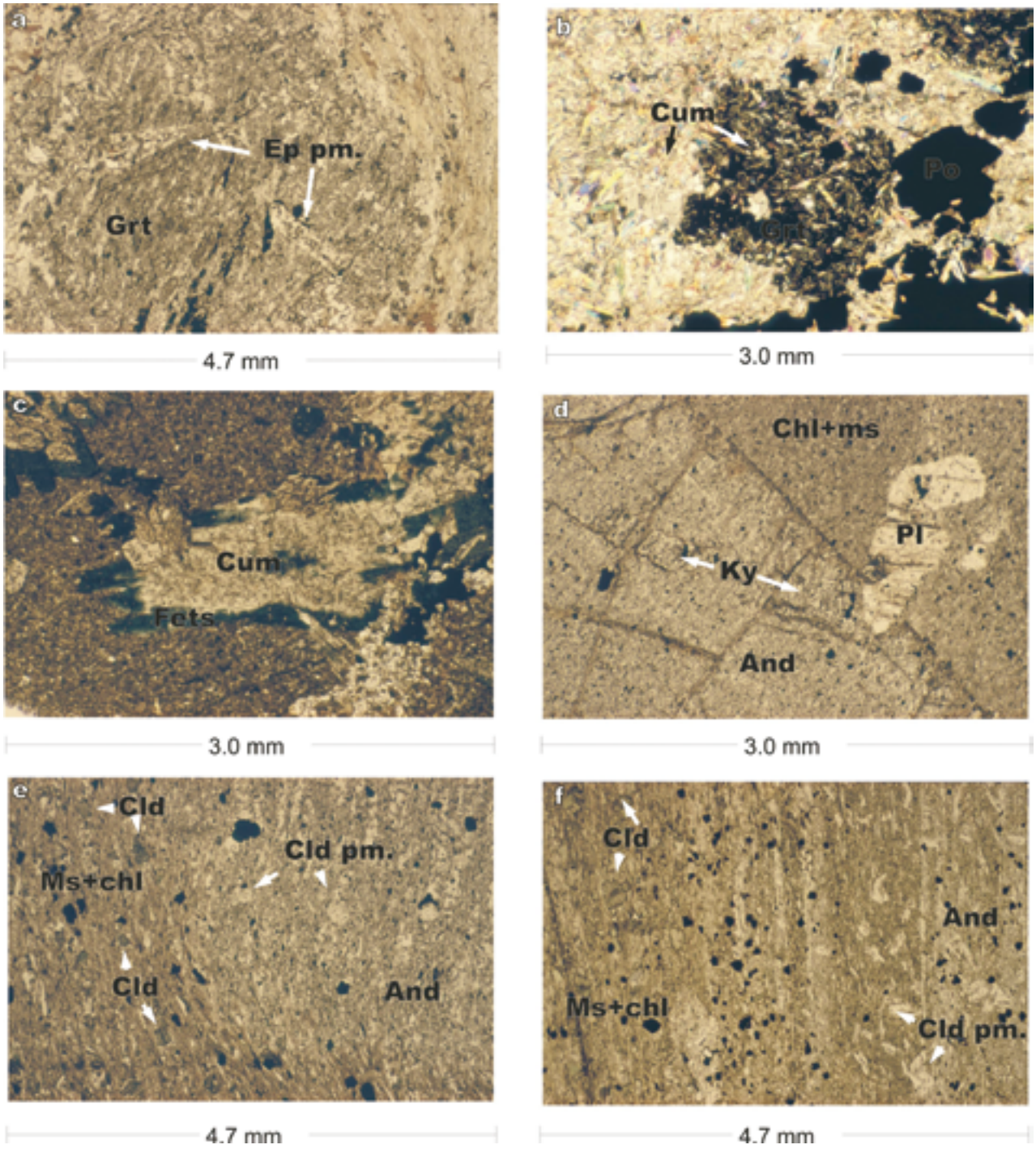

Fig. 11. Metamorphic textures and reactions in Zones III and V.1. a) A pseudomorph after epidote where the original crystal shape is preserved in garnet. Zone III, sample PSH-00-62.1, N 7548844, E 3460628, b) Cummingtonite inclusions in garnet. Sample PSH-00-1.4, N 7523465, E 2512075, c) Cummingtonite altering from rims to ferrotschermakite. Sample PSH-00-1.8, N 7525947, E 3385536, d) Kyanite inclusion in andalusite. Sample PSH-98-8.2, N 7480252, E 3486120, e) Chloritoids in the rock matrix and possible chloritoid pseudomorphs in andalusite. Sample PSH-98-4, N 7471821, E 3495325, f) Chloritoid inclusions in andalusite north of Zone IV. Sample PSH-98-59.3, N 7512570, E 3486600.

belonging to the Savukoski and Kittilä Groups, are the most abundant rock types in Zone IV. These rocks have generally preserved their primary volcanic textures with randomly oriented plagioclase phenocrysts, although in many cases these are carbonatized and epidotized. Carbonate seems to be more common in the NW part of the greenschist zone than in its eastern parts. Ultramafic rocks have usually preserved their magmatic mineral compositions, which are ol-tre-op±opx.

Pelitic schists are fine-grained, and if not pervasively sheared, they have preserved the primary structures, commonly seen as millimetre to centimetre scale sedimentary layers. Typical mineral assemblages are

chl-white mica-qtz-opaque minerals±pl±bt±tur±mnz and bt-chl-qtz-op±crb. The coarsest average grain size in the studied samples was ca. 0.05–0.1 mm, but finer-grained schists are common. Schists with the coarsest grain size are texturally granoblastic. Biotite and chlorite sometimes occur as porphyroblasts whose grain size is up to 0.5–1 mm in diameter.

Zone V

Zone V consist mostly of metapelites, and it shows a progressively increasing metamorphic grade from fine-grained andalusite schists to coarse-grained sillimanite gneisses east of the Sodankylä village (Fig. 8). Zone V.1 consists of pelitic schists which have centimetre-sized andalusites and ca 3–10 mm staurolite porphyroblasts in a fine-grained (ca 0.02–0.1 mm) matrix. The matrix of the rock is formed of chlorite, muscovite, chloritoid and quartz, and also magnetite grain aggregates are common. The matrix grain size is finest in rocks close to Sodankylä. The average grain size of the matrix generally coarsens southwards and eastwards in this Zone. Kyanite occurs as randomly oriented prisms (normally 0.2–0.5 mm in length but some prisms may be several millimetres) in the rock matrix and on andalusite grain boundaries and as inclusions in andalusite (Fig. 11d). Chloritoid inclusions in andalusite are rare, but andalusite often has inclusion free domains which have the shape of the chloritoid crystals in the matrix (Fig. 11e) which indicates that in cld-bearing rocks andalusite was formed in the reaction

(13) cld + qtz = and + chl + H_2O.

Some andalusite porphyroblasts have retrograde coronas formed of inner muscovite layer and outer chlorite layer. Plagioclase, when present, occurs like kyanite as randomly oriented idiomorphic 0.5–1 mm grains having many quartz and sometimes chloritoid inclusions. Biotite-bearing assemblages are rare, and tiny garnet was observed only in one thin section. Millimetre-sized pseudomorphs filled with chlorite, albite and muscovite are common, evidently these are hydrated plagioclases, staurolites and andalusites. Chloritoid is sometimes present in these pseudomorphs, indicating back-reaction (13). Monazite is a common accessory mineral in Zone V.1.

Prograde chloritoid occurs also north of the greenschist facies zone IV in a small area in the southern part of the zone III, where its textural relationships (inclusions in plagioclase and in andalusite, Fig. 11f) are exactly the same as in the zone V.1. It is possible that the greenschists are lying on the rocks of Zone III and Zone V, the metamorphic zonation of the pelite formation continuing under the allochthonous greenschists.

In Zone V.2, chloritoid disappears, evidently in the reactions (9), (10), (13) or in

(14) cld + qtz = chl + st + H_2O

(Fig. 23d). Metapelites in Zone V.2 are medium grained gneisses, not schists as in Zones V.1–2. Melting has not started and primary bedding is visible in many places. Staurolite and andalusite may be up to 1–2 cm in size, and kyanite prisms up to 1 cm are common. There are andalusite-bearing layers without kyanite and also kyanite-bearing layers without andalusite. Kyanite and andalusite occur also together, in these rocks kyanite is found in the matrix, as inclusions in andalusite, and as needles on andalusite rims (Fig. 12a). Kyanite inclusions found in andalusite may be an effect of two-dimensional thin sections, because on outcrops kyanite needles growing into andalusite are common.

In Zone V.3, biotite becomes stable occurring often as large flakes, and grain size the matrix of the coarsens in pelitic rocks. Sillimanite also rarely occurs as fibrolitic grains. Chlorite is less abundant in biotite-rich than in biotite-poor rocks, therefore it is possible that Zone V.3 represents the divariant KFMASH chlorite breakdown reaction (11) chl + mu = bt + st + qtz + H_2O, (Fig. 23d) that has consumed chlorite in some layers but not completely everywhere. In some outcrops andalusite, kyanite and sillimanite are found in the same thin section; in these rocks fibrolitic sillimanite is crystallized on plagioclase and mica rims rather than replaces kyanite or andalusite (Fig. 12b). This texture indicates that temperature increased into the field where the divariant KFMASH reaction

(15) st + ms = bt + als + H_2O

took place (Fig. 23d). Chlorite is often a retrograde phase, and in some exposures staurolites have almost completely altered into chlorite and muscovite, indicating back-reaction (11).

In Zone V.4, garnet was observed in one exposure where it occurs in textural equilibrium with relatively coarse-grained kyanite in the assemblage ky-st-bt-ms-pl-qtz-grt (Fig. 12c). This texture indicates that garnet was formed in reaction (5) bt + st + q = grt + ms + ky + H_2O. The assemblage and absence of other Al_2SiO_5 minerals indicates similar metamorphic conditions as in Zone II, differing clearly in pressure from the progressive zoning in V.1–3 and V.4.

In Zone V.5 andalusite was not detected any more and kyanite occurs only as small relics. Staurolites up to 1 cm and garnets and plagioclases up to 5–6 mm are common. Sillimanite is fibrolitic and replaces

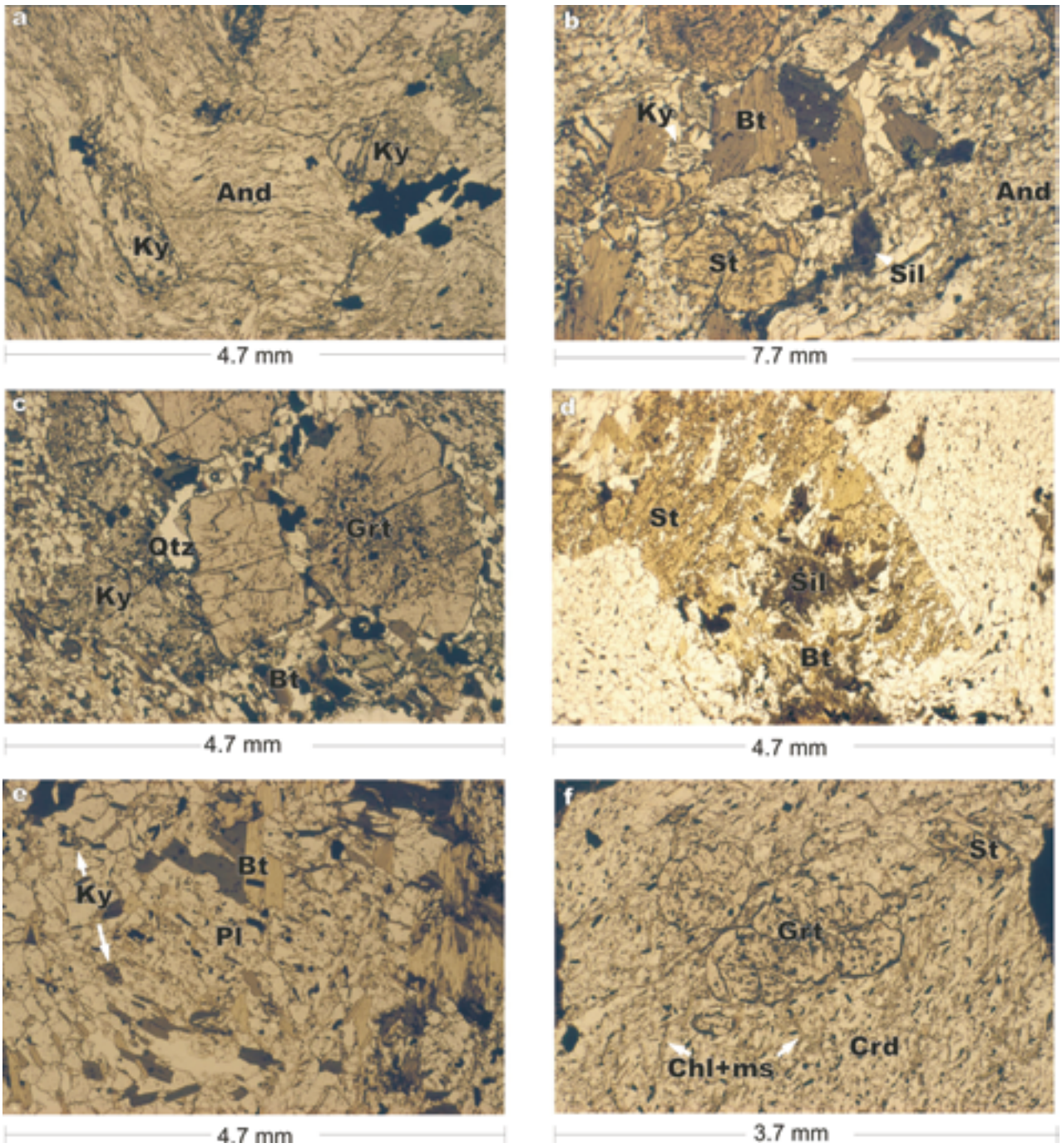

Fig. 12. Metamorphic textures and reactions in the zones V and VI. a) kyanite-andalusite assemblage, zone V.3, sample PSH-99-72.1, N 7485560, E 3511380; b) kyanite-andalusite-sillimanite-staurolite-biotite assemblage, zone V.4, sample PSH-00-113.2, N 7491153, E 3503060; c) garnet-kyanite-biotite-muscovite assemblage, zone V.4, sample PSH-98-53.2, N 7494530, E 3505680; d) fibrolitic sillimanite and biotite replacing staurolite, zone V.5, sample PSH-01-17.1, N 7521105, E 3535306; e) kyanite inclusions in plagioclase, zone V.5, sample PSH-01-17.2, N 7521105, E 3535306; f) garnet inclusions in cordierite, zone VI.2, sample PSH-98-69.1, N 7469020, E 3472710.

sometimes staurolite porphyroblasts together with biotite (Fig. 12d). These assemblages indicate that the reactions (5) and (15) locally consumed all staurolite in the sillimanite field. The matrix micas have strong preferred orientation (S3) but matrix quartz and feldspar have a granoblastic texture. Some garnet porphyroblasts are helisitic, containing plenty of quartz inclusions, but others are almost inclusion-free. When present, kyanite occurs locally as randomly oriented, small grains, and it commonly exists as inclusions in plagioclase, probably representing prograde relics (Fig. 12e).

Zone VI

Zone VI covers the area around granitoids of the central and western Lapland. At the western margin of Central Lapland Granitoid Complex, the grade

of metamorphism increases progressively towards the complex without abrupt change. In the eastern and northern side of the Central Lapland Granitoid Complex the change in grade from Zone IV and from Zone V is connected with shear zones.

In Zone VI.1, metapelites are fine-grained schists (average matrix grain size < 0.1 mm). Locally, biotite forms flakes up to 5 mm in a fine-grained matrix, and in one exposure there was one ca 10 mm cordierite; tiny andalusites and garnets are very rare in this Zone. In the country rock of the Pahtavuoma Cu-ore, garnet is locally present in the alteration zone as 1–3 mm idiomorphic grains, in skarns that are formed between amphibole-rich and carbonate-rich layers. The garnet-bearing assemblage is grt-bt-crb±cum±Fets. Garnet has often cummingtonite inclusions and cummingtonite is altered from rims to bluish green ferrotschermakite, which occurs also as idiomorphic grains, several millimetres in size (Figs 11b–c). These textures indicate that garnet and ferrotschermakite were formed in the reaction

(16) cum + cal = grs + Fets.

Another garnet-bearing locality is in the southern side of Zone IV, where garnet occurs in an iron-rich rock in the assemblage grt-amph-qtz. In the Pahtavuoma area schists with the matrix assemblage bt-qtz-cc locally have scapolite porphyroblasts 3–7 mm in diameter. Scapolite is not restricted only in this zone and in these assemblages but occurs also elsewhere in the Central Lapland area. Descriptions of the scapolite-bearing rocks are given by Tuisku (1985) and Frietsch et al. (1997).

In Zone VI.2, metapelites are medium grained gneisses with granoblastic matrix. Andalusite is a common Al-silicate but it often co-exist with fibrolitic sillimanite. Cordierite was observed only in a few localities. In the cordierite-bearing rocks garnet, when rarely present, occurs as inclusions in cordierite and on andalusite rims (Fig. 12f). Cordierite has also many muscovite inclusions, whose optical orientation does not differ from muscovite in the matrix, and it seems to replace andalusite from rims. It has also some chlorite inclusions, so the univariant KFMASH reaction

(17) chl + ms + and + qtz = bt + crd + H_2O

may have produced cordierites. In the cordierite-bearing rocks garnet, when rarely present, occurs as inclusions in cordierite and on andalusite rims (Fig. 12f). Because cordierite has some staurolite inclusions, the garnet may also have been a reactant and earlier mineral than cordierite in a reaction such as

(18) grt + and + H_2O = crd + st + qtz.

Fibrolitic sillimanite often replaces andalusite from rims, indicating reaction

(19) and = sil

Kyanite was observed only in one outcrop (PSH-98–11). There andalusite, kyanite and sillimanite occur in the same Mg-rich, coarse-grained metapelite. Assemblages in this rock are bt-ms-ky-crd-qtz±and±sil±chl, bt-ms-crd-qtz±sil and ky-and-sil-ms-crd-qtz. Sillimanite occurs as fibrolitic grain aggregates, kyanite forms coarse-grained prisms up to 5–10 millimetres and andalusite occurs as centimetre-sized helisitic grains with abundant quartz inclusions. Sillimanite often replaces andalusite in grain boundaries (Fig. 13a) but rarely kyanite, which forms intergrowths with muscovite and cordierite. Kyanite and andalusite occur as inclusions in cordierite, and cordierite coronas are formed between kyanite and biotite, cordierite forming embayments into biotite (Figs 13b–c). Sillimanite replaces this muscovite and sometimes occurs as inclusions in cordierite together with muscovite. Although often close to each other, andalusite and kyanite were not found in contact, therefore their cystallization order is unclear. However, if they underwent similar metamorphism than Zones V.1–4, kyanite crystallization may have been roughly simultaneous with andalusite. With increasing temperature they were partly altered into sillimanite and cordierite was formed in a continuous reaction between Al-silicate (ky, and, sil) and biotite

(20) bt + als + qtz = crd + ms.

In garnet and staurolite-bearing rocks of Zone VI.2, andalusite contains inclusions of quartz, biotite, muscovite, chlorite, skeletal staurolite and euhedral garnet (Fig. 13e), indicating that andalusite was formed in reactions such as (5), (15) and

(21) chl + st + qtz = grt + and + H_2O.

In the Mertavaara area there are garnet and andalusite-bearing muscovite-free rocks, where both garnet and andalusite have staurolite inclusions, indicating reactions (5) and (21).

Strong retrogression is a typical feature in Zone VI.2. Hydration has often destroyed previous garnet, andalusite and staurolite that are now pseudomorphs, filled with fine grained muscovite, biotite and chlorite. Garnets have also been altered into plagioclase and chlorite (Fig. 13f), and sometimes staurolite, plagioclase and biotite replace garnet from rims indicating back-reaction (5). Some back-reaction (16) obviously took place in andalusite-bearing rocks, because andalusite is often rimmed by staurolite.

Zone VI.3 represents sillimanite grade, where the

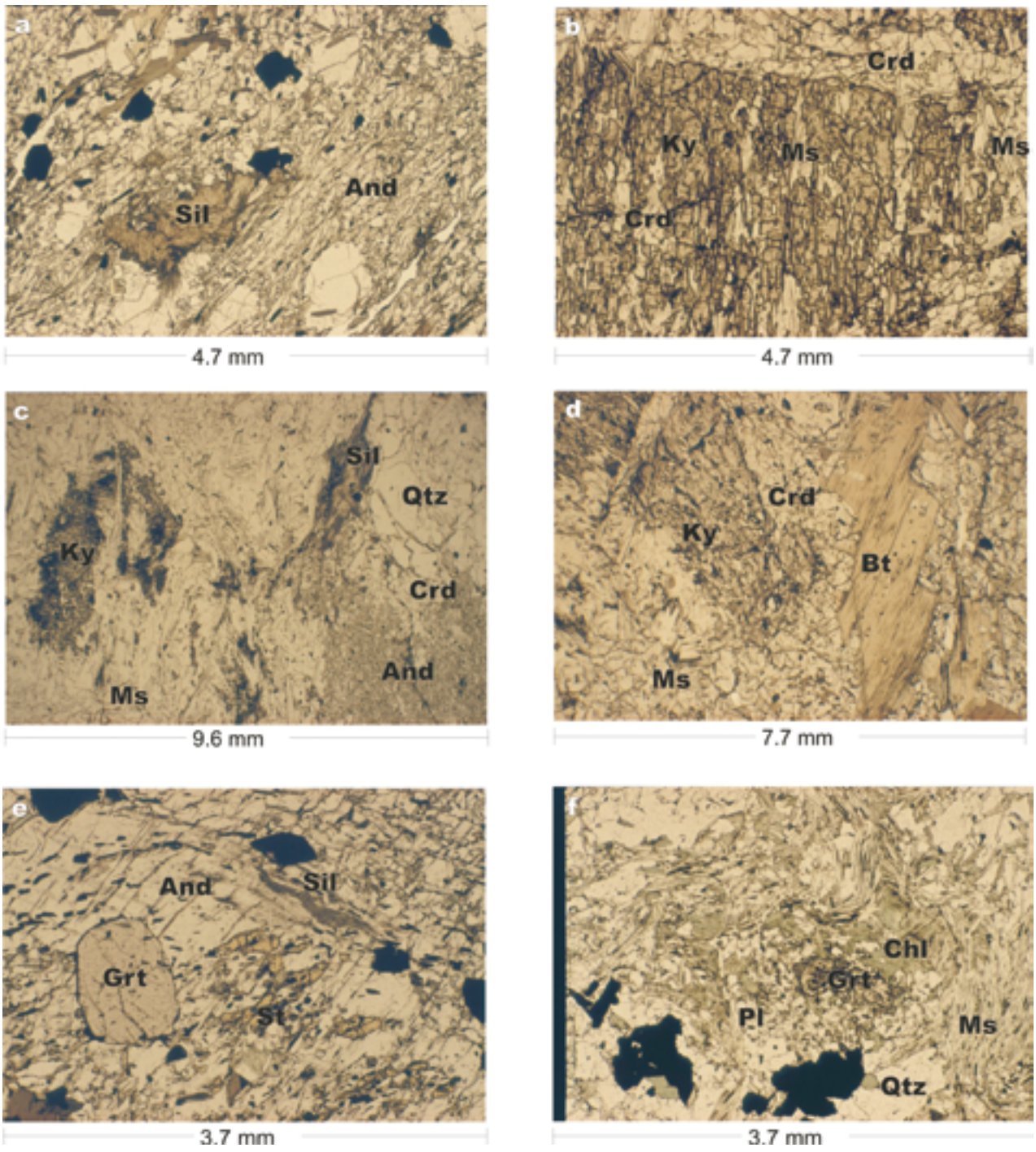

Fig. 13. Metamorphic textures and reactions in Zone VI.2 a) Fibrolite needles on andalusite rim, sample PSH-98-97.3, N 7495066, E 3416256, b) Kyanite intergrowths with cordierite and muscovite. Sample PSH-98-11B, N 7466644, E 3466995, c) Coexisting andalusite, fibrolitic sillimanite and kyanite, andalusite is replaced by cordierite corona. Sample PSH-98-11.2, N 7466644, E 3466995, d) Cordierite corona between kyanite and biotite. Sample PSH-98-11B, e) Staurolite, sillimanite and garnet inclusions in andalusite. Sample PSH-98-97.5, N 7495066, E 3416256, f) Garnet altering into plagioclase and chlorite. Sample PSH-98-18.2C, N 7485693, E 3447609.

high grade seems to be caused mainly by granitoid intrusions. Sillimanite is the only Al_2SiO_5 polymorph in this zone. There may be some changes in grade inside the zone, depending e.g. on the distance from granitoid contacts, but those variations could not be mapped during the course of this study. Locally metapelites are migmatitic, for example on the western side of the Central Lapland Granitoid Complex, where pelitic rocks become migmatitic close to the contact of granitoids, having granitic leucosomes as narrow stromatic veins. In Zone VI.3, sillimanite is the only Al_2SiO_5 mineral, although these rocks still contain grt-als-st-bt-ms-chl-pl-qtz assemblages, typical for Zone VI.2. This indicates, that the Al_2SiO_5-forming

reactions observed in Zone VI.2 started in the andalusite and continued in the sillimanite field in Zone VI.3. The western part of the zone VI.3 is characterized by potassium-feldspar-rich, reddish gneisses, which often are plagioclase-free. Idiomorphic and subidiomorphic potassium-feldspars are surrounded by interstitial quartz in these rocks, a texture suggesting that feldspars were crystallized from melt.

In mafic rocks, clinopyroxene is a rare mineral. With normally a granoblastic texture. In these rocks, epidote and chlorite are retrograde minerals, typically occurring in fractures and shear planes.

Metamorphic zones and gold mineralization

The Central Lapland area has tens of known gold occurrences; some of those are economic (Eilu, 1999). These occurrences belong to the orogenic gold deposit group following the classification of Groves et al. (1998). They argued, that orogenic gold deposits were formed during compressional to transpressional deformation processes at convergent plate margins in accretionary or collisional orogens. According to McCuaig & Kerrich (1998), the accretionary environment is indicated by the distribution of orogenic gold deposits in belts of great geological complexity, with gradients of lithology, strain, and metamorphic grade. Most – although not all – and the largest of these deposits occur in terranes that were metamorphosed in greenschist facies. In Fig. 8, there are plotted most of the known gold occurrences in the study area. This figure shows, that the majority of them are located in the greenschist facies Zone IV. The country rocks of orogenic gold deposits are mostly strongly altered, mafic and ultramafic volcanic rocks, having white mica, biotite and carbonate assemblages in the alteration zones (Korkiakoski 1992, Eilu 1994, Patison 2007).

Deformation and the growth of metamorphic minerals

In Central Lapland, the early structural evolution (D1+D2) is characterized by subhorizontal folds and foliations observed throughout the study area, although in some subareas this might have caused more steeply dipping structures. The late structural evolution (D3 and later) is characterized by highly variable strike, dip and intensity of different structural elements. Because the area is generally poorly exposed, the relationship of the metamorphic mineral growth with these deformations can be reliably demonstrated only in a few localities.

In Zone I, the rock texture is normally granoblastic, indicating annealing close to the metamorphic peak. In Zone II, the main foliation of the rock (S2) wraps around garnets and staurolites which have curved inclusion trails, suggesting syntectonic growth with D2 (Fig. 14a). Some big garnets have plenty of quartz inclusions in the core but very few in the edge (Fig. 14b), indicating rapid growth during the early stage of the garnet crystallization. Many kyanites are elongated along the S2 (Fig. 14a), but generally randomly oriented kyanites overgrow S2. Some muscovites in these rocks are similarly randomly oriented (Fig. 14c). These features suggest that kyanite growth partly took place during a static period of deformation in reactions such as (7) or (11).

In Zone III, garnet and staurolite have curved inclusion trails, indicating syntectonic growth during D2. S2 wraps around these porphyroblasts (Fig. 3a). S2 is not curved around andalusite, but andalusite growth evidently took place during D2 because the early S2 crenulation cleavage is preserved as inclusion trails in andalusite. The S2 crenulation cleavage is absent or weak in the matrix close to andalusite (Fig. 14d). Kyanite and chloritoid are fine-grained and overgrow S2 as randomly oriented crystals (Figs 10d–f and 14e) although chloritoid occurs also elongated along S2. In Zones II–III, observations could only rarely be made from fold, hinges, so e.g. Fig. 14d can record a situation on the limb of F3 fold where S2 and S3 are parallel, consequently the crenulation cleavage in andalusite in Fig. 14b could represent either S2 or S3. In the cordierite-orthoamphibole rocks of the Siltaharju area, orthoamphibole is generally elongated along S2, but may also randomly overgrow the F3 fold hinges (Fig. 15a).

Zone V is relatively well-exposed, so that observations on the porphyroblast growth could be made on the fold hinges. In this area, D3 deformation formed upright, slightly reclined and even recumbent folds, whose axial surfaces are in E-W direction and vergences to the north. F3 folds have a well developed axial plane crenulation cleavage, S3. In Zone V.1, andalusite and staurolite occur as helisitic porphyroblasts having many quartz and magnetite inclusions trails which are sometimes sligthly curved near the grain boundaries when the bedding parallel S1/S2 foliation is well developed in the matrix. Generally andalusite overgrows S1/S2, but occasionally S1/S2 foliation wraps around andalusite porphyroblasts. S1/S2 wraps clearly around chloritoid grains (Fig. 11e). In Zones V.2 and V.3, andalusite, kyanite, staurolite and plagi-

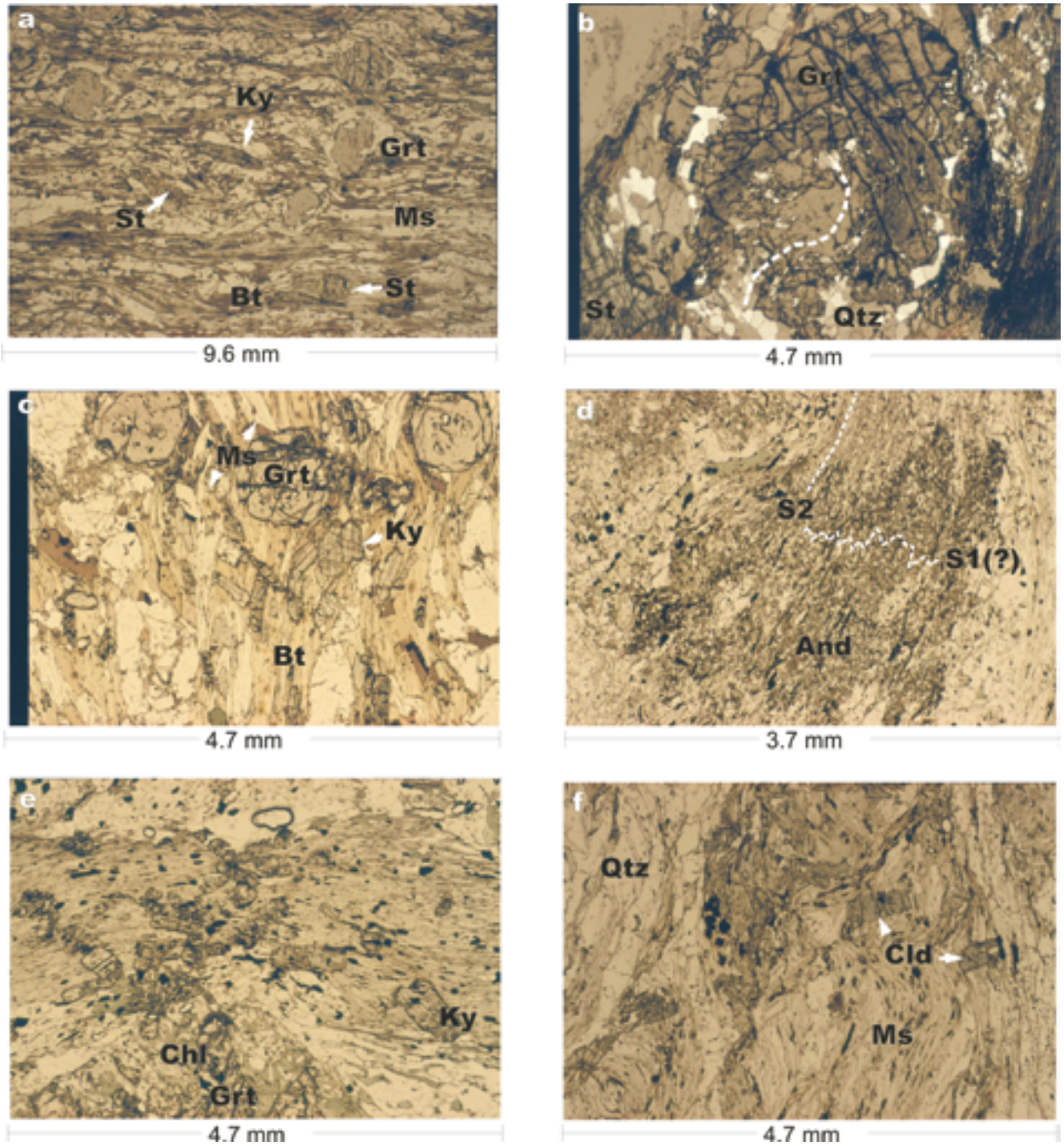

Fig. 14. Textures indicating the relationship of mineral growth with deformation phases in Zones II–III. a) Curved inclusion trails in staurolite and garnet and S2 parallel kyanite. Zone II, sample PSH-99-102.2, N 7563820, E 3450900, b) Curved quartz inclusion trails in a garnet with an inclusion-poor rim. Zone II, sample JTV-98-32.1, N 7552059, E 3457464, c) Randomly oriented kyanites and muscovites overgrowing the S2 schistosity. Zone II, sample PSH-99-99, N 7576623, E 3445579, d) S2 Crenulation in andalusite. Zone III, sample PSH-98-60, N 7518130, E 3481410, e) Randomly oriented kyanite grains overgrowing the main foliation. Zone III, sample PSH-97-11.1, N 7517280, E 3478240, f) Randomly oriented chloritoids overgrowing the main foliation. zone III, sample PSH-97-7.2, N 7528450 E 3485900.

oclase overgrow the S3 crenulation cleavage which can be seen as inclusion trails in these minerals (Figures 15b–c). This observation was also made by Evins & Laajoki (2002), their D2 corresponding with D3 of this study. The S3 crenulation cleavage sometimes wraps around andalusite and staurolite, indicating that their growth took place during D3. Kyanite mostly occurs as randomly oriented grains (Fig. 15c). The relationship of kyanite to D3 deformation is similar to that of orthoamphibole in the Siltaharju area, although this does not mean that D3 was coeval everywhere in Central Lapland. In Zones V.3–V.5, rock textures show signatures on annealing, matrix minerals forming dihedral angles. In annealed rocks, biotite sometimes occur as randomly oriented flakes.

Also in the zone VI.2, the F3 crenulation cleavage is

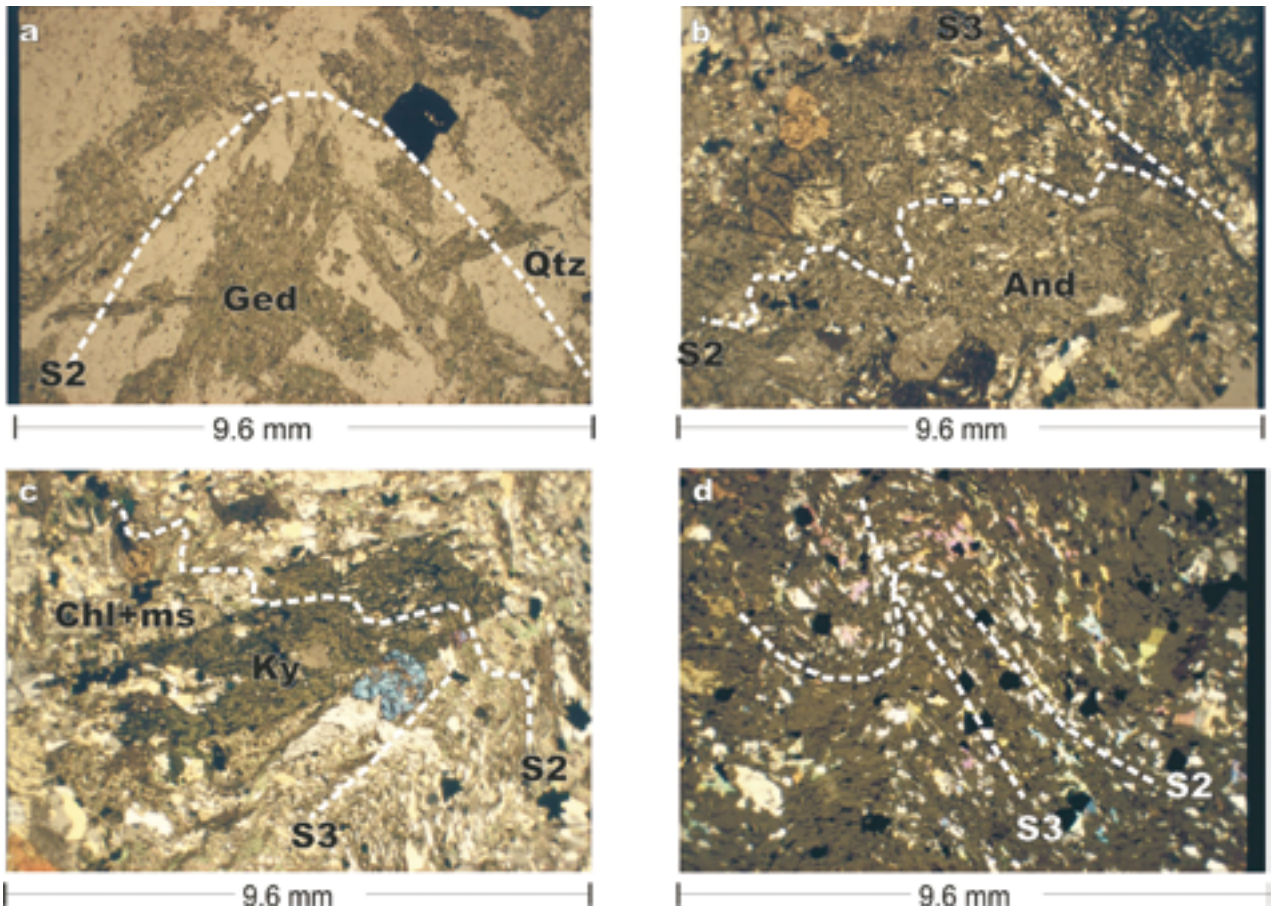

Fig. 15. Textures indicating the relationship of mineral growth with deformation phases in the zones II–VI. a) chloritized orthoamphiboles overgrowing F3 fold hinges, sample PSH-97-32.4, zone II, N 7544700, E 3494300; b) S3 crenulation as inclusion trails in andalusite, sample PSH-99-72.2, zone V.3, N 7485560, E 3511380; c) S3 crenulation as inclusion trails in kyanite prism, same exposure than in Fig. 16b, sample PSH-99-72.5; d) open S3 crenulation in andalusite, zone VI.2, sample PSH-98-97.5, N 7495066 E 3416256.

seen as inclusion trails in big andalusite porphyroblasts. In the western part of the study area, the S3 crenulation cleavage wraps around andalusites grains, which have sigmoidal quartz inclusion trails (Fig. 15d).

Above mentioned textural features indicate that regional metamorphism started during D2 and in the northern zones it may have reached its peak during the D2. In Zone V.1, the PT conditions were in the chloritoid field during D2. Some andalusite and staurolite may have crystallized already then, but as in Zone VI.2, their growth took place mainly during D3, especially in Zones V.2–V.5 where chloritoid is not stable. In Zone V.1 the D3, structures are more brittle forming shear planes where all minerals are deformed.

Mineral compositions

Analytical procedure

Mineral analyses were done in the laborotory of the Geological Survey of Finland, and at the microprobe laboratory of Department of Earth Sciences in the Uppsala University using CAMECA SX-50 microprobes. The beam width was 10 µm for micas and feldspars and 1 µm for other minerals. The sample current was 25 nA for micas, garnets and amphiboles 15 nA for feldspars and cordierites. The acceleration voltage was 15 kV. Natural standards and the ZAF correction program were used. All analyses at the Uppsala University microprobe laboratory were done using sample current of 15 nA and acceleration voltage of 20 kV and. Altogether 1700 microprobe analyses were done from the study area. Selected analyses from various metamorphic zones are presented in Appendix 1.

Garnet

Although the Lapland Granulite Belt was not included in this study, one garnet was analysed for comparison from peraluminous migmatite of this belt, whose zoning profile is presented in Fig. 16a

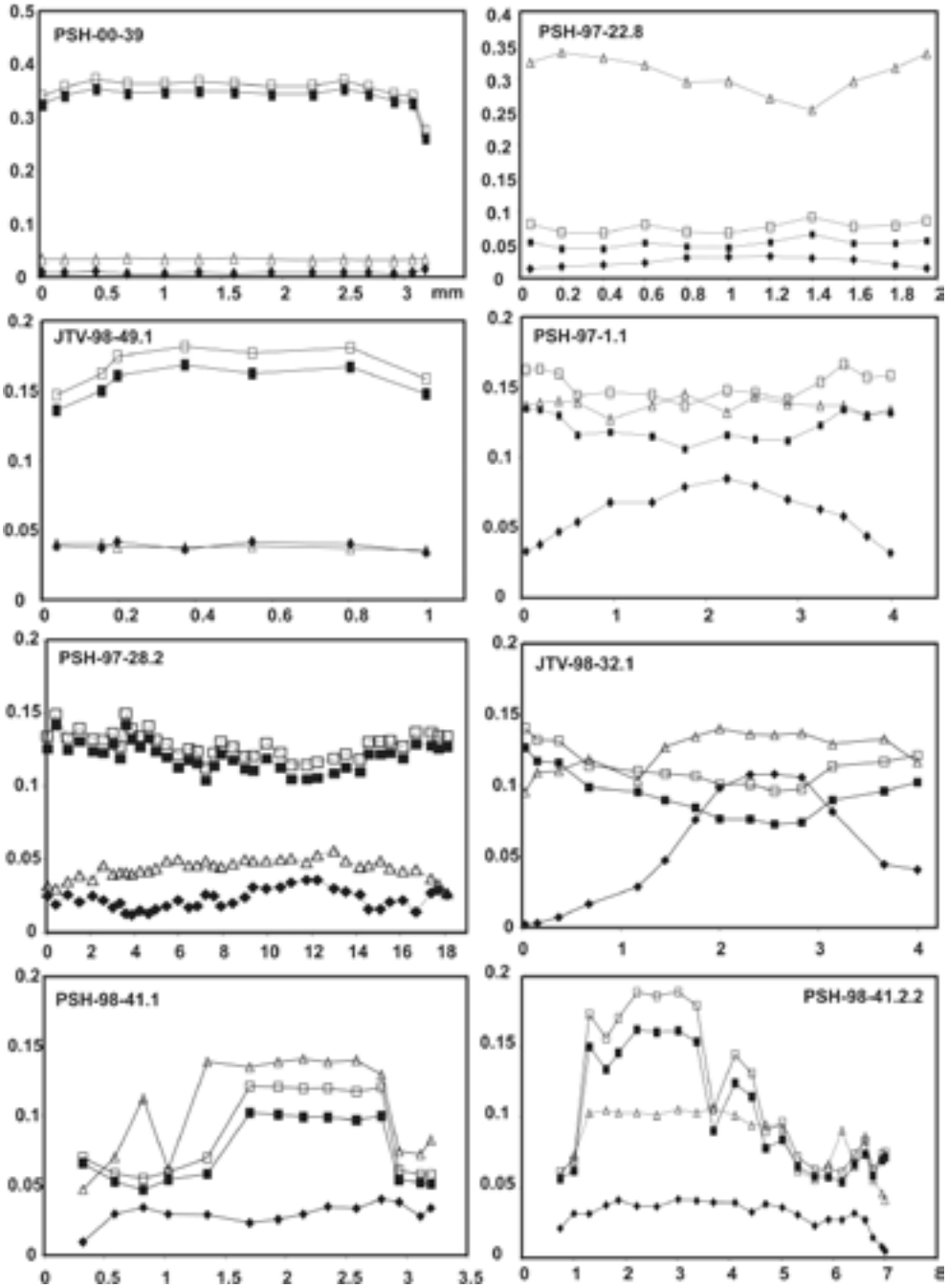

Fig. 16a. Composition profiles of garnets. Y-axis of the figures is the mole fraction. Symbols: open squares = Mg/(Mg+Fe), filled squares = Mg/(Fe+Mn+Mg+Ca), open triangles = Ca/(Fe+Mn+Mg+Ca), filled diamonds = Mn/(Fe+Mn+Mg+Ca). Sample PSH-00-39, Lapland Granulite Belt, N 7599934, E 3460762; sample PSH-97-22.8, zone I, N 756382, E 3493470; sample JTV-98-49.1, zone II, N 7576663, E 3445005; sample JTV-98-32.1 (the same garnet as in Fig. 14b), zone II, N 7552059, E 3457464; sample PSH-97-28.2, zone III, N 7543200, E 3495550; sample PSH-97-1.1, zone III, N 7544752, E 3493952; sample PSH-98-41.1, sample PSH-98-41.2, zone III, N 7517980, E 3457930.

(PSH-00–39). This garnet is Mg-rich with Mg-number (Mg/Mg+Fe) at around 0.35, which is clearly higher than in any analysed garnet in the other metamorphic zones.

In Zone I, garnets were analysed only in mafic rocks. Garnet in the sample PSH-97–22.8 is Ca-rich compared with other garnets, the X_{Ca} is from 0.25 to 0.34, increasing from core to rim (Fig. 16a). X_{Mg} in this garnet is low, from 0.05–0.07. Sample PSH-00–40 has also Ca-rich garnets with X_{Ca} from 0.31–0.32, but the X_{Mg} is higher, from 0.08 in the rim to 0.14 in the core.

In Zone II, garnets were analysed in metapelites. Compositionally, small inclusion-free garnets are only weakly zoned, but the zoning is much stronger in large garnets like JTV-98–32.1 in Fig. 16a. In this garnet, X_{Mg} is increasing and X_{Ca} and X_{Mn} decreasing from the core to the rim. In many of the zone III gar-

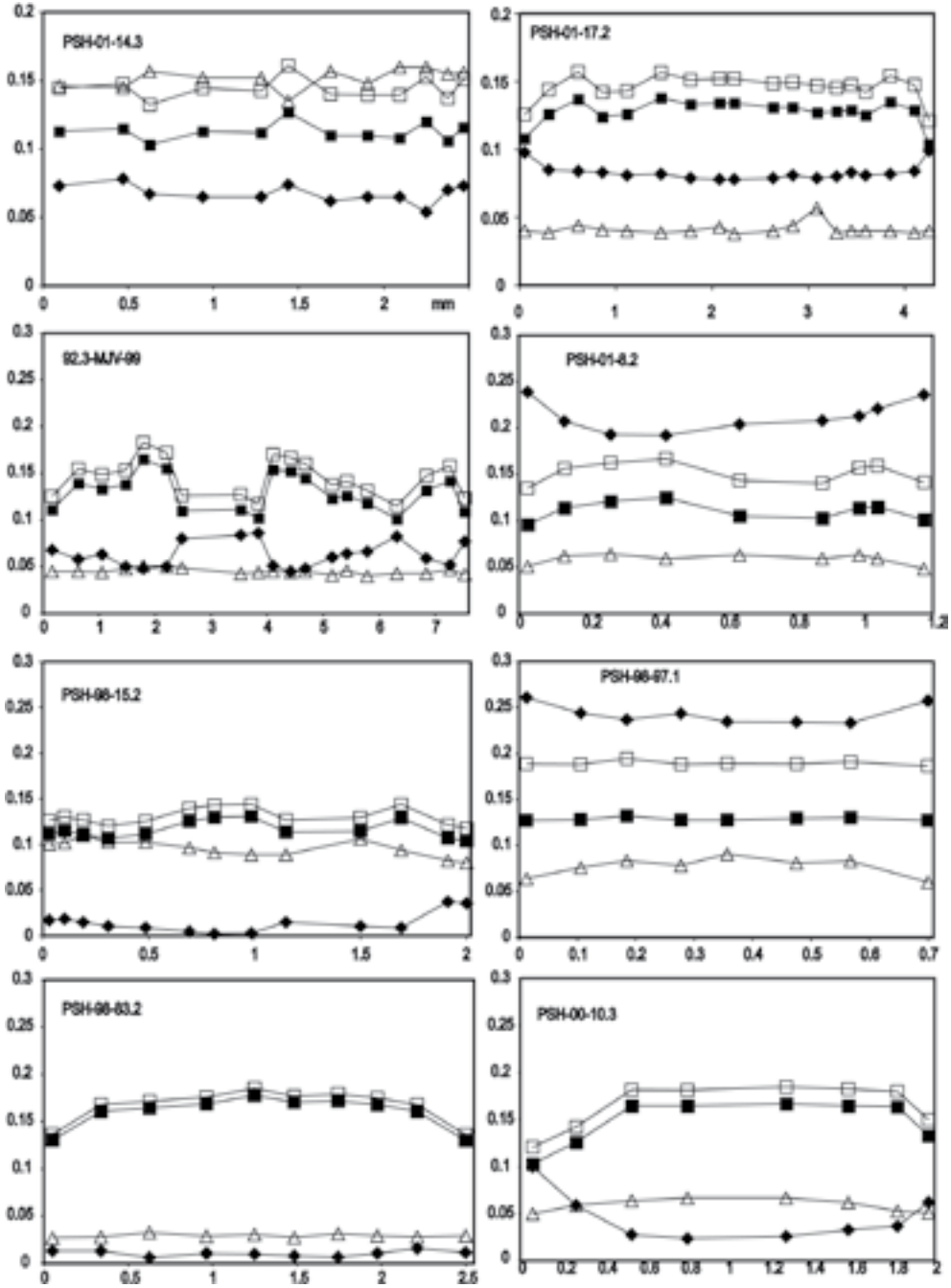

Fig. 16b. Composition profiles of garnets. Sample PSH-01-14.3, zone III, N 7521952, E 3519947; sample PSH-01-17.2, zone V.4, N 7521105, E 3535306; sample 92.3-MJV-99, zone V.4, N 7476970, E 3533028; sample PSH-01-8.2, zone V.4, N 7504537, E 3513451; sample PSH-98-15.2, zone VI.2, N 7481728, E 3449834; sample PSH-98-97.1, zone VI.2, N 7495066, E 3416256; sample PSH-98-83.2, zone VI.3, N 7493544, E 3378613; sample PSH-00-10.3, zone VI.3, N 7557588, E 3409926. Symbols as in Fig. 16a.

nets, both in pelitic and mafic compositions, the X_{Mg} is increasing from the core to the rim and the X_{Mn} is decreasing. Big garnets of the samples PSH-98–41.1 and PSH-98–41.2.2 from Zone III.1 have several decreases and increases in Ca and Mg in composition profiles that are made across large grains (Fig. 16a). This probably does not indicate several PT changes during the garnet crystallization because the decreases in X_{Mg} in the core area of the grain are near fractures which were healed during the late garnet growth. The general zoning pattern in these garnets is that that they have Ca and Mg rich core areas and these components are decreasing to the rim.

Garnet extracted from the sample PSH-97–28.2 (Fig. 16a) is from cordierite-orthoamphibole rock of Zone III. The zoning profile across this garnet is 18 mm, and it shows only a slight increase in X_{Mg} from the core (0.10–0.12) to the rim (0.12–0.14). It has Ca

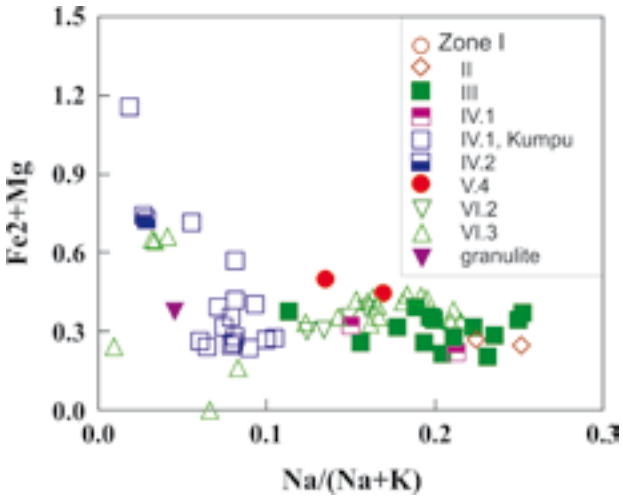

Fig. 17. Fe2++Mg vs. Na/(Na+K) plot of muscovites.

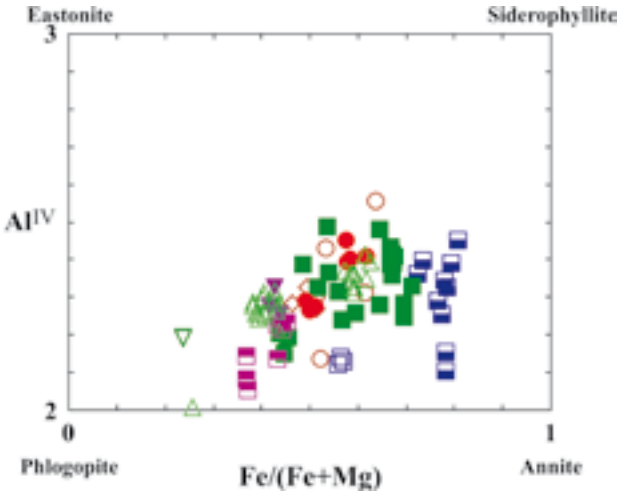

Fig. 18. Plot of biotites in the phl-ann-east-sid field. Symbols as in Fig. 17.

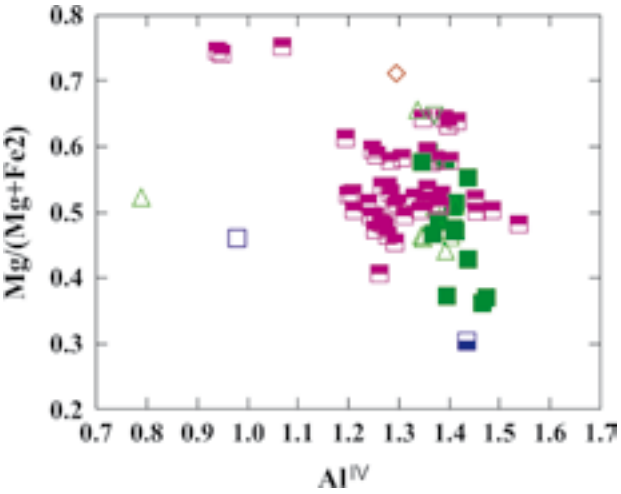

Fig. 19. AlVI vs. Si of chlorites. Symbols as in Fig. 17.

and Mn in small abundances, X_{Ca} slightly decreasing to the rim. Garnets from skarns and iron formations from Zone VI.1 are very Mg-poor and rich in grossular and almandine.

Muscovites in the rocks of the Kumpu group (Zone IV) clearly differ from most other white micas in their Na contents (Fig. 17). The Na/(Na+K) is lower than 0.1 in the white micas of the Kumpu formation in Zone IV, but higher than 0.1 in most muscovites from the other zones. Muscovites from other rocks in the zone IV have higher Na/(Na+K) ratios, indicating that their crystallization does not represent the same PT conditions than muscovites from the Kumpu formation (cf. Guidotti 1984). Some muscovites from Zone VI.3 and in the Lapland Granulite Belt also have low Na/(Na+K), which indicates a retrograde origin for these white micas. Fe and Mg contents are slightly higher in muscovites with low Na/(Na+K) than in other white micas.

Biotites have Mg-numbers roughly between $Mg_{30–60}$, depending generally on the Mg content of garnet, and therefore both the PT conditions and the whole rock Fe/Mg ratio (Table 2 and Fig. 18). Biotites in skarns and iron-formations in Zone VI.1 have the lowest Mg-numbers. Al^{VI} values are lowest in biotites from the greenschist facies zone IV. TiO_2 is from 1–3 wt% in the other zones but 3.2–3.7 wt% in the zone I samples and 4.1–4.3 wt% within biotites in the Lapland Granulite Belt.

Chlorites have highly variable Mg-numbers from Mg_{30}–Mg_{75}, mostly varying between Mg_{40}–Mg_{70}. The Si content is higher in most chlorites from the zone IV (Si 2.9–3.4) than in chlorites from the other zones (Si 2.7–2.9). Si content is high also in chlorites from one sample from Zone VI.3 (Fig. 19), indicating that these chlorites are retrograde. Al^{VI} is lower in many chlorites from zone IV (0.9–1.6) than in the other zones (1.3–1.5) but Al^{VI} also overlaps within various metamorphic zones, indicating that chlorite in amphibolite facies zones is mostly retrograde.

Calcic amphiboles are mostly actinolites in Zone IV, with a few ferroactinolitic compositions, following the amphibole classification by Leake (1978). Actinolitic and ferroactinolitic hornblendes occur close to the boundaries of Zone IV. In the other zones amphiboles are magnesiohornblendes, ferrohornblendes, tschermakitic and ferrotschermakitic hornblendes. In the analysed skarns and Fe-rich rocks from the zone VI.1 amphiboles are ferrotschermakites (Fig. 20). In Zone VI.3 Mg-rich actinolite occurs in scapolite, biotite and clinopyroxene-bearing mafic rock. In the zone III the analysed optically zoned amphiboles have bluish green magnesio-hornblende cores and lighter ferrotschermakitic rims. Orthoamphibole from Zone III (sample PSH-97–28.3) have Mg-numbers at $Mg_{33–36}$. The Na_2O content is 1.6–1.8 wt% and Al_2O_3

Table 2. Summary of the composition of garnets, plagioclases and biotites. Garnet compositions deviating remarkably from the average and their sample codes in each metamorphic zone are in italics.

Zone			**grt**	**grt**	**grt**	**grt**	**pl**	**bt**
	Rock type		$100 \cdot X_{Fe}$	$100 \cdot X_{Mn}$	$100 \cdot X_{Mg}$	$100 \cdot X_{Ca}$	$100 \cdot X_{Ca}$	100·Mg-nr
LGB	pelitic	cores	61–63	01	34–35	03	46	56–58
		rims	69–72	01–02	23–26	03		
I	mafic	cores	55–60	03–04	18–22	19–23	48–68	36–48
		rims	57–60	03–04	09–18	19–22	61–71	
PSH-00–40	mafic	core	52–55	02	13–14	31–32	62	*39*
		rim	*55–56*	*03–05*	*07–12*	*31*	*57*	
PSH-97–22.8	*mafic*	*core*	*61–65*	*02–03*	*05–07*	*25–30*	*41*	
		rim	59–61	*01–02*	*04–06*	*32–34*	*47*	
II	pelitic	cores	73–76	05–06	15–17	04–06	32–38	49–54
		rims	75–78	03–04	13–15	03–04		
III	pelitic	cores	68–75	02–11	07–12	11–16	42–53	51–59
		rims	76–89	01–07	05–14	04–11		
PSH-98-41.2.2	pelitic	core	*68–70*	*02–04*	*15–17*	*10–11*	*41*	*33*
		rim	*82–89*	*005–008*	*06–09*	*03–08*		
PSH-97-1.1	mafic	core	66–69	05–07	11–12	13–14	39	
		rim	68–70	03–04	13–14	13–14		
PSH-97-38.2	*mafic*	*cores*	*73–74*	*09–11*	*03–04*	*11–16*	*36*	*29–30*
		rims	74–75	*09–11*	*03–04*	*9–15*		
	crd-oam rocks	cores	79–82	03–05	11–14	03–06	05–19	41–48
		rims	77–82	02–06	12–14	02–06	03–20	
IV.1	mafic						01–20	
	pelitic						09–31	55–63
Kumpu	pelitic							43–44
Kumpu	quartzite							
IV.2	skarn	cores	59–67	15–25	02–03	13–17	49–57	19–22
		rims	62–67	14–17	02–03	13–16		
83.2-MJV-99	Fe-formation	core	72–73	15	04	09–10	86–87	27–28
		rim	72	14	04	11		
V.4	pelitic	cores	74–78	05–08	11–17	04–06	36–51	38–50
		rims	75–77	07–10	10–11	04–05		
PSH-01-8.2	*pelitic*	*core*	*62–63*	*19–24*	*10–13*	*06*	*49*	*49–50*
		rim	*61–62*	*24*	*10*	*05*		
VI.2	pelitic	cores	50–56	23–31	06–13	05–15	38–39	38–60
		rims	52–56	25–31	06–12	06–12		
PSH-98-15.2	pelitic	cores	76–79	*003–02*	*11–13*	*10–11*	*35–38*	*38–41*
		rims	*76*	*02–03*	*11*	*09*	*35–37*	
PSH-98-11	*pelitic*							*76*
PSH-98-16.1	mafic	cores	61–63	07–09	07–08	22–24	40–43	
		rims	61–62	06–07	08	23		
VI.3	pelitic Mn-rich	cores	51–55	23–31	12–15	05–09	40–44	57–60
		rims	52–56	26–31	12–14	04–06		
	pelitic	cores	74–80	01–06	16–18	03–07	40–43	37–58
		rims	75–83	01–04	10–15	03–05		
PSH-98-80.1	pelitic Mn-rich	cores	24–26	57–60	06–08	09–11	97–99	61–62
		rims	24–26	56–59	06–08	09–10		
PSH-98-85.3	pelitic Mn-rich	cores	25–26	41–45	07–08	22–24	97–99	55–56
		rims	27	45	05	23		
	mafic						61–92	74–75

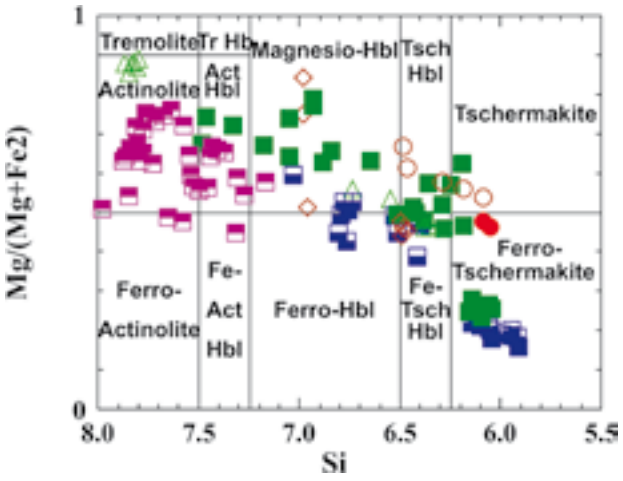

Fig. 20. Classification of the analysed amphiboles. Symbols as in Fig. 17.

14.0–16.1 wt%. Cummingtonite which is an alteration product of ferrohornblende in skarn in the zone VI.1 has Mg-number at around Mg_{30}.

Cordierite was found only in three localities in the study area. In the cordierite-orthoamphibole rock sample PSH-97–28.4 from Zone III, the Mg-number is Mg_{63} and the Na_2O is 0.41–0.42. In a Mg-rich peraluminous rock PSH-98–11B (Appendix 1) In Zone VI.3, the Mg-number is high, Mg_{87}. In Zone VI.2, one cordierite-bearing locality was found, where the cordierite has Mg_{75}. In the two latter samples the Na_2O-content is 0.10–0.14 wt%.

Clinopyroxenes were found from the zones I and VI.3. In Zone I, the Mg-numbers are $Mg_{67–68}$, Al_2O_3 2.7–2.9 wt% and Na_2O 0.58–0.66 wt%. In the zone VI.3, the scapolite-bearing rock PSH-00–69.2 has a high Mg-number, $Mg_{83–86,}$ lower Al_2O_3 (0.59–0.66 wt%) and higher Na_2O content (0.99–1.36 wt%) than other analysed clinopyroxenes, which have 1.2–1.8 wt% Al_2O_3, 0.13–0.36 wt% Na_2O and Mg-numbers of $Mg_{46–66}$. Sample PSH-00–4 which is close to the greenschist facies zone has lower Mg-number and lower Na_2O than sample PSH-00–17 which is farther from the zone IV (Appendix 1).

Plagioclases are albites in the mafic rocks of Zone IV, and also in most pelites. In other Zones, plagioclases are mostly oligoclases and andesines, but also labradorites and depending on the metamorphic grade and Ca-content of the whole rock, even anorthites. (Table 2 and Appendix 1).

Staurolites were analysed from Zones III and VI.3. Mg-numbers are $Mg_{12–19}$ in Zone III and in other Zones $Mg_{23–25}$. The MnO contents are lowest in staurolites of Zone III, 0–0.47 wt%. In Zone VI.3, MnO is from 0.83–1.03. Also the ZnO content varies from 0.04–2.44 wt%, and there is not a correlation with the metamorphic zone.

Chloritoid was analysed only in one locality from Zone III.1, where it is an alteration product of staurolite. There the Mg-number is $Mg_{09–13}$, while the MnO content is low, being 0–0.13 wt%.

Geothermometry and geobarometry

Metamorphic pressures and temperatures were calculated using the Thermocalc v. 3.1 software (Powell & Holland, 1988 1994; Powell & al. 1998). The summary of the results, mineral assemblages used in calculations, and end member activities are presented in Appendix 2. Metamorphic pressures and temperatures were calculated using both the core and rim compositions of garnets with compositions of the matrix and minerals adjacent to garnet, respectively. In Zones II–VI, this method gives a strong pressure decrease and moderate or small temperature decrease from core to rim, as indicated by the arrows in Fig. 21. These differences are mainly caused by the garnet zoning, because normally the compositional differences of other minerals are small when the matrix minerals are compared with those minerals touching garnet. This difference does not necessarily show the real PT path experienced by these rocks, because garnet core may be chemically isolated and does not represent chemical equilibrium with the present rock matrix (Marmo et al. 2002). However, most garnets have only a narrow outer rim, where there is a decvease in X_{Mg} (Fig. 16). This may record diffusion during cooling and reaction only with the adjacent minerals, not with the whole matrix. In these cases the usage of the composition of the garnet core with the matrix minerals probably gives temperatures and pressures that are close to the real maximum T and corresponding P. Some garnets have a strong zoning from the core to rim (e.g. garnets PSH-98–41.1–2 in Fig. 16a), which evidently is growth zoning during changing PT conditions. In these cases the T and P calculated using the compositions of the garnet core and matrix minerals not touching garnet may be meaningless. However, garnets in the sample PSH-98–41 have remarkably higher Mg and Ca contents in the mineral core than in the edges, which indicates higher temperatures and pressures during the early garnet growth.

In Zone I, the peak temperatures and pressures that were achieved using the core compositions of garnets

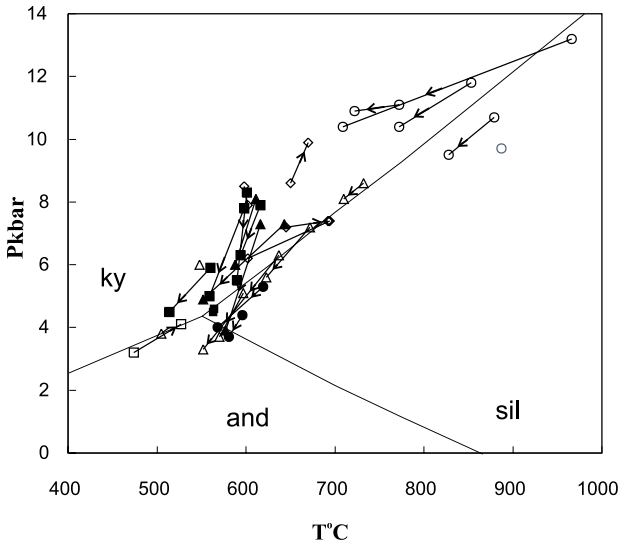

Fig. 21. Thermocalc average PT results plotted on the PT diagram. Symbols: open dots = zone I, diamonds = zone II, filled squares = zone III, filled dots = zone V.5, open triangles = zone VI.2, filled triangles = zone VI.3.

and compositions of matrix amphiboles, plagioclases and pyroxenes (when present) are mostly from 770–890 °C and 9.7–11.8 kbars. Also Tuisku and Makkonen (1999) determined a pressure of around 11 kbars for one sample from Zone I, although their temperature (670 °C), is lower, but it may represent cooling, especially because Tuisku and Makkonen (op. cit.) used double coronas on olivine in an ultramafic rock for their PT determination. One sample (PSH-00–40) gives 966 °C and 13.2 kbars, which is unrealistically high. In this sample the difference between results given by garnet core and rim compositions is greatest (257 °C and 2.8 kbars), so the garnet core may not represent equilibrium with the matrix assemblage. For the Zone I, temperatures and pressures are calculated at a_{H2O} of 0.4, because in this Zone mafic rocks are mostly migmatised, and melting evidently decreased the water activity. Temperatures and pressures calculated using the garnet rim compositions with adjacent plagioclases and amphiboles are 50–80 °C and 0.2–1.4 kbars lower than those given by garnet cores. In most garnets from Zone I, the pressure difference between the garnet core and rim results are not as remarkable as in other zones, which indicates a near-isobaric cooling as suggested also by the reactions in Figures 9a–b. The standard deviations are rather high for both pressures and temperatures because of the uncertainties in the thermodynamic properties of amphibole.

In Zone II, the Thermocalc pressures given by garnet cores are from 7.4–9.9 kbars, to some extent depending on the mineral assemblages and water activities used in calculations. In the three studied samples from Zone II the temperatures given by garnet cores are ca 600–690 °C, the highest temperature (and the lowest pressure) being from the northern part of the zone where melting has already started in metapelites. In the sample JTV-98–28, where the Mg content of garnet is increasing from core to rim the rim compositions give higher pressures and temperatures than cores. In this sample garnet has inclusion-rich core and inclusion free rim. In these kind of samples the garnet zoning represent growth during the prograde stage of metamorphism, and the 'core' pressures and temperatures may be meaningless because they probably do not represent equilibrium with the matrix assemblage.

For Zone III the 'core' temperatures are ca. 560–615 °C when the a_{H2O} is set at 1.0, which may be not far from the real value because these rocks were not melted. Otherwise the assemblage used in the Thermocalc calculations has a strong influence in the pressures. In the zone III, most peraluminous schists have both andalusite and kyanite. If one or both of the Al-silicates are eliminated, the pressures are from 6.1–7.9 kbars, which is too high for the grt-and-st-chl-pl-qtz assemblage, typical for these rocks. However, if both andalusite and kyanite are included in the assemblage used by the Thermocalc, pressures are from 3.9–4.8 kbars, which are reasonable for andalusite-bearing assemblages.

Temperatures for Zone III.1 are similar with the temperatures in Zone III, but the strong zoning in some garnets is reflected in pressures. In the samples PSH-98–41.1–2 which have the strongest garnet zoning in the studied rocks (Fig. 16a), garnet rims give 2.7–2.8 kbar lower pressures (4.5–5.5 kbars) than garnet cores (7.2–8.3 kbars), the 'rim' temperature being ca 10–40 °C lower than the 'core' temperature.

For the greenschist facies zone IV, it was not possible to calculate meaningful Thermocalc temperatures and pressures. In Table 3, there are temperatures calculated using the chlorite thermometer of Cathelineau (1988). Most of these are around 350–400 °C, which are reasonable for the greenschist facies rocks. Temperatures given by the chlorite thermometer for one rock from the Kumpu group are around 260 °C. This is clearly lower than elsewhere in the zone IV, but also chlorite from a metavolcanic rock close to Kumputunturi give a similar low temperature (Fig. 22), indicating that the area close to Kumputunturi represents the lowest metamorphic grade in the greenschist facies zone. On the other hand, most analysed chlorites also from the higher grade zones give temperatures at around 350–400 °C, which indicates the retrograde origin of chlorite and perhaps simultaneous retrogression with the greenschist facies metamorphism in Zone IV. The

Table 3. Examples of chlorite compositions and temperatures given by the chlorite thermometer of Cathelineau (1988)

Sample	**PSH-99-37**	**PSH-99-47**	**PSH-99-52**	**PSH-99-57**	**PSH-99-59**	**MJV-99-83.2**
northing	7480840	7510050	7512820	7500240	7508350	7478895
easting	3478370	3451480	3437620	3491400	3491190	3474068
SiO2	24,23	25,36	26,45	25,88	24,23	22,88
TiO2	0,01	0,07	0,04	0,1	0,12	0,12
Al2O3	23,37	20,8	19,37	21,04	21,53	22,61
FeO	25,75	24,03	25,09	22,38	25,31	32,22
MnO	0,26	0,37	0,44	0,18	0,15	0,26
MgO	14,56	15,19	15,16	17,58	15,12	7,86
Total	88,18	85,82	86,55	87,16	86,46	85,95
Cations/14 oxygens						
Si	2,545	2,716	2,823	2,693	2,596	2,566
AlIV	1,455	1,284	1,177	1,307	1,404	1,434
AlVI	1,435	1,339	1,257	1,271	1,313	1,552
Ti	0,001	0,006	0,003	0,008	0,01	0,01
Fe	2,261	2,152	2,239	1,947	2,268	3,022
Mn	0,023	0,034	0,04	0,016	0,014	0,025
Mg	2,279	2,425	2,412	2,727	2,415	1,314
T°C	407	352	317	359	390	400

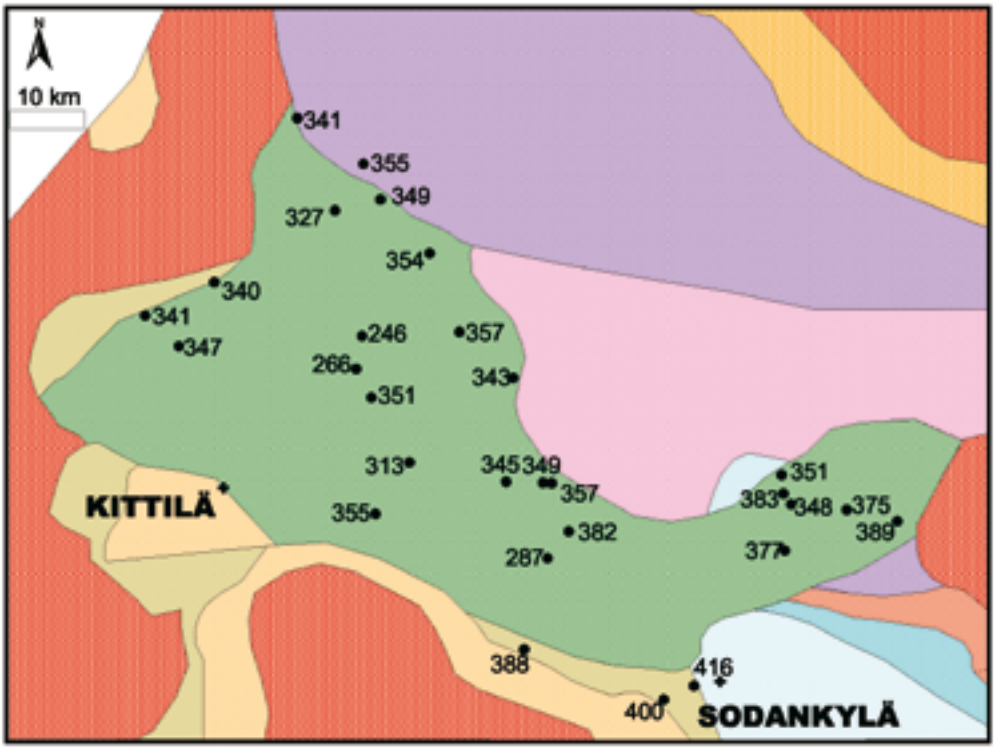

Fig. 22. Regional distribution of the temperatures given by the chlorite thermometer for the greenschist facies Zone IV. Colours for the metamorphic zones are as in Fig. 8.

temperatures are close to 400 °C in Zone VI.1 on the southern side of Zone IV. The sample PSH-00–1.7 (Appendix 2) is from the zone VI.1, located in the western part of the zone IV, where the temperature has been high enough for garnet growth in skarns. The Thermocalc pressure for the core of this garnet is 3.2 kbars, which probably is close to the pressure for the greenschist facies metamorphism before garnet crystallized, probably as a consequence of heat flow from the adjacent granitoids.

Rocks from the sillimanite grade Zone V.5 give Thermocalc pressures which are of the same order (3.7–5.3 kbars when a_{H2O} =1) than those given by grt-st-and-ky assemblages in Zone III. Advective heat flow from granitoids probably caused the sillimanite grade metamorphism in this zone. Thermocalc average PT calculations were not done in this study for Zones V.1-3 because of the absence of garnet, but the coexistence of andalusite and kyanite (Fig. 12a) indicates, however, that metamorphic pressures were close to the andalusite-kyanite boundary also in these rocks.

Both sillimanite-bearing and Al-silicate-absent pelitic rocks as well as garnet amphibolites from Zones VI.2–3 give relatively high 'peak' Thermocalc pressures, (6.1–8.1 kbars at ca 610–730 °C), and similar decreasing pressure trends as other zones in the core-rim thermobarometry (Fig. 21). However, when these rocks have both andalusite and sillimanite (sample PSH-98–97.1, Fig. 13a) or all three Al_2SiO_5 polymorphs (sample PSH-98–11B, Fig. 13c) and all minerals present are used in the Thermocalc calculation, the pressures are low (from 3.3–3.8 kbars), which is in accordance with the presence of andalusite. Cordierite and andalusite-bearing, plagioclase-free sample PSH-98–69.1 gives pressures and temperatures of 4.1–5.1 kbars and 534–627 °C. The high pressures in some samples, as well as the reaction (21) bt + als + qtz = crd + ms which has a relatively flat dP/dT slope indicate decompression also for this zone. The temperatures and pressures in many other samples from Zones V–VI, especially those given by garnet rims, plot in the sillimanite field in Fig. 21.

Phase diagrams

The core-core and rim-rim thermobarometry fits relatively well with the petrogenetic grids for the zones II, III, V and VI in Figures 23a–e, which were constructed using the Thermocalc 3.25 software (Powell & Holland 1988, 1994; Powell et al., 1998; see the web page *http://www.earthsci.unimelb.edu.au/tpg/thermocalc/)*. The whole rock compositions are from samples analysed using the XRF method. These compositions are examples, e.g. a higher Mg/Fe ratio in the whole rock would raise in each case the univariant curves and divariant fields to higher pressures. In Zone II the maximum temperature conditions are interpreted to have been close the reaction boundary bt + ms + st + pl + qtz = grt + ky + liq (Fig. 23b), which fits well with the average pressures and temperatures given by the garnet cores. Neither sillimanite nor andalusite was observed in the zone II, so the post-peak cooling took evidently place in the kyanite field, as illustrated by the arrow in Fig. 23a.

In Zone III, the garnet zoning does not clearly indicate the early high pressure, and kyanite is a late retrograde phase. However, some garnets have chloritoid inclusions, which may indicate that they were reactants in the reaction (8) cld + qtz = grt + st + chl + H_2O, which takes place in pressures ≥ 7 kbars in the compositions represented by the analysed metapelites. Therefore the early pressure in the PT path may have been as high as given by those average PT calculations where the Al-silicate is absent. Same rocks have andalusite, retrograde kyanite and chloritoid which indicates cooling down to conditions, where the univariant cooling reaction chl+st+qtz+H_2O = cld+als took place, straddling at the andalusite-kyanite boundary (Fig. 23c).

In Zone III.1, garnets have altered from rims into biotite, and staurolites are close to these garnets, which indicates that PT conditions were in the field where the divariant KFMASH reaction grt + ms + H_2O = bt + st + qtz takes place (field grt-bt-st in Fig. 23d). This is in accordance with the 7.2–8.3 kbar average pressures given by the garnets that have Mg and Ca rich cores. Because the average Thermocalc pressure for the garnet rims were around 5 kbars, and there seems to be late biotite growth in chlorite-muscovite filled staurolite pseudomorphs, caused by the reaction (15) chl + mu = bt + st + qtz (field chl-bt-st in Fig. 23d), the PT path was probably as indicated by the arrow in Fig. 23d, with some reheating before cooling to the chloritoid field.

In Zone V, the metamorphic field gradient from the chloritoid grade to the sillimanite grade is demonstrated by the dashed arrow in Fig. 23e. Andalusite was produced at least partly by the divariant KFMASH reaction (13) cld + qtz = and + chl + H_2O (field chl-cld-als-ms in Fig. 23e), and chloritoid was consumed by the univariant and divariant reactions (10) als + cld = chl + st + qtz + H_2O and (14) cld + qtz = chl + st + H_2O (field chl-st-cld-ms), the PT conditions being also in these reactions close to the andalusite-kyanite boundary. With rising temperature, sillimanite was formed in the divariant reaction st + ms + qtz = bt + sil + H_2O (field bt-st-als-ms). Crossing the univariant boundary

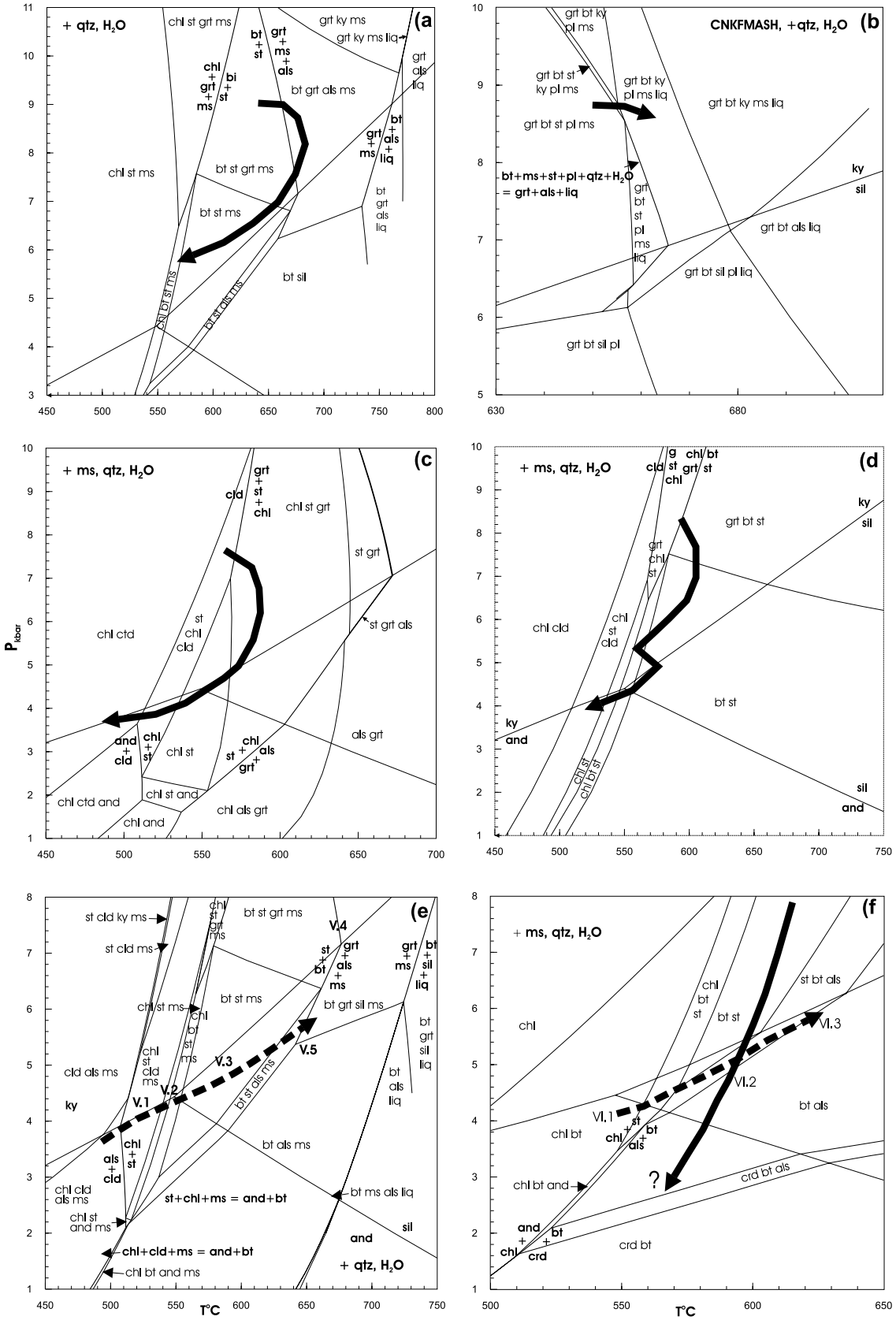

Fig. 23. Pseudosections showing the fields for some of the observed mineral assemblages and reactions in metapelites for various metamorphic zones in the system KFMASH, apart from Fig. 23b which is for the CNKFMASH. Solid arrows are for possible PT paths, dashed arrows are for the metamorphic field gradients. a) = zone II, composition SiO_2 70.16, Al_2O_3 15.57, MgO 3.44, FeO 8.82, K_2O 2.01 mol.%; b) zone II, composition SiO_2 68.15, Al_2O_3 15.12, MgO 3.34, FeO 8.57, CaO 0.63, Na_2O 2.23, K_2O 1.95, mol.%; c) zone III, composition SiO_2 70.16, Al_2O_3 15.57, MgO 3.44, FeO 8.82, K_2O 2.01 mol.%; d) zone III.1 composition SiO_2 71.18, Al_2O_3 15.13, MgO 3.24, FeO 8.72, K_2O 1.73 mol.%; e) zone V.1–5, SiO_2 69.58, Al_2O_3 18.16, MgO 2.12, FeO 7.80, K_2O 2.33 mol.%; f) zone VI.1–3, SiO_2 73.99, Al_2O_3 11.79, MgO 5.44, FeO 5.37, K_2O 3.42 mol.%. Heavy lines are for univariant reactions, narrow lines are borders of the divariant and trivariant fields.

bt + st + q = grt + ms + als + H_2O may have produced garnet-sillimanite assemblages in zone V.5.

The dashed arrow in Fig. 23f illustrates the change in PT conditions from Zones VI.1 to VI.3. Because all three Al_2SiO_5 polymorphs are present in zone VI.2, it is evident that the PT path was not far from their triple point. Because some average pressures are high, from 6.1–8.1 kbars, the PT path was probably as indicated by the solid arrow in Fig. 23f, going down to pressures where the reaction (21) bt + als + qtz = crd + ms (Fig. 13d) starts with decreasing pressure (field crd-bt-als). Reaction (21) is strongly dependent on the Fe/Mg ratio of the rock, in compositions that are Mg richer than the one used in Fig. 23f the reaction takes place in higher pressures. On the other hand, it is also possible that the reaction (21) does not represent decreasing pressure but increasing temperature in near-isobaric conditions, resulting from advective heat flow from the granitoid intrusions.

DISCUSSION

The onset of the tectonic evolution of Central Lapland is characterized by a prolonged extensional rifting of the Archaean basement and the related volcanism, magmatism and sedimentation. This stage lasted at east 500 Ma from ca 2.5 Ga to ca 2.0 Ga (papers in Vaasjoki 2001). The orogenic evolution of Central Lapland that started ca 2.0–1.89 Ga ago, is a combination of two main tectonic events: the northward or northeastward directed Svecofennian tectonic movement that thrusted the earlier formations onto the Archaean basement, and the thrusting of the Lapland Granulite Belt towards the approximately opposite direction (Ward et al. 1997). As a result, the associated structures in different parts of the Central Lapland are not straightforwardly correlated with each other. The correlation of structures is further hampered by the paucity of suitable structurally controlled granitoids that could be dated for time markers for different tectonic events.

The early structural evolution (D1+D2) of Central Lapland is characterized by subhorizontal folds and foliations observed throughout the study area, accepting the possibility that in some subareas this might have caused more steeply dipping structures (Ward et al. 1989), as is common in many younger fold-and-thrust belts. In the southern and central part of the study area, the fold vergences and other kinematic indicators suggest a N or NE directed tectonic movement during this stage. Subhorizontally deformed tonalites suggest that the age of the deformation is around 1.88–1.87 Ga, assuming that the tonalites correlate with the Haaparanta suite intrusions, indicating a typical Svecofennian age of deformation (see e.g. Nironen 1997). Close to the Lapland Granulite Belt, inclined W- to SW-vergent folds were observed, but their correlation with N-NE-vergent structures in the south is not known. It is most plausible that the thrusts were initiated at this period although they were clearly reactivated in later stages.

The late structural evolution (D3 and later) in Central Lapland caused the extreme variety concerning strike, dip and intensity of different structural elements now seen on geological and geophysical maps and observed at outcrop scale. At this stage, the thrusts that were initiated in earlier stage were reactivated and the structural pattern with opposing fold vergences and high strain shear zones developed. Simultaneous or progressive thrusting from different directions towards the oceanic Kittilä group is a peculiar feature in Central Lapland and cannot be explained by a simple head-on thrusting. During thrusting older formations were juxtaposed over younger ones in some places and vice verse in other places. Metamorphic boundaries at thrust planes indicate that thrusting was at least partly late metamorphic or postmetamorphic.

The mineral assemblages and thermobarometry show very large PT differences between metamorphic zones, especially pressure differences are remarkable. When not caused by advective heat from large granitoid massifs, the changes in metamorphic grade are connected with shear zones and D3 thrust planes. The eastward prograde increase in metamorphic grade in the zone V may reflect an oblique cut of the crust, revealed by the D3 thrusting where higher grade eastern zones represent deeper crustal sections. The increase in grade may also be caused by heat flow from granitoids which are abundant in Zone V.5.

The present structural geometry shows an inverted gradient where pressure and temperature increase upwards in the present tectonostratigraphy from greenschist facies in the zone IV through garnet-andalusite-staurolite grade in the zone III and garnet-kyanite grade amphibolite facies in Zone II to granulite facies in Zone I. The inverted gradient could be explained by crustal thickening caused by overthrusting of the hot granulite complex onto the lower grade rocks, as inferred by tectonic transport directions in Fig. 7. Krill (1985) proposed this mechanism for the Karasjok-Levajok area in the western side of the Lapland Granulite Belt in northern Norway, where the metamorphic zonation is similar to that in our study area. Tuisku & Makkonen (1999) explained the high pres-

sure at the margin of the Lapland Granulite Belt as a consequence of subduction of the Karelian foreland under the overriding Kola Plate.

These kind of 'hot-over-cold' models have been proposed also to explain the inverted gradients e.g. in Zanskar Himalaya (Searle & Rex 1989). To preserve the inverted isograds a rapid exhumation and cooling is needed (Thompson & Ridley 1987). Therefore Searle & Rex (1989) favoured a model where subsequent folding and thrusting deformed the normal upward decreasing Barrovian metamorphic sequence, causing the present inverted gradient structure. To some extent similar process may be an explanation also for the southward decreasing grade from Zone I to the zone III south of the Lapland Granulite Belt, where the higher grade gneisses may have been thrusted onto lower grade schists during the late stage of metamorphism, although the granitoids also have had a thermal input into metamorphism in Central Lapland. Thrusting probably thickened the crust in a large area and was followed by decompression as indicated by the inferred PT paths. Peraluminous metasediments were not found in the eastern part of Zone II, so it is unclear whether the eastern side of Zone II underwent similar PT evolution than its western part that exhibit many kyanite-bearing rocks. However, kyanite-bearing metasediments were described by Perchuk et al. (2000) ca 150 km east of our study area, from the southern contact of the Tanaelv belt, as well as by Krill (1985) from the western contact of the Tanaelv belt in Norway, on the western side of the granulite complex. Therefore it is probable that also in our study area, the eastern part of Zone II, represents similar PT-conditions than its western part, as indicated by the Thermocalc pressures of ca 7.5 kbars given by garnet amphibolites and orthoamphibole rocks from the Siltaharju area.

Generally, the Tanaelv belt (Zone I) has been described as a separate unit not belonging to the granulite complex, its metamorphism being caused by hot granulites (Barbey et al. 1980, 1982, 1984; Krill 1985, Perchuk et al. 2000). However, the structures in the Tanaelv belt are similar to those in the Lapland Granulite Belt (Nironen and Mänttäri 2003) and the metamorphic conditions do not differ from those in lower parts of the granulite complex. The lithology of the Tanaelv belt differs from that of the Lapland Granulite Belt but evidently they were metamorphosed together in the same thickening process.

There is a several kbar change in the metamorphic pressure from the kyanite grade Zone II to the andalusite grade Zone III, but the zoning profiles of garnet and the thermobarometry indicate that the zone III also underwent a higher pressure stage, reaching the 'peak' temperatures after thickening and decompression. Zone II may represent the upper plate in thickening which was cooled more rapidly without reaching the andalusite field while still reactive. Lower grade rocks further from the granulites stayed close to their maximum temperature down to the andalusite field or to the andalusite-kyanite boundary, and this period was followed by a near-isobaric cooling to the kyanite field, maybe representing decompression and cooling after extensional collapse. In Zone I, the near-isobaric cooling period took place in much higher pressure, but these cooling events (Figs. 9a–b and 10b) were not necessarily simultaneous in Zones I and II.

During the thickening, the greenschist facies rocks (the Kittilä Group) were probably not in their present position, but they represent a late metamorphic allocthon that was accreted to Zones II and III during late D3. Lithological boundaries around the Kittilä Group are mostly also metamorphic boundaries which supports this idea. However, the rocks Kittilä of the group have been proposed to continue north to the Karasjok area in Norway (Lehtonen et al. 1998) through Zone II, although there is a major change in PT conditions from Zone IV to Zone II. This may mean that the volcanic rocks in Zone II do not belong to the Kittilä Group, but it is also possible that some parts of the oceanic unit were included in the thickening that produced high pressure ampibolite facies rocks in Zone II, and other parts were juxtaposed later with Zones II and III.

ACKNOWLEDGEMENTS

The authors want to express their cordial thanks to Pekka Tuisku, Mikko Nironen and Eero Hanski for critical reviews, which considerably improved the manuscript, to Lassi Pakkanen and Hans Harryson for microprobe analyses, and to Veikko Keinänen, Eelis Pulkkinen, Vesa Kortelainen, Nicole Patison and the GTK technical staff in Kittilä and Sodankylä for help and stimulating discussions in the field. Prof. Pekka Nurmi is thanked for the help in planning and realization of the project, and Director General Elias Ekdahl for the original initiative for studying the metamorphic structure of Central Lapland.

REFERENCES

Barbey, P., Convert, J., Moreau, B., Capdevila, R. & Hameurt, J. 1980. Relationships between granite-gneiss terrains, greenstone belts and granulite belts in the Archaean crust of Lapland (Fennoscandia). Geologische Rundschau 69, 648–658.

Barbey, P., Capdevila, R. & Hameurt, J. 1982. Major and transition trace element abundances in the khondalite suite of the granulite belt of Lapland (Fennoscandia). Evidence for an early Proterozoic flysch-belt. Precambrian Research 16, 273–290.

Barbey, P., Convert, J., Moreau, B., Capdevila, R. & Hameurt, J. 1984. Petrogenesis and evolution of an early Proterozoic collisional orogenic belt : the granulite belt of Lapland and the Belomorides (Fennsocandia). Bulletin of the Geological Society of Finland 56, 161–188.

Barbey, P. & Raith, M. 1990. The granulite belt of Lapland. In: Vielzeuf, D. & Vidal, Ph. (eds.) Granulites and crustal evolution, Kluwer Academic Publishers. NATO ASI Series, Vol. 311, 111–132.

Burg, J-P. 1999. Ductile structures and instabilities; their implications for Variscan tectonics in the Ardennes. Tectonophysics 309, 1–25.

Cathelineau, M. 1988. Cation site occupancy in chlorites and illites as a function of temperature. Clay Minerals 23, 471–485.

Eilu, P. 1994. Hydrothermal alteration in volcano-sedimentary rocks in the Central Lapland Greenstone Belt, Finland. Geological Survey of Finland, Bulletin 374. 145 p.

Eilu, P. 1999. FINGOLD – a public database on gold deposits in Finland. Geological Survey of Finland, Report of Investigation 146. 224 p.

Eskola, P. 1952. On the granulites of Lapland. American Journal of Science, Bowen Volume, Part 1, 133–171.

Evins, P. M. & Laajoki, K. 2002. Early Proterozoic nappe formation: an example from Sodankylä, Finland, northern Baltic Shield. Geological Magazine 139, 73–87.

Frietsch, R., Tuisku, P., Martinsson, O. & Perdahl, J.-A. 1997. Early Proterozoic Cu-(Au) and Fe ore deposits associated with regional Na-Cl metasomatism in northern Fennoscandia. Ore Geology Reviews 12 (1), 1–34.

Gaál, G., Berthelsen, A., Gorbatschev, R., Kesola, R., Lehtonen, M. I., Marker, M. & Raase P. 1989. Structure and composition of the Precambrian crust along the POLAR Profile in the northern Baltic Shield. Tectonophysics 162, 1–25.

Gaál, G., Mikkola, A. & Söderholm, B. 1978. Evolution of the Archean crust in Finland. Precambrian Research 6, 199–215.

Groves, D. I., Goldfarb, R. J., Gebre-Mariam, M., Hagemann, S. G. & Robert, F. 1998. Orogenic gold deposits: A proposed classification in the context of their crustal distribution and relationship to other gold deposit types. Ore Geology Reviews 13, 7–27.

Guidotti, C. V. 1984. Micas in metamorphic rocks. In Ribbe, P.H. (ed.) Micas. Mineralogical Society of America. Reviews in Mineralogy 13, 357–456.

Haapala, I., Front, K., Rantala, E. & Vaarma, M. 1987. Petrology of Nattanen-type granite complexes, northern Finland. Precambrian Research 35, 225–240.

Hanski, E. S. 1997. The Nuttio Serpentinite Belt, Central Lapland: an example of Paleoproterozoic ophiolitic mantle rocks in Finland. Ofioliti 22, 35–46.

Hanski, E. 2001. History of stratigraphical research in northern Finland. In: Vaasjoki, M. (ed.) Radiometric age determinations from Finnish Lapland and their bearing on the timing of Precambrian volcano-sedimentary sequences. Geological Survey of Finland, Special Paper 33, 15–43.

Hanski, E., Huhma, H., & Vaasjoki, M. 2001. Geochronology of northern Finland: a summary and discussion. In: Vaasjoki, M. (ed.) Radiometric age determinations from Finnish Lapland and their bearing on the timing of Precambrian volcano-sedimentary sequences. Geological Survey of Finland, Special Paper 33, 255–279.

Hanski, E., Mänttäri, I., Huhma H. & Rastas, P. 2000. Post-1.88 Ga deposition of the Kumpu and Lainio Group molasse-type sediments in northern Finland: evidence from conventional and NORDSIM zircon dating. 24th Geological Winter Meeting, Trondheim, January 6–9, 2000, Abstracts, p. 75.

Hölttä, P. & Väisänen, M. 2000. Tectonic evolution of the Central Lapland Grenstone Belt – metamorphic and structural observations. In: Lauri J. Pesonen, Annakaisa Korja and Sven-Erik Hjelt (Eds.) Lithosphere 2000: A symposium on the structure, composition and evolution of the lithosphere in Finland. Geological Survey of Finland, Espoo, October 4–5, 2000. Institute of Seismology, University of Helsinki, Report S-41, 161–163.

Hörmann, P.K., Raith, M., Raase, P., Ackermand, D. & Seifert, F. 1980. The granulite complex of Finnish Lapland, Petrology and metamorphic conditions in the Ivalojoki-Inarijärvi area. Geological Survey of Finland, Bulletin 308, 100 p.

Huhma, H. 1986. Sm-Nd, U-Pb and Pb-Pb isotopic evidence for the origin of the early Proterozoic Svecokarelian crust in Finland. Geological Survey of Finland, Bulletin 337. 48 p.

Korja, T., Tuisku, P., Pernu, T. & Karhu, J. 1996. Field, petrophysical and carbon isotope studies on the Lapland Granulite Belt: implications for deep continental crust. Terra Nova 8, 48–58.

Korkiakoski, E. 1992. Geology and geochemistry of the metakomatiite-hosted Pahtavaara gold deposit in Sodankylä, northern Finland, with emphasis on hydrothermal alteration. Geological Survey of Finland. Bulletin 360, 96 p.

Korsman, K. (ed.), Koistinen, T. (ed.), Kohonen, J. (ed.), Wennerström, M. (ed.), Ekdahl, E. (ed.), Honkamo, M. (ed.), Idman, H. (ed.), Pekkala, Y. (ed.) 1997. Suomen kallioperäkartta = Berggrundskarta över Finland = Bedrock map of Finland 1:1 000 000. Espoo. Geological Survey of Finland.

Kretz, R. 1983. Symbols for rock-forming minerals. American Mineralogist 68, 277–279.

Krill, A.G. 1985. Svecokarelian thrusting with thermal inversion in the Karasjok-Levajok area of the Northern Baltic Shield. Norges Geologiske Undersøkelse Bulletin 403, 89–101.

Kärkkäinen, N. 1982. Kittilän vihreäkivien ja niihin liittyvien metapeliittien metamorfoosista. In: Laajoki, K., Paakkola, J. & Tuisku, P. (eds.) Suomen kallioperän ja malmien metamorfoosi ja deformaatio. Res Terrae. Ser. B 5, 98–107 (in Finnish).

Leake, B. E. 1978. Nomenclature of amphiboles. American Mineralogist, 63, 1023–1053.

Lehtonen, M., Airo, M.-L., Eilu, P., Hanski, E., Kortelainen, V., Lanne, E., Manninen, T., Rastas, P., Räsänen, J. & Virransalo, P. 1998. Kittilän vihreäkivialueen geologia: Lapin vulkaniittiprojektin raportti. Summary: The stratigraphy, petrology and geochemistry of the Kittilä greenstone area, northern Finland: a report of the Lapland Volcanite Project. Geological Survey of Finland, Report of Investigation 140. 144 p.

Marker, M. 1988. Early Proterozoic thrusting of the Lapland granulite belt and its geotectonic evolution, northern Baltic Shield . Geologiska Föreningens i Stockholm Förhandlingar 110, 405–410.

Marmo, B. A., Clarke, G. L. & Powell, R. 2002. Fractionation of bulk rock composition due to porphyroblast growth: effect on eclogite facies mineral equilibria, Pam Peninsula, New Caledonia. Journal of Metamorphic Geology 20, 151–165.

McCuaig, T. C. & Kerrich, R. 1998. P-T-t-deformation-fluid characteristics of lode gold deposits: evidence from alteration systematics. Ore Geology Reviews 12 (6), 381–453.

Mouri, H. & Korsman, K. 1999. Partial melting and P-T-t evolution of LP/HT metamorphic terranes: an example from

the Svecofennian K-feldspar-poor leucosome migmatite belt, southern Finland. In: Understanding granites: integrating new and elassic techniques. Geological Society Special Publications, 168. London, 239–253.

Nironen, M. 1997. The Svecofennian Orogen: a tectonic model. Precambrian Research 86, 21–44.

Nironen, M. & Mänttäri, I. 2003. Structural evolution of the Vuotso area, Finnish Lapland. Bulletin of the Geological Society of Finland 75, 93–101.

Patison, N. L. 2007. Structural controls of gold mineralisation in the Central Lapland greenstone belt. Geological Survey of Finland, Special Paper 44, 105–122.

Pattison, D. 2003. Petrogenetic significance of orthopyroxene-free garnet+clinopyroxene+plagioclase±quartz-bearing metabasites with respect to the amphibolite and granulite facies. Journal of Metamorphic Geology 21, 21–34.

Perchuk, L. L., Gerya, T. V., Van Reenen, D. D., Smit, C. A. & Krotov, A.V. 2000. P-T paths and tectonic evolution of shear zones separating high-grade terrains from cratons: examples from Kola Peninsula (Russia) and Limpopo Region (South Africa). Mineralogy and Petrology 69, 109–142.

Powell, R., Holland, T. & Worley, B. 1998. Calculating phase diagrams involving solid solutions via non-linear equations, with examples using THERMOCALC. Journal of Metamorphic Geology 16, 577–588.

Powell, R. & Holland, T. 1994. Optimal geothermometry and geobarometry. American Mineralogist 79, 120–133.

Powell, R. &Holland, T. J. B. 1988. An internally consistent dataset with uncertainties and correlations; 3, Applications to geobarometry, worked examples and a computer program. Journal of Metamorphic Geology 6, 173–204.

Raith, M., Raase, P. & Hörmann, P. K. 1982. The Precambrian of Finnish Lapland: evolution and regime of metamorphism. Geologische Rundschau 71, 230–244.

Rastas, J. & Kilpeläinen, T. 1991. Tektonis-metamorfiset tutkimukset Mertavaarassa, Puljun liuskejaksolla. Institute of Geology and Mineralogy, University of Turku, Publication No 25, 19 p. (in Finnish).

Räsänen, J. & Huhma, H. 2001. U-Pb datings of the Sodankylä schist area, central Finnish Lapland. Geological Survey of Finland, Special Paper 33, 153–188.

Searle, M. P. & Rex, J. 1989. Thermal model for the Zanskar Himalaya. Journal of Metamorphic Geology 7, 127–134.

Sorjonen-Ward, P., Nironen, M. & Luukkonen, E. 1997. Greenstone Associations in Finland. In: Maarten de Wit & Lewis Ashwal (eds.) Greenstone Belts. Clarendon Press, London, 677–698.

Thompson, A. B. & Ridley, J. R. 1987. Pressure-temperature-time histories of orogenic belts. Philosophical Transactions of the Royal Society, London, A321, 27–45.

Tuisku, P. 1985. The origin of scapolite in the Central Lapland schist area, Northern Finland : preliminary results. In: Laajoki, K. & Paakkola, J. (eds.) Proterozoic exogenic processes and related metallogeny : proceedings of the symposium held in Oulu, Finland, August 15–16, 1983. Geological Survey of Finland, Bulletin 331, 159–173.

Tuisku, P. & Makkonen, H. 1999. Spinel-bearing symplectites in Palaeoproterozoic ultramafic rocks from two different geological settings in Finland : thermobarometric and tectonic implications. Geologiska Föreningens i Stockholm Förhandlingar 121 (4), 293–300.

Vaasjoki, M. 2001 (ed.). Radiometric age determinations from Finnish Lapland and their bearing on the timing of Precambrian volcano-sedimentary sequences. Geological Survey of Finland. Special Paper 33, 279 p.

Väisänen, M. 2002. Structural features in the central Lapland greenstone belt, northern Finland. Geological Survey of Finland, Archive report K 21.42/2002/3. 20 p.

Ward, P., Härkönen, I., Nurmi, P., & Pankka, H. S. 1989. Structural studies in the Lapland greenstone belt, northern Finland and their applications to gold mineralizations. Geological Survey of Finland. Special Paper 10, 71–78.

Wennerström, M., & Airo, M-L. 1998. Magnetic fabric and emplacement of the post-collisional Pomovaara Granite Complex in northern Fennoscandia. Lithos 45 (1–4), 131–145.

Whitney, D. L. & Irving, A. J. 1994. Origin of K-poor leucosomes in a metasedimentary migmatite complex by ultrametamorphism, syn-metamorphic magmatism and subsolidus processes. Lithos 32, 173–192.

Appendix 1. Electron microprobe analyses of minerals. n.d. = not determined.

Sample	Rock type	Northing	Easting	Mineral	Zone	Site	SiO2	TiO2	Al2O3	Cr2O3	FeO	MnO	MgO	CaO	Na2O	K2O	BaO	NiO	ZnO	SrO	F	Cl	Total
Biotites																							
JTV-98-47.2	metapelite	7563830	3450920	bt	II	core	36,45	1,68	19,07	0,03	17,27	0,00	11,17	0,00	0,02	9,84	0,16	0,05	n.d.	0,00	0,57	0,03	96,33
JTV-98-49.1	metapelite	7576663	3445005	bt	II	core	36,13	1,79	18,89	0,09	19,18	0,00	10,18	0,03	0,13	9,22	0,07	0,00	0,10	0,00	0,48	0,05	96,35
JTV-98-28.2	metapelite	7552687	3458503	bt	III	core	37,22	1,35	18,58	0,00	16,77	0,10	12,00	0,00	0,26	8,66	0,00	0,01	0,01	0,00	0,69	0,33	95,97
PSH-01-14.3 A	metapelite	7521952	3519947	bt	III	matrix, core	34,68	1,57	18,63	n.d.	18,20	0,09	10,83	0,00	0,10	9,20	0,25	n.d.	n.d.	n.d.	n.d.	n.d.	93,54
PSH-97-28.3	crd-oam rock	7543200	3495550	bt	III	matrix, core	34,45	1,39	16,30	n.d.	22,78	0,03	8,75	0,01	0,08	9,23	0,15	n.d.	n.d.	n.d.	n.d.	n.d.	93,18
PSH-97-28.4 B	crd-oam rock	7543200	3495550	bt	III	matrix, core	35,89	1,33	18,89	n.d.	20,03	0,00	10,46	0,00	0,31	8,77	0,18	n.d.	n.d.	n.d.	n.d.	n.d.	95,86
PSH-98-41.1	metapelite	7517980	3457930	bt	III	core	34,37	1,64	18,99	0,18	23,57	0,08	6,56	0,00	0,26	9,41	0,00	0,09	0,12	0,00	0,24	0,16	95,68
PSH-98-41.1	metapelite	7517980	3457930	bt	III	rim	34,68	1,24	19,39	0,00	24,01	0,04	6,44	0,01	0,19	9,14	0,00	0,11	0,08	0,00	0,34	0,12	95,81
PSH-98-41.2.2	metapelite	7517980	3457930	bt	III	matrix	34,31	1,46	19,17	0,08	24,41	0,00	6,60	0,06	0,29	8,97	0,06	0,20	0,04	0,03	0,32	0,18	96,16
PSH-98-41.2.2	metapelite	7517980	3457930	bt	III	alt. from grt	34,45	1,68	18,89	0,14	24,18	0,00	6,63	0,06	0,25	8,93	0,09	0,07	0,09	0,10	0,47	0,16	96,20
92.3-MJV-99	metapelite	7482200	3529044	bt	VI	alt. from grt	33,95	1,62	18,15	n.d.	23,25	0,02	8,09	0,01	0,05	8,76	0,15	n.d.	n.d.	n.d.	n.d.	n.d.	94,05
92.3-MJV-99 B	metapelite	7482200	3529044	bt	VI	core	34,23	1,56	18,30	n.d.	21,92	0,08	8,79	0,00	0,34	8,65	0,29	n.d.	n.d.	n.d.	n.d.	n.d.	94,16
PSH-01-17.2 B	metapelite	7521105	3535306	bt	VI	core	34,71	1,70	19,40	n.d.	21,63	0,07	8,93	0,00	0,44	8,81	0,30	n.d.	n.d.	n.d.	n.d.	n.d.	95,98
PSH-01-8.2	metapelite	7504537	3513451	bt	VI	at grt	36,30	1,59	18,69	n.d.	19,21	0,18	10,33	0,00	0,21	9,35	0,10	n.d.	n.d.	n.d.	n.d.	n.d.	95,97
PSH-01-8.2	metapelite	7504537	3513451	bt	VI	matrix, core	36,23	1,55	18,44	n.d.	18,93	0,16	10,63	0,00	0,26	9,06	0,01	n.d.	n.d.	n.d.	n.d.	n.d.	95,27
PSH-98-11B	metapelite	7466644	3466995	bt	VI.2	core	38,62	1,88	18,78	0,08	9,47	0,00	17,17	0,00	0,18	9,15	0,00	0,08	n.d.	0,00	0,29	0,04	95,73
PSH-98-15.2	metapelite	7481728	3449834	bt	VI.2	matrix, core	34,88	1,93	18,35	0,11	22,32	0,11	7,77	0,09	0,04	9,69	0,08	0,04	0,08	0,00	0,34	0,19	96,02
PSH-98-15.2	metapelite	7481728	3449834	bt	VI.2	at grt	34,90	1,57	18,34	0,04	21,66	0,04	8,39	0,00	0,11	9,42	0,13	0,03	0,00	0,00	0,34	0,12	95,08
PSH-98-69.1	metapelite	7469020	3472710	bt	VI.2	matrix, core	37,24	1,38	18,93	0,04	15,38	0,26	13,01	0,00	0,24	9,32	0,12	0,16	n.d.	0,03	0,38	0,00	96,50
PSH-98-97.1B	metapelite	7495065	3416255	bt	VI.2	at grt	37,43	1,63	18,91	0,05	15,29	0,27	13,41	0,11	0,22	9,23	0,00	0,00	n.d.	0,00	0,26	0,01	96,82
PSH-98-97.1B	metapelite	7495065	3416255	bt	VI.2	matrix, core	37,17	1,50	18,80	0,09	16,06	0,28	13,00	0,09	0,20	9,07	0,00	0,02	n.d.	0,03	0,33	0,02	96,64
JTV-98-38.1A	metapelite	7498984	3391353	bt	VI.3	core at st	36,31	1,84	18,64	0,00	15,70	0,17	12,39	0,08	0,22	8,99	0,32	0,04	0,05	0,00	0,28	0,17	95,20
JTV-98-38.1B	metapelite	7498984	3391353	bt	VI.3	core	37,13	1,81	18,96	0,08	16,58	0,18	12,22	0,04	0,24	9,35	0,29	0,12	0,05	0,00	0,33	0,22	97,61
PSH-00-10.3	metapelite	7557588	3409925	bt	VI.3	at grt	26,62	0,80	21,49	n.d.	28,42	0,06	11,13	0,09	0,00	1,13	0,05	0,06	0,06	n.d.	0,00	0,13	90,04
PSH-00-10.3	metapelite	7557588	3409925	bt	VI.3	core	34,23	1,86	18,45	n.d.	23,22	0,02	7,78	0,09	0,04	8,40	0,21	0,01	0,04	n.d.	0,00	0,21	94,61
PSH-98-85.3	metapelite	7505446	3378078	bt	VI.3	core	36,55	2,25	16,66	0,00	16,79	0,65	12,20	0,00	0,00	10,14	0,00	0,15	0,03	0,05	0,33	0,25	96,06
PSH-98-98.3	metapelite	7494615	3418736	bt	VI.3	at grt	36,60	1,49	18,49	0,01	16,76	0,17	12,43	0,09	0,20	9,15	0,18	0,01	n.d.	0,08	0,39	0,13	96,20
PSH-98-98.3	metapelite	7494615	3418736	bt	VI.3	matrix, core	36,83	1,28	18,92	0,07	16,10	0,34	12,56	0,02	0,15	9,58	0,12	0,11	n.d.	0,06	0,35	0,20	96,67
Chlorites																							
PSH-00-54	meta-andesite	7555569	3431031	chl	II	core	26,70	0,17	22,40	0,08	15,39	0,00	21,39	0,06	0,00	0,06	0,00	0,04	n.d.	0,00	0,14	0,02	86,45
PSH-01-14.3 B	metapelite	7521952	3519947	chl	III	core	24,62	0,08	23,71	n.d.	23,04	0,23	15,92	0,00	0,00	0,00	0,00	n.d.	n.d.	n.d.	n.d.	n.d.	87,60
PSH-98-60.4	metapelite	7518130	3481410	chl	III	alt. from grt	23,94	0,07	22,53	0,09	29,35	0,03	12,33	0,00	0,00	0,00	0,05	0,07	0,00	0,13	0,14	0,07	88,79
PSH-98-61.2	metapelite	7517370	3478400	chl	III	core	24,46	0,13	22,67	0,12	27,18	0,15	13,60	0,00	0,00	0,00	0,00	0,02	n.d.	0,00	0,34	0,02	88,68
PSH-99-47	metabasalt	7510050	3451480	chl	IV.1	core	25,36	0,07	20,80	0,02	24,03	0,37	15,19	0,06	0,00	0,00	0,00	0,06	n.d.	0,00	0,23	0,00	86,21
PSH-00-101.2	metabasalt	7511014	3490940	chl	IV.1	core	26,94	0,05	20,73	0	20,15	0,1	17,91	0,13	0	0,03	0,08	0,12	n.d.	0,03	0,18	0,05	86,51
PSH-00-32	metabasalt	7531488	3444800	chl	IV.1	core	24,62	0,07	20,66	0,03	25,38	0,44	13,89	0,06	0,00	0,03	0,00	0,00	n.d.	0,00	0,16	0,00	85,34

Appendix 1. Continued

Sample	Rock type	Northing	Easting	Mineral	Zone	Site	SiO2	TiO2	Al2O3	Cr2O3	FeO	MnO	MgO	CaO	Na2O	K2O	BaO	NiO	ZnO	SrO	F	Cl	Total
PSH-00-46.2	metabasalt	7542782	3440573	chl	IV.1	core	25,22	0,09	20,96	0	24,72	0,44	14,68	0,04	0	0,02	0	0,07	n.d.	0	0,08	0,02	86,34
PSH-00-67	metabasalt	7524944	3452524	chl	IV.1	core	25,81	0,14	21,7	0,17	20,35	0,25	16,2	0,04	0	0,01	0	0,03	n.d.	0,09	0,11	0,01	84,9
PSH-00-82	metabasalt	7538649	3409705	chl	IV.1	core	25,61	0,06	19,82	0,04	24,9	0,35	14,1	0,08	0	0	0,04	0	n.d.	0	0,18	0,01	85,17
PSH-00-84	metabasalt	7529460	3404642	chl	IV.1	core	24,76	0,01	19,82	0	29,45	0,41	11,33	0,05	0	0	0,07	0,06	n.d.	0	0,15	0,01	86,13
PSH-00-86	metabasalt	7509896	3456787	chl	IV.1	core	25,48	0,06	20,94	0,03	23,36	0,48	15,37	0,03	0	0,03	0,05	0	n.d.	0,11	0,22	0	86,16
PSH-00-88	metabasalt	7509862	3458002	chl	IV.1	core	25,17	0	20,53	0,13	25,82	0,4	13,55	0,04	0	0,05	0	0	n.d.	0,04	0,15	0,02	85,89
PSH-98-101	metabasalt	7533821	3399791	chl	IV.1	core	25,72	0,03	21,08	0,06	21,9	0,29	16,86	0,04	0	0,02	0	0	n.d.	0,16	0,16	0,02	86,34
PSH-99-107	metabasalt	7550487	3433491	chl	IV.1	core	24,98	0,15	19,49	0,00	26,75	0,25	13,49	0,02	0,00	0,00	0,00	0,00	n.d.	0,09	0,19	0,02	85,41
PSH-99-88.1	metabasalt	7562138	3421613	chl	IV.1	core	25,38	0,13	20,66	0,07	25,07	0,28	13,8	0,05	0	0	0	0	n.d.	0,03	0,14	0,07	85,68
83.2-MJV-99	Fe-formation	7478895	3474068	chl	IV.2	core	22,95	0,02	22,62	0,02	32,38	0,14	7,96	0,02	0	0,03	0,01	0	n.d.	0	0,09	0,05	86,29
PSH-98-15.2	metapelite	7481728	3449834	chl	VI.2	alt. from grt	24,71	0,12	21,95	0,00	27,30	0,12	13,06	0,06	0,00	0,07	0,03	0,00	0,01	0,00	0,23	0,02	87,68
PSH-98-18.2B	metapelite	7485693	3447609	chl	VI.2	alt. from grt	24,27	0,17	22,70	0,03	24,07	0,50	15,40	0,05	0,00	0,01	0,00	0,12	0,11	0,00	0,32	0,02	87,77
PSH-98-69.1	metapelite	7469020	3472710	chl	VI.2	matrix, core	25,62	0,00	23,08	0,01	18,54	0,46	19,08	0,00	0,00	0,02	0,00	0,03	n.d.	0,05	0,29	0,06	87,25
PSH-98-69.1	metapelite	7469020	3472710	chl	VI.2	matrix, core	25,62	0,00	23,08	0,01	18,54	0,46	19,08	0,00	0,00	0,02	0,00	0,03	n.d.	0,05	0,29	0,06	87,25
PSH-00-10.3	metapelite	7557588	3409925	chl	VI.3	at grt	24,82	0,14	21,45	n.d.	27,73	0,23	13,31	0,00	0,00	0,00	0,05	0,10	0,05	n.d.	0,00	0,07	87,96
PSH-98-97.1B	metapelite	7495065	3416255	chl	VI.3	at grt	26,26	0,20	22,47	0,03	17,99	0,48	19,80	0,00	0,00	0,00	0,07	0,01	n.d.	0,05	0,18	0,00	87,54
Clinopyroxene																							
PSH-97-19.1L	amphibolite	7574600	3494935	cpx	I	core	49,50	0,19	2,71	n.d.	12,91	0,14	10,98	21,06	0,66	0,00	0,00	n.d.	n.d.	n.d.	n.d.	n.d.	98,15
Cordierites																							
PSH-97-28.4 B	crd-oam rock	7543200	3495550	crd	3	matrix, core	47,69	0,00	32,96	n.d.	8,79	0,06	8,24	0,03	0,42	0,01	0,00	n.d.	n.d.	n.d.	n.d.	n.d.	98,20
PSH-98-11B	metapelite	7466644	3466995	crd	VI.2	core	49,05	0,03	33,13	0,00	3,00	0,09	11,63	0,03	0,13	0,01	0,00	0,00	n.d.	0,06	0,12	0,03	97,31
PSH-98-69.1	metapelite	7469020	3472710	crd	VI.2	at grt	49,27	0,00	32,80	0,00	5,33	0,62	9,93	0,00	0,18	0,02	0,00	0,00	n.d.	0,05	0,00	0,01	98,22
PSH-98-69.1	metapelite	7469020	3472710	crd	VI.2	matrix, core	48,94	0,02	33,02	0,00	5,42	0,80	9,78	0,02	0,14	0,01	0,00	0,00	n.d.	0,11	0,01	0,00	98,25
Epidotes																							
PSH-99-88.1	metabasalt	7562138	3421613	ep	II	core	37,63	0	25,41	0	8,84	0,08	0,04	23,73	0	0,02	0	0	n.d.	0	0,06	0,02	95,83
PSH-99-47	metabasalt	7510050	3451480	ep	IV.1	core	38,57	0,14	28,44	0,03	5,40	0,07	0,03	23,41	0,00	0,01	0,02	0,00	n.d.	0,04	0,04	0,00	96,20
PSH-00-101.2	metabasalt	7511014	3490940	ep	IV.1	core	37,43	0,03	24,5	0,11	10,34	0,14	0,02	23,23	0,02	0	0,04	0,06	n.d.	0,12	0,08	0,03	96,14
PSH-00-32	metabasalt	7531488	3444800	ep	IV.1	core	38,08	0,00	27,81	0,02	6,43	0,03	0,04	23,67	0,00	0,02	0,05	0,00	n.d.	0,05	0,09	0,00	96,27
PSH-00-46.2	metabasalt	7542782	3440573	ep	IV.1	core	38,02	0,07	28,03	0	6,24	0,1	0,04	23,47	0	0,01	0,03	0,01	n.d.	0,03	0,12	0	96,16
PSH-00-67	metabasalt	7524944	3452524	ep	IV.1	core	38,39	0,08	28,44	0,06	5,8	0,15	0	23,39	0	0	0	0	n.d.	0	0,11	0,03	96,45
PSH-00-82	metabasalt	7538649	3409705	ep	IV.1	core	37,72	0	24,41	0,03	9,6	0,06	0	23,41	0	0,02	0	0,01	n.d.	0,13	0,14	0	95,54
PSH-00-86	metabasalt	7509896	3456787	ep	IV.1	core	38,22	0,25	28,64	0	5,5	0,01	0,03	23,86	0	0,03	0,01	0	n.d.	0	0,11	0,03	96,68
PSH-00-88	metabasalt	7509862	3458002	ep	IV.1	core	38,05	0,04	27,93	0	6,32	0,25	0,03	23,2	0	0,03	0	0	n.d.	0,21	0,07	0	96,11
PSH-98-101	metabasalt	7533821	3399791	ep	IV.1	core	38,14	0,04	29,11	0,02	4,63	0	0,02	24	0	0	0	0	n.d.	0,08	0,1	0,01	96,14
PSH-99-107	metabasalt	7550487	3433491	ep	IV.1	core	37,36	0,06	22,51	0,06	12,55	0,17	0,00	22,47	0,00	0,00	0,00	0,00	n.d.	0,32	0,07	0,00	95,58

Appendix 1. Continued

Sample	Rock type	Northing	Easting	Mineral	Zone	Site	SiO2	TiO2	Al2O3	Cr2O3	FeO	MnO	MgO	CaO	Na2O	K2O	BaO	NiO	ZnO	SrO	F	Cl	Total
Garnets																							
PSH-00-40	amphibolite	7596329	3455725	grt	I	core	37,87	0,16	20,91	n.d.	25,24	0,96	3,60	11,07	0,00	0,00	0,00	n.d.	n.d.	n.d.	n.d.	n.d.	99,80
PSH-00-40	amphibolite	7596329	3455725	grt	I	corona	37,28	0,06	20,92	n.d.	26,06	2,32	1,86	10,96	0,00	0,00	0,00	n.d.	n.d.	n.d.	n.d.	n.d.	99,45
PSH-00-42.1	amphibolite	7590218	3440182	grt	I	core	36,88	0,19	21,23	n.d.	27,37	0,69	5,46	7,50	0,00	0,00	0,00	n.d.	n.d.	n.d.	n.d.	n.d.	99,32
PSH-00-42.1	amphibolite	7590218	3440182	grt	I	rim	36,95	0,11	21,30	n.d.	28,12	1,37	4,35	7,52	0,00	0,00	0,00	n.d.	n.d.	n.d.	n.d.	n.d.	99,73
PSH-97-19.1L	amphibolite	7574600	3494935	grt	I	core	37,38	0,08	21,26	n.d.	29,12	1,11	4,94	6,99	0,00	0,00	0,00	n.d.	n.d.	n.d.	n.d.	n.d.	100,88
PSH-97-20.2 A	amphibolite	7572940	3494520	grt	I	core	37,56	0,07	21,19	n.d.	27,77	0,98	4,54	8,01	0,00	0,00	0,00	n.d.	n.d.	n.d.	n.d.	n.d.	100,12
PSH-97-20.2 A	amphibolite	7572940	3494520	grt	I	rim	37,59	0,04	21,03	n.d.	28,79	1,39	3,89	7,54	0,05	0,00	0,00	n.d.	n.d.	n.d.	n.d.	n.d.	100,33
PSH-97-20.2 B	amphibolite	7572940	3494520	grt	I	corona	37,04	0,05	20,92	n.d.	27,92	1,40	4,68	7,64	0,00	0,00	0,00	n.d.	n.d.	n.d.	n.d.	n.d.	99,65
PSH-97-22.8	amphibolite	7563820	3493470	grt	I	core	35,88	0,02	21,00	n.d.	31,10	1,29	1,59	8,45	0,00	0,00	0,00	n.d.	n.d.	n.d.	n.d.	n.d.	99,33
PSH-97-22.8	amphibolite	7563820	3493470	grt	I	rim	37,47	0,03	21,58	n.d.	28,53	0,65	1,35	11,27	0,05	0,00	0,01	n.d.	n.d.	n.d.	n.d.	n.d.	100,93
JTV-98-47.2	metapelite	7563830	3450920	grt	II	core	36,61	0,10	20,58	0,00	32,86	2,41	3,70	1,83	0,00	0,01	0,00	0,00	n.d.	0,15	0,33	0,00	98,59
JTV-98-47.2	metapelite	7563830	3450920	grt	II	rim	37,19	0,00	20,70	0,06	34,36	1,29	3,90	2,62	0,00	0,03	0,00	0,09	n.d.	0,12	0,20	0,00	100,55
JTV-98-49.1	metapelite	7576663	3445005	grt	II	core	37,33	0,04	20,65	0,00	34,63	1,62	4,31	1,34	0,00	0,00	0,00	0,04	0,11	0,12	0,20	0,01	100,39
JTV-98-49.1	metapelite	7576663	3445005	grt	II	rim	36,78	0,04	20,49	0,00	35,56	1,71	3,44	1,42	0,00	0,00	0,03	0,03	0,00	0,05	0,24	0,00	99,79
JTV-98-28.2	metapelite	7552687	3458503	grt	III	core	36,87	0,00	20,35	0,02	30,80	4,69	2,25	4,32	0,00	0,03	0,00	0,00	0,00	0,00	0,24	0,03	99,61
JTV-98-28.2	metapelite	7552687	3458503	grt	III	rim	37,36	0,00	20,72	0,02	32,56	0,14	3,40	5,00	0,00	0,00	0,08	0,00	0,00	0,03	0,29	0,00	99,61
PSH-00-38.2	amphibolite	7528956	3454965	grt	III	core	36,67	0,02	20,51	n.d.	33,60	3,84	0,76	3,90	0,07	0,15	0,04	0,00	0,05	n.d.	0,00	0,07	99,68
PSH-00-38.2	amphibolite	7528956	3454965	grt	III	rim	36,84	0,18	20,15	n.d.	32,40	3,92	0,88	5,21	0,00	0,04	0,03	0,00	0,04	n.d.	0,00	0,02	99,70
PSH-01-14.3 B	metapelite	7521952	3519947	grt	III	core	36,10	0,00	20,87	n.d.	31,74	3,14	3,09	4,56	0,00	0,00	0,00	n.d.	n.d.	n.d.	n.d.	n.d.	99,50
PSH-01-14.3 B	metapelite	7521952	3519947	grt	III	rim	36,69	0,10	20,67	n.d.	31,15	3,00	2,63	5,35	0,00	0,00	0,00	n.d.	n.d.	n.d.	n.d.	n.d.	99,59
PSH-97-1.1	amphibolite	7544752	3493952	grt	III	core	36,27	0,16	20,94	n.d.	31,52	3,68	2,83	4,49	0,00	0,00	0,00	n.d.	n.d.	n.d.	n.d.	n.d.	99,88
PSH-97-1.1	amphibolite	7544752	3493952	grt	III	rim	37,06	0,05	20,82	n.d.	33,17	1,43	3,33	4,71	0,09	0,01	0,00	n.d.	n.d.	n.d.	n.d.	n.d.	100,66
PSH-97-28.3	crd-oam rock	7543200	3495550	grt	III	rim	35,63	0,07	20,74	n.d.	36,45	1,44	3,37	1,76	0,00	0,00	0,00	n.d.	n.d.	n.d.	n.d.	n.d.	99,46
PSH-97-28.4 B	crd-oam rock	7543200	3495550	grt	III	rim	35,82	0,05	21,18	n.d.	37,36	0,99	3,50	0,71	0,08	0,00	0,00	n.d.	n.d.	n.d.	n.d.	n.d.	99,69
PSH-98-41.1	metapelite	7517980	3457930	grt	III	core	37,23	0,00	20,45	0,00	33,22	1,15	2,56	4,90	0,00	0,00	0,00	0,00	0,00	0,08	0,19	0,01	99,78
PSH-98-41.1	metapelite	7517980	3457930	grt	III	near-rim	36,72	0,08	20,24	0,13	39,46	0,42	1,67	1,66	0,00	0,00	0,00	0,08	0,02	0,10	0,19	0,00	100,78
PSH-98-41.1	metapelite	7517980	3457930	grt	III	rim	36,59	0,00	20,15	0,04	39,12	0,20	1,77	1,43	0,00	0,03	0,03	0,06	0,02	0,00	0,31	0,00	99,75
PSH-98-41.2.2	metapelite	7517980	3457930	grt	III	core	37,17	0,00	20,30	0,02	32,35	1,92	4,23	3,85	0,00	0,00	0,06	0,00	0,00	0,00	0,24	0,02	100,16
PSH-98-41.2.2	metapelite	7517980	3457930	grt	III	rim	36,59	0,00	20,09	0,02	38,59	1,01	1,45	1,95	0,00	0,02	0,00	0,04	0,01	0,05	0,33	0,00	100,17
PSH-98-60.4	metapelite	7518130	3481410	grt	III	rim	36,67	0,00	20,02	0,00	33,37	1,16	2,59	4,87	0,00	0,02	0,00	0,02	0,00	0,07	0,19	0,04	99,01
PSH-98-61.2	metapelite	7517370	3478400	grt	III	rim	37,02	0,04	20,30	0,00	34,18	0,99	2,78	4,01	0,00	0,00	0,00	0,00	n.d.	0,02	0,21	0,00	99,56
83.2-MJV-99	Fe-formation	7478895	3474068	grt	IV.2	rim	37,12	0,35	20,82	0,01	31,33	5,95	0,87	3,01	0	0,05	0	0	n.d.	0	0,2	0	99,72
83.2-MJV-99	Fe-formation	7478895	3474068	grt	IV.2	core	37,02	0,11	20,97	0	31,15	6,26	0,91	3,3	0	0,02	0	0,05	n.d.	0	0,15	0	99,93
PSH-00-1.7	skarn	7525947	3385536	grt	IV.2	core	36,63	0,11	20,76	n.d.	29,78	7,08	0,63	5,46	0,00	0,00	0,00	0,00	0,00	n.d.	0,00	0,01	100,45
PSH-00-1.7	skarn	7525947	3385536	grt	IV.2	rim	37,20	0,13	20,71	n.d.	28,19	7,65	0,58	6,46	0,00	0,00	0,06	0,01	0,00	n.d.	0,00	0,00	100,97
92.3-MJV-99	metapelite	7482200	3529044	grt	V.5	core	35,94	0,03	20,39	n.d.	34,78	2,07	3,99	1,71	0,00	0,00	0,00	n.d.	n.d.	n.d.	n.d.	n.d.	98,91
92.3-MJV-99	metapelite	7482200	3529044	grt	V.5	rim	36,18	0,01	20,60	n.d.	35,35	2,89	2,69	1,50	0,08	0,00	0,00	n.d.	n.d.	n.d.	n.d.	n.d.	99,28
98.3-MJV-99	metapelite	7486916	3449031	grt	V.5	rim	36,24	0,01	19,95	n.d.	35,45	3,40	2,65	1,64	0,10	0,00	0,00	n.d.	n.d.	n.d.	n.d.	n.d.	99,44

Appendix 1. Continued

Sample	Rock type	Northing	Easting	Mineral	Zone	Site	SiO2	TiO2	Al2O3	Cr2O3	FeO	MnO	MgO	CaO	Na2O	K2O	BaO	NiO	ZnO	SrO	F	Cl	Total
PSH-01-17.2 A	metapelite	7521105	3535306	grt	V.5	core	36,17	0,00	20,66	n.d.	34,43	3,34	3,24	1,44	0,04	0,00	0,00	n.d.	n.d.	n.d.	n.d.	n.d.	99,31
PSH-01-17.2 A	metapelite	7521105	3535306	grt	V.5	rim	35,90	0,02	20,53	n.d.	34,73	4,16	2,61	1,33	0,00	0,00	0,05	n.d.	n.d.	n.d.	n.d.	n.d.	99,33
PSH-01-8.2	metapelite	7504537	3513451	grt	V.5	core	37,31	0,03	20,56	n.d.	29,09	8,49	3,14	2,07	0,00	0,00	0,00	n.d.	n.d.	n.d.	n.d.	n.d.	100,68
PSH-01-8.2	metapelite	7504537	3513451	grt	V.5	rim	37,24	0,00	20,65	n.d.	27,97	10,35	2,54	1,68	0,00	0,01	0,00	n.d.	n.d.	n.d.	n.d.	n.d.	100,44
PSH-98-15.2	metapelite	7481728	3449834	grt	VI.2	core	37,44	0,05	20,61	0,00	35,07	0,09	3,29	3,21	0,00	0,00	0,07	0,00	0,06	0,01	0,18	0,00	100,08
PSH-98-15.2	metapelite	7481728	3449834	grt	VI.2	rim	37,12	0,11	20,19	0,02	35,29	0,67	2,88	3,13	0,00	0,02	0,00	0,00	0,03	0,06	0,20	0,01	99,73
PSH-98-16.1	amphibolite	7481654	3450010	grt	VI.2	core	37,12	0,18	20,11	0,00	28,16	3,91	1,73	8,11	0,00	0,00	0,00	0,00	0,00	0,10	0,19	0,00	99,60
PSH-98-16.1	amphibolite	7481654	3450010	grt	VI.2	rim	37,16	0,09	20,08	0,01	28,25	3,05	1,94	8,07	0,00	0,02	0,05	0,00	0,01	0,08	0,17	0,02	99,01
PSH-98-18.2B	metapelite	7485693	3447609	grt	VI.2	near rim	36,78	0,22	20,02	0,00	25,60	10,16	1,68	4,80	0,00	0,00	0,00	0,04	0,00	0,17	0,17	0,01	99,63
PSH-98-69.1	metapelite	7469020	3472710	grt	VI.2	core	36,91	0,00	20,45	0,05	24,56	12,80	3,22	1,80	0,00	0,00	0,00	0,02	n.d.	0,13	0,12	0,00	100,08
PSH-98-69.1	metapelite	7469020	3472710	grt	VI.2	rim	36,96	0,01	20,27	0,00	23,44	13,56	2,87	1,89	0,01	0,03	0,00	0,00	n.d.	0,15	0,13	0,03	99,35
PSH-98-97.1B	metapelite	7495065	3416255	grt	VI.2	core	37,02	0,26	20,40	0,03	24,88	10,87	3,24	2,76	0,00	0,02	0,02	0,01	n.d.	0,11	0,11	0,00	99,72
PSH-98-97.1B	metapelite	7495065	3416255	grt	VI.2	rim	37,07	0,00	20,52	0,00	25,01	11,44	3,22	2,12	0,00	0,00	0,00	0,00	n.d.	0,06	0,19	0,03	99,66
JTV-98-38.1B	metapelite	7498984	3391353	grt	VI.3	core	37,02	0,20	20,47	0,04	24,41	10,63	3,59	2,93	0,05	0,00	0,00	0,00	0,06	0,08	0,07	0,00	99,54
JTV-98-38.1B	metapelite	7498984	3391353	grt	VI.3	rim	37,11	0,00	20,36	0,06	25,49	11,42	3,53	1,24	0,00	0,00	0,04	0,03	0,00	0,03	0,14	0,01	99,44
PSH-00-10.3	metapelite	7557588	3409925	grt	VI.3	core	37,87	0,01	21,08	n.d.	33,62	1,17	4,26	2,36	0,00	0,01	0,05	0,00	0,00	n.d.	0,00	0,00	100,44
PSH-00-10.3	metapelite	7557588	3409925	grt	VI.3	rim	37,37	0,00	20,74	n.d.	33,74	4,46	2,58	1,74	0,00	0,02	0,03	0,00	0,01	n.d.	0,00	0,01	100,70
PSH-98-85.3	metapelite	7505446	3378078	grt	VI.3	core	36,99	0,13	18,79	0,00	14,07	19,13	2,08	7,87	0,00	0,00	0,07	0,00	0,03	0,07	0,07	0,00	99,30
PSH-98-98.3	metapelite	7494615	3418736	grt	VI.3	core	37,29	0,10	20,16	0,00	23,72	12,23	2,99	3,16	0,04	0,03	0,09	0,07	n.d.	0,08	0,06	0,05	100,08
PSH-98-98.3	metapelite	7494615	3418736	grt	VI.3	rim	37,19	0,02	20,54	0,01	25,45	11,65	3,53	1,33	0,00	0,02	0,03	0,00	n.d.	0,08	0,25	0,02	100,12
Amphiboles																							
PSH-00-40	amphibolite	7596329	3455725	amph	I	core	39,04	1,62	14,48	n.d.	21,44	0,23	6,23	11,36	1,53	1,76	0,00	n.d.	n.d.	n.d.	n.d.	n.d.	97,70
PSH-00-42.1	amphibolite	7590218	3440182	amph	I	core	43,63	1,00	11,83	n.d.	16,01	0,13	10,66	11,65	1,37	1,02	0,02	n.d.	n.d.	n.d.	n.d.	n.d.	97,30
PSH-00-42.1	amphibolite	7590218	3440182	amph	I	rim	44,14	0,88	11,55	n.d.	15,86	0,09	11,22	11,36	1,31	0,92	0,01	n.d.	n.d.	n.d.	n.d.	n.d.	97,34
PSH-97-19.1L	amphibolite	7574600	3494935	amph	I	core	41,39	1,51	11,25	n.d.	18,67	0,10	9,47	11,20	1,62	0,79	0,00	n.d.	n.d.	n.d.	n.d.	n.d.	96,00
PSH-97-20.2 A	amphibolite	7572940	3494520	amph	I	core	39,00	1,62	13,45	n.d.	20,08	0,20	7,67	11,14	1,44	1,41	0,11	n.d.	n.d.	n.d.	n.d.	n.d.	96,13
PSH-97-20.2 A	amphibolite	7572940	3494520	amph	I	rim	39,49	1,63	13,33	n.d.	20,09	0,22	7,46	11,09	1,65	1,31	0,00	n.d.	n.d.	n.d.	n.d.	n.d.	96,27
PSH-97-20.2 B	amphibolite	7572940	3494520	amph	I	rim	40,04	1,05	13,93	n.d.	19,07	0,17	8,18	11,20	1,54	0,88	0,00	n.d.	n.d.	n.d.	n.d.	n.d.	96,06
PSH-97-22.8	amphibolite	7563820	3493470	amph	I	core	37,58	0,90	14,64	n.d.	25,55	0,14	3,82	11,12	1,59	1,53	0,00	n.d.	n.d.	n.d.	n.d.	n.d.	96,88
PSH-97-22.8	amphibolite	7563820	3493470	amph	I	rim	37,13	0,52	16,02	n.d.	25,21	0,13	3,63	11,11	1,25	1,56	0,00	n.d.	n.d.	n.d.	n.d.	n.d.	96,56
PSH-00-54	meta-andesite	7555569	3431031	amph	II	core	49,56	0,29	7,75	0,15	10,92	0,04	14,72	11,01	0,62	0,08	0,05	0,00	n.d.	0,01	0,16	0,05	95,41
PSH-00-38.2	amphibolite	7528956	3454965	amph	III	core	39,55	0,24	16,75	n.d.	23,52	0,18	3,45	10,66	1,22	0,55	0,00	0,02	0,04	n.d.	0,00	0,06	96,23
PSH-00-38.2	amphibolite	7528956	3454965	amph	III	rim	40,18	0,40	16,69	n.d.	23,43	0,30	3,24	10,25	1,16	0,55	0,00	0,03	0,00	n.d.	0,00	0,00	96,23
PSH-97-1.1	amphibolite	7544752	3493952	amph	III	core	42,29	0,60	14,22	n.d.	19,49	0,07	8,72	10,28	1,85	0,29	0,00	n.d.	n.d.	n.d.	n.d.	n.d.	97,80
PSH-97-1.1	amphibolite	7544752	3493952	amph	III	rim	42,00	0,46	13,59	n.d.	20,00	0,19	8,17	10,59	1,65	0,27	0,00	n.d.	n.d.	n.d.	n.d.	n.d.	96,91
PSH-97-28.3	crd-oam rock	7543200	3495550	ged	III	rim	40,23	0,15	16,30	n.d.	29,59	0,38	8,03	0,21	1,77	0,01	0,00	n.d.	n.d.	n.d.	n.d.	n.d.	96,67
PSH-97-28.3	crd-oam rock	7543200	3495550	ged	III	core	42,09	0,17	14,03	n.d.	30,26	0,31	9,34	0,20	1,55	0,00	0,00	n.d.	n.d.	n.d.	n.d.	n.d.	97,95
PSH-99-47	metabasalt	7510050	3451480	amph	IV.1	core	53,00	0,00	2,01	0,07	13,56	0,34	14,23	12,12	0,02	0,05	0,00	0,00	n.d.	0,00	0,19	0,02	95,59

Appendix 1. Continued

Sample	Rock type	Northing	Easting	Mineral	Zone	Site	SiO2	TiO2	Al2O3	Cr2O3	FeO	MnO	MgO	CaO	Na2O	K2O	BaO	NiO	ZnO	SrO	F	Cl	Total
PSH-00-101.2	metabasalt	7511014	3490940	amph	IV.1	core	51,54	0,35	4,31	0,15	11,65	0,14	15,02	12,06	0,49	0,13	0	0,03	n.d.	0,18	0,11	0,09	96,25
PSH-00-32	metabasalt	7531488	3444800	amph	IV.1	core	53,18	0,07	1,95	0,00	13,09	0,23	14,43	12,49	0,08	0,03	0,00	0,00	n.d.	0,05	0,17	0,01	95,78
PSH-00-46.2	metabasalt	7542782	3440573	amph	IV.1	core	52,87	0,05	2,15	0,03	14,67	0,29	13,58	12,42	0,12	0,08	0	0	n.d.	0,1	0,12	0,02	96,49
PSH-00-67	metabasalt	7524944	3452524	amph	IV.1	core	51,9	0,2	4,44	0,12	11,84	0,28	14,47	11,87	0,29	0,09	0	0,03	n.d.	0	0,21	0,01	95,76
PSH-00-82	metabasalt	7538649	3409705	amph	IV.1	core	52,32	0,12	2,99	0,07	14,31	0,33	13,28	12,38	0,25	0,05	0	0	n.d.	0	0,19	0,01	96,31
PSH-00-84	metabasalt	7529460	3404642	amph	IV.1	core	51,96	0	1,48	0,07	19,04	0,56	10,61	11,91	0,08	0,11	0	0,05	n.d.	0,15	0,17	0,01	96,19
PSH-00-86	metabasalt	7509896	3456787	amph	IV.1	core	51,22	0,19	4,8	0	12,77	0,2	13,99	12,64	0,32	0,18	0	0,05	n.d.	0	0,12	0	96,46
PSH-00-88	metabasalt	7509862	3458002	amph	IV.1	core	48,67	0	7,04	0,06	16,72	0,34	10,5	12,05	0,46	0,32	0	0,02	n.d.	0	0,2	0,04	96,42
PSH-98-101	metabasalt	7533821	3399791	amph	IV.1	core	53,64	0,03	2,16	0,26	11,1	0,25	15,64	12,7	0,07	0,08	0	0,05	n.d.	0,05	0,13	0,01	96,17
PSH-99-107	metabasalt	7550487	3433491	amph	IV.1	core	49,03	0,15	5,55	0,15	17,08	0,24	11,36	11,75	0,73	0,14	0,00	0,00	n.d.	0,00	0,18	0,03	96,39
PSH-99-88.1	metabasalt	7562138	3421613	amph	IV.1	core	42,57	0,37	12,72	0	19,19	0,3	7,4	11,09	1,29	0,1	0	0,05	n.d.	0,09	0,22	0	95,38
83.2-MJV-99	Fe-formation	7478895	3474068	amph	IV.2	core	39,49	0,19	19,21	0	21,94	0,38	2,47	10,65	0,83	0,39	0	0,14	n.d.	0,01	0,25	0,12	96,07
83.2-MJV-99	Fe-formation	7478895	3474068	amph	IV.2	rim	39	0,5	19,41	0,03	21,67	0,32	2,59	11,26	0,87	0,53	0	0	n.d.	0,12	0,29	0,17	96,75
PSH-00-1.7	skarn	7525947	3385536	amph	IV.2	core	37,83	0,35	15,90	n.d.	25,79	0,48	2,60	10,49	1,48	0,71	0,14	0,07	0,10	n.d.	0,00	1,16	97,10
PSH-00-1.7	skarn	7525947	3385536	amph	IV.2	rim	38,05	0,46	14,04	n.d.	27,13	0,53	2,51	10,51	1,53	1,00	0,00	0,00	0,09	n.d.	0,00	1,56	97,40
PSH-98-16.1	amphibolite	7481654	3450010	amph	VI.2	core	41,87	0,59	12,87	0,02	20,92	0,19	7,05	10,94	1,34	0,34	0,00	0,06	0,00	0,11	0,25	0,03	96,58
PSH-98-16.1	amphibolite	7481654	3450010	amph	VI.2	rim	42,06	0,40	12,95	0,00	20,66	0,22	7,11	11,07	1,38	0,31	0,00	0,00	0,00	0,01	0,24	0,03	96,45
Muscovites																							
JTV-98-47.2	metapelite	7563830	3450920	ms	II	core	46,07	0,50	35,43	0,00	0,99	0,02	0,69	0,01	1,78	8,43	0,28	0,07	n.d.	0,07	0,10	0,01	94,46
JTV-98-28.2	metapelite	7552687	3458503	ms	III	core	46,52	0,34	35,43	0,10	1,09	0,05	0,68	0,04	1,05	8,66	0,33	0,04	0,00	0,07	0,09	0,02	94,49
PSH-01-14.3 A	metapelite	7521952	3519947	ms	III	matrix c.	45,51	0,35	33,83	n.d.	2,55	0,00	0,92	0,00	1,15	9,49	0,28	n.d.	n.d.	n.d.	n.d.	n.d.	94,06
PSH-01-14.3 B	metapelite	7521952	3519947	ms	III	core	45,43	0,18	36,02	n.d.	2,40	0,01	0,55	0,00	0,78	9,42	0,67	n.d.	n.d.	n.d.	n.d.	n.d.	95,46
PSH-98-41.1	metapelite	7517980	3457930	ms	III	core	46,73	0,49	33,80	0,06	2,09	0,02	0,79	0,04	1,39	9,13	0,33	0,08	0,02	0,10	0,07	0,01	95,17
PSH-98-41.2.2	metapelite	7517980	3457930	ms	III	matrix	46,19	0,44	34,45	0,09	1,38	0,00	0,62	0,01	1,57	8,94	0,34	0,00	0,00	0,08	0,08	0,00	94,20
PSH-98-41.2.2	metapelite	7517980	3457930	ms	III	alt.	46,58	0,16	35,99	0,09	1,20	0,06	0,38	0,00	1,77	8,95	0,07	0,06	0,00	0,02	0,08	0,02	95,41
PSH-98-60.4	metapelite	7518130	3481410	ms	III	core	45,69	0,30	34,32	0,00	2,12	0,03	0,50	0,02	1,49	9,13	0,29	0,00	0,06	0,11	0,12	0,00	94,20
PSH-98-61.2	metapelite	7517370	3478400	ms	III	core	46,44	0,30	35,16	0,03	2,02	0,02	0,30	0,00	1,73	8,54	0,15	0,07	n.d.	0,02	0,13	0,00	94,92
92.3-MJV-99	metapelite	7482200	3529044	ms	V.5	alt.from g	45,98	0,70	35,18	n.d.	2,51	0,00	0,54	0,00	1,14	9,15	0,31	n.d.	n.d.	n.d.	n.d.	n.d.	95,50
92.3-MJV-99	metapelite	7482200	3529044	ms	V.5	core	46,22	0,42	35,12	n.d.	2,36	0,00	0,45	0,00	1,04	9,03	0,48	n.d.	n.d.	n.d.	n.d.	n.d.	95,12
PSH-01-8.2	metapelite	7504537	3513451	ms	V.5	at grt	46,12	0,58	34,01	n.d.	2,85	0,00	0,62	0,01	1,25	9,31	0,48	n.d.	n.d.	n.d.	n.d.	n.d.	95,24
PSH-01-8.2	metapelite	7504537	3513451	ms	V.5	matrix, core	45,60	0,42	34,17	n.d.	2,97	0,00	0,82	0,00	0,95	9,24	0,21	n.d.	n.d.	n.d.	n.d.	n.d.	94,38
PSH-98-11B	metapelite	7466644	3466995	ms	VI.2	core	45,66	0,70	34,35	0,06	1,57	0,02	0,64	0,03	1,02	10,01	0,30	0,09	n.d.	0,00	0,12	0,03	94,60
PSH-98-15.2	metapelite	7481728	3449834	ms	VI.2	matrix, core	46,32	0,54	34,80	0,00	2,06	0,03	0,54	0,00	1,56	8,94	0,28	0,06	0,06	0,01	0,10	0,02	95,32
PSH-98-15.2	metapelite	7481728	3449834	ms	VI.2	alt. from g.	46,21	0,11	37,09	0,01	1,18	0,00	0,17	0,08	0,61	10,20	0,44	0,01	0,00	0,00	0,07	0,00	96,18
PSH-98-18.2B	metapelite	7485693	3447609	ms	VI.2	alt. from grt	46,46	0,24	35,37	0,04	2,71	0,07	0,42	0,05	1,03	9,70	0,29	0,08	0,00	0,09	0,08	0,00	96,63
PSH-98-69.1	metapelite	7469020	3472710	ms	VI.2	at grt	45,95	0,35	34,64	0,00	2,85	0,09	0,54	0,05	1,48	9,31	0,30	0,02	n.d.	0,02	0,10	0,02	95,73
PSH-98-69.1	metapelite	7469020	3472710	ms	VI.2	matrix, core	46,81	0,18	34,70	0,01	2,75	0,01	0,55	0,03	1,37	9,39	0,28	0,11	n.d.	0,00	0,00	0,00	96,18
PSH-98-97.1B	metapelite	7495065	3416255	ms	VI.2	at grt	46,20	0,40	34,55	0,02	2,32	0,00	0,54	0,09	1,46	9,20	0,58	0,00	n.d.	0,04	0,06	0,01	95,47

Appendix 1. Continued

Sample	Rock type	Northing	Easting	Mineral	Zone	Site	SiO2	TiO2	Al2O3	Cr2O3	FeO	MnO	MgO	CaO	Na2O	K2O	BaO	NiO	ZnO	SrO	F	Cl	Total
PSH-98-97.1B	metapelite	7495065	3416255	ms	VI.2	matrix, core	46,26	0,48	34,19	0,06	2,70	0,00	0,67	0,01	1,43	9,16	0,53	0,02	n.d.	0,03	0,14	0,00	95,66
JTV-98-38.1A	metapelite	7498984	3391353	ms	VI.3	core	45,93	0,76	34,23	0,04	2,70	0,07	0,64	0,03	1,20	9,29	0,96	0,08	0,01	0,00	0,02	0,04	95,99
JTV-98-38.1A	metapelite	7498984	3391353	ms	VI.3	rim	45,80	0,51	33,96	0,00	2,56	0,00	0,62	0,00	1,19	9,44	1,19	0,02	0,01	0,00	0,12	0,00	95,43
PSH-00-10.3	metapelite	7557588	3409925	ms	VI.3	at grt	45,64	0,34	35,09	n.d.	2,71	0,00	0,58	0,06	1,08	9,03	0,60	0,00	0,07	n.d.	0,00	0,00	95,19
PSH-00-10.3	metapelite	7557588	3409925	ms	VI.3	core	47,31	0,39	36,14	n.d.	2,30	0,01	0,40	0,04	1,13	8,88	0,61	0,00	0,02	n.d.	0,00	0,00	97,22
PSH-98-85.3	metapelite	7505446	3378078	ms	VI.3	core	45,51	0,00	36,29	0,04	1,62	0,04	0,13	0,32	0,03	11,62	0,00	0,00	0,00	0,05	0,09	0,00	95,75
PSH-98-98.3	metapelite	7494615	3418736	ms	VI.3	at grt	45,74	0,94	34,48	0,09	2,60	0,03	0,55	0,06	1,17	9,44	0,95	0,00	n.d.	0,00	0,15	0,01	96,22
PSH-98-98.3	metapelite	7494615	3418736	ms	VI.3	matrix, core	44,74	0,49	37,19	0,08	2,23	0,01	0,43	0,02	0,83	9,03	0,66	0,03	n.d.	0,03	0,11	0,00	95,89
Plagioclases																							
PSH-00-40	amphibolite	7596329	3455725	pl	I	core	56,64	0,01	26,59	n.d.	0,05	0,03	0,04	9,26	6,00	0,25	0,00	n.d.	n.d.	n.d.	n.d.	n.d.	98,86
PSH-00-40	amphibolite	7596329	3455725	pl	I	rim	57,61	0,00	25,99	n.d.	0,08	0,03	0,03	8,48	6,82	0,25	0,02	n.d.	n.d.	n.d.	n.d.	n.d.	99,31
PSH-00-42.1	amphibolite	7590218	3440182	pl	I	core	59,88	0,00	25,39	n.d.	0,07	0,00	0,00	6,66	7,85	0,06	0,02	n.d.	n.d.	n.d.	n.d.	n.d.	99,93
PSH-97-19.1L	amphibolite	7574600	3494935	pl	I	core	56,55	0,00	26,87	n.d.	0,11	0,00	0,00	9,12	6,23	0,17	0,03	n.d.	n.d.	n.d.	n.d.	n.d.	99,07
PSH-97-20.2 A	amphibolite	7572940	3494520	pl	I	core	54,37	0,00	28,08	n.d.	0,09	0,00	0,00	10,60	5,99	0,14	0,03	n.d.	n.d.	n.d.	n.d.	n.d.	99,30
PSH-97-20.2 A	amphibolite	7572940	3494520	pl	I	rim	53,75	0,00	28,60	n.d.	0,14	0,00	0,00	10,80	5,71	0,11	0,00	n.d.	n.d.	n.d.	n.d.	n.d.	99,11
PSH-97-20.2 B	amphibolite	7572940	3494520	pl	I	rim	54,28	0,00	27,96	n.d.	0,20	0,00	0,00	10,77	5,50	0,11	0,00	n.d.	n.d.	n.d.	n.d.	n.d.	98,83
PSH-97-22.8	amphibolite	7563820	3493470	pl	I	core	60,89	0,00	23,96	n.d.	0,01	0,01	0,01	5,49	8,55	0,14	0,00	n.d.	n.d.	n.d.	n.d.	n.d.	99,07
PSH-97-22.8	amphibolite	7563820	3493470	pl	I	rim	59,98	0,00	24,75	n.d.	0,19	0,00	0,00	6,55	8,13	0,22	0,00	n.d.	n.d.	n.d.	n.d.	n.d.	99,81
JTV-98-47.2	metapelite	7563830	3450920	pl	II	core	63,62	0,00	22,26	0,00	0,00	0,00	0,00	3,60	9,31	0,14	0,00	0,00	n.d.	0,15	0,05	0,00	99,13
JTV-98-49.1	metapelite	7576663	3445005	pl	II	core	63,76	0,02	22,56	0,02	0,04	0,00	0,00	4,15	9,16	0,04	0,01	0,01	0,02	0,18	0,08	0,00	100,04
PSH-00-54	meta-andesite	7555569	3431031	pl	II	core	53,61	0,00	28,89	0,00	0,18	0,00	0,07	11,10	5,18	0,10	0,07	0,00	n.d.	0,08	0,01	0,02	99,30
PSH-99-88.1	amphibolite	7562138	3421613	pl	II	core	67,11	0,09	20,35	0	0,04	0	0,01	1,09	11,19	0,04	0	0	n.d.	0	0,06	0	99,97
JTV-98-28.2	metapelite	7552687	3458503	pl	III	core	60,64	0,00	24,28	0,02	0,04	0,00	0,01	6,00	8,03	0,06	0,00	0,03	0,13	0,19	0,00	0,00	99,42
PSH-00-38.2	amphibolite	7528956	3454965	pl	III	core	64,38	0,03	22,40	n.d.	0,49	0,01	0,00	3,46	9,56	0,17	0,06	0,00	0,00	n.d.	0,01	0,03	100,59
PSH-01-14.3 A	metapelite	7521952	3519947	pl	III	matrix c.	56,67	0,00	26,85	n.d.	0,07	0,00	0,02	8,93	6,97	0,04	0,00	n.d.	n.d.	n.d.	n.d.	n.d.	99,56
PSH-01-14.3 B	metapelite	7521952	3519947	pl	III	core	57,61	0,00	26,05	n.d.	0,06	0,00	0,03	7,97	7,64	0,06	0,03	n.d.	n.d.	n.d.	n.d.	n.d.	99,45
PSH-97-1.1	amphibolite	7544752	3493952	pl	III	core	61,42	0,00	23,25	n.d.	0,00	0,01	0,00	4,64	9,29	0,04	0,00	n.d.	n.d.	n.d.	n.d.	n.d.	98,66
PSH-97-1.1	amphibolite	7544752	3493952	pl	III	rim	62,29	0,00	22,77	n.d.	0,02	0,04	0,03	4,17	9,71	0,06	0,00	n.d.	n.d.	n.d.	n.d.	n.d.	99,09
PSH-97-28.3	crd-oam rock	7543200	3495550	pl	III	matrix, core	64,83	0,02	21,50	n.d.	0,00	0,00	0,00	2,19	10,49	0,05	0,00	n.d.	n.d.	n.d.	n.d.	n.d.	99,09
PSH-97-28.4 A	crd-oam rock	7543200	3495550	pl	III	at grt	67,00	0,00	20,24	n.d.	0,02	0,00	0,02	0,53	11,57	0,03	0,06	n.d.	n.d.	n.d.	n.d.	n.d.	99,48
PSH-98-41.1	metapelite	7517980	3457930	pl	III	core	61,46	0,00	23,86	0,02	0,07	0,01	0,00	5,61	8,41	0,13	0,00	0,00	0,00	0,14	0,03	0,02	99,75
PSH-98-41.2.2	metapelite	7517980	3457930	pl	III	alt. from grt?	61,85	0,08	23,60	0,02	0,10	0,00	0,00	5,40	8,52	0,11	0,00	0,00	0,00	0,17	0,02	0,00	99,88
PSH-98-41.2.2	metapelite	7517980	3457930	pl	III	alt. from grt?	61,85	0,08	23,60	0,02	0,10	0,00	0,00	5,40	8,52	0,11	0,00	0,00	0,00	0,17	0,02	0,00	99,88
PSH-98-60.4	metapelite	7518130	3481410	pl	III	core	60,00	0,00	24,69	0,03	0,04	0,00	0,00	6,70	7,70	0,02	0,05	0,00	0,00	0,21	0,00	0,01	99,48
PSH-98-61.2	metapelite	7517370	3478400	pl	III	core	60,59	0,06	24,31	0,05	0,19	0,07	0,00	6,17	7,95	0,08	0,00	0,01	n.d.	0,22	0,00	0,00	99,69
PSH-99-47	metabasalt	7510050	3451480	pl	IV.1	core	67,42	0,00	19,82	0,02	0,16	0,00	0,00	0,31	11,73	0,09	0,00	0,00	n.d.	0,00	0,05	0,01	99,60
PSH-00-101.2	metabasalt	7511014	3490940	pl	IV.1	core	67,41	0	19,94	0,04	0,14	0	0	0,82	11,43	0,04	0	0	n.d.	0,04	0	0,02	99,89
PSH-00-32	metabasalt	7531488	3444800	pl	IV.1	core	70,12	0,12	18,27	0,00	0,12	0,00	0,01	0,67	10,31	0,05	0,00	0,00	n.d.	0,00	0,07	0,04	99,80

Appendix 1. Continued

Sample	Rock type	Northing	Easting	Mineral	Zone	Site	SiO2	TiO2	Al2O3	Cr2O3	FeO	MnO	MgO	CaO	Na2O	K2O	BaO	NiO	ZnO	SrO	F	Cl	Total
PSH-00-46.2	metabasalt	7542782	3440573	pl	IV.1	core	67,4	0,09	20,08	0	0,06	0	0,11	1,02	11,06	0,04	0	0	n.d.	0,11	0,01	0	99,98
PSH-00-67	metabasalt	7524944	3452524	pl	IV.1	core	66,8	0,03	20,59	0,03	0,09	0,02	0	1,51	10,32	0,09	0	0	n.d.	0	0,17	0,01	99,67
PSH-00-82	metabasalt	7538649	3409705	pl	IV.1	core	67,63	0	19,56	0	0,19	0,01	0,01	0,41	11,54	0,06	0	0	n.d.	0,01	0,04	0,05	99,51
PSH-00-84	metabasalt	7529460	3404642	pl	IV.1	core	67,66	0	19,85	0	0,22	0	0,04	0,47	11,09	0,05	0	0,04	n.d.	0,13	0,09	0,02	99,66
PSH-00-86	metabasalt	7509896	3456787	pl	IV.1	core	67,39	0	19,96	0,01	0,1	0	0,01	0,4	11,88	0,06	0	0,04	n.d.	0	0	0	99,86
PSH-00-88	metabasalt	7509862	3458002	pl	IV.1	core	66,11	0,1	20,78	0	0,17	0	0	1,7	10,72	0,08	0	0	n.d.	0,12	0,07	0,01	99,86
PSH-98-101	metabasalt	7533821	3399791	pl	IV.1	core	67,82	0,02	19,67	0,01	0,11	0,03	0	0,42	11,39	0,03	0,05	0	n.d.	0	0,05	0,02	99,6
PSH-99-107	metabasalt	7550487	3433491	pl	IV.1	core	67,60	0,01	19,77	0,03	0,07	0,00	0,00	0,35	11,73	0,07	0,00	0,06	n.d.	0,07	0,00	0,00	99,74
83.2-MJV-99	Fe-formation	7478895	3474068	pl	IV.2	core	48,83	0,01	32,62	0,01	0,3	0	0	15,5	2,58	0,02	0	0	n.d.	0,07	0,05	0	99,99
PSH-00-1.7	skarn	7525947	3385536	pl	IV.2	core near grt	60,15	0,00	25,40	n.d.	0,23	0,00	0,00	6,91	7,90	0,06	0,00	0,06	0,00	n.d.	0,00	0,03	100,74
PSH-00-1.7	skarn	7525947	3385536	pl	IV.2	core, matrix	57,94	0,08	26,83	n.d.	0,33	0,00	0,00	8,29	6,85	0,02	0,00	0,01	0,00	n.d.	0,00	0,00	100,34
92.3-MJV-99	metapelite	7482200	3529044	pl	V.5	incl. in grt	63,42	0,00	23,16	n.d.	0,01	0,00	0,00	4,80	9,04	0,07	0,00	n.d.	n.d.	n.d.	n.d.	n.d.	100,52
92.3-MJV-99	metapelite	7482200	3529044	pl	V.5	core	61,36	0,00	23,05	n.d.	0,04	0,00	0,00	4,85	9,37	0,05	0,00	n.d.	n.d.	n.d.	n.d.	n.d.	98,73
PSH-01-17.2 B	metapelite	7521105	3535306	pl	V.5	core	59,64	0,00	25,48	n.d.	0,04	0,00	0,04	7,17	7,62	0,04	0,00	n.d.	n.d.	n.d.	n.d.	n.d.	100,03
PSH-01-8.2	metapelite	7504537	3513451	pl	V.5	matrix, core	59,14	0,00	25,25	n.d.	0,02	0,03	0,00	6,81	7,75	0,05	0,00	n.d.	n.d.	n.d.	n.d.	n.d.	99,05
PSH-98-15.2	metapelite	7481728	3449834	pl	VI.2	matrix, core	62,56	0,06	23,15	0,00	0,06	0,04	0,00	4,53	8,81	0,07	0,13	0,00	0,00	0,14	0,11	0,02	99,68
PSH-98-15.2	metapelite	7481728	3449834	pl	VI.2	alt. from g.	62,74	0,00	23,21	0,00	0,02	0,00	0,01	4,60	8,72	0,14	0,02	0,01	0,00	0,13	0,01	0,01	99,62
PSH-98-16.1	amphibolite	7481654	3450010	pl	VI.2	core, matrix	61,88	0,02	23,45	0,00	0,14	0,04	0,02	5,27	8,58	0,08	0,01	0,01	0,00	0,15	0,08	0,00	99,74
PSH-98-16.1	amphibolite	7481654	3450010	pl	VI.2	core, next to grt	61,28	0,04	23,64	0,06	0,11	0,07	0,00	5,30	8,46	0,04	0,00	0,00	0,06	0,29	0,03	0,02	99,40
PSH-98-18.2B	metapelite	7485693	3447609	pl	VI.2	alt. from grt	62,55	0,00	23,43	0,00	0,03	0,00	0,00	5,05	8,72	0,03	0,00	0,07	0,03	0,07	0,03	0,01	100,02
PSH-98-97.1B	metapelite	7495065	3416255	pl	VI.2	at grt	61,87	0,04	23,74	0,00	0,13	0,03	0,00	5,53	8,29	0,02	0,00	0,04	n.d.	0,24	0,03	0,01	99,98
PSH-98-97.1B	metapelite	7495065	3416255	pl	VI.2	at grt	61,87	0,04	23,74	0,00	0,13	0,03	0,00	5,53	8,29	0,02	0,00	0,04	n.d.	0,24	0,03	0,01	99,98
JTV-98-38.1A	metapelite	7498984	3391353	pl	VI.3	core at st	61,08	0,01	23,61	0,01	0,06	0,00	0,00	5,54	8,37	0,07	0,06	0,06	0,00	0,20	0,10	0,00	99,18
JTV-98-38.1B	metapelite	7498984	3391353	pl	VI.3	core	61,59	0,00	23,82	0,08	0,09	0,03	0,00	5,67	8,22	0,03	0,08	0,00	0,00	0,12	0,08	0,01	99,82
PSH-00-10.3	metapelite	7557588	3409925	pl	VI.3	core	62,07	0,00	24,34	n.d.	0,00	0,00	0,01	5,35	8,67	0,09	0,09	0,02	0,00	n.d.	0,00	0,00	100,64
PSH-00-10.3	metapelite	7557588	3409925	pl	VI.3	rim	63,19	0,06	25,25	n.d.	0,06	0,00	0,00	5,55	8,39	0,05	0,02	0,03	0,00	n.d.	0,00	0,00	102,61
PSH-98-85.3	metapelite	7505446	3378078	pl	VI.3	core	44,07	0,00	35,25	0,00	0,28	0,00	0,00	19,21	0,34	0,02	0,00	0,07	0,03	0,10	0,02	0,02	99,43
PSH-98-98.3	metapelite	7494615	3418736	pl	VI.3	matrix, core	61,69	0,03	23,89	0,00	0,05	0,01	0,00	5,89	8,21	0,04	0,00	0,09	n.d.	0,07	0,07	0,00	100,03
PSH-98-98.3	metapelite	7494615	3418736	pl	VI.3	rim	61,46	0,00	24,09	0,02	0,00	0,04	0,00	5,80	8,26	0,11	0,00	0,00	n.d.	0,20	0,00	0,00	99,99
Staurolites																							
PSH-01-14.3 A	metapelite	7521952	3519947	st	III	core	27,53	0,54	53,72	0,07	13,16	0,29	1,78	0,01	0,05	0,00	0,01	n.d.	0,04	n.d.	n.d.	n.d.	97,19
PSH-01-17.2 B	metapelite	7521105	3535306	st	III	core	27,95	0,57	52,50	0,10	15,28	0,25	1,65	0,00	0,00	0,00	0,00	n.d.	0,10	n.d.	n.d.	n.d.	98,40
PSH-98-69.1	metapelite	7469020	3472710	st	VI.2	matrix, core	27,77	0,47	51,87	0,05	12,01	0,87	1,97	0,00	0,42	0,03	0,00	0,10	2,44	0,03	0,10	0,00	98,12
PSH-98-97.1B	metapelite	7495065	3416255	st	VI.2	core, at grt	27,46	0,64	52,33	0,01	13,12	1,03	2,33	0,03	0,01	0,00	0,00	0,05	0,34	0,10	0,06	0,00	97,53
PSH-98-97.1B	metapelite	7495065	3416255	st	VI.2	rim	27,12	0,48	52,71	0,08	13,07	0,93	2,23	0,00	0,06	0,00	0,00	0,07	0,38	0,07	0,08	0,00	97,28
JTV-98-38.1A	metapelite	7498984	3391353	st	VI.3	core	27,21	0,52	52,11	0,00	12,84	1,01	2,28	0,01	0,10	0,02	0,00	0,00	0,78	0,10	0,17	0,01	97,16
JTV-98-38.1A	metapelite	7498984	3391353	st	VI.3	core	26,74	0,62	52,52	0,13	12,81	0,76	2,26	0,00	0,11	0,03	0,01	0,02	0,81	0,11	0,11	0,00	97,05
PSH-98-98.3	metapelite	7494615	3418736	st	VI.3	core	27,19	0,44	52,89	0,08	12,18	0,93	2,08	0,00	0,15	0,04	0,01	0,00	1,00	0,00	0,12	0,01	97,12
PSH-98-98.3	metapelite	7494615	3418736	st	VI.3	rim	27,01	0,46	52,59	0,00	12,65	0,83	2,32	0,03	0,17	0,04	0,00	0,09	0,73	0,05	0,15	0,02	97,13

Appendix 2

Appendix 2. THERMOCALC average P-T results for mafic rocks.

Sample	**PSH-00-42**		**PSH-00-42**		**PSH-97-19.1L**		**PSH-97-20.2A**		**PSH-97-20.2A**		**PSH-97-20.2B**		**PSH-97-22.8**		**PSH-97-22.8**		**PSH-00-40**	
P-T stage	Peak		Cooling		Peak		Peak		Cooling		Cooling		Peak		Cooling		Peak	
Zone	I		I		I		I		I		I		I		I		I	
Activities	at 850°C		at 800°C		at 850°C		at 850°C		at 800°C		at 800°C		at 850°C		at 800°C		at 850°C	
Garnet	core		rim		core		core		rim		grt corona		core		rim		core	
prp	0.0205		0.0115		0.0141		0.0126		0.00790		0.0121		0.000750		0.000560		0.00770	
grs	0.0149		0.0143		0.0105		0.0160		0.0122		0.0119		0.0170		0.0360		0.0350	
alm	0.130		0.150		0.160		0.150		0.180		0.150		0.230		0.200		0.120	
Amphibole	core		rim		core		core		rim		rim		core		rim		mean	
tr	0.0250		0.0362		0.0161		0.00809		0.00640		0.0152		0.000533		0.000833		0.00268	
fact	0.000520		0.000420		0.000960		0.000720		0.000900		0.00100		0.00360		0.00399		0.00100	
ts	0.00230		0.00170		0.000300		0.000200		0.000300		0.000800		0.00007		0.000130		0.000300	
parg	0.0490		0.0610		0.0224		0.0202		0.0166		0.0417		0.00271		0.00512		0.0113	
gl	-		0.000813		-		-		-		0.0007595		-		-		-	
Plagioclase	mean		mean		core		core		rim		rim		core		rim		core	
an	0.410		0.410		0.560		0.630		0.650		0.660		0.340		0.400		0.570	
ab	0.690		0.690		0.560		0.520		0.500		0.490		0.740		0.690		0.540	
Clinoprproxene					core													
di	-		-		0.510		-		-		-		-		-		-	
hed	-		-		0.300		-		-		-		-		-		-	
cats	-		-		0.0400		-		-		-		-		-		-	
Other	qtz H2O		qtz H2O		qtz H2O		qtz H2O		qtz H2O		qtz H2O		qtz H2O		qtz H2O		qtz H2O	
Results																		
*a*H2O	1.0	0.4	1.0	0.4	1.0	0.4	1.0	0.4	1.0	0.4	1.0	0.4	1.0	0.4	1.0	0.4	1.0	0.4
T°C	**894**	**853**	**807**	**772**	**943**	**887**	**911**	**879**	**858**	**828**	**848**	**812**	**794**	**772**	**743**	**722**	**1011**	**966**
s.d.(T)	99	89	112	80	79	70	118	109	110	102	99	90	117	110	105	99	146	133
P kbar	**12.7**	**11.8**	**11.1**	**10.4**	**10.5**	**9.7**	**11.6**	**10.7**	**10.3**	**9.5**	**9.7**	**9.0**	**11.8**	**11.1**	**11.6**	**10.9**	**14.4**	**13.2**
s.d.(P)	1.8	1.7	2.0	1.5	1.4	1.3	1.9	1.8	1.8	1.7	1.6	1.5	2.0	1.9	1.8	1.7	2.2	2.0
correl.	0.527	0.487	0.607	0.574	0.372	0.328	0.552	0.495	0.532	0.478	0.538	0.490	0.738	0.699	0.753	0.715	0.698	0.639
fit	0.83	0.58	1.27	0.93	0.90	0.61	0.83	0.62	0.97	0.74	0.84	0.69	0.37	0.21	0.40	0.27	0.63	0.43
NR	4	4	4	4	7	7	4	4	4	4	4	4	4	4	4	4	4	4
end members eliminated	-	-	-	gl	-	-	-	-	-	-	gl	gl	-	-	-	-	-	-

Appendix 2. Continued

Appendix 2. THERMOCALC Average P-T results for mafic rocks.																		
Sample	**PSH-00-40**		**PSH-97-1.1**		**PSH-97-1.1**		**PSH-00-38.2**		**PSH-00-38.2**		**PSH-98-16.1**		**PSH-98-16.1**		**PSH-00-1.7**		**PSH-00-1.7**	
P-T stage	Cooling		pre-peak		Peak		pre-peak		Peak		pre-peak		Peak		pre-peak		Peak	
Zone	I		II		II		III.1		III.1		VI.2		VI.2		IV.2		IV.2	
Activities	at 800°C		at 650°C		at 700°C		at 550°C		at 550°C		at 650°C		at 650°C		at 550°C		at 550°C	
Garnet	corona		core		rim		core		rim		core		rim		core		rim	
prp	0.00134		0.00310		0.00450		0.000068		0.000107		0.000910		0.00130		0.000044		0.000035	
grs	0.0330		0.00300		0.00300		0.00150		0.00330		0.0120		0.0130		0.00400		0.00600	
alm	0.160		0.250		0.280		0.410		0.360		0.210		0.220		0.260		0.230	
Amphibole	mean		core		rim		core		rim		core		rim		core		rim	
tr	0.00315		0.0456		0.0338		0.00280		0.00169		0.0205		0.0213		0.00125		0.000899	
fact	0.00100		0.00196		0.00297		0.0123		0.0107		0.00620		0.00590		0.0223		0.0245	
ts	0.000300		0.00150		0.00130		0.00110		0.00110		0.00110		0.00130		0.000120		0.00002	
parg	0.0119		0.106		0.0784		0.00898		0.00669		0.0359		0.0371		0.00494		0.00216	
gl	-		0.00952		0.00418		0.00141		0.00143		0.00125		0.00130		0.00166		0.000632	
Plagioclase	rim		core		rim		core		core		matrix		next to grt		matrix		next to grt	
an	0.520		0.320		0.350		0.280		0.280		0.380		0.380		0.640		0.530	
ab	0.590		0.790		0.760		0.830		0.830		0.750		0.750		0.610		0.680	
Other	qtz H2O		qtz H2O		qtz H2O		qtz H2O		qtz H2O		qtz H2O		qtz H20		qtz H2O		qtz H2O	
Results																		
*a*H2O	1.0	0.4	1.0	0.4	1.0	0.4	1.0	0.4	1.0	0.4	1.0	0.4	1.0	0.4	1.0	0.4	1.0	0.4
T°C	**733**	**709**	**645**	**615**	**692**	**666**	**514**	**493**	**560**	**533**	**710**	**673**	**732**	**693**	**474**	**456**	**527**	**507**
s.d.(T)	96	90	55	50	62	57	62	56	66	64	72	61	70	62	46	43	57	54
P kbar	**11.1**	**10.4**	**7.2**	**6.8**	**7.4**	**7.0**	**4.5**	**4.1**	**5.9**	**5.4**	**8.1**	**7.4**	**8.6**	**7.9**	**3.2**	**2.8**	**4.1**	**3.7**
s.d.(P)	1.7	1.5	1.4	1.4	1.5	1.5	1.5	1.5	1.8	1.8	1.7	1.4	1.6	1.5	1.0	1.0	1.1	1.1
correl.	0.669	0.624	0.672	0.666	0.647	0.638	0.590	579	0.656	0.651	0.706	0.688	0.711	0.692	0.544	0.536	0.594	569
fit	0.95	0.73	0.79	0.60	0.69	0.51	1.22	1.19	1.28	1.33	1.09	0.88	1.04	0.84	0.70	0.78	0.45	41
NR	4	4	5	5	5	5	5	5	5	5	5	5	5	5	5	5	5	5
end members eliminated	gl	-	-	-	-	-	-	-	-	-	-	-	-	-	-	-	-	-

Appendix 2. Continued

Appendix 2 (cont.). THERMOCALC Average P-T results for pelitic rocks.																		
Sample	**JTV-98-47**		**JTV-98-47**		**JTV-98-49**		**JTV-98-49**		**JTV-98-28**		**JTV-98-28**		**PSH-98-41.1**		**PSH-98-41.1**		**PSH-98-41.2**	
P-T stage	pre-peak		Peak		Peak		Cooling		Pre-peak		Peak		peak, M1		cooling, M2		Peak	
Zone	II		II		II		II		II		II		III.1		III.1		III.1	
Activities	at 650°C		at 650°C		at 650°C		at 650°C		at 650°C		at 650°C		at 650°C		at 650°C		at 650°C	
Garnet	core		rim		core		rim		core		rim		core		rim		core	
prp	0.00500		0.00570		0.00650		0.00360		0.00138		0.00490		0.00210		0.000530		0.00750	
grs	0.00026		0.00059		0.000088		0.000098		0.00210		0.00410		0.00330		0.000079		0.00160	
alm	0.390		0.360		0.400		0.440		0.280		0.340		0.360		0.650		0.270	
Biotite	core		core		core		core		core		core		core		core		core	
phl	0.0700		0.0700		0.0520		0.0520		0.0800		0.0800		0.0210		0.0210		0.0198	
ann	0.0390		0.0390		0.0510		0.0510		0.0330		0.0330		0.110		0.110		0.120	
east	0.0570		0.0570		0.0450		0.0450		0.0560		0.0560		0.0220		0.0220		0.0220	
Muscovite	core		core						core		core		core		core		core	
mu	0.690		0.690		-		-		0.680		0.680		0.640		0.640		0.690	
pa	-		-		-		-		0.680		0.680		0.700		0.700		0.800	
cel	0.0160		0.0160		-		-		0.0160		0.0160		0.0210		0.0210		0.0160	
Plagioclase	core		core		core		core		core		core		core		core		core	
an	0.260		0.260		0.300		0.300		0.430		0.430		0.400		0.400		0.380	
ab	-		-		-		-		0.710		0.710		0.730		0.730		0.740	
Other	ky qtz H2O		ky qtz H2O		ky qtz H2O		ky qtz H2O		ky qtz H2O		ky qtz H2O		qtz H2O		qtz H2O		qtz H2O	
Results																		
*a*H2O	1.0	0.4	1.0	0.4	1.0	0.4	1.0	0.4	1.0	1.0	1.0	1.0	1.0	0.4	1.00	0.4	1.00	0.4
T°C	**602**	**602**	**598**	**598**	**694**	**694**	**602**	**602**	**650**	**602**	**670**	**643**	**601**	**551**	**590**	**536**	**598**	**549**
s.d.(T)	78	78	76	76	120	120	102	102	29	30	22	30	32	35	47	44	65	64
P kbar	**7.9**	**7.9**	**8.5**	**8.5**	**7.4**	**7.4**	**6.2**	**6.2**	**8.6**	**7.6**	**9.9**	**9.3**	**8.3**	**7.6**	**5.5**	**5.0**	**7.8**	**7.2**
s.d.(P)	1.4	1.4	1.4	1.4	2.1	2.1	1.8	1.8	1.4	1.1	1.0	1.1	1.1	1.4	1.8	1.8	2.4	2.6
correl.	0.737	0.736	0.760	0.76	0.831	0.831	0.821	0.821	0.785	0.785	0.764	0.794	0.752	0.760	0.734	0.759	0.726	0.740
fit	0.33	0.33	0.34	0.34	0.19	0.19	0.19	0.19	1.33	0.93	0.76	0.53	1.1	1.42	1.75	1.87	2.34	2.68
NR	5	5	5	5	3	3	3	3	6	5	6	5	5	5	5	5	5	5
end members eliminated	-	-	-	-	-	-	-	-	-	ky	-	ky	-	-	-	-	-	-

Appendix 2. Continued

Appendix 2 (cont.). THERMOCALC Average P-T results for pelitic rocks.																		
Sample	**PSH-98-41.2**		**PSH-98-60.4**		**PSH-98-61.2**		**PSH-98-61.2**		**PSH-98-61.2**		**PSH-01-14.3**		**PSH-01-14.3**		**PSH-01-14.3**		**PSH-01-17.2**	
P-T stage	cooling, M2		M2		M2		M2		M2		Peak		Peak		cooling, M2		Peak	
Zone	III.1		III		III		III		III		III		III		III		V.5	
Activities	at 650°C		at 550°C		at 550°C		at 550°C		at 550°C		at 650°C		at 650°C		at 550°C		at 650°C	
Garnet	rim		rim		rim		rim		rim		core		core		rim		core	
prp	0.000300		0.00240		0.00260		0.00260		0.00260		0.00450		0.00450		0.00280		0.00340	
grs	0.000170		0.00300		0.00180		0.00180		0.00180		0.00330		0.00330		0.00460		0.000107	
alm	0.600		0.350		0.390		0.390		0.390		0.240		0.240		0.260		0.370	
Biotite	core										matrix, core		matrix, core				core	
phl	0.0194		-		-		-		-		0.0580		0.0580		-		0.0350	
ann	0.110		-		-		-		-		0.0410		0.0410		-		0.0650	
east	0.0210		-		-		-		-		0.0600		0.0600		-		0.0380	
Muscovite	core		alt. from g		alt. from g		alt. from g		alt. from g		matrix, core		matrix, core		alt. from g			
mu	0.730		0.690		0.690		0.690		0.690		0.650		0.650		0.690		-	
pa	0.890		0.950		0.970		0.970		0.970		0.780		0.780		0.591		-	
cel	0.00930		0.0130		0.00740		0.00740		0.00740		0.0230		0.0230		0.00850		-	
Chlorite			alt. from g		alt. from g		alt. from g		alt. from g						alt. from g			
clin	-		0.0114		0.0180		0.0180		0.0180		-		-		0.040		-	
daph	-		0.0450		0.0330		0.0330		0.0330		-		-		0.0150		-	
ames	-		0.0197		0.0270		0.0270		0.0270		-		-		0.0480		-	
Plagioclase	core		core		core		core		core		core		core		core		core	
an	0.380		0.530		0.490		0.490		0.490		0.660		0.660		0.590		0.500	
ab	0.740		0.680		0.710		0.710		0.710		0.600		0.600		0.640		-	
Other	qtz H2O		and ky qtz H2O		and ky qtz H2O		and ky qtz H2O		and ky qtz H2O		mst 0.0019 fst 0.39 ky and qtz H2O		mst 0.0019 fst 0.39 ky and qtz H2O		mst 0.0011 fst 0.45 ky and qtz H2O		mst 0.00089 fst 0.470 sill qtz H2O	
Results																		
*a*H2O	1.0	0.4	1.0	1.0	1.0	0.4	1.0	0.4	1.0	0.4	1.0	1.0	1.0	0.4	1.0	0.4	1.0	0.4
T°C	**559**	**509**	**576**	**563**	**564**	**507**	**582**	**528**	**584**	**530**	**616**	**586**	**588**	**543**	**594**	**537**	**596**	**553**
s.d.(T)	27	24	23	23	17	15	13	13	20	18	27	20	27	30	25	21	32	29
P kbar	**5.0**	**4.5**	**6.3**	**4.5**	**4.6**	**3.9**	**6.8**	**6.1**	**6.1**	**5.5**	**7.9**	**4.8**	**7.3**	**6.9**	**6.3**	**5.6**	**4.4**	**4.1**
s.d.(P)	1.1	1.0	1.4	0.3	0.2	0.2	0.8	0.9	1.0	1.0	1.2	0.3	1.1	1.3	1.3	1.2	1.5	1.4
correl.	0.744	0.769	0.579	0.657	0.901	0.853	0.622	0.690	0.780	0.816	0.776	0.904	0.740	0.758	0.666	0.720	0.940	0.946
fit	0.52	0.43	1.75	1.81	1.88	1.74	1.07	1.17	1.42	1.46	1.11	1.70	1.00	1.27	1.69	1.64	0.55	0.83
NR	5	5	6	7	7	7	6	6	6	6	7	9	5	5	7	7	5	5
end members eliminated	-	-	ky	-	-	-	and	and	ky	ky	ky and	-	mst ky fst and	mst ky fst and	-	-	-	-

Appendix 2. Continued

Appendix 2 (cont.). THERMOCALC Average P-T results for pelitic rocks.																		
Sample	**PSH-01-17.2**		**PSH-01-8.2**		**PSH-01-8.2**		**MJV-99-98**		**MJV-99-98**		**PSH-98-15.2**		**PSH-98-15.2**		**PSH-98-69.1**		**PSH-98-69.1**	
P-T stage	Cooling		Peak		Cooling		Peak		Cooling		Peak		Cooling		Peak		Peak	
Zone	V.5		V.5		V.5		VI.2		VI.2		VI.2		VI.2		VI.2		VI.2	
Activities	at 650°C		at 600°C		at 600°C		at 650°C		at 600°C		at 600°C		at 600°C		at 600°C		at 600°C	
Garnet	rim		core		rim		core		rim		core		rim		core		core	
prp	0.00180		0.00270		0.00140		0.00610		0.00180		0.00380		0.00250		0.00290		0.00290	
grs	0.000079		0.000260		0.000140		0.000180		0.000110		0.00115		0.000910		0.00018		0.00018	
alm	0.390		0.230		0.220		0.340		0.380		0.440		0.440		0.130		0.130	
Biotite	core		matrix, core		core, at grt		core		alt. from g		matrix, core		at grt		matrix, core		matrix, core	
phl	0.0350		0.0570		0.0540		0.0320		0.0241		0.0276		0.0350		0.0950		0.0950	
ann	0.0650		0.0500		0.0530		0.0640		0.0690		0.0920		0.0840		0.0250		0.0250	
east	0.0380		0.0470		0.0450		0.0350		0.0310		0.0280		0.0330		0.0710		0.0710	
Muscovite			matrix core		core, at grt		core		alt. from g		matrix, core		alt. from g		matrix, core		matrix, core	
mu	-		0.630		0.640		0.670		0.650		0.670		0.800		0.660		0.660	
pa	-		0.566		0.710		0.570		0.660		0.830		0.518		0.77		0.77	
cel	-		0.0180		0.0150		0.0105		0.0120		0.0130		0.00410		0.014		0.014	
Chlorite													alt. from g.		matrix, core		matrix, core	
clin	-		-		-				-		-		0.0164		0.0850		0.0850	
daph	-		-		-				-		-		0.0360		0.00460		0.00460	
ames	-		-		-				-		-		0.0205		0.0770		0.0770	
Plagioclase	core		core		core		core		incl. in g		matrix, core		alt.from g		-		-	
an	0.500		0.500		0.500		0.330		0.360		0.350		0.350		qtz crd 0.61		qtz crd 0.61	
ab	-		0.680		0.680		0.780		0.780		0.780		0.770		fcrd 0.048		fcrd 0.048	
Other	mst 0.00089		sill qtz		sill qtz		sill qtz		sill qtz		qtz H2O		qtz H2O		mncrd 0.0016		mncrd 0.0016	
	fst 0.470		H2O		H2O		H2O		H2O						mst 0.0051		mst 0.0051	
	sill qtz H2O														fst 0.29 H2O		fst 0.29 H2O	
															spss 0.023 and		spss 0.023 and	
Results																		
*a*H2O	1.0	0.4	1.0	0.4	1.0	0.4	1.0	0.4	1.0	0.4	1.0	0.4	1.0	0.4	1.0	0.4	1.0	0.4
T°C	**581**	**539**	**619**	**562**	**568**	**518**	**672**	**609**	**623**	**565**	**611**	**560**	**588**	**532**	**597**	**542**	**591**	**531**
s.d.(T)	32	30	27	25	25	23	29	26	28	26	27	29	22	22	15	19	33	43
P kbar	**3.7**	**3.4**	**5.3**	**4.9**	**4.0**	**3.6**	**7.2**	**6.6**	**5.6**	**5.1**	**8.1**	**7.5**	**6.0**	**5.3**	**5.1**	**4.2**	**5.1**	**4.1**
s.d.(P)	1.4	1.4	1.1	1.1	1.0	1.0	1.2	1.1	1.1	1.1	1.1	1.2	1.3	1.4	0.5	0.7	0.8	1.1
correl.	0.943	0.951	0.908	0.918	0.916	0.929	0.907	0.917	0.913	0.932	0.732	0.748	0.529	0.641	0.831	0.851	0.917	0.920
fit	0.23	0.45	0.93	1.08	0.85	0.98	0.70	0.98	0.51	0.72	0.89	1.23	1.59	1.70	1.19	1.70	1.18	1.77
NR	5	5	6	6	6	6	6	6	6	6	5	5	8	8	12	12	9	9
end members eliminated	-	-	-	-	-	-	-	-	-	-	-	-	-	-	grs pa	grs pa	grs pa chl	grs pa chl

Appendix 2. Continued

Appendix 2 (cont.). THERMOCALC Average P-T results for pelitic rocks.																		
Sample	**PSH-98-69.1**		**PSH-98-18.2**		**PSH-98-11B**		**PSH-98-97.1**				**PSH-98-97.1**				**PSH-98-98.3**			
P-T stage	Cooling		Cooling		Cooling		Peak				Cooling				Peak			
Zone	VI.2		VI.2		VI.2		VI.2				VI.2				VI.3			
Activities	at 600°C		at 600°C				at 650°C				at 650°C				at 650°C			
Garnet	rim		rim				core				rim				core			
prp	0.00210		0.000600		-		0.00310				0.00290				0.00250			
grs	0.00021		0.00260		-		0.000670				0.000310				0.000850			
alm	0.130		0.170		-		0.150				0.160				0.120			
Biotite					core		core				at grt							
phl	-		-		0.200 0.00450		0.0900				0.0990				0.0910			
ann	-		-		0.113		0.0260				0.0230				0.0300			
east	-		-		core		0.0660				0.0700				0.0660			
Muscovite	at grt		alt. from g		0.720		core				at grt							
mu	0.650		0.680		0.72		0.640				0.670				0.670			
pa	0.82		0.660		0.0170		0.700				0.750				0.479			
cel	0.0130		0.00990				0.0160				0.0130				-			
Chlorite	matrix, core		alt. from g		-						at grt							
clin	0.0850		0.030		-		-				0.0920				-			
daph	0.00460		0.0157		-		-				0.00360				-			
ames	0.0770		0.0410				-				0.0750				-			
Plagioclase	-		alt. from g		-		core				at grt							
an			0.380		-		0.400				0.400				0.420			
ab	and qtz H2O		0.760				0.740				0.740				0.720			
Other	crd 0.620				crd 0.800													
	fcrd 0.0480				fcrd 0.0150		mst 0.0065				mst 0.0056				mst 0.0058			
	mncrd 0.00098				ky and sill		fst 0.26				fst 0.28				fst 0.27			
	spss 0.028				qtz H2O		and sill qtz H2O				and sill qtz H2O				sill qtz H2O			
Results																		
*a*H2O	1.0	0.4	1.0	0.4	1.0	1.0	1.0	1.0	1.0	0.4	1.0	1.0	1.0	0.4	1.0	1.0	1.0	0.4
T°C	**570**	**511**	**548**	**501**	**505**	**492**	**549**	**637**	**595**	**549**	**552**	**591**	**608**	**562**	**646**	**666**	**617**	**566**
s.d.(T)	21	21	27	24	8	36	12	35	29	26	7	14	24	22	53	47	31	28
P kbar	**3.7**	**2.6**	**6.0**	**5.4**	**3.8**	**3.5**	**3.3**	**6.3**	**6.6**	**6.2**	**3.3**	**5.4**	**6.1**	**5.8**	**6.9**	**6.7**	**6.6**	**6.1**
s.d.(P)	0.7	0.7	1.5	1.4	0.1	0.7	0.3	1.2	1.1	1.0	0.2	0.7	1.1	1.0	2.3	1.9	1.1	1.1
correl.	0.931	0.955	0.499	0.579	0.754	0.990	0.129	0.948	0.766	0.783	0.186	0.877	0.941	0.948	0.941	0.911	0.773	0.790
fit	0.99	1.08	1.83	1.82	0.75	0.84	1.73	1.23	0.31	0.35	1.25	0.83	0.79	0.71	2.00	1.59	0.38	0.19
NR	7	7	5	5	6	5	9	8	5	5	12	11	8	8	7	5	4	4
end members eliminated	grs pa	grs pa	-	-	pa	and	-	sill	mst fst sill and	mst fst sill and	-	and	and ames clin daph	and ames clin daph	-	fst mst	fst mst sill	fst mst sill

Appendix 2. Continued

Appendix 2 (cont.). THERMOCALC Average P-T results for pelitic rocks.																		
Sample	**PSH-98-98.3**		**JTV-98-38.1**				**JTV-98-38.1**		**PSH-00-10**		**PSH-00-10**							
P-T stage	Cooling		Peak				Cooling		Peak		Cooling							
Zone	VI.3		VI.3				VI.3		VI.3		VI.3							
Activities	at 650°C		at 650°C				at 650°C		at 650°C		at 650°C							
Garnet	rim		core				rim		core		rim							
prp	0.00290		0.00440				0.00350		0.00710		0.00150							
grs	0.000310		0.000830				0.000067		0.000530		0.000160							
alm	0.160		0.130				0.170		0.390		0.400							
Biotite	at grt		matrix, core				alt. from st		matrix core		at grt							
phl	0.0990		0.0780				0.0840		0.0234		0.0223							
ann	0.0230		0.0310				0.0270		0.0740		0.0450							
east	0.0700		0.0600				0.0650		0.0280		0.0380							
Muscovite	at grt		core				rim		matrix core		at grt							
mu	0.670		0.630				0.660		0.660		0.650							
pa	0.750		0.620				0.650		0.590		0.580							
cel	0.0130		0.0150				0.0160		0.00880		0.0120							
Chlorite											at grt							
clin	-		-				-		-		0.0160							
daph	-		-				-		-		0.0360							
ames	-		-				-		-		0.0201							
Plagioclase	rim		matrix, core				at st		core		rim							
an	0.400		0.410				0.400		0.380		0.400							
ab	0.740		0.730				0.740		0.750		0.740							
Other	mst 0.0056		mst 0.0065				mst 0.0055		sill qtz		sill qtz							
	fst 0.28		fst 0.26				fst 0.280		H2O		H2O							
	sill qtz H2O		sill qtz H2O				sill qtz H2O											
Results																		
*a*H2O	1.0	0.4	1.0	0.4	1.0	0.4	1.0	0.4	1.0	1.0	1.0	1.0						
T°C	**608**	**562**	**643**	**591**	**611**	**526**	**598**	**552**	**616**	**667**	**577**	**574**						
s.d.(T)	24	22	32	27	30	26	24	22	32	34	18	18						
P kbar	**6.1**	**5.8**	**7.3**	**6.9**	**6.9**	**6.5**	**5.1**	**4.9**	**7.3**	**8.1**	**3.9**	**4.3**						
s.d.(P)	1.1	1.0	1.4	1.3	1.1	1.0	1.1	1.0	1.4	1.3	0.9	1.0						
correl.	0.941	0.948	0.936	0.941	0.765	0.781	0.945	0.950	0.911	0.737	0.847	0.611						
fit	0.79	0.71	1.29	1.20	0.36	0.64	0.94	0.92	1.29	1.08	1.19	1.22						
NR	8	8	8	8	5	5	8	8	6	5	9	8						
end members eliminated	-	-	-	-	mst fst sill	mst fst sill	-	-	-	sill	-	sill						

Gold in the Central Lapland Greenstone Belt, Finland
V. Juhani Ojala (ed.)
Geological Survey of Finland, Special Paper 44, 57– 106, 2007.

CHARACTERISTICS OF GOLD MINERALISATION IN THE GREENSTONE BELTS OF NORTHERN FINLAND

by
Pasi Eilu[1], Heikki Pankka[2], Veikko Keinänen[3], Vesa Kortelainen[4],
Tero Niiranen[5], Eelis Pulkkinen[6]

Eilu, P., Pankka, H., Keinänen, V., Kortelainen, V., Niiranen, T. & Pulkkinen, E. 2007. Characteristics of gold mineralisation in the greenstone belts of northern Finland. *Geological Survey of Finland, Special Paper 44, 57−106, 31 figures, one table, 4 appendices.*

More than 60 drilling-indicated gold occurrences have been discovered in the Palaeoproterozoic greenstone belts (orogenic belts) of northern Finland during 1985–2004. Genetic deposit types detected in the region include the orogenic, iron oxide-copper-gold (IOCG) and palaeoplacer type. The orogenic type can be further divided into the gold only and the atypical metal association subtypes.

Most of the features of gold occurrences in northern Finland are similar to those detected in Palaeoproterozoic greenstone belts globally. In all epigenetic occurrences in northern Finland, structure is the regionally the most significant control for mineralisation. Locally, the two most significant controls are structure and rock type. Fluid compositions suggest variable, mixed, origins for volatiles and metals with no obvious indications of a local source. The orogenic gold-only type is characterised by carbonatisation with sericitisation or biotitisation, PT conditions at 300–450°C and 1–3 kbar, pyrite, pyrrhotite and arsenopyrite being the main ore minerals, consistent enrichment of Ag, Au, As, CO_2, K, Rb, S, Sb, and Te, and a low-salinity fluid with hydrothermal quartz showing $\delta^{18}O$ at +11 – +13‰ and carbonate $\delta^{13}C$ at -8 – -1‰. Orogenic gold occurrences with atypical metal association are similar to the gold-only type, except having significant chalcopyrite ± cobaltite, gersdorffite and/or uraninite contents, enrichment also in Cu and, in some cases, in Co, LREE, Ni and/or U, and intense albitisation predating the gold-related alteration. The iron oxide-copper-gold (IOCG) occurrences are characterised by regional albitisation ± scapolitisation, multi-stage local alteration, formation T at 400–600°C, main ore minerals of magnetite, pyrite, pyrrhotite, chalcopyrite ± cobaltite, consistent enrichment in Ag, Au, Bi, Cu, Fe, S, and Te, and an aqueous high-salinity mineralising fluid with variable salinity and Eh, and $\delta^{18}O$ at +9.6 – +17.5‰. The palaeoplacers are Au-only, sedimentary facies-controlled, occurrences in molasse-like sediments of the uppermost stratigraphic formation of the Central Lapland greenstone belt.
Timing of gold mineralisation in northern Finland is not well-constrained. Most or all of orogenic gold mineralisation took apparently place during the continental collision epoch of the evolution of the Fennoscandian shield, at 1.85–1.79 Ga, although some orogenic mineralisation may be related to the earlier compressional stage, the microcontinent accretion, at 1.92–1.88 Ga. For the IOCG type of mineralisation, both of the extensional epochs of the Palaeoproterozoic orogenic evolution seem to be possible: the occurrences were formed during the continental extension at 1.88–1.85 Ga, or orogenic collapse and stabilisation at 1.80–1.77 Ga, or both. For the IOCG deposits in the Kolari area, the ca. 1.80 Ga timing appears to be the most probable. The probable time frame for the palaeoplacer mineralisation covers the 1.88–1.85 Ga epoch and the early parts (pre-D_3?) of the 1.85–1.79 Ga epoch.

Key words (GeoRef Thesaurus AGI): gold ores, greenstone belts, mineral deposits,

genesis, alteration, structural controls, lithologic controls, tectonics, Paleoproterozoic, Northern Finland.

[1-4,6] *Geological Survey of Finland, P.O. Box 96, FI-02151 Espoo, Finland*
[5] *Northland Exploration Finland Oy, Teknotie 14-16, tsto 11, FI-96930 Rovaniemi, Finland*

E-mail: pasi.eilu@gtk.fi, [5]TNiiranen@goldgroup.com

INTRODUCTION

Exploration for gold in northern Finland was boosted during the 1980's for three major reasons: 1) significant increase in the price of gold during the late 1970's, 2) globally extensive research into the formation of gold deposits, which has resulted in a range of genetic exploration models, and 3) technical developments in exploration and analytical methods (e.g., Hirvas et al. 1977, Kontas 1981, Boulton 1984, Niskavaara & Kontas 1990).

Glacial drift covers about 95% of the bedrock in northern Finland. The drift is, on average, 5 m thick and is mostly composed of till. Central Lapland was an ice divide area during the Pleistocene glaciations. The basal ice velocity is relatively slow within an ice divide area, and glacial erosion is minimal (Boulton 1984). Consequently, the preglacial weathered crust between the till blanket and the fresh bedrock is common in Central Lapland (Hirvas et al. 1977). In areas of highly altered rocks, which contain abundant carbonate and sulphide minerals, the thickness of the weathered crust may extend from one metre to up to the depth of hundred metres. Till and bedrock-surface geochemical surveys, combined with low-altitude airborne (flight altitude 30–40 m) and ground geophysical survey and bedrock mapping, have, hence, proved to be the most effective tools in the pre-drilling stages of gold and base-metal exploration in Lapland (e.g., Eilu 1999).

The discovery of palaeoplacer gold in the conglomerates of the uppermost, less than 1.9 Ga old quartzites of the Central Lapland greenstone belt (Härkönen 1984) initiated modern gold exploration in the region, at first in the Kittilä and Sodankylä area and later on elsewhere in Lapland. In the late 1980's, exploration targets changed from palaeoplacer to orogenic types mineralisation (then called mesothermal).

As a result of exploration during 1985–2004, more than 60 gold occurrences with >1 ppm Au per metre of drill core have been reported in the Palaeoproterozoic volcano-sedimentary (greenstone) belts of northern Finland. Of these, 36 have been discovered in the Central Lapland greenstone belt, 24 in the Kuusamo schist belt and 5 in the Peräpohja schist belt (Fig. 1).

Table 1. Main gold belts in northern Finland. Location of the orogenic belts and gold deposits mentioned are indicated in Figure 1.

Belt	Genetic deposit types[1]	Major deposits
Central Lapland greenstone belt	Orogenic	Pahtavaara, Saattopora, Suurikuusikko
	Iron oxide-copper-gold	Laurinoja
	Palaeoplacer	none major
Kuusamo schist belt	Orogenic	Juomasuo
Peräpohja schist belt	Orogenic	none major
	Iron oxide-copper-gold	Vähäjoki

[1] Genetic types as defined in this report

All together, 14 of them have been regarded as economical or nearly economical. The gold deposit types detected in northern Finland include orogenic gold (including many with atypical metal associations), iron oxide-copper-gold and palaeoplacer gold (Table 1 and App. 1). The most important gold occurrences of northern Finland are described in this paper and other reports in this volume.

The object of this paper is to provide a summary and review of the characteristics of Palaeoproterozoic gold deposits in northern Finland. First, based on publicised information, we briefly describe the general geological setting and give descriptions of selected deposits. Then, we review the existing data to provide an up to date synthesis on genetic aspects of gold mineralisation in the region. With a review, we attempt to reclassify the gold occurrences according to the present views in research on economic geology and to relate the gold mineralisation with the general crustal evolution of the region.

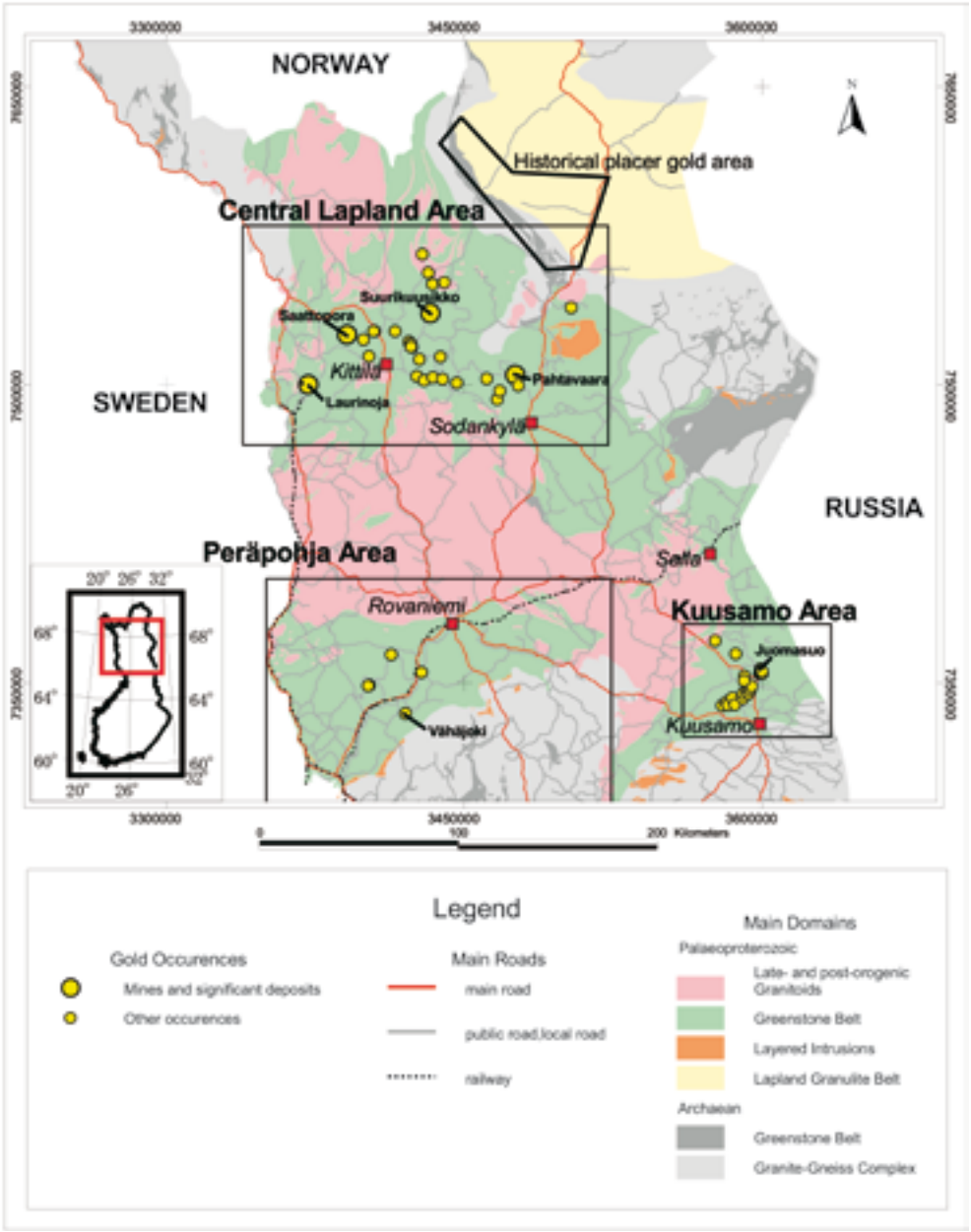

Fig. 1. General geological map of northern Finland, and gold occurrences in the area. Rectangles indicate the areas shown in Figures 3–5. Coordinates according to Finnish National Grid (ykj-grid) metric values. Compiled by Vesa Nykänen. Basemap © National Land Survey 521/MYY/07.

GENERAL FEATURES OF THE PALAEOPROTEROZOIC GREENSTONE BELTS OF NORTHERN FINLAND

Four major components form the bedrock of northern Finland (Fig. 1): 1) Archaean granite-gneiss complexes and greenstone belts, 2) Palaeoproterozoic greenstone belts, 3) the 1.9 Ga Lapland Granulite Belt, and 4) Svecokarelian syn- to late- (1.89–1.80 Ga) and post-orogenic (1.80–1.77 Ga) granitoids (Hanski et al. 1997). In this section, we concentrate on the Palaeoproterozoic greenstone belts, as they form the host to gold in the region. For more comprehensive descriptions of the general geological evolution and setting of northern Finland, see the papers by Hölttä et al., and Patison in this volume.

Finnish Lapland, which comprises a significant portion of the northern part of the Archaean Karelian craton (Fig. 2), records a prolonged and episodic history of sedimentation, rifting and magmatism throughout the Palaeoproterozoic times. The Palaeoproterozoic greenstone belts in northern Finland include the Central Lapland greenstone belt, and Kuusamo and Peräpohja schist belts (Figs. 1 and 3–5, Table 1). These belts

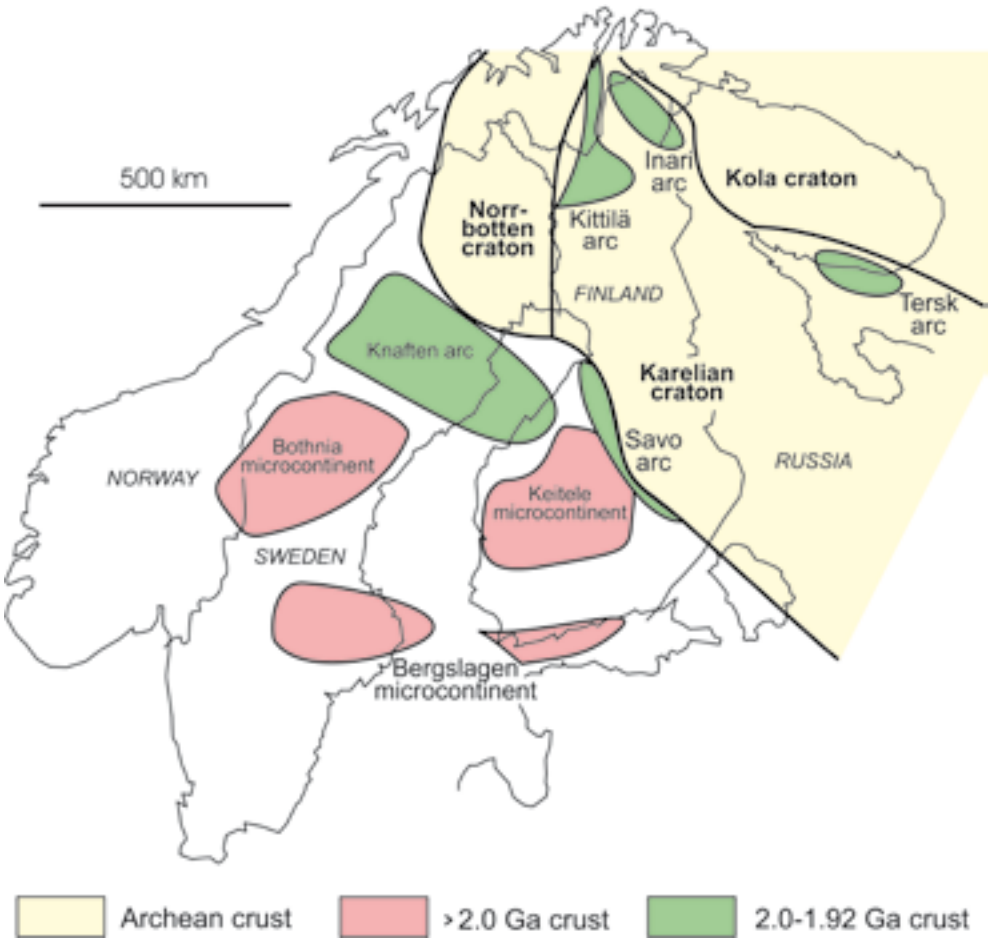

Fig. 2. Present position of pre-1.92 Ga crustal components of the Fennoscandian shield. Modified from Lahtinen et al. (2003).

were all initially formed in intracratonic rift settings related to the Archaean craton (Hanski et al. 1997, Sorjonen-Ward et al. 2003).

According to Lahtinen et al. (2003), the Palaeoproterozoic evolution of the region after 1.92 Ga includes the following major epochs or orogens: 1) microcontinent accretion (1.92–1.88 Ga), 2) continental extension (1.88–1.85 Ga), 3) continent-continent collision (1.85–1.79), and 4) orogenic collapse and stabilisation (1.80–1.77 Ga). The first epoch includes collision of the Kola and Karelian cratons in the northeast and collision of the Norrbotten and Karelian cratons in the west (Fig. 2). This resulted in the amalgamation of the Archaean parts of the Fennoscandian shield. This was followed by the formation of extensional basins in Lapland, in the far hinterland of subduction in the west (epoch 2). The third epoch is defined by the collision of Fennoscandia, Sarmatia and Amazonia (the latter being later rifted away). The 1.80–1.77 Ga epoch was a period of thermal resetting and post-orogenic magmatism. We consider all of the above-mentioned epochs as potentially significant for gold mineralisation in northern Finland, as also is suggested by Lahtinen et al. (2003) and by Weihed and Eilu (2003). Sorjonen-Ward et al. (2003) present two major orogenic epochs for the region: 1) crustal-plate collision and compression during 1.91–1.86 Ga, and 2) active deformation and regional metamorphism during 1.84–1.80 Ga due to crustal thickening or mantle underplating; they also suggest that orogenic mineralisation took place during the latter epoch.

The Central Lapland greenstone belt (CLGB; Figs. 1 and 3) is the largest mafic volcanic-dominated province preserved in Finland. The sequence starts with bimodal komatiitic and felsic volcanic rocks, dated at ca. 2.5 Ga (zircon U–Pb data from felsic volcanic rocks, Peltonen et al. 1988, Manninen et al. 2001), which unconformably overlie Archaean basement and represent the onset of rifting (Peltonen et al. 1988, Lehtonen et al. 1998). Continued rifting of the Archaean crust resulted in the widespread emplacement of gabbro-norite layered intrusions in the

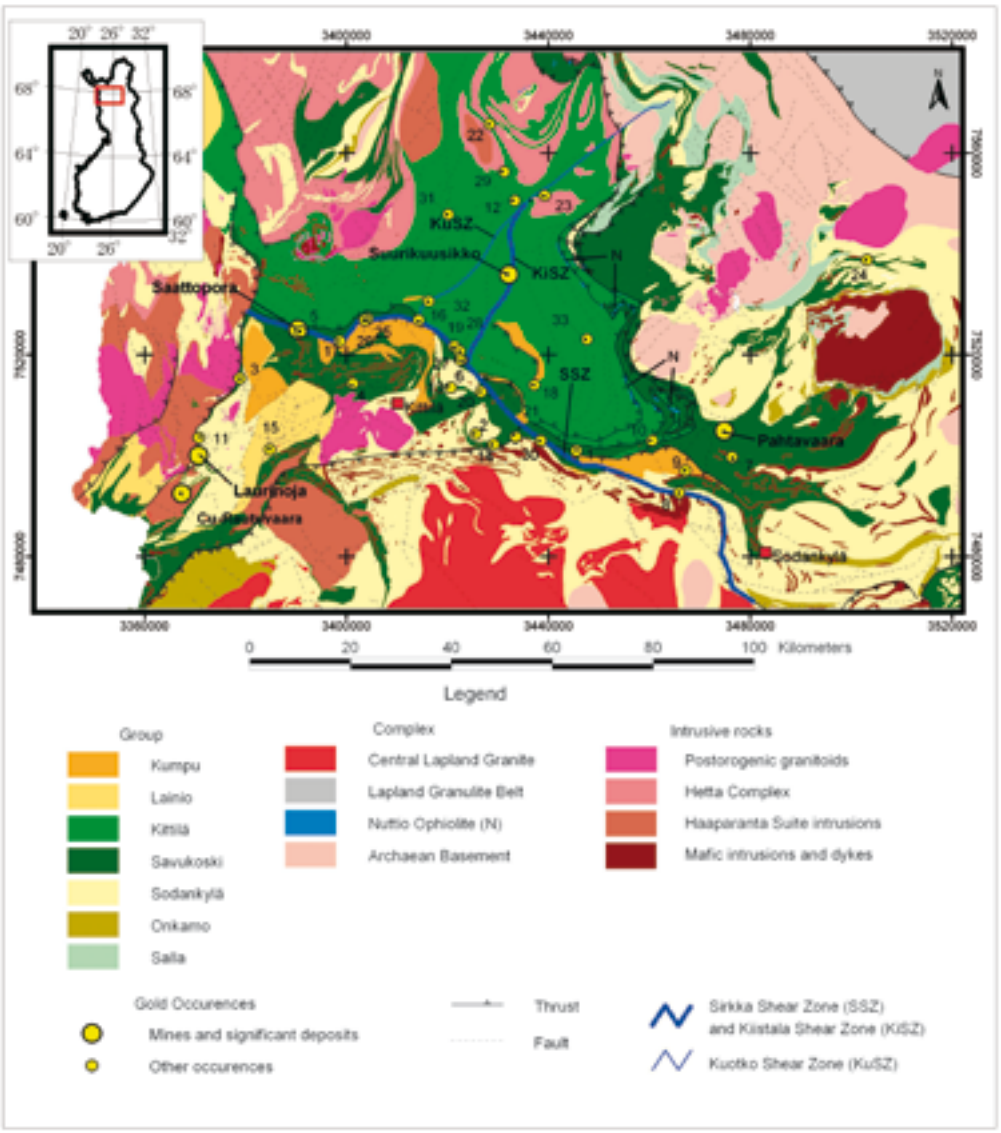

Fig. 3. Gold occurrences in the Central Lapland greenstone belt. Numbers identify occurrences listed in Table 3. Coordinates according to Finnish National Grid (ykj-grid) metric values. Geology after Lehtonen et al. (1998).

region between 2.45–2.39 Ga (Alapieti & Lahtinen 1989). Terrigenous clastic sedimentary rocks discordantly overlie these layered intrusions, with further episodes of mafic magmatism recorded as sporadic lavas and sills dated at ca. 2.2 Ga, ca. 2.10 Ga, and ca. 2.05 Ga (single-zircon U-Pb data, Huhma 1986, Vuollo et al. 1992, Huhma et al. 1996, Räsänen et al. 1996, Lehtonen et al. 1998, Vaasjoki 2001). All mafic igneous episodes mentioned above coincided with rifting and subsidence along the whole of the Karelian craton margin, recorded by coarse-clastic turbidites, carbonate rocks, iron formations and graphitic schists. Rifting culminated in extensive mafic and ultramafic volcanism and the formation of oceanic crust at ca. 1.97 Ga. Fragments of oceanic crust were subsequently emplaced back onto the Karelian craton, as the Nuttio ophiolite in Lapland and the Jormua and Outokumpu ophiolites further south (Kontinen 1987, Gaál 1990, Sorjonen-Ward et al. 1997, Lehtonen et al. 1998). The emplacement of the ophiolites was followed by the main compressional deformation associated with the Svecofennian synorogenic plutonism, between 1.90–1.86 Ga (Vaasjoki 2001). If we apply the scheme of Lahtinen et al. (2003) into above, the ophiolite emplacement and the compressional deformation in the present area of the CLGB belong to the accretional and collisional epochs at 1.92–1.88 Ga and 1.85–1.79 Ga, respectively.

Deformation evolution of the CLGB for 1.90–1.77 Ga is discussed in detail by Patison (2007). The main deformational stages took apparently place as follows (Ward et al. 1989, Sorjonen-Ward et al. 1992, Mänttäri 1995, Patison 2007): D_1 and D_2 during 1.90–1.88 Ga, D_3 either during 1.90–1.88 Ga or 1.84–1.80, and the

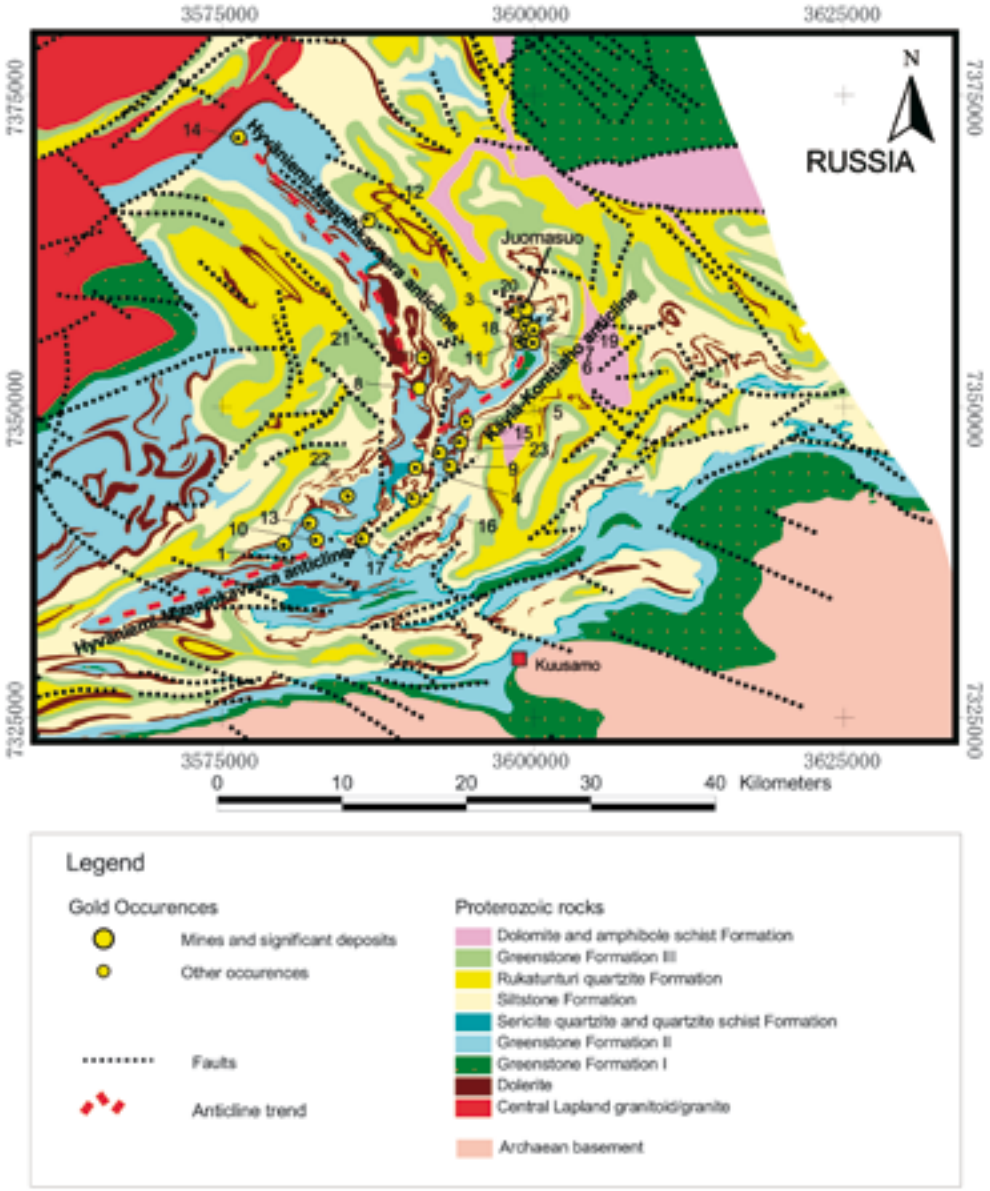

Fig. 4. Gold occurrences in the Kuusamo schist belt. Numbers identify occurrences listed in Table 4. FM = Formation. Coordinates according to Finnish National Grid (ykj-grid) metric values. Geology after Vanhanen (2001).

latest, completely brittle, D_4 in ca. 1.77 Ga or slightly post-1.77 Ga. The D_1–D_4 evolution appears to fit into the evolutional epochs of Lahtinen et al. (2003) fairly well. Note, however, that the timing for D_1 to D_4 is chiefly indirect with a very few robust radiometric dates setting definite values for any of the stages; especially, the timing of D_3 may either be 1.90–1.88 Ga or 1.84–1.80 Ga (Patison 2007). Similar geotectonic evolution, as for the CLGB, can be envisioned for both the Kuusamo and Peräpohja belts for the entire Proterozoic (e.g., Lahtinen et al. 2003).

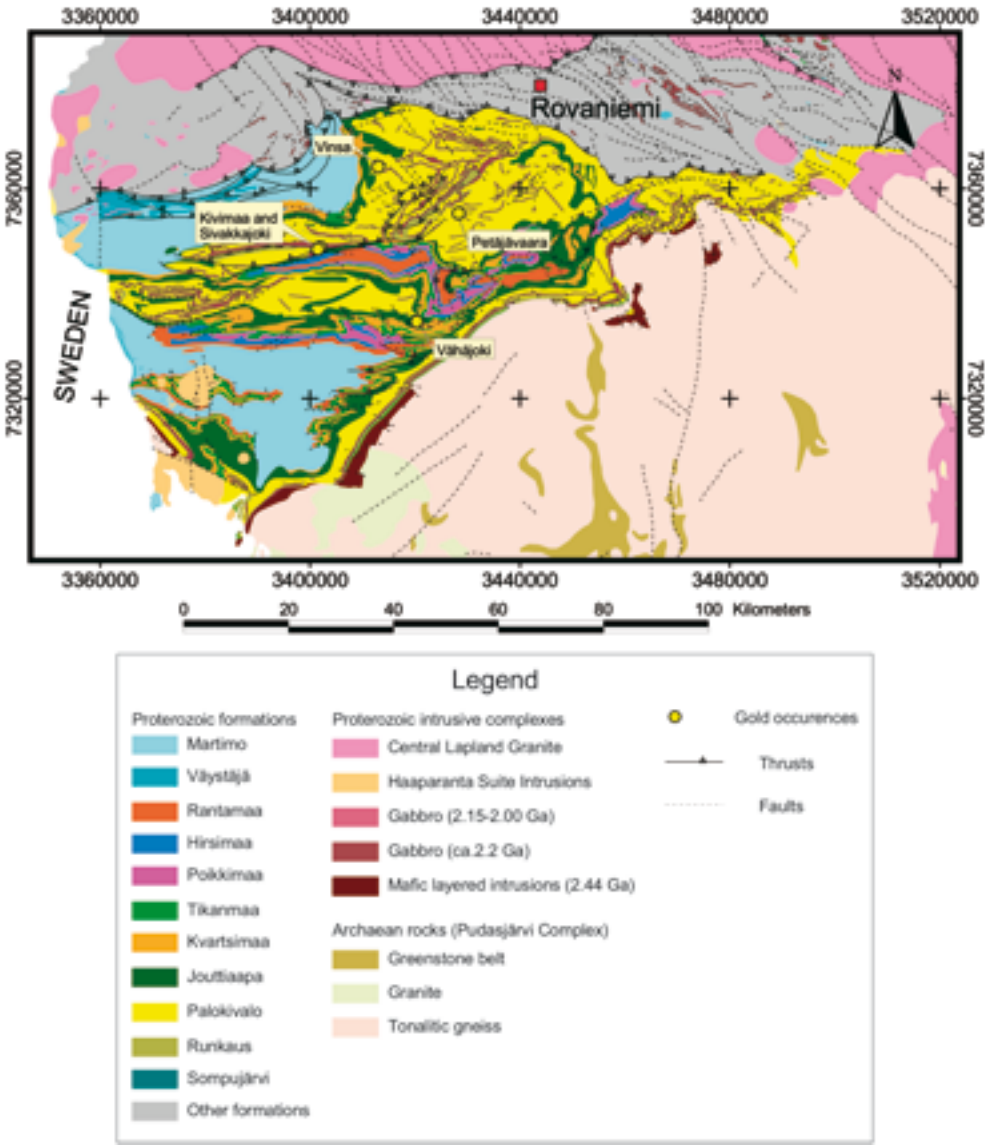

Fig. 5. Gold occurrences in the Peräpohja schist belt. Geology after Perttunen (1989, 2002, 2003). The grey areas ('Other formations' in the legend) contain no signs of gold mineralisation. Coordinates according to Finnish National Grid (ykj-grid) metric values.

GOLD IN CENTRAL LAPLAND GREENSTONE BELT

Geological setting

In the CLGB, the majority of the deposits and drilling-indicated occurrences discovered (Fig. 3) are spatially associated with the 0.2–2 km wide Sirkka Shear Zone (SSZ). Some occurrences are within the SSZ, but a large number is in shear and fault zones subsidiary to it, within three km from the main structure. The SSZ represents a major, crustal-scale, long-lived shear zone with a distinct thrust reverse component to the south and, in detail, a complex zone involving several parallel faults and fault segments (Lanne 1979, Ward et al. 1989, Lehtonen et al. 1998, Patison 2007). In addition to the gold deposits, the SSZ is also characterised by intense alteration (albitisation, sericitisation and carbonatisation), and anomalous Au along its entire length.

A number of gold occurrences are further away from the SSZ, hosted by strike-slip faults at a high angle to the SSZ, and interpreted as reactivated transfer faults or reoriented early thrusts (Ward et al. 1989, Patison 2007). Of these structures, one of the most notable is the Kiistala Shear Zone (KSZ; Fig. 3) which hosts the 3 Moz Suurikuusikko deposit (App. 2). The NNE-trending KiSZ extends for about 30 km; in the south crosses the SSZ near the Hirvilavanmaa gold occur-

rence and in the north it seems to converge or ends with the longer, NE-trending, Kuotko Shear Zone. Along strike, the KiSZ is consistently anomalous in gold for at least 15 km (Härkönen 1992, 1997, Riddarhyttan 2005).

Below, we briefly describe selected gold occurrences within the CLGB; their structural control is discussed in detail by Patison in this volume. Suurikuusikko is not discussed here, as it is described in detail in the paper by Patison et al. in this volume. Note also, that the deposits at Kaaresselkä, Levijärvi-Loukinen and Päivänenä-Hirvilavanmaa are described in more detail in this volume by Holma & Keinänen, Hulkki & Pulkkinen, and Hulkki & Keinänen. Detailed information on all drilling-indicated gold occurrences is listed in Appndix 2 and is also available from the FINGOLD database at: http://en.gtk.fi/ExplorationFinland/Commodities/Gold/gtk_gold_map.html.

Gold deposits and occurrences

Saattopora

The Saattopora mine is located in the western, E-W trending section of the SSZ (Figs. 3 and 6). The deposit was mined by Outokumpu during 1988–1995. A total of 2.1 Mt ore was exploited. The bulk grade of the ore prior to treatment was 3.29 ppm Au and 0.28% Cu (App. 2), yielding a total of 6278 kg Au and 5177 t Cu (Korvuo 1997b).

The area around Saattopora is hosted by metavolcanic and metasedimentary rocks of the Matarakoski Formation (Savukoski Group), here located between Linkupalo Formation (Savukoski Group) and Vesmajärvi Formation (Kittilä Group) metavolcanic rocks in the south and north, respectively. The Au-Cu lodes are hosted by intensely albitised, graphitic phyllite or intermediate tuffite units, close to partially carbonated but not albitised, tholeiitic and komatiitic, metalavas

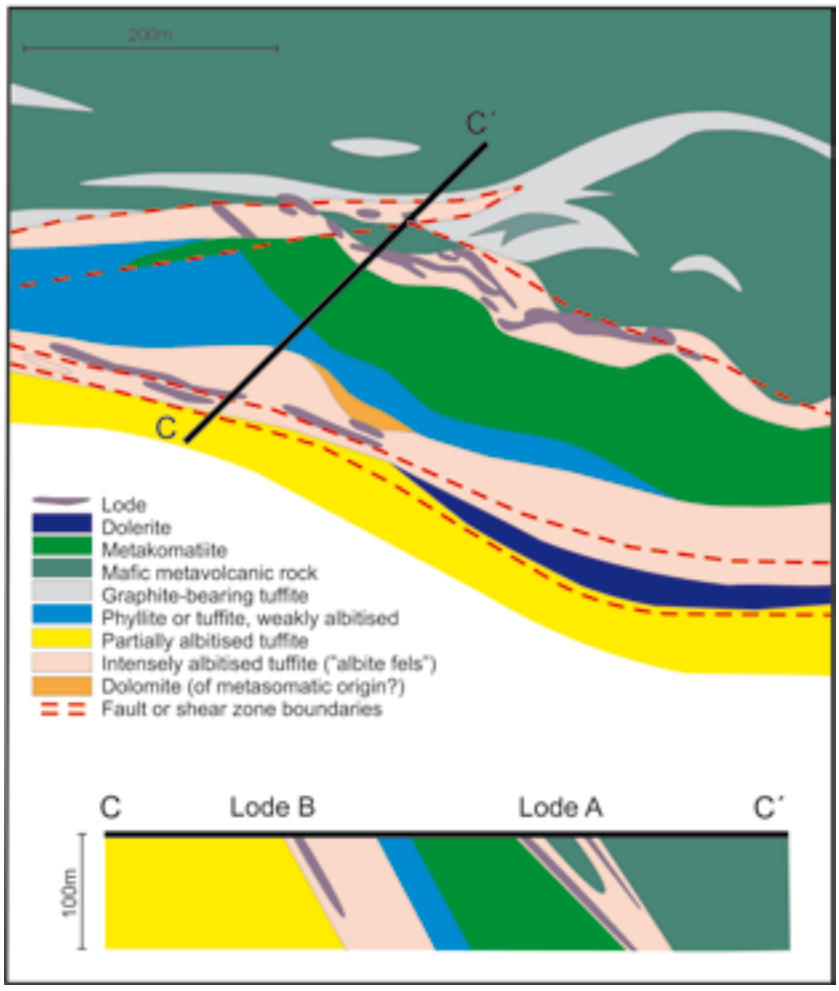

Fig. 6. Plan view and cross section at Saattopora. The mafic metavolcanic rock apparenlty belongs to the Vesmajärvi Formation of Kittilä Group; the rest of the lithological units depicted belong to the Matarakoski Formation of the Savukoski Group. Geology based on Korvuo (1997b), stratigraphy on Lehtonen et al. (1998).

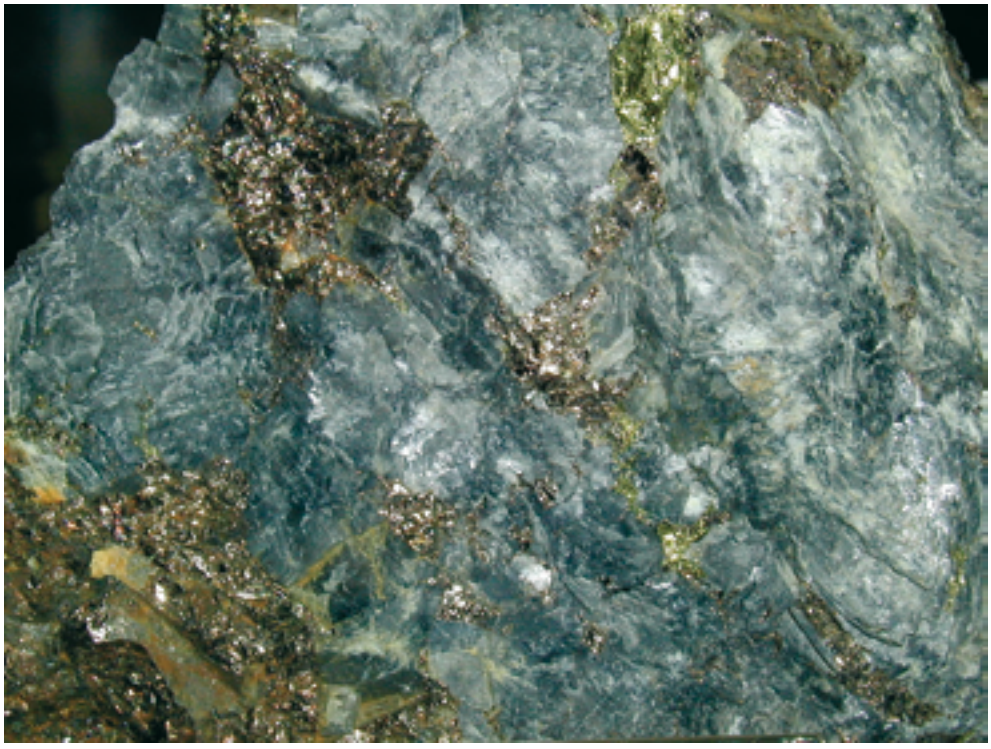

Fig. 7. Pyrrhotite-chalcopyrite dominated ore in brecciated massive albite rock at Saattopora. Field of view 7 cm. Photo: Jari Väätäinen.

(Fig. 6). The host rocks are metamorphosed and altered under lower- or mid-greenschist facies conditions. Brittle deformation characterises the deposit.

The ore bodies at Saattopora comprise two subparallel sets of lodes, a southern (B) and a northern (A) set, which are separated by a weakly albitised tuffite and a metakomatiite unit (Fig. 6). Native gold occurs in a few millimetres to several metres thick quartz-ankerite-dolomite-pyrite-pyrrhotite veins and their immediate, brecciated wallrock, closely associated with quartz and carbonate gangue (Fig. 7). The veins have a N-S trend, but form E-W trending clusters which also define the trend of mineable ore bodies. The ore bodies are 1–25 m wide and up to 250 m long. The auriferous veins have preferentially developed in the most competent rock units in the area, i.e. in the most intensely albitised rocks. This is in accordance with the deformation and alteration sequence at Saattopora suggesting that albitisation predated gold mineralisation (Patison 2007).

The ore minerals are dominated by pyrite and pyrrhotite with minor chalcopyrite, gersdorffite, arsenopyrite, pentlandite, tucholite, uraninite, bismuthinite, niccolite, tellurides and native gold (Korvuo 1997b, Grönholm 1999). Alteration related to gold mineralisation, and overprinting the albitisation, is characterised by the formation of the mineral assemblage quartz – sericite – albite – Fe dolomite/ankerite – sulphides.

In addition to gold, the deposit is enriched, in variable degree, in a large number of elements, as listed in Appendix 2 (Nurmi et al. 1991, Korvuo 1997b). However, it remains to be investigated which elements, and to what degree, were enriched during the different stages of alteration at Saattopora. Mineral assemblages from ore and unmineralised rock suggest that most or all Na enrichment took place before gold mineralisation, some carbonatisation also predates gold, and that most or all Ag, As, Au, Bi, Cu, S, Se, and Te enrichment took place during gold mineralisation.

Other occurrences within Sirkka Shear Zone

The **Sirkka kaivos** and **Sirkka W** copper-gold occurrences (Fig. 3, App. 2) are about 1.5 km apart, along the SSZ, in Matarakoski Formation rocks. They comprise sets of 10–20 m wide lodes formed by mineralised quartz-carbonate-albite veins and their altered wallrocks (Vesanto 1978). The Sirkka kaivos deposit comprises, at least, eight distinct lodes within a kilometre of the strike of the SSZ. Two lodes have been reported from the Sirkka W (Hugg 1987b). Main host to mineralisation in both occurrences is intermediate metatuffite with komatiitic and tholeiitic metalavas forming minor hosts to ore (Vesanto 1978, Lehtinen 1987). Alteration mineral assemblages documented (Vesanto 1978, Inkinen 1985) suggest that mineralisa-

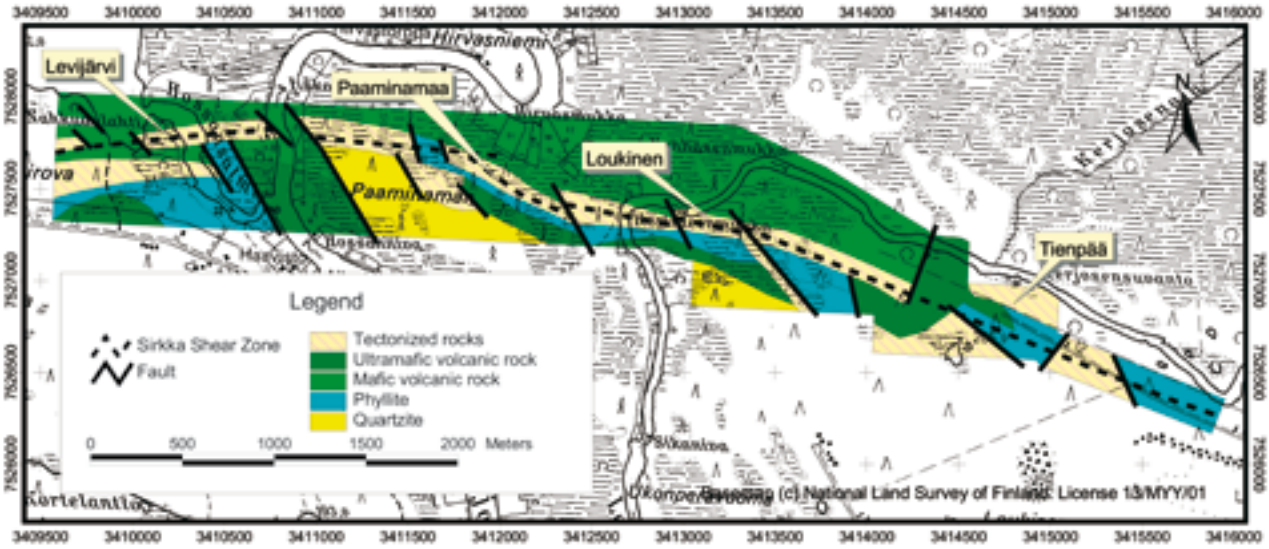

Fig. 8. Geological map of the Levijärvi-Loukinen area. Coordinates according to Finnish National Grid (ykj-grid) metric values. Compiled by Veikko Keinänen. Basemap © National Land Survey 521/MYY/07.

tion took place under mid- or upper-greenschist facies conditions. Main ore minerals are pyrite, pyrrhotite and chalcopyrite, with minor to trace amounts of gersdorffite, pentlandite, Ag pentlandite, sphalerite, mackinawite, violarite, cobaltite, melnikovite and native gold (Hänninen 1977, Vesanto 1978, Inkinen 1985, Lehtinen 1987).

Four major gold (± Cu, Ni) lodes have been detected in the **Levijärvi-Loukinen area**, a 5 km long section of the SSZ (Figs. 8 and 9, App. 2). The lodes are depicted as separate occurrences in Figure 8 but, in fact, gold mineralisation of variable grade is continuous through the entire area shown in Figure 8 (V. Keinänen, pers. comm. 2002). The lodes are formed by quartz-carbonate veins and sulphidised quartz-carbonate breccia zones hosted by komatiitic (main host) and tholeiitic metavolcanic rocks, graphitic phyllite, and contact zones between the lithological units. The potentially economic lodes are up to a few hundreds of metres long and tens of metres wide. They are within the SSZ, in and close to locations where dextral NNW- to N-trending strike-slip faults cut across the main shear zone (Patison 2007). Alteration is characterised by carbonatisation and sericitisation in the metavolcanic rocks and albitisation and sericitisation in the phyllite. Typical ore minerals are pyrrhotite, pyrite,

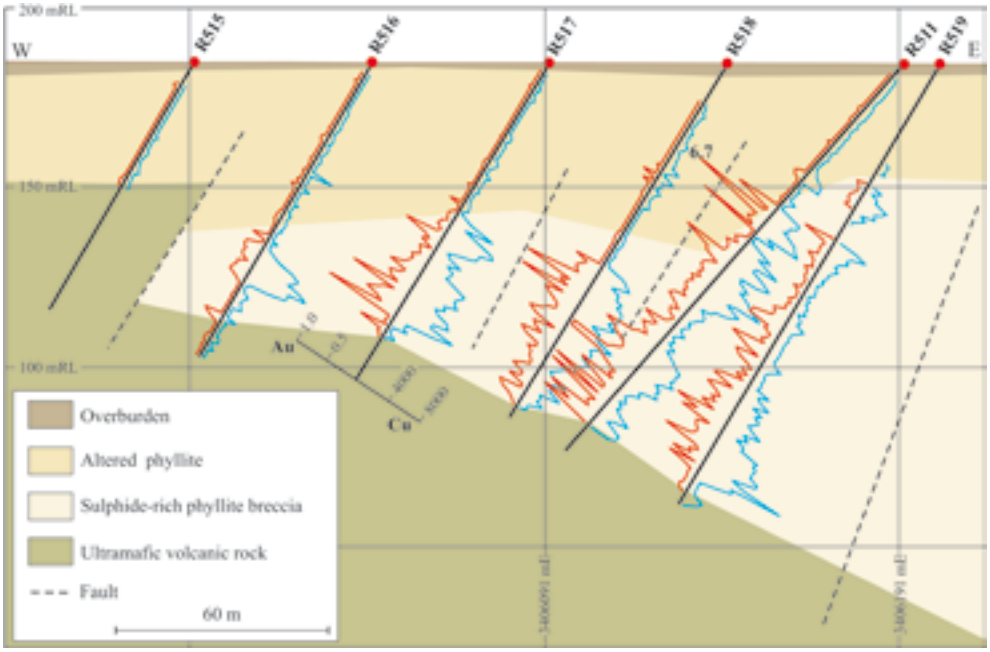

Fig. 9. A long section along the Loukinen lode. Au and Cu in ppm. Compiled by Veikko Keinänen.

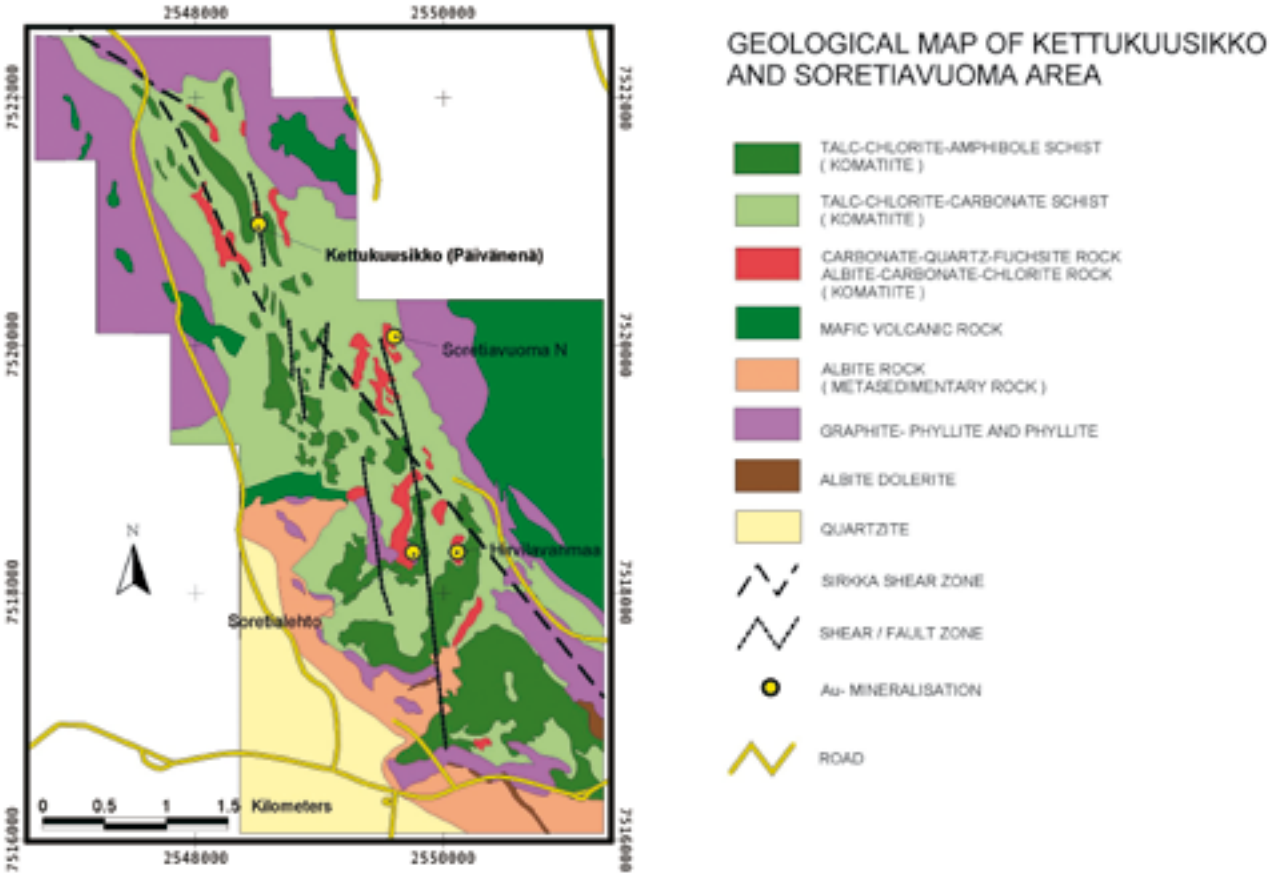

Fig. 10. Geological map of the Kettukuusikko-Soretialehto area. Contacts between the lithological units are based on ground-geophysical surveys. The 'shear zone' indicates the local trend of the SSZ; its location is based on a local negative IP anomaly. Coordinates according to Finnish National Grid (ykj-grid) metric values. Compiled by Veikko Keinänen. Basemap © National Land Survey 521/MYY/07.

chalcopyrite, gersdorffite and native gold. Minor and trace ore minerals detected in the lodes include pentlandite, violarite, Ag pentlandite and sphalerite. Holma and Keinänen describe the deposit in more detail in this volume.

Four gold occurrences have been discovered in a three-kilometre-long, NW-trending, dominantly extensional, section of the SSZ in the **Päivänenä-Hirvilavanmaa area**: Hirvilavanmaa, Päivänenä, Soretialehto and Soretiavuoma (Figs. 3, 10 and 11, App. 2, and Hulkki & Keinänen 2007); the Päivänenä occurrence has also been known by the names Lälleävuoma and Kettukuusikko. The main host rock in all occurrences is metakomatiite, with graphitic phyllite (Soretialehto) and tholeiitic metabasalt (Hirvilavanmaa, Päivänenä, Soretialehto) forming minor hosts to ore (Härkönen & Keinänen 1989, Hugg 1991, Keinänen 1997). Silicate mineral assemblages indicate lower- to mid-greenschist facies metamorphic and alteration conditions. Intense carbonatisation and sericitisation characterise the occurrences, except at Hirvilavanmaa where the degree of sericitic alteration is exceptionally low. In metakomatiites, a distinct alteration sequence can be indicated, from the distal chlorite-dolomite-talc through the intermediate chlorite-Fe dolomite-ankerite-quartz to the proximal Fe dolomite-ankerite-fuchsite-albite-quartz-pyrite (Fig. 11). Mineral assemblage quartz-albite-sericite-ankerite characterises the phyllites proximal to and hosting gold mineralisation. Brittle style of deformation dominates and the host rocks are cut, even brecciated, by sets of pyrite- and gold-bearing quartz-carbonate veins (Fig. 11, and Hulkki & Keinänen 2007). At least three generations of quartz veins are known, but only the second generation contains gold. The dominant ore mineral is pyrite. Native gold, pyrrhotite, chalcopyrite, arsenopyrite, gersdorffite, galena, tetrahedrite, bismuthinite, ulmannite, molybdenite, millerite, violarite and vaesite occur in minor and trace amounts (Härkönen & Keinänen 1989, Keinänen & Hulkki 1992). Gold is closely associated with pyrite or occurs free within the quartz-carbonate gangue in all four occurrences (Härkönen & Keinänen 1989, Keinänen & Hulkki 1992, Hulkki & Keinänen 2007).

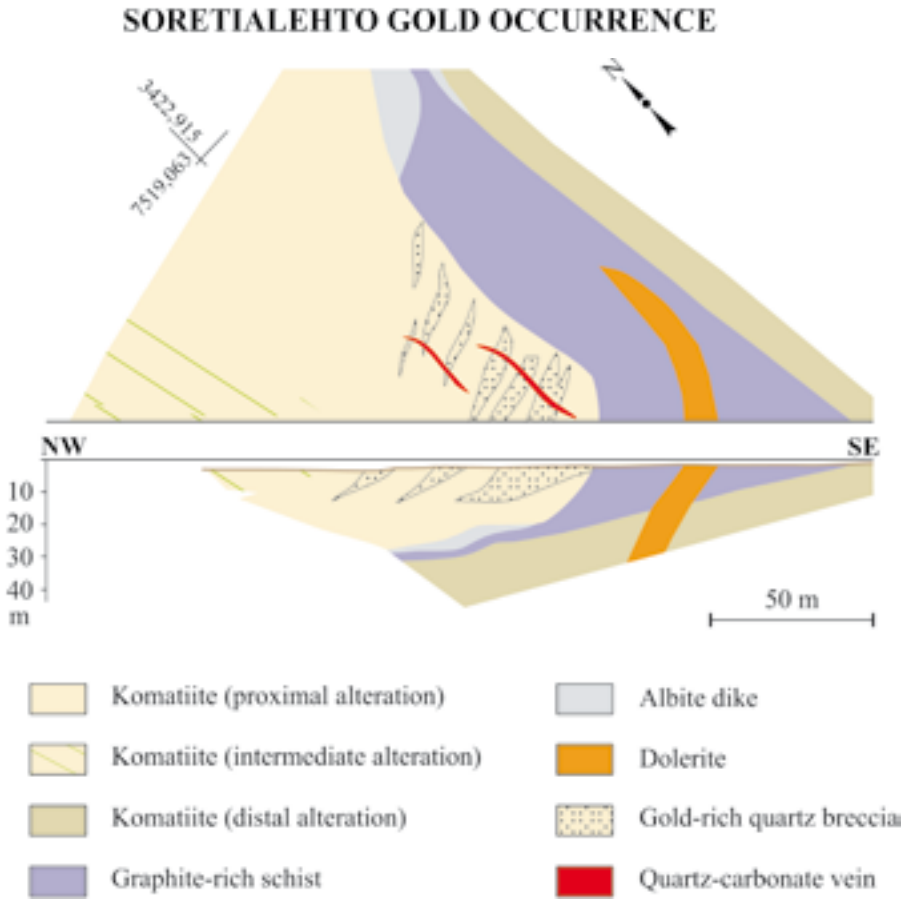

Fig. 11. Geological map of Soretialehto. Coordinates according to Finnish National Grid (ykj-grid) metric values. Compiled by Veikko Keinänen.

Kaaresselkä

Kaaresselkä is hosted by the volcano-sedimentary sequence of the Matarakoski Formation of the Savukoski Group rocks (Fig. 3). It is located just to the south of the SSZ, in minor, W- to WNW-trending, shear zones branching from the SSZ. Several N-trending faults, also mineralised, cut these shear zones. Brittle-ductile to ductile deformation characterises the deposit. There are eight individual lodes in the area, hosted chiefly by mafic tuffite (Figs. 12 and 13). Other hosts to ore are metadolerite, metakomatiite, metaconglomerate and sericitic quartzite (Pulkkinen 1998, 1999). Hulkki and Pulkkinen describe the deposit in more detail in this volume.

The host rocks are intensely sheared and altered by K metasomatism. Free-milling gold dominates and is chiefly associated with chlorite and carbonates, but also occurs with sericite, adularia(?), pyrite, chalcopyrite, arsenopyrite and, in the weathered zone, goethite (Fig. 4 in Hulkki & Pulkkinen 2007). Significant gold occurs both in quartz-carbonate and pyrite-carbonate veins and in the altered host rock. When associated with the sulphides, gold grains are mainly in small fractures of the sulphides and in contacts between sulphide grains. At the Vanha lode, there also are 1–3 m wide discrete chalcopyrite-carbonate lenses with a high gold concentration. These are associated with altered ultramafic rocks outside the core of the local shear zone.

Two less extensive auriferous shear zones occur 500 m to the SW and to the NW of the Vanha lode (Fig. 12). The SW lodes (‘Lampi’) are hosted by volcanogenic metaconglomerate and by the contact zone between quartzite and the conglomerate. The NW lodes (‘Tienvarsi’) are at the contact zone between volcanogenic metaconglomerate and mafic metavolcanic rocks. In the SW and NW lodes, the gold is closely associated with pyrite.

Gold-related alteration at Kaaresselkä is characterised by biotitisation and carbonatisation with minor chlorite, sericite, tourmaline, adularia and sulphides. Regional albitisation of variable degree, detected in all rock types, has preceded gold mineralisation. The mineral assemblages, except the presence of adularia, suggest that metamorphism and mineralisation took place under greenschist facies PT conditions. Extensive presence of biotite in both altered and unaltered

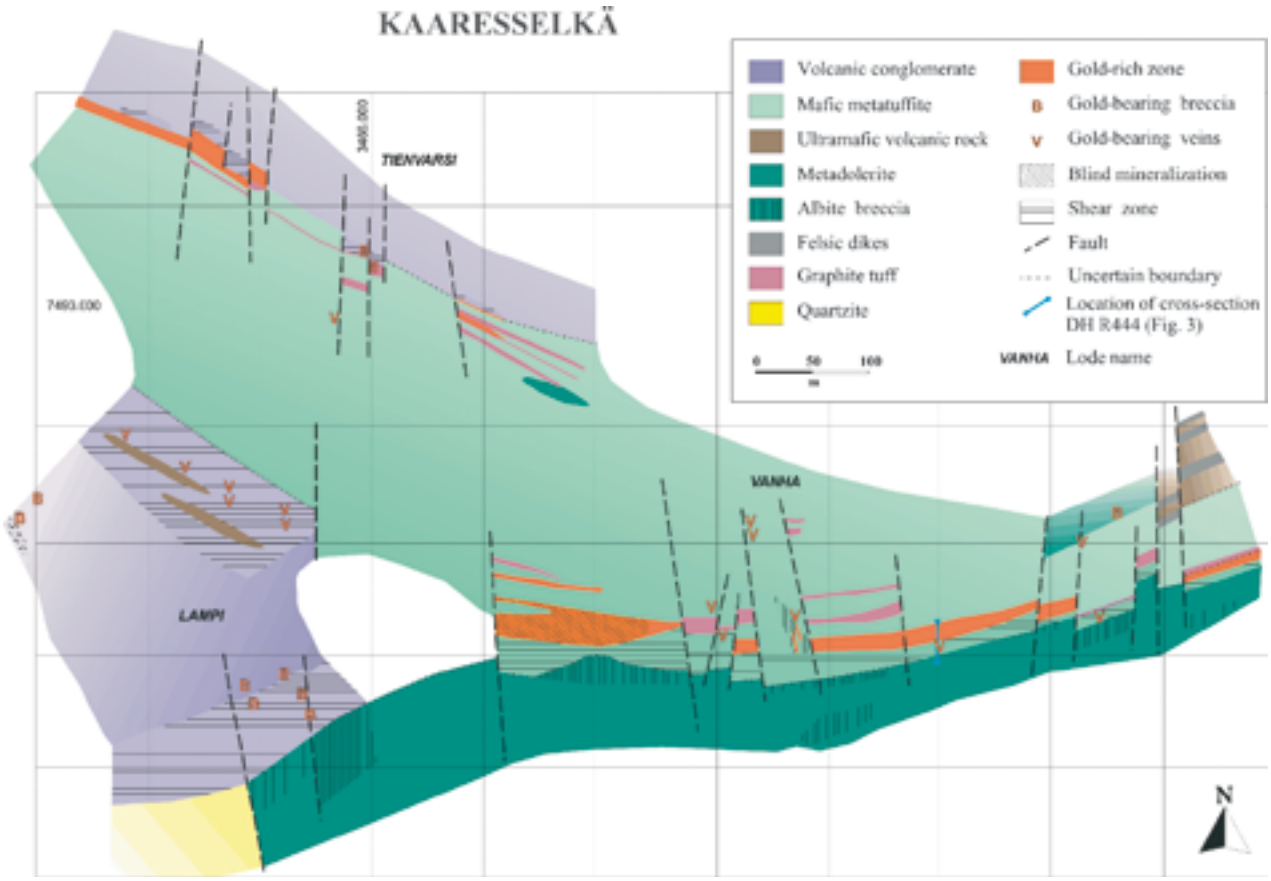

Fig. 12. Geological map of the Kaaresselkä area. The three main lodes, Lampi, Tienvarsi and Vanha, are shown. The albite breccia comprises carbonatised dolerite fragments in albite-dominated matrix. The location of the section presented in Figure 13 is indicated by a heavy line. Compiled by Eelis Pulkkinen.

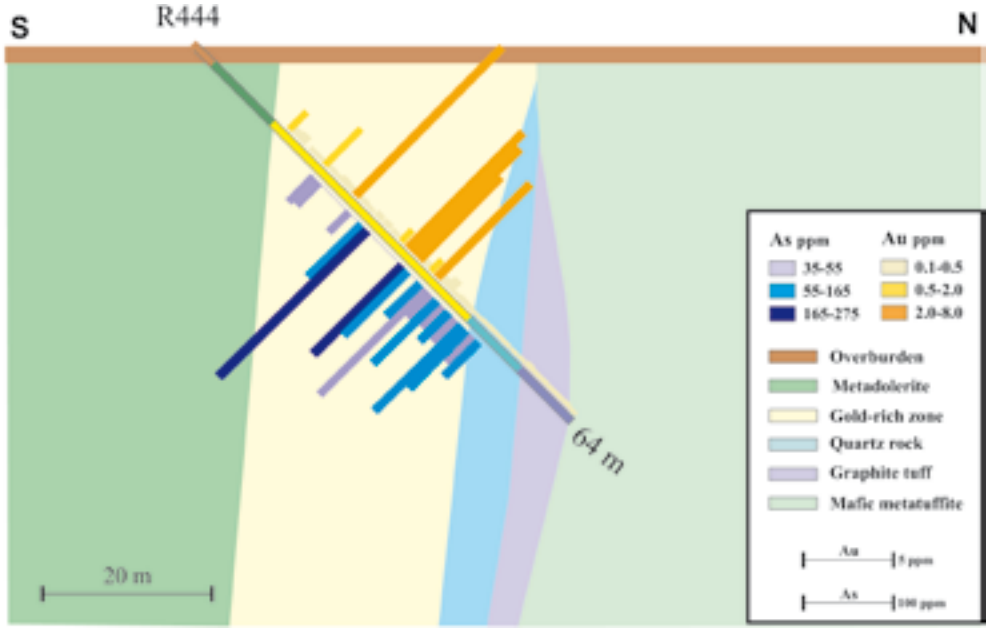

Fig. 13. A section across the Vanha lode at Kaaresselkä. Compiled by Eelis Pulkkinen.

rocks, and absence of fuchsite in ultramafic rocks point towards upper-greenschist facies conditions. An open question is, how the adularia fits into the picture, as it is a mineral normally only formed in conditions prevailing at or very close to the surface, under lower temperature and much lower pressure than those at greenschist facies (e.g., Deer et al. 2001) and being, for example, part of the diagnostic alteration

assemblage in low-sulphidation epithermal systems (Hedenquist et al. 1996). At Kaaresselkä, adularia has been identified by polarisation microscopy and microprobe work (H. Hulkki, pers. comm. 2002). Post-metamorphic, post-mineralisation formation at near-surface conditions might provide an explanation for the presence of adularia at Kaaresselkä.

Pahtavaara

The Pahtavaara mine (Fig. 14) is located 25 km NW from the town of Sodankylä in the eastern central part of the CLGB, within the extensive, predominantly pyroclastic Sattasvaara metakomatiite complex. The mine was active in 1996–2000 and was reopened in 2003. During 1996–2000, total production was 3300 kg gold from the average grade of 4 ppm Au (H. Alaniska, pers. comm. 1998, 1999, H. Vartiainen, pers. comm. 2001). In the end of 204, the mine had an indicated resource and reserve of 2.985 Mt @ 3.2 ppm gold (Scanmining 2005).

The deposit is hosted by the Sattasvaara Formation (Savukoski Group), which here forms an E–W trending, 40 km long, 5 km wide, several kilometres thick sequence of metakomatiitic lava flow and pyroclastic units, and komatiite-related mafic metavolcanic rocks (Korkiakoski 1992, Lehtonen et al. 1998). The deposit is near the northern margin of the volcanic sequence, in the contact zone between a pyroclastic and a lava flow units (Hulkki 1990, Korkiakoski 1992).

The host rocks have been metamorphosed under upper-greenschist facies conditions. The regional-metamorphic mineral assemblages in the area include chlorite – tremolite – antophyllite and tremolite – talc – chlorite – dolomite(?) – antophyllite in pyroclastic rocks, and tremolite – antophyllite(?) ± chlorite, carbonate, plagioclase in the lava flow units (Hulkki 1990, Korkiakoski 1992, Lehtonen et al. 1998). Ductile deformation dominates in unaltered komatiites whereas brittle-ductile deformation characterises the gold-mineralised domain. The Pahtavaara deposit comprises a set of lodes generally 5–10 m wide, trending roughly NW-SE and dipping to the north at about 70–80° (Korkiakoski & Kilpelä 1997). This and the regional structures suggest that the local control for ore is formed by locations where NW-trending faults cut across an E-W trending shear zone possibly branching from the SSZ.

The ore is characterised by biotite-talc ± magnetite breccias that typically are surrounded by a more massive tremolitic amphibole rock with irregular dilational arrays of barite-carbonate-quartz veins. All this is surrounded by biotite-carbonate-magnetite alteration of the komatiitic host rock. Nearly all gold is free native, and occurs between silicate, carbonate and barite grains, locally also as inclusions in magnetite;

Fig. 14. Pahtavaara mine, Sodankylä. View to the NW. Photo Terra Mining Oy.

gold grains and grain aggregates are also present in coarse-grained amphibole rock. Less than 10 % of gold is present as inclusions in pyrite and chalcopyrite (Kojonen & Johanson 1988, Hulkki 1990, Korkiakoski 1992). The most common ore mineral at Pahtavaara is magnetite which may form up to 5–10 % of ore, particularly in intensely biotitised komatiite. Pyrite is the second ore mineral forming up to 1% of rock volume. Minor and trace ore minerals detected at Pahtavaara include chalcopyrite, rutile, pentlandite, pyrrhotite, violarite, millerite, cubanite, native gold, clausthalite, and merenskyite (Kojonen & Johanson 1988, Hulkki 1990, Korkiakoski 1992). The presence of most of the latter minerals reflects the relatively high primary Cu, Ni and PGE contents of the ultramafic host rock – there are no indications of Cu, Ni or PGE enrichment during gold mineralisation at Pahtavaara.

Two stages of alteration have been described at Pahtavaara (Hulkki 1990, Korkiakoski 1992, Eilu 1997): 1) Partial albitisation and carbonatisation which preceded gold mineralisation. This stage possibly prepared ground for gold mineralisation by making the Na-CO_2 altered komatiite more competent than the surrounding talc- and chlorite-dominated komatiites and, hence, a structurally favourable site for the mineralising fluids to precipitate gold. 2) Biotitisation, formation of nematoblastic tremolite in breccia zones, and additional carbonatisation, with formation of abundant quartz veins, are related to the gold mineralisation. This stage produced the assemblage biotite-talc-dolomite/ankerite-tremolite/actinolite-quartz-pyrite-rutile ± albite, richterite, barite, magnetite, tourmaline in the host rock.

Kuotko

The Kuotko deposit is hosted by the NE-trending, brittle-ductile, Kuotko Shear Zone (KuSZ, Figs. 3 and 15), in a location where a NW-trending, lower-order, shear or fault zone branches from the KuSZ. The

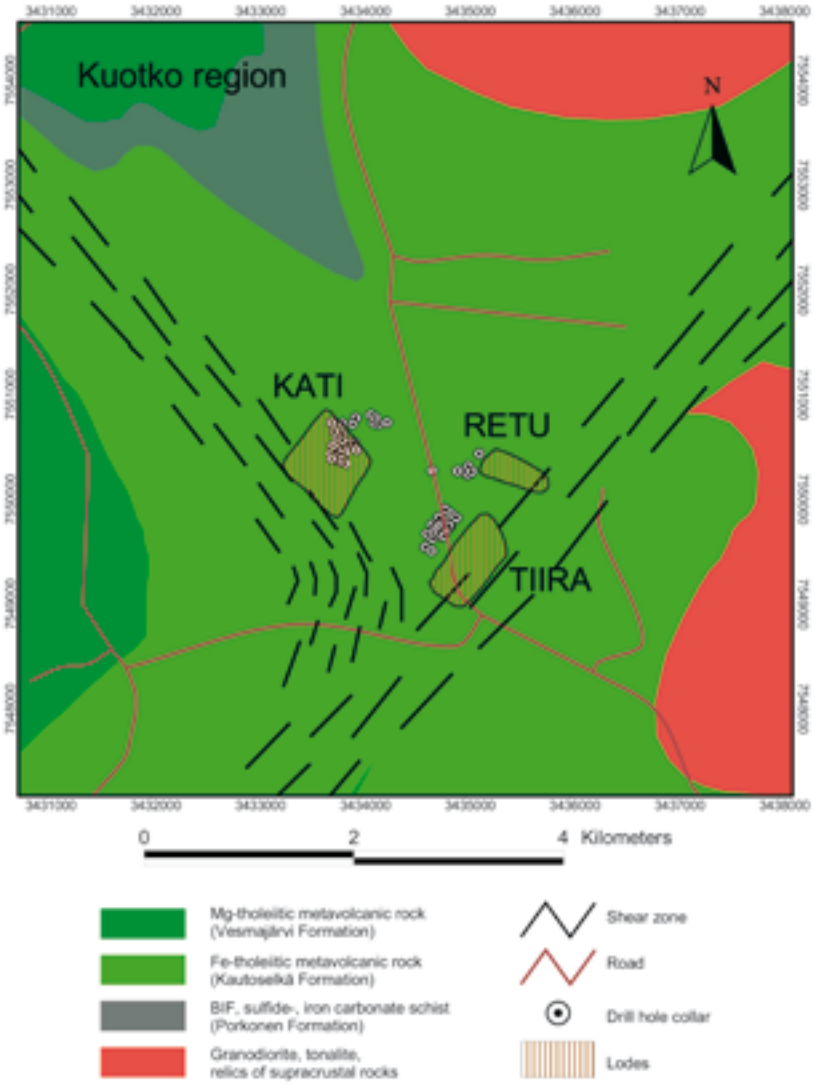

Fig. 15. Geological map of the Kuotko area (Härkönen et al. 2001). Coordinates according to Finnish National Grid (ykj-grid) metric values. Compiled by Veikko Keinänen.

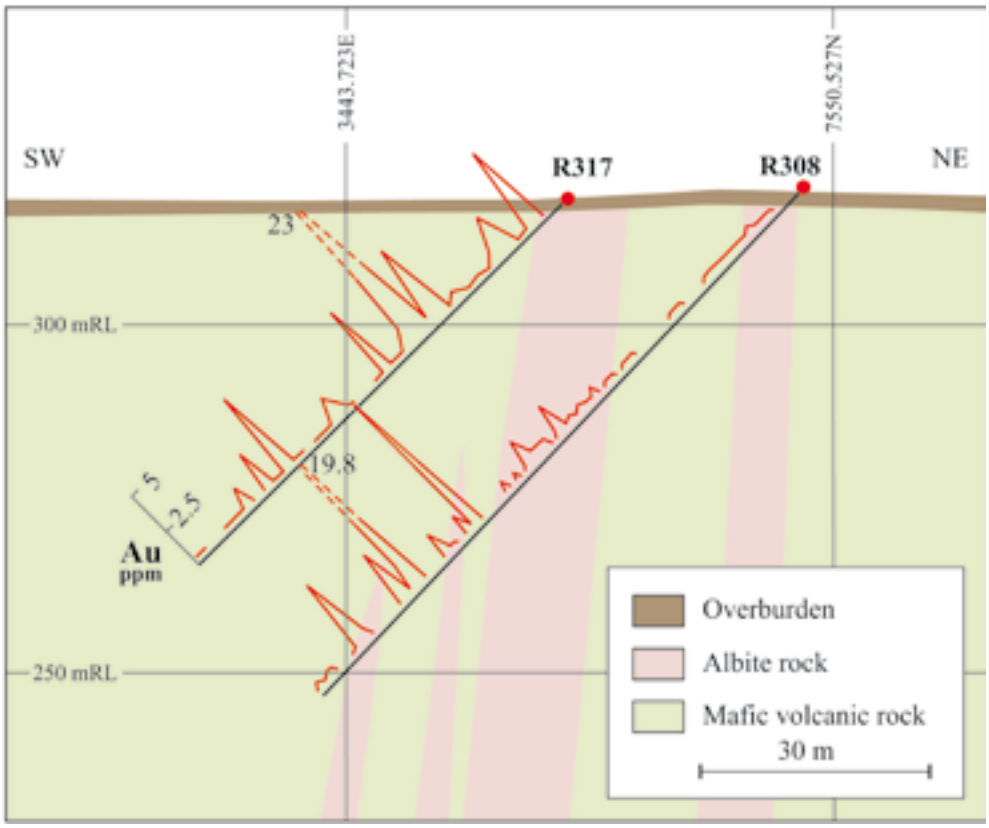

Fig. 16. Section across the Kati lode at Kuotko (Härkönen et al. 2001).

deposit is hosted by the Kittilä Group rocks (Fig. 3). Pyroclastic Fe-tholeiitic metabasalts form the major host and felsic dykes minor host to ore (Härkönen & Keinänen 1989, Härkönen 1994, Lehtonen et al. 1998, Härkönen et al. 2001). Mineral assemblages at Kuotko indicate that both regional metamorphism and gold mineralisation have taken place at lower- to mid-greenschist facies conditions.

Four subparallel lodes have been discovered at Kuotko. For two of them, enough drilling was performed until 2001 to warrant a preliminary resource estimate for the upper 40–50 m of bedrock (Härkönen et al. 2001): this is the resource indicated in Appendix 2 for Kuotko. All lodes detected are open at depth and along strike. The main lode, Kati (Fig. 16), is up to 15 m wide, and has been followed by drilling for 150 m along strike. According to in-hole geophysical survey, the Kati lode extends to the depth of 100–300 m or even into greater depths (Härkönen et al. 2001). Auriferous quartz-ankerite veins characterise the deposit (Härkönen & Keinänen 1989). The main sulphide minerals are pyrite, arsenopyrite, gersdorffite and pyrrhotite. Native gold occurs as free grains (60%) among gangue and as inclusions in arsenopyrite.

Ruosselkä

The Ruosselkä gold prospect is located about 65 km north from the town of Sodankylä. The area is dominated by metavolcanic and metasedimentary rocks of the Sodankylä and Savukoski Groups and by the post-orogenic Nattanen-type granites (Figs. 3 and 17) (Lehtonen et al. 1998).

The first gold in the area was found in 1988 when several gold grains were discovered by panning till from areas which were detected anomalous in gold in regional geochemical till survey (Salminen 1995). In January 1999, GTK started a new project to investigate the gold anomalies in the region. The old till samples were reanalysed for Au and Te. The concentrations of both elements were found to be tens of times higher than the regional background in about 100 samples. In addition, a major part of the gold anomalies in till appeared to be associated with Cu and Mo anomalies detected previously in the region (Pulkkinen et al. 2005).

The supracrustal sequence at Ruosselkä includes komatiitic metavolcanic rocks, mafic metatuff, and graphitic felsic metatuff forming a large fold opening to the east (Fig. 17). The sequence is intruded by a

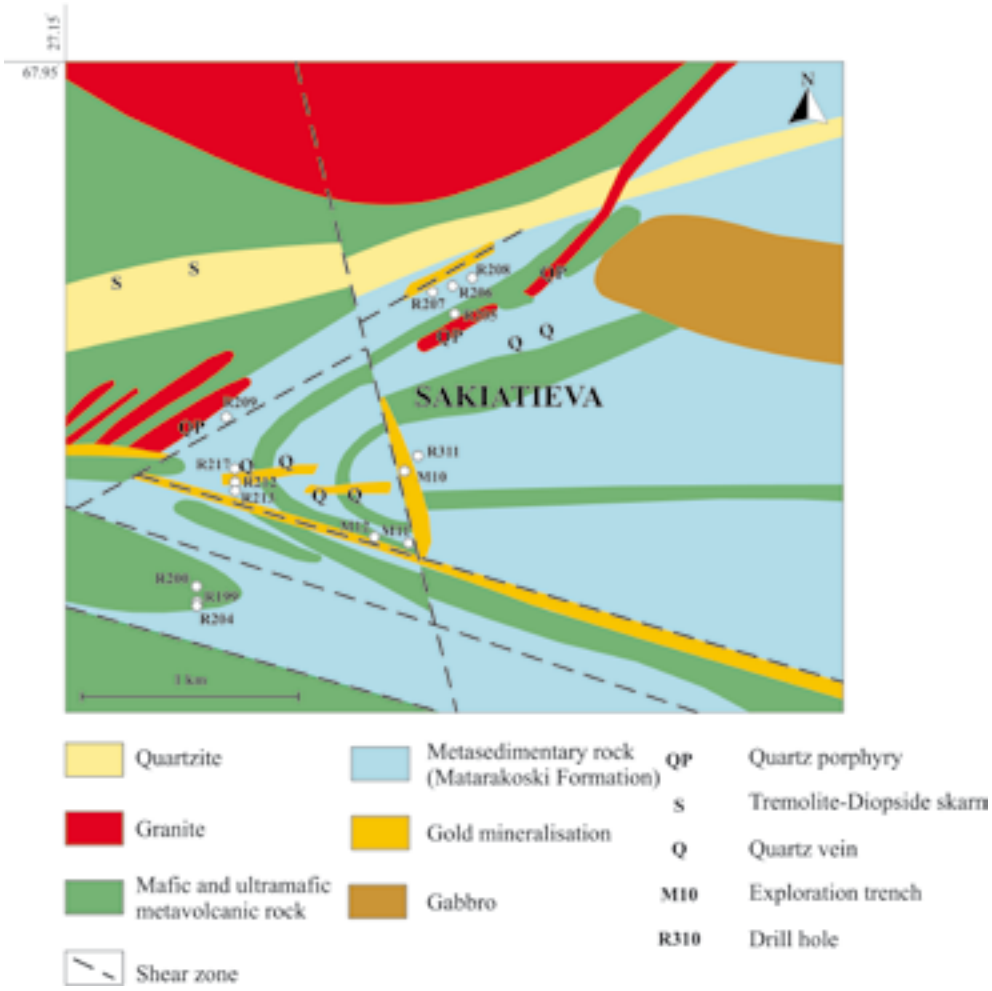

Fig. 17. Geological map of the Ruosselkä area. The map is chiefly based on ground-magnetic and electromagnetic survey with controlling data from exploration trenches, drill holes and the few outcrops present in the area. Compiled by Eelis Pulkkinen.

ca. 1.77 Ga granite pluton in the north, 1–20 m wide quartz porphyry, pyrite-disseminated monzogranite and granite dykes, and cut by a set (or sets) of barren quartz veins. Drilling and trenching in the area revealed altered, auriferous, W-, WNW-, NNW- and NE-trending, up to 200 m wide, shear and fault zones apparently concentrating in the hinge area of the eastward-opening fold (Fig. 17). Some of the granite dykes cut across the WNW-trending shear zones, whereas others are parallel to them. These features indicate that, at least, most of the deformation along the shear zones took place before granite intrusion. Gold grades in the WNW-trending shear zone locally range from 0.3 to 1.5 ppm Au forming lodes 1–10 m wide. The NNW-trending auriferous shear zone contains an 8 m wide zone with 3–11 ppm Au (Fig. 18, App. 2). Native gold has also been detected as inclusions in hornblende sampled from an outcrop 0.5 km northeast of the above-mentioned shear zones (Rantala 2003), apparently in the NE-trending shear zone(s) shown in Figure 17. The latest results from diamond drilling in the Ruosselkä area include a 3 m section with 244 ppm Ag and 0.1 % Zn, and an 1 m section with 7 ppm Au; both of these sections are closely associated with felsic dykes (E. Pulkkinen 2003, pers. comm., Pulkkinen et al. 2005).

One of the lodes at Ruosselkä, at the Sakiatieva locality, is 150 m long and 10 m wide, but it is open at depth and along strike at both ends. Based on the ground geophysical survey, the entire altered zone there is 50–200 m wide and 400 m long. The Sakiatieva lode is hosted by mafic volcanic rocks and graphitic phyllites. The main gangue minerals are carbonate, quartz, diopside, biotite, feldspar and chlorite. Main sulphide mineral is pyrrhotite. Gold occurs as native, free grains with gangue and pyrrhotite. Other ore minerals detected at Sakiatieva are chalcopyrite, pyrite, tellurides galena, sphalerite, scheelite and molybdenite (Pulkkinen et al. 2005).

Alteration in the auriferous parts of the shear zones

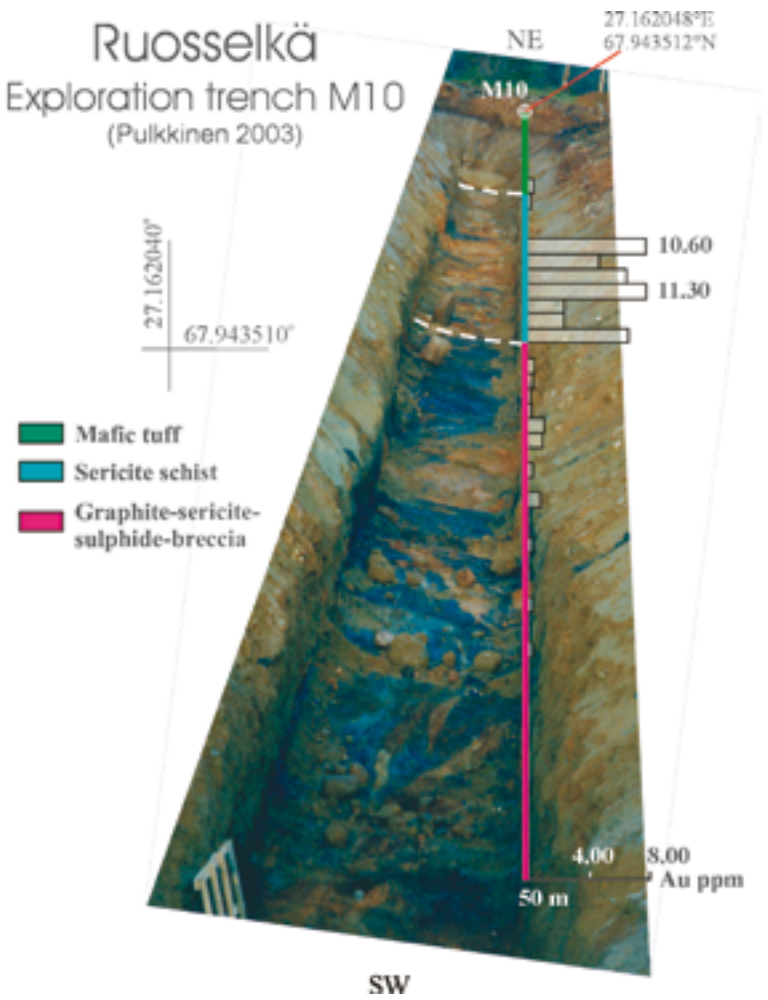

Fig. 18. A 50 m long, 2 m wide exploration trench across gold mineralisation in a shear zone at the Sakiatieva locality at Ruosselkä. Compilation by Eelis Pulkkinen, photo: V. Mäntynen.

has produced a mineral assemblage of hornblende-biotite-chlorite in the metakomatiites (Sattasvaara Formation), chlorite-sericite-quartz-Fe sulphides and disappearance of graphite in the metatuffs (Matarakoski Formation). The latter is represented by the 'sericite schist' in Figure 18. Alteration in the granite dykes is minimal suggesting that the dykes postdate gold and gold-related alteration in the area.

Iron oxide-copper-gold in Kolari area

Several magnetite orebodies (ironstone) and skarn-like units of diopside-hornblende rock in the Kolari area of the westernmost Central Lapland greenstone belt host Cu-Au mineralisation (Figs. 19–24). All deposits have a structural control and are located in or close to a fault or shear zone. The ironstone bodies are hosted by a supracrustal sequence containing abundant mafic metavolcanic rocks and marbles (calcitic and dolomitic), and are close to, or at the contact with, a ca. 1.86 Ga synorogenic monzonite intrusion (Hiltunen 1982, Lehtonen et al. 1998, Niiranen et al. 2007). Magnetite deposits at Rautuvaara and Hannukainen have been exploited as iron ores, but gold and copper have been extracted only from the Laurinoja orebody (Figs. 20 and 21) at Hannukainen (Hiltunen 1982).

Magnetite content in the ironstones is 20–80%, and that of sulphides 1–5%. Gangue chiefly comprises diopside and hornblende with minor tremolite-actinolite, albite, biotite, K feldspar, scapolite, calcite, quartz, garnet and epidote. At Cu-Rautuvaara, the gangue comprises albite, antophyllite and biotite with minor diopside, quartz and titanite. The main sulphide minerals are chalcopyrite, pyrite and pyrrhotite which form dissemination, millimetre-wide veins and weak stockworks. Gold is closely associated with sulphides, particularly chalcopyrite, occurs in native form, and has been detected as inclusions or in cracks in chalcopyrite, magnetite, diopside and amphibole (Fig. 23) (Hiltunen 1982, Niiranen & Eilu 2003, Niiranen et al. 2007).

Early regional, structurally-controlled alteration

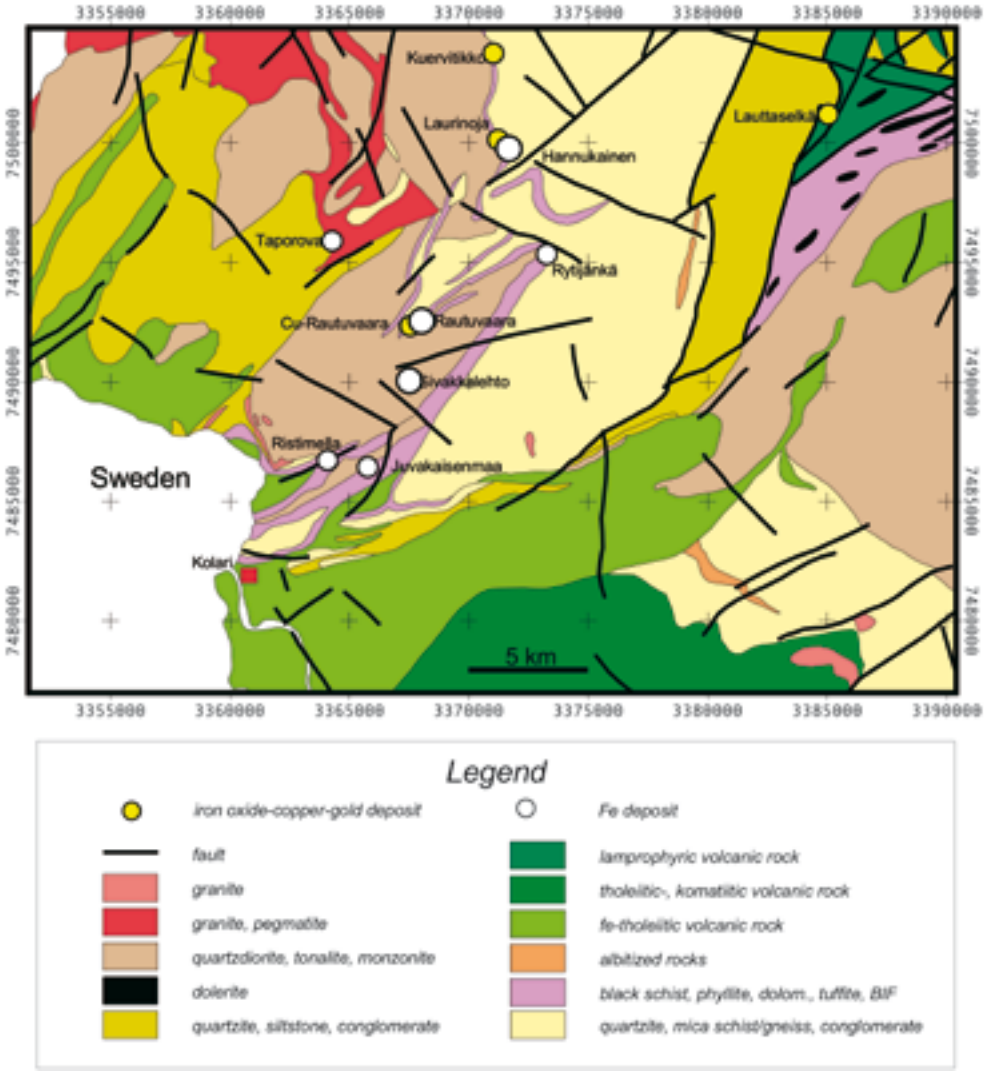

Fig. 19. Geological map of the Kolari region, westernmost CLGB. Geology based on Lehtonen et al. (1998), location of Fe deposits from Hiltunen (1982).

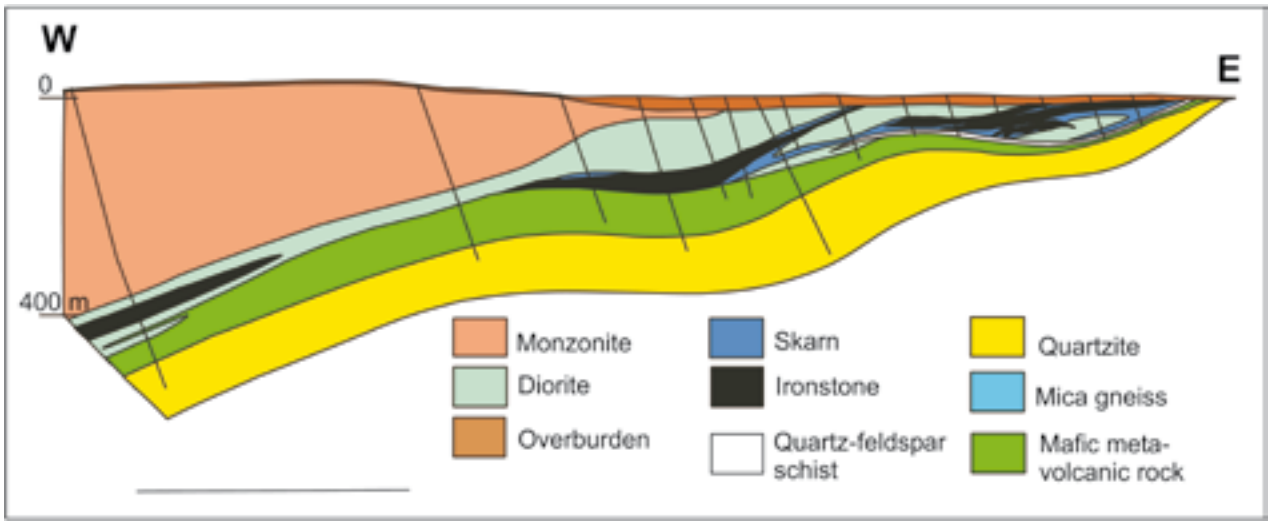

Fig. 20. Section across the Hannukainen mine area, which includes the Laurinoja Fe-Cu-Au orebody, Kolari area, western Central Lapland greenstone belt. Modified from Hiltunen (1982).

Fig. 21. Chalcopyrite- and native gold-rich, massive magnetite rock at Laurinoja. The pen is 12 cm long. Photo: Pasi Eilu.

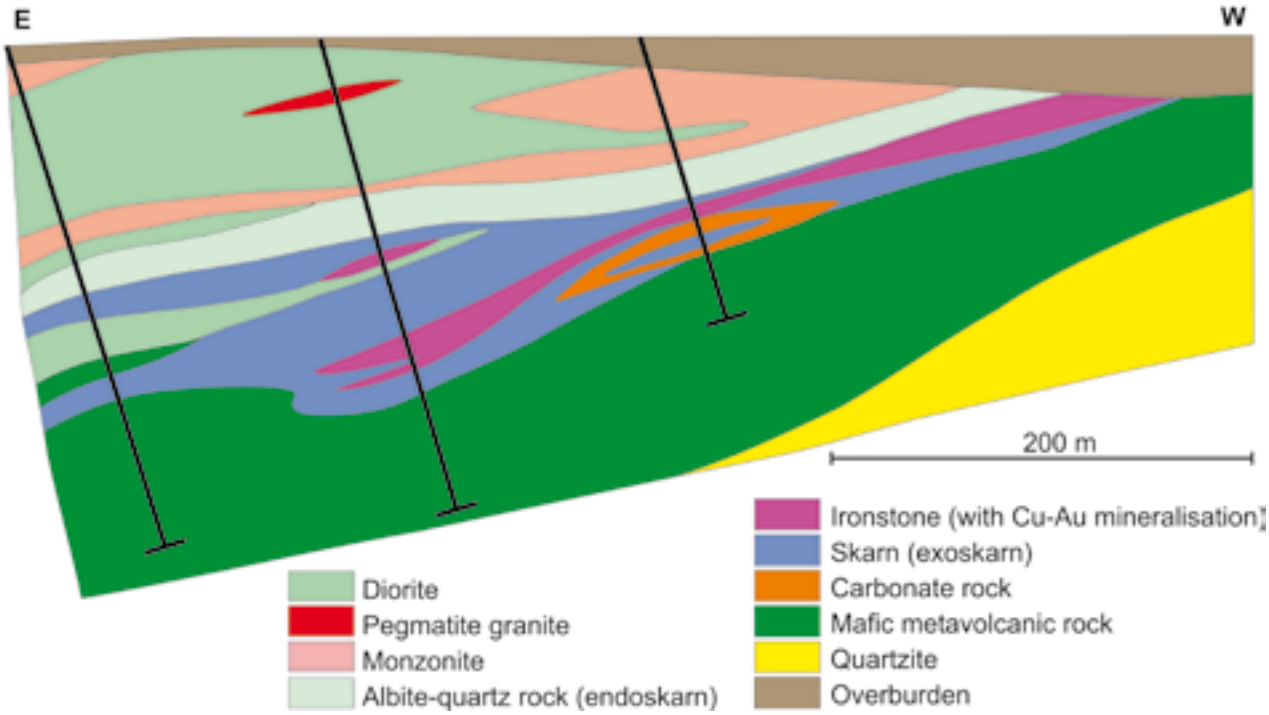

Fig. 22. A section across the Kuervitikko occurrence, after Hiltunen (1982). Most of the gold and copper is hosted by the ”Iron ore” unit.

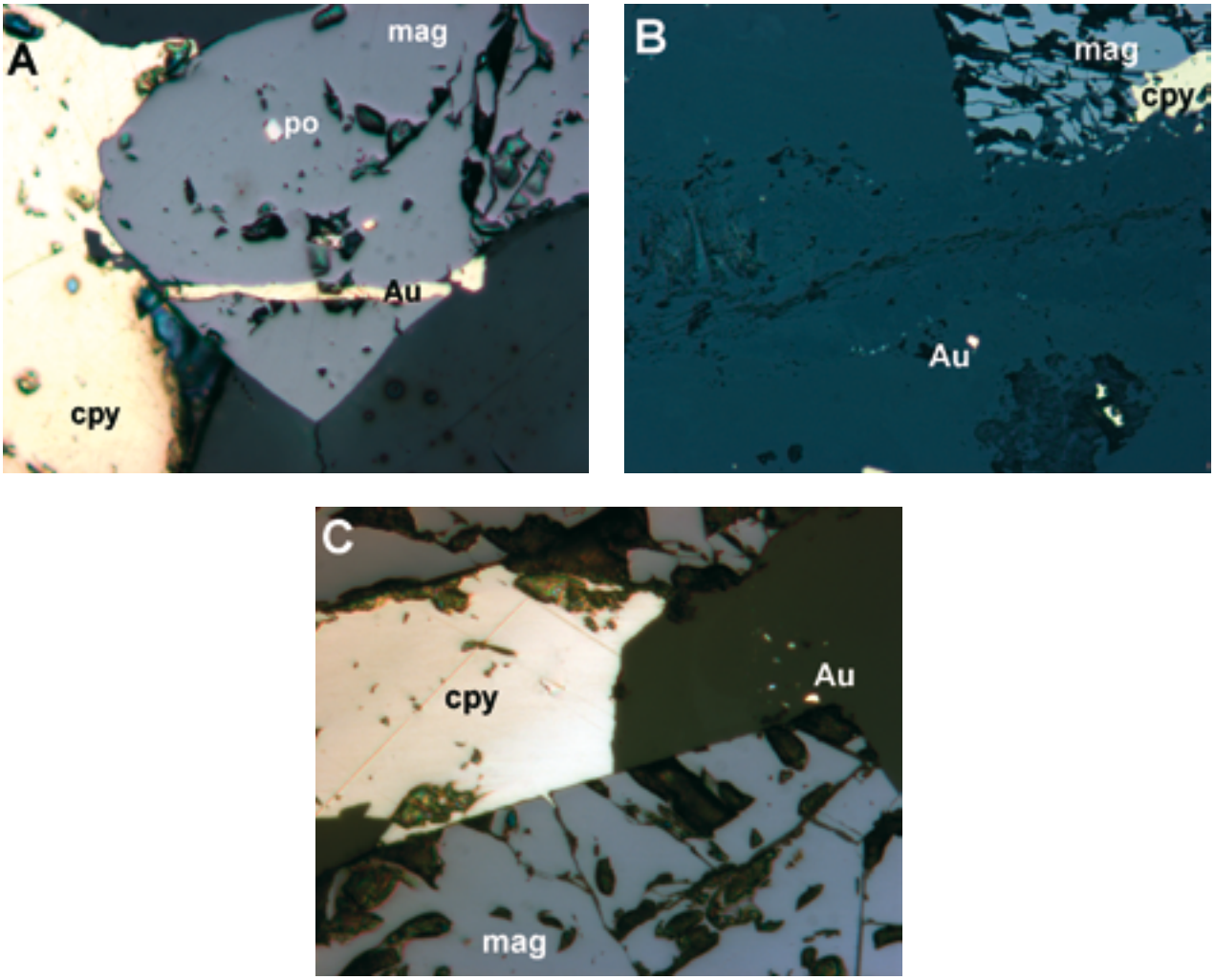

Fig. 23. Siting of native gold in the Kolari IOCG occurences. A) Gold in a crack in magnetite, associated(?) with chalcopyrite, Laurinoja. B) Gold in silicate gangue, Laurinoja. C) Gold in gangue near magnetite, Kuervitikko. Field of view in A 0.4 mm, in B and C 0.2 mm. Abbreviations: Au = gold, cpy = chalcopyrite, mag = magnetite, po = pyrrhotite. All imaging by Tero Niiranen.

in nearly all rock types in western Lapland includes weak-to-moderate albitisation and scapolitisation. This Na-Ca alteration is followed by at least two stages of local alteration extending for hundreds of metres to kilometres along strike and tens to hundreds of metres across the strike of the host rocks in Kolari. The first stage produced magnetite, diopside, titanite and minor iron sulphides in the ironstones surrounded by abundant hornblende, diopside and plagioclase, and minor K feldspar, biotite, garnet, titanite, magnetite and scapolite ('skarn' in Figs. 20, 22, 24). In the second stage, most of the sulphides and gold, with hornblende and variable but minor amounts of albite, quartz, calcite, K feldspar, biotite, calcite, talc and epidote, overprint the ironstone. The adjacent granitoids also show the effects of hydrothermal alteration, including formation of albite, quartz, hornblende, epidote, biotite, ± pyrite and chalcopyrite ('albite-quartz rock' in Fig. 22) (Niiranen et al. 2007).

Palaeoplacer gold

Palaeoplacer gold deposits are hosted by mono- and polymictic conglomerates of the uppermost unit, the Kumpu Group (Fig. 3), of the CLGB (Lehtonen et al. 1998). The conglomerates were deposited in deltaic and fluvial fan environments after ca. 1913 Ma and before ca. 1800 Ma (Härkönen 1984, 1986, Rastas et al. 2001). Most of the gold is hosted by the central major unit of the Kumpu Group, in up to 3 m thick and 30 m long conglomerate lenses. Within these lenses, the Au grade in most cases varies from 0.1 to 5 ppm, but locally reaches 22 ppm (Härkönen 1984). However, only in two cases, Outapää and Kaarestunturi (Fig. 3, App. 2), does the Au content exceed 1 ppm for an interval more than 1 m across a lode.

Gold nearly exclusively occurs as free, detrital grains with a size of 0.03–0.4 mm and, in minor amounts, as smaller inclusions in quartz clasts (Härkönen 1984).

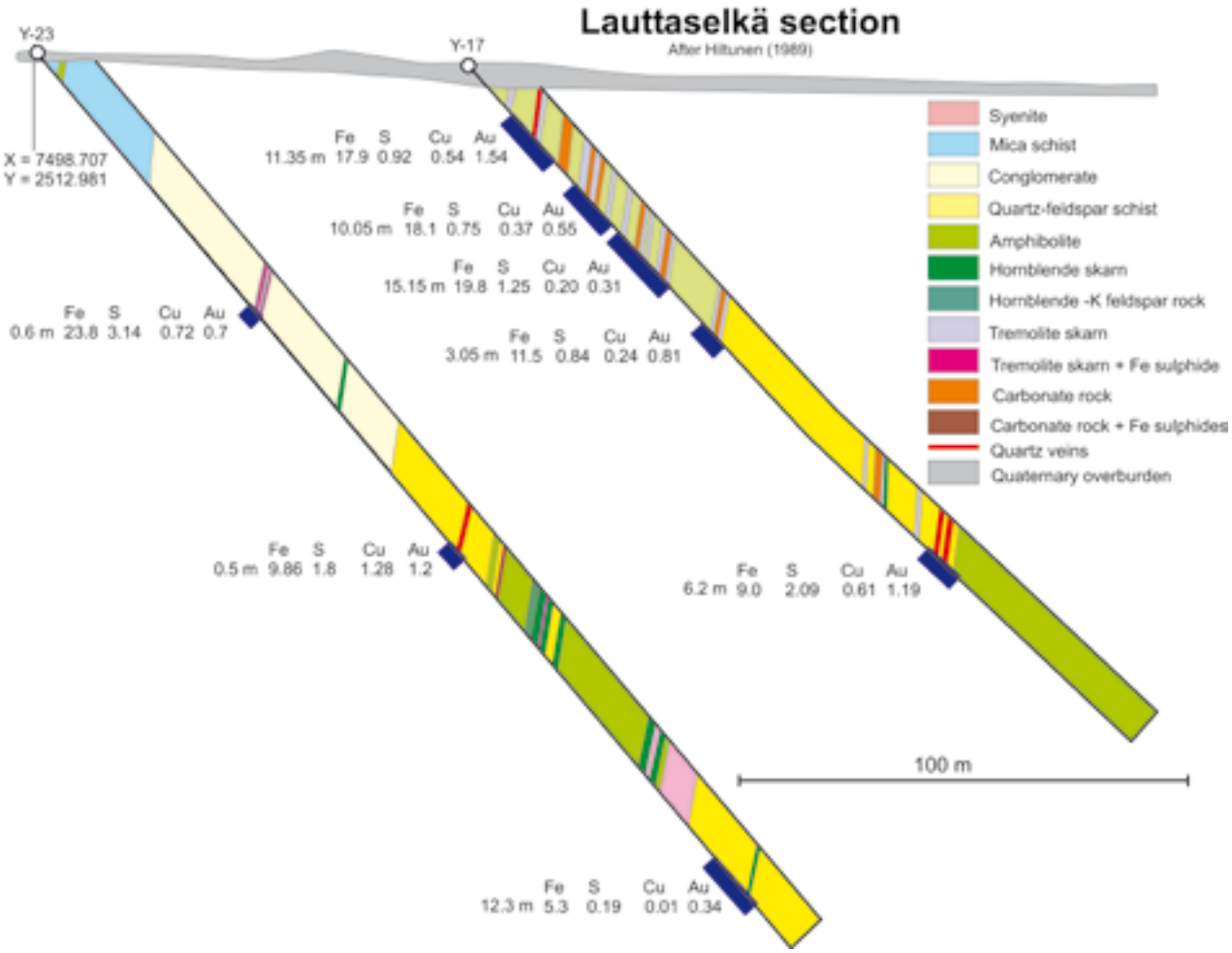

Fig. 24. A section drilled across the Lauttaselkä Cu-Au occurrence. The Cu-Au mineralisation is hosted by both amphibole-rich, skarn-like, mafic volcanic(?) rocks and by felsic rocks of sedimentary origin. The Cu, Fe and S concentrations are in %, Au in ppm. After Hiltunen (1989). Coordinates according to Finnish National Grid (kkj-grid) metric values.

Heavy minerals occurring in the same beds as the gold are magnetite, haematite, uraninite, pyrite, ilmenite, rutile, native silver, tourmaline, monazite, titanite and zircon (Härkönen 1984). The host rocks are metamorphosed under greenschist-facies conditions. No alteration of the host rock or any mobilisation or hydrothermal precipitation of Au has been reported in these occurrences.

GOLD IN KUUSAMO SCHIST BELT

General geological features of the Kuusamo schist belt

The formation of the stratigraphic sequence of the KSB is summarised here based on Silvennoinen (1972, 1991), Pankka (1992), and Räsänen and Vaasjoki (2001). It started with the deposition of a thin, discontinuous polymictic conglomerate unit directly on Archaean crust. This was followed by Greenstone Formation I (Fig. 4) which chiefly comprises mafic and intermediate amygdaloidal and massive lava units with tuffitic interlayers deposited in a subaerial environment. The volcanic activity ended with the formation of tuffites. The following unit, the Sericite Quartzite Formation, was deposited under transgressive conditions and is now composed of sericitic quartzite, feldspathic quartz-pebble conglomerates, sericite schists, carbonate rocks (dolomitic marbles) and felsic volcaniclastic rocks. Prior to ca. 2206 Ma (U-Pb zircon, baddeleyite and titanite ages in cross-cutting dolerites; Silvennoinen 1991), eruption of a

thin, but extensive, basalt (the Greenstone Formation II) followed the sedimentary formation. Then the sedimentation continued during regressive conditions, producing the Siltstone Formation, which now is composed of meta-arkose, orthoquartzite, phyllite and dolomitic marble members. This was followed by eruption(s) of extensive, continental tholeiitic basalt (Greenstone Formation III), and deposition of arenaceous sediments, the present Rukatunturi Quartzite Formation comprising sericitic and arkosic quartzites and orthoquartzite. These, in turn, were covered by the Dolomite Formation which separates the quartzites from the uppermost stratigraphic unit of the KSB, the volcanogenic Amphibole Schist Formation.

Differentiated dolerite sills and dykes, 'albite diabases', intruded into all of the formations of the KSB, except into the Amphibole Schist Formation. According to Silvennoinen (1991), the mafic intrusives belong to two age groups, 2206±9 Ma and 2078±8 Ma (U-Pb zircon, baddeleyite and titanite ages). These intrusive stages probably represent major rifting stages of the intracratonic Kuusamo basin, as the dolerite units are voluminous, up to tens of metres thick, and occur throughout the belt (Pankka and Vanhanen 1992).

The KSB was probably subjected to the same orogenic epochs as the CLGB during Palaeoproterozoic (cf., Lahtinen et al. 2003). During the compressive epochs (1.92–1.88, 1.85–1.79 Ga), the degree of regional metamorphism varied from lower-greenschist to upper-amphibolite facies (Silvennoinen 1972, 1991). The highest metamorphic grade was attained in the W and NW, near the contact with the Central Lapland Granite Complex. From there, the metamorphic grade at the present surface decreases towards the central parts of the belt which also hosts all gold occurrences (Fig. 4). From the central parts, the metamorphic grade again increases towards the eastern flank of the belt.

Gold mineralisation

The Kuusamo gold occurrences (App. 3) are mainly hosted by the two lowermost, dominantly sedimentary, supracrustal formations (Sericite Quartzite and Siltstone Formation). Although the known deposits are preferentially in certain stratigraphic units, the main regional and local control for mineralisation is structure: two roughly SW- to NW-trending antiforms in the middle of the KSB, Hyväniemi-Maaninkavaara and Käylä-Konttiaho anticline (Fig. 4), control all gold occurrences. In deposit scale, the main controls for mineralisation are the intersections between antiforms and shear and fault zones and, probably, also the regional pre-gold albitisation (Pankka 1992, Pankka & Vanhanen 1992). Most of the deposits are strongly elongated along the local shearing lineation. Individual lodes may be controlled by smaller structures; for example, the mineralised pipes at Konttiaho appear to be in hinges of meso-scale folds (J. Ojala, pers. comm. 2001).

Uranium, Fe-sulphide and Au-Co-Cu±U deposits have been discovered in the KSB (Pankka 1992, Pankka & Vanhanen 1992, Korteniemi 1993, Vanhanen 2001). Except for most of the uranium deposits, which belong to the stratiform sandstone type, the deposits are epigenetic. The Au-Co-Cu±U deposits can be divided into two end members based on structural setting: 1) replacement mineralisation (e.g., Juomasuo) in a ductile deformation regime, and 2) breccia mineralisation (e.g., Konttiaho) in a brittle deformation regime (Vanhanen 2001). The Fe-sulphide deposits are essentially comprised of pyrrhotite and pyrite, are weakly enriched in cobalt but lack precious metals or uranium.

Alteration is extensive and multistage in the KSB. The whole belt was affected by the first three main stages of alteration (Vanhanen 2001): 1) Diagenetic, partial albitisation of feldspars and sericitisation of clay minerals in all sedimentary units. 2) Local, partial to total albitisation of clastic sedimentary units and spilitisation of volcanic units when the ca. 2.206 Ga mafic sills and dykes generated fluid circulation near the contacts of the intrusions. 3) The early spilitisation and diagenetic albitisation are overprinted by much more extensive albite and scapolite alteration and variable carbonatisation across the belt. Intensity of the latter alteration varied from weak (<10% albite) to strong, locally resulting in almost pure albite rocks (99% albite + traces of carbonate, rutile, quartz).

In addition to the regional styles of alteration, the sites of structurally controlled fluid flow have been affected by a number of hydrothermal alteration stages of local extent. The best known of such areas are the gold occurrences and their immediate surroundings. Below, we use the Juomasuo and Konttiaho deposits as examples to describe typical alteration directly related to the KSB gold occurrences, as these two are among the most intensely investigated deposits in the belt.

At **Juomasuo** (Figs. 25 and 26), the alteration sequence postdating the two regional alteration events is, from the earliest to the latest (Korteniemi 1993, Vanhanen 2001): A) Local carbonatisation controlled by structures formed in early stages of orogeny (1.92–1.88 Ga ?). B) Formation of the assemblage magnetite-albite-quartz-chlorite-phlogopite-biotite-amphibole-talc. This stage is distinctly controlled by the same structures that control gold mineralisation. At Juomasuo, this alteration extends only up to

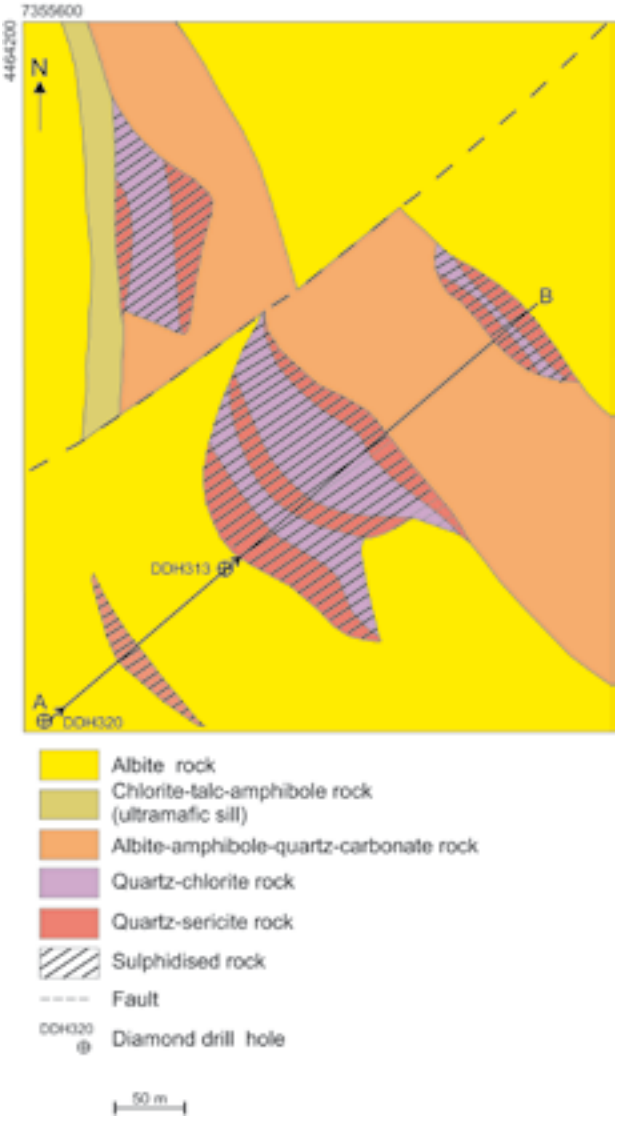

Fig. 25. Geological map of the Juomasuo area; after Pankka (1992). Line AB indicates the location of the section shown in Figure 25.

50 m away from gold mineralisation. C) The main mineralising stage: formation of the assemblage albite-quartz-chlorite-pyrrhotite-cobaltite-Co pentlandite-chalcopyrite-gold ± uraninite. D) Formation of the mineral assemblage quartz-sericite-pyrite ± gold, uraninite, and tellurides; this assemblage formed very locally in the domain characterised by the Stage C mineral assemblage.

At **Konttiaho**, the local alteration comprises the following stages (Vanhanen 2001): A) Local carbonatisation similar to that at Juomasuo. B) Main mineralised stage with proximal biotitisation and chloritisation, and formation of Fe sulphides, chalcopyrite, uraninite, gold, enveloped by distal, partial albitisation. C) Second stage of biotitisation and chloritisation, associated with formation of Fe sulphides, molybdenite, tellurides and minor gold.

Similar sequences, as at Juomasuo or Konttiaho, have been detected in practically all gold-mineralised localities in the KSB. This is also the case at **Meurastuksenaho** (Fig. 27), except for a higher temperature during gold mineralisation. There, the proximal, gold-related alteration mineral assemblage is chlorite-biotite-garnet-staurolite-amphibole-magnetite-cobaltite-gold (Vanhanen 2001).

The most common ore minerals in the Kuusamo deposits are pyrrhotite and pyrite (App. 3). They also are the only sulphides in the barren Fe-sulphide deposits which in their style of alteration and structural control resemble the Au-Co-Cu±U deposits (Vanhanen 2001). Gold is dominantly in free native form, associated with gangue (Pankka 1992, Korteniemi 1993, Vanhanen 2001). In only a few deposits, significant volumes of gold occurs as inclusions in pyrite and cobaltite. Chalcopyrite is the only significant carrier for Cu and cobalt pentlandite and cobaltite are the main carriers of Co. In the U-rich deposits, native gold, uraninite, galena, and various tellurides are typical accessory minerals. Molybdenite is a typical accessory mineral in some deposits but absent from others. Magnetite and rutile are the typical oxides of the KSB Au deposits forming dissemination in the altered rocks.

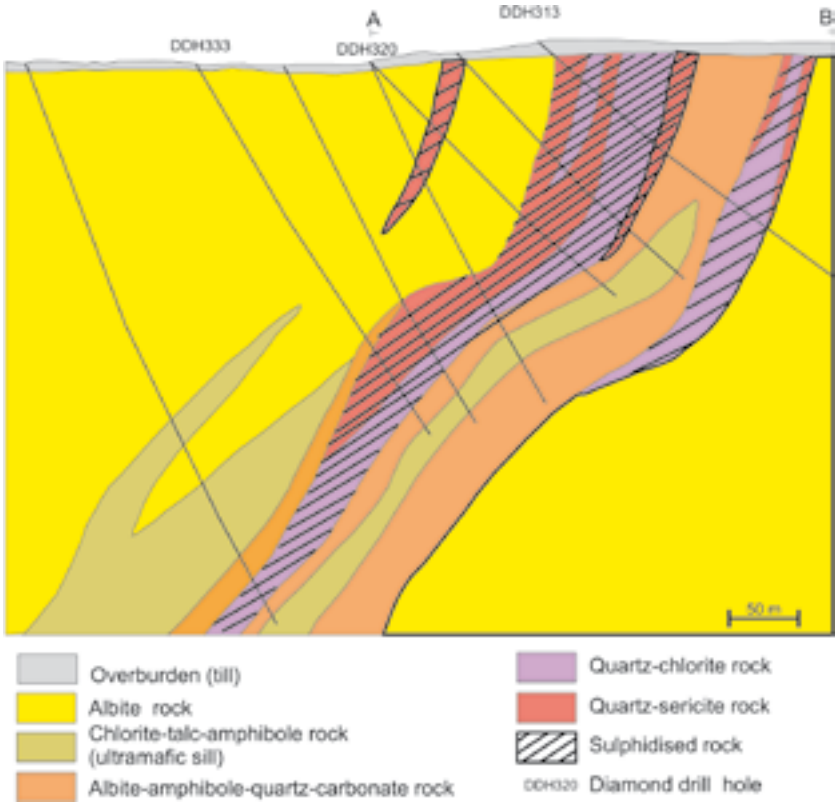

Fig. 26. Section across the Juomasuo Co-Au deposit; after Pankka (1992).

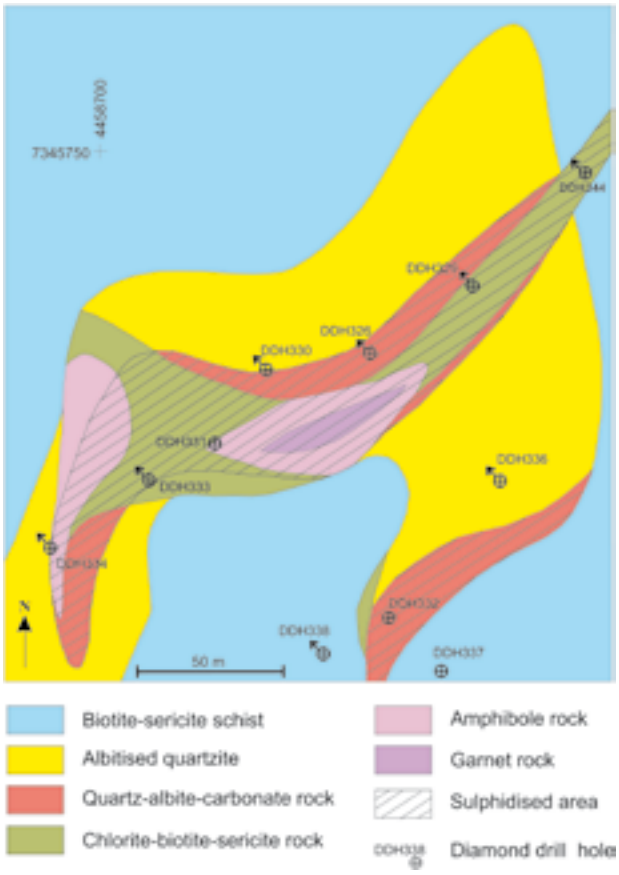

Fig. 27. Geological map of Meurastuksenaho; after Vanhanen (2001).

GOLD IN PERÄPOHJA SCHIST BELT

General geological features of the Peräpohja schist belt

The Palaeoproterozoic Peräpohja schist belt (PSB) forms the southwesternmost corner of the Lapland domain of the Precambrian of Finland. It covers a triangular area bounded in the S and SE by the Archaean Pudasjärvi Gneiss complex. To the N and NE, it has a gradational boundary with the Central Lapland Granitoid Complex (Figs. 1 and 5). To the west of the Finland–Sweden international border, the PSB is bounded by the N-S trending Baltic–Bothnian Megashear (Berthelsen & Marker 1986).

The formation of the stratigraphic sequence of the PSB is summarised below based on Perttunen (1989, 2002, 2003), and Perttunen and Vaasjoki (2001). The central, western and southern parts of the belt, where all gold occurrences are, is composed of a distinct sequence of volcanic and sedimentary formations (Fig. 5): The stratigraphic sequence started by the deposition of a thin polymictic conglomerate, the Sompujärvi Formation, unconformably on the Archaean Pudasjärvi gneisses. The overlying volcanic rocks of the Runkaus Formation are subaerial amygdaloidal tholeiitic basalts with evolved compositions. The following formation is the Palokivalo quartzite. The Jouttiaapa Formation, which consists of dozens of subaerial tholeiitic basalt flows, covers the Palokivalo quartzite. The overlying Kvartsimaa Formation is composed of pure orthoquartzite with local dolomitic quartzite and dolomite interbeds. It is covered by mafic tuffitic rocks of the Tikanmaa and Hirsimaa Formations, with the dolomite-dominated Poikkimaa Formation located between the two tuffitic formations. The Rantamaa Formation consists of stromatolitic dolomite with thin quartzite interlayers. The Martimo and Väystäjä Formations are the uppermost of the main units of the PSB; the former is composed of turbiditic greywackes with black shale interbeds and the latter chiefly of mafic pillow lavas.

The PSB is intruded by 2.2 Ga and 2.1 Ga differentiated sills, albite-rich dolerites, which cut across all formations up to the quartzite of the Palokivalo Formation (Perttunen & Vaasjoki 2001). As like as in Central Lapland and Kuusamo, these mafic intrusive stages most probably represent major rifting stages in the belt (Huhma et al. 1990). In the west and north, the belt is intruded by orogenic (1.89–1.80 Ga) granitoids. Also, a number of felsic dykes have been detected throughout the belt, but all which have been investigated contain xenocrystic, Archaean zircons, and their emplacement age is unknown (Perttunen & Vaasjoki 2001). Regional metamorphic grade varies from mid-greenschist to upper-amphibolite facies increasing from south to north across the belt.

Gold deposits and occurrences

Five drilling-indicated gold occurrences are known from the PSB (Fig. 5; App. 4), four of which are orogenic and one, Vähäjoki, is of iron oxide-copper-gold (IOCG) type. The overall control on gold mineralisation is not well known because of scarcity of detailed investigations, but the control possibly is the antiform structures and the cross-cutting faults, a situation similar to the KSB. All deposits are in rocks metamorphosed under upper-greenschist facies conditions, and all orogenic gold deposits are hosted by metadolerites and have a metal association of Au-Cu.

The **Kivimaa** deposit (Fig. 28) is essentially defined by an E-W trending, 350 m long and 1–6 m wide, auriferous calcite-quartz vein in metadolerite (Rouhunkoski & Isokangas 1974). The vein is in a dip-slip fault and is enveloped by an alteration halo that is characterised by the mineral assemblage calcite-chlorite-biotite-albite-pyrite. The main ore minerals at Kivimaa are pyrite and chalcopyrite with minor to trace amounts of arsenopyrite, pyrrhotite, ilmenite, rutile, bismuthinite, native bismuth, native gold, galena and fahlore (Rouhunkoski & Isokangas 1974, Lehtinen & Eilu 1987). Native gold and bismuth occur as inclusions in arsenopyrite. The deposit was exploited in 1969

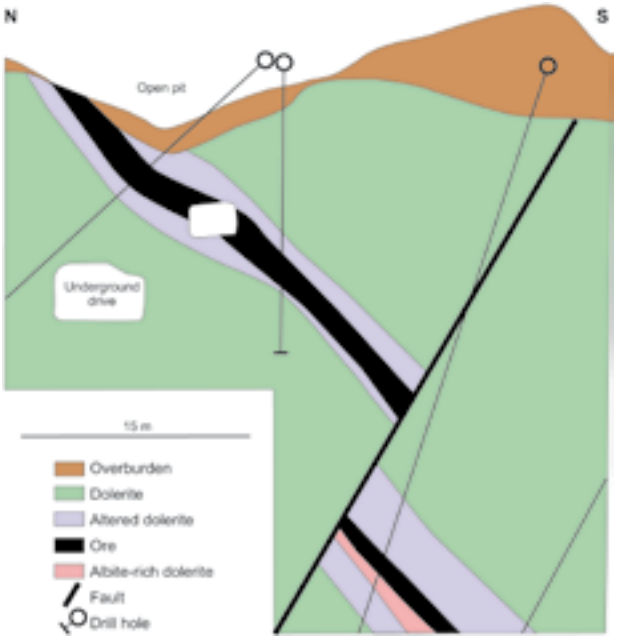

Fig. 28. Section across the Kivimaa Cu-Au deposit (Rouhunkoski & Isokangas 1974).

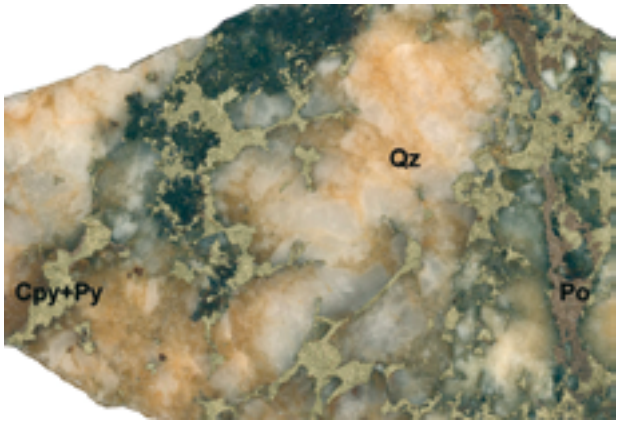

Fig. 29. Sample from the main gold- and copper-rich quartz vein from Vinsa. Quartz (Qz) – pyrite (Py) – chalcopyrite (Cpy) – pyrrhotite (Po) assemblage in the vein. The black domains are intensely altered host rock (dolerite). Field of view 9 cm. Imaging Jari Väätäinen.

when 18000 t of Au-Cu ore was mined (Rouhunkoski & Isokangas 1974). Other orogenic gold occurrences in the PSB include **Petäjävaara, Sivakkajoki** and **Vinsa** (Figs. 5 and 29) which in nearly all features are similar to Kivimaa (App. 4).

More than 30 individual ore bodies, with sizes from 0.04 to 1.0 Mt, comprise the **Vähäjoki** Fe-Cu-Co-Au occurrence (Fig. 30) in the SE part of the PSB (Korvuo 1982). The first lodes were discovered by ground-magnetic survey in 1943 (Laitakari 1943, 1944), and Vähäjoki was for a long time investigated essentially as an iron deposit. Only in early 1980's other metals were seriously evaluated and some of lodes we found to contain significant concentrations of gold, cobalt and copper (App. 4; Korvuo 1982).

The ore bodies at Vähäjoki comprise magnetite with gangue dominated by tremolite-actinolite, cummingtonite and hornblende (Liipo & Laajoki 1991), and are hosted by skarn-like rocks within dolomitic marble and mafic tuffite units of the ca. 2.14–2.0 Ga(?) Tikanmaa Formation (Perttunen 1989, Huhma et al. 1990). Structural control of the deposit is not well defined, but the ore bodies seem to be hosted by N- to NNE-trending shear zones within a major, N-trending fault zone. According to Liipo and Laajoki (1991), the peak metamorphic conditions at Vähäjoki were 400–500°C and 2–4 kbar.

All alteration detected at Vähäjoki is of local extent,

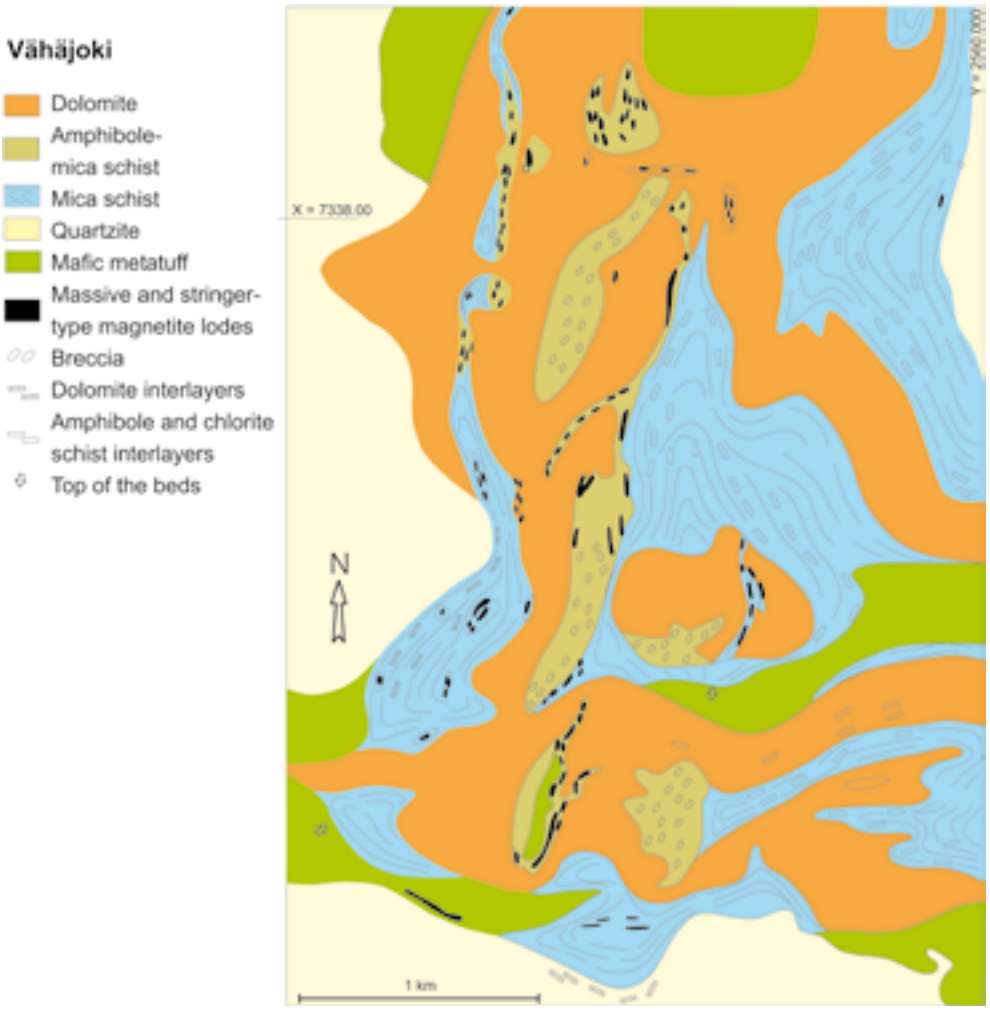

Fig. 30. Surface geology at Vähäjoki. The Au-Co-Cu mineralisation is hosted by the magnetite lodes. Coordinates according to Finnish National Grid, Zone 2, metric values. After Liipo and Laajoki (1991).

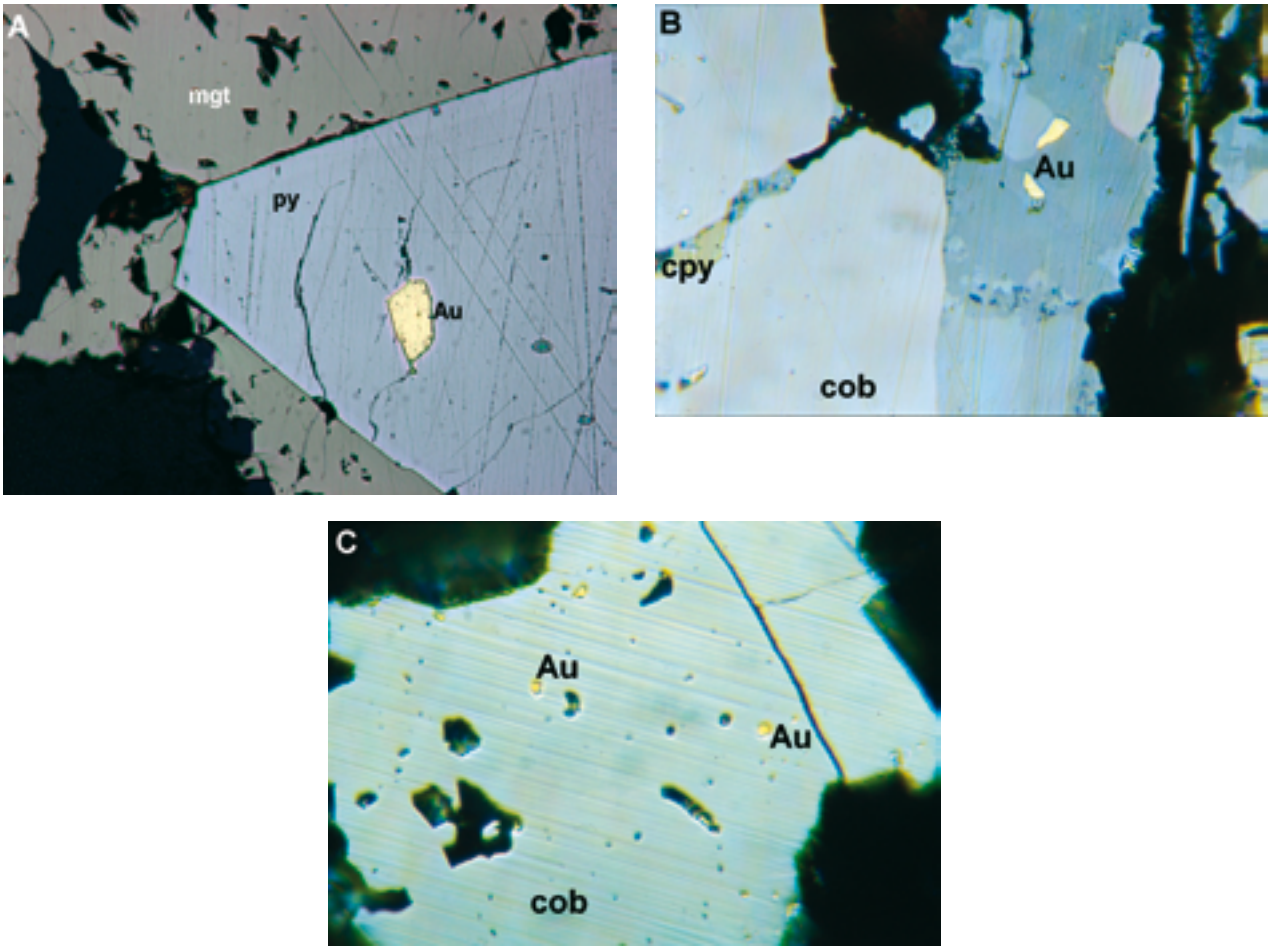

Fig. 31. Siting of native gold in the Vähäjoki IOCG occurrence. A) Gold in pyrite surrounded by magnetite. B) Gold (yellow) as inclusions in haematite; drill hole R42, 53 m down-hole depth. C) Gold (yellow) as inclusions in linneaite or cobaltite (pale grey). Field of view in all images 0.2 mm. Abbreviations: Au = gold, cob = cobaltite, cpy = chalcopyrite, haem = haematite, py = pyrite. All imaging by Tero Niiranen.

characterised by Ca-Fe±K metasomatism expressed by formation of magnetite, cummingtonite, tremolite, hornblende, biotite and chlorite. No extensive albitisation has been detected; only low-degree scapolitisation and albitisation has been observed in the rocks adjacent to the magnetite bodies (Niiranen & Eilu 2003).

Magnetite forms breccia matrix, veins, small blobs and larger masses in the country rocks at Vähäjoki (Vornanen 1963, Korvuo 1982). The main ore minerals are magnetite and pyrite with locally significant volumes of chalcopyrite and cobaltite. Ilmenite, haematite, arsenopyrite, sphalerite, galena, mackinawite, linneaite, bornite, marcasite, pyrrhotite, and native gold are present as minor to trace volumes (Vornanen 1963, Korvuo 1982). Native gold occurs as inclusions in cobaltite (chalcopyrite is common in the same inclusions), and locally associated with arsenopyrite, chalcopyrite, pyrite, haematite and quartz (Fig. 31) (Vornanen 1963, Korvuo 1982, T. Niiranen unpublished data). Ore mineral assemblages suggest that precipitation of the sulphides and gold postdate the formation of magnetite at Vähäjoki (Niiranen & Eilu 2003).

DISCUSSION

Three genetic types of gold mineralisation have been detected in the Palaeoproterozoic of northern Finland: orogenic, iron oxide-copper-gold (IOCG) and palaeoplacer. The orogenic type we have further divided into the normal (gold only) and the atypical metal association subtype. The latter term is from Groves et al. (2003); in northern Finland, we have included into that subtype those gold occurrences

where all significant features except the potential commodities are characteristic for a classic orogenic mineralisation (App. 1).

Certain features are common to all epigenetic gold occurrences in the Palaeoproterozoic greenstone belts of northern Finland: 1) Structure is regionally the most significant and locally one of the two significant controls of the siting of a gold occurrence: deposits and occurrences are hosted by fault or shear zones, intersections of these, and intersections of anticlines and faults. 2) Rock type, especially where competence is enhanced by pre-gold albitisation, is the other significant local control of mineralisation. 3) Mineralisation is related to Palaeoproterozoic orogenic evolution of the Lapland Domain of the Fennoscandian Shield during ca. 1.92–1.77 Ga. 4) Alteration related to mineralisation is intense. Albitisation and carbonatisation of variable degree are related to all occurrences, but the timing relationship between gold and albitisation and carbonatisation stages varies between the types of mineralisation and between individual deposits.

Orogenic gold

Host rocks

Sedimentary, volcanogenic sedimentary, and mafic to ultramafic volcanic rocks are the dominant hosts to orogenic gold in Central Lapland and Kuusamo (App. 2 and 3). In most cases, there is more than one host rock although, generally, one rock type is dominant. These features are typical for any Precambrian region in the world hosting orogenic gold deposits (Groves et al. 1998, McCuaig & Kerrich 1998, Goldfarb et al. 2001). In contrast to many other Precambrian shields (cf., McCuaig & Kerrich 1998), there is nearly a complete lack of banded iron formation-hosted deposits. A significant difference regarding the host rocks also occurs between CLGB and KSB: in the latter, sedimentary rocks dominate whereas mafic to ultramafic volcanic rocks and volcanogenic sedimentary rocks form the overwhelming majority in the former area (App. 2 and 3). A notable exception of the extensive variation in host rock type occurs in the Peräpohja schist belt where the orogenic gold occurrences are exclusively hosted by dolerite (App. 4).

The importance of different host-rock types reflects the general distribution and abundance of rock types in the greenstone belts of northern Finland: BIF is relatively uncommon, komatiites are more abundant in the CLGB than elsewhere, and metasedimentary units in Kuusamo are extensive and located in structurally favourable position for gold mineralisation (Vanhanen 2001). Another reason for increasing the share of metasedimentary rocks as hosts to gold is the extensive albitisation predating gold mineralisation in some areas in the CLGB and, especially, in the KSB (Pankka 1992, Grönholm 1999, Vanhanen 2001, Holma & Keinänen 2007). This albitisation is thought to have, at least in some cases, rendered the metasedimentary units more competent than other lithological units and, hence, mechanically favourable for localising mineralisation.

Ore mineralogy and metal association

A characteristic feature of orogenic gold deposits anywhere is that, in spite of enrichment of an extensive suite of elements, gold is usually the only metal present in economically significant amounts (Colvine et al. 1988, Goldfarb et al. 1997, Groves et al. 1998). Gold-only occurrences dominate in the CLGB, too (App. 2). Also the other components typically enriched in the gold deposits of northern Finland (especially, Ag, As, Bi, CO_2, K, Rb, S, Sb, Te, W) are the same as in orogenic gold deposits in other Precambrian terrains (App. 1).

Orogenic gold deposits with an atypical metal association (App. 1) occur in all greenstone belts in northern Finland. They contain economically recoverable Co, Cu, Ni or U concentrations. Other components enriched are roughly the same as for the gold-only subtype. Only in Kuusamo the situation is different, as also Fe, Mo and/or LREE are significantly enriched there. Other components abundant in the Finnish occurrences (App. 1–4) show enrichment in only locally and only to a low degree (Nurmi et al. 1991, Vanhanen 2001). Overall, the metal association of the atypical subtype in northern Finland is similar to the representatives of the subtype elsewhere in the Fennoscandian Shield (Ettner et al. 1994, Lindblom et al. 1996), other Proterozoic terrains (Boer et al. 1995, Rowins et al. 1997, Santos et al. 2001, Sener et al. 2005), and younger areas (Haeberlin et al. 2002, Zhang 2003) with Au-Cu being the most common commodity association (App. 1).

Ore mineral association in both subtypes is dominated by pyrite, pyrrhotite or arsenopyrite or a combination of these. Pyrite is the major Fe sulphide in the CLGB and PSB and pyrrhotite in the KSB. This difference may reflect PT conditions of mineralisation with pyrite being common in lower- to mid-greenschist facies and pyrrhotite in upper-greenschist facies de-

posits (Eilu et al. 1998). Alternatively, or in addition, it reflects variation in oxidation state and amount of sulphur available in the mineralising system.

The variation in the commodity association is reflected in the major ore minerals present (App. 2–4). Chalcopyrite is abundant in all Cu-enriched deposits, whereas the volume of other Cu minerals is insignificant. Cobalt minerals, notably cobaltite and cobaltian pentlandite, are among the main ore minerals in the Co-rich deposits in Kuusamo (Vanhanen 2001). In the CLGB, only cobaltite is significant in Co-rich and gersdorffite in Ni-rich deposits (Vesanto 1978, Holma & Keinänen 2007). In addition, uraninite is a significant ore mineral in some of the KSB deposits (Vanhanen 2001).

Among ore minerals present in minor to trace volumes, only native gold is significant for the economy of the deposits. Detailed mineralogical studies indicate that, although gold grains in many deposits occur intergrown with As minerals, gold is in most cases present in free-milling form (Nurmi et al. 1991, Korkiakoski 1992, Pankka 1992, Vanhanen 2001). Only in a few of the deposits, in Central Lapland, the gold-arsenopyrite association can be problematic. This is the case at Suurikuusikko where about 73 % of Au is in the crystal lattice of arsenopyrite and 23 % as inclusions in pyrite (Kojonen & Johansson 1999).

Metamorphism and structural style

Orogenic gold occurrences in northern Finland are hosted by rocks metamorphosed and altered at lower-greenschist to lower-amphibolite facies conditions (App. 2–4). The style of deformation varies from brittle through brittle-ductile to ductile with increasing PT conditions with the brittle-ductile style being the most common. Practically all deposits studied in detail show an elongated, plate-like, shape along the host structure (e.g., Grönholm 1999, Patison et al. 2007). The lodes within the mineralised shear or fault zones tend to form en echelon swarms and follow the dominant lineation within the structure, as exemplified by the Suurikuusikko deposit (Patison et al. 2007). All these features are typical for the majority of Precambrian greenstone belts (Anhaeusser and Maske 1986, Groves et al. 1998 and 2003, McCuaig & Kerrich 1998).

Alteration

Palaeoproterozoic greenstone belts of northern Fennoscandian Shield has been subject to several stages and styles of alteration. Those detected in and around orogenic gold occurrences can be divided into 1) syngenetic, 2) orogenic albitisation ± carbonatisation ± scapolitisation ('Na-Ca alteration'), and 3) syn-orogenic gold styles.

The **syngenetic styles** comprises synvolcanic spilitisation of volcanic rocks, diagenetic albitisation of feldspars in clastic sedimentary rocks and other supracrustal sequences, and albitisation and carbonatisation in the contact zones of the ca. 2.2 Ga metadolerites possibly soon after the intrusion of the dykes and sills in, at least, central parts of the CLGB and the KSB. Albitisation and carbonatisation took possibly place also in the contact zones of the ca. 2.10 Ga and 2.05 Ga dolerites in the region. The spilitic and diagenetic alteration styles have a regional character, and have been detected in throughout the greenstone belts in northern Finland (Perttunen 1989, Eilu 1994, Vanhanen 2001).

Partial to total **albitisation** with (or without) minor carbonatisation, surrounded by scapolitisation, characterises structures active during the ca. 1.84–1.80 Ga(?) orogenic stage of the evolution of the region (Sorjonen-Ward et al. 1992, 2003) especially in the CLGB and KSB and, also, the orogenic belts in northern Sweden and Norway. Alteration was extensive: domains of structurally controlled albitisation and scapolitisation extend for up to tens of kilometres along major structures (>100 km along the SSZ) and, laterally, kilometres away from them (Pankka & Vanhanen 1992, Ettner et al. 1994, Frietsch et al. 1997, Korvuo 1997b, Bergman et al. 2001, Vanhanen 2001). Pankka and Vanhanen (1992) and Vanhanen (2001) have interpreted the alteration to be a product of greenstone belt-scale, orogenic, hydrothermal circulation of magmatic and/or basinal brines. Timing of alteration is not well-constrained, however, and there are two main views on it: 1) it is coincident with the orogenic gold mineralisation and the peak-compressional deformation associated with the Svecofennian synorogenic plutonism of the accretional epoch (Ettner et al. 1994, Frietsch et al. 1997), or 2) it predates orogenic gold mineralisation (Ward et al. 1989, Hulkki 1990, Pankka 1992, Grönholm 1999, Vanhanen 2001). If the latter is correct, then the intense albitisation prepared ground for orogenic gold mineralisation near structurally favourable locations, such as along and around the Sirkka Shear Zone (Figs. 3, 6 and 8) and the central antiforms of the KSB (Fig. 4). Because the gold-mineralising fluids were of low-salinity, near neutral and H_2O-CO_2-rich (Korkiakoski 1992, Grönholm 1999) in many localities, it is unlikely that these fluids could have directly been responsible for the albitisation. Also the textural relationship between

albitisation- and gold-related mineral assemblages suggest that, at least in most cases, the extensive albitisation preceded gold mineralisation.

Style of **alteration directly related to orogenic gold** mineralisation and the relationship between alteration mineral assemblages and metamorphic grade are largely similar to those recorded in orogenic gold deposits in other parts of the world (App. 1) reflecting the low-salinity, neutral to slightly alkaline, H_2O-CO_2-dominated, mineralising fluid (cf., Groves et al. 1998, McCuaig & Kerrich 1998). Alteration includes sericitisation and carbonatisation at lower- to mid-greenschist facies, and biotitisation and carbonatisation in upper-greenschist to lower-amphibolite facies rocks (Korkiakoski 1992, Vanhanen 2001, Hulkki & Keinänen 2007). Also the low-degree sulphidation is a characteristic feature; typically the ores contain 1–5 % sulphides. The main exception to the typical orogenic-gold alteration is formed by the Fe-rich alteration assemblages in the Kuusamo deposits which are characterised by the formation of magnetite, and Fe-rich biotite and chlorite (Korteniemi 1993, Vanhanen 2001). The unusual alteration assemblages in Kuusamo reflect the Fe-enriched atypical metal association subtype of orogenic gold mineralisation and a saline fluid.

Structural and lithological control

Structural control is evident for the orogenic gold occurrences in northern Finland (App. 1). In the CLGB, the Sirkka Shear Zone (SSZ), a major, crustal-scale structure is located close to most of the gold occurrences (Fig. 3). Some occurrences, for example Hookana, Kaaresselkä and Pahtavaara, are in lower-order shear zones branching from the SSZ. In addition, there are occurrences in second-order(?), NNE- to NE-trending, fault zones obviously younger than the original formation of the SSZ, as the former structures also cut across the latter: Kuotko, and Rovaselkä, Ruoppapalo, Sukseton and Suurikuusikko. In Kuusamo, nearly all occurrences are located within two parallel, NE- to NW-trending, antiforms located in the central part of the greenstone belt (Fig. 4), at or near intersections between antiforms and cross-cutting faults (Pankka 1992, Vanhanen 2001). Little structural data is available from Peräpohja. Despite this, structural control is suggested also for the PSB occurrences: for example, there is a major, E-W trending, fault zone near three of the occurrences in the central part of the belt (Fig. 5). The structural control for gold mineralisation in northern Finland, for both the gold-only and the atypical metal association subtype, does not show any deviation from that detected for orogenic gold elsewhere (Groves et al. 1998, McCuaig and Kerrich 1998).

Lithological control is a significant local control for orogenic mineralisation in northern Finland. Competent rock types are the most favourable host rocks, particularly where they are chemically reactive. At Saattopora, where all lodes are in rocks that were pervasively albitised prior to gold mineralisation (Fig. 6), the pre-gold albitisation significantly increased the competency of the host tuffites and phyllites, providing pathways for the mineralising fluids where these units were brecciated (Grönholm 1999). Grönholm (1999) further suggests that precipitation of gold at Saattopora was induced by reduction-oxidation reactions between the mineralising, H_2O-CO_2-dominated, fluid and graphite in the albitised wallrock. Increased competency due to pre-gold albitisation has also been suggested for most of the Kuusamo deposits (Pankka & Vanhanen 1992, Vanhanen 2001). Reduction-oxidation reactions may also have been significant for precipitating gold in the originally graphite-rich rocks at Ruosselkä (E. Pulkkinen, unpublished data). Also favoured for mineralisation are the contact zones between chemically reactive rocks with a significant competency difference: the SSZ-related occurrences of Kutuvuoma, Levijärvi-Loukinen, Päivänenä, Pikku-Mustavaara, Saattopora, Sirkka kaivos, Sirkka W, Soretialehto and Tuongankuusikko (Fig. 3, App. 2) are all within a few metres of a contact zone between pervasively carbonated, hence competent, komatiitic metalava and plastic, graphitic, tuffite or phyllite.

Tectonic setting

The timing and the anomalous metal associations in orogenic gold occurrences in northern Finland requires special attention. These topics are closely related to the tectonic setting of the northern Fennoscandian Shield, as discussed below.

Anomalous metal associations

According to Goldfarb et al. (2001), where deformation of older, intracratonic basins are included into the processes of orogenic mineralisation, the ore fluids may become anomalously saline and produce base metal-rich orogenic gold deposits. Goldfarb et al. (2001) suggest this as an explanation for the formation of base metal-enriched gold deposits in the Sabie–Pilgrim's Rest in South Africa, and in Tennant Creek, Pine Creek and Telfer in Australia. Similar conditions may have produced many of the Au-Cu deposits in the

Tapajos–Parima orogenic belt, Amazon Craton (Santos et al. 2001) and Au ± Ag ± base metal deposits in the Pataz area in Peru (Haeberlin et al. 2002). Some of these deposits have been suggested to be genetically related to the local granitoids but recent, robust, age dating has shown that, for example in Pine Creek (Sener et al. 2005), the intrusions in question predate gold mineralisation by tens of millions of years. These data indicate that the local intrusions need not to have any part in the mineralising process when an epigenetic, base metal-enriched gold deposit is formed.

For the northern Fennoscandian Shield, the scenario by Goldfarb et al. (2001) appears as an attractive explanation for the polymetallic nature of many gold deposits whose timing, and P-T, structural and alteration features best fit with the orogenic type of mineralisation (App. 1). The northern part of the Fennoscandian Shield is characterised by Palaeoproterozoic rifted basins of intracratonic setting, extensive supracrustal sequence and probable evaporites. These sequences accumulated, compacted, were intruded by several stages of basaltic magma, and were subject to several alteration processes during the about 600 million years between the end of the Archaean and start of the Palaeoproterozoic orogenies at ca. 1.92 Ga (Vuollo et al. 1992, Eilu 1994, Huhma et al. 1996, Räsänen et al. 1996, Lehtonen et al. 1998, Vaasjoki 2001, Lahtinen et al. 2003). This means that there was an exceptionally wide range of rock types, structures, and fluid and metal sources to be subjected to the orogenic processes during 1.92–1.79 Ga. Shall an orogenic fluid meet such an sequence, it may well become more saline when meeting evaporites and/or connate brines and, hence, become able to leach, transport and precipitate both gold and base metals. No active part from the local intrusions are needed for, nor do we necessarily need local pre-orogenic enrichment for the base metals, as the brines would be able to leach metals from extensive volumes of the crust. On the other hand, in lack of evidence otherwise, we cannot completely reject the possibility that some of the base metals are derived from the local syngenetic base-metal occurrences.

Timing

Orogenic gold mineralisation takes place during terrane accretion, translation, or collision, which are related to plate subduction and/or lithospheric delamination. The mineralisation typically occurs in the latter part of the deformational and metamorphic history of an evolving orogen (Groves et al. 1998, 2003). Following the sequence of orogenies suggested by Lahtinen et al. (2003) for the Fennoscandian shield, and the ore-genetic definition above, two possible epochs for orogenic mineralisation can be suggested for the Palaeoproterozoic of northern Finland: microcontinent accretion at 1.92–1.88 Ga, and continent-continent collision at 1.85–1.79 Ga. Most of the age dating from the gold occurrences and their wallrocks suggest that mineralisation took places during the latter epoch. However, the age datings are not based on very robust direct methods but on indirect methods, chiefly sulphide Pb/Pb model ages with rare Pb/Pb whole-rock and monazite, U/Pb sulphide and U/Pb titanite ages from wallrocks (Mänttäri 1995, Rastas et al. 2001). This leaves us the possibility of, at least, some orogenic mineralisation during the 1.92–1.88 Ga, too.

Sorjonen-Ward et al. (1992, 2003) suggest the period 1.84–1.80 Ga as the probable age for orogenic gold in northern Finland. Their suggestion is based on metamorphic Ar/Ar mica and U/Pb titanite ages, timing of extensive late-orogenic granitoid magmatism and structural interpretations of the greenstone belts. This interpretation also suggests that most or all orogenic gold mineralisation is related to the 1.84–1.79 Ga collisional epoch of Lahtinen et al. (2003).

We can also try to set the timing by investigating the relationship between gold mineralisation and the main stages of deformation and regional metamorphism. Patison (2007) presents four main stages of deformation for the CLGB, and concludes that all or most of orogenic gold mineralisation took place during the D_3. The present knowledge of the timing of the D_3 is insufficient. All we know is that the D_3 took place after 1.89 Ga and before 1.77 Ga (Patison 2007). According Sorjonen-Ward et al. (2003), structurally controlled albitisation, which is pre- to syn-gold mineralisation, is associated with late-tectonic shear systems – this implies timing no earlier than 1.84–1.80 Ga for gold. On the other hand, the relationship between mineralisation and peak metamorphism seems not to be consistent throughout the northern Finland. Suurikuusikko, Kuotko, and many occurrences in the SSZ seem to be syn-peak or post-peak metamorphic, whereas mineral assemblages at Pahtavaara and some deposits in Kuusamo suggest slightly pre-peak metamorphic mineralisation (Korkiakoski 1992, Grönholm 1999, Vanhanen 2001, Holma & Keinänen 2007).

The evidence available gives the following scenario for the tectonic setting of orogenic gold mineralisation in northern Finland. Some mineralisation may have taken place during the peak or late stages of the microcontinent accretion epoch at 1.92–1.88 Ga. If this was the case, at least some of the shear zone-controlled albitisation also took place during this orogenic epoch.

Shear zone-controlled albitisation and scapolitisation may also relate to continental extension at 1.88–1.85 Ga, and/or the early to peak stages of the continent collision epoch at 1.85–1.79 Ga. In any case, most of orogenic mineralisation appears to be occurred during the peak deformation stage of the collisional epoch at 1.85–1.79 Ga. This would also mean that the age of the D_3 (Patison 2007) is between 1.85 and 1.79 Ga.

Both of the potential periods of orogenic mineralisation in northern Finland fit into one of the main global periods of orogenic gold mineralisation, at ca. 2.1–1.8 Ga, which occurred prior to the final Palaeoproterozoic cratonisation in all Precambrian cratons (Goldfarb et al. 2001). This indicates that orogenic mineralisation in Lapland may be related to a global-scale processes. In any case, more work, especially robust dating and investigations on mineralising fluids, is clearly needed for defining the timing and processes of gold mineralisation in northern Finland.

Iron oxide-Cu-Au (IOCG)

The most probable IOCG occurrences in Finland are the Kolari deposits in the westernmost CLGB and Vähäjoki in the PSB (Figs. 20–22 and 30). They have the following common features (App. 1, 2 and 4; Hiltunen 1982, Niiranen & Eilu 2003, Niiranen et al. 2007): 1) nearly all are hosted by epigenetic magnetite rock, 2) Cu-Au occurrences are in the central parts of the magnetite bodies, 3) main sulphide minerals are chalcopyrite, pyrite and pyrrhotite, 4) most of Au occurs as native gold associated with sulphides, 5) gangue is dominated by Ca amphibole, with significant diopside in Kolari, with minor albite and quartz, 5) components enriched are Ag, Au, Bi, Ca, CO_2, Cu, Fe, S, Te ± As, Ba, Cl, Co, K, LREE, Mo, Na, Pb, Rb, Sb, Se, U, 6) formation of the ironstone predates Cu-Au mineralisation, 7) multi-stage alteration, 8) formation in the P-T range of 400–600°C, 1.5–3.5 kbar, 9) structural control, 10) occur in orogenic belts that probably originally contained evaporites, and 11) the regions have experienced both extensive compression and extension. The main differences between the Kolari and PSB deposits are the extensive early albitisation and scapolitisation, highly saline fluids, and a close spatial (if not genetic) relationship with granitoids in Kolari, and the intense enrichment of As and Co in the PSB. In Kolari, the fluid inclusion data suggests that the mineralising fluids were highly saline (up to 56 % NaCl eq.) H_2O±CO_2 fluids (Niiranen et al. 2007).

All the features mentioned above fit into the extensive class of IOCG mineralisation originally defined by Hitzman et al. (1992) and further redefined by Barton and Johnson (1996), Hitzman et al. (2000), Marschink et al. (2000), and Partington and Williams (2000). Features considered typical for the IOCG category (e.g., Hitzman et al. 1992, Hitzman 2000), but missing in the Kolari and PSB deposits are the absence of F and P enrichment, and lack of sulphides with a high Cu/S ratio, such as bornite or chalcocite. At Vähäjoki, also missing from the typically diagnostic features are indications of highly saline fluids and extensive albitisation.

If the Kolari and Vähäjoki Fe-Cu-Au deposits belong to the IOCG category, they were formed during the post-accretion continental extension at 1.88–1.85 Ga, or during orogenic collapse and stabilisation at 1.80–1.77 Ga, or both. The extensional tectonic regime of both of these epochs fits into the mineralisation models of (Hitzman et al. 1992, Barton & Johnson 1996, Hitzman 2000). In Kolari, the ages of a partially mineralised pluton (1864±5 Ma) and cross-cutting granite dykes (1766±5 Ma) bracket the timing of mineralisation there. Work by Niiranen et al. (2007) further suggests that the most probable timing for the Kolari IOCG mineralisation is ca. 1.80 Ga. On the other hand, more than just one period of IOCG mineralisation in northern Finland is suggested by the presence of several stages of IOCG mineralisation in the nearby northern Sweden (Weihed & Eilu 2003).

Palaeoplacer gold

The sedimentary facies of the host rocks, and the shape of both the lodes and gold grains, strongly support the detrital, placer, origin of gold mineralisation in the Kumpu Formation of the CLGB. There are no indications of epigenetic gold. The placer mineralisation in the CLGB took place after ca. 1913 Ma and before about 1800 Ma, which are the earliest and the latest ages, respectively, for the deposition of the Kumpu Formation sediments (Härkönen 1984, 1986, Rastas et al. 2001).

It has been suggested that the palaeoplacer gold is derived from the underlying greenstones, especially from the numerous orogenic gold deposits (Fig. 3) and from small and low-grade, but even more numerous, syngenetic sulphide occurrences of the CLGB (Härkönen 1984, 1986). This is reasonable, considering the unconformity between the Kumpu Formation and the underlying, mineralised, greenstones.

The sequence hosting the palaeoplacer occurrences is metamorphosed and deformed during the late stages of orogenic evolution of the region, probably during both the D_3 and D_4, but does not show any signs of the D_1 or D_2 deformation (Lehtonen et al. 1998). If the D_1 and D_2 are related to the 1.92–1.88 Ga accretional epoch and the D_3 to the 1.84–1.78 Ga collisional

epoch, sedimentation and placer formation could be related to the continental extension during 1.88–1.85 Ga. Extensive erosion and clastic sedimentation in extensional conditions is expected for, making the 1.88–1.85 Ga timing probable for Palaeoproterozoic placer mineralisation in northern Finland. However, placer accumulation may well have continued during the early parts of the 1.85–1.79 Ga epoch, until the end of erosion and deposition of sediments derived from the possible mountains created by the collision in that time. This timing suggests that the placers may have deposited before the formation of all or majority of orogenic gold occurrences and implicates source for gold chiefly being the syngenetic base metal-dominated sulphide occurrences of the CLGB.

CONCLUSIONS

The genetic gold deposit categories detected in northern Finland include the orogenic, iron oxide-copper-gold (IOCG) and palaeoplacer type. The orogenic type can be further divided into the normal (gold only) and the atypical metal association subtype.

With a few exception, all features of the gold occurrences in northern Finland are similar to those detected in Palaeoproterozoic greenstone belts elsewhere in the world (App. 1). For all epigenetic occurrences in northern Finland, structure is the regionally most significant and locally one of the two significant controls, as all occurrences are in first- to low-order shear or fault zones, in intersections of these, or in or near to intersections between antiforms and cross-cutting fault and shear zones. Another significant local control for mineralisation is rock type. The mineralising fluid was aqueous in all cases, having a variable salinity and CO_2 content. The fluid compositions suggest variable, mixed origins for volatiles and metals with apparently no obvious local source.

When connected to the orogenic scheme of Lahtinen et al. (2003), the evolution of the Palaeoproterozoic greenstone belts and formation of gold deposits in northern Finland can be summarised as follows:

1. The Palaeoproterozoic evolution of the region during ca. 2.5–1.92 Ga is characterised by rifting of Archaean Karelian craton. Rifting took place in several stages and resulted in mafic intrusive and extrusive magmatism at ca. 2.45–2.39, 2.2, 2.10, and 2.05 Ga, and culminated in extensive mafic and ultramafic volcanism and the formation of oceanic crust at 1.97 Ga. Simultaneously, terrigenous clastic sedimentary units were deposited in the rifted basins. Also syngenetic alteration characterises the regional evolution in that time. Submarine synvolcanic spilitisation took place in volcanic rocks, and diagenetic albitisation of feldspars in clastic sedimentary rocks, throughout the supracrustal sequences. In addition, albitisation and carbonatisation took place in the contact zones of the ca. 2.2, 2.10 and 2.05 Ga dolerites apparently soon after the intrusion of the dykes and sills. No significant gold mineralisation has been detected to be taken place during the 2.5–1.92 Ga period.
2. Microcontinent accretion and extensive compressional deformation took place at ca. 1.92–1.88 Ga resulting in the amalgamation of the Archaean parts of the Fennoscandian shield. The epoch was characterised by the main deformational stages D_1 and D_2. It remains unclear whether the stage D_3 is related to the culmination of this epoch of crustal evolution, or is related to the 1.85–1.79 Ga epoch. Most evidence points towards the latter timing. Open questions also are: a) is part or all of the structurally controlled albitisation and scapolitisation (Na-Ca alteration), and b) formation of some of the orogenic gold occurrences during 1.92–1.88 Ga. Most, but not all, of the evidence is against the Na-Ca alteration and orogenic mineralisation being this early. It still remains a possibility that there has been structurally-controlled alteration and mineralisation in several stages in the region allowing for the accretion-related timing for the Na-Ca alteration and orogenic mineralisation in some parts of the greenstone belts.
3. Accretion was followed by continental extension during 1.88–1.85 Ga. This is one of the two most probable timings for extensive structurally-controlled albitisation and scapolitisation (Na-Ca alteration). This implies circulation of hydrothermal fluids in scales of tens of kilometres across the greenstone belts during the epoch. Possibly also the iron-oxide-copper-gold (IOCG) deposits in Kolari and Peräpohja were formed then. In any case, the deposits postdate the regional-scale Na-Ca alteration. In Kolari, the ca. 1.86 Ga age for an IOCG-mineralised pluton further restricts the maximum age for IOCG mineralisation there. Structural evidence and the extensional tectonic style also suggests that some or all of the gold palaeoplacers were formed during the epoch.
4. The second major compressional stage was a continent-continent collision epoch at ca. 1.85–1.79 Ga. Most of the age dating and structural evidence

indicates that the brittle-ductile D_3 and most or all of orogenic gold mineralisation and, hence, crustal-scale hydrothermal circulation of the mineralising H_2O-CO_2 fluids, is related to this orogenic epoch. This also is another of the two most probable timings for the structurally-controlled albitisation and scapolitisation. Some or all of the palaeoplacer mineralisation occurred in the pre-D_3 part of the epoch.

5. An orogenic collapse and stabilisation epoch took place during 1.80–1.77 Ga. As this was an extensional epoch, it also could have been a period of IOCG mineralisation in northern Finland, as also is supported by the age data from the Kolari IOCG deposits.
6. The entirely brittle D_4 is contemporaneous with or slightly post-dates the post-orogenic, 1.77 Ga, Nattanen-type granitoid magmatism. The D_4 also post-dates all gold mineralisation and the alteration stages described above.

The variation in metal association in orogenic gold occurrences possibly reflects variation in the environment of the hydrothermal system. The occurrences with an atypical metal association (Au ± Cu ± Co ± LREE ± Ni ± U) were probably formed as a result of the complex geologic and tectonic setting of northern Finland. The region is characterised by Palaeoproterozoic rifted basins of intracratonic setting, extensive supracrustal sequence and probable evaporites. These sequences accumulated, compacted, were intruded by magmas, and were subject to several major stages of alteration predating gold mineralisation. Hence, there was an exceptionally wide range of rock types, structures, and fluid and metal sources to be subjected to the orogenic processes. When an orogenic fluid met such an sequence, during 1.92–1.88 and/or 1.85–1.79 Ga, it became more saline when meeting the possible evaporites and connate brines, became able to leach and transport both gold and base metals. Eventually, the metals were precipitated when the brines met structural and chemical traps in the greenstone belts. On the other hand, where the fluids did not become saline, gold-only occurrences were formed.

From the work done so far, more gold deposits can be expected to be discovered in northern Finland. The areas of greatest potential for the discovery of new orogenic and IOCG deposits probably are the Central Lapland and Kuusamo belts. The real potential of the Peräpohja belt is difficult to assess, because not enough exploration has been done in the area, but indications for more gold deposits to be discovered are good also for that region. Also, it is obvious that more work, especially robust dating and investigations on mineralising fluids, is needed for defining the timing and processes of gold mineralisation in northern Finland. This would also significantly help in more precisely defining future exploration targets.

ACKNOWLEDGEMENTS

Many of figures in this paper were drawn into their final format by Viena Arvola, Pirkko Kurki, Vesa Nykänen and Heikki Salmirinne. Nicole Patison is acknowledged of a number of comments on an the early version of manuscript. Noreen Vielreicher is thanked for a thorough review of entire the manuscript. Editorial help by Juhani Ojala has been important throughout the process of writing the text and producing the figures.

REFERENCES

Alapieti, T.T. & Lahtinen, J.J. 1989. Early Proterozoic layered intrusions in the northeastern part of the Fennoscandian Shield. In: Alapieti, T.T. (ed.) 5th International Platinum Symposium. Guide to the Post-Symposium Field Trip, August 4–11, 1989. Geological Survey of Finland, Guide 29, 3–41.

Anhaeusser, C.R. & Maske, S. 1986. Mineral Deposits of Southern Africa. Geological Society of South Africa. 1314 p.

Anttonen, R. 1994. Kaivoslain 19 pyk. mukainen tutkimustyöselostus: Kittilä, Jerusaleminjänkä, kaiv. rek. n:o 4844/1, ja Jerusaleminjänkä 2, kaiv. rek. n:o 5030/1 (Exploration report: Kittilä, Jerusaleminjänkä, Mine Reg. no. 4844/1, and Jerusaleminjänkä 2, Mine Reg. no. 5030/1). Outokumpu Oy, Report 080/2734 05/RSA/94. (in Finnish)

Anttonen, R. 1995. Tutkimukset Kittilän Kutuvuomassa 1993–1995 (Report on exploration at Kutuvuoma, Kittilä, in 1993–1995). Outokumpu Oy Finnmines, Report 001/371112/RSA/95. 5 p. (in Finnish)

Äyräs, M. 1991. Geochemical prospecting at Vinsanmaa, northern Finland. Journal of Geochemical Exploration 39, 379–386.

Baker, T. & Laing, W.P. 1998. Eloise Cu-Au deposit, East Mt Isa Block: structural environment and structural controls on ore. Australian Journal of Earth Sciences 45, 429–444.

Barton, M.D. & Johnson, D.A. 1996. An evaporitic-source model for igneous-related Fe oxide(-REE-Cu-Au-U) mineralization. Geology 24, 259–262.

Bergman, S., Kübler, L. & Martinsson, O. 2001. Description of regional geological and geophysical maps of northern Norrbotten County (east of the Caledonian orogen). Sveriges Geologiska Undersökning Ba 56. 109 p.

Berthelsen, A & Marker, M. 1986. 1.9–1.8 Ga old strike-slip

megashears in the Baltic Shield, and their plate tectonic implications. Tectonophysics 128, 163–181.

Boer, R.H., Meyer, F.M., Robb, L.J., Graney, J.R., Vennemann, T.W. & Kessler, S.S. 1995. Mesothermal-type mineralization in the Sabie–Pilgrim's Rest Gold Field, South Africa. Economic Geology 90, 860–876.

Boulton, G.S. 1984. Development of a theoretical model of sediment dispersal by ice sheets. In: Prospecting in Glaciated Terrain. The Institution of Mining and Metallurgy, London. 213–223.

Colvine, A.C., Fyon, J.A., Heather, K.B., Marmont, S., Smith, P.M. & Troop, D.G. 1988. Archean lode gold deposits in Ontario, Canada. Ontario Geological Survey Miscellaneous Paper 139. 136 p.

Deer, W.A., Howie, R.A. & Zussman, J. 2001. Rock-forming minerals – 2nd edition. Vol. 4A: Frame-work silicates: feldspars. Geological Society, London. 972 p.

Dragon Mining NL 2004. Annual Report 2003. Perth, Australia. 46 p.

Dragon Mining NL 2005. Annual Report 2004. Perth. 80 p. online: www.dragon-mining.com.au/pdf/Dragon2004Annual.pdf

Eilu, P. 1994. Hydrothermal alteration in volcano-sedimentary associations in Central Lapland greenstone belt. Geological Survey of Finland, Bulletin 374. 145 p.

Eilu, P. 1997. Orogenic lode-gold deposits: Notes to accompany samples from deposits located on the Fennoscandian Shield. University of Turku, Department of Geology and Mineralogy, Publication 35, 1st edition. 14 p.

Eilu, P. 1999. FINGOLD – a public database on gold deposits in Finland: Geological Survey of Finland, Report of Investigation 146. 224 p.

Eilu, P., Mathison, C.I., Groves, D.I. & Allardyce, W. 1998. Atlas of Alteration Assemblages, Styles and Zoning in Orogenic Lode-Gold Deposits in a Variety of Host Rock and Metamorphic Settings. Geology Department & University Extension, The University of Western Australia, Publication 30. 64 p.

Ettner, D.C., Björlykke, A. & Andersen, T. 1994. Fluid evolution and Au-Cu genesis along a shear zone: a regional fluid inclusion study of shear zone-hosted alteration and gold and copper mineralization in the Kautokeino greenstone belt, Finnmark, Norway. Mineralium Deposita 29, 16–29.

Ferenczi, P.A. & Ahmad, M. 1998. Geology and mineral deposits of the Granites-Tanami and Tennant Creek Inliers, Northern Territory. AGSO Journal of Australian Geology & Geophysics 17, 19–33.

Frietsch, R., Tuisku, P., Martinsson, O. & Perdahl, J-A. 1997. Early Proterozoic Cu-(Au) and Fe ore deposits associated with regional Na-Cl metasomatism in northern Fennoscandia: Ore Geology Reviews 12, 1–34.

Gaál, G. 1990. Tectonic styles of Early Proterozoic ore deposition in the Fennoscandian Shield: Precambrian Research 46, 83–114.

Goldfarb, R.J., Miller, M.L., Leach, D.L. & Snee, L.W. 1997. Gold deposits in metamorphic rocks of Alaska. In: Goldfarb, R.J. & Miller, M.L. (eds.) Mineral Deposits of Alaska. Economic Geology Monograph 9, 151–190.

Goldfarb, R.J., Groves, D.I. & Gardoll, S. 2001. Orogenic gold and geologic time: a global synthesis. Ore Geology Reviews 18, 1–75.

Grönholm, P. 1999. The mesothermal Saattopora copper-gold deposit in the Palaeoproterozoic Central Lapland greenstone belt, Northern Finland. In: Cook, N.J. & Sundblad, K. (eds.) Precambrian gold in the Fennoscandian and Ukrainian Shields and related areas. Gold '99 Trondheim, Norway, 4–6 May 1999. Geological Survey of Norway, Trondheim, p. 83.

Groves, D.I., Goldfarb, R.J., Gebre-Mariam, M., Hagemann, S. & Robert, F. 1998. Orogenic gold deposits: A proposed classification in the context of their crustal distribution and relationship to other gold deposit types. Ore Geology Reviews 13, 7–27.

Groves, D.I., Goldfarb, R.J., Robert, F. & Hart, C.J.R. 2003. Gold deposits in metamorphic belts: overview of current understanding, outstanding problems, future research, and exploration significance. Economic Geology 98, 1–30.

Haeberlin, Y., Moritz, R. & Fontbote, L. 2002. Paleozoic orogenic gold deposits in the Central Andes and its foreland, South America. Ore Geol. Rev. 22, 41–59.

Hagemann, S.G. & Cassidy, K.F. 2000. Archean orogenic lode gold deposits. In Hagemann, S.G. & Brown, P.E. (eds.) 2000. Gold in 2000. Reviews in Economic Geology 13, 9–68.

Hänninen, E. 1977. Kittilän Sirkan malmityypeistä (Types of mineralisation at Sirkka). Outokumpu Oy, Report 070/2741 10B/EH/77. (in Finnish)

Hanski, E., Perttunen, V. & Sorjonen-Ward, P. 1997. Overview of the geology of northern Finland. Geologian tutkimuskeskus, Opas – Geological Survey of Finland, Guide 43, 7–-9.

Härkönen, I. 1984. The gold-bearing conglomerates of Kaarestunturi, Central Finnish Lapland. In: R.P. Foster (ed.) Gold '82; the Geology, Geochemistry and Genesis of Gold Deposits. Geological Society of Zimbabwe, Special Publication 1, 239–247.

Härkönen, I. 1986. Gold in the Proterozoic conglomerates of Finnish Lapland. Terra Cognita 6, 538.

Härkönen, I. 1988. Tutkimustyöselostus Kittilän kunnassa valtausalueella Outapää 1, kaiv. rek. n:o 3529/1 suoritetuista malmitutkimuksista (Exploration report: Kittilä, Outapää 1, Mine Reg. no. 3529/1). Geological Survey of Finland, Report M06/3712/-88/2/10. 3 p. (in Finnish)

Härkönen, I. 1992. Tutkimustyöselostus Kittilän kunnassa valtausalueella Suurikuusikko 1, kaiv.rek. n:o 4283/1 suoritetuista malmitutkimuksista (Exploration report: Kittilä, Suurikuusikko 1, Mine Reg. no. 4283/1). Geological Survey of Finland, Report M06/2743/-92/1/10. 5 p. (in Finnish)

Härkönen, I. 1994. Tutkimustyöselostus Kittilän kunnassa valtausalueilla Kuotko 3, kaiv.rek. n:o 4319, Kuotko 4, kaiv. rek. n:o 4333/1, ja Kuotko 5, kaiv.rek. n:o 4333/2, suoritetuista malmitutkimuksista (Exploration report: Kittilä, Kuotko 3–5, Mine Reg. no. 4319, 4333/1–2). Geological Survey of Finland, Report M06/2743/ -95/1/10. 5 p. (in Finnish)

Härkönen, I. 1997. Tutkimustyöselostus Kittilän kunnassa valtausalueilla Suurikuusikko 2 ja Rouravaara 1–10 (kaivosrekisterinumerot 5965/1, 6160/1, 6288/1–6288/9) suoritetuista kultatutkimuksista vuosina 1987–1997. English summary: Gold exploration during 1987–1997 within the exploration claims Suurikuusikko 2 and Rouravaara 1–10 (Mine reg. nos. 5965/1, 6160/1, 6288/1–6288/9). Geological Survey of Finland, Report M 06/2743/97/1. 47 p.

Härkönen, I. & Keinänen, V. 1989. Exploration of structurally controlled gold deposits in the Central Lapland greenstone belt. Geological Survey of Finland, Special Paper 10, 79–82.

Härkönen, I., Pankka, H. & Keinänen, V. 2001. Summary report. The Iso-Kuotko gold prospects, Kittilä, Finnish Lapland. http://en.gtk.fi/ExplorationFinland/Tender/iso_kuotko/iso-kuotko.htm

Hedenquist, J.W., Izawa, E., Arribas, A. & White, N.C. 1996. Epithermal gold deposits: Styles, characteristics, and exploration. Resource Geology Special Publication 1. 16 p.

Hiltunen, A. 1982. The Precambrian geology and skarn iron ores of the Rautuvaara area, northern Finland: Geological Survey of Finland, Bulletin 318. 133 p.

Hiltunen, A. 1989. Report on exploration at Lauttaselkä. Rautaruukki Oy, Report 21.12.1989. 2 p. (in Finnish)

Hirvas, H., Alfthan, A., Pulkkinen, E., Puranen, R & Tynni, R. 1977. Raportti malminetsintää palvelevasta maaperätutkimuk-

sesta Pohjois-Suomessa vuosina 1972–1976. Summary: A report on glacial drift investigations for ore prospecting purposes in northern Finland 1972–1976. Geological Survey of Finland, Report of Investigation 19. 54 p.

Hitzman, M.W., Oreskes, N. & Einaudi, M.T. 1992. Geological characteristics and tectonic setting of Proterozoic iron oxide (Cu-U-Au-REE) deposits. Precambrian Research 58, 241–287.

Hitzman, M.W. 2000. Iron oxide-Cu-Au deposits: what, where, when, and why. In: Porter, T.M. (ed.) Hydrothermal Iron Oxide Copper-Gold & Related Deposits: A Global Perspective. Australian Mineral Foundation, Adelaide. 9–25.

Holma, M. & Keinänen, V. 2007. The Levijärvi-Loukinen gold occurrence: An example of orogenic gold mineralisation with atypical metal association. Geological Survey of Finland, Special Paper 44, 165–186.

Hölttä, P. & Karhu, J. 2001. Oxygen and carbon isotope compositions of carbonates in the alteration zones of orogenic gold deposits in central Finnish Lapland. In: Autio, S. (ed.) Geological Survey of Finland, Current Research 1999-2000. Geological Survey of Finland. Special Paper 31, 25–29.

Hölttä, P., Väisänen, M., Väänänen,j. & Manninen, T. 2007. Paleoproterozoic metamorphism and deformation in Central Finnish Lapland. Geological Survey of Finland, Special Paper 44, 9−44.

Hugg, R. 1987a. Kaivoslain 19 pyk. mukainen tutkimustyöselostus: Kittilä, Lammasvuoma 1, Lammasvuoma 2 ja Lammasvuoma 3, kaiv. rek. n:o 4576/1, 4627/1 ja 4765/1 (Exploration report: Kittilä, Lammasvuoma 1, Lammasvuoma 2 and Lammasvuoma 3, Mine Reg. nos. 4576/1, 4627/1 and 4765/1). Outokumpu Oy, Report. 2 p. (in Finnish)

Hugg, R. 1987b. Kaivoslain 19 pyk. mukainen tutkimustyöselostus: Kittilä, Sirkka, kaiv. rek. n:o 3912/1. (Exploration report: Kittilä, Sirkka, Mine Reg. no. 3912/1). Outokumpu Oy, Report 080/2741 10/REH/1987. 2 p. (in Finnish)

Hugg, R. 1991. Kaivoslain 19§:n mukainen tutkimustyöselostus; Päivänenä kaiv.rek.nro 3750/2 (Exploration report: Päivänenä Mine Reg. no. 3750/2). Outokumpu Oy Finnmines, Report 080/2743 01/REH/91. 1 p. (in Finnish)

Huhma, H. 1986. Sm-Nd, U-Pb and Pb-Pb isotopic evidence for the origin of the Early Proterozoic Svecokarelian crust in Finland. Geological Survey of Finland, Bulletin 337. 48 p.

Huhma, H., Cliff, R.A., Perttunen, V. & Sakko, M. 1990. Sm-Nd and Pb isotopic study of mafic rocks associated with early Proterozoic continental rifting: the Peräpohja schist belt in northern Finland. Contributions to Mineralogy and Petrology 104, 369–379.

Huhma, H., Mutanen, T., Hanski, E., Räsänen, J., Manninen, T., Lehtonen, M., Rastas, P. & Juopperi, H. 1996. Isotopic evidence for contrasting sources of the prolonged Palaeoproterozoic mafic-ultramafic magmatism in Central Finnish Lapland, in Papunen, H., ed., IGCP Project 336 Symposium in Rovaniemi, Finland, August 21–23, 1996: program and abstracts: University of Turku, Department of Geology, Publication 38. p. 17.

Hulkki, H. 1990. Sodankylän Sattasvaaran komatiittikompleksin Au-kriittinen muuttumisvyöhyke (The Au-enriched alteration domain in the Sattasvaara Komatiite Complex in Sodankylä). Unpublished MSc thesis. Department of Geology, University of Helsinki. 190 p. (in Finnish)

Hulkki, H. 2002a. Tutkimustyöselostus Kittilän kunnassa, valtausalueella Mantovaara 1, kaiv.rek.n:o 5637/1 suoritetuista malmitutkimuksista. English summary: Exploration report covering the claim area Mantovaara 1, Mine Reg. 5637/1 in the municipality of Kittilä. Geological Survey of Finland, Report M 06/2743/2002/1/10. 7 p.

Hulkki, H. 2002b. Tutkimustyöselostus Kittilän kunnassa, valtausalueilla Palolaki 1-3, kaiv.rek.n:o 5623/1-3 ja Sinoselkä 1-2, kaiv.rek.n:o 5631/1-2 suoritetuista malmitutkimuksista. English summary: Exploration report covering the claim areas Palolaki 1-, Mine reg. no. 5623/1-3, and Sinoselkä 1-2, Mine Reg. no. 5631/1-2, in the municipality of Kittilä. Geological Survey of Finland, Report M 06/3721/2002/1/10. 8 p.

Hulkki, H. & Keinänen, V. 2007. The alteration and fluid inclusion characteristics of the Hirvilavanmaa gold deposit, Central Lapland Greenstone Belt, Finland. Geological Survey of Finland, Special Paper 44, 137–153.

Hulkki, H. & Pulkkinen, E. 2007. Exploration history of the Kaaresselkä gold-copper occurrence, Central Lapland. Geological Survey of Finland, Special Paper 44, 155–164.

Inkinen, O. 1985. Kittilän Sirkan kulta-kupariesiintymästä. Summary: Gold-copper occurrence at Sirkka, Kittilä. Geologi 37, 8–11.

Inkinen, O. 1987. Kaivoslain 19 pyk. mukainen tutkimustyöselostus: Lavasuo, Kuusamo (Exploration report: Kuusamo, Lavasuo). Outokumpu Oy, Report 080/4611 12/OI/87. 1 p. (in Finnish)

Inkinen, O. 1991. Kaivoslain 19 pyk. mukainen tutkimustyöselostus: Kittilä, Hanhilampi 1, Hanhilampi 2 ja Hanhilampi 3, kaiv. rek. n:o 4481/1, 4481/2 ja 4516/1 (Exploration report: Kittilä, Hanhilampi 1, Hanhilampi 2 and Hanhilampi 3, Mine Reg. nos. 4481/1, 4481/2 ja 4516/1). Outokumpu Oy, Report 080/2732/OI/91. 2 p. (in Finnish)

Inkinen, O. 1992a. Kaivoslain 19 pyk. mukainen tutkimustyöselostus: Kittilä, Tuongankuusikko, kaiv. rek. n:o 4570/1 (Exploration report: Kittilä, Tuongankuusikko, Mine Reg. no. 4570/1). Outokumpu Oy, Report 080/3712/OI/92. 2 p. (in Finnish)

Inkinen, O. 1992b. Kaivoslain 19 pyk. mukainen tutkimustyöselostus: Sodankylä, Koppelonkangas, kaiv. rek. n:o 4440/1 (Exploration report: Sodankylä, Koppelonkangas, Mine Reg. no. 4440/1). Outokumpu Oy, Report 080/3712/OI/92. 1 p. (in Finnish)

Keinänen, V. 1990. Tutkimustyöselostus Kittilän kunnassa valtausalueella Pikku-Mustavaara (Kaivosrekisterinumero 4296/1) suoritetuista kupari- ja kultatutkimuksista vuosina 1987–89 (Report on copper and gold exploration at Pikku-Mustavaara, Kittilä, (Mine Reg. no. 4296/1) during 1987–89). Geological Survey of Finland, Report M06/2734/-90/1/10. 2 p. (in Finnish)

Keinänen, V. 1995. Tutkimustyöselostus Kolarin kunnassa valtausalueella Kuervitikko 1 (Kaivosrekisterinumero 5082/1) suoritetuista kulta-kuparimalmitutkimuksista vuosina 1992–93 (Report on copper and gold exploration at Kuervitikko 1 (Mine Reg. no. 5082/1), Kolari, during 1992–93). Geological Survey of Finland, Report M06/2714/-95/1/10. 2 p. (in Finnish)

Keinänen, V. 1996. Tutkimustyöselostus Muonion kunnassa valtausalueella Äkäsaivo 1 (Kaivosrekisterinumero 4795/1) suoritetuista tutkimuksista vuosina 1990–92 (Report on exploration at Äkäsaivo 1 (Mine Reg. no. 4795/1), Muonio, during 1990–92). Geological Survey of Finland, Report M06/2732/96/1/10. 3 p. (in Finnish)

Keinänen, V. 1997. Tutkimustyöselostus Kittilän kunnassa valtausalueella Soretiavuoma 3 (kaiv.rn:o 5290/1) suoritetuista malmitutkimuksista (Report on exploration at Soretiavuoma 3 (Mine Reg. no. 5290/1), Kittilä). Geological Survey of Finland, Rreport M06/2734/-97/1/10. 8 p. (in Finnish)

Keinänen, V. 2002. Report on mineral exploration carried out in Kittilä Parish on Exploration Claims Naakenavaara 1, Mine Register no. 5522/1, Naakenavaara 2, Mine Register no. 5522/2, Naakenavaara 3, Mine Register no. 6089/1, Naakenavaara 4 and 5, Mine Register nos. 6159/1 and 2, Naakenavuoma 1 and 2, Mine Register nos. 6089/1 and 2, Putaanperä 1, Mine Register no. 5686/1. Geological Survey of Finland, Report M06/2734/2002/1/10. 6 p. (in Finnish, with English summary)

Keinänen, V. & Hulkki, H. 1992. Main features of the three geochemically different gold mineralizations in Soretiavuoma, Finnish Lapland. 20:e Nordiska Geologiska Vintermötet, Reykjavik. Abstracts. p. 96.

Kojonen, K. & Johanson, B. 1988. Pahtavaaran Au-malmiaiheen malmimineraaleista (Ore minerals in the Pahtavuoma deposit). Geological Survey of Finland, Report M40/3714/-88/1/41.2. 2 p. (in Finnish)

Kojonen, K. & Johanson, B. 1999. Determination of refractory gold distribution by microanalysis, diagnostic leaching and image analysis. Mineralogy and Petrology 67, 1–19.

Koljonen, T. (ed.) 1992. The Geochemical Atlas of Finland, Part 2. Geological Survey of Finland, Espoo. 218 p.

Kontas, E. 1981. Rapid determination of gold by flameless atom absorption spectrometry in the ppb and ppm ranges without organic solvent extraction: Atomic Spectroscopy 2, 59–61.

Kontinen, A. 1987. An early Proterozoic ophiolite – the Jormua mafic-ultramafic complex, northeastern Finland. Precambrian Research 35, 313–341.

Korkiakoski, E. 1992. Geology and geochemistry of the metakomatiite-hosted Pahtavaara gold deposit in Sodankylä, northern Finland, with emphasis on hydrothermal alteration. Geological Survey of Finland, Bulletin 360. 96 p.

Korkiakoski, E. & Kilpelä, M. 1997. The komatiite-hosted Pahtavaara gold mine near Sodankylä, northern Finland. In: Korkiakoski, E. & Sorjonen-Ward, P. (eds.) Ore deposits of Lapland in northern Finland and Sweden: Geological Survey of Finland, Guide 43, 27–29.

Korteniemi, J. 1993. Kultaesiintymien ympäristön hydroterminen muuttuminen Käylän alueella Kuusamossa (Hydrothermal alteration around gold occurrences in the Käylä region, Kuusamo). Unpublished MSc thesis. Department of Geology, University of Turku. 90 p. (in Finnish)

Korvuo, E. 1982. Vähäjoen rautamalmialueen tutkimukset 1979–1982 (Exploration in the Vähäjoki iron ore camp in 1979–1982). Lapin Malmi Oy, Report. 49 p. (in Finnish)

Korvuo, E. 1997a. Kaivoslain 19§:n mukainen tutkimustyöselostus valtausalue Harrilommol 1, kaiv.rek.nro 4519/1 (Exploration report: Harrilommol 1, Mine Reg. no. 4519/1). Outokumpu Oy, Report 080/2741/EK/91. 3 p. (in Finnish)

Korvuo, E. 1997b. The Saattopora gold ore and the Pahtavuoma Cu-Zn-U occurrences in the Kittilä region, northern Finland. In: E. Korkiakoski and P. Sorjonen-Ward (eds.) Ore deposits of Lapland in northern Finland and Sweden: Geological Survey of Finland, Guide 43, 21–25.

Lahtinen, R., Korja, A. & Nironen, M. 2003. Paleoproterozoic orogenic evolution of the Fennoscandian Shield at 1.92–1.77 Ga with notes on the metallogeny of FeOx-Cu-Au, VMS, and orogenic gold deposits. In: D.G. Eliopoulos et al. (eds) Mineral Exploration and Sustainable Development. Proceedings of the Seventh Biennial SGA Meeting, Athens, Greece, 24-28. August 2003. Millpress, Rotterdam. 1057–1060.

Laitakari, A. 1943. Geologisen toimikunnan muistio Tervolan Vähäjoen rautamalmilöydöistä (Memoir on the discovery of the Vähäjoki iron deposit in Tervola). Geological Survey of Finland, Report Dc N:o 33. 2 p. (in Finnish)

Laitakari, A. 1944. Selostus Tervolan Vähäjoen rautamalmialueella vuosina 1943 ja 1944 suoritettujen tutkimusten tuloksista (Report on exploration during 1943–1944 in the Vähäjoki iron ore area in Tervola). Geological Survey of Finland, Report Dc N:o 34. 7 p. (in Finnish)

Lanne, E. 1979. Vuotoksen ja Kittilän alueiden geofysikaalisten tietojen tulkinnasta. Summary: On the interpretation of geophysical data from the Vuotos and Kittilä areas, northern Finland. Geological Survey of Finland, Report of Investigation 25. 38 p.

Lehtinen, M. 1987. Kittilän tutkimusalue: Sirkka. In: H. Papunen (ed.) Lapin vulkaniittien tutkimusprojekti. (The Kittilä study area: Sirkka. Final Report of the Lapland Volcanite Research Project). Department of Geology, University of Turku, Report. 85–96. (in Finnish)

Lehtinen, M. & Eilu, P. 1987. Diabaaseihin liittyvät malmiaiheet: Kivimaa. In: H. Papunen (ed.) Lapin vulkaniittien tutkimusprojekti. Loppuraportti. (Prospects related to dolerites: Kivimaa. Final Report of the Lapland Volcanite Research Project). Department of Geology, University of Turku, Report. 346–352. (in Finnish)

Lehtonen, M. I., Airo, M-L., Eilu, P., Hanski, E., Kortelainen, V., Lanne, E., Manninen, T., Rastas, P., Räsänen, J. & Virransalo, P. 1998. Kittilän vihreäkivialueen geologia. Lapin vulkaniittiprojektin raportti. Summary: The stratigraphy, petrology and geochemistry of the Kittilä greenstone area, northern Finland. A report of the Lapland Volcanite Project. Geological Survey of Finland, Report of Investigation 140. 144 p.

Liipo, J. & Laajoki, K. 1991. Mineralogy, geochemistry and metamorphism of the early Proterozoic Vähäjoki iron ores, northern Finland. Geological Society of Finland, Bulletin 63, 69–85.

Lindblom, S., Broman, C. & Martinsson, O. 1996. Magmatic-hydrothermal fluids in the Pahtohavare Cu-Au deposit in greenstone at Kiruna, Sweden. Mineralium Deposita 31, 307–318.

Manninen. T., Pihlaja, P. & Huhma, H. 2001. U-Pb geochronology of the Peurasuvanto area, northern Finland. Geological Survey of Finland, Special Paper 33, 189–200.

Mänttäri, I. 1995. Lead isotope characteristics of epigenetic gold mineralization in the Palaeoproterozoic Lapland greenstone belt, northern Finland. Geological Survey of Finland, Bulletin 381. 70 p.

Marschink, R., Leveille, R.A. & Martin, W. 2000. La Candelaria and the Punta del Cobre district, Chile: early Cretaceous iron-oxide Cu-Au(-Zn-Ag) mineralization. In: T.M. Porter (ed) Hydrothermal Iron Oxide Copper-Gold & Related Deposits: A Global Perspective. Australian Mineral Foundation, Adelaide, 160–175.

McCuaig, T.C. & Kerrich, R. 1998. P-T-t-deformation-fluid characteristics of lode gold deposits: evidence from alteration systematics: Ore Geology Reviews 12, 381–453.

Niiranen, T. & Eilu, P. 2003. Iron oxide-copper-gold deposits in northern Finland. In: D.G. Eliopoulos et al. (eds) Mineral Exploration and Sustainable Development. Proceedings of the Seventh Biennial SGA Meeting, Athens, Greece, 24-28. August 2003. Millpress, Rotterdam. 1091–1094.

Niiranen, T., Poutiainen, M. & Mänttäri, I. 2007. Geology, geochemistry, fluid inclusion characteristics, and U–Pb age studies on iron oxide–Cu–Au deposits in the Kolari region, northern Finland. Ore Geology Reviews 30, 75–105.

Niskavaara, H. & Kontas, E. 1990. Reductive coprecipitation as a separation method for the determination of gold, palladium, platinum, rhodium, silver, selenium and tellurium in geological samples by graphite furnace atomic absorption spectrometry. Analytica Chemica Acta 231, 273–282.

Nurmi, P. A., Lestinen, P. & Niskavaara, H. 1991. Geochemical characteristics of mesothermal gold deposits in the Fennoscandian Shield, and a comparison with selected Canadian and Australian deposits. Geological Survey of Finland, Bulletin 351. 101 p.

Pankka, H. 1989. Tutkimustyöselostus Kuusamon kunnassa valtausalueella Ollinsuo 1, kaiv.rek. n:o 3693, suoritetuista malmitutkimuksista (Exploration report on Ollinsuo 1, Kuusamo, Mine Reg. no. 3693). Geological Survey of Finland, Report M06/4522/-89/1/10. 5 p. (in Finnish)

Pankka, H. 1992. Geology and mineralogy of Au-Co-U deposits in the Proterozoic Kuusamo volcanosedimentary belt, northeastern Finland. PhD thesis. Geology. Michigan Technological

University. 233 p.

Pankka, H. 2000. Exploration report covering the claim area Kantosuo 1, Mine Reg. no. 5633/1 in the municipality of Kuusamo. Geological Survey of Finland, Report M06/4611/00/1/10. 4 p. (in Finnish with English summary)

Pankka, H., Puustinen, K. & Vanhanen, E. 1991. Kuusamon liuskealueen kulta-koboltti-uraaniesiintymät. Summary: Au-Co-U deposits in the Kuusamo volcano-sedimentary belt, Finland. Geological Survey of Finland, Report of Investigation 101. 53 p.

Pankka, H.S. & Vanhanen, E.J. 1992. Early Proterozoic Au-Co-U mineralization in the Kuusamo district, northeastern Finland: Precambrian Research 58, 387–400.

Partington, G.A. & Williams, P.J. 2000. Proterozoic lode gold and (iron)-copper-gold deposits: a comparison of Australian and global examples. SEG Reviews 13, 69–101.

Patison, N.J. 2007. Structural controls on gold mineralisation in the Central Lapland Greenstone Belt. Geological Survey of Finland, Special Paper 44, 107–124.

Patison, N.J., Salamis, G. & Kortelainen, V.J. 2007. The Suurikuusikko gold deposit: Project development summary of northern Europe's largest gold resource. Geological Survey of Finland, Special Paper 44, 125–136.

Peltonen, P.T., Manninen, T. & Pihlaja, P. 1988. The late Archean volcaniclastic Rookkiaapa formation in Peurasuvanto, northern Finland. In: Laajoki, K. & Paakkola, J. (eds.) Sedimentology of the Precambrian formations an eastern and northern Finland. Geological Survey of Finland, Special Paper 5, 165–176.

Perttunen, V. 1989. Peräpohjan alueen vulkaniitit. Summary: Volcanic rocks in the Peräpohja area, northern Finland. Geological Survey of Finland, Report of Investigation 92. 40 p.

Perttunen, V. & Vaasjoki, M. 2001. U-Pb geochronology of the Peräpohja Schist Belt, northwestern Finland. Geological Survey of Finland, Special Paper 33, 45–84.

Perttunen, V. 2002. Törmäsjärvi. Geological Map of Finland 1:100 000, Pre-Quaternary Rocks, Sheet 2631. Geological Survey of Finland.

Perttunen, V. 2003. Koivu. Geological Map of Finland 1:100 000, Pre-Quaternary Rocks, Sheet 2633. Geological Survey of Finland.

Pulkkinen, E. 1998. Sodankylän kultaesiintymät. In: Proterotsooisten nikkeli- ja kultamalmien etsintä sekä orogeniavyöhykkeiden tektonomagmaattinen kehitys (Gold occurrences in Sodankylä). Geological Survey of Finland, Excursion Guide 15–18.9.1998. (in Finnish)

Pulkkinen, E. 1999. Summary report. The Kaaresselkä gold and copper prospects, Sodankylä, Finnish Lapland. Geological Survey of Finland, Report C/M 06/3714/-99/2. http://en.gtk.fi/ExplorationFinland/Tender/kaaresselka/kaaresselka.htm

Pulkkinen, E., Keinänen, V. & Salmirinne, H. 2005. The Sakiatieva gold prospect in the Central Lapland Greenstone Belt, Finland. Geological Survey of Finland, Report CM06/3741/2005/1/10. 23 p.

Rantala, S. 2003. Vihreäkiven muuttuminen Nattas-tyypin graniitin kontaktissa Sodankylässä. (Alteration and mineralisation in greenstones near their contact to the Nattanen granites in Sodankylä). Unpublished MSc thesis. Department of Geology, University of Helsinki. 70 p. (in Finnish)

Räsänen, J., Hanski, E., Juopperi, H., Kortelainen, V., Lanne E., Lehtonen, M.I., Manninen, T., Rastas, P. & Väänänen, J. 1996. New stratigraphical map of central Finnish Lapland. Abstracts: 22nd Nordic Geological Winter Meeting in Turku 1996, p. 182.

Räsänen, J. & Vaasjoki, M. 2001. The U-Pb age of a felsic gneiss in the Kuusamo Schist Area: reapprisal of local lithostratigraphy and possible regional correlations. Geological Survey of Finland, Special Paper 33, 143–152.

Rastas, P., Huhma, H., Hanski, E., Lehtonen, M.I., Härkönen, I., Kortelainen, V., Mänttäri, I. & Paakkola, J. 2001. U-Pb isotopic studies on the Kittilä greenstone area, Central Lapland, Finland. Geological Survey of Finland, Special Paper 33, 95–141.

Riddarhyttan Resources AB 2005. Press release 02 June 2005.

Roos, S. 1987. Lapista valitut vertailukohteet: Apajalahti ja Lemmonlampi. In: H. Papunen (ed.) Lapin vulkaniittien tutkimusprojekti. Loppuraportti (Apajalahti and Lemmonlampi. In: H. Papunen (ed.) Final Report of the Lapland Volcanite Research Project). Department of Geology, University of Turku, Report. 275–281. (In Finnish)

Rossi, S. 1993. Kultalohkareaiheen malmitutkimukset Peräpohjan liuskealueella Sivakkajoen varressa Kivimaassa Tervolan kunnan luoteisosassa vuosina 1989–1992 (Gold exploration at Kivimaa, by the Sivakkajoki river in Tervola municipality, Peräpohja Schist Belt, during 1989–1992). Geological Survey of Finland, Report M19/2631/-93/1/10. 33 p. (in Finnish)

Rossi, S. 1998. Tutkimustyöselostus Rovaniemen maalaiskunnassa valtausalueella Petäjävaara 1 kaiv.rek. nro 5471/1 suoritetuista kulta-kupari-kobolttimalmitutkimuksista vuosina 1992–1994 (Report on gold-copper-cobalt exploration at Petäjävaara, Mine Reg. no. 5471/1, Rovaniemi rural municipality, during 1992–1994). Geological Survey of Finland, Report M06/2633/-98/1/10. 12 p. (in Finnish)

Rouhunkoski, P. & Isokangas, P. 1974. The copper-gold vein deposit of Kivimaa at Tervola, N-Finland. Bulletin of the Geological Society of Finland 46, 29–35.

Rowins, S., Groves, D.I. & McNaughton, N.J. 1997. A reinterpretation of the role of granitoids in the genesis of Neoproterozoic gold mineralization in the Telfer Dome, Western Australia. Economic Geology 92, 133–160.

Salminen, R. (ed.) 1995. Alueellinen geokemiallinen kartoitus Suomessa 1982–1994. Summary: Regional geochemical mapping in Finland in 1982–1994. Geological Survey of Finland, Report of Investigation 130. 47 p.

Santos, J.O.S., Groves, D.I., Hartmann, L.A., Moura, M.A. & McNaughton, N.J. 2001. Gold deposits of the Tapajos and Alta Floresta domains, Tapajos–Parima orogenic belt, Amazon Craton, Brazil. Mineralium Deposita 36, 278–299.

Scanmining AB 2002. Press release 9 September 2002.

Scanmining AB 2005. Press release 3 March 2005.

Sener, A.K., Young, C., Groves, D.I., Krapez, B. and Fletcher, I.R. 2005. Major orogenic gold episode associated with Cordilleran-style tectonics related to the assembly of Paleoproterozoic Australia? Geology 33, 225–228.

Silvennoinen, A. 1972. On the stratigraphical and structural geology of the Rukatunturi area, northeastern Finland. Geological Survey of Finland, Bulletin 257. 48 p.

Silvennoinen, A. 1991. Kuusamon ja Rukatunturin kartta-alueiden kallioperä. Pre-Quaternary rocks of the Kuusamo and Rukatunturi map-sheet areas. Geological Map of Finland 1:100000. Explanation to the Maps of Pre-Quaternary Rocks, Sheets 4524+4542 and 4613. Geological Survey of Finland. 62 p.

Skirrow, R.G. & Walshe, J.L. 2002. Reduced and oxidised Au-Cu-Bi iron oxide deposits of the Tennant Creek Inlier, Australia: an integrated geologic and chemical model. Economic Geology 97, 1167–1202.

Sorjonen-Ward, P., Nurmi, P., Härkönen, I. & Pankka, H. 1992. Epigenetic gold mineralization and tectonic evolution of a lower Proterozoic greenstone terrain in the northern Fennoscandian (Baltic) Shield. In: Sarkar, S.C. (Ed.) Metallogeny Related to Tectonics of the Proterozoic Mobile Belts. Oxford & IBH Publishing, New Delhi, 37–52.

Sorjonen-Ward, P., Nironen, M. & Luukkonen, E. 1997. Greenstone associations in Finland. In: de Wit, M.J. & Ashwal, L.D.

(eds.) Greenstone Belts. Clarendon Press, Oxford. 677–698.

Sorjonen-Ward, P., Ojala, V.J. & Airo, M.-L. 2003. Structural modelling and magmatic expression of hydrothermal alteration in the Paleoproterozoic lapland greenstone belt, northern Fennoscandian Shield. In: D.G. Eliopoulos et al. (eds) Mineral Exploration and Sustainable Development. Proceedings of the Seventh Biennial SGA Meeting, Athens, Greece, 24–28. August 2003. Millpress, Rotterdam. 1107–1110.

Taranis Resources Inc. 2005. Press release 26 May 2005.

Vaasjoki, M. (ed.) 2001. Radiometric age determinations from Finnish Lapland and their bearing on the timing of Precambrian volcano-sedimentary sequences. Geological Survey of Finland, Special Paper 33. 279 p.

Vanhanen, E. 1990a. Kuusamon Iso-Rehvin kultaesiintymän malmitutkimukset vuosina 1988–1989 (Exploration report on work done during 1988–1989 at Iso-Rehvi, Kuusamo). Geological Survey of Finland, Report M19/4611/90/3/10. 17 p. (in Finnish)

Vanhanen, E. 1990b. Sulfidimalmi- ja kultatutkimukset Kuusamon ja Sallan kuntien alueella vuosina 1983–1988 kohteissa Vilkaslampi, Painanteenniitty, Maitokoski, Perttuma-aapa, Juhonlampi, Pullealampi, Manalanniemi, Kotikumpu, Saarilampi, Paukuttaja, Ylimmäinen Kokalampi, Murronmaa, Kotisuo ja Riihilampi-Rovavaara (Exploration report on work done during 1983–1988 at Vilkaslampi, Painanteenniitty, Maitokoski, Perttuma-aapa, Juhonlampi, Pullealampi, Manalanniemi, Kotikumpu, Saarilampi, Paukuttaja, Ylimmäinen Kokalampi, Murronmaa, Kotisuo and Riihilampi-Rovavaara, Kuusamo). Geological Survey of Finland, Report M19/4522, 4611, 4612, 4613/-90/2/10. 2 p. (in Finnish)

Vanhanen, E. 1991a. Kuusamon Konttiahon ja sen lähiympäristön kultamalmitutkimukset vuosina 1985–1990 (Exploration report on work done during 19885–1990 at Konttiaho and its surroundings, Kuusamo). Geological Survey of Finland, Report M19/4611/-91/1/10. 12 p. (in Finnish)

Vanhanen, E. 1991b. Cobalt-, gold- and uranium-bearing mineralizations and their relation to deep fractures in the Kuusamo area. Geological Survey of Finland, Special Paper 13, 91–97.

Vanhanen, E. 1992. Kuusamon Juomasuon kulta-kobolttiesiintymien lähiympäristön kultamalmitutkimukset vuosina 1986–1991 (Exploration report on work done during 1986–1991 in the surroundings of the Juomasuo deposit, Kuusamo). Geological Survey of Finland, Report M19/4613/-92/1/10. 51 p. (in Finnish)

Vanhanen, E. 2001. Geology, mineralogy and geochemistry of the Fe-Co-Au-(U) deposits in the Paleoproterozoic Kuusamo Schist Belt, northeastern Finland. Geological Survey of Finland, Bulletin 399. 229 p.

Vesanto, J. 1978. Sirkan malmi ja sitä ympäröivä kallioperä (Sirkka gold deposit and the surrounding bedrock). Unpublished MSc thesis, Department of Geology, University of Oulu. 89 p. (in Finnish)

Vornanen, E. 1963. Vähäjoen malmin ja sen lähiympäristön kivilajien geologiaa (Vähäjoki deposit and the surrounding bedrock). Unpublished MSc thesis. Department of Geology, University of Helsinki. 84 p. (in Finnish)

Vuollo, J., Piirainen, T. & Huhma, H. 1992. Two Early Proterozoic tholeiitic dyke swarms in the Koli-Kaltimo area, Eastern Finland – their geological significance. Geological Survey of Finland, Bulletin 363, 1–32.

Ward, P., Härkönen, I. & Pankka, H.S. 1989. Structural studies in the Lapland greenstone belt, northern Finland and their application to gold mineralization: Geological Survey of Finland, Special Paper 10, 71–78.

Weihed, P. & Eilu, P. 2003. Gold, Fe oxide-Cu-Au and VMS metallogeny of the Fennoscandian Shield. In: D.G. Eliopoulos et al. (eds) Mineral Exploration and Sustainable Development. Proceedings of the Seventh Biennial SGA Meeting, Athens, Greece, 24-28. August 2003. Millpress, Rotterdam. 1123–1126.

Zhang, L., Shen, Y. & Ji, J. 2003. Characteristics and genesis of Kanggur gold deposit in the eastern Tianshan mountains, NW China: evidence from geology, isotope distribution and chronology. Ore Geology Reviews 23, 71–90.

Appendix 1.

Comparison of gold deposits in northern Finland with the globally detected features of orogenic gold deposits, orogenic(?) gold deposits with atypical metal association, and IOCG deposits.

	Orogenic gold		Orogenic gold with atypical metal association		Iron oxide-copper-gold	
Critical features	**Global[1]**	**Northern Finland[2]**	**Global[3]**	**Northern Finland[2]**	**Global[4]**	**Northern Finland[2]**
Tectonic setting	Accretionary to collisional	Accretionary to collisional	Accretionary to collisional	Accretionary to collisional	Extensional: orogenic collapse, anorogenic magmatism, subduction	Extensional(?) hinterland extension ± orogenic collapse
Structural control	Second- to fourth-order fault and shear zones, fold hinges	First(?)- to third-order fault and shear zones, fold hinges	First- to lower-order shear and fault zones	First- to lower-order shear and fault zones, fold hinges	First- to lower-order shear and fault zones	First- and second-order fault zones?
Spatial association with intrusions	Variable: some hosted by, some with a distance of up to 200 km from nearest intrusion	No distinct relationship; some hosted by dolerites much older than mineralisation	Strong association with granitoids and/or lamprophyres in many, but not all, cases	No distinct relationship; some hosted by dolerites much older than mineralisation.	Strong association with granitoids common	Immediate contact with a synorogenic pluton in CLGB. None within several km at Vähäjoki
Style of mineralisation[5]	Single veins, vein arrays, saddle reefs, dissemination	Large veins, vein arrays, dissemination	Disseminated to vein styles. Single to multistage mineralisation	Vein arrays, breccia pipes, dissemination, saddle reefs? Single- to two-stage mineralisation	Disseminations, breccias, massive, vein arrays. Mgt±Apa typically predate Au-Cu mineralisation	Disseminations and breccias
Timing related to stages of orogeny	Late-tectonic, syn-peak to slightly post-peak metamorphic	Syn-peak to slightly post-peak metamorphic	Single-stage, syn-peak or late orogenic. Multistage VMS, porphyry style or early orogenic overprinted by peak- to late orogenic	Syn-peak to slightly post-peak metamorphic?	Typically late- to post-orogenic ± anorogenic	Late-orogenic?
Potential commodities	Au	Au	Au ± Ag, Bi, Co, Cu, Pb, Sb, Zn; Au-Cu typical	Au-Cu ± Co, Ni, U	Fe-Cu-Au ± Ag, Bi, Co, F, LREE, Mo, U, Zn	Fe-Cu-Au ± Co
Metal zoning	Rare	None detected	Variable, from non-existent to strong	Typically none. Partial to complete overlap of Au, Co and Cu zones in some cases in Kuusamo.	None, Au-Cu in central parts only, or Au-, Cu- and Bi-rich parts only partially overlap	Au-Cu-Fe ± Co in central sulphidised parts, Fe only in outer parts
Proximal alteration[6]	Low T: Ank/Dolo-Musc-Qz-Ab-Rut Mid T: Calc-Biot-Plag-Qz-Act-Tit/Rut High T: Calc-Biot-Plag-Di-Hbl-Tit	Low T: Ank/Dolo-Musc-Qz-Ab-Rut Mid T: Calc-Biot-Plag-Qz-Act-Tit/Rut High T: none detected	Variable, multistage in most cases. Ank/Dolo-Musc-Qz-Ab common.	Two-stage. Early intense albitisation overprinted by Ank/Dolo-Musc-Qz-Ab-Rut	Multistage. Early albitisation overprinted by 2–7 stages of K ± Na ± Ca ± Fe ± Si metasomatism; sodic at depth, potassic in higher levels	Multistage. Earlier Ab, Mgt-Di ± Biot, Kfsp, Scap; later Hbl/Act ± Carb, Biot, Musc, Scap, Talc, Ep
P-T conditions	220–600°C, 0.5–4.5 kbar	300–450°C, 1–3 kbar	200–650°C, <1–4 kbar	300–500°C, 1–3 kbar	200–800°C, 0.5–2.5 kbar	400–600°C, 1.5–3.5 kbar
Dominant ore minerals[5]	Py, Po, Apy	Py, Po, Apy	Py, Po, Cpy ± Cob, Gn, Sp, Sti	Py, Po, Cpy ± Apy, Cob, Cpy, Grs	Mgt or Hm ± Py, Po, Cpy, Bor, Cha, Bit, Ura	Mgt, Py, Po, Cpy, Cob, Apy

Appendix 1. Continued

Enriched in ore	Ag, As, Au, CO_2, K, Rb, S, Sb, Te ± B, Ba, Bi, Cs, Hg, Na, Pd, Pt, Se, W	Ag, Au, As, CO_2, K, Rb, S, Sb, Te ± B, Ba, Bi, Cs, Hg, Li, Na, Se, W	Ag, As, Au, CO_2, Cu, K, Rb, S ± Ba, Bi, Co, LREE, Mo, Ni, Pb, Sb, Tl, V, W, Zn	Ag, As, Au, CO_2, Cu, K, Rb, S, Sb, Te ± B, Ba, Bi, Cd, Ce, Cs, Co, Fe, Hg, La, Mn, Mo, Nb, Pd, Se, Sn, U, W	Au, Cu, Fe, S ± Ag, As, Ba, Bi, Ca, Co, F, LREE, Mg, Mo, Na, P, Pb, Te, U, W, Zn	Ag, Au, Bi, Ca, CO_2, Cu, Fe, S, Te ± As, Ba, Cl, Co, K, Mo, Na, Pb, Rb, Sb, Se, U, Zn
Ore fluids	H_2O-CO_2-H_2S ± CH_4, N_2; neutral to slightly alkaline; reducing; <10% NaCl eq.	H_2O-CO_2-H_2S; <10% NaCl eq.	H_2O-H_2S to H_2O-CO_2-H_2S ± CH_4, N_2; alkaline to acidic; reducing; 5–55% NaCl eq.	H_2O-CO_2; low to high salinity; early oxidising; late reducing?	H_2O±CO_2±CH_4 with Na, Ca ± Ba, Fe, K, Mg, Mn; dominantly oxidising; low-S, 20-60% NaCl eq.; lower-salinity; reducing stages possible	H_2O±CO_2 with Na, Ca, K ± As, Fe, Mn, Sr; oxidising (Vähäjoki); high- (Kolari) to low-(Vähäjoki) salinity
Fluid stable isotope data	$\delta^{18}O$ +4 – +15‰ $\delta^{13}C$ -11 – +2‰ δD -80 – -30‰	$\delta^{18}O$ +5 – +8‰ $\delta^{13}C$ -6 – +2‰	$\delta^{18}O$ +0 – +15‰ $\delta^{13}C$ -12 – -1‰ δD -100 – -15‰	$\delta^{18}O$ +7 – +8‰ $\delta^{13}C$ -6 – +2‰	$\delta^{18}O$ +1 – +10‰ δD -80 – -10‰	Kolari: $\delta^{18}O$ +9.6 – +11.2‰; Vähäjoki: $\delta^{18}O$ +12.8 – +17.5‰
Heat sources	From astenospheric upwelling to mid-crustal intrusions	Not investigated	Early- or late-orogenic intrusion, later deep crustal or lithospheric source	Not investigated	Local intrusions	Local intrusions suggested in CLGB, deep source in PSB
Fluid and metal sources	Subducted crust, mid- to lower crust and/or upper mantle	Local and deep sources suggested	Variable, from local magmatic and metamorphic to deep crustal suggested	Local and deep sources, intrusions and metamorphic, suggested	Local intrusions and/or local supracrustal sequence (evaporites); ± meteoric in shallowest levels	Metamorphic and/or magmatic
Deposit examples	Bendigo, Golden Mile (AUS), Homestake, Mother Lode (USA), Kolar (India), Björkdal (Sweden)	Kuotko, Pahtavaara, Surikuusikko	Pine Creek, Telfer (AUS), Sabie–Pilgrim's Rest (RSA), Guarim (Brazil), Hemlo (Canada), Pahtohavare (Sweden), Bidjovagge (Norway)	Kivimaa, Kaaresselkä, Levijärvi-Loukinen, Saattopora, Sirkka, Vinsa; most or all of the Kusamo deposits	Tennant Creek, Ernest Henry, Olympic Dam (AUS), NICO, Sue-Dianne (Canada), Candelaria (Chile), Alemao–I. Bahia (Brazil)	Kuervitikko, Laurinoja, Vähäjoki

1) Groves et al. (1998, 2003), McCuaig & Kerrich (1998), Partington & Williams (2000), Goldfarb et al. (2001)
2) FINGOLD-database (http://en.gtk.fi/ExplorationFinland/Commodities/Gold/gtk_gold_map.html) and references therein, Hölttä & Karhu (2001), Lahtinen et al. (2003); for the IOCG type, also Hiltunen (1982), Niiranen & Eilu (2003) and Niiranen et al. (2007)
3) Ettner et al. (1994), Boer et al. (1995), Lindblom et al. (1996), Rowins et al. (1997), Goldfarb et al. (2001), Santos et al. (2001), Groves et al. (2003), Sener et al. (2003), Zhang (2003)
4) Hitzman et al. (1992), Ferenczi & Ahmad (1998), Hitzman (2000), Partington & Williams (2000), Skirrow & Walshe (2002)
6) Mineral abbreviations: Ab = albite, Act = actinolite, Ank = ankerite, Biot = biotite, Calc = calcite, Di = diopside, Dolo = dolomite, Ep = epidote, Hbl = hornblende, Kfsp = K feldspar, Musc = muscovite, Qz = quartz, Plag = calcic plagioclase, Rut = rutile, Scap = scapolite, Tit = titanite
5) Mineral abbreviations: Apa = apatite, Apy = arsenopyrite, Bit = bismuthinite, Bor = bornite, Cha = chalcocite, Cob = cobaltite, Copn = cobalt pentlandite, Cpy = chalcopyrite, Gn = galena, Hm = haematite, Mgt = magnetite, Po = pyrrhotite, Py = pyrite, Sp = sphalerite, Sti = stibnite, Ura = uraninite

Appendix 2.

Main features of drilling-indicated gold occurrences in Palaeoproterozoic northern Finland

Gold deposits and drilling-indicated occurrences in the Central Lapland area. Location of the occurrences is indicated in Figure 3.

Deposit / Prospect (parallel name)	Size / Best section	Main host rocks	Metamorphic grade	Main ore minerals[1]	Gold mainly occurs as[1]	Commodity association	Enriched compounds[2] * incomplete data available	Genetic type[3]	No. in Fig. 3
Mine									
Kutuvuoma[4]	0.03 Mt @ 3 ppm Au; 4–16 m @ 11 ppm Au	Metakomatiite	Greenschist	Py, Po	Free native	Au only	*Int: Au *Mod: K, S	Orogenic	1
Laurinoja[5]	4.6 Mt @ 0.95 ppm Au, 0.88% Cu, 43 % Fe	Magnetite skarn or ironstone	Lower-amphibolite	Mgt, Py, Cpy	Free native + inclusions in Cpy	Fe-Cu-Au	Int: Au, Cu, S Mod: Ag, Bi, Ca, CO_2, Fe, Mo, Na, Pb, Te	IOCG	
Pahtavaara[6]	3 Mt @ 4 ppm Au	Metakomatiite	Upper-greenschist	Mgt, Py	Free native assoc. with gangue	Au only	Int: Au, Se Mod: Ba, CO_2, K, S, Te, U, W	Orogenic	
Saattopora[7]	2.163 Mt @ 3.0 ppm Au, 0.24 % Cu	Intermediate metatuffite	Lower- to mid-greenschist	Py, Po, Cpy	Free native assoc. with gangue	Au-Cu	Int: As, Au, S, Te, Mod: Ag, B, Bi, CO_2, Cu, K, La, Pd, Se, U, W	Orogenic, anomal. metal assoc.	
Major deposit									
Suurikuusikko[8]	12.7 Mt @ 5.1 ppm Au; 79 m @ 8.4 ppm Au	Mafic metavolc. rocks	Lower-greenschist	Apy, Py	In Apy lattice, inclusions in Py	Au only	*Int: As, Au, S *Mod: CO_2, Na, Sb, Te	Orogenic	
Other prospects									
Ahvenjärvi (Isomaa)[9]	1 m @ 4.9 ppm Au; 5 m @ 1.3 ppm Au	Quartzite	Greenschist	Py	No data	Au only	*Int: Au	Orogenic	2
Äkäsaivo[10]	0.9 m @ 6.2 ppm Au	Diopside skarn	Lower-amphibolite	Mgt, Cpy	No data	Fe-Au-Cu	*Int: Au, Cu *Mod: Ca?, CO_2, Fe, S	IOCG	3
Hanhilampi (Jolhikko)[11]	1 m @ 13.3 ppm Au	Metadolerite	Greenschist	Py, Po	No data	Au only	*Int: Au *Mod: CO_2	Orogenic	4
Harrilommol[12]	3 m @ 5.0 ppm Au	Intermediate metatuffite	Lower- to mid-greenschist	Py, Po, Cpy?	Free native assoc. with gangue	Au-Cu ?	*Int: Au *Mod: CO_2, Cu?, K, S	Orogenic, anomal. metal assoc.?	5
Hirvilavanmaa[9]	3.5 m @ 6.5 ppm Au; 28 m @ 5.2 ppm Au	Metakomatiite	Lower- to mid-greenschist	Py	Free native with Py, Te	Au only	Int: Au, Mod: CO_2, S, Sb, Te	Orogenic	6
Hookana[13]	1 m @ 1 ppm Au	Metadolerite	Upper-greenschist?	Py, Cpy	No data	Au-Cu	*Int: Au, Cu *Mod: S	Orogenic, anomal. metal assoc.	7
Kaaresselkä[14]	0.3 Mt @ 1–10 ppm Au, <0.1–3.0% Cu, several 3 m @ >10 ppm Au	Mafic metatuffite	Upper-greenschist	Py	Free native assoc. with gangue, Py, Cpy, Apy	Au-Cu	*Int: Au, Cu *Mod: CO_2, K, S	Orogenic, anomal. metal assoc.	8

Appendix 2. Continued.

Deposit / Prospect (parallel name)	Size / Best section	Main host rocks	Metamorphic grade	Main ore minerals[1]	Gold mainly occurs as[1]	Commodity association	Enriched compounds[2] * incomplete data available	Genetic type[3]	No. in Fig. 3
Kaarestunturi[15]	?	Conglomerate	Upper-greenschist?	none	Free native in matrix	Au only	*Int: Au	Palaeoplacer	9
Kellolaki[32]	10.6 m @ 4.86 ppm, 11.7 m @ 4.5 ppm	Metatuffite(?)	Lower- to mid-greenschist(?)	Py(?)	No data	Au only	*Int: Au	Orogenic	31
Koppelokangas (Rimpelä)[16]	2 m @ 1 ppm Au	Metasedimentary rocks	Greenschist	Py	No data	Au only	*Int: Au	Orogenic	10
Kuervitikko[17]	1.2 Mt @ 0.2–5 ppm Au, 0.11–8.3% Cu, 36–53 % Fe	Magnetite skarn or ironstone	Lower-amphibolite	Mgt, Cpy, Po, Py	Free native + inclusions in Cpy, Mgt	Fe-Cu-Au	Int: Au, Cu, S, Te Mod: Ag, Bi, Cl, Co, Fe, K, LREE, Mo, Na, Se, Te	IOCG	11
Kuotko (Iso-Kuotko)[18]	0.17 Mt @ 4.3 ppm Au + 0.121 Mt @ 2.7 ppm Au	Mafic metavolcanic rocks	Greenschist	Apy, Py, Po	Free native assoc. with Apy, Py	Au only	Int: As, Au, Bi, Sb Mod: CO_2, K, S, Te	Orogenic	12
Naakenavaara[9]	10 m @ 1.4 ppm Au; 2 m @ 1.8 % Cu	Phyllite	Lower- to mid-greenschist	Py, Po	No data	Au-Cu	*Int: Au, Cu *Mod: CO_2, K, S	Orogenic, anomal. metal assoc.	13
Lammasvuoma[19]	1.2 m @ 25 ppm Au; 10 m @ 1.7 ppm Au	Metakomatiite	Greenschist	Py, Cpy	No data	Au-Cu	*Int: Au *Mod: CO_2, Cu, S	Orogenic, anomal. metal assoc.	14
Lauttaselkä[20]	0.6 Mt @ 0.48 ppm Au, 0.23% Cu, 21% Fe	Metakomatiite(?)	Lower-amphibolite	Mgt, Cpy	No data	Fe-Cu-Au	*Int: Au, S *Mod: CO_2, Cu, Fe	IOCG	15
Levijärvi-Loukinen[9]	0.11 Mt @ 0.4 ppm Au, 0.45 % Ni; 20 m @ 0.5 ppm Au; 76 m @ 0.53 % Cu	Metakomatiite	Lower- to mid-greenschist	Py, Cpy, Grs	Free native + inclusions in Grs, Py	Au-Cu-Ni	*Int: Au, Cu *Mod: CO_2, K, Ni, S	Orogenic, anomal. metal assoc.	16
Mantovaara[33]	1 m @ 1.61 ppm Au	Mafic metatuff or tuffite	Lower- to mid-greenschist	No data	No data	Au-Cu	*Int: As, Au, S *Mod: Cu, Ni, Mo, Pb, Sb, Te, Zn	Orogenic, anomal. metal assoc.	32
Muusanlammit[21]	1.7 m @ 7.9 ppm Au	Graphitic phyllite and tuffite	Greenschist	Py	No data	Au only	*Int: Au	Orogenic	17
Outapää[22]	Several 1 m sections @ 1–6 ppm Au	Conglomerate	Greenschist	none	Free native in matrix	Au only	*Int: Au	Palaeoplacer	18
Päivänenä (Kettukuusikko)[23]	28.9 m @ 1.4 ppm Au, 1.8 m at 27.7 ppm Au	Metakomatiite	Lower- to mid-greenschist	Py	Free native assoc. with quartz, Py	Au only	Int: Au, Te Mod: Ag, CO_2, K, S, Sb, W	Orogenic	19
Palolaki[34]	1 m @ 1.46 ppm Au	Intermediate metatuffite	Upper-greenschist?	No data	No data	Au only	*Int: As, Au, S *Mod: Cu, Ni, Mo, Pb, Sb, Te	Orogenic	33

Appendix 2. Continued

Deposit / Prospect (parallel name)	Size / Best section	Main host rocks	Metamorphic grade	Main ore minerals[1]	Gold mainly occurs as[1]	Commodity association	Enriched compounds[2] * incomplete data available	Genetic type[3]	No. in Fig. 3
Palovaara[24] (Jerusaleminjänkä)	2 m @ 4.8 ppm Au	Intermediate metatuffite	Greenschist	Py	No data	Au only	*Int: Au *Mod: CO_2, K, S	Orogenic	20
Pikku-Mustavaara[25]	2.5 m @ 10 ppm Au; 5 m @ 2.8 ppm Au, 0.3% Cu	Graphitic phyllite	Greenschist	Py, Apy	Free native assoc. with Py, Apy	Au-Cu	*Int: Au *Mod: As, CO_2, S	Orogenic	21
Rovaselkä[26]	1.2 m @ 2.1 ppm Au	Sulphide-rich schists	Upper-green-schist?	Po ?	No data	Au only	Int: As, Au, S, Se Mod: B, Bi, Cu, Mo, Pb, Pd, Te, U	Orogenic	22
Ruoppapalo[27]	4 m @ 2.7 ppm Au	Intermediate dykes	Greenschist	Py	Free native assoc. with carbonates	Au only	*Int: Au	Orogenic	23
Ruosselkä (Sakia-tieva)[13]	7 m @ 13.7 ppm Au; 8 m @ 6 ppm Au	Mafic metatuff and metakomatiite	Greenschist + contact-metam. overprint	Py	Free native	Au only	Int: Au, S, Sb Mod: Ag, As, Cu, K, La, Mo, Te, Th	Orogenic	24
Sirkka kaivos[21]	?	Intermediate metatuffite	Mid- to upper-greenschist	Py, Po, Cpy	Native as inclusions in Grs, Apy	Au-Cu	Int: As, Au, Bi, Cu, Te Mod: Co, CO_2, K, Ni, S	Orogenic, anomal. metal assoc.	25
Sirkka W[21,28]	11.6 m @ 0.5 ppm Au, 0.5% Cu	Intermediate metatuffite	Mid- to upper-greenschist?	Py, Po, Cpy	Native as inclusions in Grs, Apy	Au-Cu	Int: As, Au, Bi, Cu, Te Mod: CO_2, K, Mn, S	Orogenic, anomal. metal assoc.	26
Soretialehto[9]	0.013 Mt @ 3.5 ppm Au; 8 m @ 3–4 ppm Au	Metakomatiite	Lower- to mid-greenschist	Py	Free native assoc. with quartz, Py	Au only	*Int: Au *Mod: CO_2, K, S	Orogenic	27
Soretiavuoma N[29]	3 m @ 5 ppm Au; 1.1 m @ 48 ppm Au	Metakomatiite	Lower- to mid-greenschist	Py	Native assoc. with Py	Au only	Int: As, Au, Bi, Te Mod: Ag, CO_2, Cu, K, Pb, Sb, S, W	Orogenic	28
Sukseton[30]	4.6 m @ 2.8 ppm Au	Intermediate metatuff	Greenschist	Py, Po	Free native assoc. with gangue	Au only	Int: As, Au Mod: Ag, Bi, CO_2, K, Pd, S, Sb, Te, W	Orogenic	29
Tuongankuusikko[31]	17.5 m @ 1.18 ppm Au and 1.73% Cu	Graphitic phyllite	Greenschist	Po, Cpy	No data	Au-Cu	*Int: Au, Cu *Mod: CO_2, S	Orogenic, anomal. metal assoc.	30

1) Apy = arsenopyrite, Cpy = chalcopyrite, Grs = gersdorffite, Mgt = magnetite, Po = pyrrhotite, Py = pyrite, Te = tellurides. Minerals are mentioned in the order of descending abundance
2) Bulk ore compared to average unmineralised and unaltered basalt (Koljonen 1992); Int = intense enrichment, enrichment factor >50; Mod = moderate enrichment, enrichment factor 5–50 (3–50 for major elements)
3) Orogenic: as defined by Groves et al. (1998); Orogenic with atypical metal association: as defined by Goldfarb et al. (2001); IOCG = Iron oxide-copper-gold category as defined by Hitzman et al. (1992), Barton & Johnson (1996), Hitzman et al. (2000), Marschink et al. (2000), and Partington & Williams (2000)
4) Anttonen (1995), M. Kilpelä, pers. comm. (1998)

Appendix 2. Continued

5) Hiltunen (1982), Niiranen et al. (2007)
6) H. Alaniska, pers. comm. (1998, 1999)
7) Korvuo (1997b)
8) Riddarhyttan Resources AB (2005), Patison et al. (2007)
9) Keinänen (2002), Scanmining (2002)
10) Keinänen (1996)
11) Inkinen (1991)
12) Korvuo (1997a)
13) Pulkkinen et al. (2005)
14) Pulkkinen (1999); reserves mentioned only include the uppermost 40–50 m of two lodes, Vanha and Tienvarsi (Fig. 17)
15) Härkönen (1984)
16) Inkinen (1992b)
17) Keinänen (1995), Niiranen et al. (2007)
18) Härkönen et al. (2001)
19) Hugg (1987a)
20) Hiltunen (1989)
21) Vesanto (1978), Inkinen (1985), Lehtinen (1987)
22) Härkönen (1988)
23) Hugg (1991), Taranis Resources (2005)
24) Anttonen (1994)
25) Keinänen (1990)
26) Nurmi et al. (1991)
27) I. Härkönen, pers. comm. (1998)
28) Hugg (1987b)
29) Keinänen (1997)
30) T. Korkalo, pers. comm. (1998)
31) Inkinen (1992a)
32) Dragon Mining (2005)
33) Hulkki (2002a)
34) Hulkki (2002b)

Appendix 3.

Gold deposits and drilling-indicated occurrences in the Kuusamo Schist Belt. Genetic type column not included as all seem to be of same class, i.e. orogenic with atypical metal association. Location of the occurrences is indicated in Figure 4.

Deposit / Prospect	Size, grade / Best section	Main host rocks	Metamorphic grade	Main ore minerals[1]	Gold mainly occurs as[1]	Commodity association[2]	Enriched compounds[3] * incomplete data available	No. in Fig. 4
Major deposit								
Juomasuo[4]	0.86 Mt @ 5.2 ppm Au, 0.15 % Co, <0.05 % Cu	Sericite quartzite	Greenschist	Po, Py, Cob	Native as inclusions in Py, Cob, Ura, gangue	Au-Co-Cu-U	Int: As, Au, S, Se, Te, U, W Mod: B, Co, Cu, K, La, Mo, Pb	
Other prospects								
Apajalahti[5]	0.1 Mt @ 10 ppm Au	Sericite quartzite	Greenschist	Po, Py	Free native assoc. with gangue	Au-Co-Cu	*Int: Au *Mod: Co, CO_2, Cu, S	1
Hangaslampi[2]	0.28 Mt @ 4.8 ppm Au, 0.1% Co; 0.1 % Cu, 300 ppm U	Sericite quartzite	Greenschist	Py, Po, Copn	Native as inclusions in Py + assoc. with gangue	Au-Co-Cu-U	Int: Au, Se, Te Mod: As, Bi, Cs, Co, CO_2, Fe, La, Mo, S, U	2
Hangaspuro[6]	3 m @ 4 ppm Au, 1 m @ 0.95% Mo	Sericite quartzite	Greenschist	Po, Py, Cpy, Mol	No data	Au-Co-Cu-U	Int: Au Mod: Co, CO_2, Cu, Mo, S, U	3
Hanhilampi[7]	5 m at 3 ppm Au	Sericite quartzite	Greenschist	Py	No data	Au-Co-Cu-U	*Int: Au, S *Mod: Co, CO_2, Cu, U	11
Honkilehto[7]	<0.01 Mt @ 4 ppm Au, 0.15 % Co, 0.3 % Cu	Sericite quartzite	Greenschist	Po, Py, Cpy	Free native	Au-Co-Cu	Int: Au, S, Se, W Mod: Ag, As, Bi, Co, CO_2, Cu, Fe, La, Th	4
Iso-Rehvi[8]	0.04 Mt @ 4 ppm Au, <0.05-0.1 % Co, 0.6-0.18 % Cu	Sericite quartzite	Greenschist	Po, Py, Cpy	Native	Au-Co-Cu	*Int: Au *Mod: Co, CO_2, Cu, S	5
Isoaho 1[9]	3 m @ 4 ppm Au	Sericite quartzite	Greenschist	Po, Py	No data	Au-Co-Cu-U	*Int: Au *Mod: Co, CO_2, Cu, S, U	6
Isoaho 2[9]	?	Sericite quartzite	Greenschist	Po, Py	Free native	Au-Co-Cu-U	*Int: Au *Mod: Co, CO_2, Cu, S, U	7
Kantolahti (Kantosuo)[10]	2 m @ 4.7 ppm Au, 1 m @ 13.4 ppm Au, 4.7 m at 0.20% Co; ≤0.15 % Cu	Mafic to intermediate metatuffite	Greenschist	Py, Po, Cpy, Cob	No data	Au-Co-Cu	*Int: Au *Mod: Co, CO_2, Cu, S	8
Konttiaho[11]	8 m @ 10 ppm Au: 0.02 % Co, 0.02 % Cu, 0.05 % Mo, 100 ppm U	Sericite quartzite and interm. tuffite	Greenschist	Po, Py	Free native assoc. with gangue	Au-Co-Cu-U	Int: Au, Bi, Mo, Se, Te, U, W Mod: B, Co, CO_2, La, Pb, Pd, S	9

Appendix 3. Continued

Kouvervaara[12]	1.58 Mt @ 0.4 ppm Au, 0.1% Co, 0.2 % Cu	Sericite quartzite	Upper-green-schist	Po, Cpy, Cob, Copn	Free native assoc. with gangue	Au-Co-Cu	Int: Au, Bi, S, Sb, Se, Te Mod: Ag, As, Co, CO_2, Cu, Fe, La, Pb, U	10
Lavasuo[13]	1 m @ 2 ppm Au; 0.1–0.2 % Co, 0.1–0.2 % Cu	?	Lower-amphi-bolite	?	No data	Au-Co-Cu	*Int: Au *Mod: Co, CO_2, Cu, S	12
Lemmonlampi[2]	0.09 Mt @ 0.15 ppm Au, 0.3% Co, 0.4% Cu	Dolerite, mica schist	Upper-green-schist	Py, Po, Mgt, Cpy	No data	Au-Co-Cu	*Int: Au *Mod: Co, CO_2, Cu, S	13
Likalampi[2]	0.5-1 ppm Au, 0.4-0.7% Cu (extent not reported)	?	Lower-amphi-bolite	Po, Cpy	No data	Au-Co-Cu	*Int: Au, Cu *Mod: Co, CO_2, S	14
Meurastuksenaho[2]	1 Mt @ 0.6 ppm Au, 0.13% Co including 0.12 Mt @ 4.4 ppm Au and 0.27% Co; 25 m @ 1.0 ppm Au, 0.35 % Co, 0.38 % Cu	Sericite quartzite and metasiltstone	Greenschist	Po, Py, Cpy, Copn	Free native in most Co-rich parts of the deposit	Au-Co-Cu	Int: As, Au, Co, Cu, S, Sb, Te Mod: Ag, Ca, Cd, Cs, CO_2, Fe, La, Mn, Nb	15
Murronmaa[14]	2 m @ 6 ppm Au	Conglomerate(?)	Greenschist	?	No data	Au-Co-Cu-U	*Int: Au *Mod: Co, CO_2, Cu, S, U	16
Ollinsuo[16]	14 m @ 3.3 ppm Au; 16 m @ 1.7 ppm Au, 0.11 % Co and 0.12 % Cu	Sericite quartzite	Greenschist	Po, Py	Free native assoc. with gangue	Au-Co-Cu	Int: Au Mod: Ag, Co, CO_2, Cu, S	17
Pohjaslampi[6]	4 m @ 4 ppm Au; ? m @ 5.8 ppm Au, 0.26 % Cu, 860 ppm U	Intermediate metatuffite	Greenschist	Py, Po	No data	Au-Co-Cu-U	*Int: Au *Mod: Co, CO_2, Cu, S, U	18
Pohjasvaara[16]	0.082 Mt @ 3.2 ppm Au, 0.10 % Co, 0.30% Cu; 11 m @ 5.1 ppm Au, 0.88 % Co, 0.2 % Cu	Mafic metavolcanic rock	Greenschist	Po, Cpy, Py	Free native	Au-Co-Cu-U	Int: Au, S, Se, Te Mod: Ag, Bi, Cd, Co, CO_2, Cu, Hg, K, La, Mo, Pd, U	19
Sakarinkaivu-lamminsuo[6]	2 m @ 5 ppm Au; 9 m @ 0.13% Co; 5.5 m @ 0.45% Cu	Sericite quartzite	Greenschist	Po, Py, Cpy, Cob	Free native	Au-Co-Cu-U	*Int: Au, Co, Cu, *Mod: CO_2, S, U	20
Sarkanniemi[2]	Several metres @ 10 ppm Au	Metasedimentary rocks	Greenschist	Po, Py	No data	Au-Co-Cu-U	*Int: Au *Mod: Co, CO_2, Cu, S, U	21
Säynäjävaara[17]	0.03 Mt @ 4.5 ppm Au or 0.4 Mt @ 1 ppm Au, 0.06% Co; 25 m @ 4.5 ppm Au, 0.04 % Co	Mafic metavolcanic rock	Greenschist	Po, Py, Copn	Free native assoc. with gangue	Au-Co-Cu	Int: Au, S, Se, Te Mod: Bi, Co, CO_2, La, Mo, U, W	22
Sivakkaharju[2]	0.04 Mt @ 8 ppm Au, 0.12% U; 4.5 m @ 5.2 ppm Au, 0.015 % Co, 0.11 % Cu	Sericite quartzite	Greenschist	Po, Ura	Free native assoc. with gangue	Au-Co-Cu-U	Int: Au, Bi, Mo, Se, Te, U, W Mod: As, B, CO_2, Cu, Pb, Pd, S, Sb, Sn	23

1 Apy = arsenopyrite, Cob = cobaltite, Copn = cobalt pentlandite, Cpy = chalcopyrite, Mgt = magnetite, Mol = molybdenite, Po = pyrrhotite, Py = pyrite, Ura = uraninite. Minerals are mentioned in the order of descending abundance.

2 As classified by Vanhanen (2001)

3 Bulk ore compared to average unmineralised and unaltered basalt (Koljonen 1992); Int = intense enrichment, enrichment factor >50; Mod = moderate enrichment, enrichment factor 5–50 (3–50 for major elements)

4 Pankka & Vanhanen (1992), Vanhanen (2001)

Appendix 3. Continued

5 Roos (1987)
6 Vanhanen (1992)
7 H. Pankka, pers. comm. (1998)
8 Vanhanen (1990a)
9 Korteniemi (1993)
10 Pankka (2000)
11 Vanhanen (1991a)
12 Vanhanen (1991b)
13 Inkinen (1987)
14 Vanhanen (1990b)
15 Pankka (1989)
16 H. Pankka, pers. comm. (1993), Dragon Mining (2004)
17 Pankka et al. (1991)

Appendix 4.

Gold deposits and drilling-indicated occurrences in the Peräpohja Schist Belt. Location of the occurrences is indicated in Figure 5.

Deposit / Prospect (parallel name)	Size / Best section	Main host rocks	Metamorphic grade	Main ore minerals1	Gold mainly occurs as1	Commodity association	Enriched compounds2 * incomplete data available	Genetic type3
Mine								
Kivimaa4	0.022 Mt @ 5.3 ppm Au, 1.87 % Cu; 6.2 m @ 4.9 ppm Au, 2.2% Cu	Metadolerite	Upper-greenschist	Py, Cpy	Native as inclusions in Apy + free native	Au-Cu	Int: As, Au, Bi, Cu, S Mod: Ag, CO2, Hg, K, Mn, Mo, Rb, Se, Te, W	Orogenic, anomal. metal association
Other prospects								
Petäjävaara (Rosvohotu)5	1 m @ 19.6 ppm, 1 m @ 3 ppm Au	Metadolerite	Upper-greenschist	Py, Cpy	No data	Au-Cu	*Int: Au, Co, Cu, S, Te *Mod: CO2, K, Rb	Orogenic, anomal. metal association
Sivakkajoki6	1 m @ 2.2 ppm, 1 m @ 1.5 ppm Au	Metadolerite	Upper-greenschist	Py, Cpy	Free native with vein quartz	Au-Cu	*Int: Au, Cu, S *Mod: CO2, K, Te	Orogenic, anomal. metal association
Vähäjoki7	>1 Mt @ 0.2–2 ppm Au, 0.38% Cu, 0.12% Co; 11 Mt @ 40 % Fe	Magnetite skarn or ironstone	Upper-greenschist	Mgt, Py, Cpy, Cob, Apy	Native as inclusions in Cob	Fe-Au-Cu-Co	Int: As, Au, Co, Cu, S Mod: Ag, Ba, Bi, Fe, K, Mo, Te, U, Zn	IOCG
Vinsa4,8	4000(?) t @ 3 ppm Au, 4% Cu	Metadolerite	Upper-greenschist	Py, Cpy, Po	Free native with vein quartz	Au-Cu	*Int: Au, Cu, S *Mod: CO2, K	Orogenic, anomal. metal association

1 Apy = arsenopyrite, Cob = cobaltite, Cpy = chalcopyrite, Mgt = magnetite, Po = pyrrhotite, Py = pyrite. Minerals are mentioned in the order of descending abundance.
2 Bulk ore compared to average unmineralised and unaltered basalt (Koljonen 1992); Int = intense enrichment, enrichment factor >50; Mod = moderate enrichment, enrichment factor 5–50 (3–50 for major elements)
3 Orogenic with atypical metal association: as defined by Goldfarb et al. (2001); IOCG = Iron oxide-copper-gold category as defined by Hitzman et al. (1992), Barton & Johnson (1996), Hitzman et al. (2000), Marschink et al. (2000), and Partington & Williams (2000)
4 Rouhunkoski & Isokangas (1974)
5 Rossi (1998)
6 Rossi (1993)
7 Korvuo (1982), Liipo & Laajoki (1991)
8 Äyräs (1991)

Gold in the Central Lapland Greenstone Belt, Finland
V. Juhani Ojala (ed.)
Geological Survey of Finland, Special Paper 44, 107–122, 2007.

STRUCTURAL CONTROLS ON GOLD MINERALISATION IN THE CENTRAL LAPLAND GREENSTONE BELT

by
N. L. Patison

Patison, N. L. 2007. Structural Controls on Gold Mineralisation in the Central Lapland Greenstone Belt. *Geological Survey of Finland, Special Paper 44,* 107–124, 7 figures and 4 tables.

Early Proterozoic gold mineralisation in the Central Lapland Greenstone Belt (CLGB) has a distinct spatial correlation with structural features generated by convergence events, and by subsequent wrench deformation during the orogenic development of the CLGB. This research aims to provide basic guidelines for assessing the prospectivity of CLGB structures, and involves examining the deformation history and timing of gold mineralisation at 10 locations. Mineralisation at these occurrences is in or near discrete strike-slip shear zones, or other deformation products of a similar relative age developed within zones of complex earlier deformation. Gold-bearing structures are typically part of the final regional deformation phase to affect the CLGB (D_3), and are overprinted by only minor (low-displacement) brittle faults.

While identifying D_3 shear zones is a useful exploration guideline, the localised effects of earlier deformation and alteration events also need to be considered. In many cases, the combined effect of early and late events constrains mineralisation to a particular location. The late orogenic timing of mineralisation is one of many features making CLGB gold mineralisation comparable to well-documented global examples of orogenic greenstone-hosted gold mineralisation.

Key words (GeoRef Thesaurus AGI): gold ores. structural controls, deformation, shear zones, Central Lapland Greenstone Belt, Paleoproterozoic, Kittilä, Sodankylä, Lapland Province, Finland.

N. L. Patison, Economic Geology Research Unit, School of Earth Sciences, James Cook University, Townsville QLD 4811 Australia. Current address: Geological Survey of Finland, P.O. Box 77, FI-96101 Rovaniemi, Finland.

E-mail: nicole.patison@gtk.fi

INTRODUCTION

Gold mineralisation occurs at numerous sites within the Central Lapland Greenstone Belt (CLGB) of northern Finland. The area has clear potential for further discoveries, exemplified by the discovery of the now 2+ million ounce Suurikuusikko gold deposit. The Geological Survey of Finland found the deposit in 1996 after ten years of exploration in the region. The Ministry of Trade and Industry sold it to Riddarhyttan Resources in 1998 and it is currently owned by Agnico-Eagle Mines Limited. Mining of the deposit will begin in 2008, targeting 14.2 million tonnes of estimated probable reserves with an average gold grade of 5.16 grams per tonne (Agnico-Eagle Mines Ltd. media release 06.05.2006).

Known CLGB gold occurrences are orogenic greenstone-hosted gold mineralisations, analogous in many ways to those in more established mineral districts such as the Yilgarn region of Western Australia (e.g., Witt

Table 1. Comparison of selected features defining the 'orogenic gold' deposit class (after Groves et al. 1998) and CLGB gold occurrences

Orogenic gold mineralisation	**CLGB mineralisation**
Host terrane: • Volcano-plutonic rocks (greenstone belts hosting Archaean deposits interpreted as most commonly having an oceanic back-arc setting, dominated by back-arc basalt and felsic to mafic arc rocks)	• Ultramafic to mafic volcanic (tholeiitic) host rocks, + minor clastic marine sediments and BIFs. Pre-, syn-, and post-tectonic plutonic rocks present but not hosting known deposits. Depositional environment evolves from intra-cratonic rifts (Onkamo and Salla Groups) to an opening ocean phase (Kittilä Group), followed by collision (Laino Group) and foreland basin development (Kumpu Group). Plutonic rocks with island-arc affinities occur within the Haaparanta Suite (Lehtonen et. al. 1998). See Figure 1
• Convergence-dominated deformation	• At least three major deformation events, two of which (D_1 and D_2) which are clearly related to convergence events
• Typically greenshist-facies metamorphic grade	• Typically greenschist-facies metamorphic grade (see Hölttä et al., this volume)
Host structures: • Hosted by second- or third-order brittle-ductile structures near large-scale compressive structures • Mineralised structures have vertical and down-plunge extents of several 100 m to 2 km	• Known deposits are near first-order thrusts and within later strike-slip shear zones. Mineralisation within/near first-order thrusts generally hosted by crosscutting D_3 shears or D_3 veins • Suurikuusikko mineralisation has a down plunge extent of at least 500 m (open at depth), and the host strike-slip shear zone is mineralised for a strike-length of at least 5 km
Deposit mineralogy and alteration: • Au in Qtz-dominated vein systems	• Au in carbonate-dominated vein systems (with quartz ± albite) or sulfide disseminations
• Au mostly in Fe and As sulfides (but reflecting host rock composition)	• Au mostly within pyrite and arsenopyrite, and also in gersdorffite (Ni-Co-As sulfide) at some sites. Au occurs as inclusions and/or within the lattice of sulfide phases. Free Au is less common
• Au-Ag ratio 10-1 (usually high within this range)	• Insufficient data, but Suurikuusikko values are within this range (ratio increases with increasing Au grade)
• Au grades 5 – 30 g/t	• Similar
• Element enrichments typically As, Bi, B, Hg, Sb. Te and minor W, Cu, Pb, Zn)	• Limited available data, but As, Cu, Ni, Fe, and Ag typically enriched, ± Sb, Te, Ni, and W. Cu and/or Ni enrichment common at several occurrences (see Eilu 1999)
• Alteration involving CO_2, S, K, H_2O, SiO_2, Na and LILE addition Typical phases pyrite, pyrrhotite, arsenopyrite, sericite, fuchsite, biotite, k-spar, albite, and amphibole	• CO_2 (distal calcite, and proximal ankerite/dolerite±amorphous 'graphitic' carbon), S (sulfide), Na (albite) and Si (quartz) addition dominates. Potassic alteration limited except for areas with fuchsite alteration (Cr+K). Biotite, sericite, potassic feldspar, amphibole, leucoxene and tourmaline at some sites only
• Low salinity, near-neutral pH, H_20-CO_2±CH_4 ore fluids	• Insufficient data. Ore fluids likely to be similar given the abundance of carbonate associated with mineralisation. High base-metal content (Cu) at some sites may suggest more saline fluids for these areas[1]. Reducing fluids likely at occurrences with 'graphitic' alteration
Timing: • Late orogenic Au mineralisation • Precambrian Au typically 20-70 million years after the youngest volcanism	• Gold is late (related to D_3 structural features present at each location) • Insufficient dating, but probably <35 million years after the majority of mafic volcanism (see Table 4)

[1]. Low salinity fluids have been attributed as responsible for the common lack of base-metal enrichments within orogenic lode-gold deposits (Kerrich and Fryer 1981). However, CLGB Cu-rich gold occurrences are also proximal to Savukoski Group sediments that cold be a source of base metal enrichment in there deposits. Documented orogenic deposits in other regions with high-salinity fluids have a spatial association with sedimentary basin sequences (see Groves et al. 2000 and references within).

& Vanderhor 1998) and Superior Province of Canada (e.g., Robert & Poulsen 1997). A brief comparison of CLGB greenstone-hosted gold mineralisation and features documented as defining the orogenic gold deposit type (Groves et al. 1998) is presented in Table 1. In detail some CLGB gold occurrences, particularly those in the western part of the Belt, display features that could be considered transitional between orogenic gold deposits and iron-oxide copper-gold (Hitzman et al. 1992) deposits. These include high copper-gold ratios and extensive albite alteration. Iron-oxide copper-gold deposits are the dominant deposit type in the northern Norrbotten region of northern Sweden (e.g., Frietsch et al. 1997), immediately west of the CLGB.

The CLGB remains under-explored compared to other greenstone belt terrains, despite being a region of proven resource potential in a country with levels of economic development and political stability equal to any major developed nation. Little CLGB-focused research or exploration activity occurred until the mid-1980s, and levels in 2001 remain low. To improve background information available on the CLGB, in

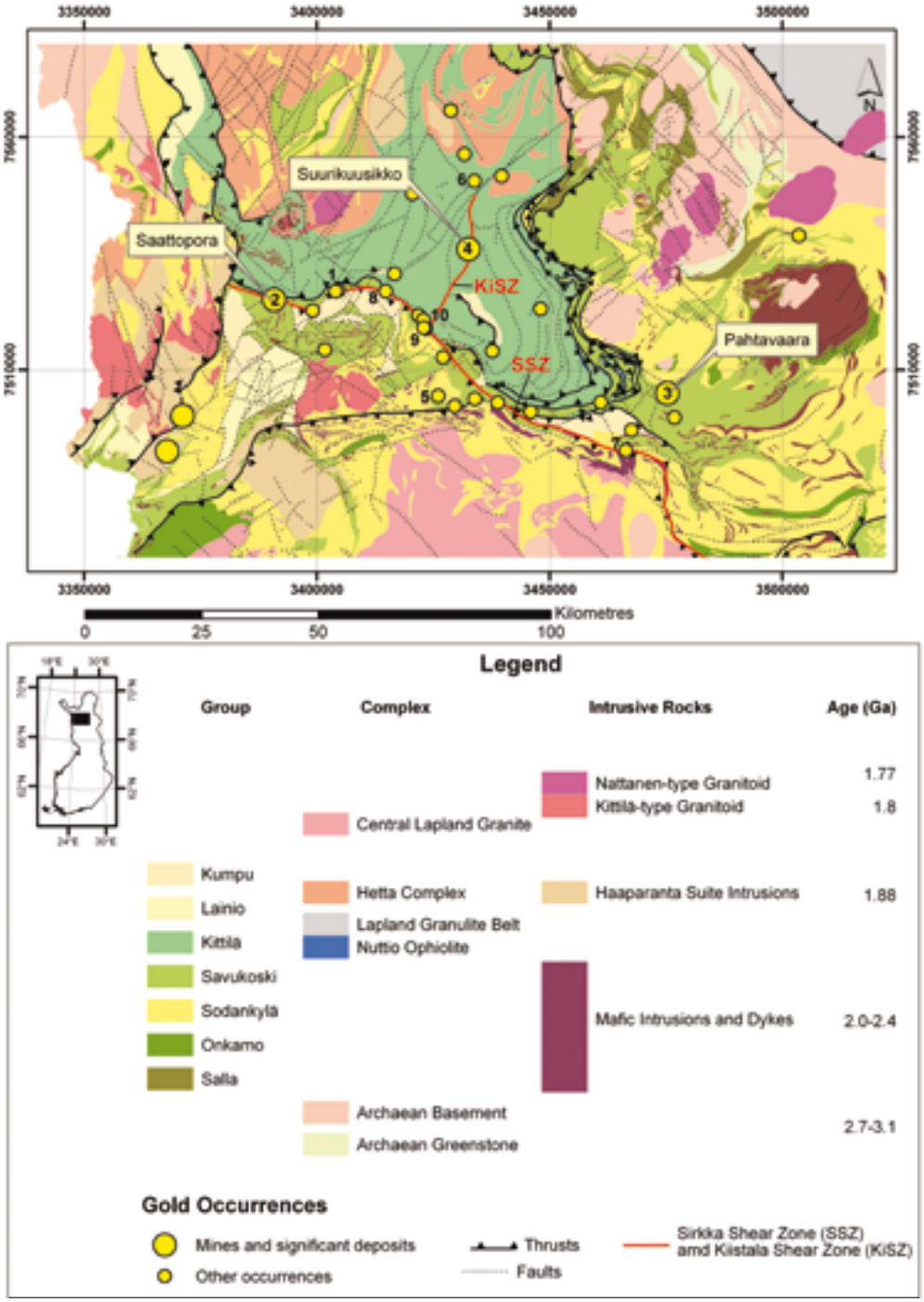

Fig. 1. Simplified lithostratigraphic map of the Central Lapland Greenstone Belt (afer Lehtonen et al 1998), showing the location of the gold prospects included in this work and major fault zones. Only basic fault traces are shown in this figure. The detailed morphologies of these are more complex, as demonstrated by their appearance in Figure 2. A detailed discussion of stratigraphic elements is provided by Hölttä et al. (this volume). Deposits: 1. Sirkka, 5. Isomaa, 6. Iso-Kuotko, 7. Kaaresselkä, 8. Loukinen, 9. Soretialehto, 10. Soretiavuoma North.

1998 the Geological Survey of Finland initiated a multidisciplinary research project aiming to generate new information on regional structure and deformation events, metamorphic events, and deposit-scale structure and fluid-flow. Combined with the revised stratigraphic reinterpretation of the CLGB (Lehtonen et al. 1998), the results of this project will provide solid background information of benefit to both future research and exploration in the region. This article presents the initial results for a component of this research entitled 'Structural and fluid-chemical characteristics of gold mineralisation in the CLGB, northern Finland'.

The gold occurrences included in this research are the three gold mines – Sirkka (Sirkka Kaivos) which underwent test mining 1955–1956 (Räisänen 2001), Saattopora (mined 1988–1995), and Pahtavaara (mined 1996–2000, reopened 2003–); the Suurikuusikko

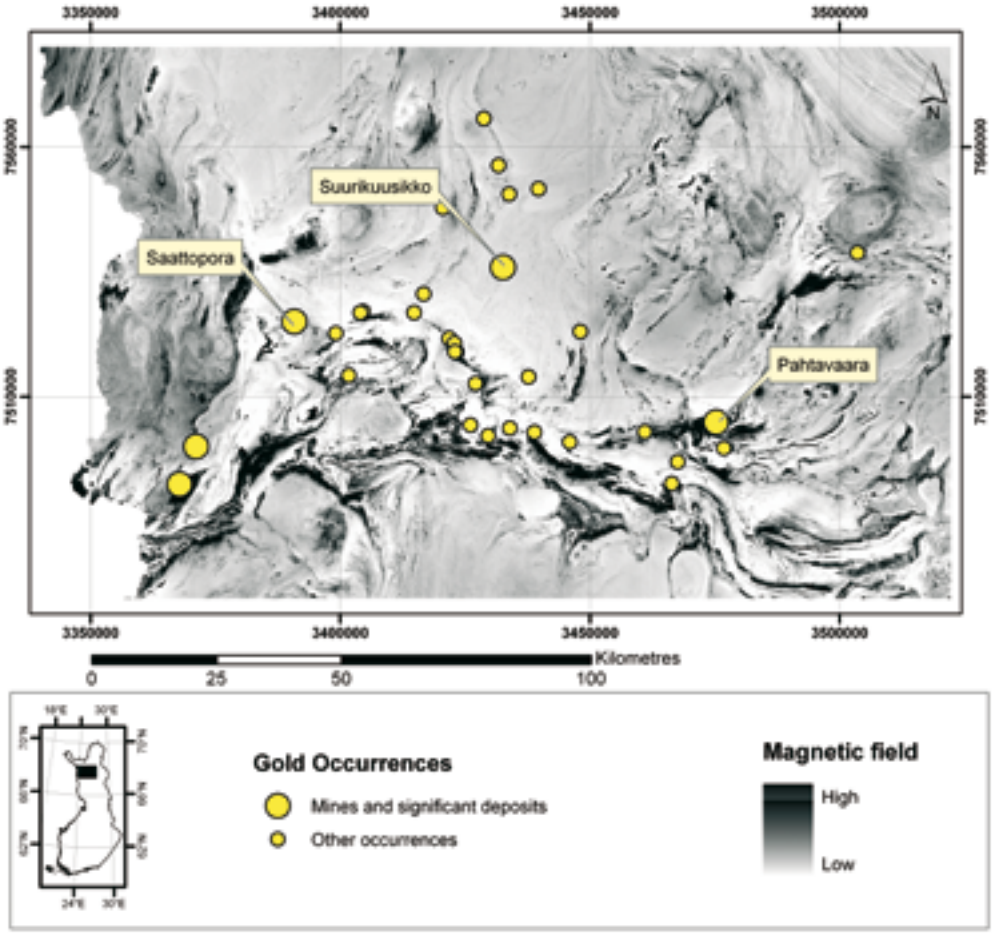

Fig. 2. Aeromagnetic map of the area shown in Figure 1, with prospect locations (Aerogeofysical data, GTK).

deposit; and six mineralised prospects – Isomaa, Iso-Kuotko, Kaaresselkä, Loukinen, Soretialehto and Soretiavuoma North (Figs. 1 & 2). Gold mineralisation at these sites is usually associated with intense albite- and carbonate-rich alteration assemblages. At some occurrences mineralised rocks also contain fine 'graphitic' carbon indicating extremely reduced conditions. This carbon is extremely fine-grained amorphous carbon with a graphitic appearance and it is referred to as graphitic alteration within this article, but the material is not crystalline graphite. In most occurrences gold is within sulfide minerals (mainly pyrite, arsenopyrite and gersdorffite (Ni-Co-As sulfide)) and less commonly as free gold grains.

The data presented here was derived from detailed mapping of man-made bedrock exposures of limited extent, from sporadic natural outcrops, from drill core, and from aeromagnetic images. The aim of this paper is to briefly summarise the field-based results of this research, and other information relating to the structural setting of a selection of CLGB occurrences. Basic conclusions regarding host structures and regional-scale guidelines to the likely prospectivity of CLGB deformation features will be presented.

REGIONAL DEFORMATION EVENTS – KEY FEATURES

The following sequence of deformation events, modified and simplified from interpretations by Ward et al. (1989) and Väisänen (2002), is used as the regional structural framework for the occurrence-scale work reviewed here, and is consistent with current results of this project. Extensional deformation relating to volcanism and some intrusions can be expected to have occurred during the deposition of CLGB rocks, and there is some evidence for later extensional events. The summary presented here does not include extensional events as these are yet to be clearly documented. The compressional deformation phases are simplistically correlated with the regional event likely to be generating deformation. See Hölttä et al. (this volume) for details of individual deformation products assigned to each phase.

The oldest mappable deformation features relate to thrusting at CLGB margins. N- to NE-directed thrusting occurred at the southern margin, driven by Svecofennian orogenic events occurring to the south. The Lapland Granulite Belt was placed over the N and NE margins of the CLGB by S- to SW-directed thrusting during another collision event at a similar time. Belt-wide thrusts and related deformation were produced by each event. A lack of clear overprinting relationships and precise geochronology discriminating these two events currently prevents denoting either as D_1 or D_2 respectively, but these are the first two major regional deformation events after volcanism ceased for which clear evidence exists. Away from CLGB margin areas correlating to convergent zones, it is difficult to assign deformation products formed at this time specifically to D_1 or D_2. This is mostly because although the tectonic transport directions of each event were opposite, the bulk strain orientations during each event were approximately parallel, resulting in the generation of structural features with similar strike orientations. The D_1 phase reported by Hölttä et al. (this volume) is here grouped with the major thrust events of D_1/D_2.

The Sirkka 'Line' or Sirkka Shear Zone (Figs. 1 & 2) includes a series of closely spaced S-dipping, sub-parallel thrusts and fold structures relating to convergence at the southern margin of the CLGB. Thrusts within this zone have average dips of approximately 40°, interpreted from seismic refraction profiles (Berthelsen and Marker 1986; Gaál et al. 1989). The Sirkka Line is the main rheological boundary within CLGB stratigraphy, separating a sequence of sediment-dominated rocks to the south (Savukoski Group) from a volcanic-dominated package to the north (Kittilä Group). In detail it is a complex structural zone involving several parallel shear zones and shear zone segments. Some segments along this zone were at least partially reoriented and/or reactivated during subsequent deformation, although interpreting exact movement histories on these shear zones is difficult. Thrust zones shown on regional maps for the western and eastern margins of the CLGB (Fig. 1) have unresolved origins and are poorly understood.

D_3 involved the development of strike-slip shear zones (e.g., Kiistala Shear Zone, Fig. 1) that displace or intersect D_1/D_2 thrust zones. D_3 shear zones generally strike NW-SE, N-S and NE-SW, at high angles to the strike of most D_1/D_2 thrusts. Neither the external events driving the development of these shear zones nor the exact timing of their initiation is clearly understood. It has been suggested that these shears may utilise segments of early thrusts (Väisänen 2002), or transfer shear zones formed during pre-D_1 extension relating to volcanism (Ward et al. 1989). It is also possible that these shears were initiated as a response to the opposing compressions operating during D_1/D_2 as a compensating response to thrusting. Strike-slip shear zones relating to CLGB deformation and potentially correlatable events further south were also recognised by early researchers, although interpreted using a variety of theoretical frameworks (e.g., Tuominen et al. 1973; Talvitie 1976; Mikkola & Vuorela 1977). Other deformation products were also generated during D_3 (e.g., Väisänen et al. 2002), but strike-slip shear zones are the most obvious features. D_3 is a complex and incompletely understood deformation phase, with shear zones here classified as D_3 likely to have formed late within this phase.

Ward et al. (1989) proposed that movement on large D_3 shears produced a dextral rotation of the entire CLGB, generating its SE-bulging geometry and controlling the distribution of high and low strain zones associated with D_3 shears. A dextral rotation of maximum principle stress (σ_1) throughout the development and/or activity of D_3 shears is supported by observations made during this research for the Kiistala Shear Zone, where σ_1 rotates through NW- and NNW-directed to a final NE-directed σ_1 for deformation events observed in the immediate area of the Suurikuusikko occurrence. Favourably oriented sections of D_1/D_2 thrusts were potentially reactivated during this rotation, in particular a NW-striking section of the Sirkka Line coinciding with several gold occurrences (section containing the Soretialehto and Soretiavuoma North occurrences labeled in Fig. 1). The orientation of D_3 features is strongly influenced at a local scale by pre-existing structures, especially in areas south of the Sirkka Line.

Importantly, an association between gold mineralisation and D_3 shearing has been recognised by this and other studies (e.g., Sorjonen-Ward et al. 1992; Väisänen 2002). A summary of selected key features associated with D_1 to D_3 deformation is given in Table 2. D_4 involved numerous discontinuous, low displacement brittle shear zones (usually conjugate sets).

CLGB stratigraphy ranges in age from 2.5 Ga to 1.88 Ga (Lehtonen et. al. 1998). The absolute ages of deformation events require further constraint, but a maximum age for deformation (D_1/D_2) of 1.89 Ga has been proposed (Lehtonen et. al. 1998). Possible D_3 deformation ages include 1.89 to 1.88 Ga (for CLGB deformation, Sorjonen-Ward et al. 1997); 1.88 Ga (for similar structures adjacent to the CLGB, Wikström et al. 1996); 1.90–1.85 Ga and 1.84–1.80 Ga (for successive movements on the Kolari Shear Zone, a strike-slip shear zone similar in orientation to CLGB D_3 shear zones but located at the western

Table 2. Key deformation events, inferred σ1 directions and/or tectonic transport directions of these events, and typical strike orientations of the structures generated

Major deformation phase	**Regional σ_1 direction or tectonic transport direction**	**Strike of key structures**
D_1/D_2	N-NE transport in south	Sirkka Line, containing E-striking to NW-striking segments. NW-striking sections may reflect later deformation of the Sirkka Line
	S-SW transport in north	NW-striking margin thrusts at the northeastern CLGB/Lapland Granulite Belt contact
D_3	Generally NW-SE to NE-SW σ_1 (oldest to youngest movements respectively), but variably modified by local conditions	E.g., N- to NE-striking Kiistala Shear Zone. D_3 shears are most likely to have more variable strikes south of the Sirkka Line, and WNW- to NW-striking D_3 structures are common in this area

margin of the CLGB, Berthelsen & Marker 1986; not shown in Fig. 1), and a minimum age of 1.77 Ga (for an undeformed felsic dyke intruding D_1/D_2 thrust related folds within the CLGB (Väisänen 2002)). Post-collisional Nattanen-type granites (Fig. 1) cut by D_4 faults also have an age of 1.77 Ga (Lehtonen et al. 1998), providing a minimum age for D_3 and a maximum age for D_4.

Estimated age ranges for mineralisation based on the isotopic composition of lead in sulfides include 1.99–1.87 Ga for mineralisation in the Saattopora area; 1.89–1.85 Ga for mineralisation in the Soretiavuoma, Kiistala (Suurikuusikko) and Iso-Kuotko areas; and 1.85–1.82 Ga for mineralisation in the Pahtavaara area (Mänttäri 1995; locations in Fig. 1). The resolution offered by the available age dates for mineralisation is

Table 3. Summary of available dates and timing relationships between CLGB deposition, deformation, metamorphic, and mineralising events. Plotted date ranges include error bars. Only post-tectonic intrusions (1.77 Ga Nattanen granites) have been included due to their relevance to age dates, but pre- and syn-tectonic intrusions are also present within CLGB stratigraphy. Data sources: columns 1, 2 and 3 Lehtonen et. al. 1998; column 4 (date ranges left to right, exact values quoted previously in text) Sorjonen-Ward et al 1997, Wikström et al. 1996, Berthelsen and Marker 1986, maximum age Väisänen et al. 2002; column 5 Väisänen et al. 2002; column 6 Mänttäri 1995, ranges left to right for Saattopora (1.990–1.870 Ga), Soretiavuoma North/Kiistala/Kuotko (1.890–1.852 Ga), and Pahtavaara (1.850–1.820 Ga) areas respectively

Age ~Ga	**Host rock deposition phase**	**D_1/D_2**	**D_3**	**D_4**	**Mineralisation (Pb-sulfide age range)**
1.70					
1.80	Post-tectonic intrusions		Minimum D_3 age 1.77 Ga	Maximum D_4 age 1.77 Ga	
	Foreland basin	Maximum D_1/D_2 age 1.89 Ga	Possible D_3 ages		
1.90	Collision				
	Opening ocean basin				
2.00					
2.10	Cratonic/ cratonic margin phase				
2.20	Intra-cratonic rifting 2.5-2.2 Ga				

insufficient and requires better paragenetic constraint. More analyses of the dominant gold-bearing sulfide phases and alteration minerals at individual occurrences are needed to constrain the absolute age(s) of mineralisation.

Peak regional metamorphism in areas containing gold occurrences also requires further constraint, but results to date suggest that peak metamorphism began during D_1/D_2 thrusting in some areas (Hölttä et al., this volume). Table 3 presents a brief timeline of CLGB events as constrained from available age dates. This data, though insufficient, suggests a late orogenic timing for gold mineralisation.

STRUCTURAL CONTROLS ON MINERALISATION

A clear regional spatial relationship exists between shear zones and mineralised sites within the CLGB (Fig. 2). Gold occurrences at Saattopora, Sirkka, Soretialehto and Soretiavuoma North are located on or immediately adjacent to Sirkka Line structures, and at least 12 other gold occurrences are located within 3 kilometres of the Sirkka Line (Eilu 1999). A significant spatial relationship between regional lineaments such as the Sirkka Line and gold has also been reported for other orogenic gold districts (e.g., Eisenlohr et al. 1989).

The Suurikuusikko and Iso-Kuotko occurrences occur on D_3 shear zones. The Pahtavaara, Kaaresselkä and Isomaa gold occurrences also coincide with shear zones with interpreted strike-slip movements, although whether these features represent shear zones generated or reactivated during D_3 is less clear. The Loukinen occurrence is spatially associated with both the Sirkka Line and an intersecting D_3 shear zone. The task for this project and for exploration within the CLGB is to understand the causes and practical implications of these spatial correlations.

Deposits spatially associated with the Sirkka Line

Saattopora

The Saattopora deposit (Figs. 1 & 2) is on an E- to ESE-striking section of the Sirkka Line, and provides a good introduction to the complexities of dealing with Sirkka Line-associated deposits. D_3 structures are not obvious on regional map sheets of the immediate area of Saattopora, or clearly seen in regional aeromagnetic images. It might therefore be assumed that the location of Saattopora is wholly influenced by Sirkka Line structures, but in detail this connection is not so clear.

Surface Sirkka Line structures at Saattopora are sub-vertical, as are the Sirkka Line aeromagnetic features in the immediate area (Airo M-L., pers. com. 2001), unlike the moderately south-dipping structures that would be expected in a simple thrust zone. The envelope of intense albite alteration associated with and containing the Saattopora ore lodes strikes parallel to the Sirkka Line, but dips steeply to the north (Korvuo 1997; Fig. 3). This distribution of alteration may reflect a preferentially altered stratigraphic unit that obtained its current strike during thrusting, but the dip of the zone is opposite to that expected within a simple thrust-interlayered stratigraphy.

A detailed alteration and deformation history exists at Saattopora, with an early carbonate-dominated (low-iron carbonate) alteration phase overprinted by the strongly albitised envelope to ore-bearing veins (Fig. 3), followed by further carbonate (high-iron carbonate) alteration hosting gold mineralisation. In order of formation, a WNW- to NW-striking foliation, E-verging and N- to NNW-verging folds, and a NE-striking cleavage all predate mineralisation and have variable timing with respect to alteration events. Gold occurs in late, brittle carbonate-rich veins, and in associated breccia zones in the immediate wall rock of the veins. These veins have several orientations but are usually vertical, very planar N-S-striking veins approximately orthogonal to Sirkka Line structures in the area. The veins are not fibrous and their mechanism of formation is not certain. Gold-bearing veins are not deformed at a macroscopic scale, and appear to be the youngest structural feature observed at Saattopora.

Most features within this complex deformation sequence cannot be fully explained by a simple, causative relationship between N- to NE-directed D_1/D_2 thrust-related deformation and mineralisation. As is evident from the numerous broken and displaced Sirkka Line segments visible in Figure 2, Sirkka Line thrusts have undergone significant post-thrusting deformation and/or reactivation. This and the complex nature of deformation at Saattopora, compared to the undeformed nature of ore veins, suggest that the veins were emplaced after most of the deformation and support a D_3 timing for mineralisation.

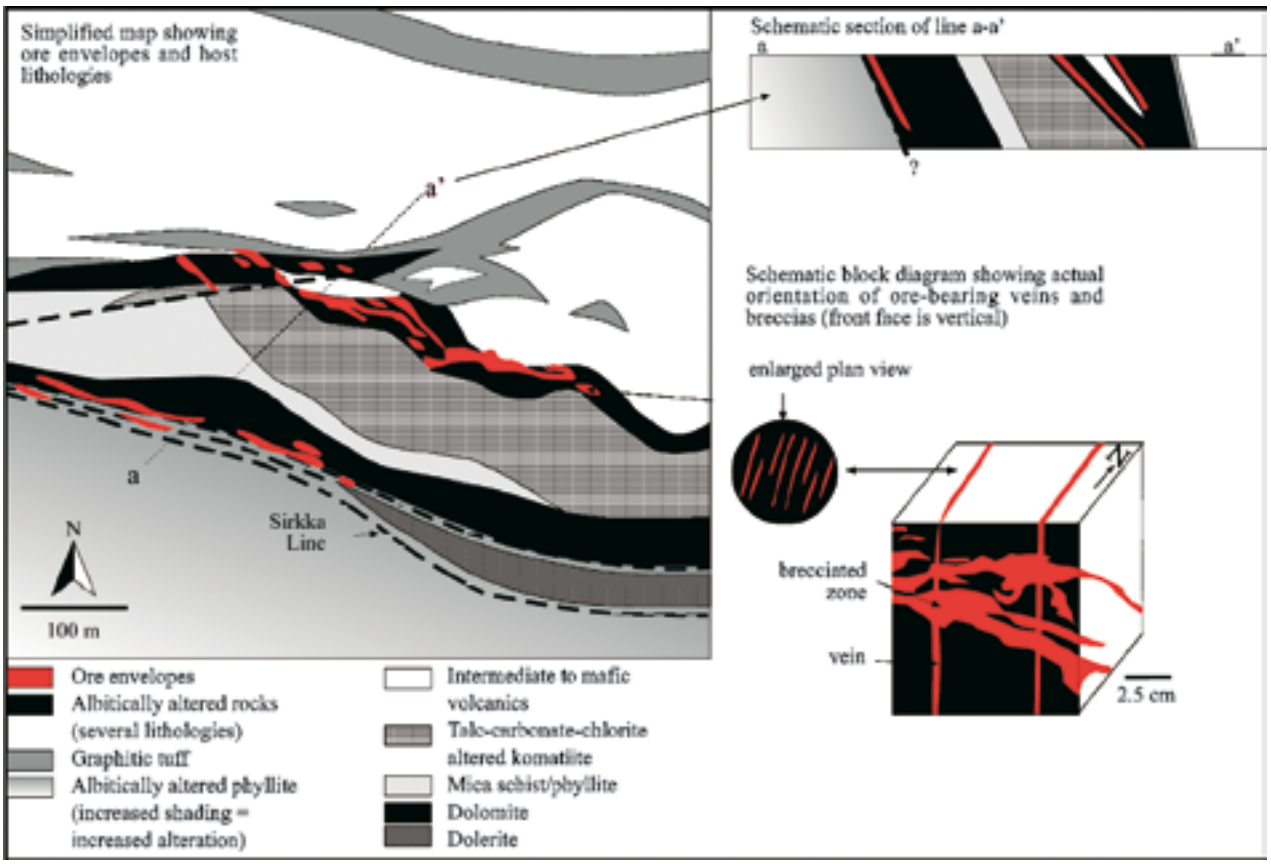

Fig. 3. Simplified surface geological map and cross-section of the Saattopora mine area. Block diagram illustrates the morphology of the ore. Gold is contained within pyrite, pyrrhotite and lesser amounts of chalcopyrite hosted by planar carbonate-rich veins and vein-associated quartz-carbonate-sulfide breccias intruding and cross cutting earlier layering. Surface map and cross section modified after Korvuo (1997)

Sirkka (Sirkka Kaivos)

Mineralisation at Sirkka also has a close spatial association with the Sirkka Line (Figs. 1 & 2). An obvious characteristic here and at other locations along the Sirkka Line is an intense cleavage that gives rocks a banded appearance. This fabric is well developed in meta-sedimentary and meta-basic host rocks, has an E-W to NW-SE strike and moderate to steep dip, and is interpreted as an early deformation feature associated with Sirkka Line thrusting. Evidence for gold-rich mineralisation clearly synchronous with or pre-dating this fabric has not been found at any location during this research. At Sirkka, mineralised quartz-carbonate-sulfide breccias containing gold as inclusions within gersdorffite and arsenopyrite (Vesanto 1978) post-date this fabric, as does the associated pervasive carbonate alteration of host rocks, implying that mineralisation post-dates D_1/D_2 thrusting.

Gold is also present in veins within Kumpu Group sediments (Hugg R., pers. com. 2003) deposited during the late collisional to early foreland basin stage of CLGB evolution, and which disconformably overlie the ore-host sequence at Sirkka. These veins are similar in composition to mineralised breccias at Sirkka, and may provide further evidence for mineralisation post-dating thrusting if belonging to the same phase of mineralisation.

Loukinen

East of Saattopora and Sirkka, the Loukinen occurrence (Figs. 1, 2, & 4), provides a clear example of the role of D_3 strike-slip shear zones in influencing deposit location within D_1/D_2 deformation zones. Loukinen is located on an E- to ESE-striking section of the Sirkka Line that contains several gold occurrences. Limited interpretive modelling of drill core data suggests the envelope of mineralised zones is steeply dipping, and strikes approximately parallel to the trend of the Sirkka Line (Keinänen V., pers. com. 2001). However, available surface exposures provide evidence constraining mineralised breccias to intersection points between the Sirkka Line and N- to NNE-striking D_3 dextral strike-slip shear zones (Figs. 4a & 4c). Gold at Loukinen occurs as free gold, or in pyrite and gersdorffite

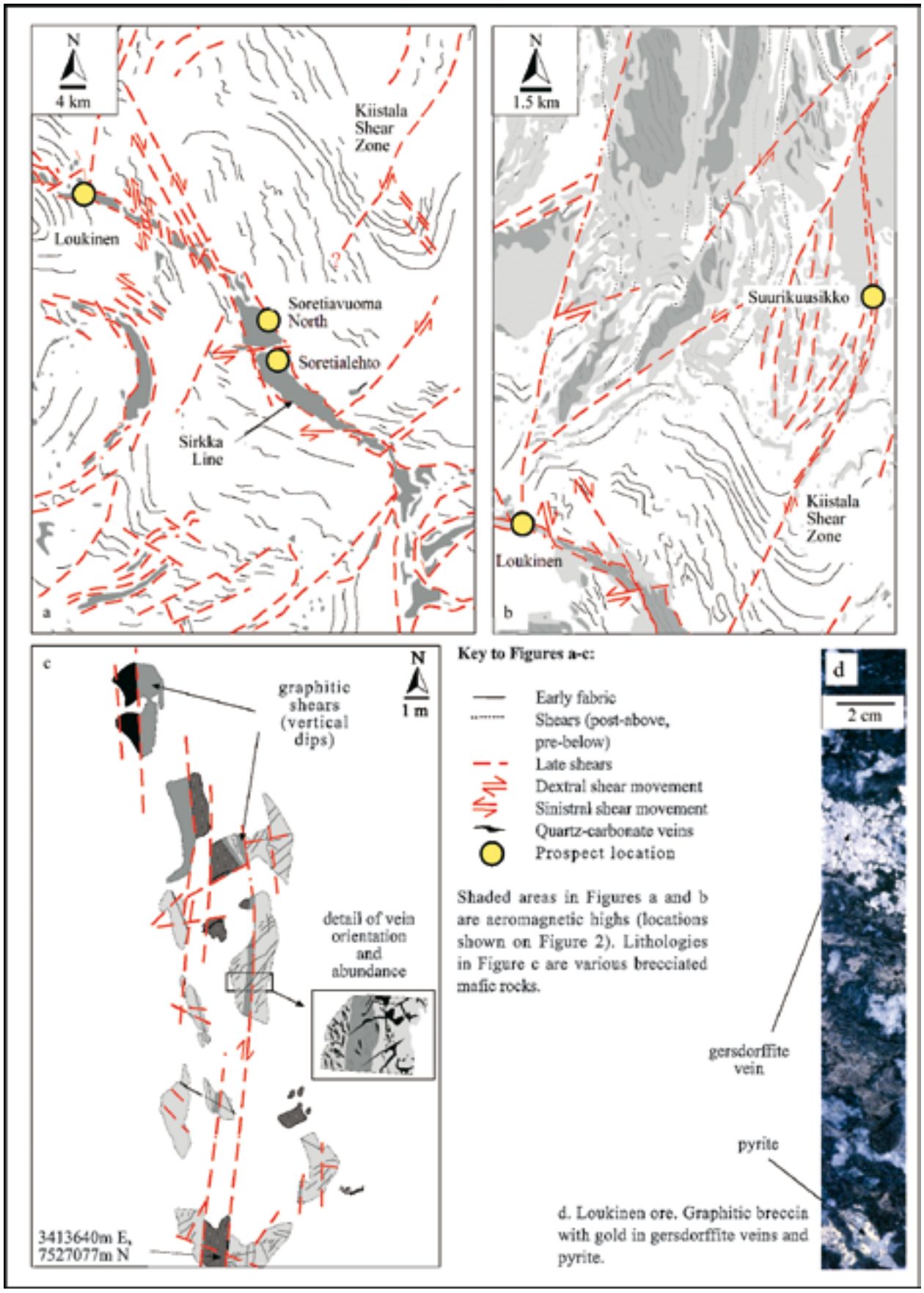

Fig. 4. Simplified interpretation of features present in aeromagnetic images (a) in the vicinity of the Loukinen, Soretiavuoma North, and Soretialehto prospects (circled). A similar interpretation to that shown in Figure 4a, covering an area further north and including the Suurikuusikko property (b). Figures 4a and 4b are designed to highlight the location of prospects relative to major faults. Simplified map of surface exposure at the Loukinen prospect (c), showing the presence of N- to NNE-striking shears associated with graphitic alteration and brecciated zones. Example of Loukinen ore (d; Dark aversin fig a + b = magnetic high)

(as inclusions or within the lattice; Eilu 1999) within graphitic quartz-sulfide breccia zones generated by movement on these D_3 shears.

Soretialehto and Soretiavuoma North

Southeast of Loukinen, Sirkka Line structures bend to strike NW and decrease in dip (Airo M-L. pers. com. 2001; Figs. 1 & 2). This bend in the Sirkka Line has been interpreted to result from deformation (folding and shearing) of this zone during the rotation of the CLGB associated with D_3 (Ward et al. 1989). More information is required to establish whether the current orientation of this bend relates totally to D_3 deformation, to a combination of D_3 deformation and pre-D_3 events, or preserves an original thrust segment orientation +/- syn-thrusting deformation.

Common in parts of this area are rocks with intense potassic alteration. Ultramafic protoliths have been variably altered to fuchsite-carbonate-rich assemblages. The timing of this alteration event relative to early Sirkka Line movements is unclear. However, the distribution of alteration visible in drill core from this area indicates that it is more sporadic than would be expected if it were a syn-depositional alteration event. Some gold deposition has accompanied this alteration event, with altered rocks outside concentrated occurrences having gold grades averaging up to 0.5 ppm (Pekkala & Puustinen 1978). Higher grade gold mineralisation in these rocks is restricted to zones cross-cutting the altered hosts, but it is not clear if the background and high gold grades represent discrete mineralisation phases, or stages of the same event.

Elevated gold grades at the Soretialehto occurrence (Figs. 1 & 2) occur adjacent to a contact between fuchsite-carbonate-altered meta-komatiites and sericitised and carbonate-altered graphitic phyllite. At Soretialehto, gold occurs in pyrite within quartz-carbonate-rich breccia zones cutting the altered komatiites, and in pyrite or as free gold within later planar quartz-carbonate extensional veins. Apart from some evidence for early E-W compression, fabrics at this site strike NE, and are overprinted by mineralised breccia zones bound by N- to NE-striking shear zones. These shear zones experienced strike-slip movements, with variable displacement senses indicated. The gold-bearing veins are not folded and have a similar orientation to mineralised veins at Saattopora, striking N to NNE. No NW-striking fabrics paralleling the orientation of the Sirkka Line in this area were seen at Soretialehto.

The nearby Soretiavuoma North occurrence (Figs. 1, 2, & 5) occurs along a similar NW-striking lithological contact as Soretialehto, but the meta-komatiitic host rocks here do not appear to show the extreme potassic alteration expressed as fuchsite-rich rocks at Soretialehto. An early WNW- to NW-striking folded fabric (local S_1) is the oldest structural feature preserved. This fabric appears to reflect non-coaxial strain, with a poorly preserved s-c fabric indicating strike-slip movement evident in some samples. The nature of this fabric suggests an association with the strike-slip dominated D_3 phase of deformation. What remains to be established is whether S_1 initially developed during D_3, or was a fabric produced in association with D_1/D_2 thrusting that was later sheared (perhaps during the folding seen at this site). S_1 is approximately parallel to the Sirkka Line, but resolving the cause of the Sirkka Line orientation here is also required before the origins of this local S_1 can be understood.

Folds of S_1 have sub-vertical axial planes striking NE, and axes typically plunging ~45° NE. An axial-planar, NE-striking crenulation cleavage is associated with these folds, and numerous quartz-carbonate shear veins with similar orientations to the crenulation cleavage cut the limbs and hinges of the folds. Pervasive iron-rich carbonate alteration occurred pre- to syn-vein formation, and intensifies at the margins of veined zones and sections of tighter folding.

Folded S_1 and the crenulation cleavage are in turn are cut by a series of NW- and NE- striking shears, followed by or synchronous with NNE- to N-striking shears. These are strike-slip shears, with movement lineations pitching less than 20°. The dominant movement sense is ambiguous, with both sinistral and dextral senses observed for all shear zone orientations, and no clear timing relationships observed between the two senses of movement. Gold-bearing quartz-carbonate-sulfide infill zones have developed within these shears. The highest gold grade in outcrop at Soretiavuoma North occurs at the intersection points between the shear zones labelled a and b in Figure 5.

The inferred σ_1 direction associated with folding at Soretiavuoma North is approximately NW-SE. Such a compression orientation is similar to that required to dilate the section of the Sirkka Line hosting Soretialehto, Soretiavuoma North, and other occurrences, as it is approximately parallel to the NW-strike of this zone (Fig. 1). The map of altered lithologies in Figure 5 also suggests a widening of the altered zone around Soretiavuoma North in NW-striking sections, and the simplified envelopes of gold-bearing zones (veins and breccias) are consistent with the orientation of failure zones predicted to result from dilation of this zone, either as internal breccia zones or breccias associated with shearing at the margins of a dilated zone.

At least the NW-striking mineralised shear zones

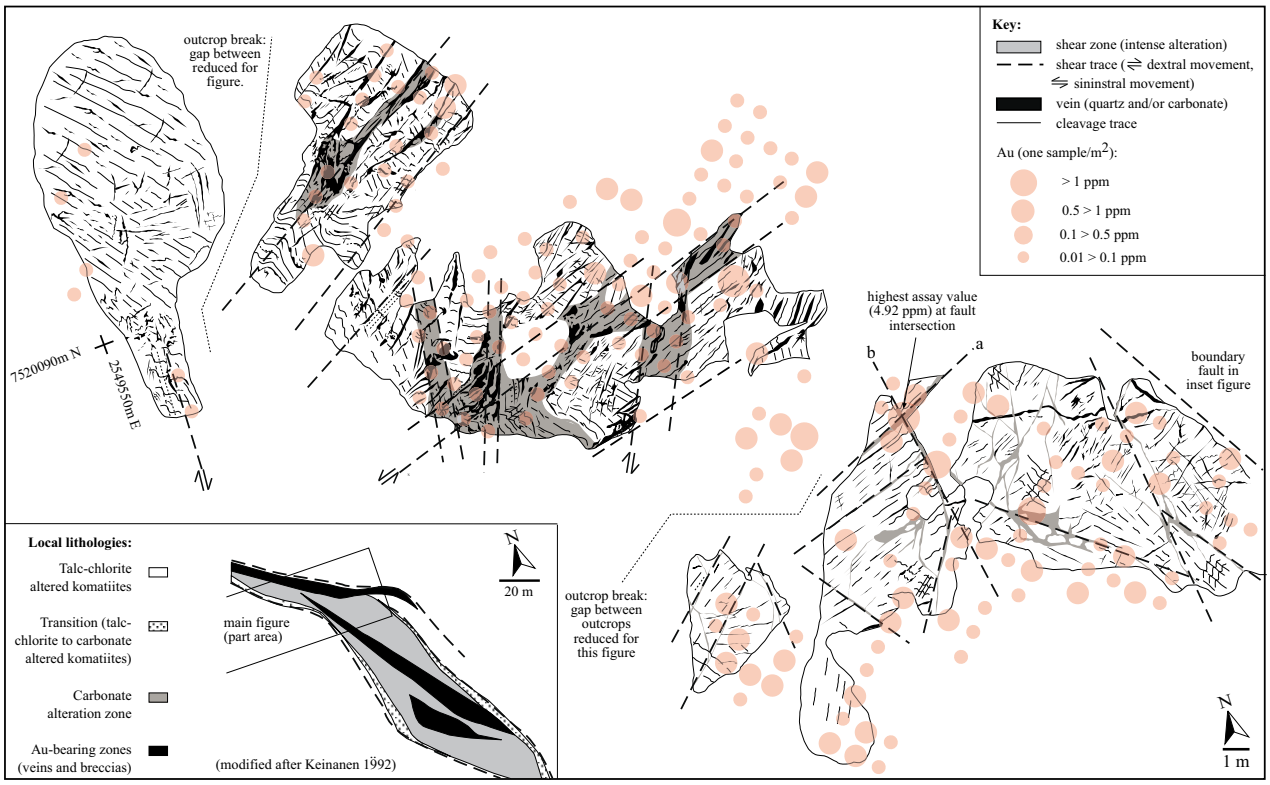

Fig. 5. A simplified map of surface exposures at Soretiavuoma North with gold values shown as an overlay. Shear zones have strike-slip movement with low-angle vectors (pitch values < 20°), and are steeply dipping or vertical. Veins are pre-shear quartz-rich quartz-carbonate veins and earlier carbonate-rich veins of variable dip. Pre-shear fabrics have moderate to vertical dips. Folds of S_1 plunge approximately 45° NE. Note scale difference between the main and inset figure. Assay values relate to nine combined mini-core samples taken for each square meter of outcrop. Values shown outside mapped areas correspond to exposure that is now covered

at Soretiavuoma North fit the above suggestion, with shears in other orientations possible relating to these NW-striking shears, or to other D_3 shear zones in the immediate area. The strike of late shear zones associated with mineralisation at Soretialehto and Soretiavuoma North most resemble the orientation of D_3 shear zones north of the Sirkka Line, including the N- to NE-trending Kiistala Shear Zone hosting the Suurikuusikko deposit. The Kiistala Shear Zone potentially intersects the Sirkka Line near both Soretialehto and Soretiavuoma North (although its exact southern termination point is unclear), further supporting the existence of D_3 deformation in this area.

In the case of the Kiistala Shear Zone, D_3 is expressed as a distinct shear zone, but at Soretialehto and Soretiavuoma North D_3 may be expressed either as re-use of earlier structures and/or an overprinting of early features by D_3 deformation. As at the previous occurrences described, complex post-thrusting deformation is again suggested by the features present at Soretialehto and Soretiavuoma North, making a D_1/D_2 timing for mineralisation unlikely.

Deposits spatially associated with strike-slip shear zones in the south and southeastern CLGB

The deformation history of the southern and southeastern CLGB is clearly complex (Fig. 2) and remains to be investigated in detail. However, mineralisation at these sites shows similar features to the other occurrences discussed so far. In each case, mineralisation is spatially constrained to strike-slip shear zones, and occurs late in the sequence of deformation and alteration events recorded for each occurrence.

Isomaa

At Isomaa (Figs. 1 & 2), an auriferous quartz-pyrite breccia occurs near an E-striking bend of a NE-striking shear zone interpreted from surface mapping. It is likely that the breccia occurs within this shear but this could not be proven from current surface exposures. The shear zone bend is defined by intensely sheared

quartz-tourmaline-sericite-sulfide altered host rocks, and is also mineralised. Recorded movements on this shear zone were dextral strike-slip on a sub-horizontal elongation lineation, and the locations of mineralisation are consistent with deposition in a dilatant zone generated by movement on this shear zone. The mineralised breccia is paragenetically late and only partially deformed, probably by later movement on the host shear zone. The relationship of this shear zone to Sirkka Line structures is not known.

Kaaresselkä

The Kaaresselkä area (Figs. 1, 2, & 6) contains several gold occurrences, and the timing of mineralisation at each is the same relative to the local deformation sequence. No concrete evidence for N-NE-directed thrust-related deformation was encountered during mapping, but several fabrics older than the mineralised structures exist. It is possible but not demonstrable due to lack of outcrop that one of these older fabrics may relate to early thrusting, and the Kaaresselkä area lies near a complex WNW-striking southeastern continuation of the Sirkka Line (Figs. 1 & 2).

Gold occurs as free gold or within pyrite and chalcopyrite (as lattice substitutions; Eilu 1999) in intensely foliated zones associated with WNW-striking, steep- to vertically-dipping sinistral strike-slip shear zones; and in late NE-striking, steep- to vertically-dipping brittle carbonate-rich veins. Both features cut all earlier fabrics, and are not themselves deformed apart from minor displacement by late faults. Pervasive carbonate alteration is also associated with mineralisation.

Mineralised sites and NW- to WNW-striking shear zones in the area are concentrated within a steeper western limb section of a fold (sketched in detail in Fig. 6, and evident in Fig. 2). These shears may have been initiated on this limb in response to fold tightening, but the timing of this folding relative to D_3 is not clear. Mineralised shears at Kaaresselkä have a similar orientation to Sirkka Line thrust remnants in this area, but the movements immediately pre- to syn-mineralisation are clearly strike-slip. This and the generally undeformed nature of ore hosting structures suggest a connection between mineralisation and D_3 deformation.

Pahtavaara

The Pahtavaara occurrence (Figs. 1 & 2) is also in a structurally complicated location. Units of the Sattasvaara komatiite complex host the deposit, and extension-related structures associated with the evolution of this complex are likely to have provided an

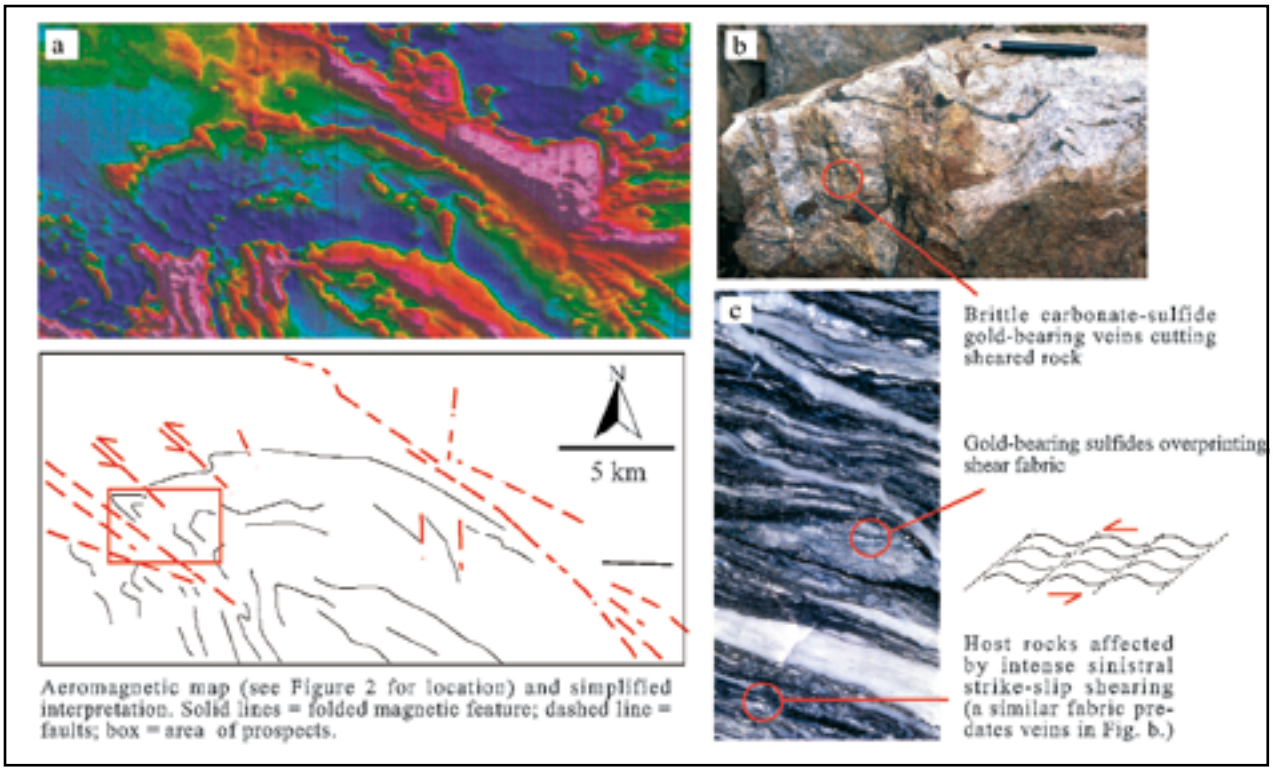

Fig. 6. Aeromagnetic image of the Kaaresselkä area (a). Equivalent faults in surface exposures have sub-vertical to vertical dips. Gold-bearing carbonate-rich veins cutting sheared quartzite (b; pencil is approximately five centimetres long). Sheared ore host (c). Gold occurs in sulfides overprinting the dark shear fabric and augen-shaped clasts. In detail the shear fabric displays an s-c fabric (sketch) indicative of sinistral fault movement (figure width on short side is three centimetres)

inherent crustal weakness utilised by later deformation events. This complex is interpreted to have formed in an E- striking rift system, the products of which now lie in an E-striking, refolded syncline (Räsänen 1999). Rifts and shear zones striking ENE and NE also existed during deposition (Saverikko 1985). The northern and western margins of the complex are described as intensely folded and overthrusted (Räsänen 1999), and geophysical data suggests that the northern contact may be a reverse fault (Lehtonen et al. 1998).

A NE-striking cleavage, followed by an ENE-striking cleavage occur in this area, and an E-striking shear zone generating a segregation layering overprints both. In the area of most intense shearing, two types of mineralised structures occur. The oldest hosts the A-type (higher grade) mineralisation, which occurs within a series of E-striking alteration zones dipping 70° to 80° N (Korkiakoski & Kilpelä 1997). Gold-bearing, irregularly oriented barite-carbonate-quartz veins and infill breccias cut biotite-talc altered rock and tremolite-altered rock within these zones. The overprinting, lower-grade B-type mineralisation within the same alteration zones is hosted by a series of NNW-striking quartz-dominated veins and less abundant E-striking veins of the same composition (Niiranen K., pers. com. 2001). Gold in both mineralisation types occurs as discrete native grains at the grain boundaries of silicates and along micro-fracture surfaces (Korkiakoski & Kilpelä 1997), suggesting paragenetically late mineralisation. It is not certain if the two mineralisation phases are parts of the same fluid event.

Shear sense on the host shear zone is unknown, but the relatively regular repetition of NW- to NNW- striking B-ore veins suggests a dextral sense if the stress field generating the host shear also produced these veins. A NW-SE σ_1 for the Sattasvaara area was also suggested from a study of magnetic lineaments, the results of which also indicate dextral movement on several NW- to WNW-striking lineaments in the area (Airo 1990). Sorjonen-Ward et al. (1992) suggested that the shear zone hosting Pahtavaara evolved as a high-strain zone during reorientation of a regional strike-slip foliation (D_3). The timing of mineralisation and nature of the host shear zone suggest that Pahtavaara mineralisation was a late (D_3) event in a zone with a long history of deformation and alteration. However, an earlier timing for gold mineralization (even potential formation during a sea floor alteration phase) cannot be excluded for this deposit (Korkiakoski 1992).

D_3 shear-shear hosted deposits north of the Sirkka Line

Occurrences associated with strike-slip shear zones north of the Sirkka Line have relatively clearer and less complex settings than those further south. Discrete N- to NE-striking D_3 strike-slip shears are the dominant tectonic feature north of the Sirkka Line, where the voluminous Kittilä Group rocks provide a large volume of relatively homogenous stratigraphy. The extent of discrete D_3 shear zones into areas south of the Sirkka Line is not clear although, as discussed above, strike-slip shears or movements on shear zones are present there as well.

Suurikuusikko

Suurikuusikko, the largest known gold resource in the CLGB, is hosted by a shear zone similar in orientation to that which truncates the Sirkka Line at Loukinen (Figs. 1, 2 & 4). Suurikuusikko occurs within a mostly N-striking segment of an otherwise NE-striking D_3 structure (the Kiistala Shear Zone). All parts of this N-striking shear segment (and associated NE-striking segments to the south) are mineralised where drilled to date (<2001; along a strike length of 5.5 kilometres).

The Kiistala Shear Zone has a complex movement history, with the youngest D_3 movements recording dextral strike-slip shearing. Early folding, a sub-regional NW-striking shear fabric, and sinistral movements on the Kiistala Shear Zone all pre-date the latest shear movements. A direct correlation appears to exist between the intensity of shearing within the Kiistala Shear Zone and the amount of gold-bearing arsenopyrite present. As with mineralisation at Loukinen, 'graphitic' alteration also accompanies intense shearing and mineralisation at Suurikuusikko. Intense albite and carbonate alteration is also present in ore zones, decreasing sharply away from intensely deformed zones. Gold occurs as inclusions and lattice substitutions (Chernet et al. 1999) within arsenopyrite (73.2%) and as inclusions in pyrite (22.7%), with the remainder as free gold (Kojonen & Johanson 1999). Gold-bearing arsenopyrite and pyrite occur disseminated on microfractures, shear fabrics, and stylolitic features, all spatially bound between N- to NE-striking sections of the Kiistala Shear Zone.

Known ore zones at Suurikuusikko plunge moderately north, but the mechanisms controlling this plunge are not completely resolved. Ore zones are likely to occupy high strain zones generated during D_3 shearing on the Kiistala Shear Zone, although

other factors including preferential host lithologies, and shear zone/lithological contacts also influence the location and orientation of ore lodes. A more detailed discussion of Suurikuusikko is given by Patison et al. (this volume).

Iso-Kuotko

The Kiistala Shear Zone can be followed north until it joins others at a complex intersection of shear zones. The Iso-Kuotko occurrences lie close to the junction of these shears (Fig. 7). All of these shear zones are likely to be D_3 in age, but have not been studied in exposures with the exception of the Kiistala Shear Zone. The NE-trending shear zone shown in Figure 7 continues to the NE, causing sinistral displacement of D_1/D_2 thrust structures at the Lapland Granulite Belt/CLGB contact (Fig. 1), indicating a D_3 age for this structure.

Several phases of mineralisation have been reported at Iso-Kuotko, all of which overprint a series NW-striking fabrics evident in surface exposures. However, considering paragenetic and compositional similarities evident in all mineralised sections of drill core, it is likely that these 'phases' indicate that a series of structures have been utilized or generated by one mineralising event. Most mineralisation occurs in identical quartz-carbonate-sulfide veins and associated breccia zones, with over 60% of gold occurring as free gold between the grain boundaries of the vein and breccia minerals. (Härkönen et al. 2001). The first phase is reported occurring within a shear fabric dipping approximately 45° NE and containing parallel gold-bearing veins (Härkönen et al. 2001). Subsequent mineralisation phases include shear-hosted sub-vertical NW- and N-striking veins (Härkönen et al. 2001). Shear senses in outcrops indicate dextral strike-slip movement on some host shears.

The NW-striking shear-related mineralised structures are likely to relate to the NW-striking shear zone in the area seen in Figure 7. The N-striking veins are contained within shear zones of the same orientation to the Kiistala Shear Zone in the Suurikuusikko area immediately south of Iso-Kuotko. Apart from the ore veins and breccias described above, disseminated arsenopyrite is also present at Iso-Kuotko. These disseminations are more like Suurikuusikko mineralisation than the Iso-Kuotko ore veins and breccias, but the gold-bearing potential of disseminations needs further testing. The timing of all shears in the Iso-Kuotko area, and the undeformed nature of ore-bearing veins and breccias support a D_3 age for mineralisation in this area.

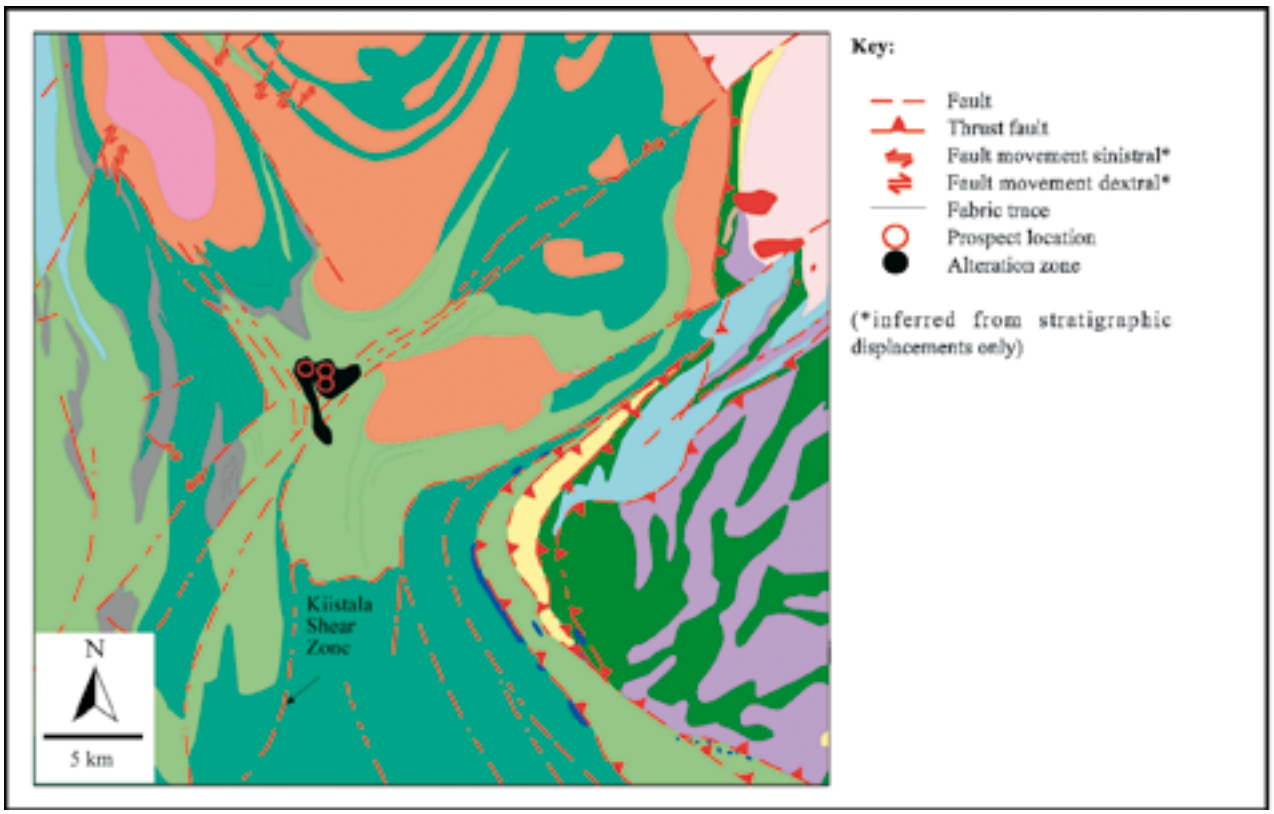

Fig. 7. Simplified map showing the location of prospects at Iso-Kuotko (after Härkönen and Keinänen 1988, and Sorjonen-Ward et al. 1992)

CONCLUSIONS

These examples provide a good introduction to the structural characteristics of CLGB gold occurrences. Clearly much work remains to be done to fully understand many aspects of deformation and mineralisation within the CLGB. However, several useful findings have emerged form this work to date, and these are reviewed below.

1. Strike-slip shear zones are prospective for mineralisation throughout the CLGB

From the summary of key gold-bearing structures presented in Table 4, it is clear that shear zones with strike-slip displacements are the most common host structures for gold occurrences, a correlation that exists throughout the CLGB. However, the complexity of this correlation varies.

Occurrences hosted by strike-slip shear zones away from the Sirkka Line, such as Suurikuusikko and Iso-Kuotko, provide clear examples of this correlation. These occurrences are also within sections of fairly uniform (dominantly mafic volcanic rocks) stratigraphy. However, among other features, the localised effects of lithological variations, of intersecting structures, and of early structures in constraining mineralisation to particular sites needs to be investigated further to aid identification of the most favourable locations for mineralisation within these long host shears.

Areas south of the Sirkka Line and in the south-eastern CLGB are the most complicated to interpret. The mix of lithologies (Fig. 1), and the variety and abundance of deformation features present here (Fig. 2) make these areas substantially more heterogeneous than areas north of the Sirkka Line. Occurrences such as Isomaa, Kaaresselkä and Pahtavaara indicate that D_3 strike-slip shear movement is also associated with mineralisation in these areas. However, at some of these occurrences (e.g., Kaaresselkä), the orientation of strike-slip shear zones may be partially inherited from the orientation of pre-D_3 deformation zones. Similarities in occurrence-specific paragenetic events that can be correlated between most of the occur-

Table 4. Summary of structural features associated with CLGB gold occurrences

Occurrence	Dominant strike of closest pre-syn D1/D2 deformation feature	Post D1-D2 feature	
		Strike of mineralised shear zone and displacement sense (where known)	Strike of mineralised veins and type (where clear)
Saattopora	E to ESE (Sirkka Line)	–	N
Sirkka (Kaivos)	E (Sirkka Line)	Breccia zone(s) of unclear strike	
Loukinen	E (Sirkka Line)	N to NNE Mineralised breccias within dextral strike-slip shear zone(s)	–
Soretialehto	NW (Sirkka Line)	N to NE Mineralised breccias within strike-slip shear zones	N to NNE Mineralised extensional or hybrid veins cutting mineralised breccias
Soretiavuoma North	NW (Sirkka Line)	NW to N and NE Mineralised shear infill within dextral + sinistral strike-slip shear zones	–
Isomaa	Multiple	NE Mineralised infill within a dextral strike-slip shear zone	–
Kaaresselkä	WNW (Sirkka Line – very fragmented)	WNW Disseminated mineralisation within sinistral strike-slip shear zone(s)	NE
Pahtavaara	E-striking rift? Pre-D1	E Mineralised breccia within sub-vertical shear zone	NW Mineralised veins cutting shear-related breccia
Suurikuusikko	n/a?	N-NE Disseminated, fabric and micro-veinlet hosted mineralisation within a strike-slip shear zone with early sinistral and late dextral movements	–
Iso-Kuotko	n/a?	NW and N Shear infill and breccias/shear veining associated with dextral (exclusively?) strike-slip shears	NW and N Mineralised shear veins synchronous with shear zones

rences reviewed here, regardless of location, suggest that strike-slip shear movements in southern areas are likely to be the same age as D_3 shearing north of the Sirkka Line.

2. The Sirkka Line is a prospective area, but has a more complicated relationship to mineralisation than might be assumed from the spatial association between gold occurrences and Sirkka Line structures

Sirkka Line structures represent the major zone of prolonged deformation within the CLGB. Through its role in aligning volcanic-dominated mafic rocks to the north against a sediment-rich sequence to the south, the Sirkka Line also generates the major stratigraphic and litho-chemical boundary in the area containing most gold occurrences. These two factors alone are enough to increase the likely prospectivity of areas proximal to the Sirkka Line. Highly deformed zones, and the most deformed areas within these (e.g., fault jogs and splays), are widely acknowledged as the most likely sites for concentrating mineralising fluids (e.g., Cox et al. 2001).

However, occurrences coinciding with the Sirkka Line demonstrate that while it is in general a prospective zone, care must be taken to understand the more detailed events constraining mineralisation to specific locations. This is essential because mineralisation appears to post-date the D_1/D_2 structures which dominate these areas. For example, despite the Sirkka Line-parallel alteration envelopes associated with mineralisation at the Loukinen, Saattopora and Sirkka occurrences, the N- to NE-striking strike-slip shear zones containing mineralised breccias at Loukinen clearly suggests that D_3 structures determined the final location of mineralisation at this occurrence. Additional timing criteria at Saattopora and Sirkka (as discussed) also indicate a post-D_1/D_2 age for mineralisation.

The Soretiavuoma North occurrence also provides some evidence for reactivation of D_1/D_2 segments of the Sirkka Line during D_3. Like Kaaresselkä, this occurrence is associated with strike-slip shearing that lies parallel to pre-existing structures evident in regional aeromagnetic images that are within or near the Sirkka Line. Regardless of whether these occurrences are or are not hosted by reactivated Sirkka Line segments, the late timing of mineralisation supports a post-D_1/D_2 age for mineralisation.

The focusing of fluids into pre-existing, localised irregularities (structural or lithological) during later deformation events, and an association between reactivation of earlier structures and mineralisation have been documented as common occurrences in similar deformed belts elsewhere (e.g., Colvine 1989; Vearncombe et al. 1989; Groves et al. 2000). The potential for such events is high in areas of Sirkka Line deformation, and these are critical questions to consider when exploring within these areas in order to determine which zones were more favourable for mineralisation during D_3.

3. Most gold occurrences studied were generated during D_3

The relative timing of mineralisation and deformation features reviewed here indicates that gold occurrences throughout the CLGB region are typically related to D_3 events, the Pahtavaara deposit being a possible exception. D_3 deformation also appears to have coincided with the general CLGB-wide evolution from ductile to brittle deformation conditions. Post-D_3 ductile deformation events were not documented during this work, and D_3 strike-slip shears are typically the last major deformation features observed in the local deformation sequences established at individual gold occurrences. Low-displacement D_4 brittle faults were occasionally present, but these have little impact on mineralised structures.

Mineralised strike-slip shears are often associated with semi-synchronous brittle deformation products, which are also mineralised (e.g., mineralised shears and veins at Kaaresselkä – Fig. 6; and at Soretialehto). These veins are similar in composition to the ore breccias they crosscut, and/or to proximal alteration mineralogy relating to the shear-associated mineralisation at these sites. Mineralised veins at these occurrences are also very planar and undeformed. These points suggest that these examples of vein-hosted gold mineralisation are products of the late stages of D_3. The loose cluster of Pb-sulfide ages shown in Table 3 are reasonably consistent with the timing of D_3, and favours mineralisation that is synchronous with or immediately post-dating the convergent margin phase of CLGB development.

There is much scope for reviewing the observations and ideas presented here by applying theoretical concepts proposed for structurally controlled gold deposits. More information and interpretations are required regarding the impact of regional and local scale stress and fluid pressure variations, fluid-chemical histories, and the effects of pre-existing structural and lithological variations in localising deposits. These and other factors have been identified as determining sites most likely to become mineralised. (e.g., Cox et al. 2001). Such a review was not the purpose of this paper, but understanding how structural features associated with CLGB gold mineralisation have acted

as fluid transporting and focusing mechanisms is an overall aim of this research project. The results of investigations using whole-rock geochemistry, stable isotopes, fluid inclusions and other relevant techniques are being added to the initial observations presented here to address some of these questions.

ACKNOWLEDGEMENTS

Relevant Geological Survey of Finland staff are thanked for their ongoing contributions to this project, particularly Pentti Hölttä, Vesa Kortelainen, and Veikko Keinänen. Vesa Nykänen is thanked for preparing Figures 1 and 2. This work is part of PhD research being undertaken at the Economic Geology Research Unit (James Cook University (JCU), Australia), supervised by Dr Nick Oliver and funded by the Geological Survey of Finland and JCU School of Earth Sciences. The author also received an Australian Postgraduate Award. Riddarhyttan Resources AB granted site and data access to allow work on the Suurikuusikko property to be included in this research. The quality of this article had been improved thanks an excellent review by John Mair.

REFERENCES

Agnico-Eagle Ltd. 2006. Media release 06.05.2006. Agnico-Eagle to build Kittila Gold Mine in Finland and complete construction of Lapa Gold Mine in Quebec; to raise $250 million in marketed equity offering.

Airo, M-L. 1990. Alueellisen geofysikaalisen tulkinnan menetelmistä: esimerkkinä Rajalan alue Keski-Lapissa. Geologian tutkimuskeskus, arkistoraportti Q19/37/90/1/22.27. 13s., 31 liites. (in Finnish)

Berthelsen, A. & Marker, M. 1986. 1.9–1.8 Ga old strike-slip megashears in the Baltic Shield, and their plate tectonic implications. Tectonophysics 128 (3–4), 163–181.

Chernet, T., Kojonen, K. & Pakkanen, L. 1999. Applied mineralogical study on the near-surface Suurikuusikko refractory gold ore, Kittilä, western Finnish Lapland (Phase 1). Geological Survey of Finland Report C/MA9/2743/2000/10.

Colvine, A.C. 1989. An empirical model for the formation of Archean gold deposits: products of final cratonization of the Superior Province, Canada. Economic Geology Monograph 6, 37–53.

Cox, S.F., Knackstedt, M.A. & Braun, J. 2001. Principles of structural control on permeability and fluid flow in hydrothermal systems. Society of Economic Geologists Reviews 14, 1–24.

Cox, S.F., Wall, V.J., Etheridge, M, A. & Potter, T.F. 1991. Deformation and metamorphic processes in the formation of mesothermal vein-hosted gold deposits – examples from the Lachlan fold belt in central Victoria, Australia. Ore Geology Reviews 6, 391–423.

Eilu, P. (ed.) 1999. FINGOLD – a public database on gold deposits in Finland. Geological Survey of Finland, Report of Investigation 146, 224 p. Web address: www.gtk.fi/explor/gold

Eisenlohr, B.N., Groves, D.I. & Partington, G.A. 1989. Crustal-scale shear zones and their significance to Archaean mineralisation in Western Australia. Mineralium Deposita 24, 1–8.

Frietsch, R., Tuisku, P, Martinsson, O. & Perdahl, J-A. 1997. Early Proterozoic Cu-(Au) and Fe ore deposits associated with regional Na-Cl metasomatism in northern Fennoscandia. Ore Geology Reviews 12 (1), 1–34.

Gaál, G., Berthelsen, A., Gorbatschev, R., Kesola, R., Lehtonen, M. I., Marker, M. & Raase, P. 1989. Structure and composition of the Precambrian crust along the POLAR Profile in the northern Baltic Shield. Tectonophysics 162 (1–2), 1–25.

Groves, D. I., Goldfarb, R.J., Gebre-Marium, M., Hagemann, S.G. & Robert, F. 1998. Orogenic gold deposits: A proposed classification in the context of their crustal distribution and relationship to other gold deposits. Ore Geology Reviews 13, 7–27.

Groves, D.I., Goldfarb, R.J., Knox-Robinson, C.M., Ojala, J., Gardoll, S., Yun, G.Y., Holyland, P. 2000. Late-Kinematic timing of orogenic gold deposits and significance for computer-based exploration techniques with emphasis on the Yilgarn Block, Western Australia. Ore Geology Reviews 17, 1–38.

Härkönen, I., Pankka, H. & Keinänen, V. 2001 Summary report. The Iso-Kuotko gold occurrences, Kittilä, Finnish Lapland. http://en.gtk.fi/ExplorationFinland/Tender/iso_kuotko/iso-kuotko.htm

Hitzman, M.W., Oreskes, N. & Einaudi, M. 1992. Geological characteristics and tectonic setting of Proterozoic iron oxide (Cu-U-Au-REE) deposits. Precambrian Research 58, 1–4, 241–287.

Keinänen, V. 1992. Tutkimustyöselostus Kittilän kunnassa valtausalueella Soretiajärvi 2, kaiv.rek.nro:4154/1, suoritetuista malmitutkimuksista. 16s, 12 liites. Geological Survey of Finland Archive Report M06/2734/92/2/10. (in Finnish)

Kerrich, R., Fryer, B.J. 1981. The separation of rare elements from abundant base metals in Archean lode-gold deposits: implications of low water/rock source regions. Economic Geology 76, 160–166.

Kojonen, K. & Johanson, B. 1999. Suurikuusikko – Determination of refractory gold distribution by microanalysis, diagnostic leaching and image analysis. Geological Survey of Finland Report, April 28, 1999.

Korkiakoski, E. A. 1992. Geology and geochemistry of the metakomatiite-hosted Pahtavaara gold deposit in Sodankylä, northern Finland, with emphasis on hydrothermal alteration. Geological Survey of Finland, Bulletin 360, 96 p.

Korkiakoski, E. & Kilpelä, M. 1997. The komatiite-hosted Pahtavaara gold mine near Sodankylä, northern Finland. In: Korkiakoski, E. & Sorjonen-Ward, P. (eds.) Research and exploration – where do they meet? 4th Biennial SGA Meeting, August 11–13, 1997, Turku, Finland. Excursion guidebook B1 : ore deposits of Lapland in northern Finland and Sweden. Geologian tutkimuskeskus, Opas – Guide 43, 21–25. 27–29.

Korvuo, E. 1997. The Saattopora gold ore and the Pahtavuoma Cu-Zn-U occurrences in the Kittilä region, northern Finland. In: Korkiakoski, E. & Sorjonen-Ward, P. (eds.) Research and exploration – where do they meet? 4th Biennial SGA Meeting,

August 11–13, 1997, Turku, Finland. Excursion guidebook B1 : ore deposits of Lapland in northern Finland and Sweden. Geologian tutkimuskeskus, Opas – Guide 43, 21–25.

Lehtonen, M., Airo, M-L., Eilu, P., Hanski, E., Kortelainen, V., Lanne, E., Manninen, T., Rastas, P., Räsänen, J. & Virransalo, P. 1998. The stratigraphy, petrology and geochemistry of the Kittilä greenstone area, northern Finland. Report of the Lapland Volcanite Project. Geological Survey of Finland Report 140.

Mänttäri I. 1995. Lead isotope characteristics of epigenetic gold mineralisation in the Palaeoproterozoic Lapland greenstone belt, northern Finland. Geological Survey of Finland, Bulletin 381, 70 p.

Mikkola, A. & Vuorela, P. 1977. Deep-seated fractures and metallogeny of Finland. In: Kortman, C. (ed.) Shear zone tectonics in the eastern part of the Baltic Shield. Proceedings of a Finnish-Soviet Symposium held in Finland, 20th–24th September 1976. Abstracts. 73–87.

Pekkala, Y., & Puustinen, K. 1978. The chromian marbles of Kittilä, Finnish Lapland. Geological Society of Finland, Bulletin 50 (1–2), 15–29.

Räsänen, J. 1999. On the Sattasvaara komatiite formation. In: Papunen, H. & Eilu, P. (eds.) Geodynamic evolution and metallogeny of the Central Lapland, Kuhmo and Suomussalmi greenstone belts, Finland: joint field excursion and workshop of the GEODE subprojects: Archaean Greenstone Belts and Ore Deposits: Palaeoproterozoic Greenstone Belts and Ore Deposits, 11–16 September 1999. Abstracts. Turun yliopiston geologian ja mineralogian osaston julkaisuja 42, 10–11.

Räisänen, K. 2001. Kun Kätkätunturin maisemissa vedettiin vesiperä. Vuoriteollisuus 59, 56–57.

Robert, F. & Poulsen, K.H. 1997. World-class Archaean gold deposits in Canada: an overview. Australian Journal of Earth Sciences 44, 329–351.

Saverikko, M. 1985. The pyroclastic komatiite complex at Sattasvaara in northern Finland. Geological Society of Finland, Bulletin 57 (1–2), 55–87.

Sorjonen-Ward, P., Nironen, M. & Luukkonen, E. 1997. Greenstone associations in Finland. In: de Wit, M & Ashwal, L.D. (eds.) Greenstone Belts. Oxford: Clarendon Press/Oxford University Press, 677–698.

Sorjonen-Ward, P., Nurmi, P.A., Härkönen, I. & Pankka, H.S. 1992. Epigenetic gold mineralisation and tectonic evolution of a Lower Proterozoic Greenstone Terrane in the northern Fennoscandian (Baltic) Shield. In: Sarkar, S.C. (ed.) Metallogeny related to tectonics of the Proterozoic mobile belts. New Delhi: Oxford and IBH Publishing, 375–452.

Talvitie, J. 1976. Fracture zone of Ladoga-Bothnian Bay. University of Oulu. Department of Geophysics. Contribution 64. 6 p. + 2 app.

Tuominen, H., Aarnisalo, J. & Söderholm, B. 1973. Tectonic patterns in the central Baltic Shield. Geological Society of Finland, Bulletin 45 (2), 205–217.

Väisänen M. 2002. Structural features in the central Lapland greenstone belt, northern Finland. 20 p., 16 plates. Geological Survey of Finland, Archive report, K 21.42/2002/3.

Vearncombe, J.R., Barley, M.E., Eisenlohr, B.N., Groves, D.I., Houston, S.M., Skwarnecki, M.S., Grigson, M.W. & Partington, G.A. 1989. Structural controls on mesothermal gold mineralisation: examples from the Archean terranes of South Africa and Australia. Economic Geology Monograph 6, 124–134.

Vesanto, J. 1978. Sirkan malmi ja sitä ympäröivä kallioperä. Unpublished pro-graduate thesis.

Ward, P., Härkönen, I., Nurmi, P.A. & Pankka, H.S. 1989. Structural studies in the Lapland greenstone belt, northern Finland and their application to gold mineralisation. Current Research. Geological Survey of Finland Special Paper 10, 71–77.

Wikström, A., Skiøld, T. & Ohlander, B. 1996. The relationship between 1.88 Ga old magnetism and the Baltic-Bothnian shear zone in northern Sweden. Precambrian Crustal Evolution in the North Atlantic Region. Geological Society of London Special Publication 112, 249–259.

Witt, W. K. & Vanderhor, F. 1998. Diversity within a unified model for Archaean gold mineralisation in the Yilgarn Craton of Western Australia: An overview of the late-orogenic, structurally-controlled gold deposits. Ore Geology Reviews 13, 29–64.

Gold in the Central Lapland Greenstone Belt, Finland
V. Juhani Ojala (ed.)
Geological Survey of Finland, Special Paper 44, 125–134, 2007.

THE SUURIKUUSIKKO GOLD DEPOSIT: PROJECT DEVELOPMENT SUMMARY OF NORTHERN EUROPE'S LARGEST GOLD RESOURCE

by
N. L. Patison[1], G. Salamis[2] & V. J. Kortelainen[3]

Patison, N. L., Salamis, G. & Kortelainen, V. J. 2007. The Suurikuusikko Gold Deposit; Project Development Summary of Northern Europe's Largest Gold Deposit. *Geological Survey of Finland, Special Paper 44,* 125–136, 6 figures and 2 tables.

The Suurikuusikko gold deposit is the largest known gold resource in northern Europe. Current resource estimates identify over of two million ounces of gold, and clear potential exists for further ounces both at depth and along strike of the host structure. The deposit occurs in Kittilä Group rocks of the Early Proterozoic Central Lapland Greenstone Belt (CLGB). The CLGB is a vastly under-explored terrane compared to similar gold-bearing districts elsewhere despite the presence of numerous gold prospects that are genetically similar to those in well-known mining districts (e.g., Yilgarn of Australia, Superior Province of Canada).

Suurikuusikko host rocks are dominantly mafic volcanic rocks. Individual ore lodes occur within an over 25-kilometre long strike-slip shear zone (Kiistala Shear Zone) active during the later stages of the orogenic development of the CLGB. Gold is refractory, occurring within arsenopyrite (majority) and pyrite as lattice-bound gold or inclusions.

The Geological Survey of Finland discovered the deposit in 1986 and the Finnish Ministry of Trade and Industry sold it to Riddarhyttan Resources AB in 1998 after an international tendering process. In preparation for mine development, Riddarhyttan expanded the resource, obtained permits and completed mine feasibility studies. In 2005, Agnico-Eagle Mines Limited took over Riddarhyttan and plans to commence mining the deposit as the 'Kittilä Mine' in 2008.

Key words (GeoRef Thesaurus AGI): gold ores, host rocks, metavolcanic rocks, shear zones, Central Lapland Greenstone Belt, Paleoproterozoic, Suurikuusikko, Lapland Province, Finland

[1]*Economic Geology Research Unit, James Cook University, Townsville QLD 4811 Australia. Current address: Geological Survey of Finland, P.O. Box 77, FI-96101 Rovaniemi, Finland.*
[2]*Riddarhyttan Resources AB (Canada). Current address: Caledon Resources PLC, 410-1111 Melville Street, Vancouver, British Columbia V6E 3V6, Canada.*
[3]*Agnico-Eagle, Finland. Pakatinie 371, FI-99100 Kittilä, Finland.*

E-mail: [1]nicole.patison@gtk.fi, [2]gsalamis@caledonresources.com [3]vesa.kortelainen@agnico-eagle.com

INTRODUCTION

The aim of this paper is to provide a practical and useful summary of the basic geological characteristics and developmental status of the Suurikuusikko gold deposit. As the next likely gold-producing deposit within the Central Lapland Greenstone Belt (CLGB), Suurikuusikko provides a good example of the gold potential of the region and the style of deposits present. Recent information about the deposit and its development is available from the following website: http://www.agnico-eagle.com (follow links to Kittilä Mine pages).

The Suurikuusikko gold deposit is located approximately 50 kilometres northeast of the town of Kittilä, in the heart of Finnish Lapland. Suurikuusikko is an orogenic gold deposit (as defined by Groves et al. 1998[1]) occurring within the Palaeoproterozoic Central Lapland Greenstone Belt (CLGB, Fig. 1). The host rocks, timing of ore formation relative to regional

1 See Patison (Table 1, this volume) for a comparison between features defining orogenic gold deposits, and the characteristics of CLGB gold mineralisation.

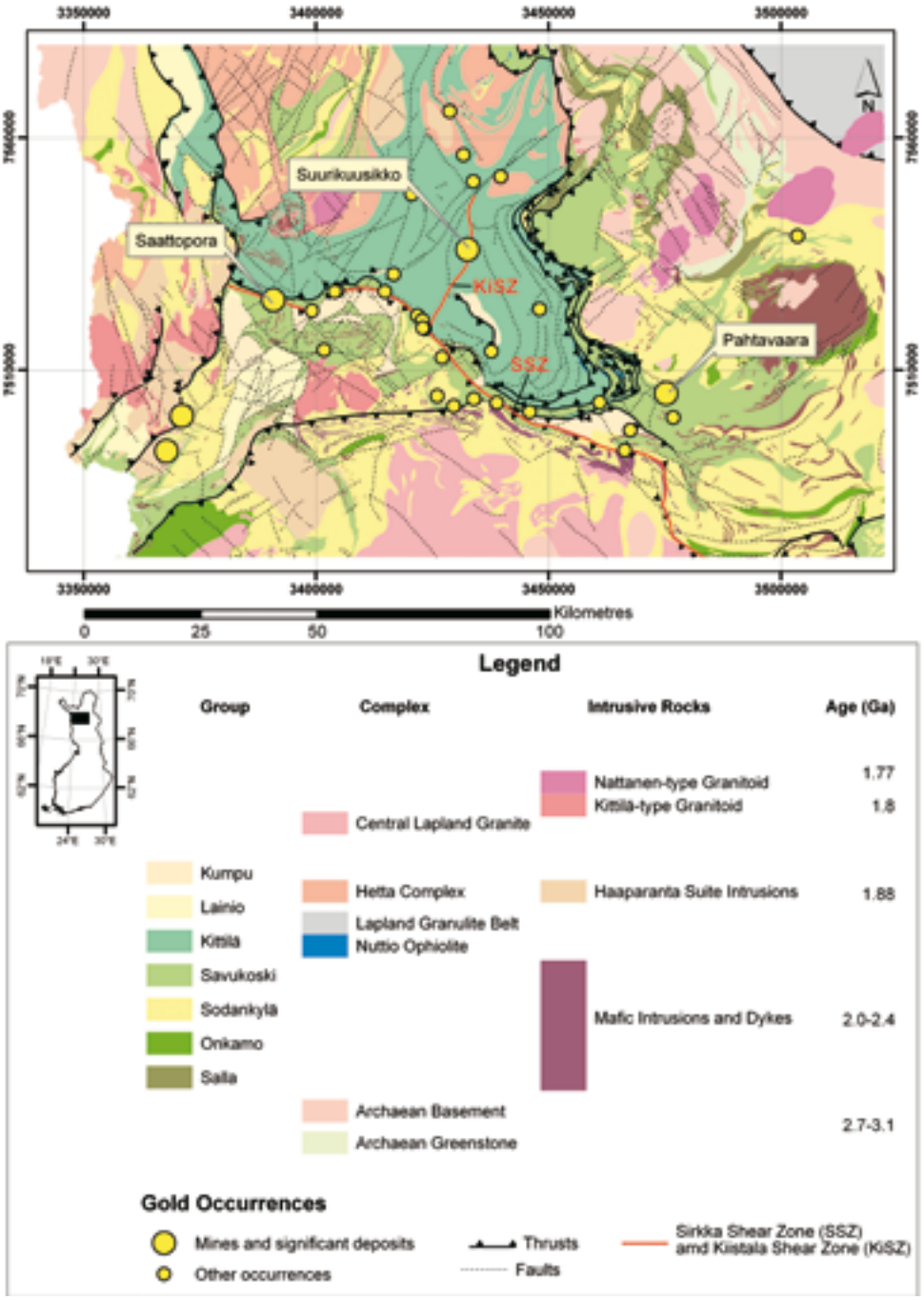

Fig. 1. Stratigraphic map of the Central Lapland Greenstone Belt, showing the location of Suurikuusikko, the Kiistala Shear Zone, and other known gold prospects. After Lehtonen et al. 1998.

deformation, metamorphic grade, alteration assemblages present, and structurally controlled nature of the deposit make it analogous to better known deposits in greenstone belts throughout the world. To illustrate this point, a brief comparison will be presented between the CLGB and the Ashanti Belt of Ghana, a region that shows particular similarities to the CLGB.

RESEARCH & EXPLORATION

Early research associated with Suurikuusikko's discovery and with preparing the prospect's release for international tender was conducted by the Geological Survey of Finland (GTK) (e.g., Härkönen & Keinänen 1989; Härkönen 1992, 1997; Härkönen et al. 1999a & b). Subsequent and ongoing studies have focused on establishing the exact location of gold within sulphides, examining the metallurgical performance of the ore as part of mine pre-feasibility studies, and on gaining an improved understanding of the host lithologies and structures, deformation history, and geophysical signatures of the deposit (e.g., Bolin & Larsson 1999; Chernet et al. 1999; Durance et al. 1999; Kojonen & Johanson 1999; Sandahl 1999; Kojonen & Pakkanen 2000; Markström et al. 2000; Markström & Larsson 2000a & b; Patison 2000; Sandahl 2000a & b; Barclay 2001; Patison 2001; & Powell 2001).

GTK Research Assistants P. Puhakka and J. Valkama discovered visible gold a few kilometres SSW of Suurikuusikko in 1986. Subsequent ground geophysical surveys and geochemical sampling lead to the identification of the Kiistala Shear Zone (KSZ), and follow-up diamond drilling by GTK along the KSZ resulted in Suurikuusikko's discovery. By 1996, a total of 77 diamond drill holes (9,320 metres) were completed by GTK, outlining a resource of 1.5 million tonnes with an average grade of 5.9 grams per tonne (g/t; or 285,000 ounces of gold). The resource boundary was defined over a strike length of just over one kilometre, and down to an average depth of approximately 75 metres.

In April 1998, the Finnish Ministry of Trade and Industry announced that Riddarhyttan Resources AB had successfully acquired the deposit and surrounding exploration permits by way of an international tender. Riddarhyttan immediately initiated an extensive program of infill and step-out drilling on the known zones of gold mineralization. Within a year of Riddarhyttan's

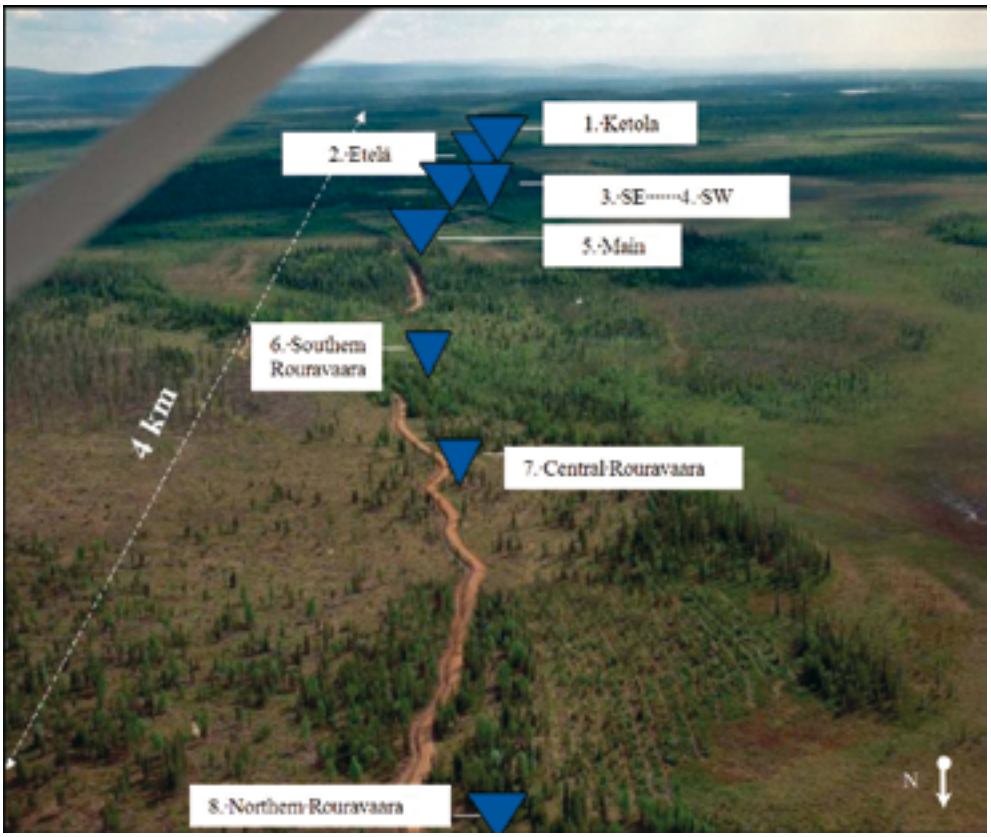

Fig. 2. Arial view of known ore zones in the Suurikuusikko area (view to the south). Dashed line shows approximate scale. Rimminvuoma area (not marked) is approximately 1.5 kilometres north of Northern Rouravaara. (photo by courtesy of Riddarhyttan Resources Ab).

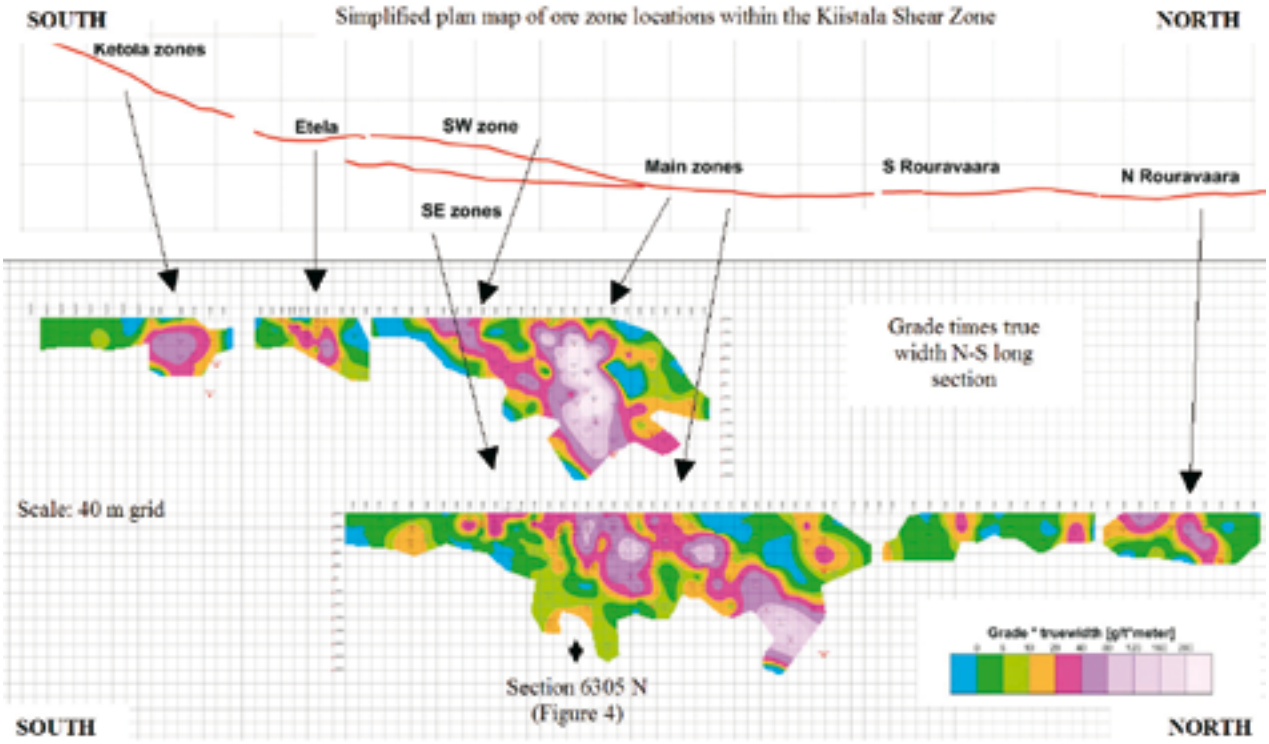

Fig. 3. Long section (vertical, N-S section) of drill core gold assay data from all larger ore zones of Suurikuusikko (as at February 2003). Southeast and Main zones appear on the lower section, the SW zone and western section of the Main zone in the upper. Colour gradations indicate grade multiplied by the true thickness of mineralised intercepts. Grid squares are 40 m^2 each. Surface elevation is approximately 210 metres, and the deepest intercepts plotted are at a vertical depth of –280 metres (~500 metres below surface). 2002/2003 Central Rouravaara drilling results and deep intercepts at the southern end of the Main Zone have not been included on this plot. A plan map of ore zone strikes is included for reference above the main figure.

acquisition of Suurikuusikko, the size of the known gold resource was more than double the original.

Exploration conducted following Riddarhyttan's acquisition of Suurikuusikko has lead to a better delineation of the original mineralised zone, and has resulted in the discovery of several new ore zones along the host structure (Figs. 2 & 3), and to an increase in the size of the resource to over two million ounces of gold (Bartlett 2002). Mineralisation has been found over a five-kilometre strike length of the host structure and the structural and stratigraphic locations of ore zones are similar. Gold grades well in excess of 10 g/t intercepted at depths of up to 400 metres below surface demonstrate the continuity of mineralised zones at Suurikuusikko.

Riddarhyttan Resources AB initiated mine feasibility studies on Suurikuusikko in the winter of 2000. The feasibility initiative encompassed a comprehensive campaign of infill drilling, metallurgical test work, and engineering studies. Riddarhyttan's studies anticipated production levels via a combined open pit and underground operation of over 125,000 ounces of gold per year for a 9.5-year period (Micon 2001). In 2004, Agnico-Eagle acquired a 14% ownership interest in Riddarhyttan, and in 2005, commenced acquisition of the remaining Riddarhyttan shares. In June 2006, a decision was made to begin mine development. At this time the estimated probable reserves for the Kittilä Mine were 2.4 million tonnes of gold ore with an average grade of 5.16 grams per tonne. The current production estimate is 150,000 ounces annually for 13 years (Agnico-Eagle Mines Ltd. media release 06.05.2006) via a combination of open pit and underground mining.

GEOLOGY

Host rocks

Suurikuusikko occurs within rocks of the Kittilä Group, a stratigraphic unit of the Central Lapland Greenstone Belt (CLGB; see Lehtonen et al. 1998). The approximately 2.0 Ga Kittilä Group is dominated by mafic volcanic rocks and contains smaller volumes of metamorphosed sediments, banded iron formation

(BIF), ultramafic, intermediate and felsic rocks (Lehtonen et al. 1998). The Kittilä Group is the thickest and most volcanic-rich package within the CLGB, and has a current thickness between six and seven kilometres (Luosto et al.1989) in the Suurikuusikko area.

The Kittilä Group is subdivided into two main formations: the Kautoselkä Formation, dominated by iron-tholeiite igneous rocks; and the Vesmajärvi Formation, dominated by magnesium-tholeiite igneous rocks. The depositional environment of each Formation has been interpreted as continental and marine respectively (Lehtonen et al. 1998). It has been speculated that Suurikuusikko occurs at the contact between the Kautoselkä and Vesmajärvi Formations, but this has not been convincingly demonstrated. Elsewhere within the CLGB, the Porkonen Formation, a thin sequence of metamorphosed and graphitic shallow water sediments, cherts, and BIF separates these two formations. Intermediate and felsic rocks also occur within the Kautoselkä and Vesmajärvi Formations. All Kittilä Group rocks have undergone greenschist-facies metamorphism, and the least-altered barren rocks in the Suurikuusikko surrounds have assemblages typical for rocks metamorphosed to this extent (see Hölttä et al. this volume). Widespread carbonate alteration and sporadic sodic (albite) and potassic alteration have accompanied regional metamorphism in many areas.

Outcrop in the Suurikuusikko area consists only of a few man-made outcrops, severely limiting local mapping. Several lithological sections through Suurikuusikko have been constructed from drill core data (Fig. 4). In the area of the 'Main' ore zone (Fig. 4), host rocks grade from mafic pillow and massive lavas west of mineralised zones to mafic transitional to intermediate lavas (andesite flows of Powell 2001) and pyroclastic material within mineralised zones. A sediment-dominated horizon including BIF, chert and argillitic material occurs at the eastern margin of mineralised zones, followed further east by more mafic lava packages and ultramafic volcanic rocks.

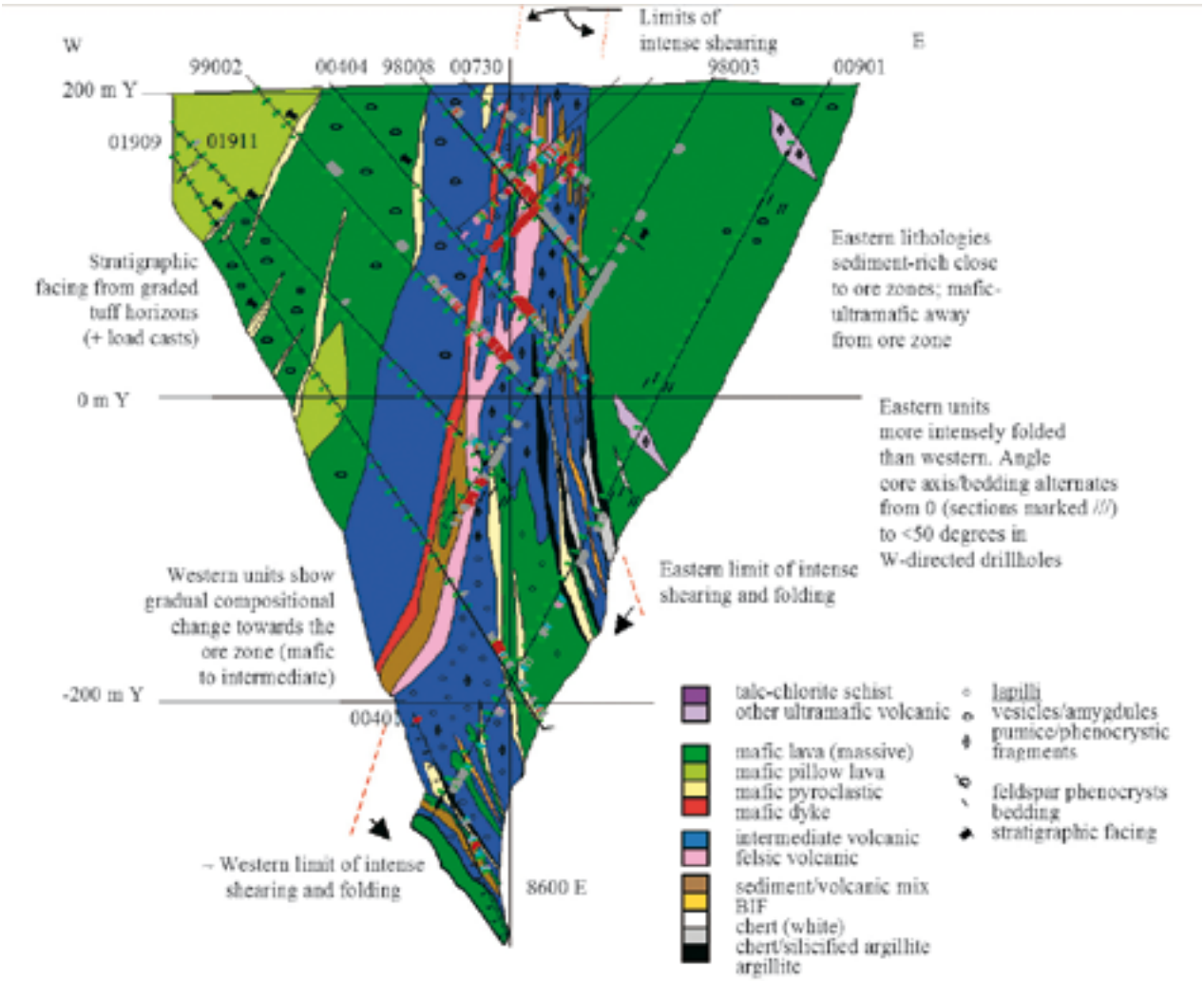

Fig. 4. Cross section of the Suurikuusikko Main ore zone. Reconstructed from core log data from numbered drill holes only. The eastern side is intensely folded and the orientation of stratigraphic units on this side represents only an approximate enveloping surface for this folding. The dip of the Kiistala Shear Zone is vertical in surface outcrop, but dips steeply to the west at depth (outer limits of intense shearing marked). Red patches parallel to drill holes indicate sampled intervals with gold grades of 5 g/t or more.

Although shearing is the main factor determining the location of mineralisation at Suurikuusikko, host rock primary texture and composition also appears to be significant. Mineralisation is preferentially concentrated within units of the host stratigraphy with pyroclastic or other clear extrusive textures and/or volcano-sedimentary origins. These include lapilli-bearing and pumaceous material, mafic lava autobreccias and slightly reworked volcano-sedimentary material. These preferential host rocks (blue units in Fig. 4) contain alteration assemblages (leucoxene-rich) and other petrographic evidence suggesting that these units have a more intermediate composition than the surrounding mafic lavas. Another preferentially mineralised unit is a narrow zone (generally under 15 metres wide) of rock with intense albite and quartz alteration that may have had a felsic primary composition (pink unit in Fig. 4). These units are currently mapped and logged as intermediate and felsic, but detailed geochemical analyses are required to confirm these assumptions.

No mineralisation occurs in ultramafic units, or within primary sedimentary material that has experienced little deformation. Zones of intense shearing typically occur at contacts between volcanic-dominated, and sediment-rich material (argillite, chert, and BIF in Fig. 4), and utilise the relatively weaker rock displaying primary textural variation (described above) or contact zones between massive lavas.

Host structure

Orogenic events relating to CLGB development have generated several phases of deformation. The earliest deformation phases preserved (D_1, D_2) involved roughly synchronous N- to NNE- and S- to SW-directed thrusting at the southern and northeastern margins of the CLGB (Ward et al. 1989). Northwest-, N-, and NE-trending D_3 strike-slip shear zones, including the Kiistala Shear Zone hosting Suurikuusikko, cut early folding and thrusting. Post-D_3 events are limited to brittle, low-displacement faults. A detailed discussion of regional deformation events and the deformation history of several individual CLGB gold prospects are provided by Hölttä et al. (this volume) and Patison (this volume).

The Kiistala Shear Zone (KiSZ) strikes N to NE for a distance of at least 25 kilometres. The dip of this shear zone in the Suurikuusikko area is steeply west to sub-vertical. Known mineralisation occurs on N-trending, and less frequently NE-trending (Ketola mineralisation only) shear zone segments. All parts of the KiSZ drilled to date (an approximately 5.5 kilometre N-trending strike section) are mineralised. The KiSZ is a complex structure, recording several phases of movement. Aeromagnetic images of the KiSZ indicate early sinistral strike-slip movement along the zone. Immediately above the widest mineralised zones, late dextral strike-slip movements are recorded on shear planes bounding mineralised zones. A minor degree of west-up movement has occurred, but movement is dominantly strike-slip. The KiSZ overprints several regional fabrics present in the Suurikuusikko area that were generated by earlier events, including regional folding.

A strong correlation exists between points of more intense shearing within the KiSZ and the amount of gold present in host rocks. It is not yet clear if the timing of mineralisation coincides with a combination of early and late shearing, or only to the later dextral shearing event which now delineates the limits of gold mineralisation in some ore zones. Ongoing work is attempting to more accurately predict the controls on the location of high-grade mineralisation within this complex shear system.

Gold mineralisation

The gold-bearing sulphides have a late timing within the paragenetic sequence at Suurikuusikko. Gold-bearing phases occur nucleated within shear fabrics and associated micro-fractures, with lesser amounts of dissemination into host rocks. Sulphides and host rocks show some evidence for deformation relating to post-mineralisation movements on host shear planes, but this does not appear to significantly affect the continuity of ore zones. Post-mineralisation brittle faults crosscut mineralised zones but are not known to cause significant displacement of ore lenses.

The majority (73,2%) of gold occurs within arsenopyrite, and visible arsenopyrite is a reliable indication of the presence of gold within samples. Remaining gold occurs in arsenian-pyrite (22,7% of gold), and as free gold (Kojonen & Johanson 1999). Sub-microscopic gold is found as inclusions or solid-solution lattice substitutions within arsenopyrite and pyrite (Chernet et al. 1999). Gold as inclusions is common in pyrite but rare in arsenopyrite. The composition of gold inclusions includes various alloys with silver and mercury (Chernet et al. 1999). The gold typi-

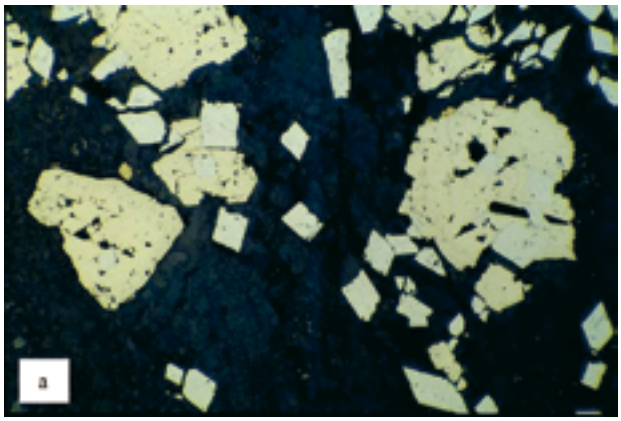

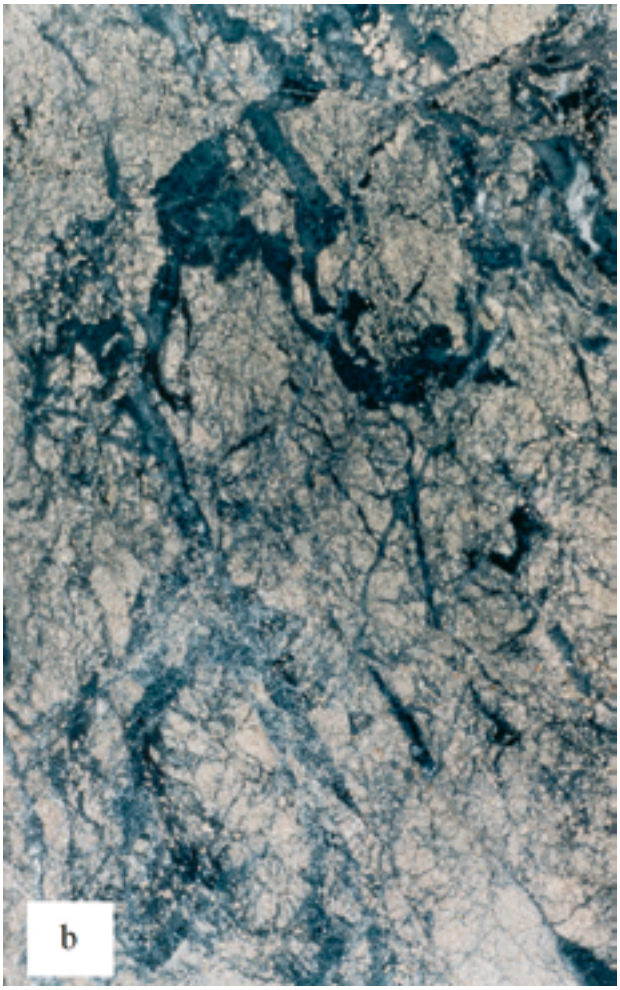

Fig. 5. Photomicrograph of gold-bearing arsenopyrite (silver), and pyrite (yellow) as seen under reflected light (a). The darkness of the non-sulfide matrix results from poor light and does not reflect the true colour of the sample. Field of view is 1.2 millimeters wide (after Chernet et al. 1999). Photographed polished block Suurikuusikko ore (b). The bleached colour of the sample reflects intense albite and carbonate (dolomite/ankerite) alteration. This sample is more competent than most ore host rocks, and has responded to deformation by fracturing rather than developing intense shear fabrics. The veining in this sample is dominantly albite-quartz-carbonate. Black material results from minor amounts of amorphous carbon within the sample. Field of view is 12 mm long.

cally has a grain size from <1 to 100 µm (Kojonen and Johanson 1999; Fig. 5a). Rare stibnite veins and amorphous grains contain extremely high gold grades and overprint the main ore-bearing sulphides.

Intense carbonate and albite alteration are associated with gold-bearing arsenopyrite and pyrite (Fig. 5b). Ore rock is intensely albitised, with albite occurring as a matrix overprint and as micro-veinlets. Intense albitisation greatly increases the hardness of the ore, but generally extends less than two metres into barren rock. Carbonate alteration includes distal calcite veins, and dolomite/ankerite veins and infill breccia proximal and within ore zones respectively. Carbonate veins and breccias are not mineralised, but infill brecciated (tectonically and hydrothermally) mineralised and albitised rock. 'Graphitic' alteration is a feature of most mineralised zones. Other alteration phases include albite, carbonates, leucoxene, and less abundant chlorite, sericite, rutile, tetrahedrite, chalcopyrite, gersdorffite, chalcocite, sphalerite, pyrrhotite, bornite, chromite, galena, talnahkite, and Fe-hydroxides (relating to weathering) in varying abundances (Chernet et al. 1999).

Free carbon (amorphic 'graphitic' carbon rather than crystalline graphite) also accompanies shearing (at least the late dextral phase) and mineralisation. The presence of this carbon suggests extremely reducing fluid conditions during shearing and mineralisation. Gold-bearing sulphides commonly nucleated on shear planes, stylolitic cleavage, and fractures bearing this material. Carbon isotope data indicates that this material is sourced from carbon-rich sediments within the host sequence (Patison, unpublished data). Argillite-rich horizons intercalated with volcanoclastic material have high primary carbon contents, and may have been chemically important for localising gold-bearing phases given the association between amorphous carbon alteration and mineralisation.

Gold-bearing phases have no known geophysical response, but the KiSZ is best detected as a total magnetic field and resistivity lows (Fig. 6). Extreme total magnetic field lows potentially relate to the intense

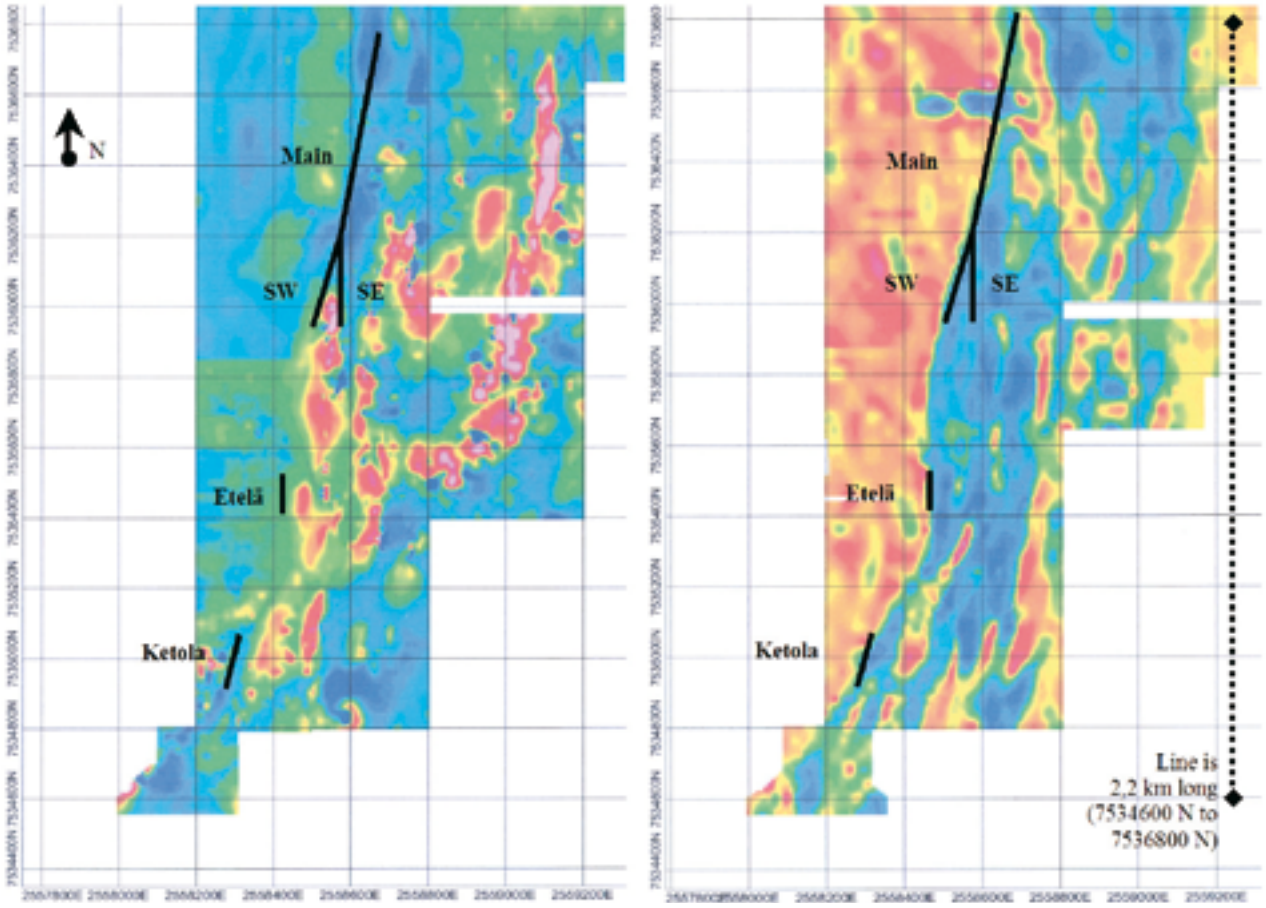

Fig. 6. Geophysical response of the Kiistala Shear Zone – magnetic total field (a), and electromagnetic (slingram) out-of-phase image (b) covering a 2.2-kilometre area including the Ketola, Etelä, SW, SE and Main ore zones. Mineralised zones correlate with lows in the total magnetic field lows (blue areas in Fig. 6a), and resistivity lows (blue areas in Fig. 6b) in electromagnetic measurements. These anomalies mostly indicate alteration associated with mineralisation (albitisation and graphitic carbon respectively). Only the western margin (best seen in Fig. 6b) of these anomalies has been explored to date. Magnetic highs (red areas) and resistivity highs (orange areas) reflect variations in host rock composition. Value ranges: Figure 6a: –50 to +400 nT; Figure 6b: –40 % to +30 % anomaly field (14 kHz at 50 metres). Data used with permission of Riddarhytten Resources AB.

albite alteration associated with mineralisation. Most highs on total magnetic field maps indicate unmineralised sulfide-bearing (pyrrhotite) metasediments, and less commonly ultramafic units. Extreme resistivity lows have a better correlation with shearing and hence mineralised zones than total magnetic field lows, and are believed to reflect the graphitic alteration associated with shearing.

Multiple mineralised zones have been discovered to date, all of which lie parallel to the margins of the KiSZ (Figs. 2 & 3). Table 1 provides examples of typical mineralised intercepts within some ore zones. The envelopes of mineralisation strike N and have a moderate northerly plunge (Fig. 3). Some zones in the Ketola area have a NE strike direction, but appear to maintain the same plunge as other zones. The control on the northerly plunge of ore zones is not completely resolved. Factors to be explored in attempts to resolve the cause of ore zone plunges include the role of intersections between multiple shear planes, and of the intersections of depositional surfaces and shear planes. The orientation of regional fold axes may also have a role in determining favourable sites for mineralisation during shearing. Such issues cannot be resolved without better exposure of the deposit.

Table 1. Example ore intersections for selected Suurikuusikko ore zones (modified after Bartlett 2002). Ore zone locations are shown in Figures 2 and 3 (except Rimminvuoma). Note that several of the holes in this table contain multiple mineralised sections, although only one section may be included in this table.

Zone	Drillhole number	Northing (m)	Example mineralised section length (m)	Averaged grade of section (g/t)
Ketola	02114	7534650	6.40	4.20
Ketola	02107	7535090	7.00	11.10
Ketola	02107	7535090	3.20	7.10
Ketola	02104	7535135	10.70	4.00
Etelä	R407	7535437	7.00	7.50
Etelä	01802	7535480	5.60	8.60
Etelä	02039	7535535	8.10	9.50
SW	R505	7535937	15.00	5.20
SW	R498	7535978	7.00	13.40
SW	R471	7536019	6.30	11.60
SE	00710	7535980	4.10	10.40
Main	R473	7536224	14.00	10.40
Main	R504	7536244	10.80	9.10
Main	00717	7536265	14.30	10.60
Main	R478	7536266	18.20	5.10
Main	99002	7536303	18.20	16.50
Main	R479	7536306	26.80	17.30
Main	00730	7536315	18.90	9.10
Main	98004	7536345	29.60	11.90
Main	00903	7536365	46.20	8.90
Main	99010	7536505	16.90	5.10
Main	99001	7536509	25.40	8.00
Main	99008	7536665	21.00	6.20
Main	99011	7536705	20.10	7.20
Main	02019	7536945	10.40	5.50
Southern Rouravaara	R507	7537203	9.10	4.30
Southern Rouravaara	02043	7537500	4.20	8.70
Central Rouravaara	02051	7537850	16.40	3.30
Northern Rouravaara	00210	7538050	9.00	8.80
Northern Rouravaara	R517	7538100	11.80	5.20
Northern Rouravaara	R514	7538200	18.00	5.40
Rimminvuoma	00307	7539400	5.40	4.50

COMPARISON BETWEEN THE CLGB AND THE ASHANTI BELT OF WEST AFRICA.

The CLGB lacks the research and exploration history to be as internationally recognised as other gold producing greenstone belts. However, the number of known prospects, the style of gold mineralisation at each, and associated host rocks and structures make the CLGB extremely similar to better-known belts. To illustrate this point, a very brief comparison will be given between the CLGB and the Ashanti Belt of Ghana (Table 2).

These two districts differ in terms of overall belt geometry, and more significantly by the amount of exploration which has occurred in each. The Ashanti

Table 2. Comparison between the Central Lapland Greenstone Belt (Finland) and Ashanti Belt (Ghana).

	Ashanti Belt (data from Oberthür et al.1998)	**Central Lapland Greenstone Belt (data as referenced)**
Ages	Host rocks: Early Proterozoic Au mineralisation: 2.1 – 2.0 Ga	Host rock: Early Proterozoic Au mineralisation: Dates cluster at 1.89-1.82 Ga (Mänttäri 1995; available data limited)
Ore types	1. Disseminated sulfide ore bodies associated with shear zones. Arsenopyrite as major gold hosting phase. E.g. Ashanti Mine (>30 million ounces); Prestea Mine (>3 million ounces); Bogosu Mine (>3 million ounces)	1. Gold in disseminated sulfides associated with shear zones. Arsenopyrite as major gold hosting phase. E.g., Suurikuusikko (>2 million ounces; Bartlett 2002)
	2. Vein-hosted gold in sulfides and/or as native gold. E.g., Ashanti Mine (> 50 million ounces); Prestea Mine	2. Vein- and associated breccia-hosted ore. Gold in sulfides and/or as native gold. E.g., Pahtavaara (> 0.5 million ounces, partly vein hosted; Eilu 1999); Saattopora (> 0.2 million ounces, mostly vein hosted; Eilu 1999); Iso-Kuotko (> 0.05 million ounces, vein and breccia hosted; Eilu 1999)
	3. Paleoplacer quartz pebble conglomerate hosted ore. E.g., Tarkwa Mine (>3 million ounces); Iduapriem Mine (> 3 million ounces)	3. Paleoplacer gold noted within the Kumpu Group, the uppermost stratigraphic unit of the CLGB (Härkönen 1984)
Estimated past resources	> 80 million ounces	<0.5 M ounces (Eilu 1999)
Estimated current resources	> 50 million ounces	>2 million ounces (Suurikuusikko current resource only)
Length of exploration activity	200+ years	Approximately 30 years (+ limited earlier activity). Accessible to foreign exploration companies for just over 10 years

Belt is a linear greenstone-dominated sequence whereas the CLGB is a non-linear section developed within the more linear Karasjok-Kittilä Greenstone Belt extending from northern Norway to western Russia. Over 200 years of geological work has been conducted in the Ashanti Belt, but the CLGB has only undergone limited exploration and study for approximately the last 30 years. This difference makes it unrealistic to compare gold production figures in each belt at this stage. However, the composition of the regional host-rock package, host-rock ages, the nature and scale of mineralised host structures, and the style of gold mineralisation present within the two Belts are similar.

The Ashanti Belt is a NNE-trending, linear, shear-bound belt of Early Proterozoic greenstones, including metamorphosed tholeiitic basalts, lesser amounts of andesites, and intercalated graphitic phyllites (Eisenlohr et al. 1992). This sequence is essentially the same as that throughout the CLGB, although meta-sedimentary rocks in close contact with mafic volcanic rocks more commonly host gold deposits within the Ashanti Belt. Intrusive rocks are present in similar volumes in each belt. Like the Sirkka Line and KiSZ (CLGB; Fig. 1), major structures within and bounding the greenstone package of the Ashanti Belt spatially correlate with known deposits. For example, the Obuasi deposit occurs within steeply dipping NNE- and NE-trending shear zones with an overall strike length of over 24 kilometres (Oberthür et al. 1997). This shear zone is similar in strike length to the KiSZ.

The most significant similarity between the CLGB and Ashanti Belt is the style of gold mineralisation occurring within each. The Obuasi area (western Ashanti Belt) has two different types of gold mineralisation, the dominant of which is disseminated auriferous arsenopyrite with associated pyrite and pyrrhotite, like the arsenopyrite-rich Suurikuusikko ore. The second type of mineralisation common to the Obuasi area is high grade, non-refractory quartz-vein hosted gold. Gold-bearing veins found in outcrop led to the discovery of Suurikuusikko, although vein-hosted gold is not a feature of the major mineralised zones. Vein-hosted free gold is present at the gold prospects immediately north and south of Suurikuusikko, at the Iso-Kuotko (dominantly vein-hosted gold) and Soretialehto (breccia and vein-hosted gold) prospects. The two mined CLGB gold resources, Saattopora and Pahtavaara, also contained vein-hosted gold as major and secondary ores respectively (Eilu 1999). Other similarities

include the presence of refractory gold (grain size of < 1 micron to 35 microns at the Bogosu and Prestea Mines; Mumin et al. 1994), and the highly reducing carbon-rich assemblages associated with most ores of the Ashanti Belt (Mumin et al. 1996).

SUMMARY

Suurikuusikko is an orogenic gold deposit comparable to deposits in gold-producing greenstone belts elsewhere in the world. It also lies within an underexplored region, but the gold potential of the CLGB is fast becoming recognised by international exploration companies. The total resource potential of the CLGB cannot yet be compared to other producing areas due the small amount of exploration and development activity conducted in the region to date. Despite this, the comparison presented between the Ashanti Belt and CLGB highlights the similarities between host rock age and type, host structures, and mineralisation styles between the CLGB and one better-known gold producing region.

Gold mineralisation at Suurikuusikko is refractory, the sub-microscopic gold occurring as lattice substitutions and inclusions mostly within arsenopyrite, but also within pyrite. Although quite evenly distributed throughout ore zones, in detail gold-bearing sulphides occur mostly on graphitic shear fabrics, stylolitic cleavages, and micro-fractures. Strong correlations exist between gold and shear intensity, intense albite alteration, the presence of free ('graphitic') amorphous carbon, and pyroclastic and volcanoclastic host units with a more intermediate composition than surrounding rocks. All ore zones are bound within the Kiistala Shear Zone, with the better-delineated zones plunging moderately north. The consistency of alteration and mineralisation styles along the strike sections of the Kiistala Shear Zone explored to date (over 5.5 kilometres of strike length), and down plunge of identified zones (to a depth of 400 metres) clearly demonstrates the potential of the KiSZ to host more gold.

Ongoing geological work is aiming to better understand controls on Suurikuusikko mineralisation by constructing three-dimensional models of the distribution of stratigraphy, alteration, sulphides (arsenopyrite and pyrite distribution) and shear zones. This work, exploratory drilling to test ideas about host structures, and the availability of new exposures as mine development proceeds will increase our current understanding of the geometry of Suurikuusikko ore lodes and ore controlling mechanisms.

ACKNOWLEDGEMENTS

All data within this article unless otherwise referenced has been sourced from Riddarhyttan Resources AB databases, and is published with the permission of Riddarhyttan Resources AB. Vesa Nykänen is thanked for preparing Figure 1. The quality of this article has been improved thanks to useful review comments supplied by Stephen Davies and Richard M. Vielreicher.

REFERENCES

Agnico-Eagle Ltd. 2006. Media release 06.05.2006. Agnico-Eagle to build Kittila Gold Mine in Finland and complete construction of Lapa Gold Mine in Quebec; to raise $250 million in marketed equity offering.

Barclay, W.A. 2001. Oriented drill core study, Suurikuusikko deposit, northern Finland. May 2001. W.A. Barclay Exploration Services Ltd. Confidential report.

Bartlett, S. 2002. Suurikuusikko gold mineral resources to 15 November 2002. Micon International Co. Ltd. Confidential internal memorandum.

Bolin, N.J. & Larsson, I. 1999. Flotation investigation of the Suurikuusikko deposit. Report TM_REP1999/080. Boliden Technology and Development, Sweden. Confidential report.

Chernet, T., Kojonen, K. & Pakkanen, L. 1999. Applied mineralogical study on the near-surface Suurikuusikko refractory gold ore, Kittilä, Western Finnish Lapland (Phase 1). Geological Survey of Finland Report C/MA9/2743/2000/10.

Durance, M-V., Morin, D., Brunet, J-F., Dictor, M-C., Foucher, S. & Brochot, S. 1999. Technical pre-feasibility study of the treatment of the Suurikuusikko refractory gold ore by flotation and bio-leaching. Final report (annexes) N 2848, August 1999. Confidential report.

Eilu, P. (ed.) 1999. FINGOLD – a public database on gold deposits in Finland. Geological Survey of Finland Report of Investigation 146, 224 p. Web address: www.gtk.fi/explor/gold

Eisenlohr, B.N. & Hirdes, W. 1992. The structural development of the Early Proterozoic Birimian and Tarkwaian rocks of southwest Ghana, West Africa. Journal of African Earth Sciences 14, 313–325.

Groves, D. I., Goldfarb, R.J., Gebre-Mariam, M., Hagemann, S.G. & Robert, F. 1998. Orogenic gold deposits: A proposed classification in the context of their crustal distribution and relationship to other gold deposits. Ore Geology Reviews 13, 7–27.

Härkönen, I. 1984. The gold-bearing conglomerates of Kaarestunturi, central Finnish Lapland. In: Foster, R. P. (ed.) Gold 82: the geology, geochemistry and genesis of gold deposits: proceedings of the symposium Gold 82, University of Zimbabwe, 24–28 May 1982. Geological Society of Zimbabwe. Special Publication 1, 239–247.

Härkönen, I. 1992. Tutkimustyöselostus Kittilän kunnassa valtausalueella Suurikuusikko 1, kaiv. rek n:o 4283/1 suoritetuista malmitutkimuksista. 5 s., 8 liites. Geological Survey of Finland confidential report. (in Finnish)

Härkönen, I. 1997. Tutkimustyöselostus Kittilän kunnassa valtausalueilla Suurikuusikko 2 ja Rouravaara 1–10 (kaivosrekisterinumerot 5965/1, 6160/1, 6288/1–6288/9) suoritetuista kultatutkimuksista vuosina 1987–1997. 47 s., 51 liites. Geological Survey of Finland confidential report.

Härkönen, I. & Keinänen, V. 1989. Exploration of structurally controlled gold deposits in the Central Lapland Greenstone Belt. Geological Survey of Finland, Special Paper 10, 79–82.

Härkönen, I., Kojonen, K. & Johanson, B. 1999a. The early Proterozoic Suurikuusikko refractory gold deposit, Kittilä, western Finnish Lapland. In: Stanley, C. J. et al. (eds.) Mineral deposits: processes to processing. Proceedings of the Fifth Biennial SGA Meeting and the Tenth Quadrennial IAGOD Symposium, London, United Kingdom, 22–25 August 1999. Vol. 1. Rotterdam: A. A. Balkema, 159–162.

Härkönen, I., Kojonen, K. & Johanson, B. 1999b. The Proterozoic Suurikuusikko refractory gold deposit in Kittilä, Western Finnish Lapland. Abstract volume, Gold´99 Trondheim, Norway May 1999.

Kojonen, K., & Johanson, B. 1999. Suurikuusikko – Determination of refractory gold distribution by microanalysis, diagnostic leaching and image analysis. Geological Survey of Finland Report, April 28, 1999.

Kojonen, K. & Pakkanen, L. 2000. Ore mineralogical study of the Rouravaara gold deposit. Geological Survey of Finland Report C/M41/2743/2000/1.

Lehtonen, M., Airo, M.-L., Eilu, P., Hanski, E., Kortelainen, V., Lanne, E., Manninen, T., Rastas, P., Räsänen, J., & Virransalo, P. 1998. Kittilän vihreäkivialueen geologia: Lapin vulkaniittiprojektin raportti. Summary: The stratigraphy, petrology and geochemistry of the Kittilä greenstone area, northern Finland. Report of the Lapland Volcanite Project. Geologian tutkimuskeskus, Tutkimusraportti 140. 144 p. + 1 app (map). (in Finnish)

Luosto U., Flueh E.R., Lund C.E. & working group. 1989. The crustal structure along the POLAR Profile from seismic refraction investigations. In: Freeman R, von Knorring M., Korhonen H, Lund C. & Mueller S. (eds) The European Geotraverse, Part 5: The POLAR Profile. Tectonophysics 162, 51–85.

Markström, P., Bolin, N.J. & Larsson, I. 2000. Suurikuusikko – Flotation pilot plant campaign. Report TM_REP2000/026. Boliden Technology and Development, Sweden. Confidential report.

Markström, S. & Larsson, I. 2000a. Laboratory tests for autogenous grinding. Report TM_REP2000/042, Boliden Technology and Development, Sweden. Confidential report.

Markström, S. & Larsson, I. 2000b. Pilot scale tests for autogenous grinding. Report TM_REP2000/047, Boliden, Sweden. Confidential report.

Micon International Co. Ltd. 2001. Suurikuusikko gold project, Interim Report 2 Scoping Study, May 2001. Confidential report.

Mumin, A., Fleet M. & Chryssoulis S. 1994. Gold mineralization in As-rich mesothermal gold ores of the Bogosu-Prestea mining district of the Ashanti Gold Belt, Ghana. Mineralium Deposita 29, 445–460.

Mumin, A., Fleet, M. & Longstaffe, F. 1996. Evolution of hydrothermal fluids in the Ashanti Gold Belt, Ghana. Stable isotope geochemistry of carbonates, graphite and quartz. Economic Geology 91, 135–148.

Oberthür, T., Vetter, U., Davis, D., & Manor, J. 1998. Age constraints on gold mineralisation and Paleoproterozoic crustal evolution in the Ashanti belt of southern Ghana. Precambrian Research 89, 3–4, 129–143.

Oberthür, T., Weiser, T., Amanour, J.A., & Chryssoulis, S.L. 1997. Mineralogical siting and distribution of gold in quartz veins and sulfide ores of the Ashanti Mine and other deposits in the Ashanti Belt of Ghana: genetic implications. Mineralium Deposita 32, 2–15.

Patison, N. L. 2000. Structural and fluid-chemical controls on gold mineralization in the Central Lapland Greenstone Belt, northern Finland: Project Report 1. Geological Survey of Finland unpublished report M16/2001/2, 27 pages.

Patison, N. L. 2001. Suurikuusikko Gold Deposit: Deformation history and preliminary paragenetic information. Report for Riddarhyttan Resources AB, 26 pages + maps. Confidential report.

Powell, W. 2001. Petrographic Report on Suurikuusikko rock types. Report for Riddarhyttan Resources AB. November 2001. Confidential report.

Riddarhyttan Resources AB. 2001. Press Release 17 April 2001. Riddarhyttan Resources AB: New calculation shows a considerable increase in tonnage at Suurikuusikko.

Salo, O. 2001. The environmental impact assessment report for the Suurikuusikko mining project. Lapland Water Research Oy (LVT Oy). Confidential report.

Sandahl, K-A. 1999. Suurikuusikko – Rouravaara. MIRAB Mineral Resources AB, Report December 12, 1999. Report number 99004. Confidential report.

Sandahl, K-A. 2000a. Suurikuusikko southern mineralization. MIRAB Mineral Resources AB, Report November 24, 2000. Report number 00004. Confidential report.

Sandahl, K-A. 2000b. Suurikuusikko – Kiistala. MIRAB Mineral Resources AB, Report December 22, 2000. Report number 00005. Confidential report.

Ward, P., Härkönen, I., Nurmi, P.A., & Pankka, H.S. 1989. Structural studies in the Lapland greenstone belt, northern Finland and their application to gold mineralization. Current Research, Geological Survey of Finland, Special Paper 10, 71–77.

Gold in the Central Lapland Greenstone Belt, Finland
V. Juhani Ojala (ed.)
Geological Survey of Finland, Special Paper 44, 137–151, 2007.

THE ALTERATION AND FLUID INCLUSION CHARASTERISTICS OF THE HIRVILAVANMAA GOLD DEPOSIT, CENTRAL LAPLAND GREENSTONE BELT, FINLAND

by
Helena Hulkki &Veikko Keinänen

Hulkki, H. & Keinänen, V. 2007. The Alteration and Fluid Inclusion Characteristics of the Hirvilavanmaa Gold Deposit, Central Lapland Greenstone Belt, Finland. *Geological Survey of Finland, Special Paper 44,* 137–153, 10 figures and 2 tables.

The Hirvilavanmaa gold deposit is situated in the southern part of the Central Lapland Greenstone Belt. First indication of mineralization in the area was a polymetallic till and stream sediment anomaly with Cu, Co, Au, As, Mo and W contents detected in 1983. The area consists mainly of pyroclastic komatiites altered into albite-carbonate-chlorite and carbonate-dominated assemblages. The area is at the intersection of the NW trending Sirkka Shear Zone and N–S trending fault. At Hirvilavanmaa, the altered rocks define a NNE trending zone 270 m long and 90 m wide where quartz breccias and veins form roughly N–S trending subzones. The rocks around the quartz breccias are impregnated with pyrite whereas hematite occurs further from the veins. Native gold occurs as small inclusions and fracture fillings both in pyrite and in vein quartz and carbonate. Four stages of alteration have been established at Hirvilavanmaa. The earliest stages of alteration are hydration and albitization. Later, the rocks were fractured and the alteration more closely associated with the gold-mineralization is pyritization, silification, carbonatization, hematitization, and minor tourmalinization and albitization. This was followed by late carbonation. During alteration chemical changes were rather small. The most intensely altered zone is clearly defined by the increased levels of CO2, S, Cl, Na and Au which are considerably higher than in the distal alteration zones. Three types of fluid inclusions were recognized at Hirvilavanmaa; Type I and II represent H2O-CO2-salt fluids with varying H2O/CO2. Type III fluids are CO2-bearing H2O-(CO2-Solid)-salt fluids. The salinities of fluid inclusions show a variation from 5 to 22 equivalent weight percent NaCl. Phase separation and interaction between wall rock and hydrothermal fluid were mechanisms which influenced gold precipitation at Hirvilavanmaa. The minimum conditions at the beginning of opening of the fracture system were 330–370ºC and about 3000 bars. After the main opening of the fracture zone, the pressure fluctuated between 1000–2200 bars due to deformation, cracking and sealing of the vein systems, and mineralization took place at 220–310ºC. At the late stages of mineralization and alteration, the late fluids migrated through the system reacting with the host rocks and causing further carbonatization.

Key words (GeoRef Thesaurus AGI): gold ores, komatiite, alteration, geochemistry, quartz veins, fluid inclusions, microthermometry, P-T conditions, Central Lapland Greenstone Belt, Paleoproterozoic, Hirvilavanmaa, Lapland Province, Finland

Geological Survey of Finland, P.O. Box 77, FI-96101 Rovaniemi, Finland
E-mail: helena.hulkki@gtk.fi, veikko.keinanen@gtk.fi

INTRODUCTION

The Hirvilavanmaa gold deposit is situated in the in the southern part of the Central Lapland Greenstone Belt, 15 km northeast from the Kittilä town (Fig. 1). The resource at Hirvilavanmaa is estimated at 0.11 Mt at 2.9 g/t (Scan Mining, 2002). Detailed geochemical studies by the Geological Survey of Finland (GTK) started in the area in 1983 (Johansson et al., 1986). These studies revealed a polymetallic till and stream moss anomaly with high Cu, Co, Au, As, Mo and W values. Further investigations (till geochemistry, ground geophysics, trenching and drilling) led to the discovery of mineralized zones; one enriched in tungsten (Soretiapulju) and three in gold (Soretiavuoma N, Hirvilavanmaa and Soretialehto). The results of the exploration activities (1985–1990) of the area have been reported by Keinänen, 1987; Keinänen et al., 1988; Härkönen and Keinänen, 1989; Keinänen and Hulkki, 1992; Keinänen, 1994, Keinänen and Holma, 2001. In this paper, only the gold deposit at Hirvilavanmaa is described and discussed in more detail.

The study area mainly consists of ultramafic rocks of komatiitic affinity (Table 1). Due to hydrothermal alteration and deformation, the ultramafic rocks are now represented by various kinds of schists, albite-carbonate-chlorite-sericite rocks and carbonate rocks including green fuchsite altered varieties (commercially marketed as "chromian marbles") (Fig. 2). The ultramafic rocks are magnetite rich and are, hence, easily identified in magnetic maps which shows that the komatiites strike NW in the area. Sulphide-bearing graphite-rich schists occur to the east of the ultramafic schists and also as intercalated lenses among the latter. Mafic volcanic rocks, predominantly tuffites, are present in the northeastern part of the area. Quartzites, with associated albite rocks, are located at the southwestern part of the study area. The supracrustal

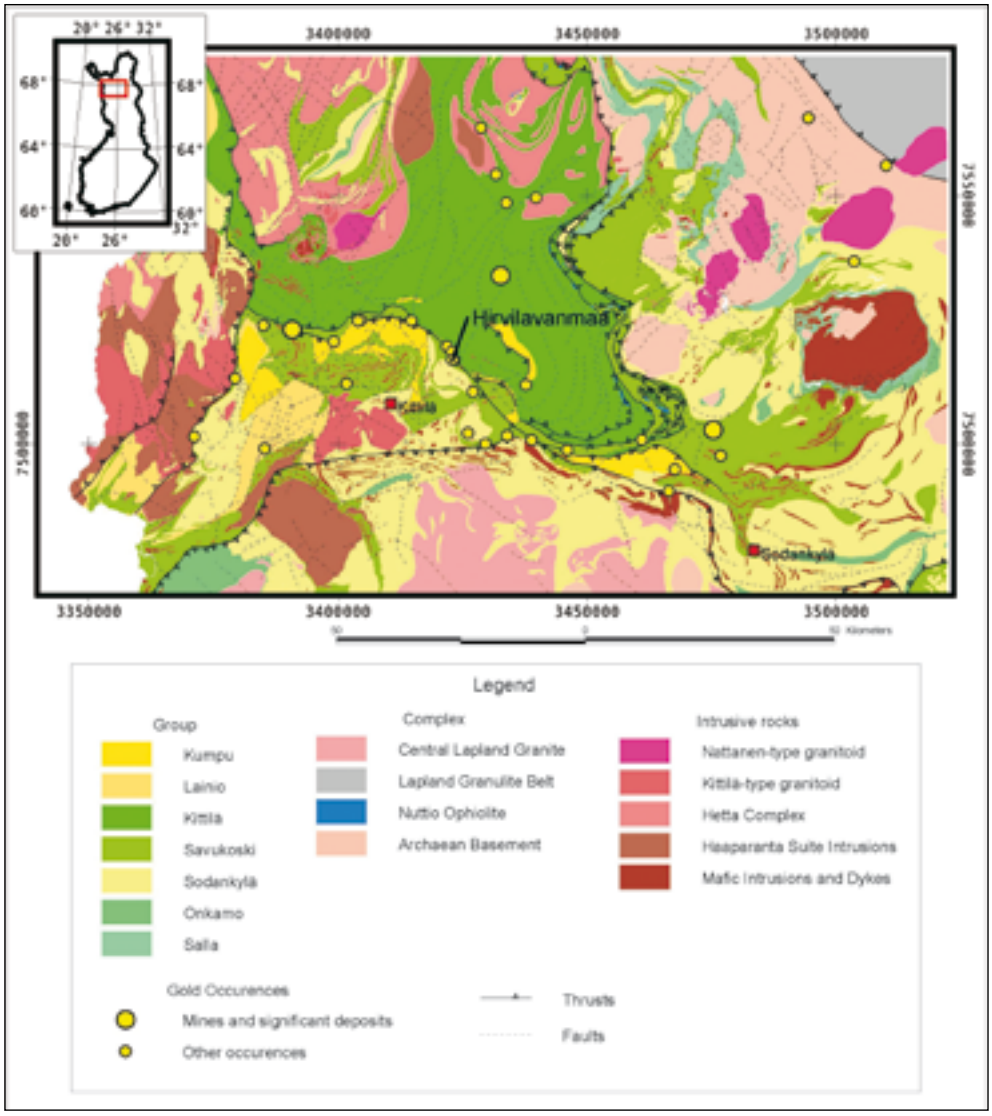

Fig. 1. Location of the Hirvilavanmaa deposit in the Central Lapland Greenstone Belt.

Table 1. Basic statistics for major and trace element data of variable altered metakomatiites from Hirvilavanmaa (drill hole DH335). DZ=distal alteration zone, POZ=proximal outer zone, PIZ=proximal inner zone. min=minimum, med=median, max=maximum, std=standard deviation. 0=very small (e.g. between minimum and maximum), – = not determined (compiled by Marko Holma).

	HANGING WALL								ORE ZONE				FOOTWALL							
	DZ (n=5)				POZ (n=4)				PIZ (n=13)				POZ (n=4)				DZ (n=4)			
	min	med	max	std	min	med	max	std	min	med	max	std	min	med	max	std	min	med	max	std
SiO2 (wt%)	40.11	42.69	43.90	1.60	35.29	40.07	44.29	3.77	31.75	35.93	47.24	4.63	39.11	41.32	43.21	1.69	40.17	43.20	50.60	4.97
TiO2	0.46	0.62	0.95	0.18	0.45	0.53	0.65	0.10	0.34	0.61	0.89	0.15	0.52	0.62	0.67	0.07	0.47	0.62	0.77	0.12
Al2O3	5.54	7.10	8.90	1.21	5.07	6.52	7.71	1.08	4.52	5.39	8.14	1.00	4.95	5.73	7.75	1.33	6.21	6.28	8.66	1.20
Fe2O3tot	8.56	11.61	13.21	1.90	7.91	10.47	12.47	2.00	7.85	10.89	12.50	1.36	9.55	10.88	11.94	1.28	9.63	10.33	13.05	1.55
MnO	0.13	0.15	0.16	0.01	0.14	0.19	0.28	0.06	0.12	0.15	0.21	0.02	0.12	0.15	0.21	0.05	0.09	0.15	0.19	0.04
MgO	23.27	24.91	25.72	1.00	20.56	24.18	25.75	2.34	12.72	19.33	25.91	3.11	23.32	24.05	25.96	1.25	22.67	26.14	27.31	2.01
CaO	3.06	5.32	7.71	1.71	4.44	7.82	16.63	5.45	0.84	4.89	10.43	2.38	3.79	6.01	8.63	2.27	1.48	4.15	8.57	2.95
Na2O	0.09	0.11	0.19	0.06	0.23	0.44	0.64	0.29	0.24	0.93	2.16	0.63	0.09	0.61	0.82	0.33	0.23	0.33	0.39	0.07
K2O	0.22	0.37	0.50	0.10	0.02	0.21	1.48	0.69	0.01	0.01	0.05	0.01	0.00	0.01	0.02	0.01	0.01	0.03	0.05	0.02
P2O5	0.02	0.04	0.05	0.01	0.02	0.03	0.04	0.01	0.02	0.03	0.13	0.03	0.03	0.04	0.04	0.01	0.02	0.03	0.05	0.01
CO2	0.16	1.16	5.31	2.05	3.33	6.58	13.04	4.07	5.50	19.75	20.78	5.20	5.97	9.34	13.19	3.39	1.34	2.63	4.69	1.47
As (ppm)	< 30	0	< 30	–	< 30	0	< 30	–	< 30	0	< 30	–	< 30	0	< 30	–	< 30	0	< 30	–
Ba	22	25	28	4	24	25	31	4	22	24	27	2	< 20	0	< 20	–	22	23	30	4
Bi	< 30	0	< 30	–	< 30	0	< 30	–	< 30	0	< 30	–	< 30	0	< 30	–	< 30	0	< 30	–
Ce	< 30	0	< 30	–	< 30	0	< 30	–	58	0	58	–	< 30	0	< 30	–	< 30	0	< 30	–
Cl	< 60	0	< 60	–	< 60	0	< 60	–	65	90	223	55	80	0	80	–	< 60	0	< 60	–
Cr	1518	2351	3236	638	1750	2013	2373	274	1113	2041	3163	529	1664	1772	1881	108	2076	2286	2998	408
Cu	38	44	137	50	54	118	257	86	30	50	85	15	108	175	313	94	52	87	171	51
Ga	22	0	22	–	< 20	0	< 20	–	< 20	0	< 20	–	< 20	0	< 20	–	< 20	0	< 20	–
La	< 30	0	< 30	–	< 30	0	< 30	–	< 30	0	< 30	–	< 30	0	< 30	–	< 30	0	< 30	–

Continues nex page

Table 1. Continues

	HANGING WALL								ORE ZONE				FOOTWALL							
	DZ (n=5)				POZ (n=4)				PIZ (n=13)				POZ (n=4)				DZ (n=4)			
	min	med	max	std	min	med	max	std	min	med	max	std	min	med	max	std	min	med	max	std
Pb	< 30	0	< 30	–	33	0	33	–	< 30	0	< 30	–	< 30	0	< 30	–	< 30	0	< 30	–
Rb	18	28	39	8	31	66	101	–	< 10	0	< 10	–	< 10	0	< 10	–	< 10	0	< 10	–
S	83	85	86	2	144	248	331	102	60	8498	34630	10354	83	253	494	169	116	165	259	73
Sb	< 100	0	< 100	–	< 100	0	< 100	–	< 100	0	< 100	–	< 100	0	< 100	–	< 100	0	< 100	–
Sc	< 30	0	< 30	–	34	0	34	–	< 30	0	< 30	–	< 30	0	< 30	–	< 30	0	< 30	–
Sn	< 20	0	< 20	–	< 20	0	< 20	–	< 20	0	< 20	–	< 20	0	< 20	–	< 20	0	< 20	–
Sr	11	20	69	27	53	94	220	78	20	55	140	32	25	42	71	19	28	80	141	56
Th	< 10	0	< 10	–	< 10	0	< 10	–	< 10	0	< 10	–	< 10	0	< 10	–	< 10	0	< 10	–
U	< 10	0	< 10	–	< 10	0	< 10	–	< 10	0	< 10	–	< 10	0	< 10	–	< 10	0	< 10	–
V	144	199	248	38	143	185	217	33	105	175	259	40	136	176	216	35	166	196	238	30
Y	< 10	0	< 10	–	10	0	11	–	10	0	12	–	11	0	13	–	10	12	12	1
Zn	60	64	87	11	64	73	84	10	46	59	94	16	71	73	86	7	90	102	111	9
Zr	22	30	48	10	18	26	32	7	14	26	48	10	23	26	34	5	20	35	37	8

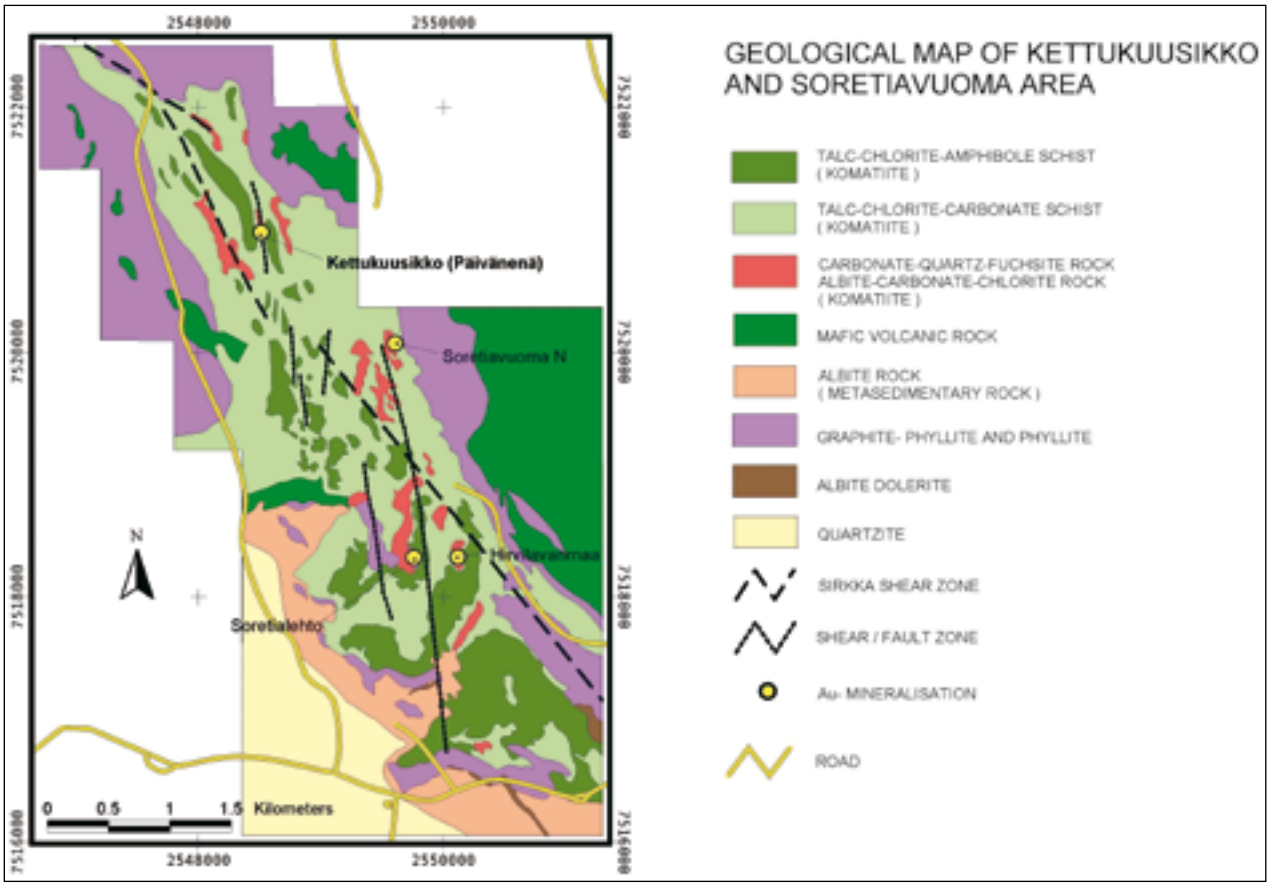

Fig. 2. Generalized geological map of the study area. Basemap © National Land Survey 521/MYY/07

sequence is intruded by dolerites of variable albite content and by albite porphyry sills. The NW trending Sirkka Shear Zone (SSZ) crosses the area. Another fault or shear zone, running roughly north-south, has been identified in induced polarization ground survey in the area. All rocks in the area have been metamorphosed under greenschist facies P-T conditions. Hence, the prefix "meta" is implied but omitted from the names of the rock types.

THE MINERALIZED ZONE AND ITS VEIN MINERALOGY

General characteristics

At Hirvilavanmaa, the altered rocks define a NNE trending zone which is 270 m long and 90 m wide (Fig. 3). The altered domain is divided into three zones: distal, proximal outer and proximal inner zone (Fig. 3). The distal zone consists of talc-chlorite-amphibole schist and the proximal outer zone of albite-carbonate-talc-chlorite schist. Albite-carbonate-chlorite rock represents the most intensely altered inner part. Quartz breccias and veins form nearly N-S trending narrow zones which commonly are located at or near the contacts between the intensely and weakly altered rocks. The rocks around the quartz veins and breccias are pyrite altered whereas hematite occurs further from the veins. The altered domain and the quartz breccias are intersected by late stage quartz veins. These younger veins are gold-rich (up to 30 g/t Au) and have a strike of N10W-N15W. The gold-rich lodes are narrow lens-like bodies which coincide with the zones of quartz breccias and veins (Fig. 3) and, typically, the highest grade ore is pyrite rich.

The altered rocks have been interepreted to be mainly pyroclastic komatiite in origin. Textural features in the sequence suggest that minor volumes of mafic rocks are present in the hosting sequence, too. The least altered komatiitic rock detected in the area has a metamorphic mineral assemblage of amphibole, chlorite, sphene, chromite, magnetite and minor amounts of carbonate and talc. Destruction of amphibole and sphene,

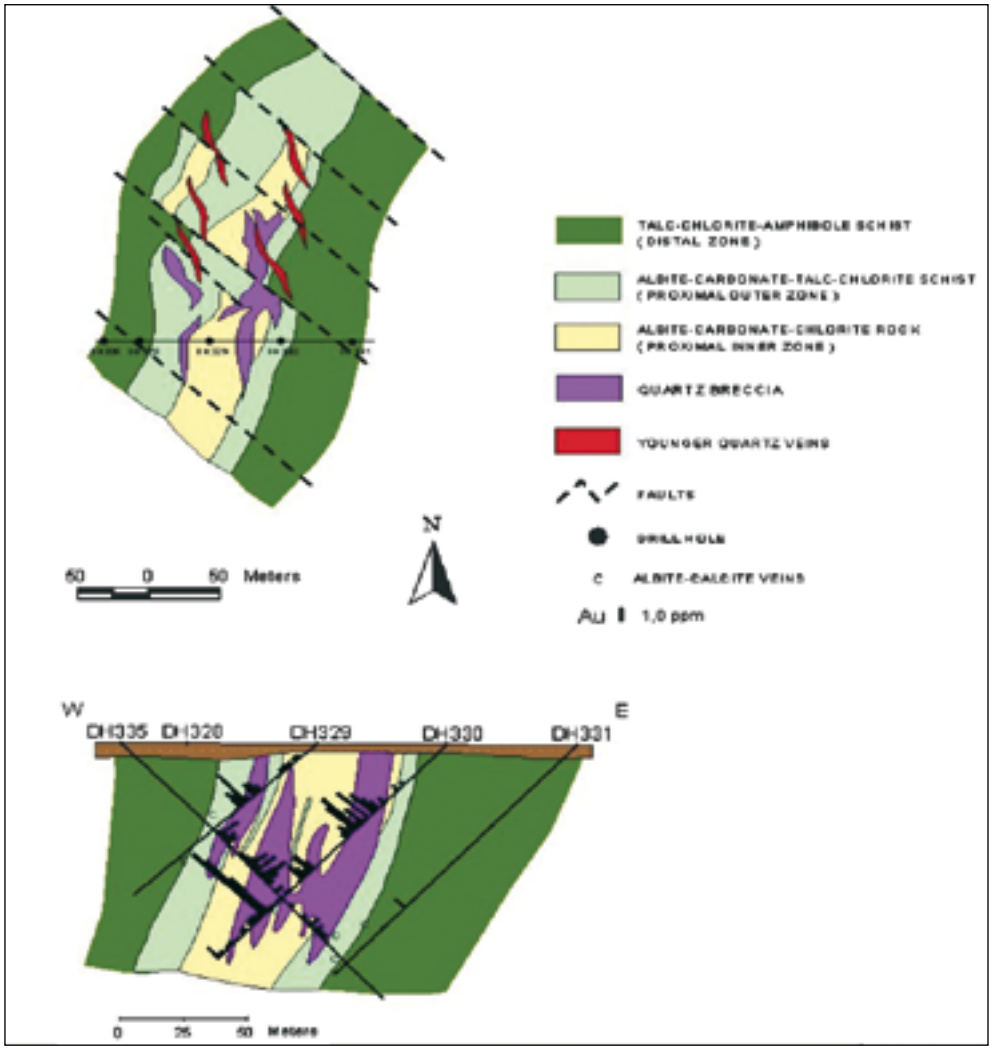

Fig. 3. Generalized geological setting of Hirvilavanmaa gold deposit and a cross-section of the alteration zone and its gold concentrations.

formation of albite, rutile and hematite and increase of the volume of carbonate and talc characterize the distal alteration zone. The transition from the distal into the proximal alteration zone is gradual and indicated by a considerable decrease in the amounts of talc, chlorite, and Cr- and Fe-oxides, and an increase in the amounts of albite, carbonate and pyrite. In the inner proximal alteration zone, rutile and quartz are common accessory minerals. The rocks of the proximal alteration zone lack the planar tectonic fabric typical for unaltered rocks and distal alteration zone and usually have coarser grain-sizes than the rocks of the distal alteration zone.

Vein mineralogy

Veins chiefly comprise quartz, carbonate and albite. Some of them are clearly deformed and boudinaged. The veins typically have marginal zones composed of albite and in some cases of carbonate and tourmaline. The veins contain pyrite and chalcopyrite whereas the late stage quartz veins contain chalcopyrite, pyrite and pyrrhotite together with carbonate in fractures in the vein quartz. Native gold occurs as small inclusions or fracture fillings (locally together with chalcopyrite and carbonate) in pyrite (Fig.4b). Gold grains have also been observed in vein quartz and carbonate. In addition to gold, chalcopyrite, rutile, galena, tetrahedrite, tellurides, molybdenite, monatzite and Y-phosphate inclusions have been documented in pyrite (Härkönen and Keinänen, 1989).

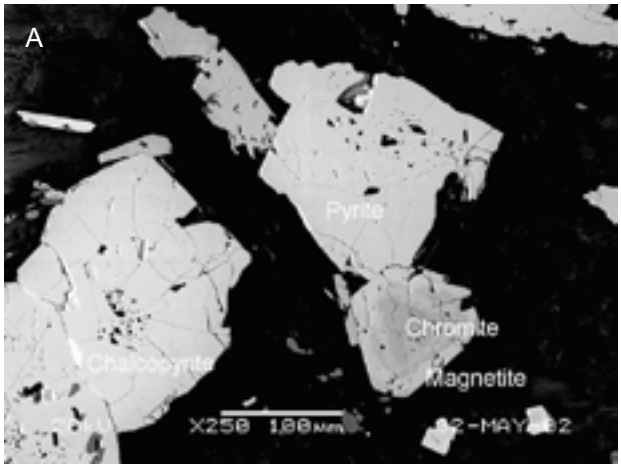

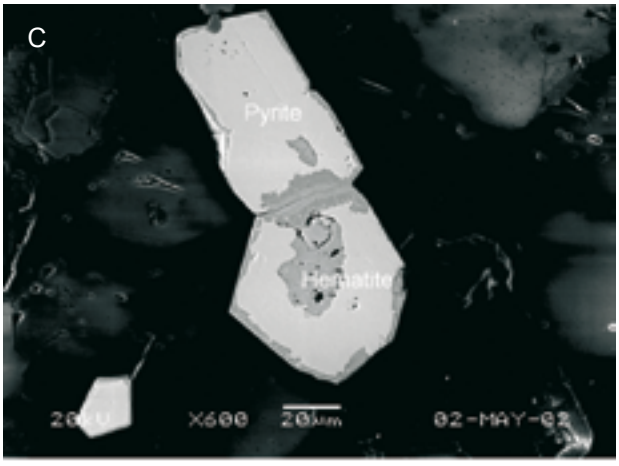

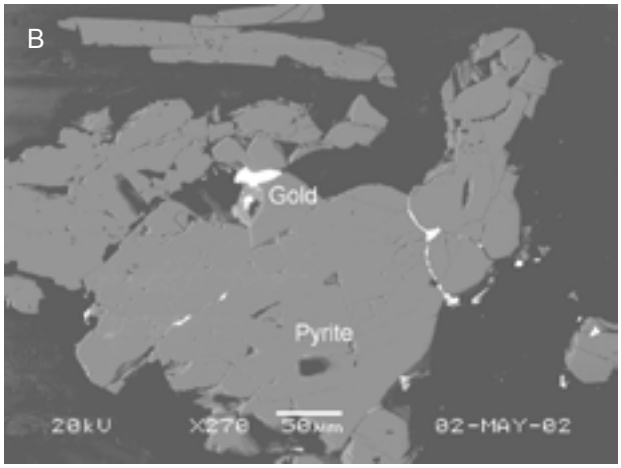

Fig. 4. Typical ore mineral parageneses at Hirvilavanmaa:
a) Chromite-magnetite-pyrite (chalcopyrite as fracture fillings).
b) Gold as fracture fill in pyrite
c) Pyrite replaced by hematite

HYDROTHERMAL ALTERATION

Hydration and albitization

Four stages of alteration have been established at Hirvilavanmaa (Fig. 5). These are described below from the earliest to the latest. The earliest stage of alteration observed in the area is hydration which caused the formation of talc and of chlorite. The hydration event is regional in nature and is not restricted to that area where the Au-mineralization took place. At that stage, the metamorphic amphibole was replaced by talc and chlorite, sphene by rutile and lath-shaped rutile-hematite clusters were formed probably as an alteration product of ilmenite grains. Low-degree carbonatization is related to this stage and is demonstrated by carbonate-talc microveinlets. In these veins, some biotite was also observed, otherwise K-metasomatism is negligible at Hirvilavanmaa.

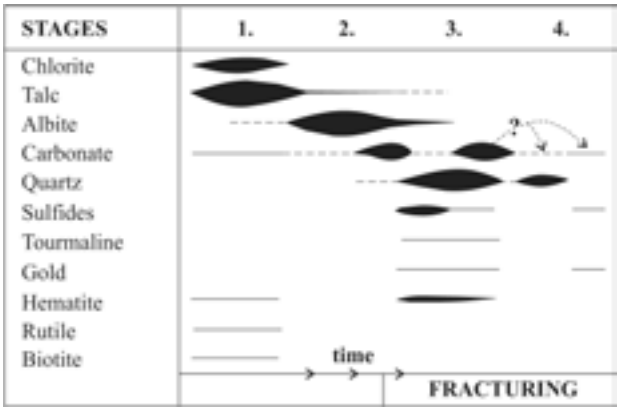

Fig. 5. Generalized sequence of alteration at Hirvilavanmaa. Line thicknesses schematically depict the relative quantities of the mineral formed. Dotted lines represent uncertainties.

Hydration was followed by the albitization. Chlorite and talc, as well as minor rutile, commonly occur as inclusions in anhedral and ragged albite grains supporting the suggestion that the main stage of albitization postdates the hydration event. However, hydration and albitization probably are more overlapping than shown in Figure 5, and albitization may just signify

a higher degree of fluid-wall rock interaction. Albite grains occur as dissemination and form discrete veins which commonly contain fan-shaped talc clusters showing that the precipitation of talc continued during the albitization. Albitization consumed chlorite causing a distinct decrease in the chlorite amount where the albitization was intense. Some of the carbonate follows the mode of occurrence of albite and seems to be in equilibrium with it. This carbonate is usually fine-grained and forms well-developed crystals. In addition, carbonate forms coatings with and without tourmaline along the quartz-rich vein walls. These observations suggest that the end of the main albitization event and the beginning of fracturing were accompanied by the carbonatization and that the early carbonatization may mark the beginning of the alteration events which are more closely related to the brittle deformation, quartz veining and gold mineralization.

Brittle deformation, and associated alteration

After hydration and albitization, the rocks were fractured and the alteration more closely associated with the Au-mineralizing fluids begun. Pyrite quite commonly contains inclusions of chlorite, albite, talc, rutile and in some cases carbonate supporting the idea that pyritization postdates hydration and albitization. Pyrite was formed at the expense of chlorite and magnetite. Pyrite grains in irregular stripes of chlorite are in some cases surrounded by talc indicating that MgO and SiO_2 released from pyritized chlorite were partly preserved in the host rock by the formation of talc. However, the formation of talc at this stage was negligible compared to the early hydration stage.

The spatial association of pyrite with quartz-rich zones suggests that silification was partly contemporaneous with pyritization. In addition to discrete quartz veins, silification caused the precipitation of secondary quartz in the wall rocks. At this stage, also some tourmaline was precipitated along the vein margins or into the wall rocks. Minor albite was formed as shown by some quartz-rich veins having albite-rich selvages. Much more hematite seems to have been formed with pyrization than during the early hydration event. However, the different spatial distribution of these minerals (pyrite occurring closer to the quartz breccias) could indicate that the fluids which were penetrating from vein fractures into wall rock changed towards more oxidating state along their fluid paths or, alternatively, there were gross changes in the redox potential of the fluid in the course of time. The change in the redox potential is also supported by the observation of pyrite locally being partly replaced by hematite (Fig. 4c).

Late carbonatization

The last major stage of alteration at Hirvilavanmaa is the carbonatization. The late carbonate has intensely replaced talc, quartz, chlorite and amphibole as well as forms overgrowths on the well-developed crystals of early carbonate. The late carbonatization has also destructed the fine-grained textures of the early carbonate by recrystallization and formation of larger grains which now replace the surrounding minerals. Due to the destructive style of the late carbonation, it is difficult to separate the two generations of carbonatization and estimate their intensities. In spite of this, it is suggested that the late carbonatization was much more pronounced than the early one.

The late carbonatization postdates the formation of quartz breccias, but the precise relationship with the late stage quartz veins remains unclear. As indicated by the dotted lines and arrows in Figure 5, it is possible that the late carbonatization is a contemporaneous event with the formation of the late stage veins. These veins could represent the latest stage of the mineralizing event gaining their quartz in response to the late CO_2-metasomatism, which released SiO_2 from carbonated minerals into circulating fluids.

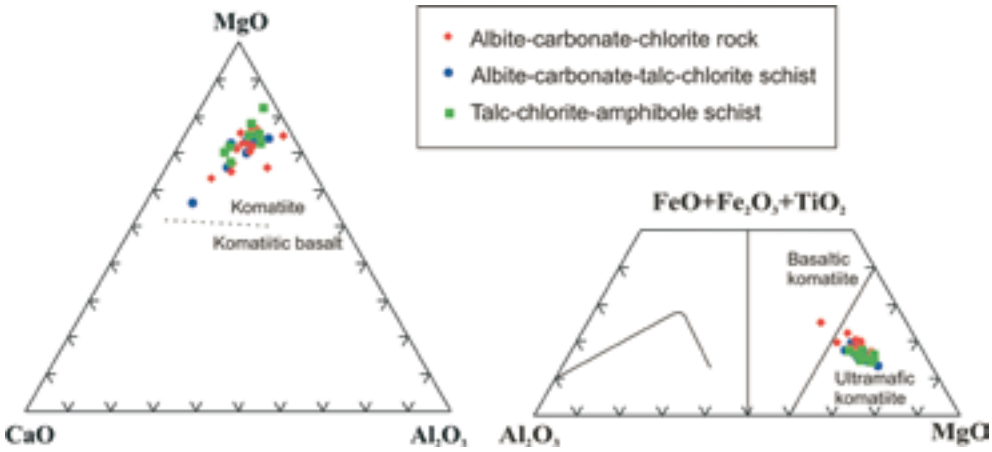

Fig. 6. Chemical compositions of altered komatiitic volcanic rocks from Hirvilavanmaa presented on Jensens cation plot and on CaO-MgO-Al_2O diagram. Compositional fields as defined by Jensen (1976), Viljoen and Viljoen (1969), and Viljoen et al. (1982).

GEOCHEMICAL FEATURES OF ALTERATION

Although intensely altered, all ultramafic rocks from Hirvilavanmaa are situated in the field of ultramafic komatiites in the Jensen (1976) cation plot (Fig. 6). The fine-grained albite-quartz-carbonate rocks detected in some of the holes drilled clearly differ from the komatiites by plotting close to the field of tholeiitic basalt.

The chemical changes related to alteration were studied in the samples from the drill hole R335 which cuts across the entire altered domain from the hanging wall to the footwall (Fig. 3). Samples (each 20-30 cm of drill core) were taken every five metres avoiding the quartz-rich types. Thus, the samples represent altered host rocks and are not diluted by vein material. Altogether 30 samples were taken representing a section 153.30 m wide. The elements Na, Mg, Al, Si, P, K, Ca, Ti, Mn, Fe, S, Cl, Sc, V, Cr, Ni, Cu, Zn, Ga, As, Rb, Sr, Y, Zr, Nb, Mo, Sn, Sb, Ba, La, Ce, Pb, Bi, Th, U were analysed by XRF, and C by Leco, in the Espoo laboratory of the GTK. Gold was analysed in the Rovaniemi laboratory of the GTK by FAAS.

The possible immobility of the elements was first checked by plotting the most common immobile elements (MacLean and Kranidiotis, 1987) against each other. This procedure indicated aluminium being the most immobile element at Hirvilavanmaa. Mobile – immobile element ratios were then used to examine the chemical changes related to alteration. By this method, the general trends of chemical changes were possible to define at Hirvilavanmaa.

The examination of the mobile element-Al_2O_3 ratio revealed that during alteration chemical changes were rather small. There are no significant differences in mobility for Mn, Ni and P across the altered domain. On the other hand Na, K, Mg, Cr, Fe, S, CO_2, Cl_2 and Cu seem to have been mobilized in contrasting way during alteration (Fig. 7), as discussed below.

The distal alteration zone both in the hanging wall and in the footwall is distinguished from the proximal outer zone by its very low CO_2, Na_2O and S levels. The level of K_2O is very low in the whole alteration zone, although clearly elevated in the hanging wall. In mineral assemblage, this relates to a weak biotitization of the rocks. The change from distal to proximal outer zone is easy to recognize with the increase in CO_2 and Na_2O. The most conspicuous is the increase of Cu and CaO, which define the proximal outer zone (see Fig. 7). Probably this is due to chalcopyrite- bearing calcitic veinlets.

The proximal inner alteration zone is clearly defined by the increased levels of CO_2, S, Cl, Na_2O and Au, as their concentrations are considerably higher than in the other parts of the area. Also, the level for Fe is slightly elevated. On the other hand, the level for MgO and SiO_2 are lower in the most intensely altered part. The depletion of SiO_2 and MgO suggests that those elements were mobilized into the fluid and were precipitated in carbonate-quartz veins.

Following trends are possible to find in the section across the altered domain and mineralization (Fig. 7). The trends of Na_2O/Al_2O_3, S/Al_2O_3 and CO_2/Al_2O_3 are similar. Clear increase from the distal zone to the proximal zones indicates that the degree of mobility of these components increases with proximity to gold

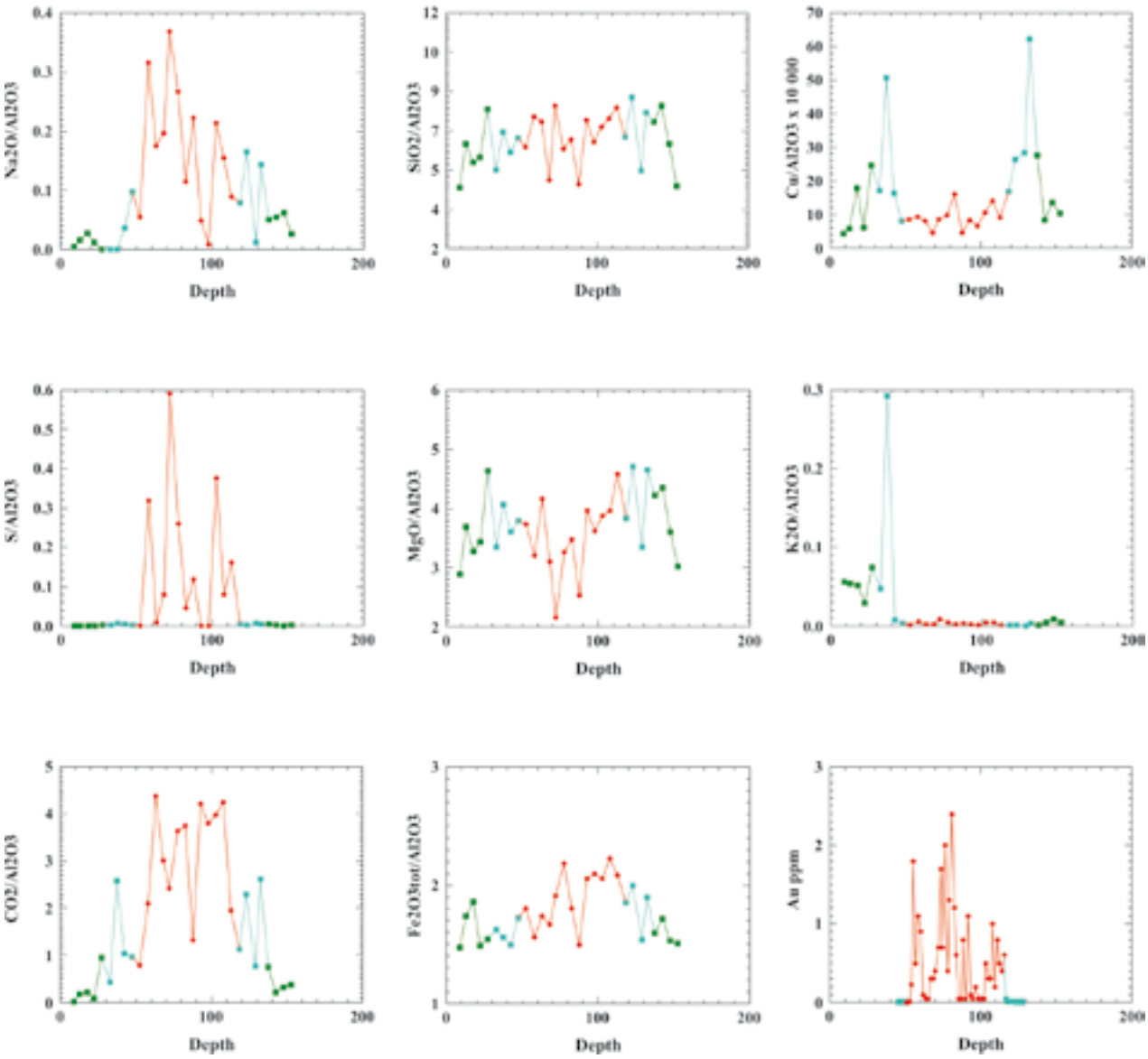

Fig. 7. Chemical trends across the drill hole DH 335. Color of the symbols as in figure 6.

mineralization. The slightly rising trend of SiO_2/Al_2O_3 and MgO/Al_2O_3 with depth is clear. Also, its worth of noticing that the level of Na_2O remains much higher in the footwall than in the hanging wall. These features may hint for another intensely altered and mineralized zone in depth.

FLUID INCLUSION STUDY

A fluid inclusion study was performed in order to provide information on the fluids associated with mineralization at Hirvilavanmaa. Temperature, composition and density data obtained from the fluid inclusions in the quartz-carbonate veins and breccias were used to estimate pressure-temperature conditions at which the gold mineralization took place. The fluid study was also intended to identify the processes which caused or influenced the gold precipitation.

Sampling and methods

The fluid inclusion study is based on seven samples. The samples were taken from gold-bearing quartz-carbonate veins and breccias and they probably represent different stages of veining during the mineralization. Altogether, nine double-polished quartz plates 0.2-0.3 mm thick were prepared from

these samples. Unfortunately, some samples were partly unfavourable for fluid inclusion study due to the deformation and recrystallization of vein quartz which had nearly completely destroyed the oldest populations of fluid inclusions. Also, the small size of inclusions in many cases restricted or prevented good and accurate measurements.

Microthermometric measurements were made on a Fluid Inc. heating-freezing stage and on a Linkam THMS 600 programmable heating-freezing stage attached to a Leitz Ortholux Pol transmitted light microscope (Shepherd et al., 1985). The stages were calibrated with synthetic fluid inclusion standards (Sterner and Bodnar, 1984). Precision in the measurements of the temperatures of phase changes ranged from 0.2ºC for temperatures below +30ºC to the maximum error of 3.0ºC for higher temperatures.

Nature and occurrence of fluid inclusions

Fluid inclusions were mainly examined in vein quartz and some inclusions were possible to identify in vein carbonate. Three types of fluid inclusions were recognized in the studied samples (Table 2). The classification of the fluid inclusions is based on their phases present at room temperature, their mode of occurrence and their cooling behavior. Commonly, fluid inclusions form intra- and intergranular trails representing healed fractures now lined by fluid inclusions, or they occur in sparsely populated clusters in relatively small areas. Some isolated individual inclusions were also recognized in the samples.

Type I–II fluid inclusions are CO_2-rich. The volumetric portion of CO_2 ranges from 5 to 100 percent. Typically, these inclusions are small (Ø <10–15 µm) with their shape varying from ellipsoidal to well-formed negative crystal shapes. In some cases, they contain transparent and opaque solid phase(s). CO_2-

Table 2. Fluid types and microthermometric data of fluid inclusions from Hirvilavanmaa

		CO_2 Vol%	T_mCO_2 °C	T_hCO_2 °C	T_mInitial °C	Salinity* Wt% NaCl equiv	T_h(L-V) °C	T_hTot** °C
Type I	**H_2O-CO_2, P-PS**							
	Breccia, P (57)	22 – 48	-56.9 – -57.3	5.5 – 24.1	-30.5	8.9 – 12.5 (c)	347 – 369	
	Breccia, PS (57)	6 – 18	-57.1 – -57.8	19.6 – 29.7	-40.5 – -28.3	16.1 – 19.2 (c)	160 – 252	
	Breccia, P-PS (59)	5 – 30	-56.5 – -57.6	13.8 – 30.4	-42.0 – -27.3	9.3 – 15.2 (i) 8.1 – 15.8 (c)	205 – 335	
	Waning phase, P (61, 63)	5 – 23	-56.7 – -59.7	19.4 – 28.3	-38.6 – -33.1	9.3 – 14.0 (i) 11.6 – 13.3 (c)	223 – 264	
	Young veins, P-PS (27, 28)	7 – 25	-57.4 – -57.9	17.3 – 26.9	-	17.7 – 19.8 (i) 16.4 – 17.1 (c)	181 – 233	
Type II	**CO_2-H_2O, P-PS**							
	Breccia, P-PS (57, 59)	70 – 100	-56.4 – -57.3	-5.5 – 22.9	-	5.0 – 6.4 (c)	246 – 319	
	Waning phase, P (61, 63)	80 – 90	-56.8 – -56.9	-3.5 – 3.6	-	-	-	
Type IIIA	**H_2O-(CO_2-Solid), P-PS**							
	Breccia, waning phase, young veins (27, 28, 57, 63)				-40.9 – -28.9	13.1 – 22.2 (i)	145 – 252	189 – 248
Type IIIB	**H_2O-(CO_2)-Solid, S**							
	Breccia, waning phase, young veins (27, 28, 57, 61, 63)				-45.2 – -32.2	19.8 – 22.5 (i)	92 – 165	153 – 235

P primary inclusions, PS pseudosecondary inclusions, S secondary inclusions
* Salinity is derived from final melting temperatures of ice (i) and clathrate (c)
** The total homogenization temperature = TmHalite (the last event is a dissolution of halite)

rich inclusions form short trails and sparsely populated small clusters and locally occur as isolated inclusions. These trails and clusters are confined to individual quartz grains and do not transect grain boundaries. This mode of occurrence indicates that the fluid inclusions may be primary and/or pseudosecondary in origin in respect to vein quartz and carbonate. In the samples of the waning stage, inclusions of Type I and II occur together in same clusters, but in the samples from breccia these two types seem to occupy somewhat different parts of thin sections. Samples taken from the late stage veins do not include inclusions of Type II and inclusions of Type I are rare.

All the samples studied contain aqueous inclusions of Type IIIB with or without a small cube of halite. In addition to small vapour bubble and halite crystal, isotropic or anisotropic daughter minerals were observed in many inclusions. Type III inclusions commonly are irregular in shape and are larger in size than the CO_2-rich inclusions. These inclusions usually form intergranular trails or they occur as dense disseminations throughout the host quartz grains. This kind of mode of occurrence indicates that the inclusions are secondary in origin in respect to vein minerals and that the fluids they represent were the latest trapped fluid phases.

Especially in the late stage intersecting quartz veins, an early generation of Type III inclusions is observed (Type IIIA) together with the late phase (Type IIIB) described above. Type IIIA is rare in other quartz veins or breccias. The Type IIIA inclusions are more regular in shape and they occur as sparsely populated short trails and small clusters in clear quartz close to sulphides or in quartz grains surrounded by sulphides. These inclusions rarely have halite as daughter mineral. Their mode of occurrence suggests that they are primary and/or pseudosecondary in origin.

Microthermometry

Some of the microthermometric data of fluid inclusions from Hirvilavanmaa are listed in Table 2. The measurements show that inclusions of Type I and II represent H_2O-CO_2-salt fluids with varying H_2O/CO_2 ratios. In the inclusions of Type III, a vapour bubble commonly shows clear expanding upon freezing suggesting the existence of compressible gases. Also, during the freezing-heating runs after the disappearance of ice, a mush composing of tiny crystals was often observed in Type III inclusions. With continued heating, this crystal mush slowly melted with the last grains usually disappearing between 12.0-25.0°C. The melting of crystals well above 0°C could be ascribed to the existence of gases in aqueous inclusions causing gas hydrates to appear. These observations imply that the vapour bubble is not water but consists of low-density CO_2 (or some other gases) and that inclusions of Type III actually are CO_2-bearing H_2O-(CO_2)-salt fluids as designated in Table 2.

The temperature of melting of CO_2 (T_mCO_2) in Type I and II inclusions varies from -56.4ºC to a maximum of -59.7ºC. The depression of melting points below the triple point of pure CO_2 (-56.6ºC) indicates the presence of other compressible gases than just CO_2. This is also supported by the observation of the above-described melting of crystal mush in some inclusions of Type I (up to 26.1°C). These high values in inclusions of Type I cannot be explained by melting of CO_2 or even CH_4 gas hydrates. The presence of H_2S in the gas phase together with CO_2 could cause the observed high values of melting of gas hydrate (Touray and Guilhaumou, 1984).

The salinities of fluid inclusions show a wide variation from 9 to 22 equivalent weight percent NaCl, and there seems to exist a rough correlation between the temperatures of homogenization of inclusions (T_h(L-V)) and the salinity (Fig. 8). The T_h(L-V)-salinity plot shows a decrease in temperature with an increase in salinity. Upon warming after complete freezing of inclusions, the first melting (T_mInitial) takes place in the range of -45.2 – -27.3ºC . The low temperatures of the first melting (below the eutectic point of the H_2O-NaCl system) indicates the presence of some other dissolved constituents besides NaCl such as Ca-, Mg-, Fe- or K-chlorides (Roedder, 1984). Thus, the salinities in Table 2 should be considered as maximum values, because the other dissolved salts result in an overestimation of the actual total salinities when they are expressed as equivalent weight percent

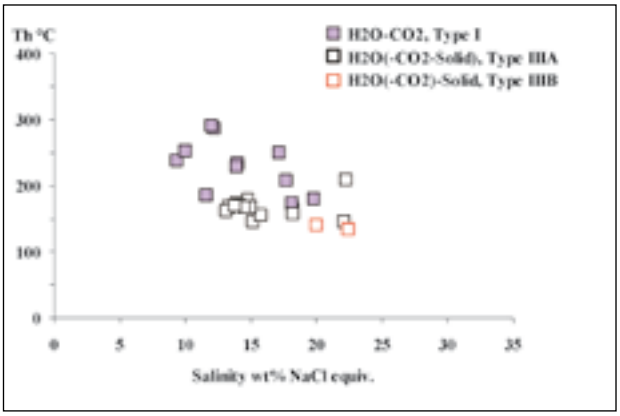

Fig. 8. Temperature of homogenization (Th(L–V) ºC) versus salinity for the Type I and III fluid inclusions.

NaCl. The spread in the T_mInitial values may indicate that the salt composition of fluids varied during the fluid entrapment.

The T_h(L-V) values of Type I and III inclusions occur over a wide interval from 92ºC to 369ºC whereas Type II only show a minor variation in the measured T_h(L-V) values (246–319ºC). The distribution in a histogram of T_h(L-V) (Fig. 9) shows five discrete populations of inclusions. These populations probably correspond to five different generations or phases of fluid. There seems to be a rough declining in the amount of CO_2 in inclusions when the oldest assumed fluid phases are compared to the youngest.

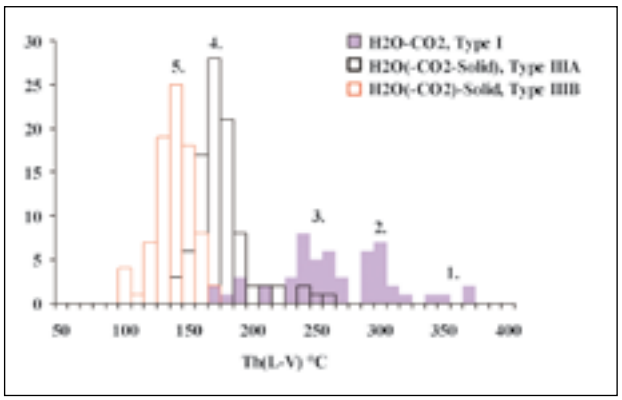

Fig. 9. Histogram of homogenization temperatures of Type I and III inclusions. The different generations of fluid phases are numbered from 1 to 5.

Relationship between fluid inclusions and mineralization

As described earlier, gold occurs in fractures of vein quartz and carbonate and is intimately associated with sulphides. This is consistent with the primary-pseudosecondary nature of the CO_2-bearing inclusions and supports the interpretation that Type I–IIIA inclusions are related to the gold mineralization. Additional support for this comes from the observation that CO_2-bearing inclusions in some cases contain opaque (sulphide?) and carbonate grains. Thus, it is believed that there is a temporal coincidence between sulphides, quartz, carbonate and gold precipitation and entrapment of Type I–IIIA inclusions.

The oldest population of inclusions observed (only present in quartz breccia) are those Type I inclusions which usually occur as isolated individual inclusions and have Th(L–V) values of 347–369ºC (Table 2, phase 1 in Fig. 9). This fluid phase is probably closely related to the beginning of brecciation and gold precipitation. Similar style of occurrence of Type II and some Type I inclusions, as well as their spatial proximity with each other suggest that Type II and some of Type I inclusions are contemporaneous. The Th(L–V) values of Type II (246–319ºC) coincide with the Th(L–V) values of fluid phases 2 and 3 presented in Figure 9. These fluid phases probably represent the main and waning phases of mineralization. Type IIIA inclusions are mostly encountered in late stage veins as primary or pseudosecondary inclusions. The intersecting nature of the young veins indicates that fluid represented by Type IIIA inclusions (phase 4 in Fig. 9) is the youngest phase, which can be directly connected to the vein formation and gold precipitation. However, there does not necessarily exist a large time gap between the fluid phases 4 and 3.

Type IIIB inclusions form a problematic group in respect to the gold mineralization. Their low Th(L–V) values (phase 5 in Fig. 9), secondary nature and the common irregular shapes point to late fluids. However, the compositional similarity of Type IIIB inclusions with Type IIIA suggest that they are in some way related to the gold mineralization. If this is the case, the Type IIIB inclusions represent the latest phase of evolving fluids, trapped during conditions of decreasing temperature and increasing salinity.

Possible mechanisms of ore deposition

Chemical changes due to the hydrothermal alteration involve interaction between wall rocks and hydrothermal fluids. We argue that the wall rock alteration was not the main cause of gold precipitation at Hirvilavanmaa because the most intense alteration predates fracturing and ore deposition. However, gold is not completely vein-hosted and interaction between wall rock and fluid (sulphidation of wallrock Fe) cannot be completely excluded as a cause of gold precipitation. A decrease in temperature cannot alone be responsible for ore deposition, as the vein and wall rock assemblages do not suggest any significant temperature variations. Chemical changes due to fluid mixing are not supported by fluid inclusions studies as a depositional process. Phase separation (unmixing) is one of the most effective ore depositional mechanisms (e.g. Drummond and Ohmoto, 1985). It has significant effects on the chemistry of a hydrothermal fluid. Phase separation

and interaction between wall rock and hydrothermal fluid are regarded as the most likely mechanisms causing the gold deposition at Hirvilavanmaa. This conclusion is supported by the fluid inclusion study as discussed below.

The observed changes in fluid salinity and overall decrease in the amount of CO_2 in inclusions over time could be explained by either phase separation or interaction between wall rock and fluid. In phase separation, a fluid will unmix to form two fluid phases, in which one is of high density and liquid-like and another of low density and gas-like. If phase separation was induced by sudden pressure drop from lithostatic to partly hydrostatic, unmixing would be appreciable leaving the residual liquid-like fluid much more saline than it would be after slow cooling. In a tectonically active environment, fluid pressure probably varies in response to deformation, fracturing and opening-sealing of the vein systems (e.g. Sibson, 1988). Such pressure fluctuations could drive fluids towards more saline by "pumping" gases out of the system over time. However, if unmixing took place at Hirvilavanmaa there should exist two different, contemporaneous, fluid phases (a liquid- and a gas-rich) with overlapping values of Th(L–V). According to the fluid inclusion investigations, Type II inclusions and some phases of Type I fulfill this criterion. Therefore, the phase separation was a possible depositional mechamism at Hirvilavanmaa during the gold mineralization.

Fluids represented by Type III inclusions are clearly associated with the gold mineralization but their origin cannot be explained by the above-described simple unmixing event. There is no contemporaneous gas-rich phase with Type III inclusions and their values of Th(L–V) are quite low, usually much less than 190ºC (Fig. 9). Also, some inclusions (especially Type IIIB inclusions) contain salt grains as daughter minerals that dissolve above the values of Th(L–V) of inclusions and, thus, they can not be the true phase of an unmixing fluid (Ramboz et al, 1982). However, if the fluid system was open enough for fluid movement, these fluids and the associated gas-rich phase could have escaped and taken a different path from the site of unmixing before trapping in vein minerals. This is supported by the overall scarcity of Type II inclusion in the studied samples. Due to its lower density and different wetting properties, the gas-rich phase of an unmixing fluid could most readily escape trapping by the same vein minerals which trapped a liquid-rich phase, if the system is open and free for fluids to flow. These escaping or migrating fluid phases could have reacted with varying extent with the host rock causing, for example, the intense late carbonatization discussed above in the section about alteration.

P–T conditions of fluids entrapment

The temperature, composition and density data obtained from the fluid inclusion study are presented in a P–T diagram in Figure 10. The Th(L–V) values of Type II inclusions, coinciding with phases 2 and 3 in Figure 9, are considered to represent true trapping temperatures due to unmixing. Type III inclusions and those Type I inclusions which have low Th(L–V) values represent evolved fluids and, thus, their Th(L–V) values can not be considered as true trapping temperatures without a pressure correction. These considerations have been taken into account in the following interpretation.

The oldest observed primary inclusions in quartz breccia samples (phase 1 in Fig. 9) were probably trapped very close to their solvus. Anyhow, the point where isochore meets the surface of the solvus gives the minimum P–T conditions for the beginning of the main fracturing event (the small box in Fig. 10). According to the fluid inclusion data, there was a major drop in pressure associated with only a minor drop in temperature, which induced the unmixing of the H_2O-CO_2-salt fluid. After the main opening of the fracture zone the pressure probably fluctuated due to deformation, fracturing and opening-sealing of the vein systems producing the fluid phases 2–3 and partly 4. At the late stage of mineralization and alteration, the late fluid phases migrated through the system reacting with the host rocks and causing the late carbonatization.

The minimum conditions for the start of opening of the fracture system are 330–370ºC and about 3000 bars. After the major drop in pressure, mineralization took place at 220–310ºC with pressure fluctuating between 1000–2200 bars (the large box in Fig. 10).

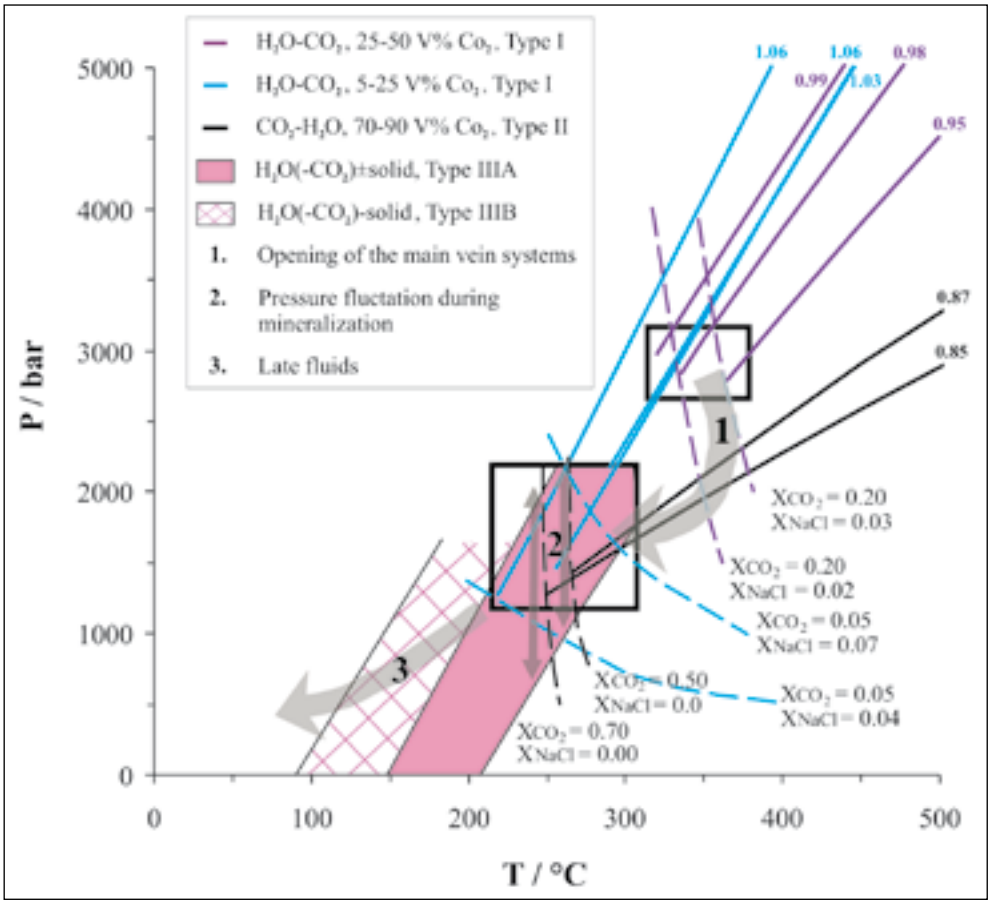

Fig. 10. P–T diagram showing sets of isochores and solvus curves for the fluid types of the Hirvilavanmaa deposit. The numbers above isochores refer to fluid densities in g/cm^3. The isochores were calculated using the program Flincor (Brown, 1989). The numbers besides solvus curves refer to fluid composition expressed as mole fractions, all possible solvus curves are not drawn. Solvus data is inter- and extrapolated after Bowers and Helgeson (1983).

DISCUSSION AND CONCLUSIONS

The general sequence of mineralogical alteration suggests that the hydrothermal events seen at Hirvilavanmaa were superimposed on the metamorphic mineral assemblage. The hydration and albitization events took place in an area larger than just the gold-mineralized localities. At this early state, the Sirkka Shear Zone may have been the main control on the fluid flow.

The more localized alteration is associated with a N–S trending deformation zone. Fracturing was controlled by the competency differences between lithological units caused by the original heterogeneity in the host rock types and further modified by the earlier hydration-albitization events. After fracturing, gold-bearing fluids flowing along fractures infiltrated into the wall rocks causing pyritization and hematization of the host rock and quartz, carbonate, sulphides, tourmaline and minor albite and gold deposition to form the quartz-dominated breccias and veins.

The late carbonatization was superimposed on the previously altered rocks. However, the late carbonatization, probably accompanying the late stage of the mineralizing event, is necessarily not restricted to the gold-mineralized parts of the area. It may be more extensive and could possibly be controlled by the Sirkka Shear Zone. However, this has not been possible to verify due to lack of outcrops in the area.

In spite of pervasive alteration, the komatiitic nature of the host rock is still obvious. By comparing the mobile element-Al_2O_3 ratios, it was possible to identify three chemically different zones: distal zone, proximal outer zone and proximal inner zone. Typical to the distal zone are very low contents of CO_2, Na_2O and S. Copper, CO_2 and Na_2O are enriched in the proximal outer zone. Elevated levels of CO2, Cl, S, Na2O and Au define the most altered, proximal inner alteration zone.

At Hirvilavanmaa, phase separation and interaction between wall rock and hydrothermal fluid were the major causes of mineralization. The circulating H_2O-CO_2-salt fluid with a high CO_2 content demands high pressures to maintain CO_2 in solution. Abrupt pres-

sure drop from about 3000 bars (and 330–370ºC) to or close to the hydrostatic pressure, due to fracturing of host rocks, induced unmixing of the fluid. Phase separation caused perturbation on the chemistry of the fluid and led to the gold deposition in the temperature range of 220–310ºC. After the main opening of the fracture zone, the pressure fluctuated between 1000–2200 bars due to fracturing and opening-sealing of the vein systems causing further unmixing and "pumping" gases out of the system. Due to density differences, the different fluid phases produced by unmixing migrated through the system and reacted with varying extent with the host rock resulting in alteration presently visible at Hirvilavanmaa.

The Hirvilavanmaa gold deposit is a typical lode-type synorogenic, post-peak metamorphic mineralization formed late in the structural history of the Central Lapland Greenstone Belt. Its geometry indicates a large scale hydrothermal fluid advection to a suitable structural trap along a well-defined channelway in the Sirkka Shear Zone in the upper crust.

ACKNOWLEDGEMENTS

Our warmest thanks are expressed to Dr. Pasi Eilu and Dr. Matti Poutiainen for helpful and critical reviews of the manuscript. MSc. Marja Lehtonen did microanalytic laboratory photos in GTK, Espoo Unit. Lars Rämö in the Department of Geology of the University of Helsinki prepared excellent polished sections for fluid inclusions study. Financial support for fluid inclusion study from the Outokumpu Foundation during the years of 1990–1993 is gratefully acknowledged.

REFERENCES

Bowers, T.S. & Helgeson, H.C. 1983. Calculation of the thermodynamic and geochemical consequences of nonideal mixing in the system H_2O–CO_2-NaCl on phase relations in geologic systems: Metamorphic equilibria at high pressures and temperatures. American Mineralogist 68, 1059–1075.

Brown, P. E. 1989. A microcomputer program for the reduction and investigation of fluid inclusions data. American Mineralogist 74, 1390–1393.

Drummond, S.E. & Ohmoto, H. 1985. Chemical evolution and mineral deposition in boiling hydrothermal systems. Economic Geology 80, 126–147.

Hulkki, H. 1990. Sodankylän Sattasvaaran komatiittikompleksin Au-kriittinen muuttumisvyöhyke. Unpublished MSc thesis. University of Helsinki, Department of Geology and Mineralogy. 190 p. (in Finnish).

Härkönen, I. & Keinänen, V. 1989. Exploration of structurally controlled gold deposits in the Central Lapland greenstone belt. In: Autio, S. (ed.) Geological Survey of Finland, Current Research 1988. Geological Survey of Finland, Special Paper 10, 79–82.

Jensen, L. S. 1976. A new cation plot for classifying subalkalic volcanic rocks. Ontario Division of Mines, Miscellaneous Paper 66, 22 p.

Johansson, P., Keinänen, V. & Lehmuspelto, P. 1986. Geochemical exploration of tungsten in glaciogenic deposits in Soretiapulju, western Finnish Lapland. In: Prospecting in Areas of Glaciated Terrain 1986: papers presented at the seventh international symposium organized by The Institution of Mining and Metallurgy and The Geological Survey of Finland, Kuopio, 1–2 September, 1986. London: The Institution of Mining and Metallurgy, 61–67.

Keinänen, V. 1987. Vein-type gold occurrence in Soretiavuoma carbonate rocks, Finnish Lapland. In: Gold '87: Program and Abstracts, Turku, Finland, May 12–13, 1987. Turun yliopiston geologian ja mineralaogian osaston julkaisuja, Opintomoniste 19, p. 8.

Keinänen, V. 1994. Shear zone-related Soretialehto gold occurrence in green carbonate rocks in the Central Lapland Greenstone Belt, Kittilä, Finnish Lapland. In: Perdahl, J.-A. (ed.) 21:a Nordiska Geologiska vintermötet 10–13 January 1994 Luleå : Abstracts of lectures and posters. Luleå: Tekniska högskolan i Luleå, p. 99.

Keinänen, V. & Holma, M. 2001. Levijärvi and Soretialehto – two epigenetic lode-gold deposits controlled by Sirkka Thrust Zone within Paleoproterozoic Central Lapland Greenstone Belt, Kittilä, northern Finland. In: Williams, P. J. (ed.) 2001 : A Hydrothermal Odyssey : new developments in metalliferous hydrothermal systems research : extended conference abstracts, May 17–19th, 2001, Townsville, Queensland, Australia. EGRU Contribution 59, 102–103.

Keinänen, V. & Hulkki, H. 1992. Main features of the three geochemically different gold mineralizations in Soretiavuoma, Finnish Lapland. In: Geirsdottir, A., Norddahl, H. & Helgadottir, G. (eds.) 20th Nordic Geological Winter Meeting, 7–10 January, Reykjavik 1992: abstracts. Reykjavik: University of Iceland. p. 96.

Keinänen, V., Johansson, P. & Lehmuspelto, P. 1988. Soretiavuoman volframi- ja kultatutkimuksista. In: V. Lappalainen and H. Papunen (eds.), Tutkimuksia geologian alalta. University of Turku, Annales Universitatis Turkuensis C 67, 69–77. (in Finnish).

Lamberg, P. & Hautala, P. 1990. Kittilän kultaesiintymien kemialliset ja petrologiset tutkimukset. Raportti, Outokumpu Mining Services, Geoanalyyttinen laboratorio, 28–38. (in Finnish).

MacLean, W. H. & Kranidiotis, P. 1987. Immobile elements as monitors of mass transfer in hydrothermal alteration: Phelps Dodge massive sulphide deposit, Mattagami, Quebec. Economic Geology 82, 951–962.

Potter, R. W., Clynne, M. A. & Brown, D. L. 1978. Freezing point depression of aqueous sodium chloride solutions. Economic Geology 73, 284–285.

Ramboz, C. Pichavant, M. & Weisbrod, A. 1982. Fluid immiscibility in natural processes: Use and misuse of fluid inclusion data: II. Interpretation of fluid inclusion data in terms of immiscibility. Chemical Geology 37, 29–48.

Roedder, E. 1984. Fluid inclusions. Reviews in Mineralogy 12, Mineralogical Society of America. 644 p.

Scan Mining 2002. Press release 9 September 2002.

Shepherd, T. J., Rankin, A. H. & Alderton, D. H. M. 1985. A practical guide to fluid inclusion studies. Glasgow: Blackie. 239 p.

Sibson, R. H. 1988. High-angle reverse faults, fluid-pressure cycling and mesothermal gold-quartz deposits. Geology 16, 551–555.

Sterner, S. M. & Bodnar, R. J. 1984. Synthetic fluid inclusions in natural quartz. I. Compositional types synthesized and applications to experimental geochemistry. Geochimica et Cosmochimica Acta 48, 2659–2668.

Touray, J. C. & Guilhaumou, N. 1984. Characterization of H_2S bearing fluid inclusions. Bulletin de Mineralogie 107, 181–188.

Viljoen, M. J. & Viljoen, R. P. 1969. The geology and geochemistry of the lower ultramafic unit of the Onverwacht Group and a proposed new glass of igneous rocks. Geological Society of South Africa, Special Publication 2, 55–86.

Viljoen, M. J., Viljoen, R. P. & Pearton, T. N. 1982. The nature and distribution of Archean komatiite volcanics in South Africa. In: Arndt. N. T. & Nisbet, E. G. (eds.) Komatiites. London: Allen & Unwin, 53–79.

Gold in the Central Lapland Greenstone Belt, Finland
V. Juhani Ojala (ed.)
Geological Survey of Finland, Special Paper 44, 155–162, 2007.

EXPLORATION HISTORY OF THE KAARESSELKÄ GOLD- COPPER OCCURRENCE, CENTRAL LAPLAND

by
Helena Hulkki and Eelis Pulkkinen

Hulkki, H. Pulkkinen, E. 2007. Exploration history of the Kaaresselkä gold-copper occurrence, Central Lapland. *Geological Survey of Finland, Special Paper 44*, 155–164, 7 figures

The Kaaresselkä Au-Cu occurrence was discovered during a Pb-Zn-Cu exploration program in 1978–1979. Assayed iron-carbonate bearing schists and pyrite-impregnated albite rocks showed anomalous gold values (50–300 ppb Au). Regional geochemical mapping of till was completed in Central Lapland in 1987 and in the Kaaresselkä area the results showed two gold-anomalous sites (11–12 ppb Au) and led to a detailed till sampling program on a 50 m x 50 m grid over the anomalous area. The results showed more than 50 sampling sites where gold concentration in till exceeds 13 ppb. Investigations of the anomalous sites lead to discovery of several gold and copper showings. The gold mineralization in the area is epigenetic and related to the shear zones at the contacts between different rock types and associated with carbonatization, sericitization, sulphidization and adularization. The mineralized shears are 4–16 m wide and form about one kilometre long zone with gold grades 1–10 g/t. The highest concentrations of gold occur in sulphide-carbonate breccias and veins as well as in chalcopyrite-quartz and pyrite-quartz veins. Because of the several assay methods used in sample preparation and analysis as well as up to 80% core loss during drilling, no reliable resource estimates could be calculated for the occurrences. Only a rough volume estimation of 160 000 m^3 of gold-rich rock can be given.

Key words (GeoRef Thesaurus AGI): shear zones, mineral exploration, geochemical methods, till, geophysical methods, Paleoproterozoic, Kaaresselkä, Lapland Province, Finland

Geological Survey of Finland
P.O. Box 77, FI-96101 Rovaniemi, Finland

E-mail: helena.hulkki@gtk.fi, eelis.pulkkinen@gtk.fi

INTRODUCTION

The Kaaresselkä gold-copper occurrence is located in Northern Finland, 20 km NW of Sodankylä (Fig. 1). The first reported gold mineralization in the Sodankylä area is at Kaarestunturi (Härkönen 1984), just to the north of Kaaresselkä (Fig. 1). The gold exploration program of the Geological Survey of Finland (GTK) in Kaaresselkä area was a continuation of a zinc and lead exploration program in 1970's which resulting in a discovery of three low-grade Pb-Zn-Cu occurrences (Härkönen 1980, Karvinen 1997). The first indications of gold mineralization in the bedrock at Kaaresselkä were detected by GTK in 1984 when assays of iron-carbonate-rich schist and pyritic albite-rock samples returned gold values up to 300 ppb.

Regional geochemical mapping of till was completed in Central Lapland in 1987 and the results

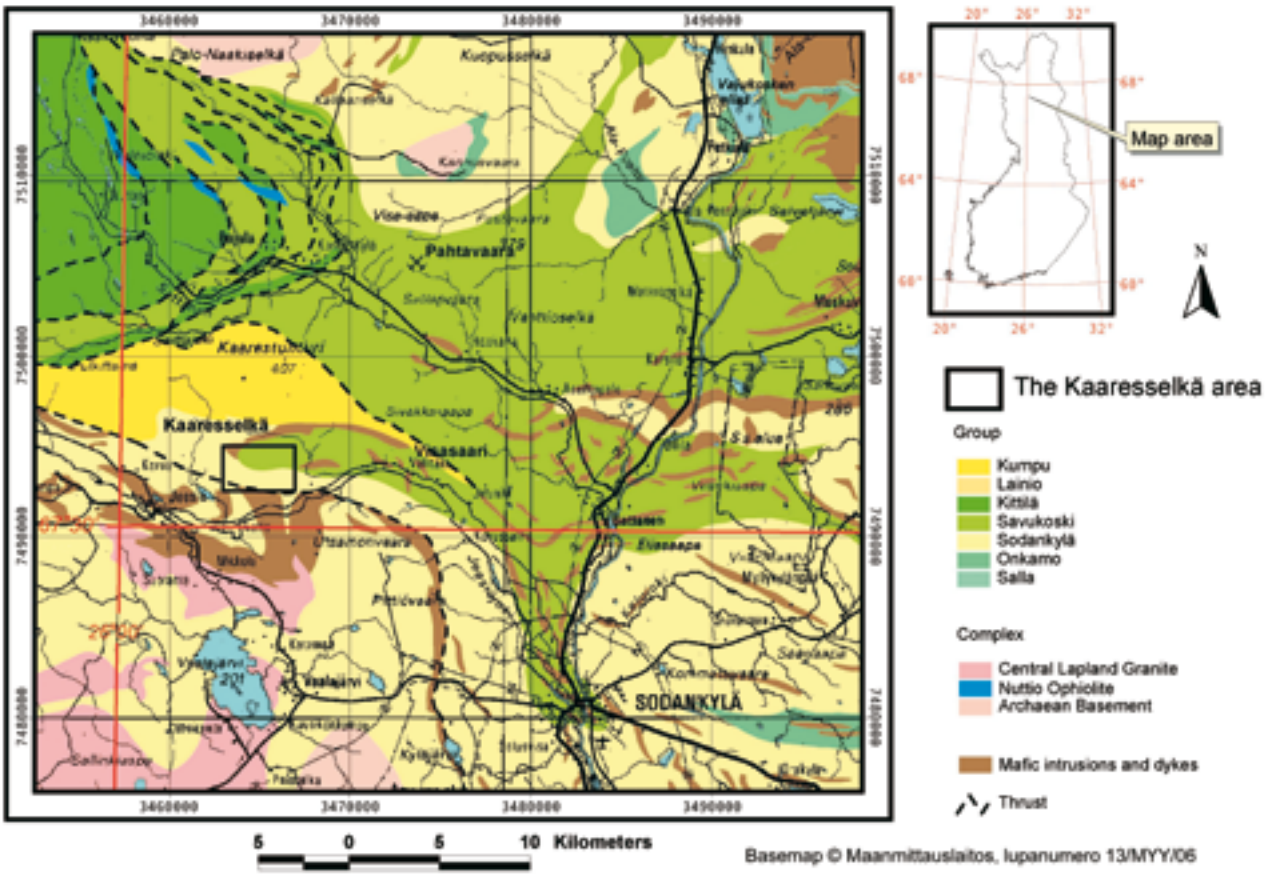

Fig. 1. Location of the Kaaresselkä prospect area and the Pahtavaara mine on the geological map by Lehtonen et al. (1998). The Sirkka Shear Zone passes through the southern part of the Kaaresselkä area. Basemap © National Land Survey 521/MYY/07

showed two gold-anomalous sites (11–12 ppb Au) in the Kaaresselkä area. This encouraged continuing exploration in the area. Consequently, a till sampling programme on a 50 m x 50 m grid was completed during the winter of 1988–89 and revealed that almost the entire Kaaresselkä exploration area is anomalous in gold. However, exploration proceeded slowly until Terra Mining Company received an exploration licence for the Pahtavaara prospect in 1991 and started gold mining in 1995, only about 15 km NE from Kaaresselkä (Korkiakoski and Kilpelä 1997). This encouraged GTK to revitalize the exploration program in the Kaaresselkä area during the 1990's.

The first six holes at Kaaresselkä intersected high-grade gold mineralization (13-16 ppm) at depths of 44 – 47 m (Pulkkinen 1998). During 1994–1998, additional drilling programs were to test anomalies based on the ground geophysical and geochemical till surveys. In all three showings (Vanha, Tienvarsi and Lampi) and five targets (Jänkä, Kumpu, Rakka, Rinne and Crossing) several targets were drilled (Fig. 2 and 7). The mineralized zones at Vanha and Tienvarsi have a combined length of approximately one kilometre and a width of 10–16 m and contain, at least, 160 000 m3 of rock with gold grades 1 – 10 g/t (Pulkkinen and Hulkki 1999).

GEOLOGICAL SETTING

The Kaaresselkä prospect (Fig. 1) is situated in a volcano-metasedimentary sequence of the Sodankylä Group of the Central Lapland Greenstone Belt, about four km north of the Central Lapland granite complex and close to the WNW-trending Sirkka Shear Zone (Lehtonen et al. 1998). The Kaarestunturi quartzite-conglomerates of the Kumpu Group lie discordantly on the Sodankylä Group rocks three km north of Kaaresselkä (Räsänen 1977). Locally, the study area is associated with the so-called "Jeesiöjoki domain"

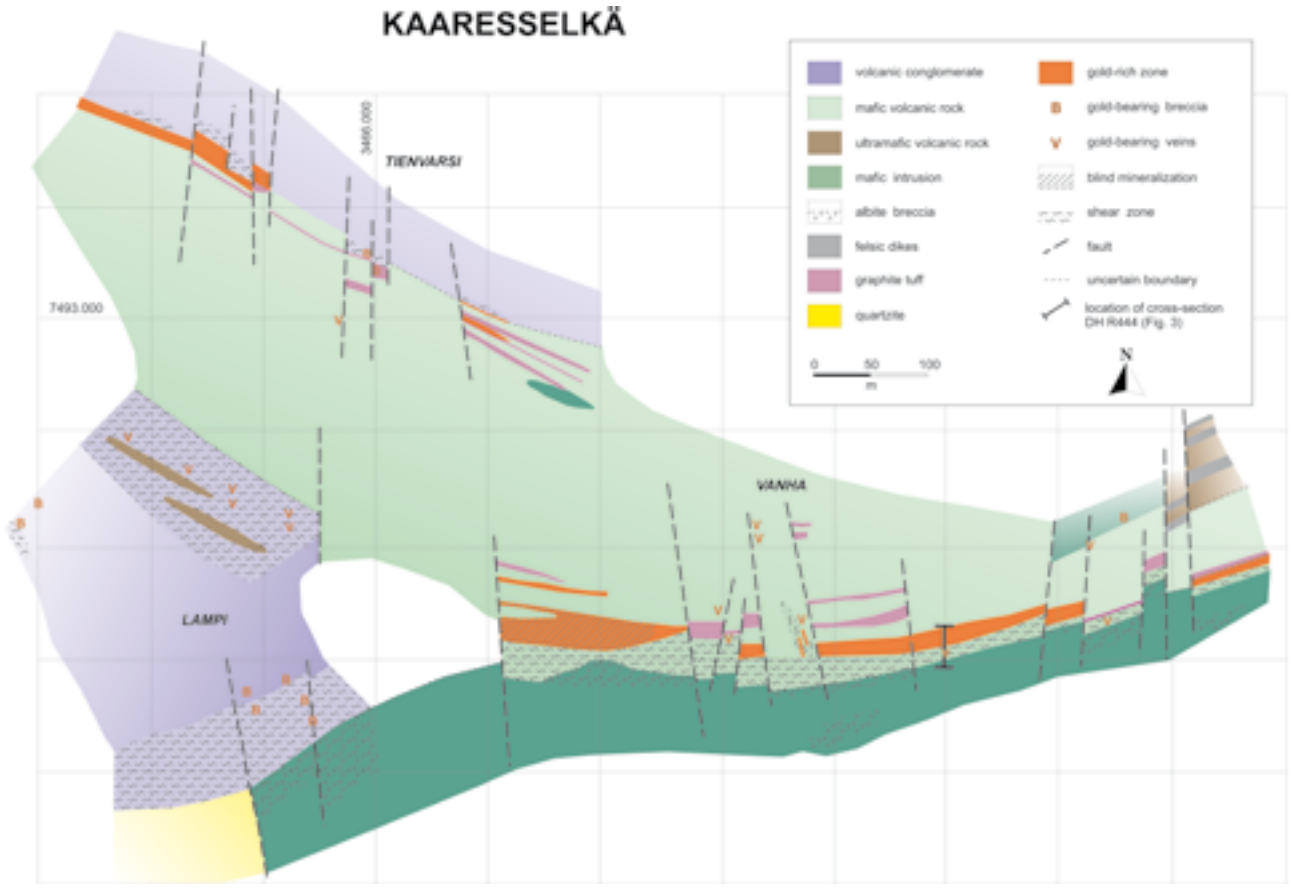

Fig. 2. Geological setting of the Vanha, Tienvarsi and Lampi prospects in the SE part of the Kaaresselkä area and the location of DH R444 (Pulkkinen and Hulkki 1999).

where dolerites and gabbros intrude the supracrustal rocks. Mafic and intermediate volcanic rocks cover the northern part (Härkönen 1980) and volcanic conglomerate is dominant in the southern part of the Kaaresselkä area. Ultramafic volcanic rocks and quartzites occur on the southern and the northern side of the study area. The only exposed rock types of the study area are quartzites with the exception of a few sites in steep-sloped terrain where volcanic conglomerate crops out.

The gold-copper deposits of Kaaresselkä are associated with layer-parallel ENE- and WNW- trending brittle-ductile shear zones. North-South trending faults cut the mineralized shear zones. The Vanha and Lampi prospects are in a broadly E-W trending shear zone, which follows the northern margin of a mafic intrusion (Fig. 2). The Tienvarsi prospect is hosted in a WNW-trending shear zone, which has developed in a contact zone between intermediate tuff and volcanic conglomerate (Fig. 2).

GLACIAL DEPOSITS IN THE AREA

The thickness of the till cover in the Kaaresselkä area is 1–4 m on hilly terrain, but mostly 4–10 m on flat, swampy areas. Glacial transport distances in Central Lapland are short (Härkönen and Pulkkinen 1991). The transport distance is remarkably short in the areas of thin glacial drift where the till cover formed mainly during the latest glaciation. An example of this short transport distance has been reported from Visasaari, which is located 10 km east of Kaaresselkä (Pulkkinen et al. 1980). In this location, the average transport distance, which was estimated from the geochemical anomalies of magnesium, chromium and nickel in the topmost till, is 270 m from a 0.5 km wide ultramafic unit in the source area.

GEOCHEMICAL METHODS

The 10 km2 study area is mostly till covered and was sampled on a 50 m x 50 m grid, which resulted as a total of 4080 samples. The samples were sieved using a nylon screen. One gram of the silt and clay fraction (<0.06 mm) was analyzed for gold after hot aqua regia dissolution by GAAS (AAS graphite furnace atomisation; Kontas 1981). Initially, the concentrations of Al, Fe, Mg, Ca, Na, Ti, V, Mn, Cr, Ni, Co, Cu, Pb, Zn and Ba were determined by the semiquantative OES-quantometer method (Danielsson and Sundkvist 1959, Gustavsson et al. 1979). Later, four samples from the corners of the grid were combined and the concentrations of these 1020 samples were assayed for Ag, Al, As, B, Ba, Ca, Cd, Co, Cr, Cu, Fe, K, La, Li, Mg, Mn, Mo, Na, Ni, P, Pb, S, Sb, Sc, Si, Sr, Th, Ti, V, Y and Zn by ICP-AES after hot aqua regia dissolution.

Diamond drill cores were logged in one-meter intervals and assayed by GAAS and ICP-AES. However, the analysing procedure included varying weights of subsample. For assaying the first six drill cores 5 g subsamples were used. As a mineralization was found a conventional drilling was applied and samples were assayed by GAAS using 20 g subsamples. In the final stage of exploration, samples of the gold-rich zone, and especially those, which contained graphite, were assayed by fire assay (FAAS) using 50 g subsamples. All analyses were carried out in the chemical laboratories of GTK.

GEOPHYSICAL METHODS

Electromagnetic (HLEM) and magnetic (Z-component) ground-geophysical measurements were completed over most of the study area during the lead-zinc exploration phase. In addition, electromagnetic VLF-R and magnetic (total field), induced polarisation (IP) and self potential (SP) methods were applied in areas of anomalous till geochemistry. Downhole geophysical measurements from 25 holes recorded magnetic, density, chargeability and radiation data.

RESULTS AND DISCUSSION

Geology of the gold-bearing zones

The **Vanha** prospect (Fig. 2) is controlled by a broadly E-W trending brittle-ductile shear zone. The shear zone has developed at the contact zone between mafic-intermediate volcanic rocks and mafic intrusion. This zone contains also some graphite tuffs and cherty-like quartz rocks (Fig. 3). Ultramafic tuffs, gabbro (mafic intrusion) and felsic dikes are present in the NE part of the target area. The gold mineralized zone is about 650 m long in the northern margin of the shear zone, but does not form a continuous lode because N-trending younger faults offset the mineralization (Fig. 2). However, there is a continuous, 200 m long and 9–16 m wide, section of gold-rich rock in the centre of the prospect.

The barren rocks in the shear zone are also sericite and albite altered whereas mineralized parts are rich in quartz, sericite, carbonate and pyrite. In addition, arsenopyrite, chalcopyrite, adularia and tourmaline are associated with the gold mineralization and define the proximal alteration zone.

The distal alteration zone in mafic-intermediate volcanic rocks is defined by albite and chlorite and pyrrhotite.

High gold values (proximal alteration) are related to altered rocks, which have at least one of the following features: (i) intense brecciation; (ii) intense pyritization and carbonation; or (iii) contain either graphite or adularia. Tiny gold grains (Ø 35–170 mm) have been found as small accumulations on the grain boundaries and fractures of pyrite, arsenopyrite, chalcopyrite and, especially, in carbonate gangue (Fig. 4). Gold visible to the naked eye (Ø 0.5–1.5 mm) has been detected in some drill cores.

The two best sections of drill core are a three metre wide zone containing 10–16 ppm Au in the western part and a six metre wide zone containing 5–6 ppm Au in the eastern part of the prospect. Based on these data, the estimated volume of gold-rich rock is, at least, 110 000 m3 when calculated to the depth of 55 m.

The gold mineralization in the **Tienvarsi** prospect is controlled by a WNW-trending shear zone, which follows the contact zone between volcanic conglom-

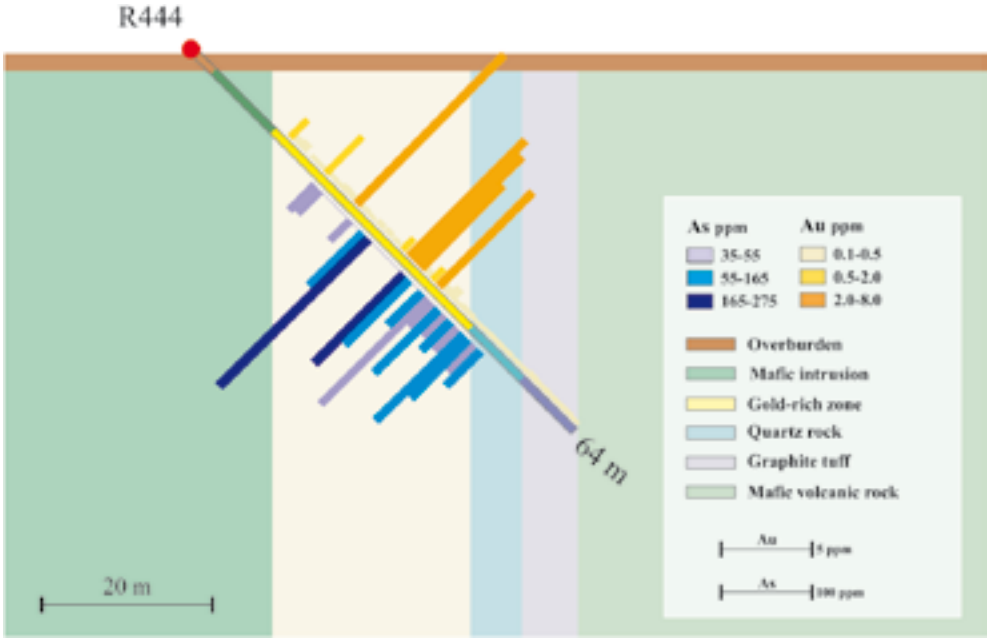

Fig. 3. A section across the Vanha prospect and its Au and As concentrations. See fig. 2 for the location of DH R444.

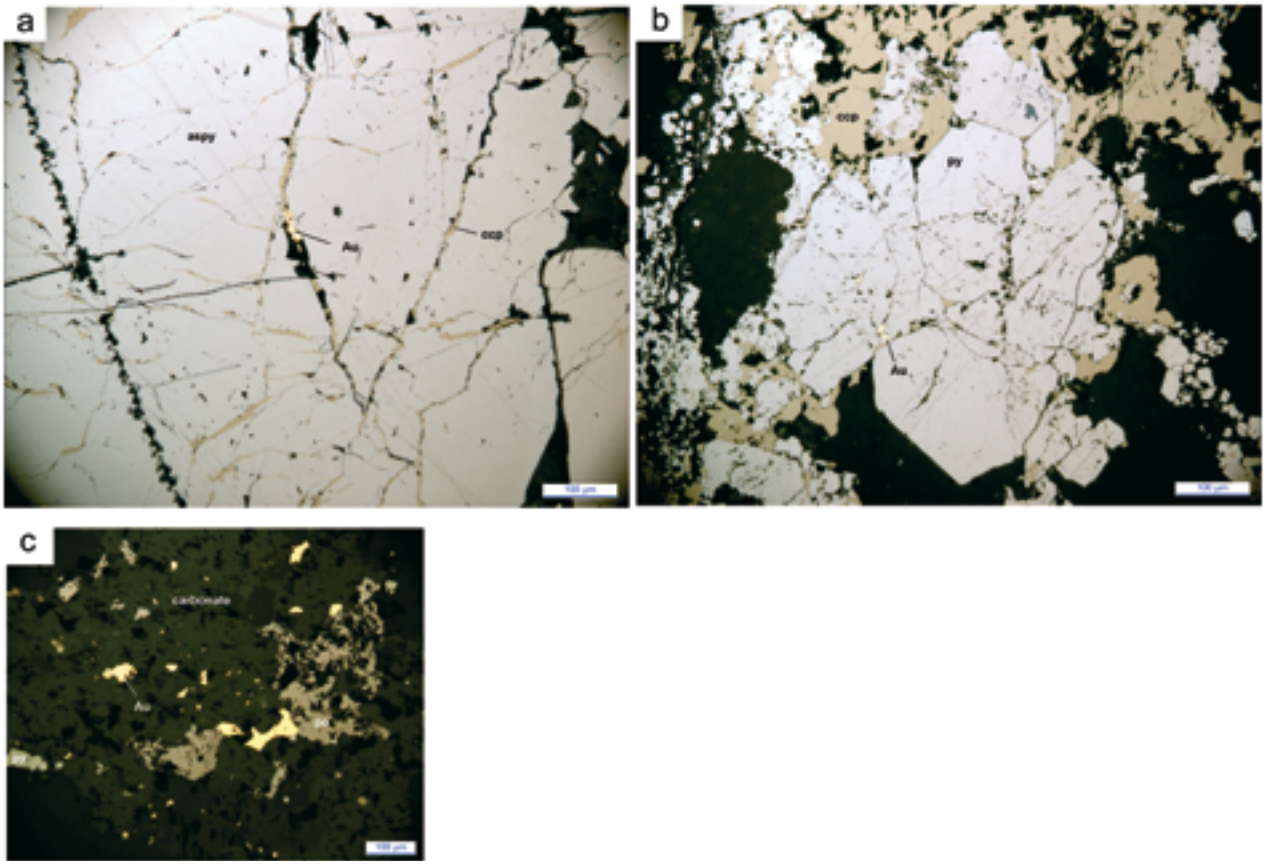

Fig. 4. Photomicrographs from the Vanha target at Kaaresselkä. A: chalcopyrite (ccp) and gold (Au) as fracture fillings in arsenopyrite (aspy) B: gold in the contact surfaces and fractures of pyrite (py) C: a small accumulation of gold grains in carbonate gangue (po; pyrrhotite). Reflected light. Photos by Helena Hulkki.

erate and mafic-intermediate tuffs (Fig. 2). Graphite tuffs are always present in the contact zone. The main mineralization is about 200 m long and 4–13 m wide. In addition, there is a separate lode of the same type about 200 m southeast from the main zone. Interpreted from the geophysical surveys and till geochemistry, this SE-lode may continue both to the NW and SE.

The mineralized parts of the shear zone are intensely carbonatized and have weathered almost completely to the 40 m depth. Gold is associated with graphite-bearing sulphide-carbonate breccias and veins. Microscopic gold grains occur in sulphide-carbonate-quartz veins and are associated with goethite. Reliable gold values and tonnages cannot be given due to intense weathering, which caused a core loss of 40–80 %. The volume of gold-rich rock is about 56 000 m3 when calculated to the depth of 40 m.

The gold mineralization in the **Lampi** prospect is controlled by an ENE-trending shear zone. The mineralization is hosted by a volcanic conglomerate unit which straddles along the northern contact of a mafic intrusion and quartzite unit (Fig. 2). The mineralization related alteration is subtle and it compose of gold rich patches in a sheared host rock. The alteration in the shear zone include albitization, chloritization, weak carbonatization, and sericitization. The best indication of gold-enrichment is the increasing amount of quartz and pyrite in the sheared rock. Quartz and very fine-grained pyrite form stringers with anomalous gold assays up to 6 ppm. Tiny gold grains have been found as small inclusions in pyrite.

In addition to above prospects, there are minor quartz-carbonate breccias and veins were located in the bedrock in other targets in the area. Samples from these targets returned gold values between 50–1430 ppb.

Geochemical results

The results of the till geochemical surveys show anomalous gold values over most of the Kaaresselkä area (Fig. 5a). The mean of the concentration of gold in till is 4.76 ppb and the 95th percentile is 13.7 ppb. There are more than 50 sampling sites where the concentration of gold exceeds 13 ppb (Fig. 5a). Copper, magnesium, chromium and nickel delineate a NW-trending zone across the area reflecting sulphide enrichments in ultramafic host rock (Fig. 5b). This zone coincides with the magnetic anomalies seen in the airborne and ground magnetic maps (Fig. 7).

Interpretation of the detailed till geochemistry results was based on the assumption that there are relatively coarse gold in till all over the Kaaresselkä area (Härkönen 1981, personal communication). This means that the sporadic, single-point, "only gold" anomalies should not be considered as important as those anomalies, which are associated with anomalies of pathfinder elements like copper and arsenic. This was verified during exploration. Alternatively, those areas where gold anomalies form consistent elongated patterns should also be considered significant.

Geochemical analyses of drill core suggest that As, Te, Cu, Zn, Pb, Mo and Ag are closely associated with gold (Fig. 3 and 6). However, a more detailed examination reveals that Cu, Te and As are only partly gold-affiliated: Cu and Te form a broad enrichment halo beside or around gold-enriched zones, whereas As is more closely associated with gold. Anomalously high Pb, Zn, Mo and Ag concentrations in gold-bearing zones are more or less associated with the graphite-rich rocks in the alteration zone.

The anomalous concentrations of Cu, Te and As, as well as in some extents also Pb, Zn, Mo and Ag, delineate the intensely altered rocks in the shear zone and do not define the exact location of the gold lodes. The Cu-Te anomalous zone typically is beside or overlaps with the gold-enriched zone. This may indicate that the Cu-Te-mineralization and Au-mineralization has taken place in different time interval or they form a distal alteration zone. This could explain why high gold concentrations occur also in sulphide-poor and apparently weakly altered rocks.

Gold values vary over a wide range. This may partly be due to the high core loss caused the strong weathering of altered rocks and partly to the varying methods used in sample preparation and analysis during the several years of exploration. This resulted in problems in estimating the tonnage of the deposit. Consequently, only the rough volume of the mineralized zones could be estimated.

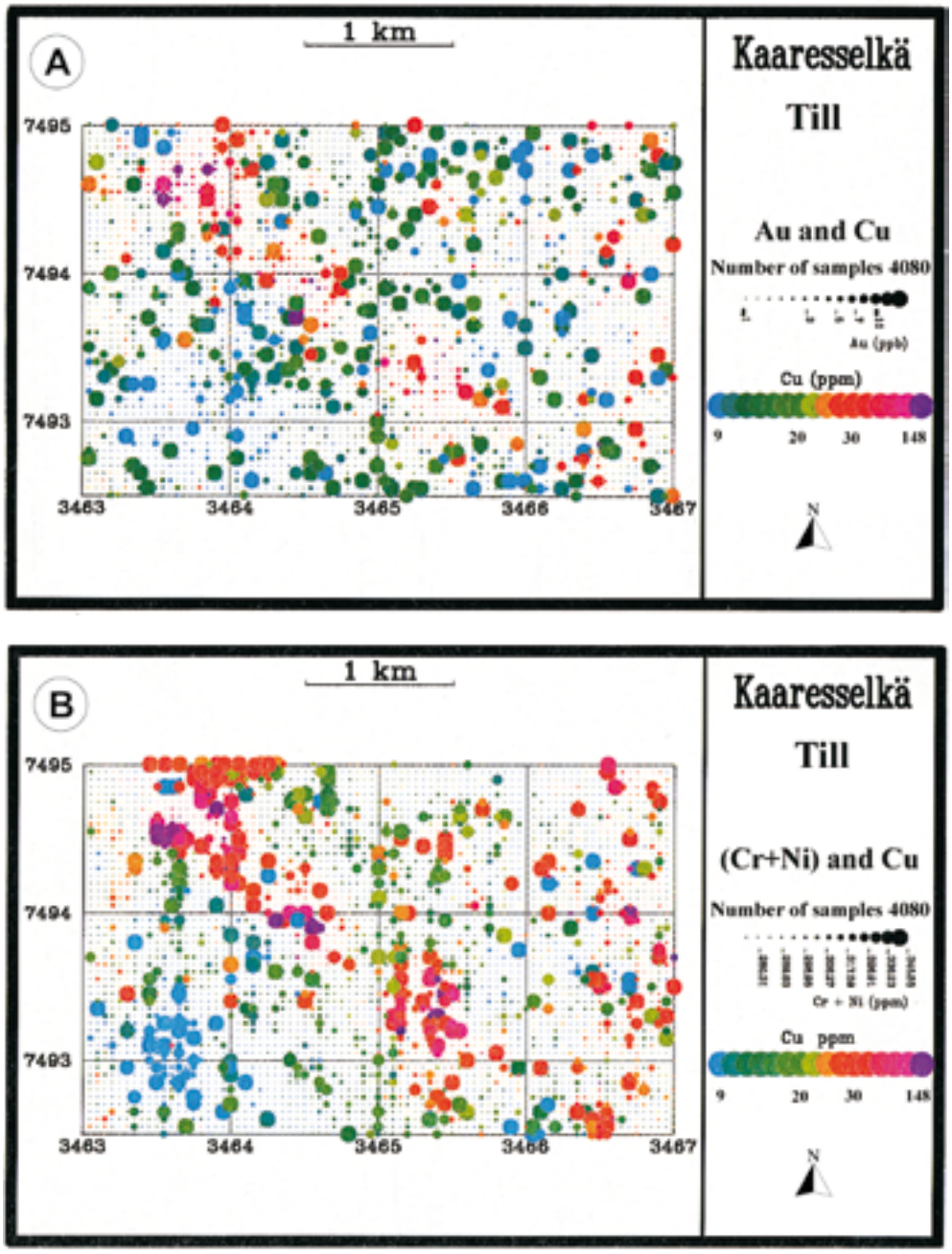

Fig. 5. Concentration of Au, Cu, Cr and Ni in till in the Kaaresselkä area. A: Geochemical map of Au and Cu in till in the Kaaresselkä area. Note the close association of gold and copper along the shear zones (compare to fig. 7) and the elongated forms of the gold anomalies. B: Geochemical map of Cr, Ni and Cu in till in the Kaaresselkä area. The size of the symbols refers to the combined concentration of chromium and nickel and the colour to the concentration of copper.

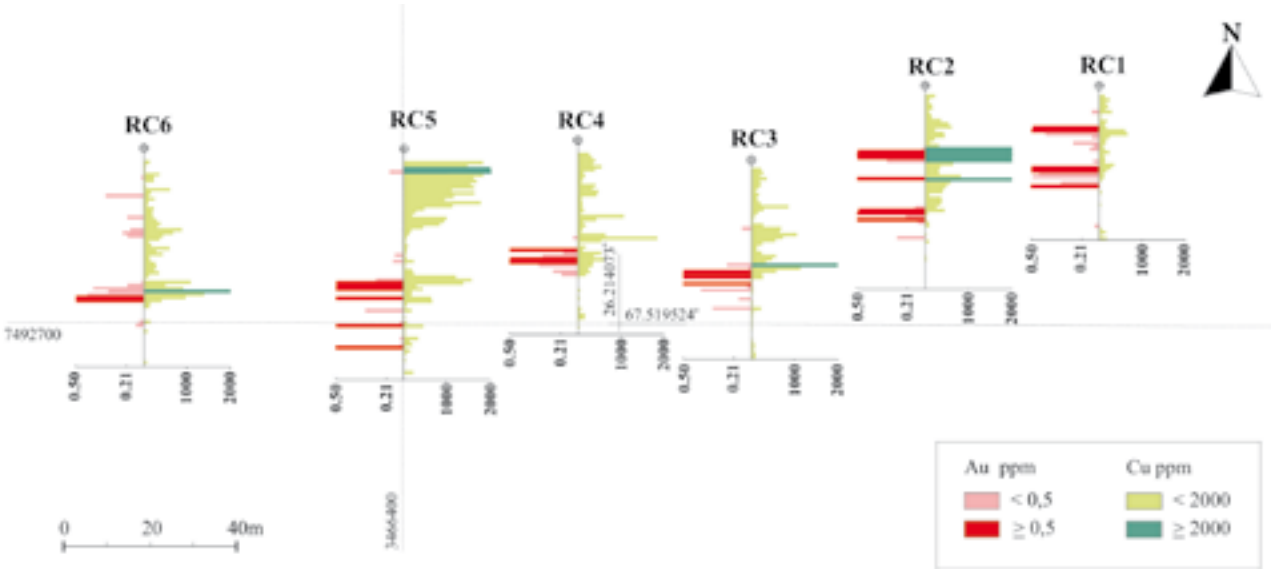

Fig. 6. Gold and copper concentrations of the drill holes RC1 – RC6 at Vanha. Note that the anomalous zones of copper and gold are only partially overlapping.

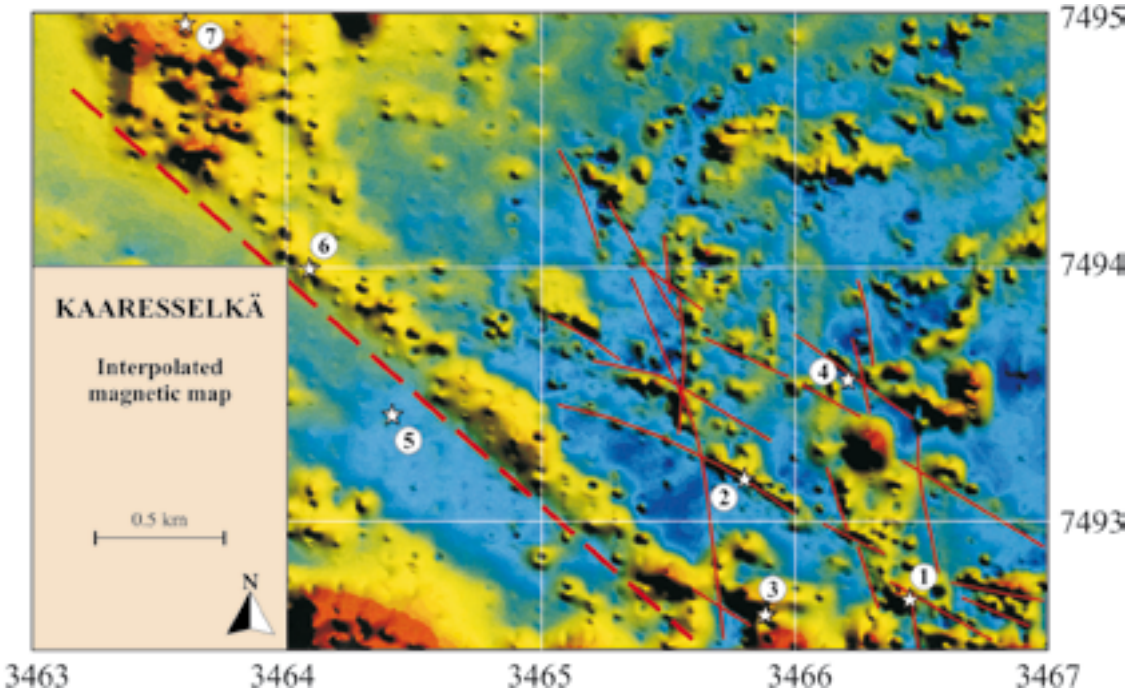

Fig. 7. Ground magnetic map of Kaaresselkä. Proven and inferred fault and shear zone lines and locations of the gold prospects (stars) are depicted. Prospects: 1. Vanha, 2. Tienvarsi, 3. Lampi, 4. Kumpu, 5. Rinne, 6. Rakka, 7. Jänkä.

Geophysical results

The SP method was the most effective in locating mineralized zones because the ground water level is at the depth of even 40 m in the area. The VLF-R method was only useful in areas where gold is associated with graphite-bearing rocks. The results of ground magnetic measurements (Jalander) delineate a positive anomaly, which almost coincides with the zone delineated by Cu, Mg, Cr and Ni (Fig. 5b and 7). This magnetic anomaly closely follows the trend of the deformation zone called the Sirkka Shear Zone.

The downhole measurements indicate that the total radiation in the gold-enriched shear zones is 15–25 μmR/h compared with 5 μmR/h within the unaltered rocks. The high radiation values may be caused by potassic alteration or monazite, which occurs as an accessory mineral in the alteration assemblage.

CONCLUSIONS

Gold mineralization in the Kaaresselkä area is epigenetic and hydrothermal in origin. Gold has precipitated in low-displacement fault and shear zones, which are probably related to the adjacent crustal-scale deformation zone called the Sirkka Shear Zone.

Elevated concentrations of Cu, Te and As, and in some extents of Pb, Zn, Mo and Ag, are spatially associated with gold mineralization. However, the gold mineralization may not to be wholly coeval with the associated trace elements and may have partly different structural control than the general trend of the shear zone.

Carbonatization, sericitization, chloritization, biotitization and formation of adularia, quartz, sulphides and tourmaline are the main alteration processes associated with the gold mineralized shear zones. These alterations were preceded by intense albitization, which may be related to intrusion of mafic intrusions (gabbros and dolerite dykes) in the region. Also carbonatization, sericitization, chloritization and biotitization may be, at least partly, related to alteration caused by the intrusion of the dolerites, as mafic-ultramafic dykes and sills can generate large-scale hydrothermal activity around them as described by Eilu (1994). The formation of adularia, quartz, tourmaline and some of the sulphides clearly are closely related to the precipitation of gold and define the proximal alteration zone. There are no indications of gold enrichment during the albitization.

The Kaaresselkä gold-copper occurrences are analogous to orogenic mesothermal gold deposits in other parts of the world in terms of geologic and structural setting, metamorphic grade, alteration and vein mineralogy (c.f. Groves et al. 1998, McCuaig and Kerrich 1998). However, Kaaresselkä shows some features that point towards an epithermal origin, such as the presence of adularia (c.f. Sillitoe 1993, Hedenquist et al. 1996), but further work is required to clarify this.

Recommendations for further exploration at Kaaresselkä

To get reliable gold assays large samples and consistency in drilling and sample preparation and analysis should be applied. More careful drilling and sampling are recommended to get more reliable resource estimates. In addition, ground-penetrating radar could be a useful tool to delineate the deeply weathered gold-bearing zones and sensitive radiation measurements could be used in tracing the gold mineralization related potassic alteration and monazite-bearing shear zones.

ACKNOWLEDGEMENTS

Mr Erkki Vanhanen the Manager of the Bedrock and Raw materials section at Rovaniemi, is thanked for the permission to publish the results of the study. Mr M. Pänttäjä and Mr H. Salmirinne are acknowledged for processing the figure data.

REFERENCES

Danielsson, A. & Sundkvist, G. 1959. The tape machine I – III. Spectrochim. Acta 15, 122 – 137.

Gustavsson, N., Noras, P. & Tanskanen, H. 1979. Seloste geokemiallisen kartoituksen tutkimusmenetelmistä. Summary: Report on geochemical mapping methods. Geological Survey of Finland, Report of Investigation 39. 20 p.

Eilu, P. 1994. Hydrothermal alteration in volcano-sedimentary rocks in the Central Lapland Greenstone Belt, Finland. Geological Survey of Finland, Bulletin 374. 145 p.

Groves, D. I., Goldfarb, R. J., Gebre-Mariam, M., Hagemann, S. & Robert, F.1998. Orogenic gold deposits: A proposed classification in the context of their crustal distribution and relationship to other deposit types. Ore Geol. Rev. 13, 1–28.

Härkönen, I. 1980. Selostus malmitutkimuksista Sodankylän Kaaresselän alueella 1979–1979. Geological Survey of Finland, unpublished report M 19/3714/–80/1/10. 20 p. (in Finnish).

Härkönen, I. 1984. The gold-bearing conglomerates of Kaaresstunturi, Central Finnish Lapland. In: Foster, R. P. (ed.) Gold '82: The Geology, Geochemistry and Genesis of Gold Deposits. Balkema, Rotterdam, 239–247.

Härkönen, I & Pulkkinen, E. 1991. Eräiden mineralisaatioiden kuvastuminen pintamoreenissa Keski-Lapissa. In: Lindroos, P. (ed.) Pintamoreenin merkitys malmilohkarekuljetuksissa. Geological Survey of Finland, Report of Investigation 55, 53–59. (in Finnish)

Hedenquist, J. W., Izawa, E., Arribas, A. & White, N. C. 1996. Epithermal gold deposits; styles, characteristics, and exploration. Resource Geol. Spec. Publ. 1. 70 p.

Karvinen, A. 1997. Tutkimustyöselostus Sodankylän kunnassa Kaaresselkä 3 nimisellä valtausalueella (kaivosrekisterinumero 4445/2) suoritetuista sinkkimalmitutkimuksista. Geological Survey of Finland, unpublished report M06/3713/97/2/10. 3 p. (in Finnish)

Kontas, E. 1981. Rapid determination of gold by flameless

atomic absorption spectrometry in the ppb and ppm ranges without organic solvent extraction. Atomic Spectroscopy 2, (2), 59–61.

Korkiakoski, E. & Kilpelä M. 1997. the komatiite-hosted Pahtavaara gold mine near Sodankylä, northern Finland. In Korkiakoski, E and Sorjonen-Ward, P. (eds.) Research and exploration – where do they meet? 4th Biennial SGA Meeting, August 11–13, 1997, Turku, Finland. Excursion guidebook B1 : ore deposits of Lapland in northern Finland and Sweden. Opas – Guide, 43, 27–29.

Lehtonen, M., Airo M-L., Eilu, P., Hanski, E., Lanne, E., Kortelainen, V., Manninen, T., Rastas, P., Räsänen, J. & Virransalo, P. 1998. Kittilän vihreäkivialueen geologia. Lapin vulkaniittiprojektin raportti. Summary: The stratigraphy, petrology and geochemistry of the Kittilä greenstone area, northern Finland. A report of the Lapland Volcanite Project. Geological Survey of Finland, Report of Investigation 140. 144 p.

McCuaig, T. C & Kerrich, R. 1998. P-T-t-deformation-fluid characteristics of lode gold deposits: evidence from alteration systematics. Ore Geol. Rev. 12, 381–453.

Pulkkinen, E., Puranen, R. & Lehmuspelto, P. 1980. Interpretation of geochemical anomalies in glacial drift of Finnish Lapland with the aid of magnetic susceptibility data. Geological Survey of Finland, Report of Investigation 47. 39 p.

Pulkkinen, E. 1998. Tutkimustyöselostus Sodankylän kunnassa, valtausalueella Kaaresselkä 2, kaiv. rek. nro 4445/1 suoritetuista malmitutkimuksista. Geological Survey of Finland, unpublished report M06/3714/–97/1/10. 7 p. (in Finnish)

Pulkkinen, E. & Hulkki, H. 1999. Tutkimustyöselostus Sodankylän kunnassa valtausalueilla Kaaresselkä 6–11, kaiv.rek. numerot 6162/1, 6162/2, 6277/1, 6277/2 ja 6771/2 suoritetuista malmitutkimuksista. Geological Survey of Finland, unpublished report C/M 06/3714/–99/1. 45 p. (in Finnish with an English summary and figure captions).

Räsänen, J. 1977. Kaarestunturi-muodostuma ja sen stratigrafinen sijainti Keski-Lapin liuskejaksossa. University of Helsinki, unpublished MSc thesis. 77 p. (in Finnish)

Sillitoe, R. S. 1993. Giant and bonanza gold deposits in the epithermal environment: assessment of potential genetic factors. Soc. Econ. Geol. Spec. Publ. 2, 125–156.

Gold in the Central Lapland Greenstone Belt, Finland
V. Juhani Ojala (ed.)
Geological Survey of Finland, Special Paper 44, 165–184, 2007.

THE LEVIJÄRVI-LOUKINEN GOLD OCCURRENCE: AN EXAMPLE OF OROGENIC GOLD MINERALISATION WITH ATYPICAL METAL ASSOCIATION

by
Marko J. Holma[1] &Veikko J. Keinänen[2]

Holma, M.J. & Keinänen, V.J. 2007. The Levijärvi-Loukinen gold occurrence: An example of orogenic gold mineralisation with atypical metal association. *Geological Survey of Finland, Special Paper 44,* 163–184, 10 figures and 2 tables.

Four adjacent polysulphidic, multimetallic lode-gold prospects within the Palaeoproterozoic Central Lapland greenstone belt have been studied. Mineralisation is continuous with variable grade along the Sirkka Shear Zone, the main structural feature in the area, for about 5 km.

The Levijärvi-Loukinen occurrence is enriched in Cu, Fe, Ni, Au ± Ag and Co, and is formed by variably sulphide-rich quartz-carbonate veins and stockworks. Deformation style is dominantly brittle. The host sequence belongs to the >2.05 Ga Savukoski Group and consists of volcano-sedimentary unit in the footwall (Matarakoski Formation) and metakomatiite unit in the hanging wall (Sattasvaara Formation). The footwall rocks can be subdivided into a sequence of phyllite, tuffite and graphitic phyllite and distal, less deformed Fe-tholeiitic rock. The most intensively altered metakomatiitic rocks are green fuchsite- and carbonate-rich rocks, listvenites. The metavolcanic rocks are partly metapyroclastic.

The proximal assemblage of quartz-carbonate-sericite/fuchsite ± albite-chlorite-pyrrhotite/pyrite-arsenopyrite-rutile chiefly characterises the alteration. Pyrrhotite, chalcopyrite, pyrite, arsenopyrite and gersdorffite are the dominant ore minerals in the occurrence. Native gold occurs mainly as inclusions and fracture fillings in the sulpharsenides and pyrite. There is no evidence of refractory gold so far. Mineralisation occurred under mid- to upper greenschist facies conditions soon after the peak of deformation and metamorphism.

Despite its unusually high base metal content and atypical metal association for orogenic gold mineralisation, the occurrence is considered to represent an epigenetic mesothermal, lode type of gold mineralisation having considerably amount of similarity with orogenic gold deposits.

Key words (GeoRef Thesaurus, AGI): gold ores, polymetallic ores, metamorphic rocks, metakomatiite, alteration, veins, shear zones, ore minerals, Central Lapland Greenstone Belt, Paleoproterozoic, Levijärvi, Loukinen, Lapland Province, Finland.

[1]*Department of Geosciences, P.O. Box 3000, FI-90014 University of Oulu, Finland.*
[2]*Geological Survey of Finland, P.O. Box 77, FI-96101 Rovaniemi, Finland.*

E-mail: [1]marko.holma@oulu.fi, [1]veikko.keinanen@gtk.fi

INTRODUCTION

The Palaeoproterozoic Levijärvi-Loukinen gold occurrence is situated in the municipality of Kittilä, northern Finland, about 145 km north of the Arctic Circle and approximately 17 km north from Kittilä, the administrative centre of the municipality (Fig. 1). During exploration it was divided into four prospects, namely Levijärvi Au-Ni, Paaminamaa Cu-Au-Ni, Loukinen Cu-Ni-Au, and Tienpää Ni-Cu-Au prospects (from now on, the *lodes*). However, as mineralised zone is about five km long without much of a change in characteristics, gold-related or otherwise, it can be defined as a single occurrence. Accordingly, in the present paper, we will follow Holma et al. (2003) by employing the name *Levijärvi-Loukinen* for this distinct group of gold lodes.

All the lodes occur in the about 150 km long Sirkka Shear Zone (SSZ), a W- to WNW-trending zone of tectonised and variably altered rocks coinciding with the southern margin of the Kittilä Group area, a major volcanic terrane in the Kittilä greenstone area of the Central Lapland greenstone belt (CLGB) (Fig. 1). Gold mineralisation is restricted to the altered intervals of fine-grained pelitic and volcanogenic metasedimentary rocks and massive and pyroclastic metavolcanic rocks. The amount of graphite in the metasedimentary rocks is in places considerably high. The metavolcanic rocks are Fe-tholeiitic and komatiitic in origin. Gold is hosted in a network of quartz-carbonate-sulphide veins and stockworks within a shear and fault zone system. In many areas, veined zones have been progressively deformed by subsequent strain localisation. In these cases the vein gangue and sulphides (± gold) have been dispersed into a shear zone.

Gold mineralisation in the area shows an unusual base metal enrichment and metal association for orogenic gold, typically Cu, Fe, Ni, Au ± Ag and Co. The single most common ore mineral is pyrrhotite, whereas chalcopyrite, the main carrier for Cu, is the second most common ore mineral. There are several nickeliferous minerals, including gersdorffite [(Co,Fe)AsS – NiAsS], nickeliferous arsenopyrite, nickeliferous cobaltite and accessory pentlandite.

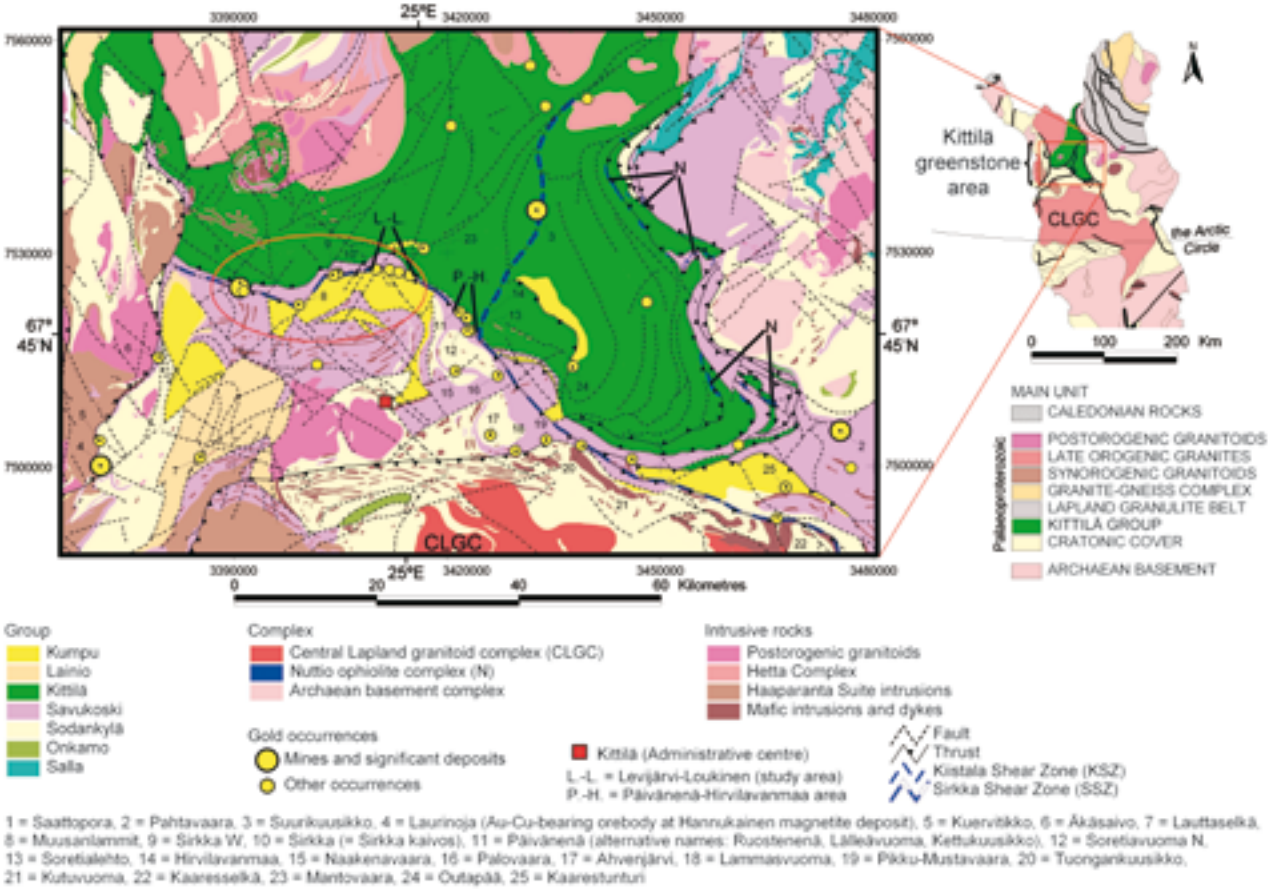

Fig. 1. Gold deposits and occurrences in the Kittilä greenstone area, the largest subarea of the Central Lapland greenstone belt that extends from this area to the Finnish-Norwegian border in the north and the Finnish-Russian border in the southeast. Most gold occurrences presented here are interpreted to be orogenic, except the No. 4 (Fe-oxide Cu-Au deposit), No. 7 (possibly an Fe-oxide Cu-Au deposit), No. 5 and 6 (skarn-hosted or Fe-oxide Cu-Au deposits), and Nos. 24 and 25 (palaeoplacers). Apart from the *multimetallic* Au-Cu and Au-Cu-Ni±Co occurrences that are surrounded here by a red oval, all orogenic occurrences are of *gold-only type*. Coordinates are in the Finnish National Grid, the ykj-grid. Geology after Lehtonen et al. (1998).

The main objectives of this study are: 1) to present the case history of the Levijärvi-Loukinen gold occurrence, and 2) to report its main field and petrographic characteristics in more detail than above.

CASE HISTORY AND PREVIOUS INVESTIGATIONS

The first indications of this distinct multimetallic[1] ore type enriched in Cu, Fe, Ni, Au ± Ag and Co were attained as early as in the 1940's–1950's when an exploration company Atri Oy performed bedrock mapping, ground magnetic and electromagnetic surveys, and diamond drilling in the region. In 1939–1953 Atri Oy explored ~4–6 km west from Levijärvi in a location nowadays known as the *Sirkka kaivos* gold occurrence (no. 10 in Fig. 1). This occurrence has been studied intermittently from ever since. After Atri Oy, Vuoksenniska Oy started underground exploration in the area. The exploration conducted by this company culminated in the establishment of a test mine and pilot plant during 1955–1956 (Lehtinen 1987). In the end, they had developed 60 m deep shaft and 600–700 m of drives down to 45 m level and produced about three kg of gold from 3000 t of ore (1 g/t Au, 0.16 % Co, 0.5 % Cu, 0.9% Ni). From these early workings stems the currently used name for this gold occurrence: "Sirkka kaivos", meaning "Sirkka mine" (Sirkka is the nearby located village). Interestingly, this occurrence has much in common with the Levijärvi-Loukinen occurrence, and particularly with the Levijärvi lode (Figs. 2 and 3).

The Levijärvi prospect was discovered in 1993 by the Geological Survey of Finland (GTK). The first indication of mineralisation was the discovery of Ni-Co-Au-rich boulders by an amateur prospector, Mr. Jalmari Tammela. They were analysed in the GTK to contain up to 25 % Ni, 3 % Co and 25 ppm Au. Magnetic and electromagnetic (VLF-R) surveys over an area of 0.42 km^2 commenced in March 1994 and continued in February 1996. The most interesting geophysical targets were studied by diamond drill-

1 Note that the term "polymetallic" has been more often used to describe this local mineralisation than is "multimetallic", the term we favour for the following reasons. In its most general usage, the word "polymetallic" has come to signify deposits that are characterised by a very specific metal association, like Cu-Pb-Zn-Ag, Cu-Mo±Au, or Cu-Zn-Au-Ag. In particularly a lot of Pb and Zn are expected from a polymetallic deposit (R. Goldfarb, pers. comm. January 2006). In many cases the polymetallic deposits *sensu stricto* are syngenetic in character (e.g. polymetallic sedex-, porphyry- and VMS-type of deposits), although not always (e.g. polymetallic epithermal gold deposits). In contrast, all gold occurrences in SSZ are distinctly epigenetic vein-type of deposits and Zn and Pb contents are not anomalous. This is confirmed by both geochemical surveys and microscopic studies (for example, only a few grains of accessory sphalerite and galena have been observed in our current occurrence). As the term "multimetallic" has not such connotations it fits better to the current context.

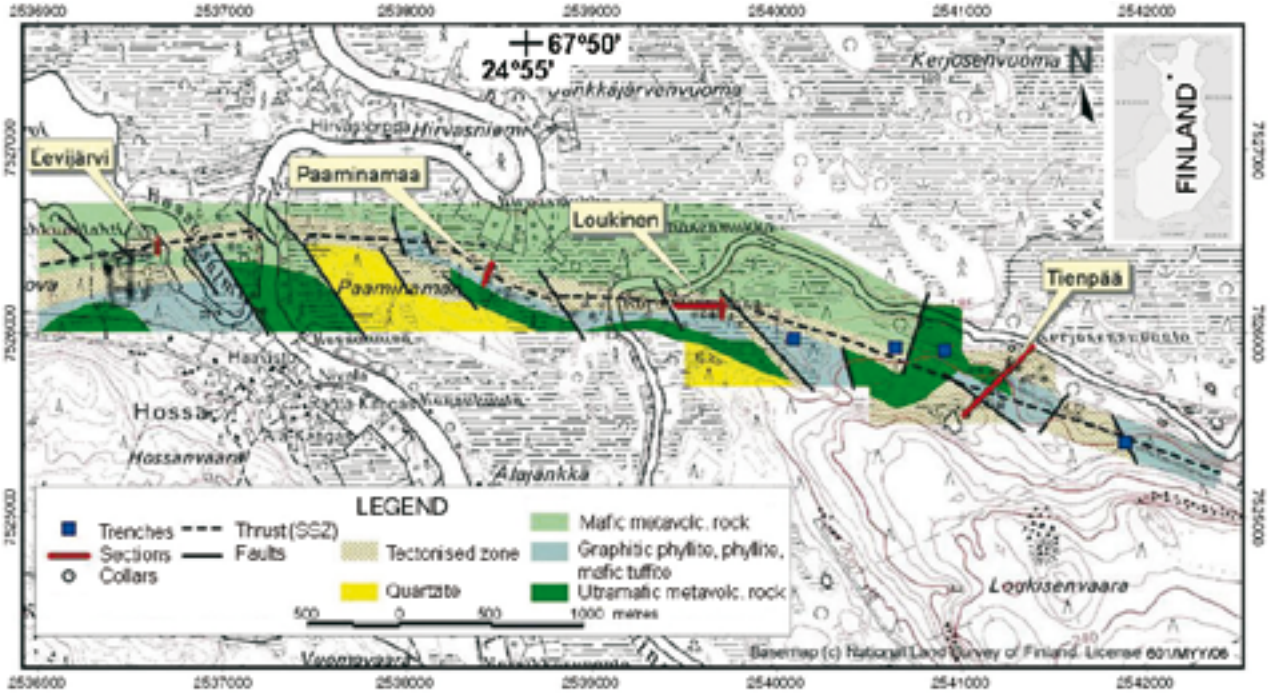

Fig. 2. Geological map of the Levijärvi-Loukinen gold occurrence (the solid square in the inset). Its four lodes (prospects) are presented with nameplates and their best sections with red bars. All rock types belong to the Savukoski Group, except the quartzites that are of the Kumpu Group. Finnish National Grid, the kkj-grid, zone 2. Modified after Keinänen et al. (2001). Topographic map@National Land Survey of Finland. Licence 521/MYY/07.

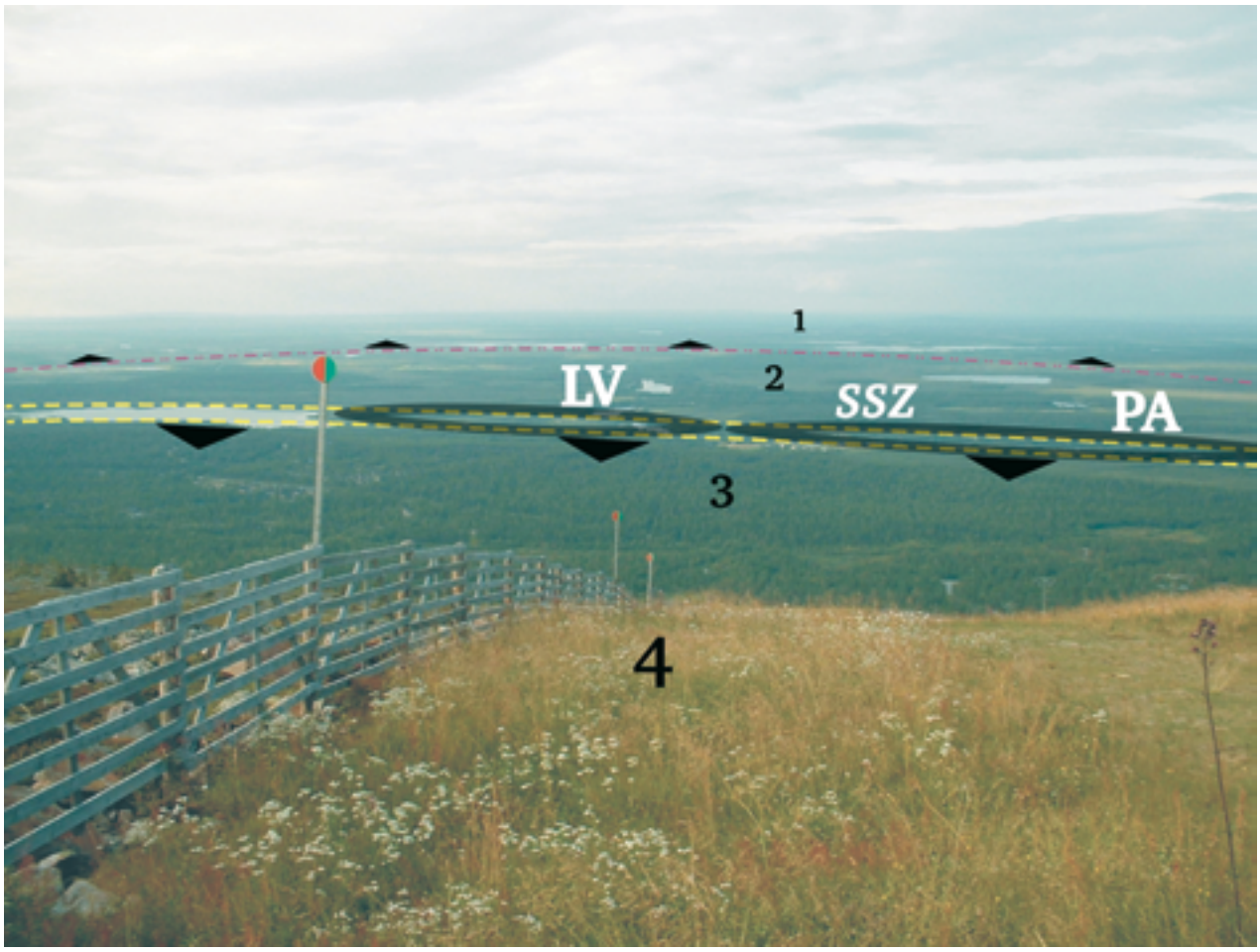

Fig. 3. Photograph looking north from the top the Levi fell. The top of this fell rises ~330 m from the surroundings (531 m a.s.l.). The landscape in view consists largely of peat bogs and till-covered low hills, the latter sheltered by coniferous forest. The trend of the Sirkka Shear Zone (SSZ) follows approximately the W-trending chain of lakes and river sections in the middle of the image (in some extent obscured by the superimposing lines and marks). The area dominated by the predominantly volcanogenic Kittilä Group (No. 1) is separated from the metasedimentary-dominated Savukoski Group (Nos. 2–3) by a tectonic zone seen in the distance (purple dashed-dot line). This tectonic zone is related to SSZ, though in the study area it curves farther north than usual (~3 km north from the main trend of SSZ). The E-trending contact between clastic rocks of the Kumpu Group (No. 4) and the older rocks lie approximately in the central part of the area 3. The shaded ovals depict the locations of the Levijärvi (LV) and Paaminamaa (PA) lodes of the Levijärvi-Loukinen gold occurrence. Solid triangles depict in which directions the tectonic zones are assumed to dip. For comparison, see Fig. 1. Geology after Lehtonen et al. (1998). Photo: Vesa Kortelainen.

ing, which started 1994 and continued periodically until 2001 (Keinänen et al. 2001). The prospects of Paaminamaa, Loukinen and Tienpää (Fig. 2) were discovered soon after as the GTK investigated the eastward continuation of the Levijärvi lode by ground geophysical methods.

Previous work on the Levijärvi–Loukinen gold occurence have been published in the following abstracts: Keinänen & Holma (2001), Holma et al. (2003), Holma (2006) and Holma & Keinänen (2006). Note also the works of Ohlson (1969), Inkinen (1985), Härkönen & Keinänen (1989), Ward et al. (1989), Nurmi et al. (1991), Mänttäri (1995), Vanhanen (2001), Weihed & Eilu (2003) and Eilu et al. (2003, 2006), the publications of which all contain data that has general significance for the understanding of gold mineralisation in the study area.

The mineralogy of SSZ's ultramafic rocks is reviewed by Riikonen (1997) (altered types) and Hanski et al. (2001b) (both the least altered and best-preserved types). A reader interested especially in local structural geology is directed to Keinänen et al. (2001), Väisänen et al. (2000) and Väisänen (2002). Some of the earliest discussions on SSZ (although then known as the Sirkka Line) can be found from Berthelsen & Marker (1986), Gaál et al. (1989) and Ward et al. (1989). The present paper has also benefited from several unpublished works in Finnish. These include Vesanto (1978), Vormisto (1969) and Lehtinen (1987), which describe the Sirkka Cu-Au occurrence, and Holma (2001) and Keinänen et al. (2001), which contain data about the Levijärvi gold lode of the Levijärvi–Loukinen gold occurrence.

MATERIAL AND RESEARCH METHODS

The study area is poorly exposed owing to the flat topography and 1–20 m thick overburden of glacial till and younger fluvial sediments (Fig. 3). In places, the fresh bedrock is also covered by preglacial weathering crust now underlying the Quaternary deposits (Ohlson 1969). Hence, geology in the Fig. 2 is mainly based on geophysics and drillings.

The main tool defining the drilling targets was the VLF-R method (Table 1). In addition, the magnetic, IP, and SP properties of the rocks were measured. In places, several borehole survey methods, including measurements of density, magnetic susceptibility, apparent resistivity, IP effect, and radiometric properties, were used to define drilling targets, contacts between the various rock types and the continuity of mineralisation at depth. All the results of these geophysical investigations were available for the current study, although they were only used as a basis for making interpretations about the local geology and character of mineralisation. Geophysical results gained during exploration have been presented in Keinänen et al. (2001).

The main methods for sampling during exploration were diamond drilling and trenching. A total of 163 diamond-drill holes, all drilled in an unoriented manner, with a total length of 11 334 m, were drilled in the area during 1994–2001. The drill holes were 35 mm, 45 mm and 56 mm in diameter. On structural interpretations the current paper relies on Väisänen et al. (2000) and Väisänen (2002) and the data reported in Keinänen et al. (2001). A summary regarding the exploration work done in the study area since 1993, together with the material and analytical methods used in this study, is shown in Table 1.

Most of the geochemical analyses were carried out in the laboratories of the GTK over a period from 1994 to 2001. The methods used were Inductively Coupled Plasma – Atomic Emission Spectroscopy

Table 1. Summary of the existing data and exploration work done in the Levijärvi-Loukinen area by the GTK during 1993–2001. The drillings are located in the following Finnish 1:20 000 base map sheets: 2741 10 (Levijärvi, Paaminamaa and part of Loukinen) and 2743 01 (Tienpää and part of Loukinen). The asterisk prefix refers to the sheet 2743 01.

	Levijärvi	**Paaminamaa**	**Loukinen**	**Tienpää**
Time of drilling:	1994–1996	1997–2000	1998–2001	1998-2000
Drill holes:				
Number of holes (hole id. code)	78 (R401–R478)	20 (R479–R494, R506–509)	37 (R495–R502, R510–R530, *R559-R561)	28 (*R519–R546)
Total length	2892 m	2152 m	3678 m	2612 m
Exploration trenches:	–	–	1	4
Geophysical surveys:				
At ground	Magnetic, VLF-R	Magnetic, VLF-R	Magnetic, VLF-R, SP	Magnetic, VLF-R, SP, IP
Borehole measurements[1]	–	9	12	12
Geochemical surveys:	–	Till geochemistry in an area of 500 x 850 m with a 50 m grid (198 sample sites)	–	Till geochemistry in a small-scale grid (~ 20 sample sites)
Geochemical and petrographic analyses:				
ICP-AES	1795 samples	1760 samples	1984 samples	1737 samples
XRF (whole-rock)	23 samples from 13 drill cores	5 samples from 1 drill core (R480)	5 samples from 1 drill core (R498)	–
GFAAS[2]	*Used constantly*	*Used constantly*	*Used constantly*	*Used constantly*
Thin sections[3]	~100	~40	~15	~30

[1] Includes measurements of density, magnetic susceptibility, apparent resistivity, IP effect, and radiometric properties. Note, however, that not all of these methods were applied to all drill holes
[2] The GFAAS method was used for gold assays whenever they were needed. The GTK's in-house method 704U, which combines the GFAAS analysis with the Pb-Fire Assay preconcentration/separation procedure, was applied every now and then
[3] The most of which are polished

(ICP-AES)[2], Graphite Furnace Atomic Absorption Spectrometry (GFAAS)[3] and X-ray Fluorescence Spectroscopy (XRF)[4]. All the ICP-AES and most of the GFAAS results were gained during exploration, but the majority of the XRF analyses were conducted during the study of Holma (2001) or later. However, as the focus of the current paper is not on geochemistry, but on the general geology, deposit characteristics and mineralogy, geochemical analyses were merely utilised here as a mean to improve the quality of geological observations on drill core and to direct mineralogical work on thin sections. Hence, a reader interested in geochemistry of the Savukoski Group and its lithostratigraphical formations is instructed to Lehtonen et al. (1998) and references therein.

Most of the mineralogical work was done with samples collected from Levijärvi (Fig. 2). Consequently most of the reported mineralogical data relates to that lode. Results from the other three lodes – Paaminamaa, Loukinen and Tienpää – are nonetheless consistent with observations from Levijärvi. Mineralogical and analytical examinations of more than 100 thin sections (from a collection of over 180 thin sections; Table 1) were done in the University of Oulu, Finland, by conventional polarising microscopy at the Department of Geosciences, Division of Geology, and by electron probe microanalyser (EPMA) JEOL JCXA-733 and scanning electron microscope (SEM) JEOL JSM-6400 at the Institute of Electron Optics[5]. In addition, many SEM-EDS analyses were done in Espoo unit of the GTK.

During the present study the authors have also examined and sampled drill core from the occurrences of Muusanlammit, Sirkka W, Päivänenä (also known by the names Kettukuusikko, Ruostenenä and Lälleävuoma), Soretiavuoma N, Soretialehto, Naakenavaara, Palovaara (= Jerusaleminjänkä), Ahvenjärvi (= Isomaa), Lammasvuoma, and Pikku-Mustavaara (Fig. 1). Since no usable drill core was available from the Sirkka occurrence, the geology regarding that occurrence was evaluated by re-examining all the written material obtainable and by studying field samples collected from the old dumps. Although the work done with these other gold occurrences is not directly related to the present study, the results gained so far have certainly led to a better understanding of our current occurrence.

2 The chemical components analysed by ICP-AES were Ag, Al, As, B, Ba, Be, Ca, Cd, Co, Cr, Cu, Fe, K, La, Li, Mg, Mn, Mo, Na, Ni, P, Pb, S, Sb, Sc, Si, Sr, Th, Ti, V, Y and Zn.

3 Gold was assayed with the GFAAS method. In addition, the Pb-Fire Assay/GFAAS method (the GTK's in-house method 704U) was occasionally used to analyse Au, Pd, Te (with detection limit of 0.01 ppm) and Pt (0.02 ppm).

4 A total of 33 whole-rock geochemical XRF analyses were performed for all major elements and the following trace elements: As, Ba, Bi, Ce, Cl, Cr, Cu, Ga, La, Mo, Nb, Ni, Pb, Rb, S, Sb, Sc, Sn, Sr, Th, U, V, Y, Zn and Zr.

5 With a few exceptions, all EPMA mineral analyses were determined using a beam diameter of 10 µm. Accelerating voltage was set to 15 kV and sample current either to 15 nA (for silicates and ore minerals) or 12 nA (for carbonates). Results were corrected using the ZAF procedures.

REGIONAL GEOLOGICAL SETTING

The study area is located in the northern part of the Fennoscandian Shield where the Palaeoproterozoic supracrustal rocks form an extensive belt across the Archaean basement. The Finnish part of this intracratonic, rift-related, 2.5–1.8 Ga volcano-sedimentary sequence is known as the Central Lapland greenstone belt (CLGB). CLGB records a prolonged and episodic history of rifting, sedimentation and magmatism before the collision and rift closure at ~1.9 Ga (Eilu et al. 2003, Weihed et al. 2005, Eilu et al. 2006, *this volume*).

Lehtonen et al. (1998) divides the supracrustal rocks of CLGB into seven lithostratigraphic groups, from which the oldest and youngest are Salla and Kumpu Groups, respectively (Fig. 1). In between these two groups lies the >2.05 Ga Savukoski Group that consists of fine-grained metasedimentary and metavolcanic rocks lying upon arkosic quartzites, orthoquartzites and mica schists of the >2.2 Ga Sodankylä Group. It is the Savukoski Group that hosts gold mineralisation in SSZ. In the northern side of SSZ the rocks belong to the ~2.02–1.99 Ga old Kittilä Group that comprises a greenstone-dominated basin up to 6 km thick (Lanne 1979, Elo et al. 1989). The evidence supports the Kittilä and Savukoski Groups were juxtaposed at ~1.92–1.91 Ga ago (Hanski et al. 1998, Rastas et al. 2001). The two uppermost groups, namely Lainio and Kumpu, the latter that deposited sometimes between 1.88–1.80 Ga (Hanski et al. 2001a), cap all the older, folded and metamorphosed rocks with unconformity.

In Finnish Lapland, the compressive stages at 1.92–1.87 Ga and 1.84–1.79 Ga (Lahtinen et al. 2003, 2005) resulted in dominantly greenschist facies regional metamorphism and a formation of a fold and thrust belt. Both of these periods are suggested to be gold-favourable in terms of orogenic gold mineralisation, but probably the latter is more profitable. These

collisional events resulted also in the emplacement of the allochthonous Lapland granulite belt from the NE (Fig. 1). This regionally important tectonic event was probably accompanied by coeval thrusting along the present SSZ to approximately NE (Lanne 1979, Ward et al. 1989, Sorjonen-Ward et al. 1992, Lehtonen et al. 1998, Eilu et al. 2006, *this volume*). At least the southern and eastern contacts of the Kittilä Group area are tectonic (eg. SSZ), and parts of it may be allocnthnous (Hanski 1997, Lehtonen et al. 1998). This is not based only on geophysics, but also on the rocks themselves along SSZ: many rocks are evidently altered in several phases, spanning from early rifting-related to later structurally controlled styles (Eilu 1994, Eilu 1999b, Eilu et al. 2006, *this volume*).

At least twenty Au, Au-Cu and Au-Cu-Ni±Co deposits and drill-indicated prospects occur within 0–3 km from SSZ indicating that it is a major deformation zone (Eilu 1999a, Eilu et al. 2003, Eilu et al. 2006, *this volume*). One of these is Levijärvi-Loukinen. Most of these mineralisations appear to be small, but, in most cases, due to lack of detailed studies, the actual size of the occurrence is open to at least some degree of speculation. The deep-seated nature of SSZ has been confirmed with the data from the deep refraction profile POLAR (Freeman et al. 1989) and the FIRE-4 transect of the Finnish Reflection Experiment (Heikkinen et al. 2004).

The most recent reviews on CLGB's lithostratigraphy, geochemistry and structural and metamorphic evolution can be found from the present publication and from Hanski & Huhma (2005) and Lahtinen et al. (2005). The radiometric age determinations from northern Finland have been presented in Vaasjoki (2001).

HOST SEQUENCE

Overview

The quartz-carbonate veins and stockworks that form the Levijärvi-Loukinen occurrence (Fig. 2) are hosted by the Savukoski Group rocks that can be assigned into two lithological units: volcano-sedimentary in the footwall and metakomatiite in the hanging wall (Fig. 4). Lithological contacts between these two units are the main locus for gold mineralisation. This holds true also elsewhere along SSZ, although in some locations either of the two might prevail. All rocks are metamorphosed in mid- to upper-greenschist facies. The stratigraphy trends E–W and dips to the south with variable angle. Also the lodes are E-W striking and have steep S-dipping orientation. The gold-related quartz-carbonate-sulphide veins are predominantly subvertical.

Other primary rock types include minor intrusives, mostly metadolerites. They are dated to be older than gold-rich vein systems (see Eilu et al. 2006, *this volume*) and none is observed to host major amount of gold-related veins. It should also be kept in mind that the clastic, late-orogenic Kumpu Group is also exposed in the area, just a few hundreds of metres south from SSZ (Figs. 1 and 2). The local topographic highs are formed from these well-preserved rocks (Fig. 3).

Volcano-sedimentary unit

This unit (Fig. 4) consists of alternating metasedimentary, volcanogenic metasedimentary and mafic metavolcanic rocks belonging to the 2.13–2.05 Ga Matarakoski Formation. Metasedimentary rocks include phyllite, variably pyrrhotite-rich graphitic phyllite[6], and minor chert. Volcanogenic metasedimentary rocks are mainly composed of tuffite. Individual beds are perhaps 10 m thick at most, but many layers are in the range of millimetres to centimetres.

The metasedimentary and volcanogenic metasedimentary rocks are part of the same fine-grained sequence, which grades into a thicker subunit comprising volcanogenic conglomerate and Fe-tholeiitic metalava (Fig. 5), the former possible being a true metapyroclastic rock. Such intermediate to mafic metavolcanic subunits can be several tens of metres thick. They mainly occur in the footwall of gold mineralisation far away from it. Accordingly, they are not as seriously altered or deformed as the other rock types in the drilled area (perhaps carbonation being as exception). For that reason they were neither studied in detail in the present work nor drilled intentionally during exploration.

It is notable that some graphitic beds comprise stratabound pyrrhotite and minor pyrite in thin discontinuous layers. These sulphides are part of the minor syngenetic mineralisation in the host sequence. From this point of view, it is noteworthy that the Matarakoski Formation is regionally known to host several syngenetic, sediment-hosted, stratabound to stratiform base-metal occurrences, like the Kortelehto

6 Owing to their high average content of graphite, these have been termed also as *graphitic schists* or *black schists*.

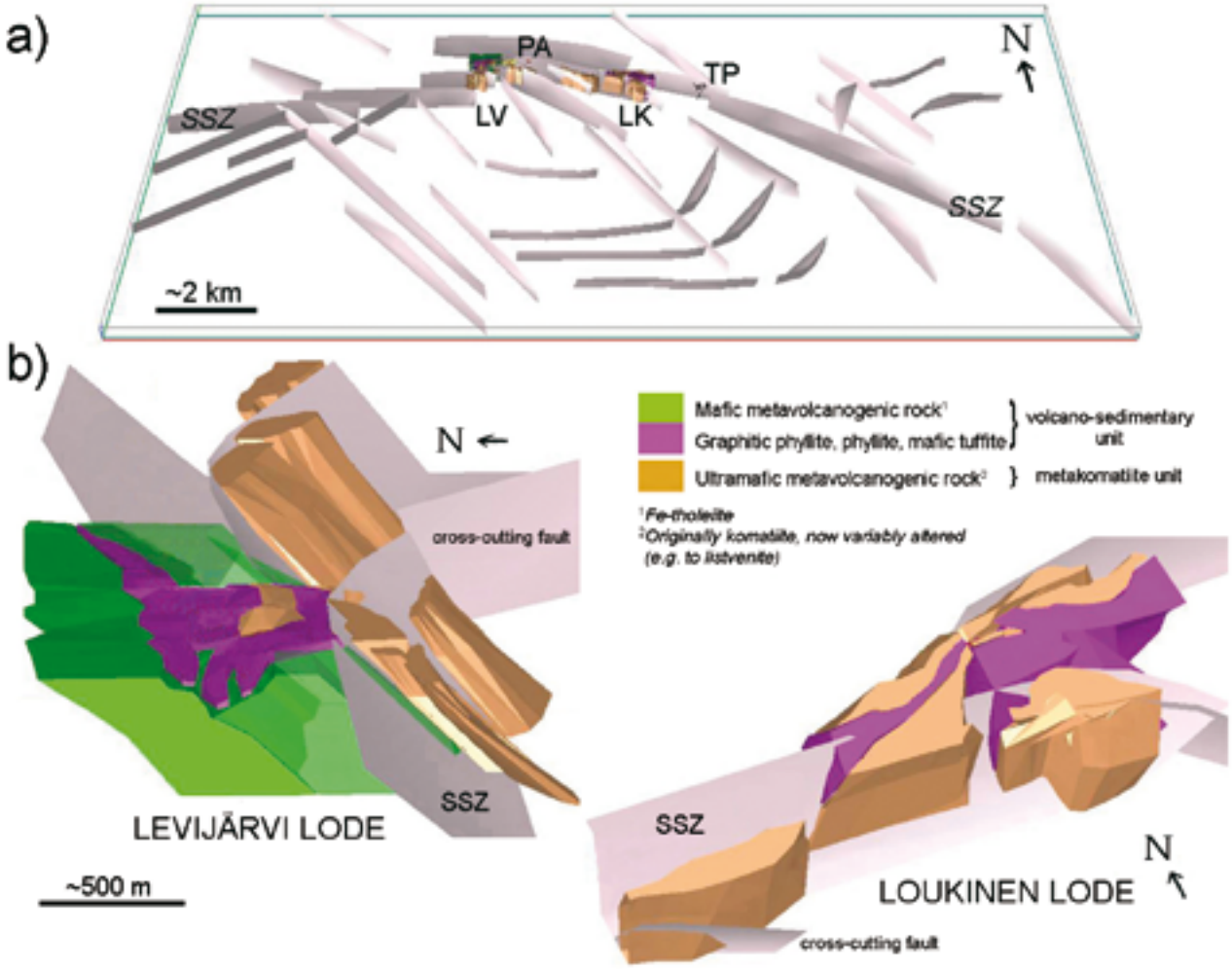

Fig. 4. Structural and lithologic 3D models for the Levijärvi-Loukinen area. **a.** Oblique view of the fault interpretation based on aeromagnetic derivative image. Pink grey planes are faults, except the "SSZ" that is the brittle-ductile Sirkka Shear Zone. Lodes: LV = Levijärvi, PA = Paaminamaa, LK = Loukinen, TP = Tienpää. **b.** Oblique view of the 3D lithologic block model based on geophysics and drillings. The Fe-tholeiitic rocks at Loukinen are located in the northern side of the view and are hence omitted. Both lodes are approximately in the same scale. Modified from Parkkinen (2002).

Zn-Cu and Pahtavuoma Cu-Zn-U occurrences near the Saattopora Au-Cu deposit (Korvuo 1997, Grönholm 1999, Eilu et al., *this volume*), and Pälkättivuoma Zn occurrence 10 km east from Kittilä (Fig. 1). The nearest of such *syngenetic* orebodies is at the Sirkka occurrence area (Fig. 1). There a sulphide-facies iron-formation occurs adjacent to Au-Cu mineralisation (Holma et al. 2006).

Metakomatiite unit

The metakomatiite unit (Fig. 4) is representative of the >2.05 Ga ultramafic Sattasvaara Formation (Hanski et al. 2001a, 2001b). These rocks lie upon those volcano-sedimentary rocks of the Matarakoski Formation that form the local footwall for gold mineralisation. Metamorphism, multistage hydrothermal alteration and tectonic movements along the host structure have destroyed most primary textures of ultramafic rocks. They are identified to be of ultramafic origin on the

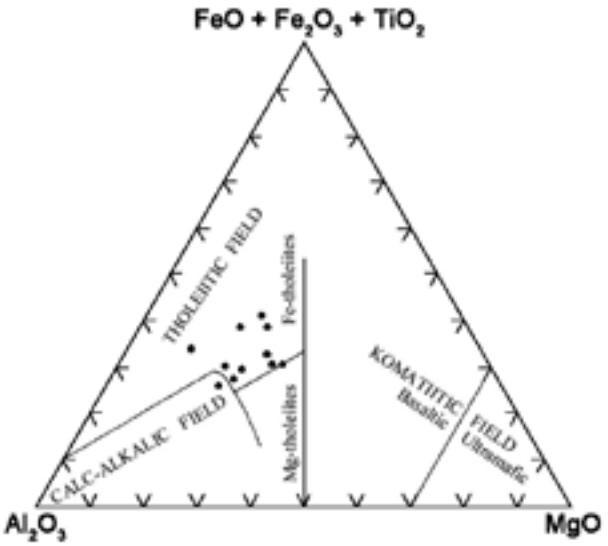

Fig. 5. Compositional diagram showing compositions of mafic metavolcanic rocks of the volcano-sedimentary unit of the Levijärvi-Loukinen gold occurrence. Given compositions are based on XRF analyses of selected drill core samples from the Levijärvi lode. Analysed samples include both fine-grained (tuffite) and massive (lava and pyroclastic rock) volcanogenic rocks. Holma (2001).

basis of their mineralogical and geochemical compositions, both of which are strikingly different from those of other rock types. The features supporting that these rocks are truly ultramafic include the relatively immobile trace elements Ni and Cr, the elements of which abundances are elevated in the altered rocks, as well as the minerals chromite (relict) and fuchsite (hydrothermal Cr mica). Besides, these strongly altered rocks grade into less altered varieties being in places talc-rich and containing magnetite impregnation. Detailed geochemical and field characteristics of the Sattasvaara rocks have been described in the literature, for instance by Saverikko (1983, 1985), Lehtonen et al. (1998) and Hanski et al. (2001b).

Summary of the lithology

The host sequence is both heterogeneous and complex. The nearest sulphide-facies iron-formation is located only ~5.5 km west from Levijärvi, close to the Sirkka occurrence, and even more importantly, within an identical supracrustal sequence (Holma et al. 2006). This suggests that some parts of the host sequence are analogous to sulphide-facies iron-formation. Hence there were, during mineralisation events, variably graphitic and sulphidic rocks present together with mafic and ultramafic rocks.

Structural, alteration and vein characteristics

Main structural features and overview of the various vein types

Structural style ranges from brittle-ductile to dominantly brittle. Plastic deformation is focused in anastomosing shear zones that may locally cut almost any rock type in the Savukoski Group. It can be said nonetheless that most of the deformation is concentrated in areas of lithological contacts between the metakomatiite and volcano-sedimentary units. Also the intensity of hydrothermal alteration and the abundance of veins continuously rise towards such contact zones. In contrast, the massive to pyroclastic Fe-tholeiitic rocks of the footwall, which are the most homogeneous rocks in the area, show the weakest intensity of deformation and alteration.

Both metakomatiites and fine-grained volcano-sedimentary schists can be highly veined, especially next to each other. Veins in them are typically deformed but they are totally destroyed only in places. Veins hosted by the volcano-sedimentary unit appear to be more numerous in areas of highest heterogeneity where grading from one rock type to another is strong. In those parts of the sequence where plastic deformation has destroyed all primary features of the rocks, along with the veins in them, if there were any, up to tens of metres broad zones of intensively sheared rocks may occur. In such shear zones, fragments of earlier emplaced veins are the only observable feature implying that also these rocks were once veined. Such shear zones are commonly rich in graphite. The country rocks between the shear zones are relatively intact and less strained (e.g. at Loukinen). They are also less altered than the rocks in the proximity of the shear zones. As a whole, SSZ is up to several hundreds of metres wide.

The three-dimensional geometry of the local bedrock is shown in Fig. 4. Note from that figure that there are metakomatiitic rocks in both sides of the volcano-sedimentary unit at Loukinen. This relationship is not observed elsewhere. It is assumed to be caused by the NW- and N-striking faults, which greatly complicate the geometry of rock units and mineralisation.

The following conclusions can be drawn by compiling data from our current study with data from Väisänen et al. (2000), Holma (2001), Keinänen et al. (2001) and Väisänen (2002): 1) the main shears have developed alongside lithological contacts, so that vein stockworks that follow structural breaks have an approximate trend from ~E-W; 2) there are two fold generations, the older folds being E-W trending and the younger ones N-S trending; 3) both the dominating fabric (E-W trending foliation) and earliest quartz-carbonate vein generations are overprinted by N-S trending folding and crenulation cleavage with accompanying shearing; 4) the N-S trending fabrics are associated with sulphidised quartz-carbonate veins that penetrate into the axial planes of the N-S trending folds or form NW- and NE-trending vein sets; 5) the N-S trending fabrics are postdated by barren coarse quartz-carbonate veins representing the last major vein generation; these well-preserved veins are rather planar in shape; 6) all previous tectonic fabrics and vein generations are affected by <1.77 Ga brittle strike-slip faults, which are of different ages or belong to a conjugate system with NW- and NE-trending components; these are D_4 faults (Patison, *this volume*). According to Patison, all or most of orogenic gold mineralisation in CLGB took place during the D_3.

Besides the auriferous veins and vein stockworks[7], which are described later on, the local bedrock hosts

7 For simplicity, these are termed *quartz-carbonate-sulphide veins* throughout the work.

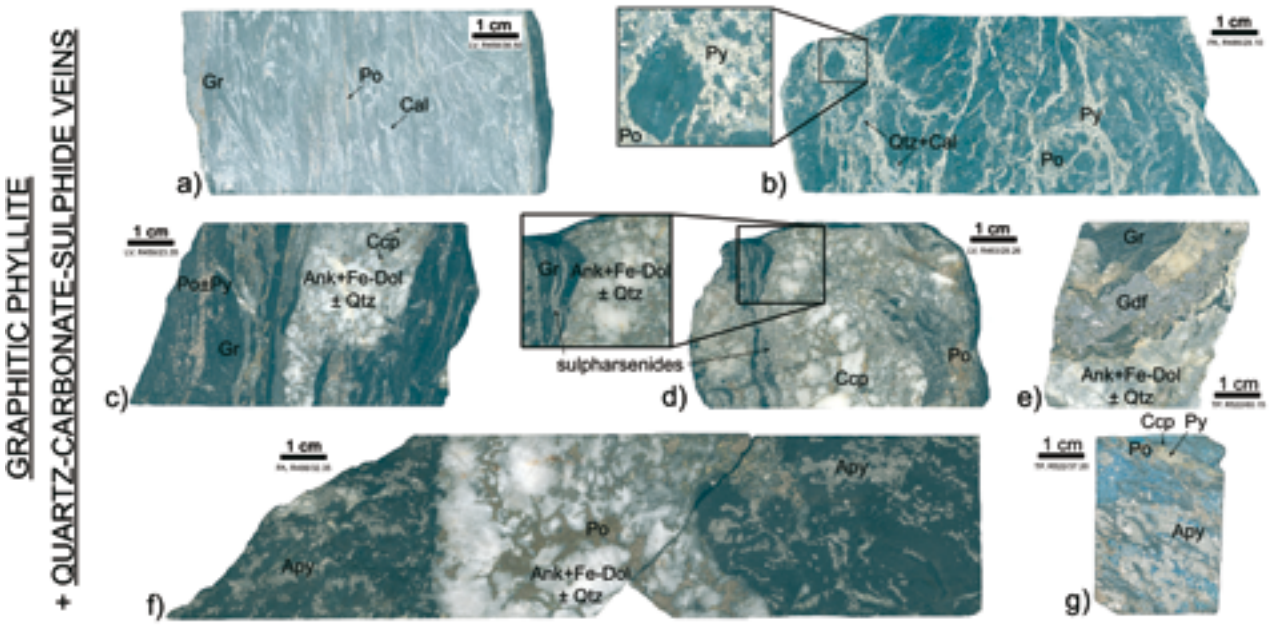

Fig. 6. Main lithologic and vein features of graphitic phyllite. In some of the figures contrast has been exaggerated to promote better distinction between different mineral phases. **a.** Pyrrhotite-bearing tightly folded graphitic phyllite containing carbonaceous interlayers or deformed calcite-pyrrhotite veins. **b.** Pyrrhotite-pyrite-rich quartz-calcite veinlets in graphitic phyllite, probably gold-related. **c.** Typical gold-related quartz-carbonate-sulphide vein that contains sulpharsenides. Note the associated pyrrhotite±pyrite veinlets in the wall rock that are similar to those in the previous figure. Gold grade: 0.03 ppm. **d.** Quartz-carbonate-sulphide vein rich in sulpharsenides, especially in Co-rich varieties (in a 0.60 m long section Co and Ni concentrations 1.4 % and 0.16 %, respectively). The graphitic slivers peeled off from the wallrock indicate repeated failure. Gold grade: 7.27 ppm. **e.** Another quartz-carbonate-sulphide vein. Here the sulpharsenide species is gersdorffite (Ni,Co,Fe)AsS. Gold grade: 0.07 ppm. **f.** Quartz-carbonate-sulphide vein with abundant arsenopyrite dissemination, no gersdorffite though. Gold grade: 0.12 ppm. **g.** Arsenopyrite, pyrrhotite, chalcopyrite and pyrite dissemination. No gersdorffite here. The blue hue is due to the usage of carbonate staining method described in Eilu et al. (1999). Abbreviations: Ab = albite, Ank = ankerite, Apy = arsenopyrite, Cal = Calcite, Ccp = chalcopyrite Fe-Dol = Fe-dolomite, Gdf = gersdorffite, Gr = graphite, Kfs = K-feldspar, Po = pyrrhotite, Py = pyrite, Rt = rutile, Ser = sericite, Qtz = quartz, LV = Levijärvi lode, PA = Paaminamaa lode, TP = Tienpää lode.

many other characteristically different vein types. Part of this variation in vein characteristics can be simply related to the lateral alteration zonation (which is also expressed in vein compositions) that surrounds the gold occurrence: examples of this are the *quartz-calcite veins and veinlets* that occur in areas distal to mineralisation, particularly in the massive Fe-tholeiitic footwall (Figs. 2 and 4). They are typically irregular in shape, fine-grained and light grey (quartz) to white (calcite) (Fig. 6a). They are a few centimetres wide at most. In addition to such veins and veinlets, there are also breccias (Figs. 7c and 8c). All these may contain minor amounts of pyrrhotite and chalcopyrite, the veins nevertheless more frequently. Breccias are commonly related to areas where alteration (interpreted to be pre-gold in timing) has made rocks more competent, but such an alteration has not been a prerequisite for brecciation (cf. Figs. 7c and 8c).

Carbonate-dominated quartz-carbonate veins are the most widespread and voluminous vein types in the area, amounting to over 70 % of all veins in drill core. However, only a small proportion of these bear *all* the characteristics of sulpharsenide-rich quartz-carbonate-sulphide veins (i.e. the vein type most of the gold is associated with). *Quartz-dominated veins* fall into two groups, one being older (Fig. 7a) and one younger than carbonate-dominated veins. The younger type of veins are broader, coarser and less deformed than any other vein type. As they also are practically barren of ore minerals, they are not dealt here in more detail.

Main alteration features

The chemical character of mafic and ultramafic rocks in the area, comprising tuffitic, pyroclastic and massive units, has contributed to the presence of biotite, chlorite, talc and especially the various carbonate species. Where alteration is absent or less intense, the mineral assemblages in the rocks are found to be typical to greenschist facies conditions.

The metakomatiite unit (hanging wall): Weakly to moderately altered metakomatiites are grey due to prevailing carbonation. More intensively altered types are green-coloured and typically also more veined, their distinct colour resulting from fuchsite (Figs. 8f and 8g). Less altered metakomatiites may contain talc and chlorite instead of fuchsite and the least altered biotite instead of fuchsite. It is interpreted here that biotite is primarily metamorphic in origin; however, a

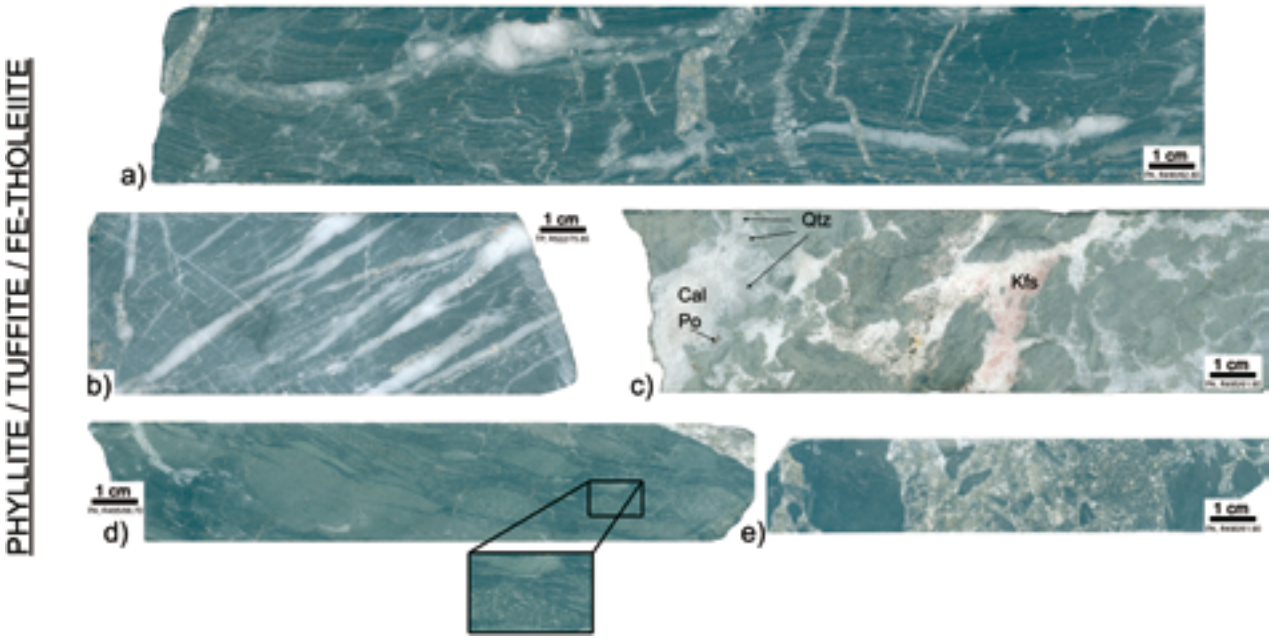

Fig. 7. Main lithologic and vein features of phyllite, tuffite and Fe-tholeiite. **a.** Carbonate-dominated quartz-carbonate veins, the most common vein type in the occurrence. Note that these veins are build upon earlier bedding-parallel, boudinaged quartz veins. Although quartz-carbonate veins in phyllite and tuffite are generally not as rich in sulphides as the quartz-carbonate-sulphide veins in graphitic phyllite (e.g. Figs. 6d–6g), these veins are part of the same veining stage(s). Such an interpretation gets support from the fact that many veins in graphitic phyllite are lacking sulphides, similarly to the veins shown in this figure and Fig. 7e. In addition, sulpharsenide-rich veins are met every now and then in phyllite and tuffite. **b.** Exceptionally hard and rigid SiO_2-rich rock. The light-grey tightly folded strips are either early quartz veins or folded chert layers. **c.** Distal quartz-calcite veinlets in the Fe-tholeiitic footwall. Note the lack of bleaching (cf. Fig. 8c). **d.** Almost an unaltered, mafic, clast-rich volcanogenic conglomerate, probably pyroclastic in origin. This rock type occures in places in the weakly altered Fe-tholeiitic footwall. Note that there is no alteration relating to the quartz-carbonate-sulphide vein in the upper right-hand corner. **e.** Relatively broad barren carbonate-dominated quartz-carbonate vein, otherwise similar to the gold-rich quartz-carbonate-sulphide veins. Note the vein breccia clasts from the wall rocks. Note also that there is no related bleaching. For abbreviations, see Fig. 6.

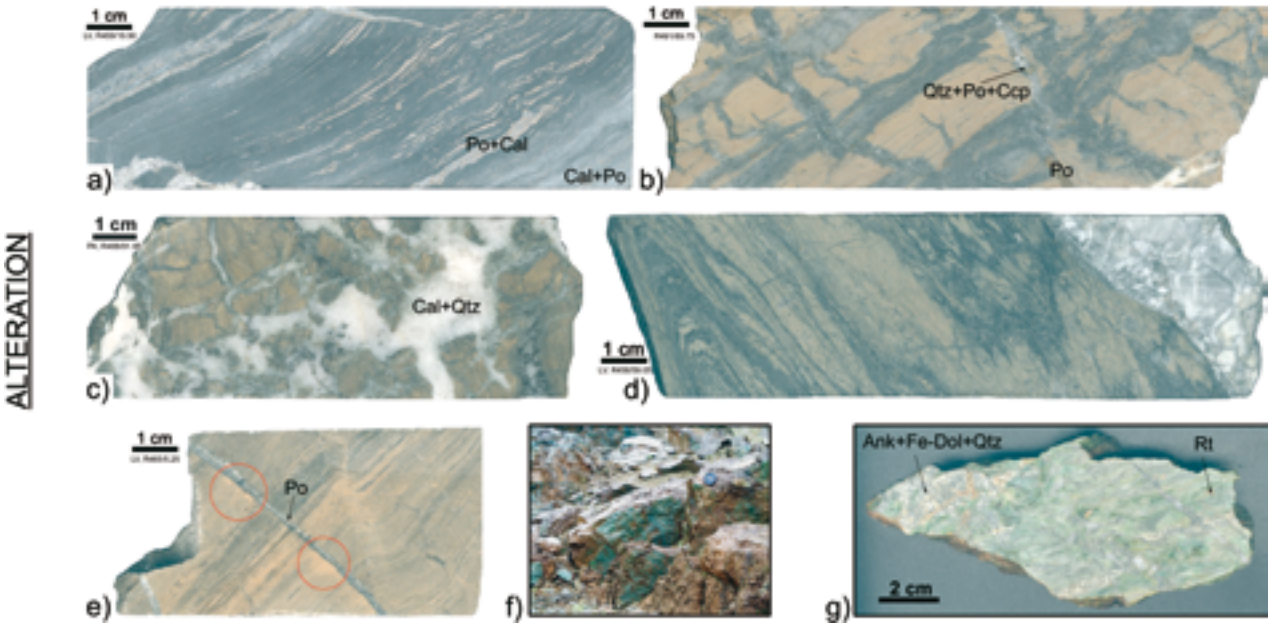

Fig. 8. Main lithologic and alteration features at Levijärvi-Loukinen. Footwall: **a.** Locally carbonated and sulphidised graphitic phyllite. **b.** Intensively bleached fine-grained schist containing hard bedding-parallel layers, which are here interpreted to be chert. The quartz-carbonate veins have pyrrhotite and chalcopyrite and the veins overprint the alteration. **c.** Intensively bleached volcanic rock where alteration predates gold mineralisation. Breccia infill is dominated by quartz and calcite, the minerals contributing to the distal alteration around the gold occurrence by occurring in narrow veins and veinlets and slightly larger breccias and as dissemination in wall rocks. **d.** Sericite-albite-altered tuffite where alteration predates gold mineralisation. The carbonate-rich vein cutting the intensively folded rock with sharp contacts contains pyrrhotite and chalcopyrite. **e.** Altered fine-grained schist. Most of the sericite-carbonate-albite-dominated alteration seen here is assumed to be earlier than gold mineralisation (cf. Figs. 8b–8d). Yet, at least part of the bleaching is related to the thin carbonate vein (red circles). Hanging wall: **f.** Intensively sericitised and carbonated metakomatiite outcrop, Tienpää. This so-called listvenite gets it distinct colour from fuchsite (Cr-muscovite) and weathered carbonate. Diameter of the lens cap is about 6 cm. **g.** Close-up from a highly sericitised and carbonated listvenite that is rich in quartz-carbonate veins, Levijärvi. For abbreviations, see Fig. 6.

more detailed study on alteration assemblages should be carried out until the question whether there exists also hydrothermal biotite, relating to one or more of the many alteration stages the host sequence has undergone, can be answered with confidence. It must be emphasised, also, that while altered metakomatiitic rocks have been found to host gold mineralisation only in the central and eastern part of the Levijärvi-Loukinen area, some of the most intensively altered types are found west at Levijärvi (Fig. 8g). Mineralogically, the carbonated and sericitised ultramafic rocks are dominated by quartz, carbonate, fuchsite and pyrite. Typical accessory minerals include one or more of the following: chalcopyrite, pentlandite, chlorite, biotite and rutile. Relict chromite is common and it is inherited from the metakomatiitic protoliths.

Terms used in the literature for describing altered ultramafic rocks of the Sattasvaara Formation include such descriptive terms as *chromian marble* (Pekkala & Puustinen 1978), *green carbonate rock* (Keinänen 1994) and *listvenite* (Riikonen 1997). We favour the term listvenite, the etymology and meaning that are discussed in Halls and Zhao (1995). Relatively weakly altered types are called *talc-carbonate schists*, *talc-magnesite schists* or *soapstones* (Ohlson 1969), all being terms that illustrate their high talc content. Note that according to Pekkala & Puustinen (1978) the intensively altered "chromian *marbles*" were primarily of sedimentary origin, but the current consensus is that these rocks are hydrothermally altered metakomatiitic rocks.

The volcano-sedimentary unit (footwall): The most common mineral assemblage in the proximal alteration zone in the clastic metasedimentary rocks is quartz-carbonate-sericite-albite. Chlorite is related to tuffaceous interbeds.

In response to the varying ratios of alteration among the highly stratified and variable strained volcano-sedimentary rocks, such descriptive field names as *sericite schist*, *albite-sericite schist*, *sericite-carbonate-albite schist*, and *carbonate-chlorite schist* have been used frequently in drill-core reports. The term *albitite* is one that has been used widely in the domestic literature to describe the regional spatial association of gold mineralisation, albite alteration and metasedimentary rocks in northern Finland. We do not use this term, because albite alteration is less wide spread at Levijärvi-Loukinen than it is illustrated to be in some other gold mineralised areas in CLGB. If there is strong albitisation somewhere in the host sequence, so intense that it bleaches the rocks, it is mainly outside the drilled area. Yet, there are some bleached rocks encountered here and there in the drill core, but their amount is relatively minor and they do not appear to be as rich in veins as some other rock types. This strongly suggests that this type of alteration predates gold mineralisation.

From all major rock types the least deformed and altered are the Fe-tholeiitic footwall rocks. They commonly show only distal alteration assemblages dominated by carbonate and chlorite (Fig. 7d). Locally, though, intense bleaching-type of alteration has taken place (Fig. 8c). As said above, this alteration is apparently an early feature; this is suggested from that there are no related veins, except some casual narrow calcite-quartz veins or breccias attributed to distal gold-related alteration. Such veins and breccias are more common in areas of low degree of bleaching-type of alteration (Fig. 7c).

The locally occurring high SiO_2 content in rocks ("silicification") is generally related to early quartz veins. Locally, if this is not the case, hard silica-rich rocks are considered to be primary chert (Figs. 7b and 8b). **Sulphidation** is generally rather weak, but in some instances the first few centimetres surrounding the veins are rich in arsenopyrite, pyrrhotite, pyrite and/or chalcopyrite. Pyrite is a major alteration phase only in carbonate-fuchsite altered metakomatiitic rocks, whereas the other three may occur in all rock types. Seemingly strong sulphidation may occur in locations where veins cut graphitic rocks that comprise stratabound sulphides (mostly pyrrhotite) or where pyrrhotite, chalcopyrite and/or pyrite have been deposited as veinlets together with quartz and calcite (Figs. 6b and 8a). Sulphidation may reach its highest intensity also in areas where sulphide-rich vein stockworks have been sheared and their sulphides mechanically dispersed and/or hydrothermally remobilised into the intensively deformed wall rocks. Pyrrhotite is more common than pyrite in the proximal alteration zones which suggests deposition in the upper greenschist facies conditions (Eilu et al. 1999). This, however, may also be a result of local variations in physico-chemical parameters.

It is evident that gold mineralisation occurred without much of a formation of **oxides**, the only notable exceptions being rutile and ilmenite, which are rather common accessory minerals in altered rocks. On the contrary, earlier formed magnetite was destroyed in all places where the rocks were altered by fluids.

To conclude proximal alteration assemblages surrounding gold-related veins and sulphidised breccias vary in accordance with lithology. The most general types of alteration are carbonation, sericitisation (or fuchsite formation), chloritisation and, in lesser extent, albitisation. Carbonation and sericitisation are especially important styles in the most altered ultramafic rocks, i.e. listvenites (Figs. 8f and 8g). These rocks

are variably bleached in places where several of these alterations occurred simultaneously. Observations on drill core suggest also that footwall albitisation is not as widespread and intense as it is in some other locations along SSZ, at least not in the drilled area. The most bleached rocks are similar to those presented in the Figures 8b–8e. It is suggested that although these rocks were probably more competent that they surroundings, they were not the best host rock for the veins related to the gold mineralisation. Current results indicate that if there are veins or breccias, they are dominated by quartz and calcite that characterise distal veins to the gold occurrence.

The given characteristics point towards mid- to upper-greenschist facies conditions during metamorphism, and that the gold mineralisation occurred slightly after the peak metamorphic conditions.

GOLD OCCURRENCE

Mineralisation styles

Two textural types of gold mineralisation have been recognised: *vein- and shear-hosted*. Most breccia-like textures simply represent multiply veined stockworks rather than large-scale true breccia veins formed in one event of extensive fracturing (Valenta et al. 1994, Robert & Poulsen 2001). Hence, the abundance, or the lack thereof, of true breccia veins is uncertain. They may exist in some structurally favourable sites nevertheless (e.g. in the most competent parts of the sequence).

Vein mineralisation: An ordinary quartz-carbonate vein stockwork is clearly formed by veins stacked on one another. Separate veins range in width from a few millimetres up to 10 centimetres, while stacked arrays of such veins can be as wide as 25 m (at Levijärvi). The sulphide content typically average 1–5 vol.%, but in some veins ore minerals dominate the vein mineralogy to the rare extreme of 100 vol.%. In many cases the sulphides are concentrated to form accumulations separated by barren gangue. Richest accumulations of sulphides are spatially related to graphite (Figs. 6d–6g).

To highlight that there exists a close spatial association between gold and sulphides, and to discriminate the gold-related veins from barren quartz-carbonate veins, gold-rich veins are termed *quartz-carbonate-sulphide veins* throughout the work.

Shear-hosted gold mineralisation: In areas where strain has progressively accumulated upon previously emplaced vein arrays, there are up to tens of metres wide zones of highly deformed rock containing fragmented and/or boudinaged veins in a fine-grained, dark and variably sulphidised matrix. The matrix is typically rich in graphite. Such sheared zones are typified by well-developed foliation and an overall brittle-ductile style of deformation (Fig. 9). Some parts of the shears are gold mineralised owing to the earlier existence of gold-hosting quartz-carbonate-sulphide veins. In places where the veins used to be sulphide-rich, the sulphides have been mechanically dispersed and/or hydrothermally remobilised into the wall rocks. This may cause the rocks to look like they are sulphidised more intensively than usual.

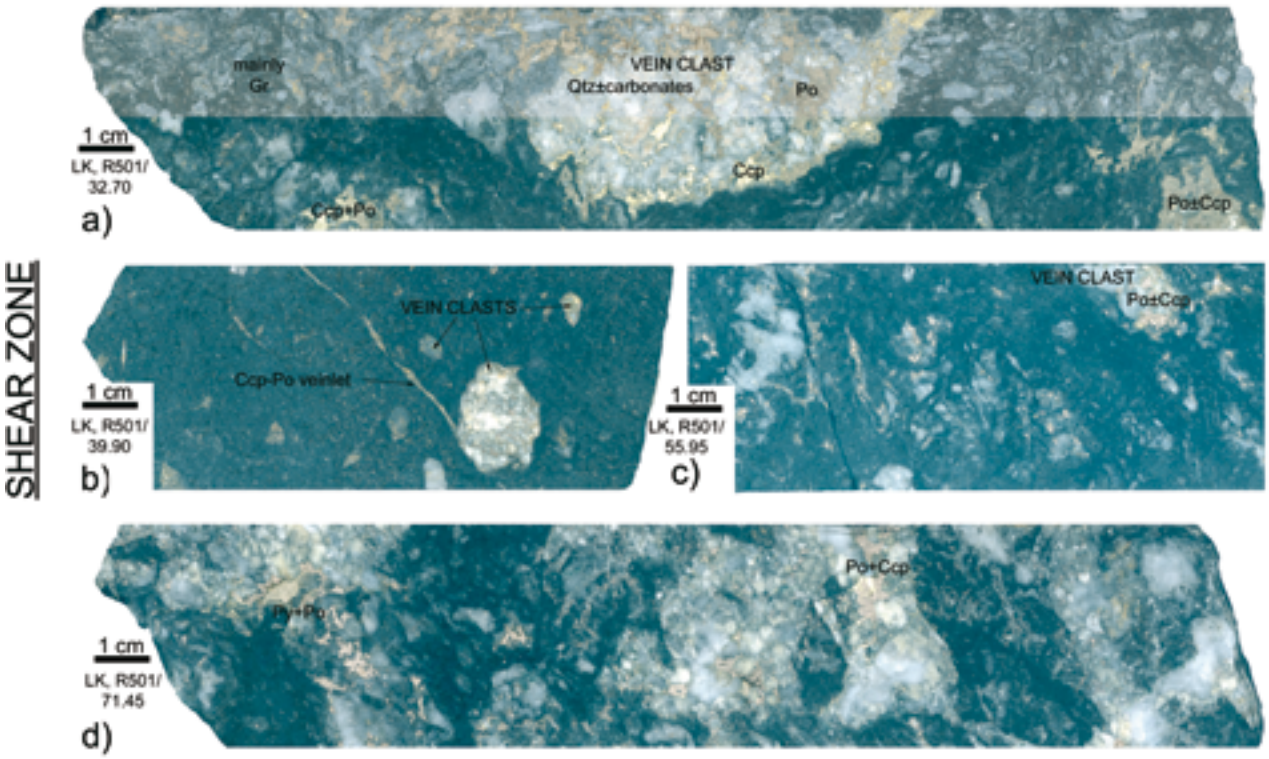

Fig. 9. Shear zone. In some of the figures contrast has been exaggerated to promote better distinction between different mineral phases. All the photographs shown here are taken from the same drill core from Loukinen (M52/2741/98/R501). This hole is drilled towards north so that it intercepts the E-striking shear zone. Although it does not reach as high gold grades as the nearby-located drill holes R515–R519, drilled towards west, it shows the same features. In the drill core R501, the section ~22–34 m is fine-grained schist (phyllite/tuffite) cut by a quartz-carbonate vein stockwork, the individual veins of which are relatively well preserved. Some veins contain sulpharsenides (at least gersdorffite). The section ~34–76 m is dominated by ductilely deformed graphitic phyllite in where most veins are sheared into tiny fragments. Although the veins are now mostly destroyed, this section was once rich in quartz-carbonate-sulphide veins containing gersdorffite, pyrrhotite and chalcopyrite. However, gold grades are noteworthy only between ~32–38 m (up to 0.24 ppm). **a.** Moderately deformed graphitic phyllite containing fragments of gold-related veins from a depth of 32.70 m. The upper half of the photo is taken from a dry surface, whereas in the lower half the surface is wet. **b.** Highly deformed graphitic phyllite from a depth of 39.90 m. Vein clasts contain pyrrhotite and chalcopyrite. These minerals occur also in the graphitic matrix. **c.** Highly deformed graphitic phyllite from a depth of 55.95 m. **d.** Moderately deformed graphitic phyllite from a depth of 71.45 m. For abbreviations, see Fig. 6.

Lodes

Mineralisation consists of four potentially economic lodes: Levijärvi, Paaminamaa, Loukinen and Tienpää (Fig. 2). Each of these is up to a few hundreds of metres long and tens of metres wide. Their continuations at depth are open. For detailed characterisation of the four lodes, see Table 2.

Of the four lodes, a mineral resource estimate has been done only for **Levijärvi** occurrence (Koistinen et al. 2000). There the up to 25 m wide mineralised zone has been delineated by diamond drilling for 700 metres along strike to a depth of 30–110 m. Its indicated mineral resources are 0.114 Mt @ 0.5 ppm Au (at a cut-off grade 0.2 ppm) and 0.45 % Ni, or, alternatively, 9 500 tons @ 1.47 ppm Au (at a cut-off grade 1.0 ppm) and 0.25 % Ni. However, both tonnages and ore grades are considered conservative, since the mineralisation is open at depth and its eastern continuations were not included into the estimation.

The best intersections in other three lodes include: **Paaminamaa:** 1.52 % Cu @ 12.4 m and 0.44 ppm Au @ 5.4 m (drill hole R479); **Loukinen:** 0.53 % Cu @ 76.1 m (R511), 0.47 ppm Au @ 20 m (R511) and 8.51 ppm Au @ 0.5 m (R498); **Tienpää:** 2.85 % Ni @ 12.75 m (R522) and 3.87 ppm Au @ 1.6 m (R522).

Table 2. List of the main features of gold mineralisation at Levijärvi-Loukinen. Some information may be inaccurate, as the availability of detailed data varies between the lodes (* = not studied as intensively as this subject category in the case of the Levijärvi lode). Note that all host rocks are metamorphosed, and the prefix meta is omitted from the rock names. Data derived from the present study and from Holma (2001), Keinänen & Holma (2001), Keinänen et al. (2001), Koistinen et al. (2000), Holma et al. (2003) and Holma (2006).

	Levijärvi	**Paaminamaa**	**Loukinen**	**Tienpää**
Commodities:	Au-Ni (± Cu)	Cu-Au-Ni	Cu-Ni-Au	Ni-Cu-Au
Sirkka Shear Zone:	E-W	WNW-ESE	E-W	WNW-ESE
Known mineralisation: Size	60 x 700 m	60 x 500 m (irregular)	70 x 250 m (mainly irregular)	40 x 80 m
Dip	Variably to south	Steeply to south	Steeply to south	Steeply to south
Ore fabric[1]	Vein stockworks	Shear-hosted: veined zones brecciated due to prolonged shearing	Shear-hosted: veined zones brecciated due to prolonged shearing	Vein stockworks
Geology: Footwall[2] / Hanging wall[3]	Volcano-sedimentary unit[4] / Metakomatiite unit[4]	Volcano-sedimentary unit[4] / Metakomatiite unit[4]	The arrangement of the metakomatiite and volcano-sedimentary units[4] is complex	The arrangement of the metakomatiite and volcano-sedimentary units[4] is complex
Major host rocks	Phyllite, tuffite and graphitic phyllite	Phyllite, tuffite and graphitic phyllite	Variably altered komatiite and phyllite, tuffite and graphitic phyllite	Variably altered komatiite and phyllite, tuffite and graphitic phyllite
Minor host rocks	Intensively altered komatiite (listvenite) may have some potential for gold	Variably altered komatiite		
Intrusives	Minor pre-gold dolerite	Not studied	Not studied	Not studied
Alteration assemblages (in major host rocks)	Quartz-carbonate-sericite-albite±sulphides in clastic sedimentary rocks, chlorite common in tuffaceous interbeds	Quartz-carbonate-sericite-albite±sulphides in clastic sedimentary rocks, chlorite common in tuffaceous interbeds	Quartz-carbonate-fuchsite-pyrite in intensively altered komatiite (listvenite); biotite, talc and/or carbonate in less altered types Quartz-carbonate-sericite-albite±sulphides in clastic sedimentary rocks, chlorite common in tuffaceous interbeds	Quartz-carbonate-fuchsite-pyrite in intensively altered komatiite (listvenite); biotite, talc and/or carbonate in less altered types Quartz-carbonate-sericite-albite±sulphides in clastic sedimentary rocks, chlorite common in tuffaceous interbeds
Mineralogy: Vein gangue	Ankerite and Fe-dolomite ± quartz, siderite, Fe-magnesite, albite, K-feldspar, chlorite	* Ankerite and Fe-dolomite ± quartz, albite, K-feldspar, chlorite	* Ankerite and Fe-dolomite ± quartz	* Ankerite and Fe-dolomite ± quartz
Major ore minerals	Pyrrhotite, chalcopyrite, pyrite[5], locally also gersdorffite and arsenopyrite	Chalcopyrite, pyrrhotite, pyrite[5], locally also gersdorffite and arsenopyrite	Pyrrhotite, chalcopyrite, pyrite[5] and locally gersdorffite	Gersdorffite, arsenopyrite, pyrite[5], pyrrhotite and chalcopyrite
Minor ore minerals	Glaucodot, cobaltite, pentlandite, violarite, safflorite, löllingite, rammelsbergite, millerite, bismuthinite, cassiterite, sphalerite, galena, rutile, ilmenite, apatite, monazite, xenotime, marcasite, Ni-Sb-Bi-S phase (hauchecornite?), Sb-bearing gersdorffite (corynite?), several U-bearing minerals (uraninite, coffinite?), several unspecified Bi-tellurides, native bismuth, native gold and maldonite	Glaucodot, pentlandite, argentopentlandite, sphalerite, ullmannite, rutile, ilmenite, apatite, monazite, U-minerals (brannerite?), hessite and native gold	* Arsenopyrite, pentlandite, argentopentlandite, galena, sphalerite, molybdenite and native gold	* Native gold
Siting of gold	Inclusions and fracture fillings in all type of sulpharsenides	* Inclusions in pyrite and gersdorffite; fracture fillings in sulphides; free gold among quartz	* Inclusions and fracture fillings in pyrite and gersdorffite; free gold	* Inclusions in pyrite, but probably also in sulpharsenides (this has not been studied yet)

[1]Only the dominant case is given
[2]Belongs to the 2.13–2.05 Ga Matarakoski Formation of the Savukoski Group
[3]Belongs to the >2.05 Ga Sattasvaara Formation of the Savukoski Group
[4]For description, see text
[5]Generally pyrite shows characteristics that refer more towards metamorphic origin (recrystallised from pyrrhotite) than to genuine hydrothermal origin. Yet, pyrite seems to be a direct hydrothermal precipitate in some veins. The latter veins are paragenetically different than the gold-hosting quartz-carbonate-sulphide veins and are possibly not related to gold at all

Ore minerals and their assemblages and textures

General characteristics of quartz-carbonate-sulphide veins

In gold-related veins, gangue mineralogy is dominated by the carbonates ankerite, Fe-dolomite and minor siderite, calcite and magnesite, the combined abundance of which generally surpasses that of quartz (Figs. 6c–6f and 7e). Quartz is grey and fine-grained and mainly concentred on vein interiors. Albite, muscovite, biotite and chlorite are typical, although non-ubiquitous, accessory constituents. In addition, minor to rare tourmaline, K-feldspar, apatite, monazite and xenotime have been met in some vein samples.

There exists a correlation between the oxidation states of ore mineral assemblages in veins and the country rocks the veins are hosted: e.g. reduced pyrrhotite-dominated mineral assemblages typically constitute the veins in graphite-bearing rocks. The main Fe-sulphide in veins hosted by carbonate-fuchsite altered metakomatiite is pyrite. Sulpharsenides are primarily related to the volcano-sedimentary unit and particularly to its graphite-rich parts. As the local sulpharsenides are typically associated with gold, the graphite-rich rocks are also the main host for gold mineralisation. Yet, similar veins are also known to cut across lithologic contacts as well as occupying shears. In places where the veins are shear-controlled, they are notably deformed (Fig. 9).

Mineralisation contains the following main paragenetic sulphide and sulpharsenide assemblages: 1) pyrrhotite, 2) pyrrhotite – chalcopyrite, 3) pyrrhotite – chalcopyrite – pyrite, 4) pyrrhotite – pyrite, 5) chalcopyrite, 6) chalcopyrite – pyrite, 7) pyrrhotite – chalcopyrite – pyrite – sulpharsenide(s), and 8) sulpharsenide(s). The sulpharsenide species is generally arsenopyrite, gersdorffite or a complex mixture of the two and cobaltite ± glaucodot. Some veins are devoid of gangue minerals so that the veins are compact sulphide/sulpharsenide veins. There is only little variation in the given patterns along this five km long mineralisation.

Sulphide and arsenic minerals

By volume, the most common ore minerals are pyrrhotite, chalcopyrite and pyrite. In the volcano-sedimentary unit, pyrite is generally associated with the other two ore minerals, while in the intensively altered ultramafics it is the most common ore mineral. All these three common sulphides may also occur as low-grade dissemination surrounding the veins and as in up to few centimetres wide compact, sulphide-only type of veins (Figs. 6b and 6c). See Table 2 for a comprehensive list of detected ore minerals.

Most of the sulpharsenides are precipitated close to the vein margins, but locally dissemination may prevail immediately adjacent to the veins (Figs. 6d–6g). Arsenopyrite [FeAsS] and gersdorffite [(Co,Fe)AsS – NiAsS] are the dominant sulpharsenide minerals. Cobaltite [CoAsS] and glaucodot [(Co,Fe)AsS)] are also met, but their distribution is much more restricted.

Only two mineral species of the löllingite group have been met: safflorite [$(Co,Fe)As_2$] and löllingite [$FeAs_2$]. They are very rare and occur only as tiny inclusions in the major sulpharsenides.

Gold and other native and intermetallic minerals

Native gold with Ag-content <25 wt.% (with at least two modes: one of relatively free of Ag and another with ~15–25 wt.% Ag) and an average grain size of 10–25 µm is by far the most common form of gold at Levijärvi-Loukinen (Fig. 10). It occurs mainly as inclusions and in narrow fractures within gersdorffite,

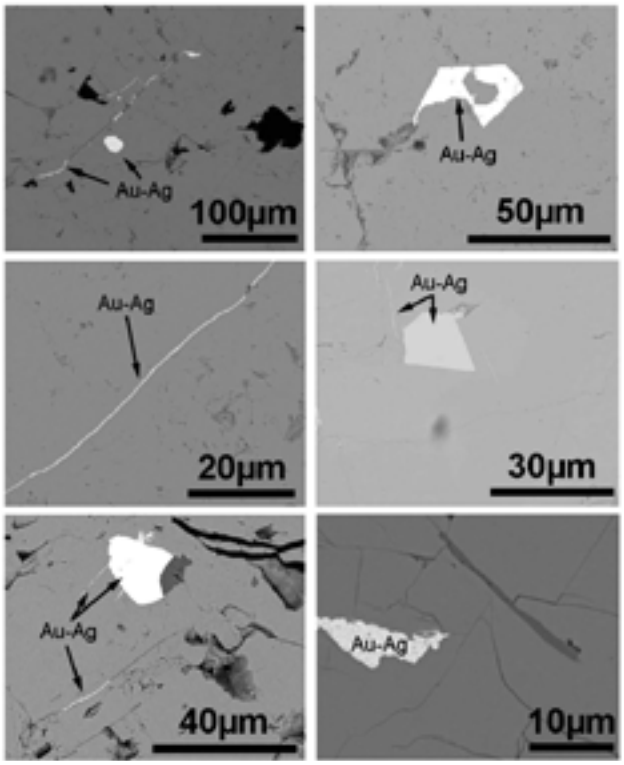

Fig. 10. Photomicrographs of native gold (Au-Ag) in Levijärvi-Loukinen. Most grains are droplet-like or somewhat angular in shape. Some grains are associated with micron-sized fractures filled by native gold. Some of these forms suggest that at least part of the gold could have been derived from the host sulpharsenide, from where it could have been exsolved into the fractures during cooling. However, so far no refractory gold has been found in any of the sulpharsenide grains. In all the given examples, gold is hosted by a sulpharsenide species (either arsenopyrite or gersdorffite). SEM BE-images.

arsenopyrite and Co-rich sulpharsenide (glaucodot and rare cobaltite). Places, also pyrite may be associated with native gold. There are also a few observations of free gold in vein quartz.

In addition to native gold, the intermetallic minerals Au_2Bi (maldonite) and Ag_2Te (hessite) have been observed in some samples. To underline that there truly exists a close association between Bi, Te and Au, some gersdorffite grains have been found to contain inclusions of native bismuth. As no refractory gold has been found on any analyses on sulpharsenides, for example, it is likely that it is a minor constituent at the most.

DISCUSSION

About the main abnormalities of the Levijärvi-Loukinen gold occurrence

The characteristics of the Levijärvi-Loukinen gold occurrence are consistent with the *atypical metal association* subtype of orogenic gold mineralisation. This term is used here in the same sense as Groves et al. (2003) uses it.

Orogenic gold mineralisation in the Kittilä greenstone area of CLGB can be subdivided into two end members: *gold-only* and *multimetallic (atypical metal association)*. Gold-only mineralisation is the dominant type. The multimetallic occurrences include Levijärvi-Loukinen and Sirkka (Fig. 1). Deposits and occurrences of this category are exceptional by having atypical metal association for orogenic gold: Cu, Fe, Ni, Au ± Ag, Co. Except their respective metal associations, the two deposit groups have overlapping characteristics. This is nowhere clearer than in SSZ (Fig. 1).

One of the uncommon features of the Levijärvi-Loukinen gold occurrence is the high abundance of gersdorffite [(Co,Fe)AsS – NiAsS] in the ore. Worldwide, gersdorffite is an unusual mineral in most of the known ore deposits, whatever the genetic background of the deposit may be. It is not that it is exceedingly rare itself, but merely that generally it is an accessory phase. However, in a small group of deposits gersdorffite may be an important ore-forming mineral (Jackson et al. 2003). Generally gersdorffite is related to magmatic ore deposits, especially if other nickeliferous minerals are present as well (e.g. pentlandite). Some gersdorffite-rich deposits – but not Levijärvi-Loukinen – are enriched in platinum group elements. The inferred genetic origins of these deposits vary from Sudbury-type of deposits to orebodies hosted by layered mafic to ultramafic igneous complexes.

The occurrence of gersdorffite in a hydrothermal vein deposit generally means that there are ultramafic rocks somewhere in the vicinity. This holds true also in the current study area. In most orogenic gold deposits gersdorffite is, if present at all, only a minor constituent of the ore. In contrast, at Levijärvi-Loukinen gersdorffite is one of the most voluminous ore minerals and there is no doubt that gold is directly associated with this mineral in particular.

According to Eilu et al. 2006 (*this volume*), pyrite is the major Fe-sulphide in CLGB. At Levijärvi-Loukinen the overall mineralogical composition of veins is a very specific one when compared to the majority of gold occurrences in the Kittilä greenstone area (if the whole northern Finland is considered, there are some similarities between the gold occurrences in the Kuusamo schist belt and the multimetallic occurrences of the Kittilä greenstone area). Besides, most of the Fe is incorporated into pyrrhotite, not in pyrite. This difference in gold-related mineral assemblages between different occurrences is a feature that seems to be closely related to different oxidation states of the deposit-hosting rocks. For example, at Levijärvi-Loukinen fractures observed in carbonate-fuchsite altered metakomatiite and other metavolcanic rocks are filled with carbonate, quartz and either pyrite or pyrrhotite, whereas otherwise similar veins in metasedimentary rocks are typically rich in pyrrhotite in lieu of pyrite. In those occurrences where majority of gold-rich veins occur in metakomatiitic rocks, pyrite in excess of pyrrhotite is the only main Fe-sulphide (e.g. at Päivänenä; Fig. 1). If this scheme is valid, then the two gold mineralisation subtypes of SSZ, i.e. the multimetallic (atypical metal association) and gold-only subtypes, are merely dissimilar in their vein characteristics because of different primary and/or altered rock types.

The enrichment of elements like Fe, Cu, Ni and Co in the occurrence can be seen as a logical consequence of the lithology built up from ultramafic and mafic volcanic rocks in close contact with reducing graphitic metasedimentary rocks. In this kind of view, the altered ultramafics are seen as the most likely source of Ni±Cu±Co. Iron could have been gathered from all rock types, including the mafic rocks. Graphitic metasedimentary rocks are a potential source for S±As as well as Cu and Fe. Highly to moderately

saline fluids are generally suggested from this type of sulphide-rich multimetallic mineralisation. The very preliminary results of the on-going fluid inclusion study on the samples from Levijärvi-Loukinen suggest saline fluids. Also previous studies on other deposits in the northern Fennoscandian Shield have shown that in many cases the fluids were anomalously saline (e.g. Frietsch et al. 1997, Martinsson 1997, Ettner et al. 1999, Vanhanen 2001).

Levijärvi-Loukinen: an example of orogenic gold mineralisation with atypical metal association

In orogenic gold systems, hydrothermal fluids are typically dilute aqueous carbonic fluids, with 5–30 mole % of $CO_2 \pm CH_4$. Fluid salinities are uniformly low (≤6 wt.% NaCl equivalent). Fluids are usually interpreted to have been derived from one or a combination of deep-seated sources. Most of the deposits are structurally hosted and generally restricted to the brittle-ductile transition in terranes that underwent greenschist facies metamorphism. Some deposits are hosted in terranes that show sub-greenschist, amphibolite, and even granulite facies metamorphism. In the orogenic gold deposit model, the deposits are seen as a logical consequence of the interaction between fluids and the rising mountain range, the mountains of which through the fluids circulate during compressional to transpressional deformation. The orogenic event is accretionary or collisional in character (Groves et al. 1998). A given orogenic gold deposit or occurrence is characteristically associated with major or lower-order tectonic structures in deformed and metamorphosed mid-crustal blocks of diverse ages (Bierlein & Crowe 2000, Hagemann & Cassidy 2000, Partington & Williams 2000).

Orogenic gold deposits are typically enriched in Au with Ag, Te, S, As, Bi, Sb, W, K, Cs, Rb and SiO_2, but rarely in base metals (Ridley 1997, McCuaig & Kerrich 1998, Eilu et al. 2006, *this volume*). As reviewed in this volume by Eilu et al., most of CLGB- and also SSZ-hosted gold occurrences show resemblance with ordinary orogenic gold deposits in their main characteristics. The main ore minerals in these so-called *gold-only* occurrences are, in order of abundance, pyrite, arsenopyrite and pyrrhotite. In the Päivänenä-Hirvilavanmaa area (Fig. 1), for example, gold is closely related to pyrite or occurs free within the quartz-carbonate gangue (Härkönen & Keinänen 1989, Keinänen & Hulkki 1992, Hulkki & Keinänen 2006, *this volume*). A typical CLGB-hosted gold-only occurrence displays enrichment in Au, Ag, As, Bi, CO_2, K, Rb, S, Sb, Te, and W (Eilu et al. 2006, *this volume*).

In contrast, occurrences of the atypical metal association type in the current study area are enriched in a larger set of metals and ore minerals. They show not only enrichment in the same suite of elements than the gold-only subtype, but also in Cu, Ni, Co and, in some localities, U. Also the amount of sulphides in them tends to surpass that in the gold-only occurrences. In short, the occurrences are polysulphidic and multimetallic compared to the gold-only occurrences.

The nearest known intrusive rocks to the Levijärvi-Loukinen occurrence, if pre-gold metadolerites are excluded, lie over 12 km to the north and northwest and 18 km to the south. Besides these, there is an obvious lack of major intrusive bodies anywhere near the occurrence, at least at the present erosional level (Fig. 1). Certainly this alone does not prove that there could not exis a genetic link between plutons and mineralisation. However, there probably is no intimate, not at least direct, relationship between the occurrence and intrusive rocks. Such a conclusion is drawn from: 1) typical skarn-related mineral associations are lacking from Levijärvi-Loukinen; 2) there is a significant scarcity of Fe-oxides; 3) mineralisation is in proximity to a large-scale fluid conduit with typical mid-crustal deformation features and mesothermal alteration patterns.

Except the composition of the fluid, most of the main features of orogenic gold deposits are met at Levijärvi-Loukinen. For example mineralisation probably took place at ~300–475°C and 1.5–3 kbar (inferred from the alteration and vein mineral assemblages) which conditions are typical to mesozonal subtype of orogenic gold mineralisation. Also the following criteria are used as basis to classify the Levijärvi-Loukinen occurrence into the category of orogenic gold mineralisation: 1) there are no indications of crustiform or colloform textures, which are diagnostic to the epizonal environment; 2) textures relating to brittle–ductile deformation and mesozonal environment are ubiquitous; 3) there is a lack of true disseminated ore bodies, which are common features of deep-seated deposits. Dissemination is notable only in ductile shear zones and in some graphite-rich rocks where there are narrow sulphide-rich veinlets. Sulphide dissemination in shear zones is traceable to distorted and fragmented veins and hence is thought to be of secondary origin. Taking all the above-mentioned aspects into account with those more specific characteristics presented in Table 2, the occurrences discussed here fall most easily into the orogenic gold category than into any other current deposit class.

SUMMARY AND CONCLUSIONS

Orogenic gold mineralisation in the Palaeoproterozoic Central Lapland greenstone belt (CLGB) of northern Finland can be divided into two subtypes: gold-only and multimetallic (atypical metal association). Most of the deposits and drilling-indicated gold occurrences are somehow related to the Sirkka Shear Zone (SSZ) (also known by the name Sirkka Line) that is considered to be a steeply southward dipping and ~150 km long collision-related shear and thrust fault system. It hosts both gold-only and multimetallic occurrences, but principally in different segments. Known multimetallic occurrences are clustered in the westernmost 35 km of SSZ and do not occur elsewhere, at least not with identical characteristics. In contrast, gold-only type of occurrences have been scattered more evenly across CLGB.

This paper describes and defines the main characteristics of the multimetallic Levijärvi-Loukinen occurrence. This undeveloped occurrence is one of the easternmost of its kind in SSZ; it locates ~25 km east of the Saattopora Au-Cu mine, which is also an atypical metal association gold deposit in CLGB (mined 1988–1995).

The Levijärvi-Loukinen occurrence comprises four lodes. The metal association of the occurrence is "atypical", because of Cu, Fe, Ni, Au ± Ag, Co, the metals the occurrence is enriched in. Potential commodities are Au, Cu ± Ni, Co. Gold grades locally exceed five ppm in drill core, but best gold grades are up to ~25 ppm (analysed from a costean sample).

The auriferous veins at Levijärvi-Loukinen have preferentially developed in the most competent and reactive rocks in the area: carbonate-fuchsite altered metakomatiite and a sequence of quartz-carbonate-sericite-albite altered phyllite, tuffite and graphitic phyllite. These rocks, which are representative of the >2.05 Ga Savukoski Group, are in close contact with each other and, due to fracturing, have offered a relatively easy passage for metal-bearing fluids. Earlier carbonation of metakomatiite and albitisation of fine-grained schists were probably both important events for the subsequent fracturing, as they could have made these rock types more competent with respect to their less-altered country rocks, which comprise mainly massive to pyroclastic Fe-tholeiites. However, albitisation is not as evident nor extent as it is elsewhere in CLGB (e.g. at Naakenavaara). The high abundance of quartz-carbonate veins in pre-carbonated metakomatiite attests to the relatively high competence of this rock type.

In areas where veining has occurred within the shears, continuous deformation has modified and possibly also partly remobilised the occurrence to its current appearance. Crosscutting faults and related brecciation further complicates the shapes of individual lodes. The width of mineralisation ranges from 25 m to 70 m.

At least five km long section of SSZ has been mineralised with the following main characteristics:

1. Structural style is dominantly brittle. Metamorphic grade and alteration assemblages imply towards mid- to upper-greenschist facies conditions. Gold-related alteration is dominated by quartz, carbonate, sericite/fuchsite ± albite, chlorite, pyrrhotite, pyrite, arsenopyrite, rutile.
2. The lodes are formed by variably sulphidised discrete veins, swarms, stockworks and complex breccia zones, the latter actually being ductilely deformed shear-hosted stockworks.
3. There is only little variation in vein gangue. Ore mineral assemblages are more varied and change according to lithology. Veins are generally dominated by carbonates over quartz, sulphides and sulpharsenides. A vein may contain any of the following: ankerite, Fe-dolomite, quartz, siderite and minor calcite, magnesite and chlorite; pyrrhotite, chalcopyrite, pyrite, arsenopyrite, gersdorffite; accessory to trace amounts of glaucodot, cobaltite, pentlandite, argentopentlandite, ullmannite, safflorite, löllingite, violarite, millerite, sphalerite, galena, bismuthinite, uraninite, brannerite, cassiterite, marcasite, monazite, xenotime, hessite, native gold, native bismuth and maldonite.
4. Native gold, the major known carrier of Au, is mainly related to sulpharsenides and pyrite. Gold hosted by sulpharsenides occurs as inclusions or as irregular forms filling voids and microcracks in their host crystals. There is no indication of refractory gold in the ore minerals so far.

The occurrence shares many geological characteristics with the orogenic gold deposit class (e.g. Groves et al. 1998, McCuaig & Kerrich 1998), whereas it lacks many key features expected from the other major gold deposit classes, including the Fe-oxide Cu-Au (IOCG) (Hitzman 2000, Partington & Williams 2000) and intrusion-related gold deposits (Lang & Baker 2001). The following characteristics point towards orogenic gold mineralisation: 1) there is an apparent lack of proximity to intrusive rocks, 2) there is scarcity of related iron oxides and absence of distinctive skarn minerals, and 3) all characteristics correspond to brittle-ductile deformation and mesothermal environment during mineralisation.

To summarise, the observed characteristics sug-

gest that mineralisation occurred under mid- to upper greenschist facies conditions at ~300–475°C and 1.5–3 kbar (inferred from the alteration and vein mineral assemblages) during brittle to brittle-ductile deformation soon after the peak of deformation and metamorphism. The close spatial association of ultramafic rocks (a likely source of Ni±Cu±Co) with mafic metavolcanic rocks (potential source of Fe) and graphitic metasedimentary rocks (a potential source for S±As as well as Cu and Fe) is the dominant cause for the observed mineralisation characteristics. By producing reducing conditions, the graphitic rocks have acted as an efficient chemical trap. Hence the entrapment of sulphides ± gold in quartz-carbonate-sulphide veins was a result of fluid-rock interaction.

ACKNOWLEDGEMENTS

This work would not have been possible without the support of the Finnish Graduate School in Geology. Holma also gratefully acknowledges the assistance of his earlier financial supporters, namely the Lappi Fund of the Finnish Cultural Foundation and the Northern Finland's Research Foundation's Fund of the Oulu University. We also thank the reviewers, Drs. Kari Kojonen, Pasi Eilu, and Gavin England, for their valuable suggestions that significantly improved the manuscript. Dr. Richard Goldfarb from the USGS deserves an acknowledgement for expressing an opinion concerning the terminology for our peculiar metal association and giving some valuable ideas about the occurrence. Dr. Jyrki Parkkinen from the GTK is kindly thanked for the 3D models and fault interpretations. Vesa Kortelainen (GTK) is gratefully acknowledged for kindly providing the photo taken from atop the Levi fell.

REFERENCES

Berthelsen, A. & Marker, M. 1986. 1.9–1.8 Ga old strike-slip megashears in the Baltic Shield, and their plate tectonic implications. Tectonophysics 128, 163–181.

Bierlein, F.P. & Crowe, D.E. 2000. Phanerozoic orogenic lode gold deposits. Reviews in Economic Geology 13, 103–139.

Eilu, P. 1994. Hydrothermal alteration in volcano-sedimentary rocks in the Central Lapland greenstone belt, Finland. Geological Survey of Finland, Bulletin 374, 145 p.

Eilu, P. 1999a. FINGOLD – a public database on gold deposits in Finland. Geological Survey of Finland, Report of Investigation 146, 224 p. Also available from Internet, updated on regular basis: URL: http://en.gtk.fi/ExplorationFinland/Commodities/Gold/gtk_gold_map.html.

Eilu, P. 1999b. Alteration in the Central Lapland greenstone belt. In: Papunen, H. & Eilu, P. (eds.) Geodynamic evolution and metallogeny of the Central Lapland, Kuhmo and Suomussalmi greenstone belts, Finland. Joint field excursion and workshop of the GEODE subprojects: Archaean Greenstone Belts and Ore Deposits, Palaeoproterozoic Greenstone Belts and Ore Deposits. 11–16 September 1999. Institute of Geology and Mineralogy, Publication No. 42, University of Turku, Finland, 89–101.

Eilu, P.K., Mathison, C.I., Groves, D.I. & Allardyce, W.J. 1999. Atlas of alteration assemblages, styles and zoning in orogenic lode-gold deposits in a variety of host rock and metamorphic settings. Geology and Geophysics Department (Centre for Strategic Mineral Deposits) & UWA Extension, The University of Western Australia, Publication No. 30, 50 p.

Eilu, P., Sorjonen-Ward, P., Nurmi, P. & Niiranen, T. 2003. A review of gold mineralization styles in Finland. Economic Geology 98, 1329–1353.

Eilu, P., Pankka, H., Keinänen, V., Kortelainen, V., Niiranen, T. & Pulkkinen, E. 2007. Characteristics of gold mineralisation in the greenstone belts of northern Finland. In: Ojala, V.J. (ed.) Gold in the Central Lapland Greenstone Belt, Finland. Geological Survey of Finland, Special Paper 44, 57–106.

Elo, S., Lanne, E., Ruotoistenmäki, T. & Sindre, A. 1989. Interpretation of gravity anomalies along the POLAR profile in the northern Baltic Shield. Tectonophysics 162, 135–150.

Ettner, D.C., Björlykke, A. & Andersen, T. 1999. Fluid geochemistry of the Bidjovagge gold-copper deposit, Norway: An example of a Proterozoic greenstone belt-hosted mesothermal gold-base metal deposit. In: Cook, N.J. & Sundblad, K. (eds.) Precambrian gold in the Fennoscandian and Ukrainian Shields and related areas. Geological Survey of Norway, Abstract volume, Gold '99 Trondheim, Norway, 4–6 May 1999, 70–71.

Freeman, R., von Knorring, M., Korhonen, H., Lund, C. & Mueller, St. 1989 (eds.). The European Geotraverse, Part 5: The POLAR profile. Tectonophysics 162, 1–171.

Frietsch, R., Tuisku, P., Martinsson, O. & Perdahl, J.-A. 1997. Early Proterozoic Cu-(Au) and Fe ore deposits associated with regional Na-Cl metasomatism in northern Fennoscandia. Ore Geology Reviews 12, 1–34.

Gaál, G., Berthelsen, A., Gorbatschev, R., Kesola, R., Lehtonen, M.I., Marker, M. & Raase, P. 1989. Structure and composition of the Precambrian crust along the POLAR Profile in the northern Baltic Shield. Tectonophysics 162, 1–25.

Grönholm, P. 1999. The mesothermal Saattopora copper-gold deposit in the Palaeoproterozoic Central Lapland greenstone belt, Northern Finland. In: Cook, N.J. & Sundblad, K. (eds.) Precambrian gold in the Fennoscandian and Ukrainian Shields and related areas. Geological Survey of Norway, Abstract volume, Gold '99, Trondheim, Norway, 4–6 May 1999, p. 83.

Groves, D.I., Goldfarb, R.J., Gebre-Mariam, M., Hagemann, S.G. & Robert, F. 1998. Orogenic gold deposits: a proposed classification in the context of their crustal distribution and relationship to other gold deposit types. Ore Geology Reviews 13, 7–27.

Groves, D.I., Goldfarb, R.J., Robert, F. and Hart, C.J.R. 2003. Gold deposits in metamorphic belts: overview of current understanding, outstanding problems, future research, and exploration significance. Economic Geology 98, 1–30.

Hagemann, S.G. & Cassidy, K.F. 2000. Archean orogenic lode

gold deposits. Reviews in Economic Geology 13, 9–68.

Halls, C. & Zhao, R. 1995. Listvenite and related rocks: perspectives on terminology and mineralogy with reference to an occurrence at Cregganbaun, Co. Mayo, Republic of Ireland. Mineralium Deposita 30, 303–313.

Hanski, E. 1997. The Nuttio serpentinite belt, Central Lapland: An example of Paleoproterozoic ophiolitic mantle rocks in Finland. Ofioliti 22, 35–46.

Hanski, E. & Huhma, H. 2005. Central Lapland greenstone belt. In: Lehtinen, M., Nurmi, P.A. & Rämö, O.T. (eds.) Precambrian geology of Finland – Key to the Evolution of the Fennoscandian Shield. Elsevier B.V., Amsterdam, 139–194.

Hanski, E., Huhma, H., Lehtonen, M. & Rastas, P. 1998. 2.0 Ga old oceanic crust in northern Finland. In: Hanski, E. & Vuollo, J. (eds.) International ophiolite symposium and field excursion – generation and emplacement of ophiolites through time. August 10–15, 1998, University of Oulu, Finland. Abstracts, excursion guide. Geological Survey of Finland, Special Paper 26, p. 24.

Hanski, E., Huhma, H. & Vaasjoki, M. 2001a. Geochronology of northern Finland: a summary and discussion. In: Vaasjoki, M. (ed.) Radiometric age determinations from Finnish Lapland and their bearing on the timing of Precambrian volcanosedimentary sequences. Geological Survey of Finland, Special Paper 33, 255–279.

Hanski, E., Huhma, H., Rastas, P. & Kamenetsky, V.S. 2001b. The Palaeoproterozoic komatiite-picrite association of Finnish Lapland. Journal of Petrology 42, 855–876.

Härkönen, I. & Keinänen, V. 1989. Exploration of structurally controlled gold deposits in the Central Lapland greenstone belt. Geological Survey of Finland, Special Paper 10, 79–82.

Heikkinen, P., Kukkonen, I.T., Ekdahl, E., Hjelt, S.-E., Korja, A., Lahtinen, R., Yliniemi, J., Berzin, R. & FIRE Working Group 2004. FIRE Transects: New images of the Precambrian crust. In: Ehlers et al. (eds.) Lithosphere 2004. Third symposium on the structure, composition and evolution of the lithosphere in Finland. Åbo Akademi University, Turku, November 10–11, 2004. Institute of Seismology, University of Helsinki, Report S-45, 11–16.

Hitzman, M.W. 2000. Iron oxide-Cu-Au deposits: what, where, when, and why. In: Porter, T.M. (ed.) Hydrothermal Iron Oxide Copper-Gold & Related Deposits: A Global Perspective. Australian Mineral Foundation, Adelaide, 9–25.

Holma, M. 2001. Kittilän Levijärven Au-Ni-esiintymän geologia ja mineralogia (Petrologic and mineralogic features of the Levijärvi Au-Ni occurrence in Kittilä). Unpublished MSc thesis. Department of Geosciences, University of Oulu, Finland, 93 p. (in Finnish with English summary)

Holma, M.J. 2006. Mineralogical composition of polymetallic gold vein ore and its adjacent wall rocks at Levijärvi-Loukinen, northern Finland. In: Peltonen, P. & Pasanen, A. (eds.) The 27th Nordic Geological Winter Meeting, January 9–12, 2006, Oulu, Finland. Abstract Volume. Bulletin of the Geological Society of Finland, Special Issue 1, p. 52.

Holma, M.J. & Keinänen, V.J. 2006. The similarity and continuation of gold mineralisation in and between the Levijärvi-Loukinen gold occurrence and old Sirkka test mine, northern Finland. In: Peltonen, P. & Pasanen, A. (eds.) The 27th Nordic Geological Winter Meeting, January 9–12, 2006, Oulu, Finland. Abstract Volume. Bulletin of the Geological Society of Finland, Special Issue 1, p. 51.

Holma, M.J., Keinänen, V.J., Ojala, V.J. & Eilu, P. 2003. The Levijärvi – Loukinen Au-Ni-Cu occurrence: A Palaeoproterozoic polymetallic orogenic gold mineralisation in the Sirkka Line tectonic structure, northern Finland. In: Eliopoulos, D.G. et al. (eds.) Mineral exploration and sustainable development. Proceedings of the seventh biennial SGA meeting, Athens, Greece, 24–28 August 2003, 1073–1076.

Holma, M.J., Törmänen, T. & Gehör, S. 2006. Characteristics of the sulphide-facies iron formation near the Sirkka kaivos gold occurrence, northern Finland. In: Peltonen, P. & Pasanen, A. (eds.) The 27th Nordic Geological Winter Meeting, January 9–12, 2006, Oulu, Finland. Abstract Volume. Bulletin of the Geological Society of Finland, Special Issue 1, p. 51.

Hulkki, H. & Keinänen, V. 2007. The Alteration and Fluid Inclusion Characteristics of the Hirvilavanmaa Gold Deposit, Central Lapland Greenstone Belt, Finland. In: Ojala, V.J. (ed.) Gold in the Central Lapland Greenstone Belt, Finland. Geological Survey of Finland, Special Paper 44, 137–153.

Inkinen, O. 1985. Kittilän Sirkan kulta-kupariesiintymästä. Summary: Gold-copper occurrence at Sirkka, Kittilä. Geologi 37, 8–11.

Jackson, D.A., Nesbitt, H.W., Scaini, M.J., Duggal, A. & Bancroft, G.M. 2003. Gersdorffite (NiAsS) chemical state properties and reactivity toward air and aerated, distilled water. American Mineralogist 88, 890–900.

Keinänen, V. 1994. Shear zone-related Soretialehto gold occurrence in green carbonate rocks in the Central Lapland Greenstone Belt, Kittilä, Finnish Lapland. In: Perdahl, J.-A. (ed.) 21st Nordic Geological Winter Meeting, 10–13 January, 1994, Luleå, Sweden. Abstracts, p. 99.

Keinänen, V. & Hulkki, H. 1992. Main features of the three geochemically different gold mineralizations in Soretiavuoma, Finnish Lapland. Geirsdóttir, Á. et al. (eds.) 20th Nordic Geological Winter Meeting, 7–10 January, Reykjavik, Iceland. Abstracts, p. 96.

Keinänen, V.J. & Holma, M.J. 2001. Levijärvi and Soretialehto – two epigenetic lode-gold deposits controlled by Sirkka Thrust Zone within Palaeoproterozoic Central Lapland Greenstone Belt, Kittilä, northern Finland. In: Williams, P.J. (ed.) 2001: A Hydrothermal Odyssey. Extended Conference Abstracts. Townsville, 17–19th May 2001. EGRU Contribution 59, 102–103.

Keinänen, V., Ojala, J. & Nykänen, V. 2001. Proterozoic greenstone-hosted Loukinen Au-Ni-Cu prospect. Geological Survey of Finland, unpublished reports CM 06/2741 and 2743/2001/1/10, Kittilä, 25 p.

Koistinen, E., Parkkinen, J. & Keinänen, V. 2000. Mineral resource assessment of the Levijärvi gold-nickel occurrence. Associated with the report M06/2741/2000/1/10, Kittilä, Levijärvi. Geological Survey of Finland, unpublished report, 14 p.

Korvuo, E. 1997. The Saattopora gold ore and the Pahtavuoma Cu-Zn-U occurrences in the Kittilä region, northern Finland. In: Korkiakoski, E. & Sorjonen-Ward, P. (eds.) Ore deposits of Lapland in northern Finland and Sweden: Geological Survey of Finland, Guide 43, 21–25.

Lahtinen, R., Nironen, M. & Korja, A. 2003. Palaeoproterozoic orogenic evolution of the Fennoscandian Shield at 1.92–1.77 Ga with notes on the metallogeny of FeOx-Cu-Au, VMS, and orogenic gold deposits. In: Eliopoulos, D.G. et al. (eds.) Mineral exploration and sustainable development. Proceedings of the seventh biennial SGA meeting, Athens, Greece, 24–28 August 2003, 1057–1060.

Lahtinen, R., Korja, A. & Nironen, M. 2005. Paleoproterozoic tectonic evolution. In: Lehtinen, M., Nurmi, P.A. & Rämö, O.T. (eds.) Precambrian geology of Finland – Key to the Evolution of the Fennoscandian Shield. Elsevier B.V., Amsterdam, 481–532.

Lang, J.R. & Baker, T. 2001. Intrusion-related gold systems: the present level of understanding. Mineralium Deposita 36, 477–489.

Lanne, E. 1979. Vuotoksen ja Kittilän alueiden geofysikaalisten tietojen tulkinnasta. Summary: On the interpretation of geophysical data from the Vuotos and Kittilä areas, northern Finland. Geological Survey of Finland, Report of Investigation 25, 38 p.

Lehtinen, M. 1987. Kittilän tutkimusalue: Sirkka. In: Papunen, H. (ed.) Lapin vulkaniittien tutkimusprojekti. Loppuraportti (The Kittilä study area: Sirkka. Final Report of the Lapland Volcanite Research Project). Department of Geology, University of Turku, 85–96. (in Finnish)

Lehtonen, M., Airo, M.-L., Eilu, P., Hanski, E., Kortelainen, V., Lanne, E., Manninen, T., Rastas, P., Räsänen, J. & Virransalo, P. 1998. Kittilän vihreäkivialueen geologia. Lapin vulkaniittiprojektin raportti. Summary: The stratigraphy, petrology and geochemistry of the Kittilä greenstone area, northern Finland. A report of the Lapland Volcanite Project. Geological Survey of Finland, Report of Investigation 140, 144 p.

Mänttäri, I. 1995. Lead isotope characteristics of epigenetic gold mineralization in the Palaeoproterozoic Lapland greenstone belt, northern Finland. Geological Survey of Finland, Bulletin 381, 70 p.

Martinsson, O. 1997. Tectonic setting and metallogeny of the Kiruna greenstones. Doctoral thesis 1997:19. Department of Environmental Planning and Design, Division of Applied Geology, Luleå University of Technology, Sweden. 49 p.

McCuaig, T.C. & Kerrich, R. 1998. P-T-t-deformation-fluid characteristics of lode gold deposits: evidence from alteration systematics. Ore Geology Reviews 12, 381–453.

Nurmi, P.A., Lestinen, P. & Niskavaara, H. 1991. Geochemical characteristics of mesothermal gold deposits in the Fennoscandian Shield, and a comparison with selected Canadian and Australian deposits. Geological Survey of Finland, Bulletin 351, 101 p.

Ohlson, B. 1969. Bedrock and Quaternary deposits of the Loukinen basin in western Finnish Lapland. Fennia 90, N:o 2, 35 p.

Parkkinen, J. 2002. Levijärvi-Loukisen rakenteista (Structural interpretation of the Levijärvi-Loukinen gold occurrence). Geological Survey of Finland, unpublished report CM19/274 1,2743/2002/1/10, 16 p. (in Finnish)

Partington, G.A. & Williams, P.J. 2000. Proterozoic lode gold and (iron)-copper-gold deposits: a comparison of Australian and global examples. Reviews in Economic Geology 13, 69–101.

Patison, N. 2007. Structural controls on gold mineralisation in the Central Lapland Greenstone Belt. In: Ojala, V.J. (ed.) Gold in the Central Lapland Greenstone Belt, Finland. Geological Survey of Finland, Special Paper 44, 107–124.

Pekkala, Y. & Puustinen, K. 1978. The chromian marbles of Kittilä, Finnish Lapland. Geological Survey of Finland, Bulletin 50, 15–29.

Rastas, P., Huhma, H., Hanski, E., Lehtonen, M.I., Härkönen, I., Kortelainen, V., Mänttäri, I. & Paakkola, J. 2001. U-Pb isotopic studies on the Kittilä greenstone area, central Lapland, Finland. In: Vaasjoki, M. (ed.) Radiometric age determinations from Finnish Lapland and their bearing on the timing of Precambrian volcano-sedimentary sequences. Geological Survey of Finland, Special Paper 33, 95–141.

Ridley, J. 1997. Syn-metamorphic gold deposits in amphibolite and granulite facies rocks. Mitteilungen der Österreichischen Mineralogischen Gesellschaft 142, 101–110.

Riikonen, S. 1997. Kittilän kromimarmorien mineralogia (Mineralogical composition of some selected chromian marbles from Kittilä). Unpublished MSc thesis. Department of Geosciences and Astronomy, University of Oulu, Finland, 61 p. (in Finnish)

Robert, F. & Poulsen, K.H. 2001. Vein formation and deformation in greenstone gold deposits. Reviews in Economic Geology 14, 111–155.

Saverikko, M. 1983. Kummitsoiva komatiite complex and its satellites in northern Finland. Bulletin of the Geological Society of Finland 55, 111–139.

Saverikko, M. 1985. The pyroclastic komatiite complex at Sattasvaara in northern Finland. Bulletin of the Geological Society of Finland 57, 55–87.

Sorjonen-Ward, P., Nurmi, P.A., Härkönen, I., Pankka, H.S. 1992. Epigenetic gold mineralization and tectonic evolution of a lower Proterozoic greenstone terrane in the northern Fennoscandian (Baltic) Shield. In: Sarkar, S.C. (ed.) Metallogeny related to tectonics of the Proterozoic mobile belts. Oxford & IBH Publishing, New Delhi, 37–52.

Vaasjoki, M. 2001 (ed.). Radiometric age determinations from Finnish Lapland and their bearing on the timing of Precambrian volcano-sedimentary sequences. Geological Survey of Finland, Special Paper 33, 279 p.

Valenta, R.K., Cartwright, I. & Oliver, N.H.S. 1994. Structurally controlled fluid flow associated with breccia vein formation. Journal of Metamorphic Geology 12, 197–206.

Vanhanen, E. 2001. Geology, mineralogy and geochemistry of the Fe-Co-Au-(U) deposits in the Palaeoproterozoic Kuusamo Schist Belt, northeastern Finland. Academic Dissertation. Geological Survey of Finland, Bulletin 399, 229 p.

Väisänen, M., Airo, M.-L. & Hölttä, P. 2000. Field investigations in the Central Lapland Greenstone Belt, northern Finland, 1998–1999. Geological Survey of Finland, unpublished report K21.43/2000/1, 19 p.

Väisänen, M. 2002. Structural features in the central Lapland greenstone belt, northern Finland. Geological Survey of Finland, unpublished report K21.42/2002/3, 20 p.

Vesanto, J. 1978. Sirkan malmi ja sitä ympäröivä kallioperä (Sirkka gold deposit and the surrounding bedrock). Unpublished MSc thesis. Department of Geology, University of Oulu, Finland, 89 p. (in Finnish)

Vormisto, K. 1969. Kittilä. Atri Oy:n tutkimukset. Yhteenvetoraportti (A summary report of the investigations conducted by the Atri Oy in the Kittilä study area). Outokumpu Oy, unpublished report, 16 p. (in Finnish)

Ward, P., Härkönen, I., Nurmi, P.A. & Pankka, H.S. 1989. Structural studies in the Lapland greenstone belt, northern Finland and their application to gold mineralization. Geological Survey of Finland, Special Paper 10, 71–77.

Weihed, P. & Eilu, P. 2003. Gold, Fe oxide-Cu-Au and VMS metallogeny of the Fennoscandian Shield. In: Eliopoulos, D.G. et al. (eds.) Mineral exploration and sustainable development. Proceedings of the seventh biennial SGA meeting, Athens, Greece, 24–28 August 2003, 1123–1126.

Weihed, P., Arndt, N., Billström, K., Duchesne, J.-C., Eilu, P., Martinsson, O., Papunen, H. & Lahtinen, R. 2005. Precambrian geodynamic and ore formation: The Fennoscandian Shield. Ore Geology Reviews 27, 273–322.

Gold in the Central Lapland Greenstone Belt, Finland
V. Juhani Ojala (ed.)
Geological Survey of Finland, Special Paper 44, 187–208, 2007.

APPLICATION OF AEROGEOPHYSICAL DATA FOR GOLD EXPLORATION: IMPLICATIONS FOR THE CENTRAL LAPLAND GREENSTONE BELT

by
Meri-Liisa Airo

Airo, M.-L. 2007. Application of Aerogeophysical Data for Gold Exploration: Implications for the Central Lapland Greenstone Belt. *Geological Survey of Finland, Special Paper 44, 187–208*, 13 figures and 2 tables.

The Central Lapland greenstone belt (CLGB) in the northern part of the Fennoscandian shield has been highly prospective for orogenic lode gold, with several occurrences already been discovered. The wide extent of the greenstone belt (100 km x 200 km) is a good reason for application of regional aeromagnetic data in characterizing the structural control on gold and investigation whether the related extensive alteration could be recognized in airborne gamma-ray spectrometric data.

Central Finnish Lapland has been covered by systematic airborne geophysical surveys since the 1970´s. The low nominal terrain clearance of 30 m, the general line spacing of 200 m, the dense sampling rate, and the practice of using a magnetic horizontal gradiometer permit interpretation in a wide range of scales from regional to prospect scale. This kind of high-resolution airborne data have widely been applied in Finland for the purposes of crustal studies, geological mapping and mineral exploration. Proven to be detailed enough, these data are nowadays being more frequently applied also for geotechnical and environmental applications. Increasing interest for gold exploration in Finnish Lapland raised the need for re-interpreting the existing airborne geophysical data in accordance with the new geological information, but also urged the need for re-surveying the most prospective areas by using modern equipment, processing and interpretation techniques. In addition to the previous 200 m line-spacing airborne measurements, test areas were (2001 – 2002) surveyed in Finnish Lapland by using line spacing of 50, 75 or 100 m and differential GPS-positioning. The results show that still more structural detail, in particular small-scale shear zones and systematics in fracturing, can be interpreted from these data. The simultaneous measurements of dual-frequency (3 kHz and 14.4 kHz) electromagnetic data give properties for interpreting the variation of electrical conductivity of the uppermost part of the crust.

Key words (GeoRef Thesaurus AGI): gold ores, mineral exploration, Central Lapland Greenstone Belt, geophysical methods, airborne methods, structural controls, hydrothermal alteration, petrophysics, Paleoproterozoic, Lapland Province, Finland.

Geological Survey of Finland, P.O. Box 96, FI-02151 Espoo, Finland

E-mail: meri-liisa.airo@gtk.fi

INTRODUCTION

This article describes application of aerogeophysical data sets in different scales: from the interpretation of the regional structural framework to the prospect scale investigation of the geophysical anomalies associated with hydrothermally altered zones. The main interest was on aeromagnetic and gamma-ray spectrometric data, and on developing routines for detecting and outlining the zones of chemical alteration. For example, a strong correlation is observed between potassic alteration of ultramafic rocks, K/Th ratios in radiometric data and magnetic reduction. The features pointed out in this study are expected to be common to other similar greenstone belts in the world. The earlier aerogeophysical survey data, carried out by using line spacing of 200 m, were compared with the re-surveys by using line spacing of 75 m. The detailed structural information increased outstandingly. The results support carrying out high precision airborne geophysical measurements at a low flying altitude (less than 50 m) and by using a line spacing of 100 m or less. The general characteristics of aerogeophysical response for chemically altered zones have been earlier reviewed in Airo (2002), with examples from both greenstone-related gold-occurrences in Lapland and base-metal bearing sulphide deposits mainly in eastern Finland.

INTERPRETATION METHODOLOGY

The first aeromagnetic high-resolution image covering the whole Central Lapland was presented as a grey-scale photomosaique map, compiled using the "photomethod" developed by Juha Korhonen and introduced at the 15th Geological Winter Meeting in Iceland (Airo and Korhonen 1982; 1983). The photomethod was extremely sensitive for detecting even the faintest magnetic variations and the map is still one the most informative presentations in describing lithological and stratigraphic variation, boundaries of signature zones, and in characterizing the main geological features in Central Lapland. Since then, along with the development of computer-based image-processing techniques, coloured shaded relief-presentations of aeromagnetic data have become more popular. The shaded relief images express, in particular, the structure displayed by the shadows, but the results are strongly conditioned by the choice of illumination azimuth. Grey-scale presentations simply portray the magnetic field data in grey tones of increasing density between white (the lowest) and black (the highest). Cordell and Knepper (1987) applied Korhonen's method for grey-scale aeromagnetic images in Missouri, and revealed totally new information even in the previously well-studied areas.

In the present study, the distribution, extent and geometry of regional scale structural patterns in Central Lapland were mainly outlined on the basis of aeromagnetic (AM) data. Measurements of both magnetometers have been utilized when preparing the magnetic data grid (50 m cell-size), which enables interpretation of even quite detailed structural features over extensive areas. The interpretation was supported by petrophysical information on the different geological units. Characterization of geophysical provinces and their boundaries was based on magnetic and electromagnetic (AEM) signatures. The AEM data were particularly useful for visual estimates of electrically conductive units and separation of magnetite-bearing units from the graphite-bearing good conductors, which may also contain variable amounts of sulphides. The interpretations are based on low-frequency (3 kHz) measurements. The general distribution of radioelements within different lithologies was inferred from airborne radiometric (AR) data. Estimated concentration of potassium is expressed as a percentage (K%), whereas U and Th are expressed in equivalent parts per million (eU and eTh), which indicates that their concentrations are deduced from daughter elements in their decay chain. Applicability of aerogeophysical data in gold or base metal exploration in general is summarized in Table 1.

The relationship between deep or surface structures was investigated by interpretation of long- and short-wavelength magnetic anomaly data, supported by regional gravity and digital topographic data. The internal structures – trends or characteristic patterns – within the outlined geophysical units were inspected and correlated with the known lithological information. Linear features forming discontinuities, offsets or terminations were interpreted as faults. Magnetic expressions of fracturing or shearing tend to be minor, often faint lineaments, which may form systematic network patterns. These are linked with late stages in the structural evolution of the area, since their magnetic counterparts crosscut all the other magnetic features. Experiences on similar aerogeophysical signatures corresponding to late stage fracturing have been obtained during projects carried out elsewhere in Finland, where aeromagnetic patterns were cor-

Table 1. Common applications of aerogeophysical and petrophysical techniques to greenstone belt gold or VMS (volcanite-associated massive sulphide) exploration problems (adapted and modified from Meju 2002).

Airborne method	Target features in VMS or gold prospects
AM (aeromagnetic)	Mapping of lithology, rock types, deformation styles and their boundaries; major structures, faults and fractures, shear zones; chemical alteration (magnetite destruction), sulphidation (increased overall magnetization in graphitic shales if pyrrhotite but locally depleted magnetization close to ore)
AEM (aeroelectromagnetic)	Structural framework, faults, shear zones; mapping of lithology: conductive or resistive bodies or mineralization
AR (aeroradiometric)	Lithological correlation: – commonly depleted K for greenstones – commonly enhanced U and Th for associated graphitic shales Zones of chemical alteration: – potassic alteration of ultramafic and mafic host rocks => increased K and K/Th – sulphidation is often associated with locally depleted Th => enhanced U/Th
Petrophysical data	Lithostratigraphic correlation; separation of deep-seated or exposed geological units; interpretation of surface geophysical exploration data; magnetic mineralogy (remanent / induced magnetization)

related with fracture and shear zone characteristics based on observations made on outcrops (Pajunen et al., 2001a and 2001b).

Interpretation methodology in Central Lapland was developed to prospect scale by examining individual flight line data. The question was if the anomalous zones displaying enrichment of potassium in the ultramafic rock sequences could be outlined in airborne data. Since a simultaneous decline in magnetite concentration was known to have taken place, local magnetic lows were expected to correlate with positive potassium anomalies in the radiometric data. Anomalous ratios of radioelements proved out to help in localizing chemically altered zones, particularly K/Th for pointing out altered ultramafic units and U/Th in localizing sulphidized rocks. These seemed to be related to intensive small scale fracturing in the host rocks.

GEOPHYSICAL OUTLINE OF CENTRAL LAPLAND AND THE MAIN GEOPHYSICAL PROVINCES

Volcanic activity in the latest Archean initiated the Central Lapland greenstone belt (CLGB). Throughout the Paleoproterozoic, it records a complex and episodic history of sedimentation, magmatic activity and hydrothermal alteration, culminating in orogenic deformation between 1.9–1.8 Ga (Sorjonen-Ward et al. 1992). From 1.84–1.80 Ga, extensive granitic magmatism occurred, particularly along the southern margin of the greenstone belt, and this magmatism is associated with active deformation and prominent metamorphic gradients. Extensive and pervasive hydrothermal alteration is found in proximity to major structures and recognized in all rock types throughout the Lapland greenstone belt (Eilu 1994; 1999).

The general geophysical characteristics of Central Lapland were described within Lehtonen et al. (1998), who report the results of the Lapland Volcanite Project (1984–1989) and define the lithostratigraphic groups in Central Lapland. The general geological map of Central Lapland in Fig. 1 is based on the results of this project. The geological characterization of these groups and their age relationships were refined by several contributors in a special publication about the radiometric age determinations from Finnish Lapland, e.g., Rastas et al. (2001). Geophysical interpretation case histories based on aeromagnetic data, concerning various areas in Central Lapland, have earlier been presented for example from the Rajala area (Korhonen et al. 1985) and the Kaunislehto metavolcanic formation (Airo 1993; Airo in Lehtonen et al. 1998). Wennerström and Airo (1998) studied the magnetic anisotropy explaining the emplacement mechanism of the porphyritic, so-called Nattanen-type granitoids in Lapland. The geology and the metamorphic and structural history of the CLGB have been investigated by Hölttä et al. (this issue). Regional geophysical data used in this study is mainly owned by the Geological Survey of Finland (GTK). In addition, the Bouguer-anomaly data of the Finnish Geodetic Institute and with the digital elevation data from the National Land Survey of Finland were available.

The magnetic signatures (Fig. 2), characterizing the

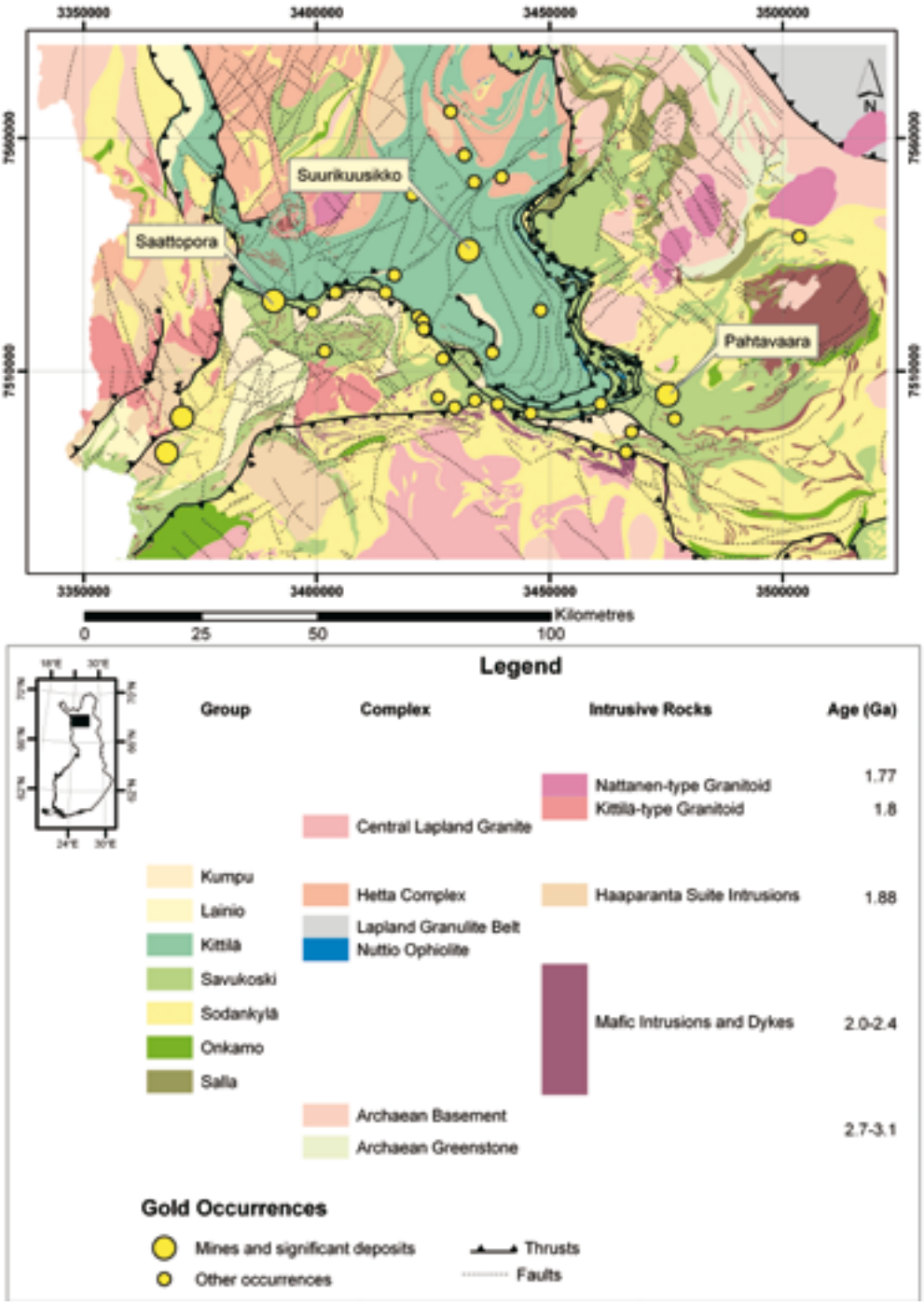

Fig. 1. Location of the study area in Lapland. The known gold occurrences and deposits marked with open circles are used as training sites. The most significant deposits are labeled.

present picture of the CLGB were mainly produced during the latest regional metamorphism, resulting both in broad regional anomalies with smooth gradients, and folded, high-frequency magnetic anomaly bands. The magnetic anomaly strikes mainly follow systematic orientations as a response to the regional stress field during the latest ductile deformation stage. Post-metamorphic tectonic and hydrothermal processes tend to disrupt or destroy the previously continuous magnetic patterns. This results in offsets or terminations of magnetic signatures represent fault and fracture zones, or zones of broken and gradually disappearing anomaly patterns and reduced anomaly amplitudes. These highly fractured zones are also susceptive for fluid injection and chemical alteration, which affects also the magnetic minerals. In general, later tectonic stress is preferably released by development of dense fracturing along the old structural weakness zones.

The general tectonic trends, interpreted from AM

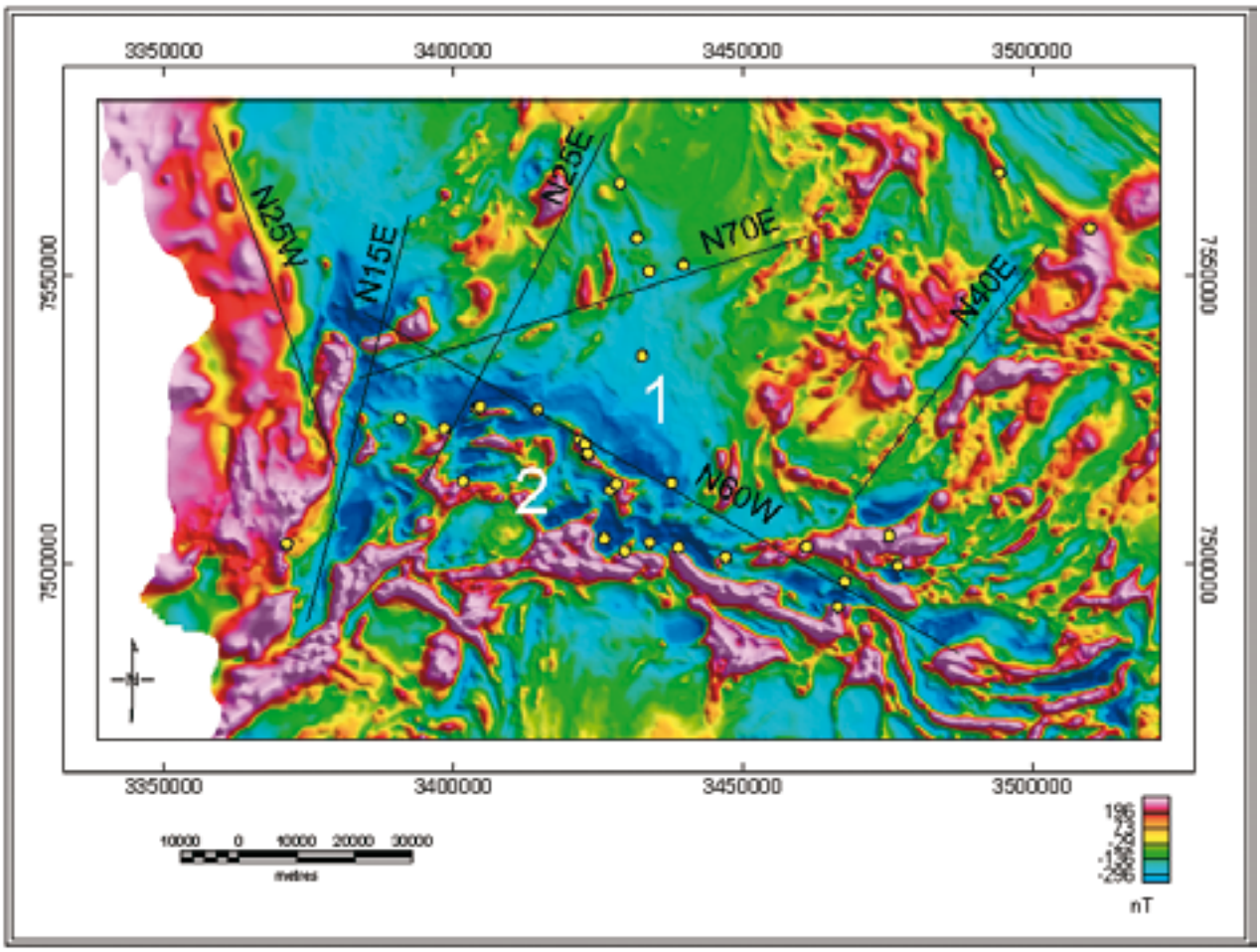

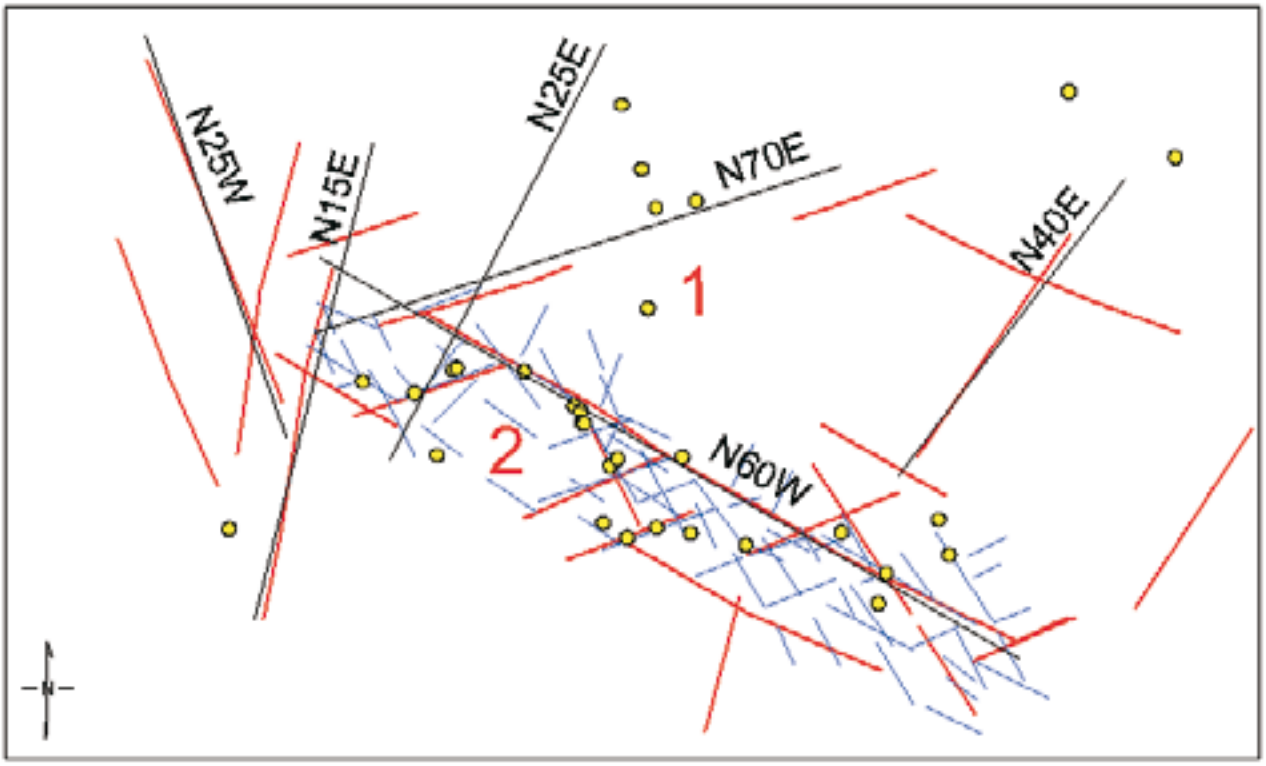

Fig. 2. Aeromagnetic image showing the CLGB (500 m upward-continuated magnetic field, illuminated from NE). Lines indicate the interpreted main tectonic trends discussed in text. Known gold occurrences are marked in yellow. Numbers denote goephysical provinces discussed in text. Aerogeohysical data, GTK.

data are schematically displayed as a separate image for more clear vision. The same trends are repeated in other regional geophysical data sets (Figs. 3–6). Two main, geophysically different Provinces 1 and 2 of the CLGB are separated by a major tectonic boundary. The weakly magnetic Province 1 (corresponding to the mainly tholeiitic metavolcanic rocks of the Kittilä Group in Fig 1; Rastas et al., 2001) is neighboured in the south by the more highly magnetic Province 2 (corresponding to metavolcanic and metasedimentary rocks of the Savukoski and Sodankylä Groups). Province 2 contains magnetite-bearing units (mafic differentiated intrusions and ultramafic metavolcanic rocks), which control the magnetic character of this province. The tectonic boundary between Provinces 1 and 2, the Sirkka line, is generally presented as a line between the Savukoski and Kittilä Groups. In geophysical sense, there is a 10–20 km wide structurally disturbed zone and, therefore, in the present paper the Sirkka zone name is used. Its main orientation corresponds to N60W, but the zone is composed of a series of thrust-faults, fracture, shear and fault zones, striking parallel to the main trend and the boundaries in the whole CLGB area. Together they form a continuous structural Z-pattern across Central Lapland, composed of N60W, N70E, N25E, N15E, N40E and N25W striking features. It is obvious that this zone was reactivated at several stages during the tectonic history of the CLGB.

The regional gravity data, from 5 km station spacing, outlines the CLGB greenstone area with a 30–40 mGal positive anomaly compared with the neighbouring basement gneisses and post-orogenic granitoids (Fig. 3). The gravity high is mainly caused by the Kittilä Group tholeiitic greenstones (Province 1), which is geophysically characterized as a high density, weakly magnetic region containing metasedimentary, graphite-bearing intercalations. According to modelling represented by Lanne (in Lehtonen et al. 1998; see also Gaál et al. 1989), the greenstones of Province 1 reach the thickness of 5–7 km with an average density of 2940 kg/m^3.

In the AEM image (Fig. 4), Province 1 is characterized by curved, folded stratigraphy-related AEM pattern caused by the graphite-bearing metasedimentary sequences. In further detail Province 1 displays division into geophysical sub-provinces 1.1, 1.2 and 1.3, delineated by mainly NS striking fault and shear zones. These sub-provinces differ chiefly in their abundance of graphitic horizons and good EM conductors, but they can also be recognized and outlined in the magnetic, gravity and topographic data. Sub-province 1.3 was more resistive against weathering or has an uplifted basement, as expressed by higher mean altitude in the digital elevation data (Fig. 5) than the other two sub-provinces. The approximately 20 km wide, fractured Sirkka zone is deeply eroded.

The magnetic mineralogy and fabrics in the geophysical provinces of the CLGB were mainly produced due to metamorphic processes of the Svecofennian orogeny, and continuous magnetic form lines represent them. Boundaries of sub-provinces 1.1, 1.2 and 1.3 were formed after the main orogenic stage, since they disrupt the continuous form line pattern. These province boundaries have reflections throughout the whole CLGB region, and are interpreted to represent features created by the regional stress field. Because of their N-S strike and coupled gradients in magnetic, gravity and electromagnetic fields, they are associated with step- or ramp-like structures, and possibly reflecting W-E compression. Their appearance in regional gravity and magnetic data, representing deep anomaly sources, refers to their great depth. Depending on the strike and competence of the rocks and old structures subjected to stresses, breaking up and fracturing occurred along the province boundaries or other structurally weak zones. The boundary between the altered ultramafic units and the graphite-bearing schists was probably especially weak horizon. Another weakness is the cleavage parallel to the general strike of bedding.

SYSTEMATICS IN FAULT AND FRACTURE PATTERNS

Structural analysis of regional geophysical data clarifies understanding of the systematics and repetition of structural trends and their relation to each other. The province outline geometry is mirrored inside the structural provinces as parallel fracture trends or thrust block geometry. Knowing the general appearance of these trends they become more visible in the field and to help evaluating their importance for the whole tectonic picture.

The main interpreted strikes of fracture and fault trends in the CLGB are: N60W, N70E, N25E, N15E, N40E and N25W (Fig. 6). NS and EW trending features are formed as combination of crosscutting strikes. NS is shown as small scale NS trending brittle fractures and shear zones, while EW is associated with fractured and altered zones of wide extent. The main fracture orientations express themselves especially clearly along the Sirkka zone, although the directions N60W and N70E dominate the geophysical fracture trends. The magnetic interference patterns are suggested to

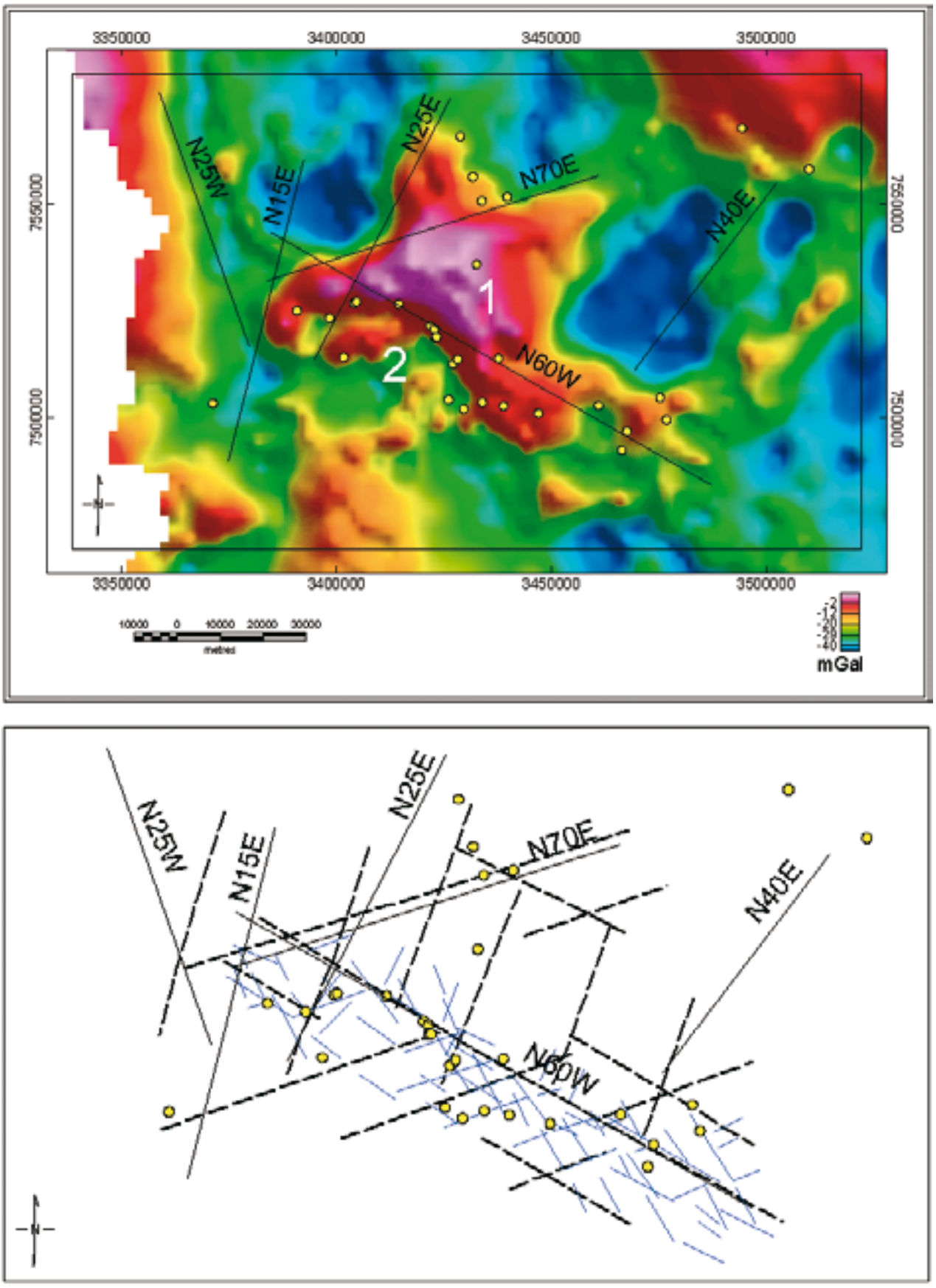

Fig. 3. Regional gravity shows the main distribution of CLGB greenstones with four corners (Finnish Geodetic Institute, 5km spacing of data points). The same tectonic trends as in Fig. 2.

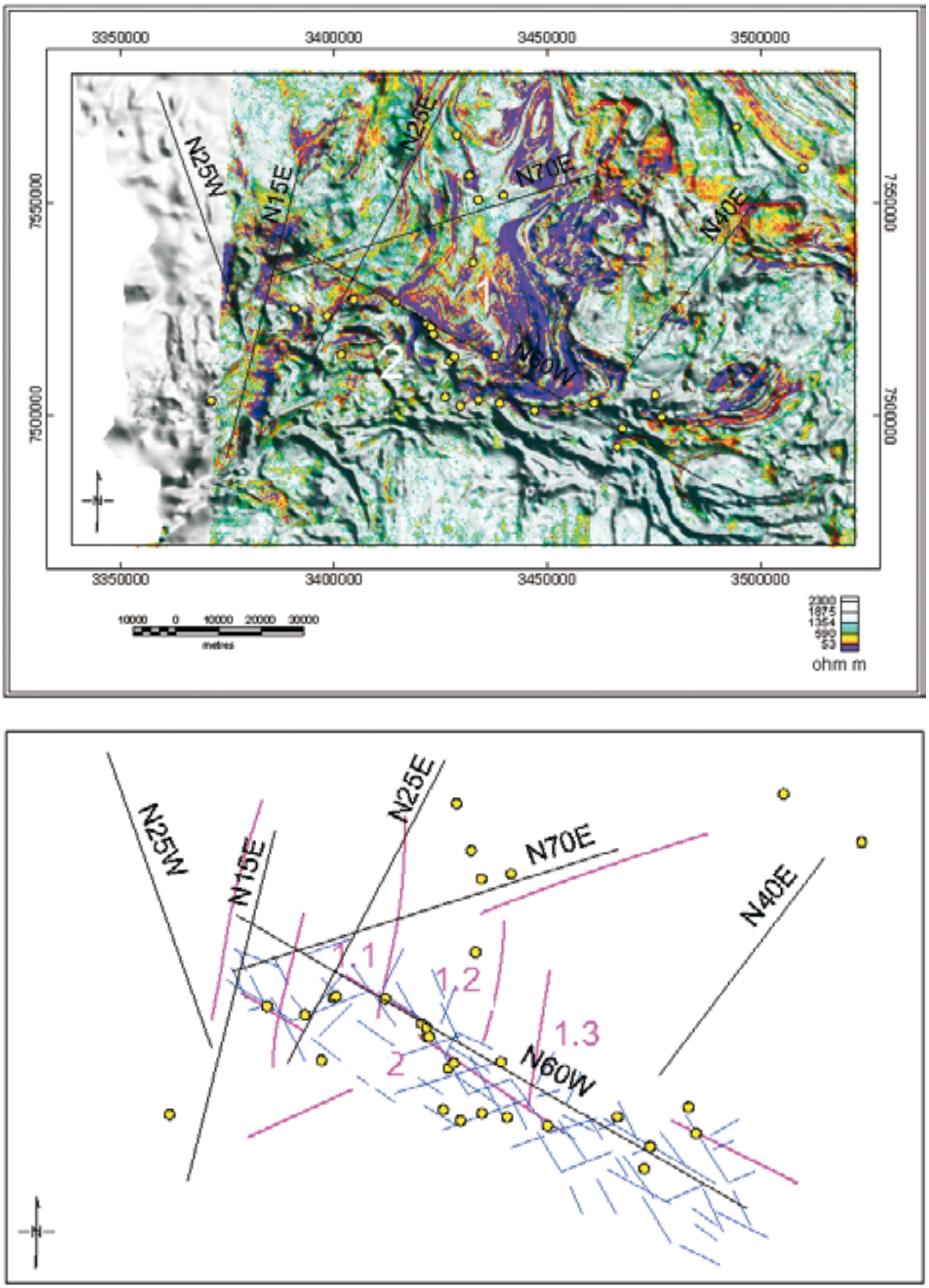

Fig. 4. Apparent resisitivity image (calculated on the basis of EM data, half-space model) superimposed on aeromagnetic shded relief. Aerogeophysical data, GTK. The same tectonic trends as in Fig. 2. Subdivision of province 1 explained in text.

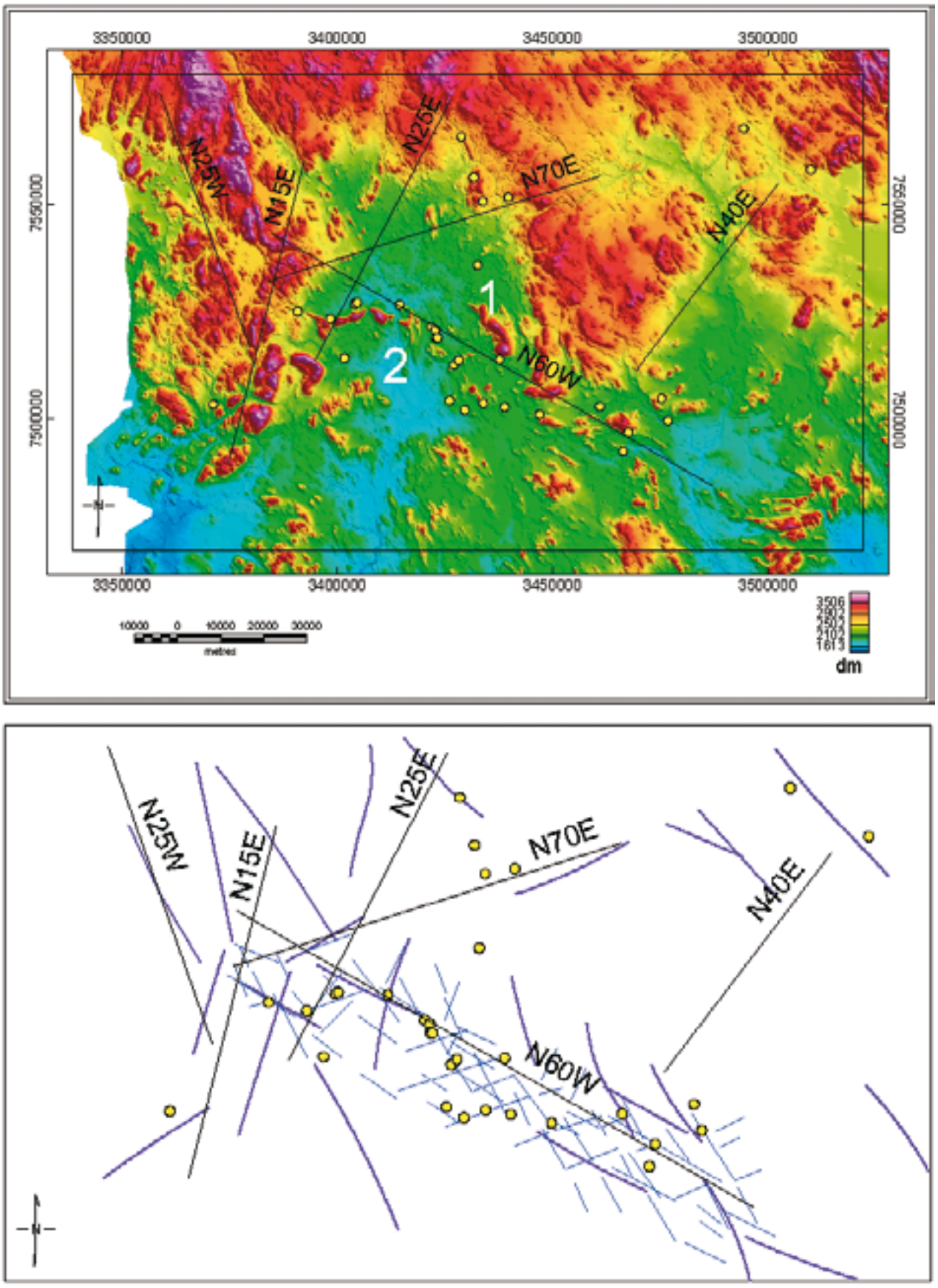

Fig. 5. Digital elevation model of Central Lapland (National Land Survey). The same tectonic trends as in Fig. 2.

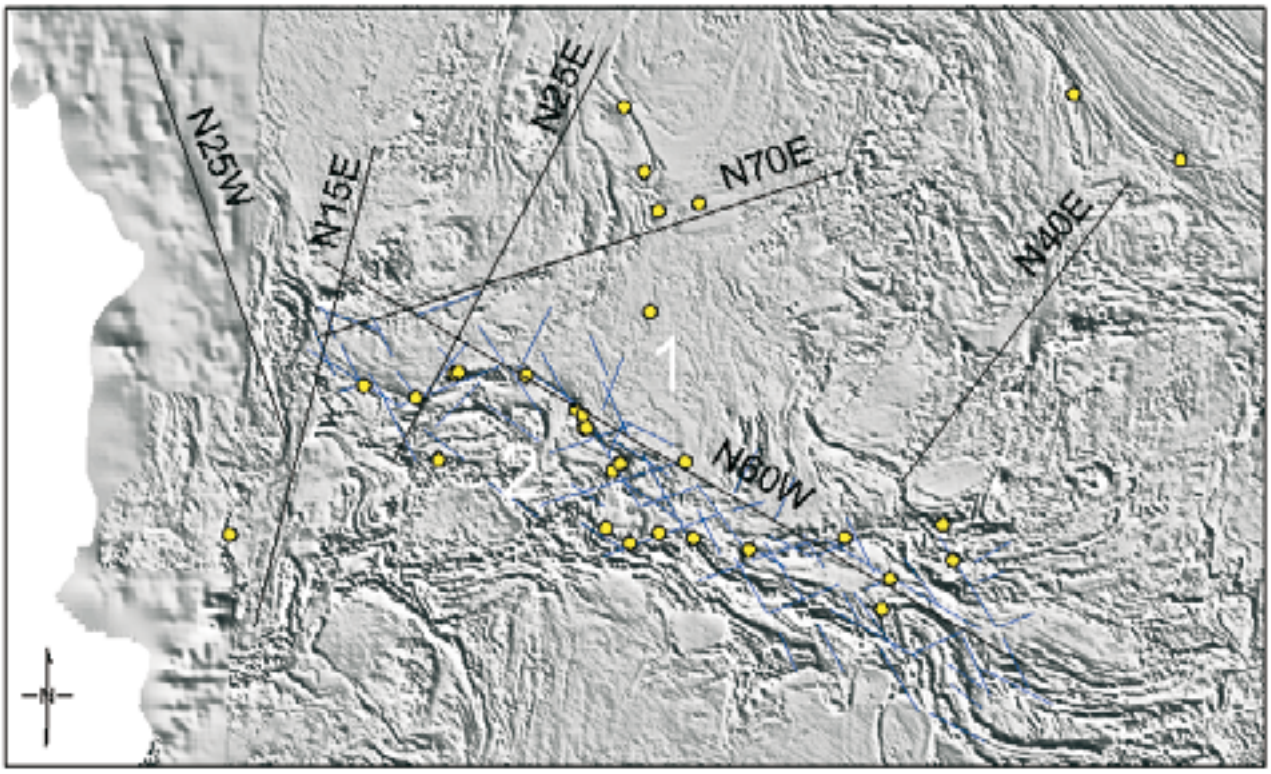

Fig. 6. Aeromagnetic gradient image (horizontal derivative) of CLGB and the main tectonic trends. Small-scala fracture trends mirror the regional fracture orientations. The map scale and other explanations as in Fig. 2. Aerogeophysical data, GTK.

be mainly due to two different stress field directions: from SW and from W. Following the latest ductile deformation stage, tectonic stress affects and tends to break the already partly cooled and rather brittle crust. The fractures and joints produced under brittle deformation stage are imaged in the aeromagnetic data as short lineaments, which cut the magnetic signatures and are coupled with topographic small-scale features. These weak expressions may be enhanced by different mathematical techniques, such as analysis of magnetic horizontal derivatives. They might be related to late stage tensile fracturing which increases with progressing deformation. One explanation for this kind of late-stage shear and tensile fracturing was represented by Satoh et al. (2000). They describe the change from shear fracturing to more tensile cracking by investigating the generation mechanism of microfractures in medium grained granite, subjected to four-fold loading and unloading of peak stresses. The relative number of shear type events was larger in the first loading cycle, while the tensile component became more important in the following cycles. They conclude, that with progressing deformation, shear fracturing becomes important irrespective of rock type. The linkage of tensile cracks could generate the shear fractures, as their density increases with deformation. This results in increasing number and extent of macroscopic fractures and joints, which inherit the microfracture geometry.

The geophysically most important structural trend in the CLGB is N60W, which is the strike of the magnetic, gravity and EM boundary between Provinces 1 and 2. This trend is expressed in regional magnetic data by linear, smooth gradients of great length, indicating also their great depth extent. They are composed of parallel, gently dipping thrust faults and thrust surfaces. Thrust ramps or terraces of the same orientation are found more northeast within Province 1, and they also have expressions in topography. More detailed-scale brittle fractures, interpreted on the basis of aeromagnetic short-wavelength data, follow the same strike. The thrust faults crosscut and disrupt the magnetic and electrical anomaly trends, suggesting that the thrusting occurred after the formation of continuous magnetic and EM signatures. Variably competent structures with different strike resulted in discrete response to tectonic stress. Where the thrust movement was perpendicular to the lithological contact between the altered ultramafic rocks and the electrically conductive schists, these structurally weak units were thrusted on each other, resulting in a wide fractured zone due to the gentle dip of structures. Where the movement was parallel to the strike of main foliation, the dips of the zone are more vertical and shearing along the foliation trend is reflected in the magnetic data as horizontal thinning.

N70E is an important trend that delineates the main part of the regional gravity anomaly due to the

greenstones. This trend is associated with dislocations and offsets in the magnetic data, expressed as sharp faults (sharp gradients) at the northern boundary of the gravity anomaly, or as highly fractured zones when crossing the Sirkka zone. N25W is related to sharp faults in magnetic data and cleavage planes with parallel strike. It is the main trend of the western boundary of the CLGB area and drainage patterns favour this trend. N25E trending sharp faults expressed as offsets in general systematic magnetic trends are found within Province 1. Some of these are seen as gradients in gravity, suggesting a great depth. N40E is an important structural trend in the eastern part of the CLGB, represented as deep faults and block boundaries in regional magnetic data.

N15E trending fault zones divide Province 1 into 3 parts according to their conductivity level; the boundaries of these parts are also recognized in magnetic data and in gravity data. In Province 1, the fracture and fault trends parallel to these sub-province boundaries cross-cut the N60W oriented thrust faults and topographic terraces. The boundary between sub-provinces 1.2 and 1.3 is also represented in gravity data as a linear gradient, meaning a deep-seated block boundary. It is obvious, that this deep structure has guided the geometry of the later, shallower structures as described by the EM and magnetic short-wave-length data. Shearing and brittle fracturing occurred along these structures, mainly in N-S orientation. These small-scale structures were determined on the basis of computed horizontal derivatives of the magnetic field. The original measured two-magnetometer data are too detailed to be used in a regional manner, but suitable when interpreting for example flight line data. In observing regional trends and repetition of structures, computed derivatives allow a quick overview on a wide area. Because of the good resolution of the magnetic grid (50 m cell-size), the derivatives are almost comparable in details with the original measured data.

Chemical alteration and petrophysics

In geophysical sense, the addition of potassium is the most important indication of chemical alteration along the Sirkka zone, coupled with a decline in the abundance of magnetite in mafic and ultramafic rocks. Geophysical indications of chemical alteration were linked to the systematic fracture pattern and individual fracture trends by studying a ca. 20 km long part of the Sirkka zone in more detail. The highly magnetic ultramafic unit in Fig. 7a, between Loukinen (see location in Fig. 1) and Sinermäjärvi is situated along the main thrust zone and hosts several lode-gold occurrences. The magnetic shaded relief presentation enhances the general structural features: the N60W trending main thrust zone (Sirkka zone) and the faults disrupting the Kittilä Group folded greenstones. The Sirkka zone outlines sharply the electrically conductive horizons belonging to Province 1, the Kittilä Group (Fig. 7b). At Loukinen the thrust zone is clearly indicated as a linear boundary where the conductive layers terminate. Chemically altered zones are expected to occur close to the structurally weak contact between the mafic/ultramafic unit and electrically conductive graphite-bearing units, but the K radiation (Fig. 7c) shows no clear increase along this zone. To be precice, there is a narrow zone of K-enrichment along the northern edge of the ultramafic unit between Hirvilavanmaa and Sinermäjärvi. This zone can be regarded as anomalous, since ultramafic rocks are commonly not associated with any K radiation. Furthermore, this addition is minor compared with the intensive K radiation produced by felsic igneous rocks, quartzites and graphite-bearing tuffitic and metasedimentary rock sequences close by. The radiation related to the covering soils may also mislead the interpretation and hence, geochemical background characteristics of various bedrock units are needed for the effective use of gamma-ray spectrometric results.

Addition of potassium was known to be associated with a decrease in magnetite content along the Sirkka zone. Therefore comparisons of fresh and altered samples were carried out to see if their petrophysical properties differ. For background, Fig. 8 illustrates density and magnetic property data for some common rock types in the CLGB. More than 8400 samples representing different rock types, collected from Central Lapland, are available in the petrophysical database provided by GTK. The densities (Fig. 8a) characterize different rock types and mainly depend on their content of mafic silicates. For example, the densities of granites (red dots) concentrate between 2500 and 2600 kg/m^3, while the mafic and ultramafic volcanic rocks (green dots) have densities above 2700 kg/m^3. A thick pile of greenstones with densities mainly above 2800 kg/m^3 cause the extensive positive gravity anomaly of the CLGB (in Fig. 3). Magnetically the samples in Fig. 8 are mainly divided into two groups, namely the weakly magnetic – concentrating at 0.001 SI – and the highly magnetic – with susceptibilities greater than 0.1 SI. Mafic and ultramafic samples show a clear division into the two magnetic groups,

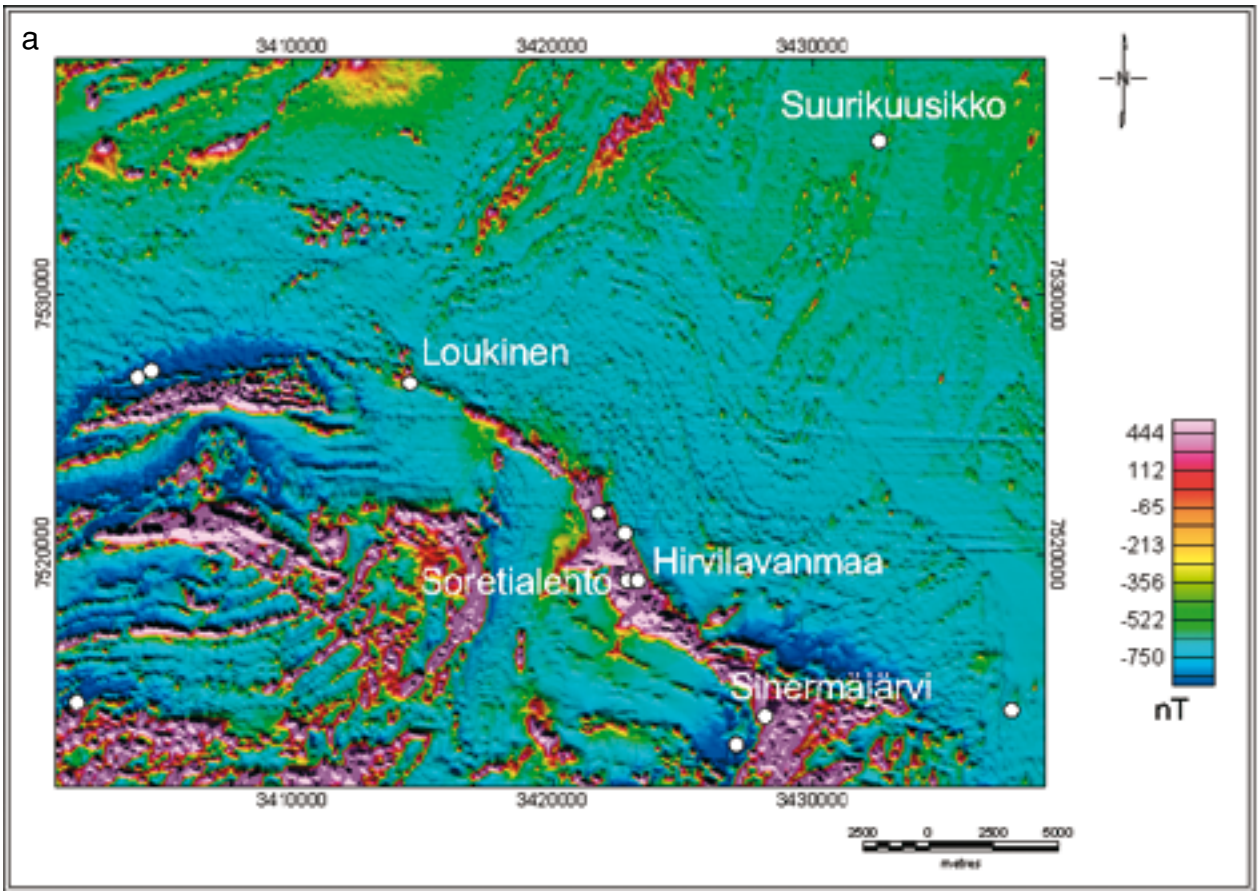
a
3410000
3420000
3430000
7530000
7520000
Suurikuusikko
Loukinen
Soretialehto
Hirvilavanmaa
Sinermajarvi
444
112
-65
-213
-356
-522
-750
nT
2500 0 2500 5000
metres

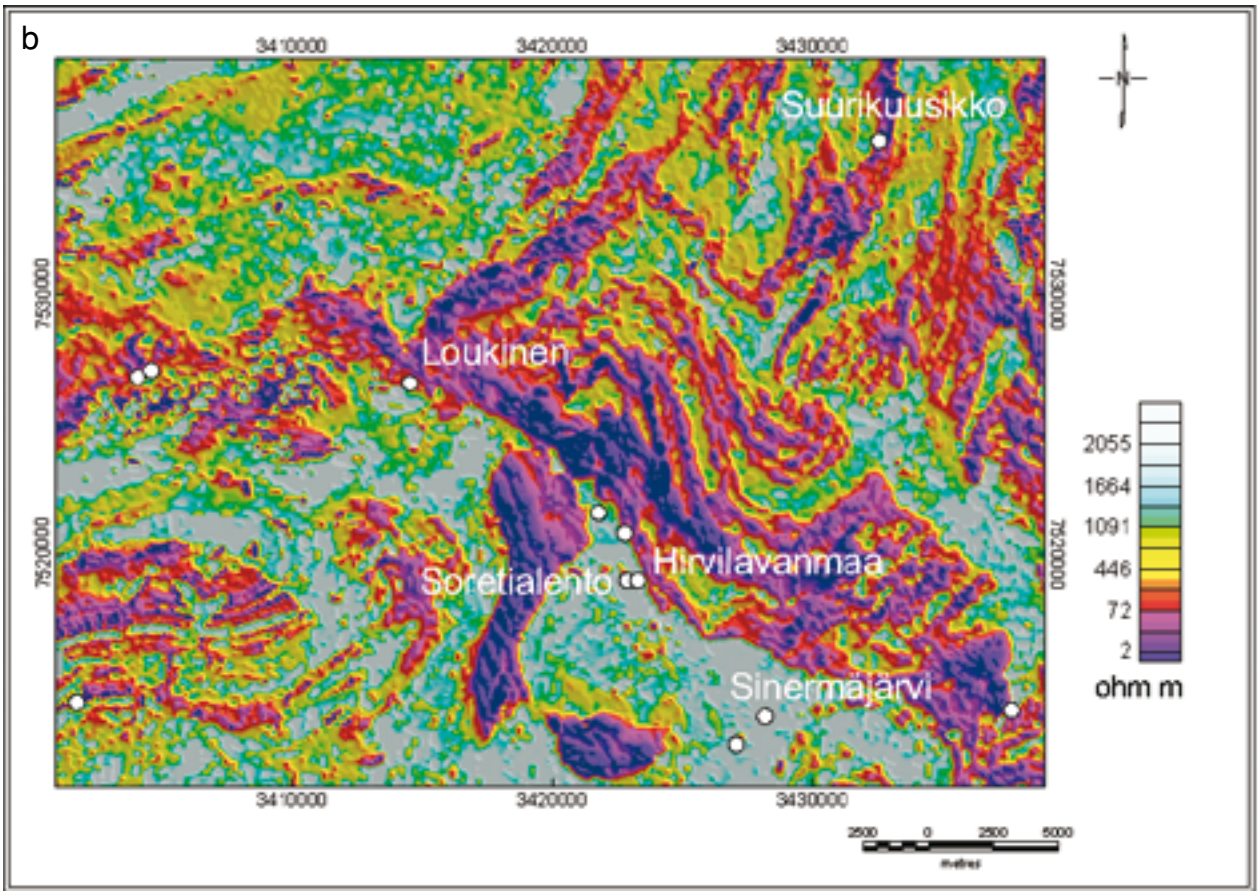
b
3410000
3420000
3430000
7530000
7520000
Suurikuusikko
Loukinen
Soretialehto
Hirvilavanmaa
Sinermajarvi
2055
1664
1091
446
72
2
ohm m
2500 0 2500 5000
metres

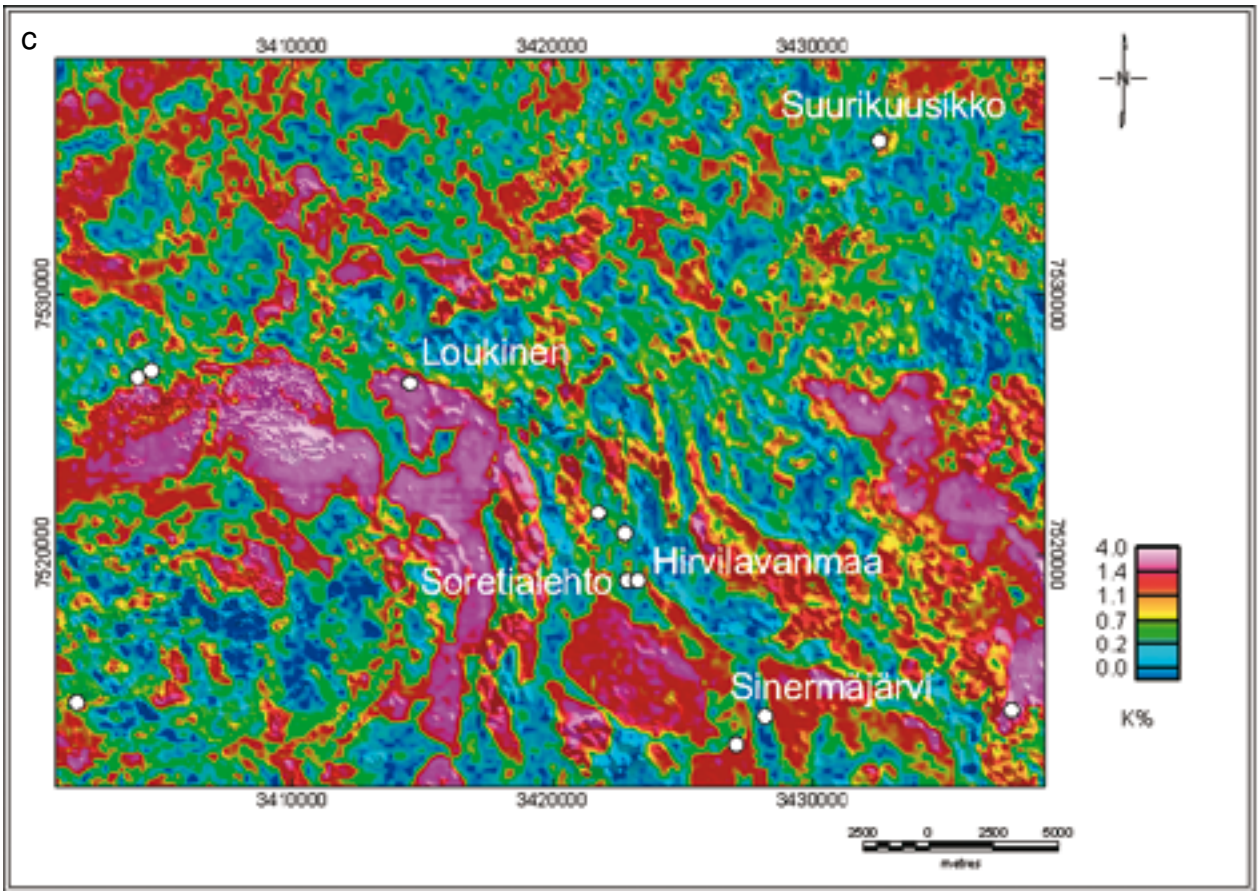

Fig. 7. a) Aeromagnetic shaded relief image of Loukinen-Sinermäjärvi; b) EM apparent resistivity image; c) Radiometric image, K concentration.

but there is also a wide magnetic distribution of granites. In general, the porphyritic granitoids in Lapland (yellow dots) are characteristically highly magnetic. Metamorphosed black shales, whose main magnetic mineral is monoclinic pyrrhotite, have a linear correlation between their densities and magnetic susceptibility. Fig. 8a shows the wide density distribution of black schists (metamorphosed black shales), with the lowest values caused by a high content of graphite. The densities of black schists grow as the content of sulphides increases.

Magnetic bimodality is typical of all magnetite-bearing metamorphosed rocks in Finland (Puranen 1989; Airo 1999), the magnetic properties being dependent on the metamorphic and alteration history of the rock (Grant, 1985). Greenstones in general are regarded as weakly magnetic, due to their low metamorphic grade, but in Central Lapland, also highly magnetic greenstones are found. To explain the variation in magnetization relative to chemical alteration of CLGB greenstones, the magnetic properties of drill-core samples were correlated to their visually estimated alteration type and degree. The density-susceptibility plot in Fig. 9 shows that originally highly magnetic komatiites and metaultramafites have susceptibilities of about 0.1 SI. The strongly altered samples have susceptibilities around 0.001, and the slightly altered ones are located between these two magnetic main groups. The effect of alteration on the studied sample set was to decrease the induced magnetization (susceptibility) and increase density. Induced magnetization is reduced along with the gradually decreased abundance of magnetite as the alteration proceeds. Although not so clearly indicated in this sample set, there is evidence from elsewhere that the intensity of the remanent magnetization may increase because of the diminished magnetic grain size. The Q-ratios of altered samples in Fig. 9 tend to grow as the susceptibilities decrease. This means a tendency of remanent magnetizations to increase. According to earlier magnetic property investigations made on samples from the CLGB metavolcanic rocks (Airo, 1993), the remanences were clearly dependent on the magnetite grain shape. Based on Curie-point determinations from thermomagnetic curves, the main ferromagnetic mineral in the highly magnetic metalavas (susceptibilities > 0.01) was pure magnetite. Hysteresis measurements referred to multi-domain behaviour of all the studied samples, both for those having Q-ratios < 0.5 and for those having Q-ratios between 1 and 10. Petrographical investigations re-

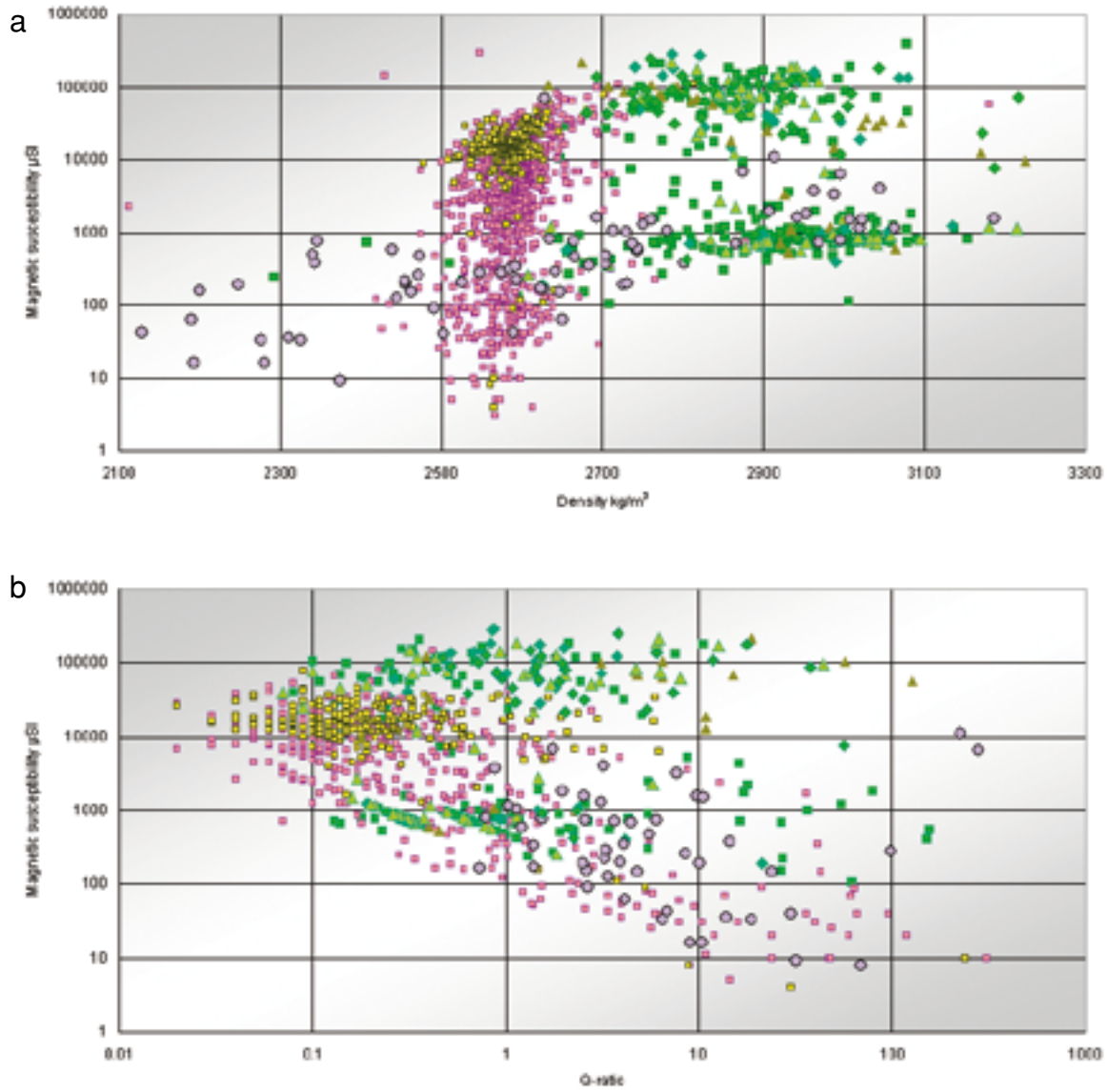

Fig. 8. Petrophysical properties for > 8400 samples collected from Central Lapland (petrpphysical data base, GTK). a) Density-magnetic susceptibility plot; b) Königsberger-ratio (remanent/induced magnetization) – magnetic susceptibility plot. Red squares = granites, Yellow dots = porphyritec granites, green dots = metavolcanic rock, purplecircles = black schists.

vealed, that magnetite grain size distributions were similar (0.01–0.5 mm) both in low-Q and higher-Q samples, but that increased irregularity in grain shape was related to high remanence intensities, despite the similarity of the magnetite contents and magnetic susceptibilities.

AERODATA APPLIED IN TARGET SCALE INTERPRETATION: FLIGHT LINE PROFILES

Airborne gamma-spectrometric data is affected by several factors, including the regolith and overburden characteristics and bedrock variation. Individual flight line data between Loukinen and Sinermäjärvi (see locations in Fig. 1 and Fig. 7) were analysed for estimating the effect of these factors on the observed radioelement variation. Fig. 10 illustrates part of the ultramafic, komatiitic unit, which is known for gold occurrences and related potassic alteration. The ultramafic unit can be outlined on the basis of its high magnetization (Fig. 10a) and the related negative EM in-phase component (Fig. 10b), which is caused by the high magnetic susceptivity due to magnetite. K-radiation profiles display anomalous K radiation along the northeastern edge of the ultramafic unit almost in every flight line (200 line spacing). In the altered zone, the magnetic anomaly intensity is decreased and illustrated as a fringed magnetic pattern. This pattern

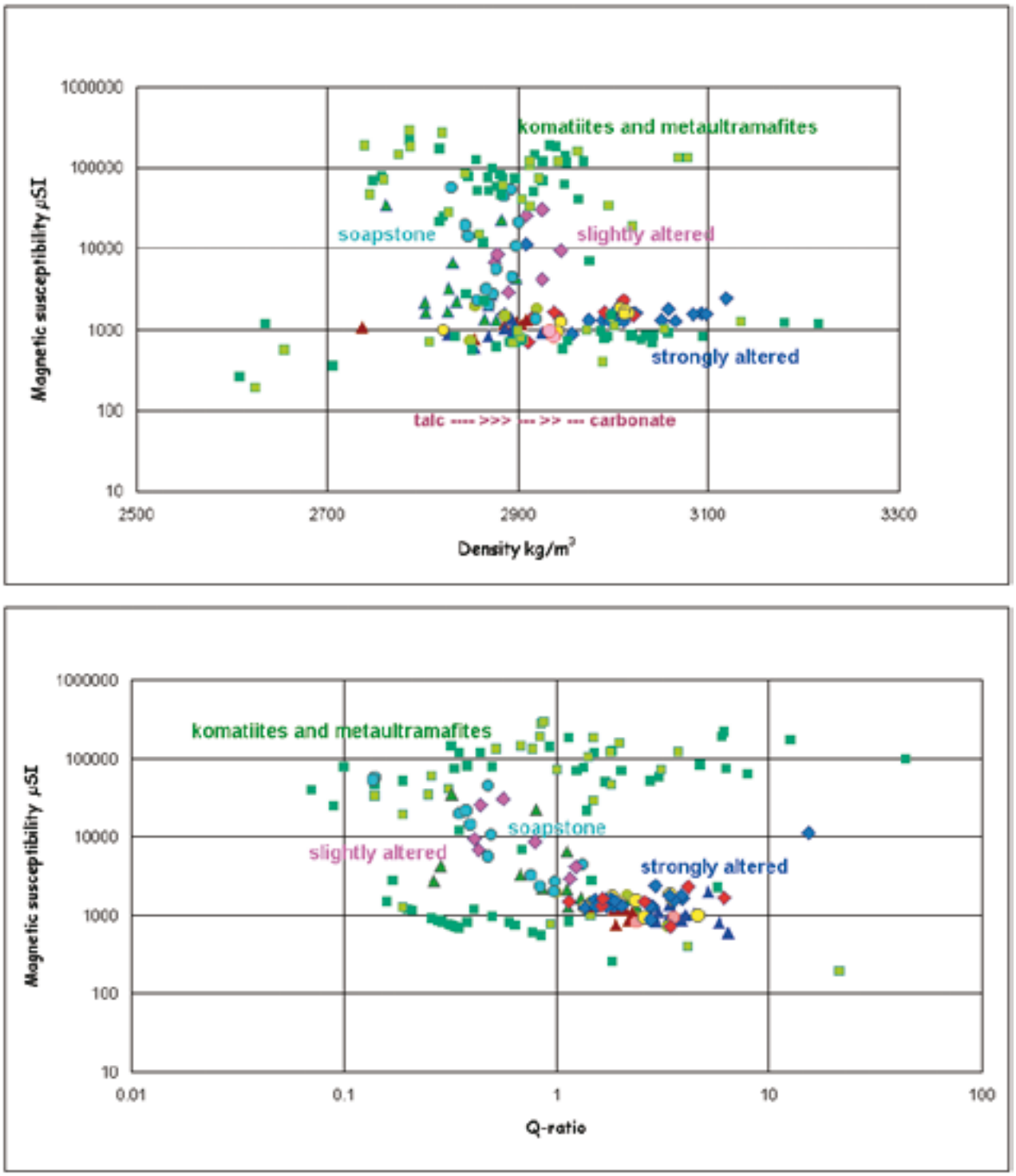

Fig. 9. Petrophysical parameters for altered greenstones. Alteration type and degree was determined optically in drill-core samples. Densities and magnetic properties of the same samples were measured in petrophysical laboratory, GTK. Komatiites and ultramafic samples (green) plot into two magnetic groups, the highly magnetic being not altered. In the present sample set, the alteration begins with the increase of talc content and proceeds with the growing amount of carbonates. Blue, red and yellow samples denote strongly altered samples having different compositions.

results partly from partial destruction of magnetite grains and partly from the fractured nature of the altered, brecciated ultramafic unit. The ultramafic unit is only occasionally exposed and it is mainly covered by several metres of till. Hence, part of the K-radiation becomes from the overburden, which is locally derived till, as was verified in the field, and it contains altered ultramafic boulders. Intensive K-radiation is also associated with quartzites south of Soretialehto and the metasedimentary rock sequences neighbouring the ultramafic unit. Opposite to magnetite-bearing ultramafic rocks, these pyrrhotite-bearing units are good

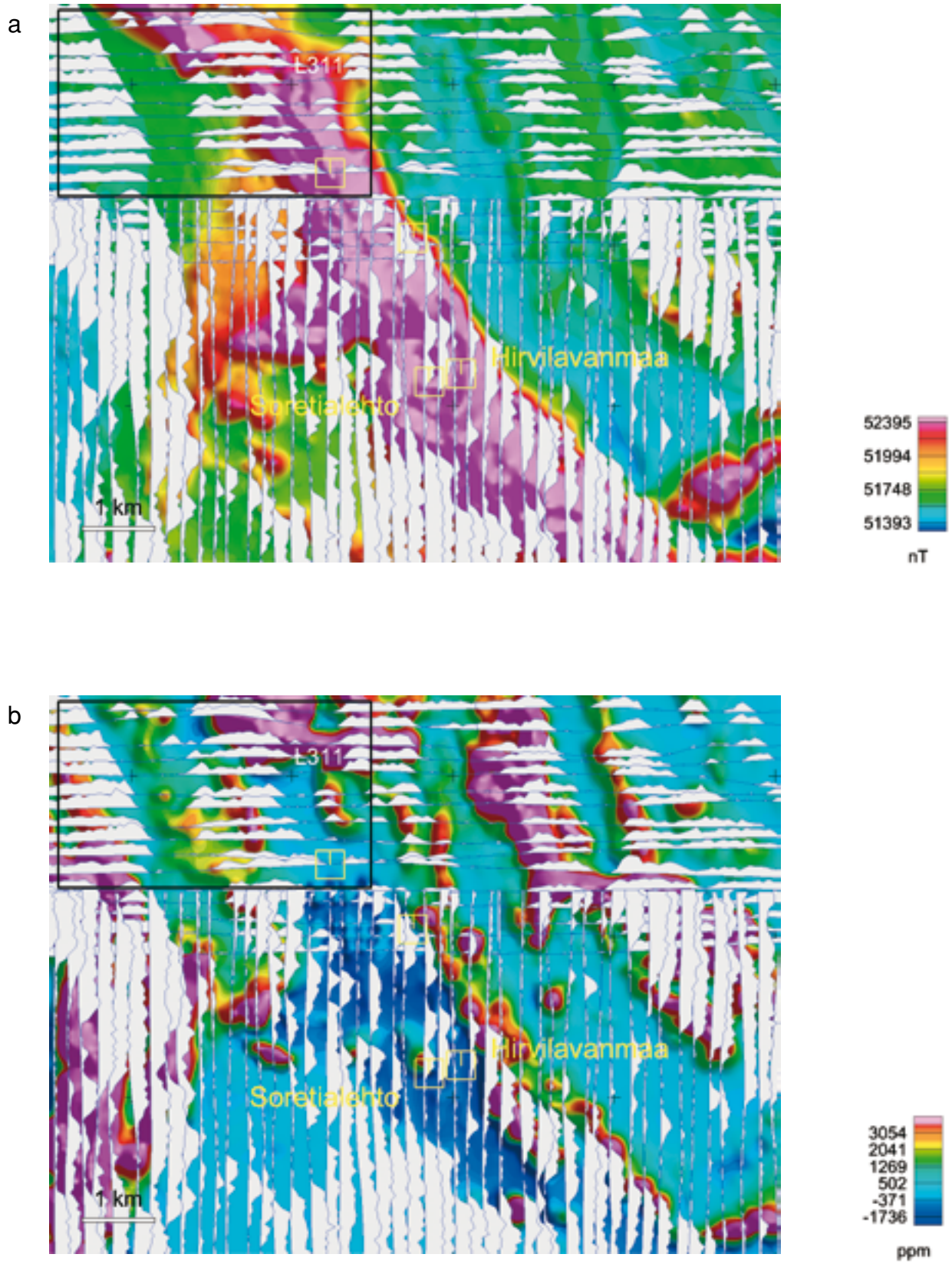

Fig. 10. Radiometric flight line profiles displaying K-radiation in light-grey (200 m line spacing, aerogeophysical data by GTK). a) Aeromagnetic map and b) AEM in-phase map. Notice the increased K-radiation along the northern edge of the highly magnetic ultramafic unit (red/purple in AM and blue in AEM in-phase). Yellow squares denote known gold occurrences. The black frame in the upper left corner outlines the Kettukuusikko site, discussed in Fig. 11 and flight line L311.

conductors and are associated with positive anomalies in the EM data. Occasionally these also may cause intense magnetic anomalies, in particular in the case of graphite-bearing metamorphosed schists, which contain monoclinic pyrrhotite.

Analysis of radioelement variations along flight lines revealed anomalous K/Th values in relation to the contact between electrically conductive zones and the altered ultramafic unit – particularly in connection of local fracturing. Important fracture trends are N40–50W, which parallels the strike of the main cleavage, e.g. the strike of bedding of the ultramafic unit, and N60E, which appears as crosscutting fractures. One major fracture zone, oriented N60E, divides the magnetic anomaly into two parts in Fig. 11. The outlined anomalous K/Th ratios along flight line L311 are related to this fracture zone. Fig. 12 illustrates the measured survey data along line L311 in detail. The framed part of L311 is located at 2547000–2548000 (in meters) and corresponds to approximately 1 km of the profile length.

The individual survey profiles in Fig. 12 correlate the AEM in-phase (LFR) and out-of-phase (LFI) data (uppermost panel). The overlapping LFR and LFI anomalies and predominance of LFR indicate, that electrically conductive schists appear as interlayers between the ultramafic units. However, it should be noted that the high LFI/LFR ratios correlate commonly with swamps and wet soils. The measured values of potassium, equivalent Th and equivalent U are compared in the centre. The high level of radiation west of 2546000 m is related to quartzites and metamorphosed schists. Between 2547000 m and 2548000 m Th is locally low, while K and U are higher. This Th low is responsible for the increase of K/Th – since K is not especially high at the same site (see the lowest panel).

The criteria represented above were applied for systematic search of intensely altered ultramafic units in the region of the CLGB along the Sirkka zone. The basic rule was to discover zones were K/Th ratios were abnormally high at several neighbouring data points and adjacent flight lines. The lowest K and Th radiation values in the data were left out because they are mainly indicators of wet soil attenuating the radiation. Additional criteria was, that anomalous K/Th peaks were related to the contact zone between the ultramafic rocks and the electrically conductive units, and to crosscutting fracture zones. In field it was observed, that distribution of brecciated and broken ultramafic boulders within the overburden may partly be responsible for the local anomalous radioelement ratios. Altogether some twenty interesting locations were selected for further geological investigations in the field. Altered ultramafic rocks were found at 8 of these sites.

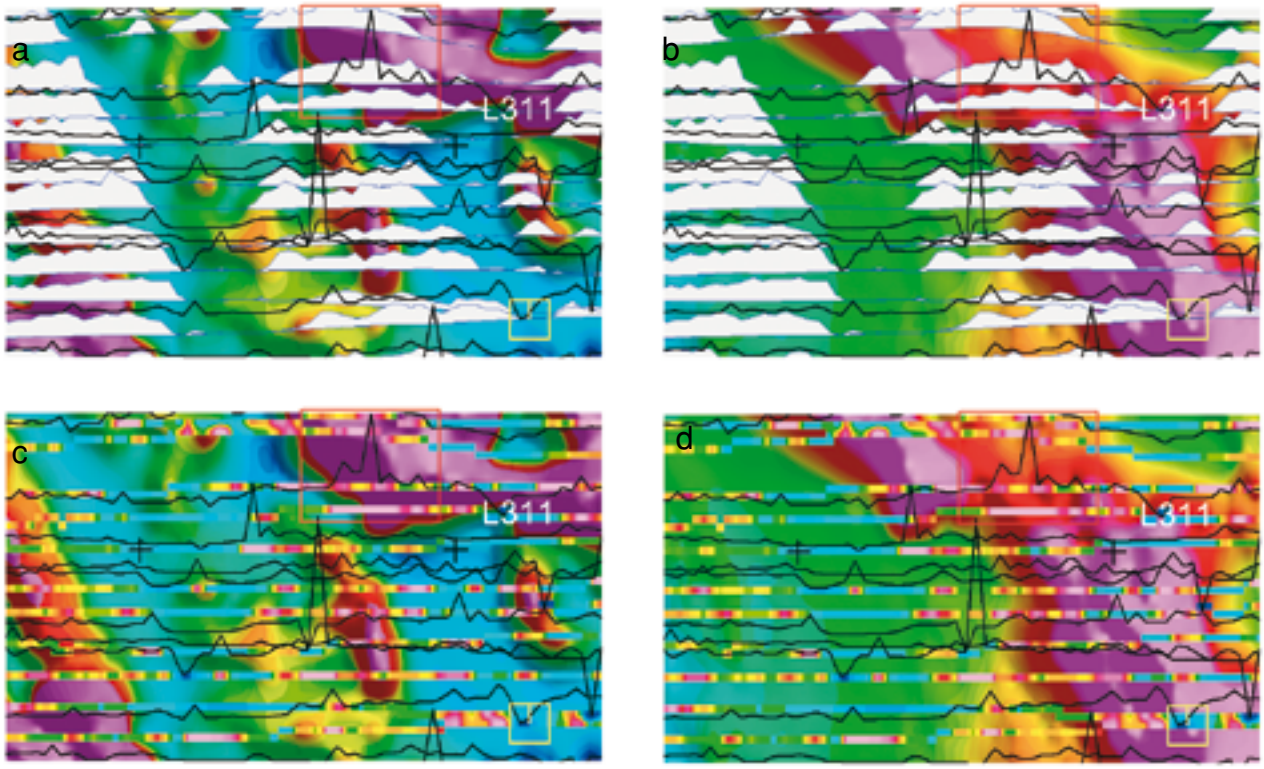

Fig. 11. Kettukuusikko, K/Th values along flight line L311 (red outline) shown in black in a) and b), and as interpolated grid (25 m on both sides of the flight line path) in c) and d). Ligh grey profiles show K-radiation. AEM in-phase in a) and c); AM in b) and c). L311 is shown in detail in Fig. 12. aerogeophysical data, GTK. 200 m line spacing. Size of view shown in Fig. 10.

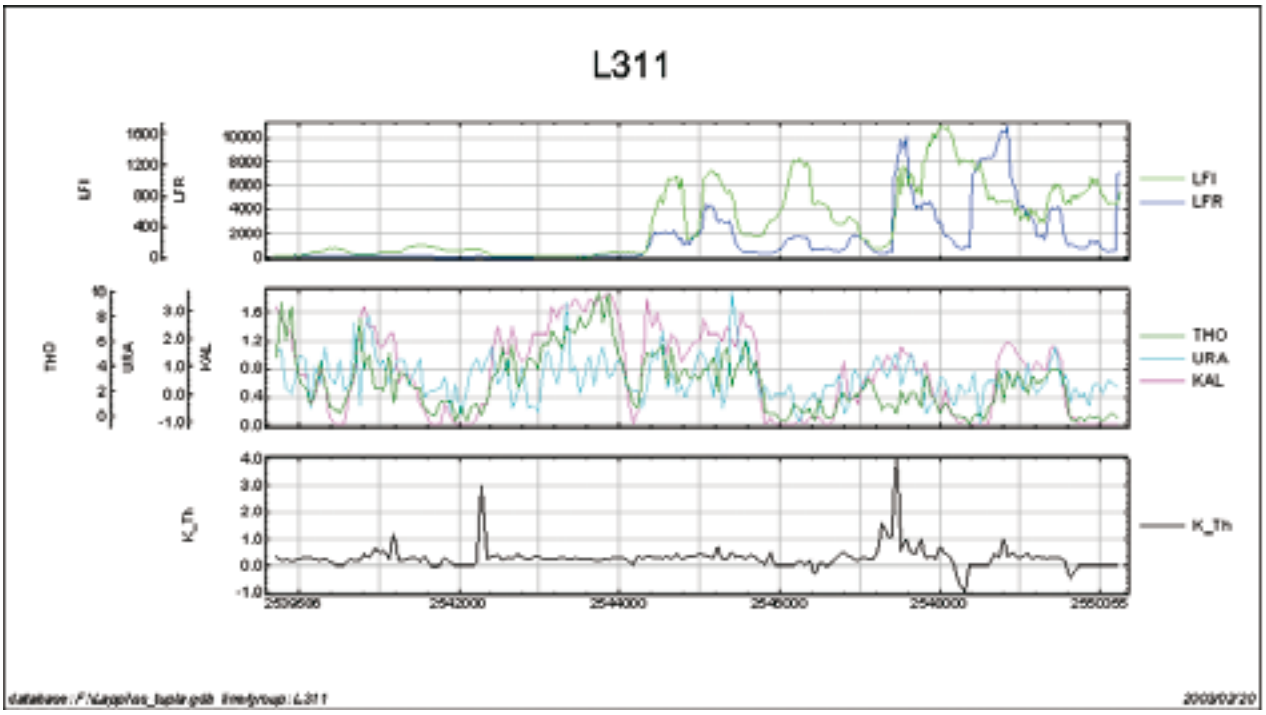

Fig. 12. Measured survey data along flight line L311. LFI = low-frequency imaginary (= out-of-phase) component in ppm; LFR = low-frequency real (=in-phase) component in ppm; THO = eTh (in ppm); URA = eU (ppm); KAL = K%; K_TH = calculated K/Th. Profile length is 10 km (displayed in metres). Notice the relatively higher K/Th values between 2547000 and 2548000, and the associated Th low at the contact zone of the good electrical conductor (indicated by the LFR anomaly much greater than LFI). Aerogeophysical data, GTK.

In summary, the correlations represented above support the idea of applying K/Th data in selecting gold exploration targets. Furthermore, based on regional studies elsewhere in Finland, anomalous U/Th ratios in aeroradiometric data were typically observed close to massive sulphide deposits. It is possible, that as sulphide-bearing geological units are expected to erode easily, the observed U radiation is preferably emitted from the highly fractured rock sequences. Hence, blocks of U-bearing rocks will be distributed into the surrounding overburden thus enhancing the radiometric results, in the same way as the brecciated ultramafic units. The importance of K/Th and U/Th as indicators of alteration zones are reviewed and compared also in Airo (2002).

Aerogeophysical test survey by using 75 m line spacing

The investigations reported above were based on airborne survey data flown at a 200 m line spacing, and results concerning structural interpretation and detection of altered greenstone units were shown to be promising. The EM results were based on low frequency (3 kHz) measurements, which were the standard before 1990´s. However, improved information on the detailed structural geology was obtained by decreasing the flight line spacing to 75 m. Additional input for interpretation is obtained from two-frequency AEM measurements (3 kHz = "low-frequency" in the following, and 14.4 kHz = "high-frequency") or, by the surrent use of four frequences since 2007. In 2001, test surveys were conducted in two areas (Kolvakero and Levijoki) in the western part of the CLGB, where Saattopora and Pahtavuoma deposits (see locations in Fig. 1) have been mined. Different airborne data sets from Kolvakero are compared in Fig. 13.

White regions in Fig. 13a correspond to moraine and sandy hills or topographically higher basement, whereas the low regions between them are commonly wet soils and swampy areas. The digital elevation data in Fig. 13b displays elevation mainly between 200 and 400 m above sea level. The magnetic image in Fig. 13c shows the E-W stratigraphy of the Kittilä Group greenstones and fracturing parallel to the main schistosity along and across the startigraphy. Kittilä Group is separated from the Savukoski Group by an almost E-W trending magnetic low, which looks like a broad fault zone. The magnetic low is situated north of the E-W valley in topography, at the southern edge of the Kittilä Group, suggesting that the magnetic low is

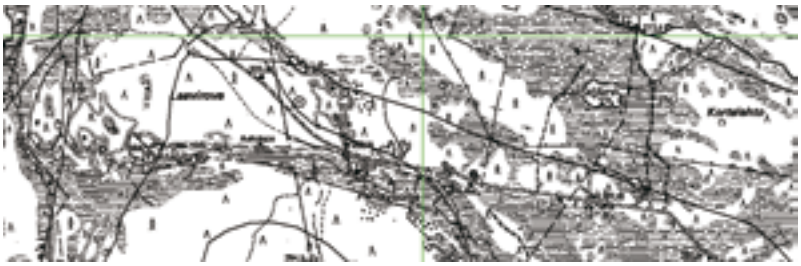

a) Topographic basemap (National Land Survey).

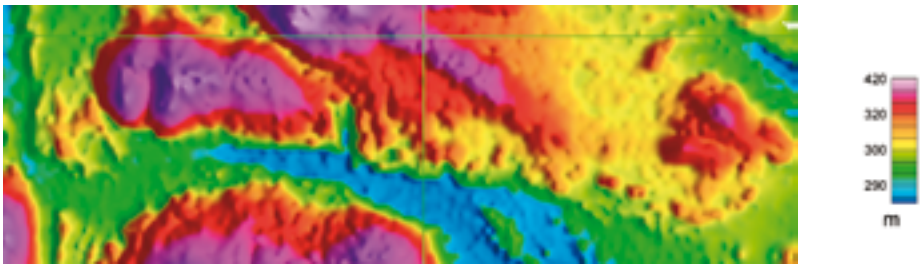

b) Digital elevation above sea level (terrain model based on data by National Land Survey).

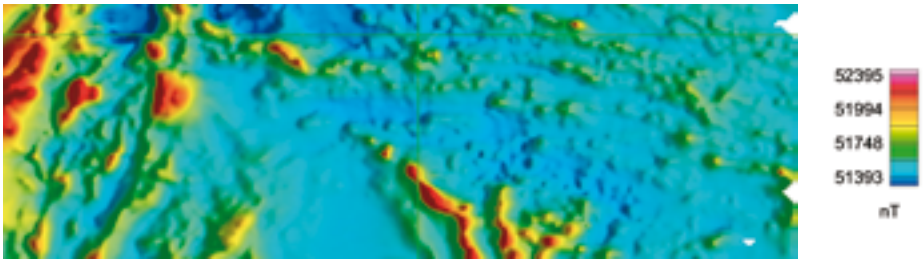

c) Aeromagnetic shaded relief image (illuminated from NE).

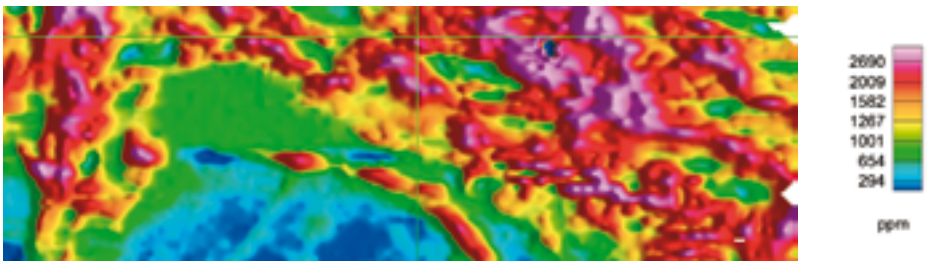

d) EM high-frequency, in ppm (14.4 kHz) quadrature.

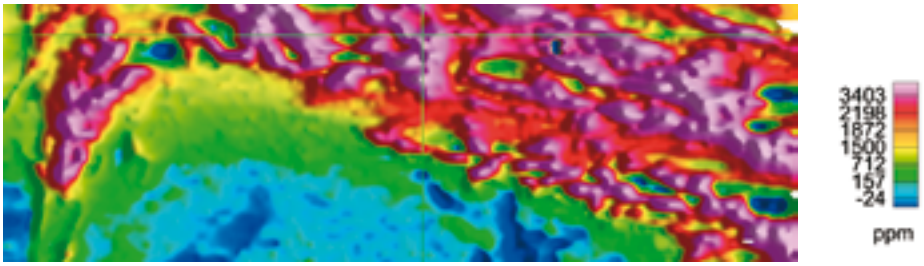

e) EM high-frequency, in ppm (14.4 kHz) in-phase.

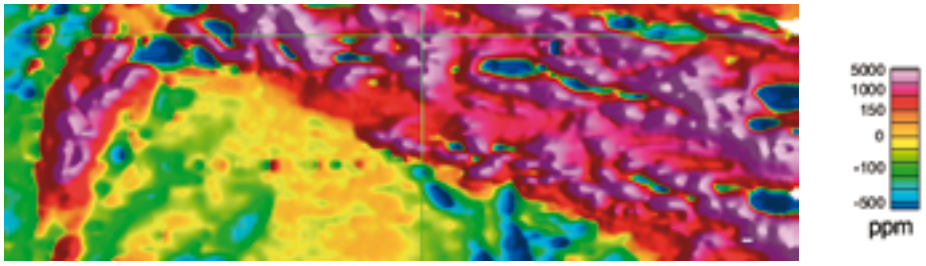

f) EM low-frequency (3 kHz) in-phase.

Continue next page

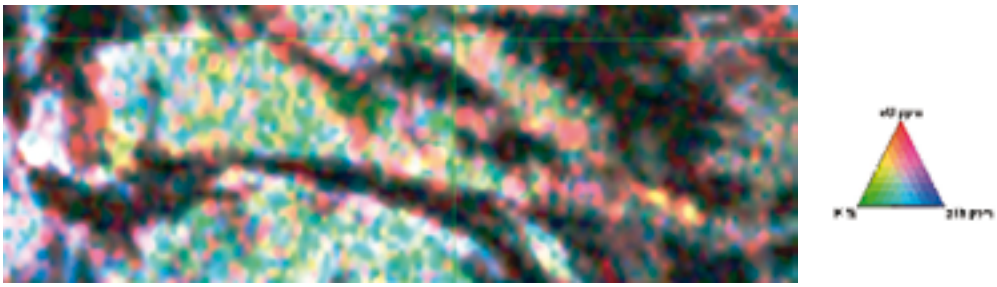

g) Aeroradiometric (AR) ternary image.

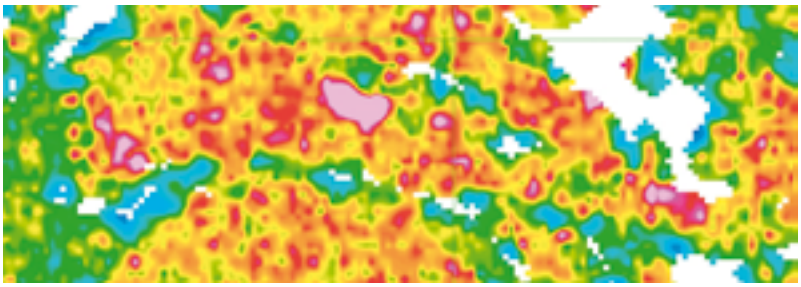

h) AR calculated K/Th.

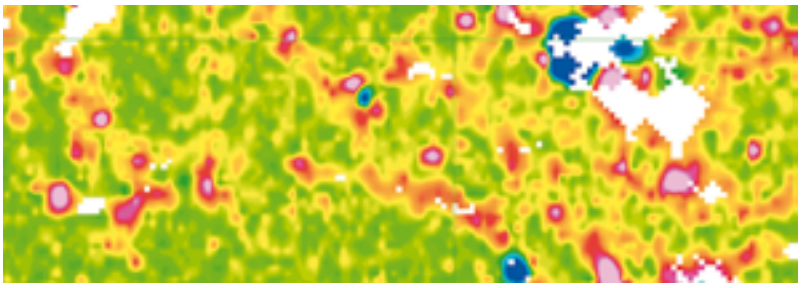

i) AR calculated U/Th.

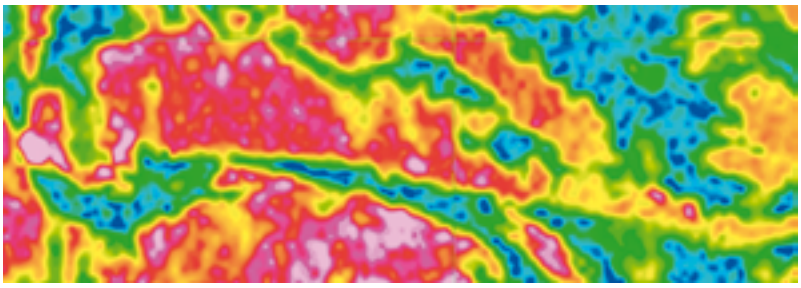

j) AR K concentration (%).

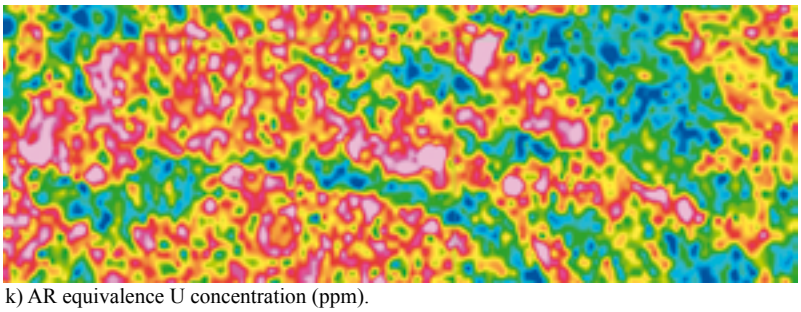

k) AR equivalence U concentration (ppm).

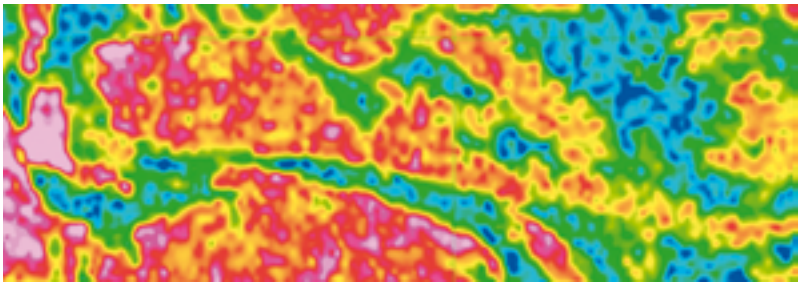

l) AR equivalence Th concentration (ppm).

Fig. 13. Kolvakero survey area, flown at 75 m line-spacing a nominal 30 m terrain clearance, GTK. Size of the area is 7.56 km by 2.5 km (green lines X=7525 and Y=2510 in Finnish co-ordinate system). Basemap © National Land Survey 521/MYY/07.

not necessarily caused by a fault zone. In the EM HFI (high-frequency quadrature), HFR (high-frequency in-phase) and LFR (low-frequency in-phase) images (Figs. 13d, e and f), the magnetic low is related to electrically conductive zones. HFI displays good correlation with wet, swampy areas in topography. The radiometric ternary image in Fig. 13g displays background radiation of bedrock and soil. Variable colours depend on the relationship between K, U and Th, whereas black regions illustrate attenuation of radiation due to water or wet soils. Deep green colour is related to enhanced potassium radiation and a high K/Th (Fig. 13h) in the area, which geologically corresponds to greenstones in the center of the image. The two yellow spots at the right hand of the image correspond with the tailings of the Pahtavuoma mine, also indicated by a relatively enhanced K/Th. Similarly, the mine is marked by enhanced U/Th in Fig. 13i. The mutual relationships of individual radioelements can be estimated in separate images of K (Fig. 13j), eU (Fig. 13k) and eTh (Fig. 13l). The relative U radiation increase along some of the river valleys, shown by red colour in the ternary image, are interpreted to be related to the increased U radiation in fractured rock, which feature is being repeatedly observed in the airborne gamma-ray data from Lapland.

SUMMARY AND CONCLUSIONS

The results stress the importance of careful analysis of regional geophysical data sets in an integrated manner. This improves understanding and evaluating the included geological information, both in a lithological and a structural sense. High-quality airborne geophysical data enable directing exploration from regional to prospect scale and selection of promising areas for detailed investigations. Correlation with geological and geochemical facts should be closely coupled to the interpretation process – already at an early stage. In particular, airborne radiometric data cannot be interpreted in a simple manner, since they are complexly affected by several factors, including bedrock and overburden properties. Background information on the influence of lithological variation and hydrothermally altered zones are necessary before estimating the reasons for the observed changes in radioelement ratios. Table 2 summarizes the applicability of various airborne methods in solving different exploration problems.

Based on magnetic interpretation, the distribution of brittle fracturing within the Central Lapland green-

Table 2. Distinctive structural, lithologic and alteration characteristics of greenstone belt gold deposits and effective airborne geophysical methods (adapted and modified from Meju 2002).

Physico-chemical features	Size of target features	Airborne method + support
Structural control (faults, folds, lineaments):		
a. Close spatial association of ore with major shear or deformation zones	10 to several 100 km long and several km wide	Regional AM, AEM + regional gravity
b. Folding may have provided extensional zones for ore deposition	All scales	Regional or detailed AM, AEM
c. Deposits found in reactivated, second or third order structures of the major shear zones especially in extensional zones	Structures up to 10 km long and several tens of metres wide; ore bodies up to 1 km long and tens of metres wide	Detailed AM (horizontal or vertical derivatives, analytic signal, shading), AEM; digital elevation model
Geological environment:		
a. Precambrian granitoid-greenstone belts	Elongate folded belts about 10 to > 100 km long	AM (commonly weak magnetization in greenstones), AEM + gravity
b. Favourable host rocks: mafic (high Fe/Fe+Mg); BIF; carbonated komatiite…	All scales	AM, AEM resisitvity
c. Carbonaceous sediments		AM, AEM, AR
d. Volcano-sedimentary schist association		AM, AEM conductivity, AR (enhanced eU and eTh)
Hydrothermal alteration:		
a. Carbonatization (extensive and most common)	Along rock boundaries and major structures; ten to 100 metres wide	AR (enhanced K for mafic host rocks), AM (commonly magnetite destruction)
b. Sulphidation (replacement of Mgt by Py/Po)	Narrow zones Cross cutting structures or zones	AEM conductivity, AM increase if Po, AM decrease when Mgt->Py, especially in BIFs;
c. Sulphidation of BIFs	Very narrow zones	AR (enhanced eU and often locally depleted eTh; locally increased U/Th)
d. Silicic alteration	Slightly less extensive than carbonation	Decreased/changed magnetization
e. Potassic alteration		

Mgt = magnetite Po = pyrrhotite AM = aeromagnetis AR = aeroradiometric
Py = pyrite BIF = bauded iron formation AEM = aero-electromagnetic

stone belt is strongly controlled by the geometry of geophysical – and structural – province boundaries. Fracture trends are also controlled by the layering and regional axial fold plane trends of the greenstones. Other important zones are the contacts between electrical conductors and altered ultramafic and tholeiitic greenstone units. These structurally weak zones have potentially been pathways also for Au-mineralising hydrothermal fluids. The resulting alteration zones create noticeable geophysical response. The NS-directed, gently curved brittle fracture trends, composed of set of small-scale shear structures, cut the other fracture trends in many places. They may represent the shallow indicators of deep block boundaries at depth.

REFERENCES:

Airo, M-L. & Korhonen, J.V. 1982. Aeromagnetic anomaly maps of Finnish Lapland. Proceedings: 15. Nord. Geol. Vintermöte, Reykjavik, Iceland, 5.–8.1.1982.

Airo, M-L. & Korhonen, J.V. 1983. On geological interpretation of aeromagnetic maps in Central Finnish Lapland. Proceedings: 14. Noftigmöte, Copenhagen, Denmark 10.–12.1.1983.

Airo, M-L. 1993. Correlation between magnetization and magnetite grain size and shape: Kaunislehto metavolcanic rocks, northern Finland. In: Autio, S. (ed.) Geological Survey of Finland, Special Paper 18, 129–132.

Airo, M-L. 1999. Aeromagnetic and petrophysical investigations applied to tectonic analysis in the northern Fennoscandian shield. Geological Survey of Finland, Report of Investigation 145. 51 p.

Airo, M-L. 2002. Aeromagnetic and aeroradiometric response to hydrothermal alteration. Surveys in Geophysics 23, 273–302.

Cordell, L. & Knepper, D.H. 1987. Aeromagnetic images: Fresh insight to the buried basement, Rolla quadrangle, southeast Missouri. Geophysics, 52, 218–231.

Eilu, P. 1994. Hydrothermal alteration in volcano-sedimentary rocks in the Central Lapland greenstone belt, Finland. Geological Survey of Finland, Bulletin 374, 1–145.

Eilu, P. 1999. FINGOLD – a public database on gold deposits in Finland. Geological Survey of Finland, Report of Investigation 146, 224 p.

Gaál, G., Berthelsen, A., Gorbatschev, R., Kesola, R., Lehtonen, M., Marker, M. and Raase, P. 1989. Structure and composition of the Precambrian crust along the POLAR profile in the northern Baltic shield. Tectonophysics 162, 1–25.

Grant, F.S. 1985. Aeromagnetics, Geology and Ore Environments, I. Magnetite in Igneous, Sedimentary and Metamorphic Rocks: an Overview. Geoexploration, 23, 303–333.

Hölttä, P., Väisänen M., Väänänen, J. & Manninen, T. 2007. Paleoproterozoic metamorphism and deformation in Central Finnish Lapland. In: Ojala, V.J. (ed): Gold in the Central Lapland Greenstone Belt, Finland 2007. Geological Survey of Finland, Special Paper 44, 7–56.

Korhonen, J.V., Airo, M-L. & Tiainen, L. 1985. Tectonic and stratigraphic interpretation of aeromagnetic and gravity data in Rajala area, Central Finnish Lapland. Geoexploration 23, 435.

Lehtonen, M., Airo, M-L., Eilu, P., Hanski, E., Kortelainen, V., Lanne, E., Manninen, T., Rastas, P., Räsänen, J. & Virransalo, P. 1998. Kittilän vihreäkivialueen geologia. Geological Survey of Finland, Report of Investigation 140. Summary: The stratigraphy, petrology and geochemistry of the Kittilä greenstone area, northern Finland. 144 p.

Meju, A.M. 2002. Geoelctromagnetic exploration for natural resources: models, case studies and challenges. Surveys in Geophysics 23, 133–205.

Pajunen, M., Airo, M-L., Wennerström, M., Niemelä, R. & Wasenius, P. 2001a. Preliminary report: The "Shear zone research and rock engineering" project, Pori area, southwestern Finland. In Autio, S. (ed.), Geological Survey of Finland, Special Paper 31, 7–16.

Pajunen, M., Elminen, T., Airo, M-L. & Wennerström, M. 2001b. Structural evolution of bedrock as a key to rock mechanical properties. In Rock Mechanics. A Challence for Society. Proceeding of Regional Symposium EUROCK 2001. A.A. Balkema, Rotterdam, 143–148.

Puranen, R. 1989. Susceptibilities, iron and magnetite content of Precambrian rocks in Finland. Geological Survey of Finland, Report of Investigation 90, 45 p.

Rastas, P., Huhma, H., Hanski, E., Lehtonen, M.I., Härkönen, I., Kortelainen, V., Mänttäri, I. & Paakkola, J. 2001. U-Pb isotopic studies of the Kittilä greenstone area, Central Lapland, Finland. In Vaasjoki, M. (ed.) Radiometric age determinations from Finnish Lapland and their bearing on the timing of Precambrian volcano-sedimentary sequences. Geological Survey of Finland, Special Paper 33, 95–141.

Satoh, T., Nishizawa, O. & Kusunose. K. 2000. Focal Mechanism of Acoustic Emission in Oshima Granite under Triaxial Compression. Tohoku Geophysical Journal, Vol. 35, Nos. 3–4, 121–131.

Sorjonen-Ward P., Nurmi P. A., Härkönen I. & Pankka H. S. 1992. Epigenetic gold mineralization and tectonic evolution of a lower Proterozoic greenstone terrane in the northern Fennoscandian Shield, in Metallogeny related to tectonics of mobile belts. Sarkar S. C. (ed) 37–52, Oxford and IBH Publishing, New Delhi.

Wennerström M. & Airo, M.-L. 1998. Magnetic fabric and emplacement of the post-collisional Pomovaara Granite Complex in northern Fennoscandia. In: Liegéois, J-P. (ed.), Lithos Vol. 45 (1998) Post-Collisional Magmatism, p. 131–145.

Gold in the Central Lapland Greenstone Belt, Finland
V. Juhani Ojala (ed.)
Geological Survey of Finland, Special Paper 44, 209–223, 2007.

GROUND GEOPHYSICAL CHARACTERISTICS OF GOLD TARGETS IN THE CENTRAL LAPLAND GREENSTONE BELT

by
Heikki Salmirinne and Pertti Turunen

Salmirinne, H. & Turunen, P. 2007. Ground Geophysical Characteristics of Gold Targets in the Central Lapland Greenstone Belt.*Geological Survey of Finland, Special Paper 44,* 209–223, 12 figures and 1 table.

A short review with some examples of petrophysical and ground geophysical work done by the Geological Survey of Finland for gold exploration in the Central Lapland Greenstone Belt (CLGB) is presented.

Although gold occurs in such low concentrations that it does not give any direct geophysical response, gold mineralized geological structures such as faults, shear zones, lithological units, alteration zones and associated minerals can usually be located by geophysical methods. The applicability of geophysical methods depends on the contrast in the physical properties of the target and the country rocks. According to regional petrophysical data the gold mineralized and altered greenstones differ slightly from the unaltered rocks in terms of density and magnetic susceptibility. Apparent resistivity, chargeability, and gamma radiation show that depending on the contrast in physical properties of the gold mineralized and the unaltered country rocks, ground geophysical methods can in many cases be used to locate and study gold mineralization indirectly. Electric or electromagnetic methods are an obvious choice in exploring for gold if sulphides are included.

The most important geophysical methods used are magnetics together with electromagnetic VLF-R or HLEM. Magnetic anomalies provide information about geological units, faults, and shear and alteration zones. Electromagnetic anomalies are caused by graphite, sulphides and fractures containing water. IP may detect disseminated sulphides and SP is used to map and classify conductive sulphide and graphite occurrences. Since gold mineralization is commonly related with potassic alteration, radiometric methods may prove to be useful.

Key words (Georef Thesaurus, AGI): gold ores, mineral exploration, Central Lapland Greenstone Belt, geophysical methods, ground methods, petrophysics, Paleoproterozoic, Kittilä, Sodankylä, Lapland Province, Finland.

Geological Survey of Finland, P.O. Box 77, FI-96101, Rovaniemi, Finland.

E-mail: heikki.salmirinne@gtk.fi, pertti.turunen@gtk.fi

INTRODUCTION

The physical properties of gold (Au), density 19300 kg/m^3 and electrical conductivity 5*10^7 S/m, are one of the most anomalous of all elements. In spite of this it is almost impossible to get direct geophysical response from gold, because of its low grade in deposits (Doyle, 1990). Nevertheless, geological structures such as faults and shear zones, lithological units, alteration zones and minerals (e.g. pyrite), that are associated with gold, can often be mapped by geophysical methods (Paterson and Hallof, 1991).

Known characteristics of orogenic gold deposits in greenstone belts are (e.g. Airo, 2002; Allibone *et al*., 2002; Groves and Foster, 1991; Paterson and Hallof, 1991)

- commonly sited adjacent to crustal-scale shear zones
- on district scale sited in affiliated smaller faults or shear zones geometrically related to crustal-scale shear zones
- host rock can be almost any rock type
- detectable geophysical anomalies can be caused by the alteration haloes (common alteration processes includes carbonatization, sericitisation and silicification)

Crustal-scale structures, faults and shear zones commonly produce observable geophysical anomalies of which aeromagnetic and gravity surveys are the most useful methods. Detailed ground geophysical surveys are used to detect smaller-scale faults and shear zones, alteration zones and minerals associated with gold to guide drilling.

Although the geophysical methods form an essential part of gold exploration, particularly where outcrops are rare, one has to remember that the usefulness of the various methods depends on the contrast between the physical properties of the target and the host rock. Because orogenic gold mineralization can occur in various rocks type, there exist a wide variety of geophysical anomalies produced by the occurrences of different types. This means that the explorer must have experience, persistence and luck; "Gold is where you find it".

PETROPHYSICAL CHARACTERISTICS OF ROCKS

Petrophysical data can be acquired by two means. The more accurate and repeatable method is to use laboratory equipment to measure the rock samples. The other way is to lower a probe into a drill hole and measure the properties, not so accurately as in the laboratory, but *in-situ*. These two methods do not replace each other as some of the physical properties can be measured only in the laboratory conditions (say, remanent magnetization), and some only in the drill holes (say, temperature). Some of the most commonly used properties, viz. density, magnetic susceptibility, and gamma radiation intensity, can be recorded in a laboratory or drillhole whereas apparent resistivity and chargeability belong to the drill hole logging category in practical mineral exploration. The electrical properties could be determined from drill core samples, but a denser spatial coverage together with practically real-time availability and lower cost make loggings more attractive.

In the national petrophysical database maintained by the Geological survey of Finland (GTK) (Korhonen *et al*., 1993; Säävuori and Hänninen, 1997) there are about 6500 rock samples gathered from the area of the CLGB. A summary of petrophysical properties (medians of bulk density, magnetic susceptibility and intensity of remanence) of different rocks types, measured in the laboratory, is presented in Table 1. 901 samples are from mafic volcanic rocks (greenstones). Density of mafic volcanic rocks is higher than other rocktypes. The density of granites is about 320 kg/m^3, and quartzites about 290 kg/m^3, lower than the average density of greenstones. Median of susceptibility presented in table 1, does not respect typical bimodal susceptibility distribution of Precambrian rocks (Puranen, 1989) into para- and ferromagnetic subsets. Susceptibility histograms should be used to identify these parts and median can be used just for a rough comparison between different rocktypes. The susceptibility of mafic volcanic rocks shows some variation, but is generally lower than in other rocks. On aeromagnetic maps, greenstones produce relatively low magnetic field values. Generally low magnetization is caused by intense regional hydrothermal alteration, predating regional metamorphism (Lehtonen *et al*., 1998). Locally, especially in marginal areas, where highly magnetic layers have been tectonically repeated and abundance of magnetite was increased in certain layers during regional metamorphism, strong magnetic varieties are more common (Lehtonen *et al*., 1998). There are no laboratory conductivity measurements in the database, but airborne electromagnetic data show numerous conductitivity anomalies within volcanic-metasedimentary rocks, mainly caused by graphite-bearing schists.

Table 1. Petrophysical properties of rocks in Central Lapland Greenstone Belt. Data from GTK's national petrophysical database.

Rocktype	Density [kg/m3]			Susceptibility [10-6 SI]		Remanence [10-3 A/m]	
	Count	Median	stddev	Count	Median	Count	Median
Quartzite	1011	2622	82	1003	240	551	32
Mica schist	344	2776	99	344	27395	182	250
Skarn	51	2821	148	51	832	36	25
Dolomite	25	2677	103	25	167	23	20
Mylonite	17	2638	178	17	376	9	10
Phyllite	27	2762	81	27	724	18	60
Carbonate rock	55	2697	129	54	565	44	23
Black schist	62	2609	257	59	290	40	29
Sericite schist	38	2700	99	38§	1104	28	186
Conglomerate	108	2736	128	107	1220	43	70
Graywacke	31	2689	94	31	1912	11	480
Granite	1830	2589	55	1829	5620	1340	50
Monzonite	32	2690	93	32	23000	12	295
Gneiss	572	2678	129	572	4450	387	80
Granodiorite	105	2615	74	105	9303	45	67
Diorite	16	2727	117	16	3775	12	20
Quartz diorite	14	2750	52	14	49867	7	400
Gabbro	426	2980	132	427	1287	260	70
Granulite	112	2702	104	112	247	111	10
Quartz-feldspar schist	42	2646	54	42	433	14	165
Pegmatite	38	2581	65	38	510	24	25
Quartz / chert	22	2690	157	22	270	18	45
Quartz porphyry	28	2570	51	28	230	27	30
Porphyry	16	2596	146	15	6060	15	30
Feldspar porphyry	10	2579	93	10	11820	9	60
Quartz dike	13	2599	125	13	30	6	17
Diabase	184	2955	112	184	1100	144	55
Serpentinite	89	2826	147	89	67280	74	3970
Acidic/felsic volcanic rock	29	2693	118	29	820	18	270
Intermediate volcanic rock	33	2806	111	33	11740	25	149
Mafic volcanic rock	901	2911	118	879	927	623	20
Ultramafic volcanic rock	237	2893	103	237	21490	218	355

In the CLGB prospects petrophysical drill hole loggings have also been done. Apparent resistivity, chargeability, and gamma radiation are typical logging parameters. Two other parameters, density and susceptibility, can be measured with better accuracy in the laboratory, but the representativeness of the two modes are in the same class. The bulk density, measured in the laboratory, is a combination of dry and saturated density depending on the saturation degree of the sample. This vagueness causes only tiny errors in density due to small porosity of crystalline rocks. In hole logging gives *in-situ* information on the physical properties, i.e. the "real" properties that produce the anomalies mapped in the field.

The gold content in rocks is, excluding exceptional cases, so low that it has neither effect on the rock's physical properties nor causes geophysical anomalies. Instead of gold, one has to explore and study such rock

units that are somehow connected to gold, in other words, to find the gold indirectly. In the three cases that are described below, gold is related to certain altered rock units or sulphide mineralizations, that can be detected by geophysical methods.

Kaaresselkä. The ground water table at Kaaresselkä is typically 50 meter below the ground surface. The overburden and bedrock above this level are poor electrical conductors, which causes the logging responses to be subdued, especially the galvanic methods. Figure 1 shows histograms of gamma-gamma density, magnetic susceptibility, Wenner apparent resistivity, chargeability, and total gamma radiation from 24 drill hole sections below the ground water table. The rocks have been classified into gold-bearing mylonites and other rocks. In the apparent resistivity and gamma radiation, there are satisfactory differences between the two classes, but in the density, susceptibility and chargeability, the distributions of the parameter values overlap too much to have use for the practical field exploration. In the case of susceptibility, the peak values are different, but the overlap of the two distributions is substantial.

Electrical and electromagnetic methods are best suited to gold exploration in the Kaaresselkä area. The use on gamma radiation is insignificant in the field mapping as the radiation attenuates to zero within 30 cm of the source. However, in drill hole logging, the gamma radiation can be used to detect the potassic alteration zone that is commonly related to the gold mineralization.

Loukinen. In the Loukinen occurrence the gold mineralization is hosted by breccias containing graphite. Rocks that contain graphite are good electrical conductors and are occasionally radioactive, because geochemical properties of uranium make it susceptible to deposit in sapropels. Figure 2 shows the physical properties logged from a borehole, together with gold content. The correlation between gamma radiation and gold content is very good. Further, apparent resistivity and chargeability correlate almost equally well with gold. The apparent resistivity minima are accompanied by chargeability maxima and vice versa. This means that both are caused by electrical conductors, and the polarization due to disseminated sulphides is not remarkable. The electrical anomalies can be explained by the black schist. Susceptibility is low and correlates weakly but positively with gold whereas the correlation between density and gold content is weakly negative.

In the Loukinen area petrophysical data suggests that the induced polarization may be effective as a ground survey method, and gamma radiation in the logging environment. The histograms in Figure 3 are based on 15 drill hole sections and show that the difference in chargeability between gold-bearing and other rocks is significant, more that one decade. Another clear difference is in the gamma radiation histograms, and the variation is even larger than shown in Figure 3, because the highest gamma peaks would go up to more than one thousand. There is, however, considerable overlap. In the three other parameters, the distributions of the gold-bearing and other rocks overlap. Below it will be shown that even if the logged chargeability seems to be a very good parameter, in practice black schists make its use difficult.

The incompatibility between the histograms of apparent resistivity and chargeability in Figure 3 is interesting. It is not clear how the gold mineralization is related to black schists and sulphides, which can be detected with electrical methods regardless of gold content. The chargeability works in much the same way, but is affected by polarization effects. For some reason, possibly mineralogical or structural, mineralized rocks polarize more than barren rocks. This phenomenon is especially clear in Figure 4, where chargeability, gamma radiation, and gold content from the drill hole R511 are shown. The data consist of samples of graphite-bearing breccias. Both the gamma radiation and gold content correlate well with chargeability. This correlation is detectable in most drill holes near R511, but its extrapolation outward should be done with care.

Iso-Kuotko. In the Iso-Kuotko area any rocktype can be mineralized and geophysical exploration is based on detecting sulphides in alteration zones with electric or preferably with electromagnetic methods.

Figure 5 shows the correlation between gold and sulfur and the associated variations in the apparent resistivity and chargeability. The correlation between gold and sulfur is clear and pronounced, which suggests that the gold mineralization is related with sulphides. Most sulphides are good conductors and polarize easily, and make finding gold possible in an indirect way. The size of the circles in the Figure 5 represents the apparent resistivities or chargeabilities as described in the legend. The lowest apparent resistivities are located in the right upper corner where sulfur and gold contents are highest. With chargeability, the situation is more complex as the largest circles are distributed evenly to cover the sulfur and gold variation range. This means that the apparent resistivity can be used to classify the sulphur, and that way gold content, but the chargeability can not. On the other hand, chargeability is more efficient in locating zones of weak gold content than apparent resistivity. The logging of chargeability together with apparent resistivity seems to be justified.

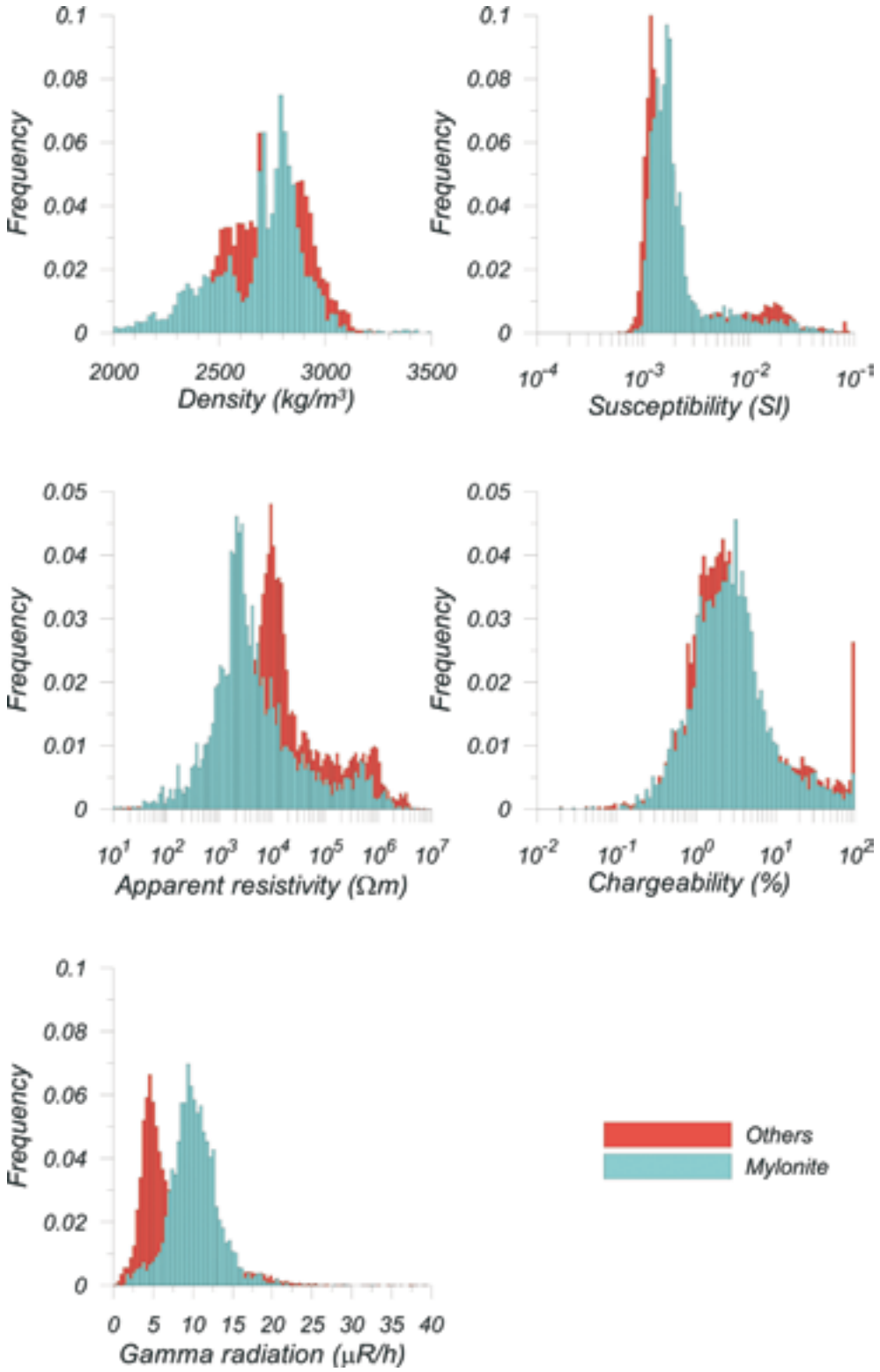

Fig. 1. Histograms of the physical properties of rocks from Kaaresselkä.

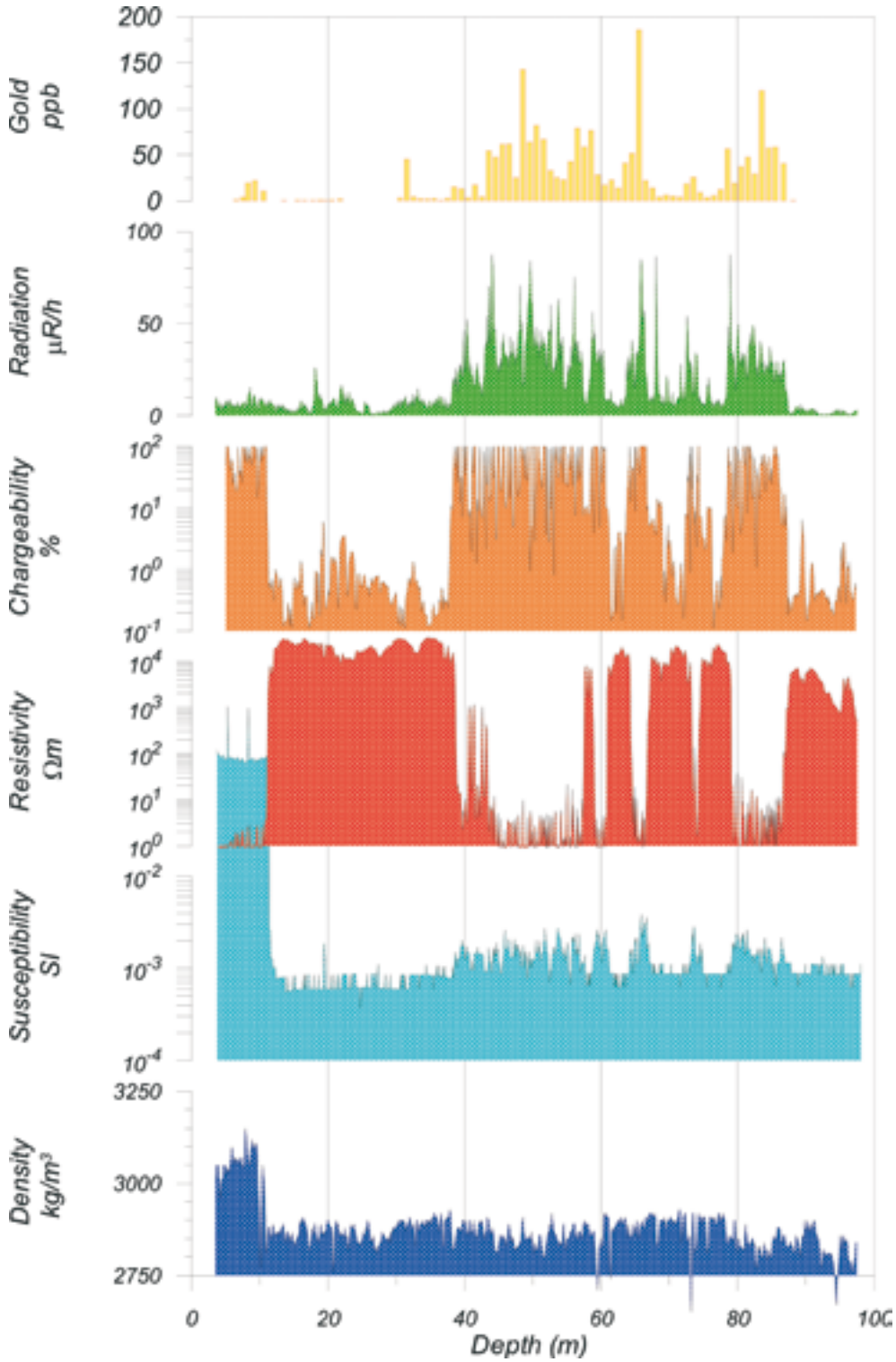

Fig. 2. Petrophysical logs and gold analyses from the drill hole R510 in Loukinen.

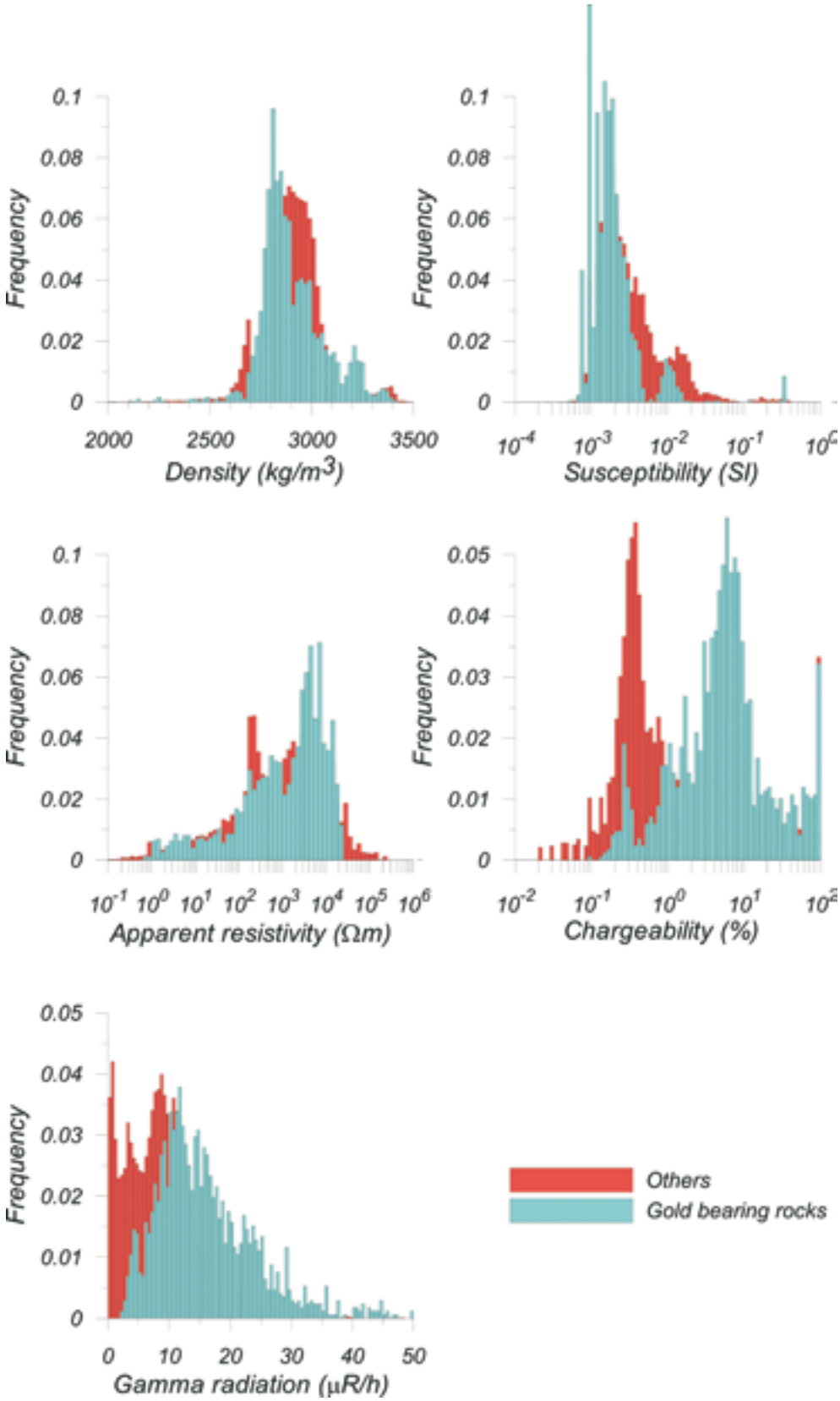

Fig. 3. Histograms of the physical properties of rocks from Loukinen.

The Iso-Kuotko area is not an ideal place for the drill hole surveys as the ground water level is very deep, almost 100 meter below the surface. Deep water table makes electric loggings difficult because there is no electrolyte present in the topmost parts of the bedrock. During surveys, water was poured into holes to make galvanic measurements somehow possible, but in spite of this the noise level at depths above the water table was rather high. This causes some noise in the logging data in Figure 5.

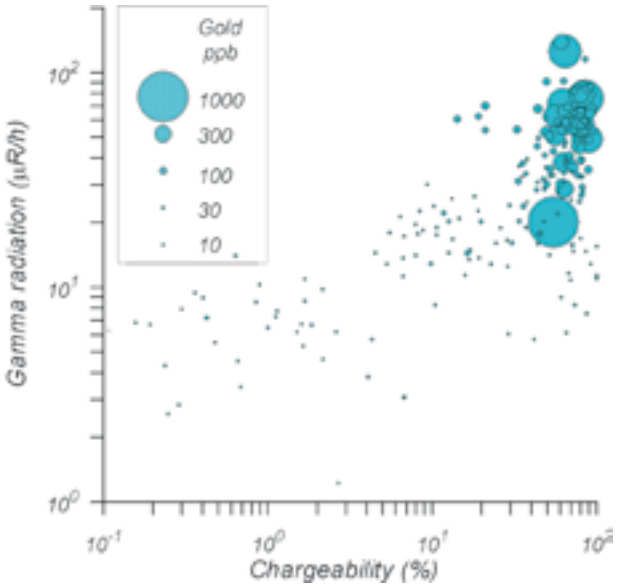

Fig. 4. Interdependence of chargeability, gamma radiation and gold content in the drill hole R511 in Loukinen.

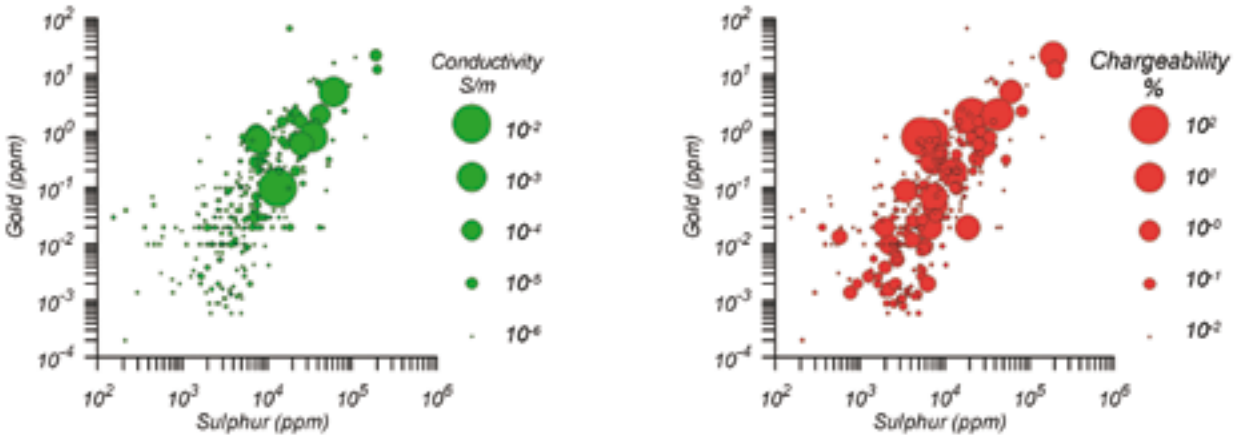

Fig. 5. Interdependence of sulfur content, gold content, conductivity and chargeability in Iso-Kuotko.

GROUND METHODS USED

In the Central Lapland Greenstone Belt proterozoic volcanic and metasedimentary rocks cover an area of about 10500 km^2. In addition to high-quality systematic airborne surveys, detailed ground geophysical surveys have been completed, for both geological mapping and exploration purposes (Fig. 6). The magnetic method, in combination with electromagnetic VLF-R or HLEM (Slingram) surveys, have been the main methods used. Other methods include gravity and Induced Polarization (IP). For these surveys line spacing has been mostly 200, 100 or 50 m and station spacing 20 or 10 m. There are also some very detailed Self Potential (SP) and Mise-à-la-Masse surveys, which are not presented in Figure 6. Below, known gold deposits are discussed in the context of regional gravity data. Examples of detailed surveys used to explore specific targets are then presented.

Regional gravity. In the early 1970's, GTK in co-operation with the Finnish Geodetic Institute began regional gravimetric surveys in which station density has varied from 1 to 6 per km^2. In CLGB area, gravimetric measurements include 14678 points in an area of about 14560 km^2, with an average point spacing of 1 point/km^2. Finnish Geodetic Institute has measured 1252 points in the same area (Kääriäinen and Mäkinen, 1997). Figure 7 has been compiled from these data sets. Volcanic rocks within CLGB are associated with higher Bouguer anomaly values compared to the surrounding granitoids. In the eastern part of the area, mafic layered intrusions, Keivitsa and Koitelainen, give

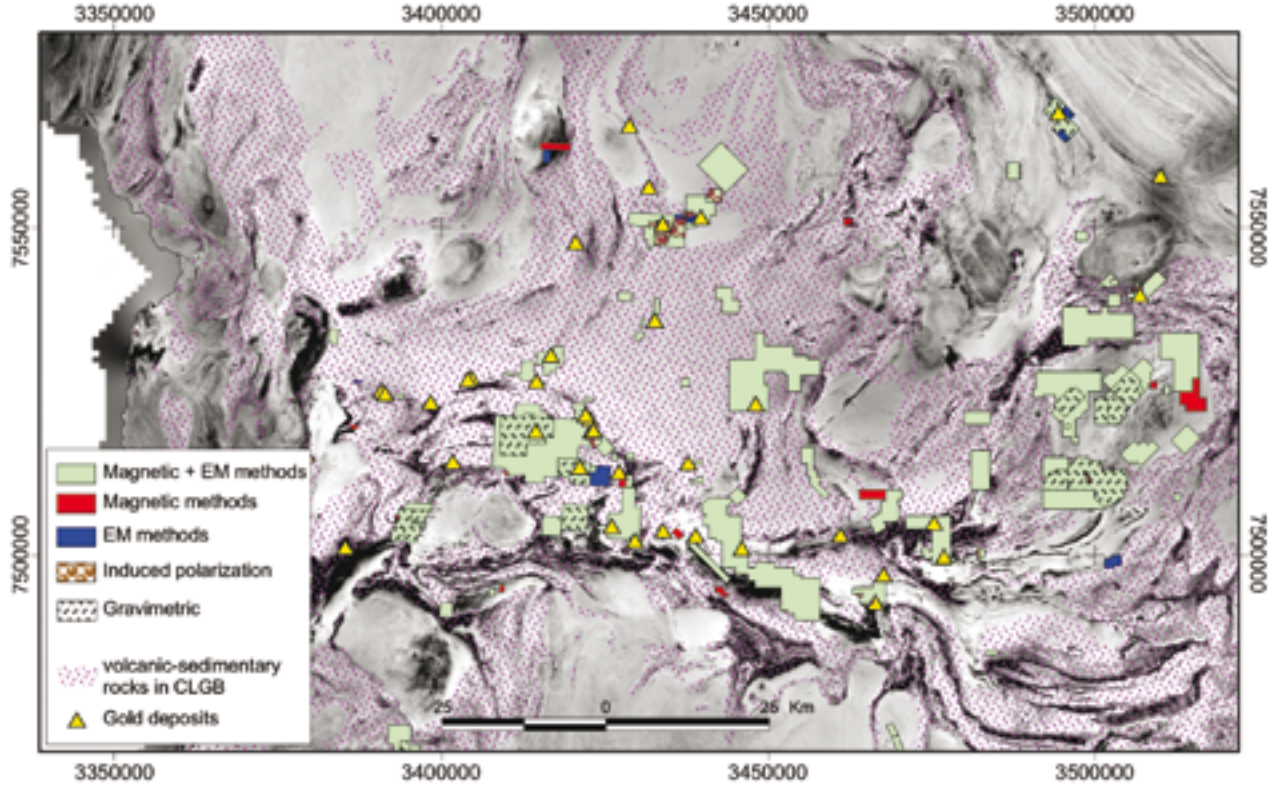

Fig. 6. Ground geophysical index map of GTK's surveys in the Central Lapland Greenstone Belt plotted on a gray scale aeromagnetic map. Gold deposits and volcanic-sedimentary rocks of the Central Lapland Greenstone Belt are shown. Aeromagnetic data by GTK.

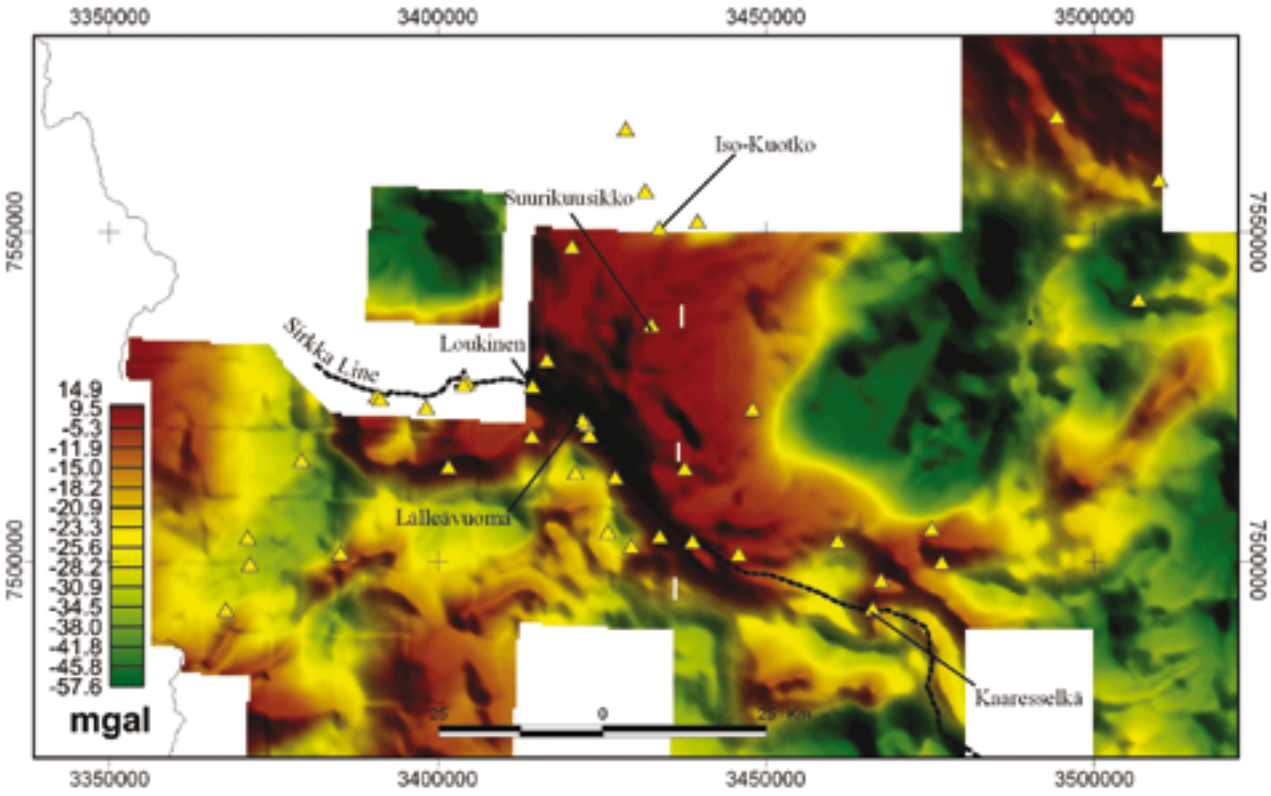

Fig. 7. Regional Bouguer anomaly map of CLGB. Station density 1 point/km^2. Sirkka Line and known gold deposits are shown as dotted line and triangles, respectively. Lälleävuoma, Loukinen, Suurikuusikko, Iso-Kuotko and Kaaresselkä deposits have been labelled separately.

rise to gravity highs, as does the Lapland granulite belt in the NE-part of the area.

Earlier geophysical interpretations (Elo *et al*., 1989, Lehtonen *et al*, 1998) suggest that the volcanic rocks dominated greenstone belt has a thickness of up to 6 km. The horizontal gradient of Bouguer anomaly indicates steep tectonic contacts between the greenstone belt and the surrounding granitoids. Most of the known gold deposits are situated along a tectonic contact zone, called the Sirkka Line, between volcanic and sedimentary rocks. However, the largest known deposit, Suurikuusikko, is situated along a N-S trending shear zone in the middle of Mg- and Fe-tholeiitic metavolcanic rocks. Weak negative Bouguer anomalies indicating shear zones and faults has been observed on gravity profiles measured across the zone (Lehtonen *et al*., 1998). These anomalies can be signals of intensely altered rocks within faults and shear zones such as in Suurikuusikko, and are worth of exploration in the future.

Magnetic, EM VLF-R and HLEM. The magnetic method is widely used geophysical tool in the gold exploration (Doyle, 1990) and in CLGB also. Magnetic data provide information on geological units, faults and shear structures. In some cases, alteration zones can be observed, because ferromagnetic minerals in mafic volcanic rocks are destroyed by alteration processes resulting in magnetic lows. Magnetic data from the Lälleävuoma deposit is presented in Figure 8. The deposit is located within a sequence of basaltic and komatiitic metavolcanic rocks and fine-grained metasedimentary rocks. The Sirkka Line occurs nearby

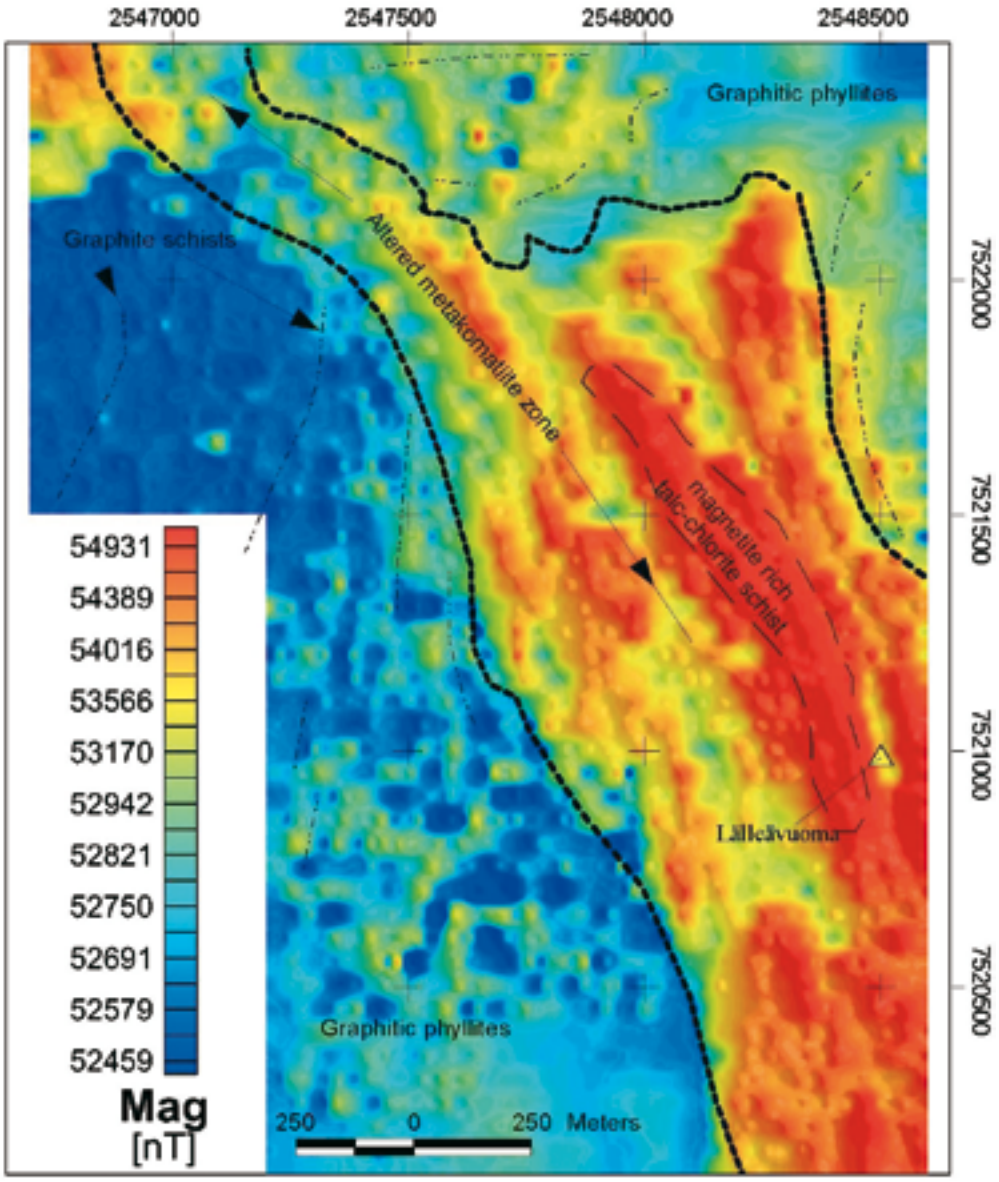

Fig. 8. Example of ground magnetic data from Lälleävuoma area. Total magnetic field was measured using proton precession magnetometer. Shaded relief map, illuminated from northeast. Line spacing 50 m and station spacing 10 m. Lälleävuoma deposit is marked by a yellow triangle.

(Eilu, 1999). Magnetite in talc-chlorite schists result in high magnetic intensity, whereas moderately carbonatizated rocks are seen as weak magnetic minima.

VLF-R is the often measured together with magnetic surveys in CLGB area by GTK. It is the most favourite electromagnetic method in northern Finland because it is cheap, fieldwork is fast and cultural noise levels are low in sparsely populated areas. In the Lälleävuoma area, Geonics EM16R instrument was used to conduct VLF-R surveys. VLF-R transmitter DHO-38 (frequency 23.4 kHz) in Germany was used. In the Lälleävuoma area, N-S trending metakomatiitic rocks stand out as a high resistive zone in the middle of the area (Fig. 9). The contacts between metakomatiites and conductive graphitic phyllites can be signified quite accurately.

An example of the ground magnetic data with electromagnetic HLEM (slingram) data is presented in Figure 10 from the Suurikuusikko deposit. The deposit is associated with a 15 km long, N-S trending shear zone chiefly located in the contact zone between major Mg- and Fe-tholeiitic metavolcanic units. The area around the deposit is dominated by mafic pyroclastic metavolcanic rocks (Härkönen, 1997). The gold deposit consists of lens-shaped, sulphide-bearing bodies striking in the main shear zone direction. Gold is associated with arsenopyrite, pyrite and gersdorffite. The sulphide-bearing tuffites or phyllites and graphitic host rocks give the major response in both magnetic and electromagnetic methods. The Suurikuusikko shear zone is indicated as a negative anomaly in magnetic maps and, due to abundant graphite vein network and pyrrhotite, as a low in the resistivity maps. Magnetite have been essentially destructed all along the shear

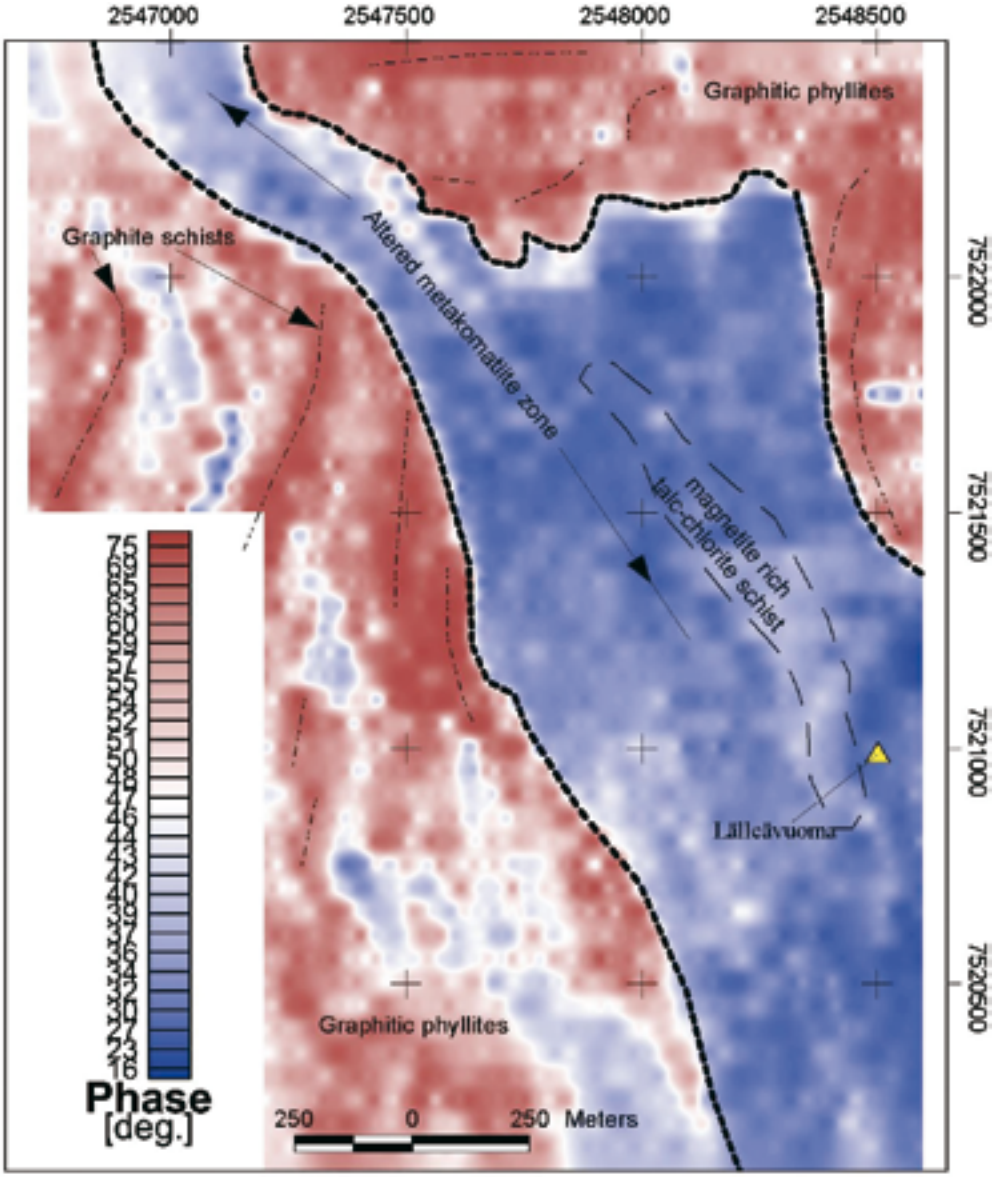

Fig. 9. Example of VLF-R phase data from Lälleävuoma area. Conductors can be seen as areas where phase angle is over 50 degrees. Line spacing 50 m, station spacing 10 m. Lälleävuoma deposit is marked by a yellow triangle.

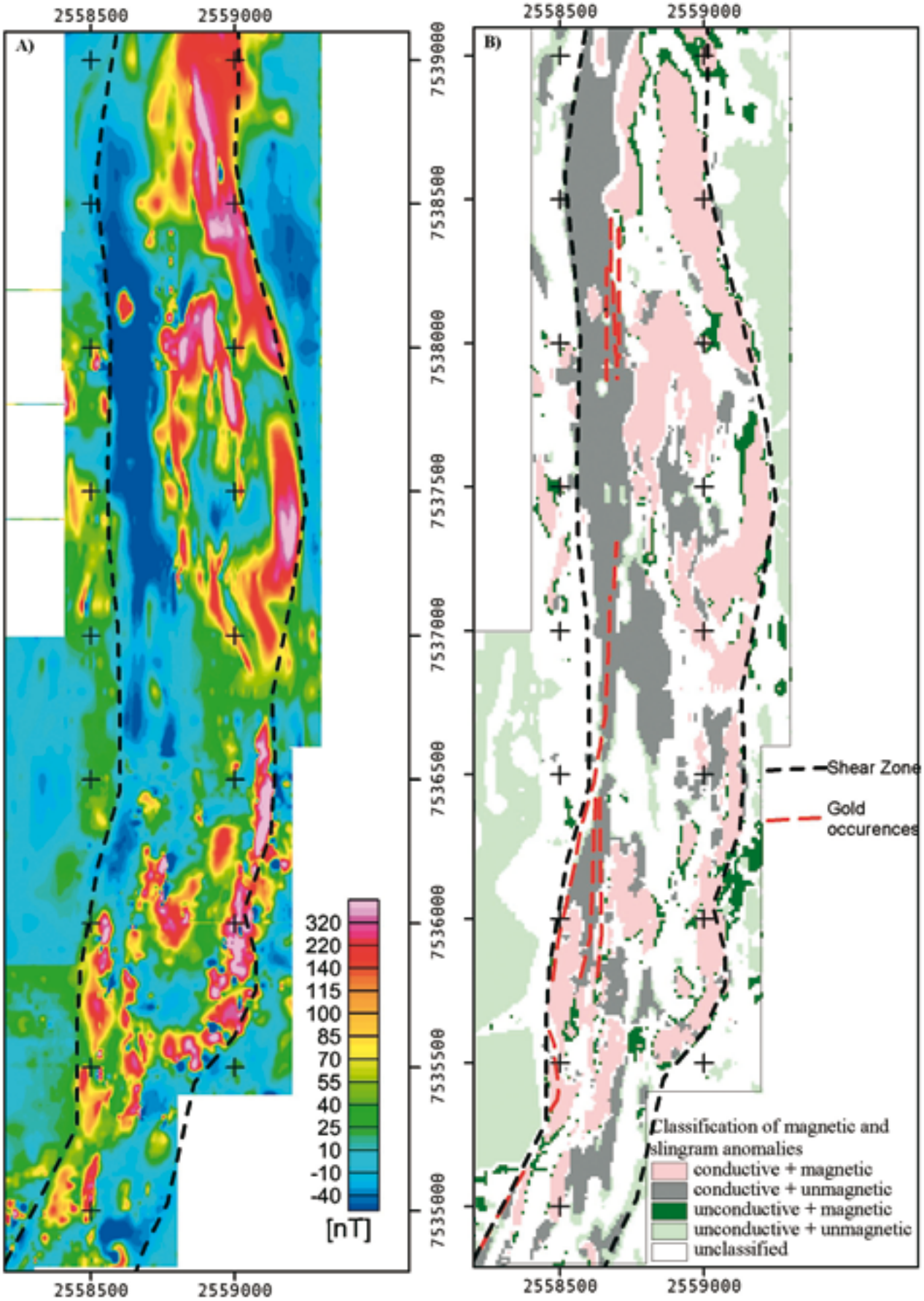

Fig. 10. A) Magnetic residual anomaly map and B) a rough classification of magnetic and HLEM (slingram) anomalies along the Suurikuusikko shear zone. Gold occurrences (Riddarhyttan Resources AB, 2002) marked by red dashed line. Data combined from GTK's and Riddarhyttan Resources AB's datasets.

zone as the result of alteration. Magnetic anomalies are caused mainly by pyrrhotite that in some places is massive (Härkönen, 1997; Eilu, 1999). Figure 10 presents the magnetic residual anomaly and a rough classification of the magnetic and HLEM anomalies measured along the Suurikuusikko shear zone.

Induced Polarization (IP). IP surveys have commonly been applied in gold exploration to locate sulphides in situations where sulphide concentration is low or moderate. Disseminated sulphide deposits in volcanic-sedimentary components of greenstone belts may not be detectable using electromagnetic methods (like VLF-R), but in some cases can be mapped using IP. In many areas of the CLGB, there are very conductive graphite-bearing schists that cause chargeability and conductivity anomalies and disturb and mask all other information. Time-domain measurements with a dipole-dipole array are commonly used, because this array is very sensitive to horizontal changes, and the effects of small local sources are larger than with other configurations.

An example of an IP survey from Iso-Kuotko deposit is presented in Figure 11. Scintrex IPR-10 receiver and dipole-dipole electrode array (a=20m, n=2) with 50 m line spacing and 20 m station spacing was used. Iso-Kuotko deposit is related to the intersection of the NW-trending Kuotko Main Shear (KMZ) and the NE-trending extension of the Suurikuusikko Shear Zone (SSZ). The mineralization and the host rocks are within a sequence of mafic metavolcanic rocks and volcanogenic metasedimentary rocks (Eilu, 1999). The Kati lode is directly related to the KMZ and strike of the Tiira lode corresponds to the SSZ. The structural geology of the area is complicated and rocks are strongly altered by albitization, carbonatization and silicification. Soil cover is thin, only up to 5 m (Härkönen *et al*., 2000).

In the Iso-Kuotko deposit, the Kati and Tiira lodes are indicated by VLF-R, HLEM and IP methods, as conductivity or chargeability anomalies. Sulphides (pyrite, arsenopyrite and pyrrhotite) are both semi-massive and disseminated, and there are no graphite. Conductive structures in the Tiira lode are subvertical and the chargeability response of IP measurements is sharp and distinctive, whilst in the Kati lode gold-bearing NW-SE trending horsetail-like thin quartz-carbonate veins with associated sulphides are dipping 40–50 degrees to NE and, consequently, the anomaly shape is more wide and fuzzy (Fig. 11). Anomalies indicate also several overlapping conducting layers near the surface to north and west of the Kati lode (Härkönen *et al*., 2000).

Self Potential (SP). In the areas where the water table is below the bedrock surface, the conditions are favourable for self potential differences to form. Anomalous potentials (hundreds of millivolts) can be observed over rocks bearing sulphide and graphite, or other conductive minerals. In many cases, large bog areas in northern Finland disturb measurements by masking the desirable response. However, the SP method has been infrequently, but successfully, used for mapping and classifying conductive sulphidic

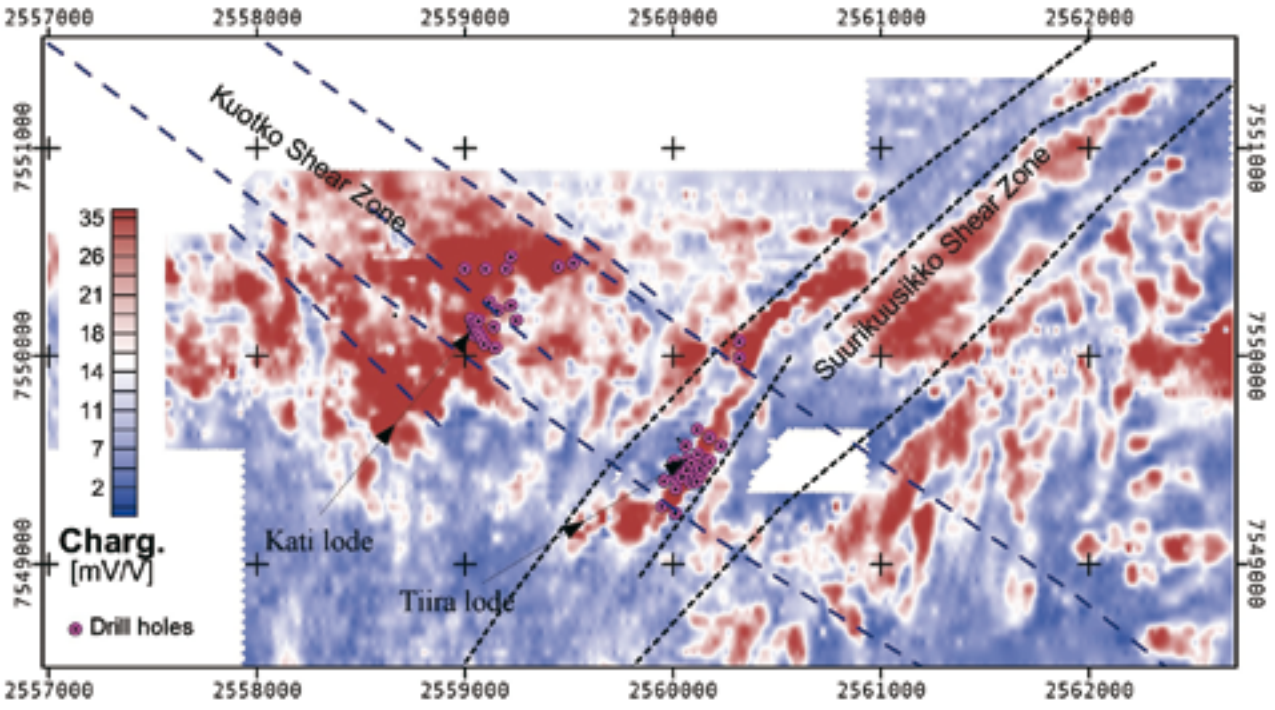

Fig. 11. IP chargeability anomaly map from Iso-Kuotko gold target. Gold-bearing sulphide lodes Kati and Tiira with drill hole locations are plotted. Trends of the Suurikuusikko and Kuotko shear zones are also shown.

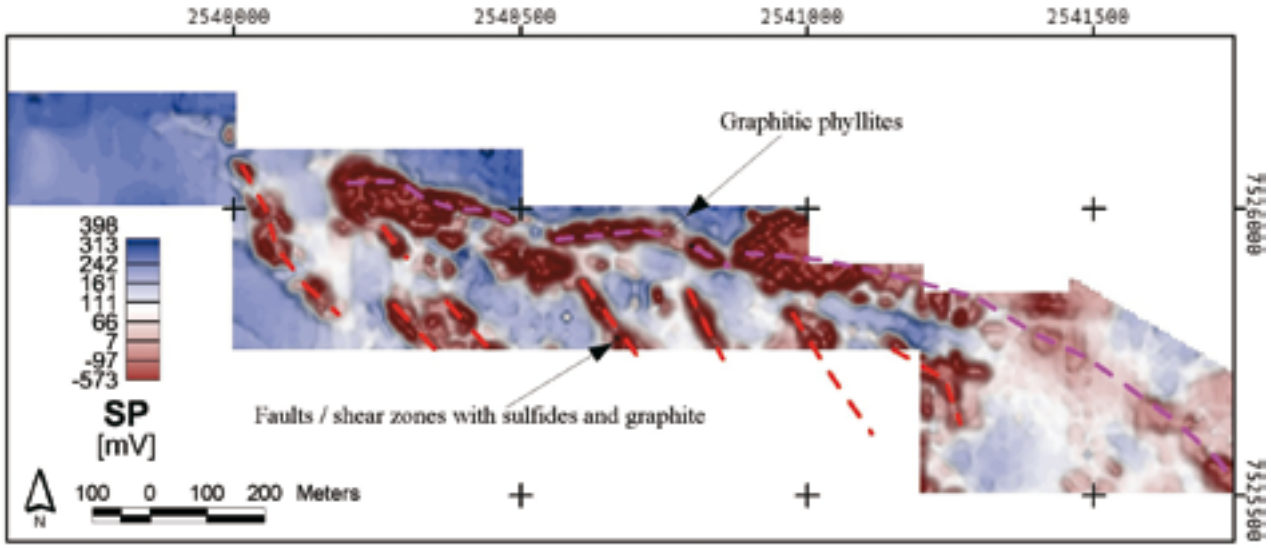

Fig. 12. SP results from the Loukinen gold occurence. Line spacing 10 m and station spacing 5 m was used. In the western part of SP-area, bogs masks and the response was not as good.

and graphitic formations. Data has been collected in the traditional manner by measuring the "absolute" potentials between nonpolarizing electrodes. One electrode is kept at a reference point while the other is moving. Commercial voltmeter with a sufficient high input impedance was used. The survey grid has usually been very dense so the resolution is good. An example from the Loukinen deposit is presented in Figure 12. Study area is located along the contact zone of ultramafic volcanic rocks and graphitic phyllites controlled by the Sirkka Line. Anomalies are caused by graphitic phyllites and partly weathered sulphides (pyrite, chalcopyrite, gersdorffite).

DISCUSSION

Geophysical methods used in the gold exploration in the CLGB have been applied quite widely. Ground magnetics in combination of EM VLF-R or HLEM have been the main methods used as the first step. Interpretation has been done mainly qualitatively, and the most interesting anomalies, assumed to be relevant for the appropriate problem, have been chosen for sampling and drilling. Magnetic anomalies provide information about geological units, faults, and shear and alteration zones. Electromagnetic anomalies are caused by graphite, sulphides and fractures containing water. As the second step other methods such as IP and SP have been used if considered to be useful. IP may detect disseminated sulphides and SP is used to map and classify conductive sulphide and graphite occurrences.

The value of the methods used depends on the petrophysical contrasts of the local rocks. Therefore petrophysical data is very useful to detect differences between gold mineralized units and barren country rocks. Examples of petrophysical drill hole loggings presented above indicate that in favourable cases it is possible to detect gold critical units indirectly. However, the selection of the methods has been done based on the geological and geophysical reasons as well as costs and equipment availability. For these reasons e.g. modern reflection seismic method has not been used for small-scale gold exploration in CLGB, although in many cases it could considered to be useful to map gold critical structures.

REFERENCES

Airo, M.-L., 2002. Aeromagnetic and aeroradiometric response to hydrothermal alteration. Surveys in Geophysics 23, 273–302.

Allibone, A.H., McCuaig, T. C., Harris, D., Etheridge, M., Munroe, S., Byrne, D., Amanor, J. & Gyapong, W. 2002. Structural Controls on Gold Mineralization at the Ashanti Deposit, Obuasi, Ghana. Society of Economic Geologist, Special Publication 9, 65–93.

Doyle, H. A. 1990. Geophysical exploration for gold – A review. Geophysics, vol 55, no 2, 134–146.

Eilu, P. 1999. FINNGOLD –a public database on gold deposits in Finland. Geological Survey of Finland, Report of Investigation 146. 224 p, 1 figure, 1 table and 2 appendices.

Elo, S., Lanne, E., Ruotoistenmäki, T. & Sindre, A. 1989. Interpretation of gravity anomalies along the POLAR Profile in the northern Baltic Shield. Tectonophysics 162 (1–2), 135–150.

Groves, D. I and Foster, R. P. 1991. Archean lode gold deposits. In: Foster, R. P. (ed.) 1991. Gold metallogeny and exploration. Blackie: 63–103.

Härkönen, I., Pankka, H.& Rossi, S. 2000. The Iso-Kuotko gold prospects, northern Finland. Sumary report, C/M06/2744/00/1/10. 18 p. + 9 appendixes.

Härkönen, I. 1997. Tutkimustyöselostus Kittilän kunnassa valtausalueilla Suurikuusikko 2 ja Rouravaara 1–10 (kaivosrekisterinumerot 5965/1, 6160/1, 6288/1–6288/9) suoritetuista kultatutkimuksista vuosina 1987–1997. English summary: Gold exploration during 1987–1997 within the exploration claims Suurikuusikko 2 and Rouravaara 1–10 (Mine reg. nos. 5965/1, 6160/1, 6288/1–6288/9). Geological Survey of Finland, unpublished report M 06/2743/97/1. 47 p. (in Finnish)

Korhonen, J.V., Säävuori, H., Wennerström, M., Kivekäs, L. & Lähde, S. 1993. One hundred seventy eight thousand petrophysical parameter determinations from the regional petrophysical programme. Geological Survey of Finland, Current research 1991–1992, 137–142.

Kääriäinen, J. & Mäkinen, J. 1997. The 1979–1996 gravity survey and results of the gravity survey of Finland 1945–1996. Publications of the Finnish Geodetic Institute. N:o 125. 24 p. + 1 app. map.

Lehtonen, M., Airo, M.-L., Eilu, P., Hanski, E., Kortelainen, V., Lanne, E., Manninen, T., Rastas, P., Räsänen, J. & Virransalo, P. 1998. Kittilän vihreäkivialueen geologia: Lapin vulkaniittiprojektin raportti. Summary: The stratigraphy, petrology and geochemistry of the Kittilä greenstone area, northern Finland: a report of the Lapland Volcanite Project. Geological Survey of Finland, Report of Investigation 140. 144 p. + 1 app. map.

Paterson, N.R. and Hallof, P.G. 1991. Geophysical exploration for gold. In: Foster, R. P. (ed.) 1991. Gold metallogeny and exploration. Blackie: 360–398.

Puranen, R. 1989. Susceptibilities, iron and magnetite content of Precambrian rocks in Finland. Geological Survey of Finland, Report of Investigation 90. 45 p. + 6 app. pages.

Riddarhyttan Resources AB. 2002. Länsprofiler av de mineraliserade zonerna i Suurikuusikko. Pressmeddelande 11.3.2002. Press release 11.3.2002, (in Swedish)

Säävuori, H. & Hänninen R. 1997. Finnish petrophysical database. In: Korhonen, J. V. (ed.) Petrophysics in potential field interpretation: First Workshop for the Finnish Geophysical Crustal Model Program, 15–16 August 1997, Espoo, Finland: abstracts. Espoo: Geological Survey of Finland, 53.

Gold in the Central Lapland Greenstone Belt, Finland
V. Juhani Ojala (ed.)
Geological Survey of Finland, Special Paper 44, 225–250, 2007.

PALAEO-STRESS MODELLING OF THE CENTRAL LAPLAND GREENSTONE BELT: IMPLICATIONS FOR GOLD EXPLORATION

by
V. J. Ojala and V. Nykänen

Ojala, V.J. Nykänen, V. 2007. Palaeo-stress modelling of the Central Lapland Greenstone Belt: Implications for gold exploration. *Geological Survey of Finland, Special Paper 44,* 225–250, 15 figures and 3 tables.

Palaeo-stress modelling applies geomechanical modelling codes to define dilatant (low stress) sites in a rock mass. These dilatational sites can be considered targets for structurally controlled mineralization. The main assumptions in the conceptual model are that the strain pattern of faults and lithological contacts has not been significantly changed since mineralization ie. that mineralization is late in the structural history, and that stress orientations and magnitudes and rheological properties of faults and rock units are known. UDEC code was applied to determine the palaeo-stress pattern caused by the fault network geometry and rheology within the Central Lapland Greenstone Belt at 1:250 000 scale to target orogenic gold mineralization. Modelling simulated E-W, N-S, NE-SW and NW-SE compression directions (D_3–D_4 deformation stage) and the minimum principal stress (σ_3) is used to indicate dilational areas.

The spatial association between the palaeo-stress modelling results of 12 different models (compression orientations and different fault classifications) and the known gold occurrences was quantified using logistic regression methods in ArcGIS. The minimum principal stress distributions of the models, which simulate E-W compression, have the highest positive weight, contrast and confidence. The maximum spatial association pattern in the best model cover 1.3% of the study area and include 11% of the known gold occurrences. In addition, the models that simulate NE-SW compression simulations give a good spatial association with known gold occurrences. This is in a good agreement with structural studies of the Central Lapland Greenstone Belt, which suggest that far field stress has varied from NE-SW to E-W during the late stages of the tectonic evolution and orogenic gold mineralization.

Key words (GeoRef Thesaurus AGI): gold ores, mineral exploration, Central Lapland Greenstone Belt, structural controls, ore-forming fluids, stress, paleostress, numerical methods, Lapland Province, Finland

Geological Survey of Finland, P.O. Box 77, FI-96101, Rovaniemi, Finland.

E-mail: juhani.ojala@gtk.fi, vesa.nykanen@gtk.fi

INTRODUCTION

Palaeo-stress modelling as a targeting tool for structurally controlled mineralization is based on geomechanical modelling for identifying areas that experienced minimum stress (maximum dilation) during periods of mineralization in a number of geological settings (Holyland 1990a,b,c,d; Holyland and Ojala 1997, Holyland et al. 1993, Groves et al. 2000).

Palaeo-stress modelling of the Central Lapland Greenstone Belt was to model the area at 1:250 000 scale using the existing geology maps (Lehtonen et al. 1998) and the solid geology and structural geology interpretations by Väisänen (2002) and Hölttä et al. (2006, this volume) for the geomechanical interpretation. Four different far field stress orientations and three different fault classifications were modelled resulting in 12 different model combinations. To quantify the spatial correlations of results to the known orogenic gold occurrences and the effectiveness of the results for targeting orogenic gold mineralization, the logistic regression model in the ArcGIS software was used. In addition, GIS modelling was to estimate which far field orientation was the most likely operational during the gold mineralization.

CONCEPTUAL MODEL

Most types of hydrothermal ore deposits are formed in structurally controlled sites in permeable fracture-systems. Typically, mineralization occurs in discrete segments of individual structures and, within the mineral deposits, some parts of the host structures are commonly better mineralized than others. Structurally controlled mineral deposits, and the high grade ore-shoots in them, are related, in general, to structurally focussed fluid flow during active deformation within the larger host structures (eg. Hodgson 1989). Hronsky et al. (1990) reviewed the common major controls on localisation of mineralization and oreshoots:

i) the intersection of host structure with a particular lithological unit (eg. BIF hosted gold deposits),
ii) intersection of two synmineralization structures,
iii) dilational jogs, divergent bends in faults or *en echelon* fault segmentation,
iv) fold hinge zones,
v) flexures in the host structure, with axes oblique to, and commonly at a high angle to, the movement direction, and
vi) zones that plunge subparallel to the stretching lineation, but in which the specific controls on their location are unclear.

In places, only one control applies to mineralization, and it may be possible to predict the location of the next one in a particular area or structure just by using the geometry of the structures. However, commonly several controls apply and the complex three-dimensional geometry of the controlling structures makes structural interpretation very difficult. In addition to geometry, competency contrast/rheological properties of host lithologies may have a significant influence. Consequently, a kinematic approach to complex structural relationships of a geological map is commonly based more on interpreter's intuition than true geometrical relationships. In addition, a purely kinematic approach fails to take into an account rheology and interaction of structural elements, which may have an effect considerable distance away (eg. large batholiths and major faults).

The observation that the orogenic gold mineralization in the Central Lapland Greenstone Belt appears to be late in structural history (D_2–D_4, Väisänen 2002, Sorjonen-Ward et al. 1992, Ward et al. 1989) suggests that, in the absence of significant subsequent tectonism, the resulting strain patterns have been preserved, and, importantly, the present geological map view represents closely the geometry at time of mineralization. Therefore, the geological map can be used for further analysis.

In summary, the current understanding of factors that control the location of structurally controlled mineral deposits indicate that if geologists can identify the areas which were dilatant zones at the time of mineralization, exploration within them would be guided by factors such as: the location of structures; rock competency and rock chemistry. Recognition of these dilatant zones (or low stress zones) is the aim of palaeo-stress modelling applied for exploration.

METHODS AND THEORETICAL CONSIDERATIONS

Irrespective of the exact origins of the fluids, the large number of common characteristics of orogenic gold deposits have led several workers to a quite similar conclusion: the hydrothermal systems which produced the gold mineralization were of crustal scale, and gold deposits possibly formed under a variety of

crustal régimes over at least a 15 km crustal profile (Colvine et al. 1984; 1988; Foster 1989; Groves et al. 1992; 2000; Goldfarb et al. 2001). This implies that the gold deposits represent a crustal continuum, and that gold mineralization in different crustal levels was broadly synchronous. This, in turn implicates a deep, sub-greenstone, crustal or mantle source for the primary ore fluid (Groves et al. 1992; 2000; Goldfarb et al. 2001). A number of fluid sources are possible, including deep-level intrusive granitoids (McNaughton et al. 1993), basal segments of greenstone belts, mid- to lower-crustal granitoid-gneisses, mantle lithosphere, or subducted oceanic lithosphere, with influx of surface water in the upper parts of the hydrothermal systems (Groves 1993; Goldfarb et al. 2001).

There is a general consensus that most orogenic gold deposits form in structurally controlled sites, and that the formation of deposits involves advection of large volumes of fluid in extensive hydrothermal systems. A number of models for fluid flow during the formation of the deposits have been proposed. Earlier models suggested that the role of faults was mainly passive as highly permeable channelways, but most models involve the active creation of high permeability during deformation or episodes of fault movement (eg. Cox et al. 1991; Hodgson 1989; Oliver et al. 1990; Phillips 1972; Ridley 1993; Sibson 1993; Sibson et al. 1975; 1988). Commonly, proposed mechanisms involve the fault valve or suction (or seismic) pump mechanisms (Sibson et al. 1975; 1988). In the fault valve model, pressure seal zones and high fluid pressure are essential requirements. Deformation is initiated by rising fluid pressure to, or above, lithostatic pressures and consequent reactivation of sealed faults and increased fracture permeability, a drop in fluid pressure and fluid flow into the fault zone (Sibson et al. 1988). In the suction pump model, the opening of extensional fractures causes the fluid pressure to drop and induces fluid flow into the dilated zone (Sibson 1987; Sibson et al. 1975). As Sibson (1993) pointed out, the fault-valve processes are more applicable to compressional deformation where the imposed load strengthens faults which are at a high angle to the maximum stress. Although rising fluid pressure can trigger faulting in the extensional régime, fluid pressures are in general closer to hydrostatic pressures in the fluid channelway.

Both these models highlight the importance of permeability, but if fluid focussing results from variations in permeability, the zones of high fluid flow will have lower fluid pressures and higher effective mean stress than surrounding rock which is at variance with inferences from quartz vein structures of high relative fluid pressures during the formation of gold deposits (Ridley 1993). Therefore, Ridley (1993) suggested, partly based on the work of Holyland (1990a) and Oliver et al. (1990), that fluid focussing into zones of low mean rock stress will be associated with high relative fluid pressures in the zone of focussed fluid flow. In addition, with progressively decreasing effective mean stress, any discontinuity, a fault or particular segment of a fault, can be a site of hydrofracturing, and subject to reactivation, within a low mean-stress domain (Ridley 1993).

Model for regional fluid focussing

Fluid inclusion studies from high crustal level deposits (Mair 1998; Ojala 1995) indicate higher pressures in the proximal parts of the mineralized zones. This appears to be in contrast to Ridley's (1993) model which predicts that absolute pressure will be lower in the fluid channel than in the wall rock. The fluid valve model of Sibson et al. (1988) can explain high fluid pressure in the upper part of the fault zone, but it does not explain why fluids are focussed in a particular fault in the first place. A combined fluid-pressure/low mean-stress activated valve model, which is broadly based on the models of Ridley (1993) and Sibson et al. (1988), and on the general approach of Holyland (1990a; 1990b; 1990c) to mean and minimum stress controlling the location of dilatant sites and fluid flow, is suggested to explain this observation. A schematic depiction of the concepts of the model are summarised in Figure 1.

The variations in mean stress result from interaction between the regional stress and overall geometry of faults and rock units, and their rheological properties. In the lithostatic régime (at depths greater than those equivalent to low to medium grade metamorphism), fluid pressure is buffered close to the confining pressure or mean stress (Etheridge et al. 1984), and, therefore, variations in the mean stress will be matched by variations in fluid pressure (Fig. 1a).

Provided that the fluid content of the rock mass stays constant, changes in fluid pressure through coupled poro-elasticity will, in general, only partly counteract changes in mean stress (Sibson 1993). Increased fluid supply, which can be a product of prograde metamorphic dehydration, magmatic sources, or mantle degassing, increases fluid pressure (Fig. 1b). Increased fluid pressure decreases effective pressure ($P_{effective} = P_{lithostactic} – P_{fluid}$) and, because permeability is controlled

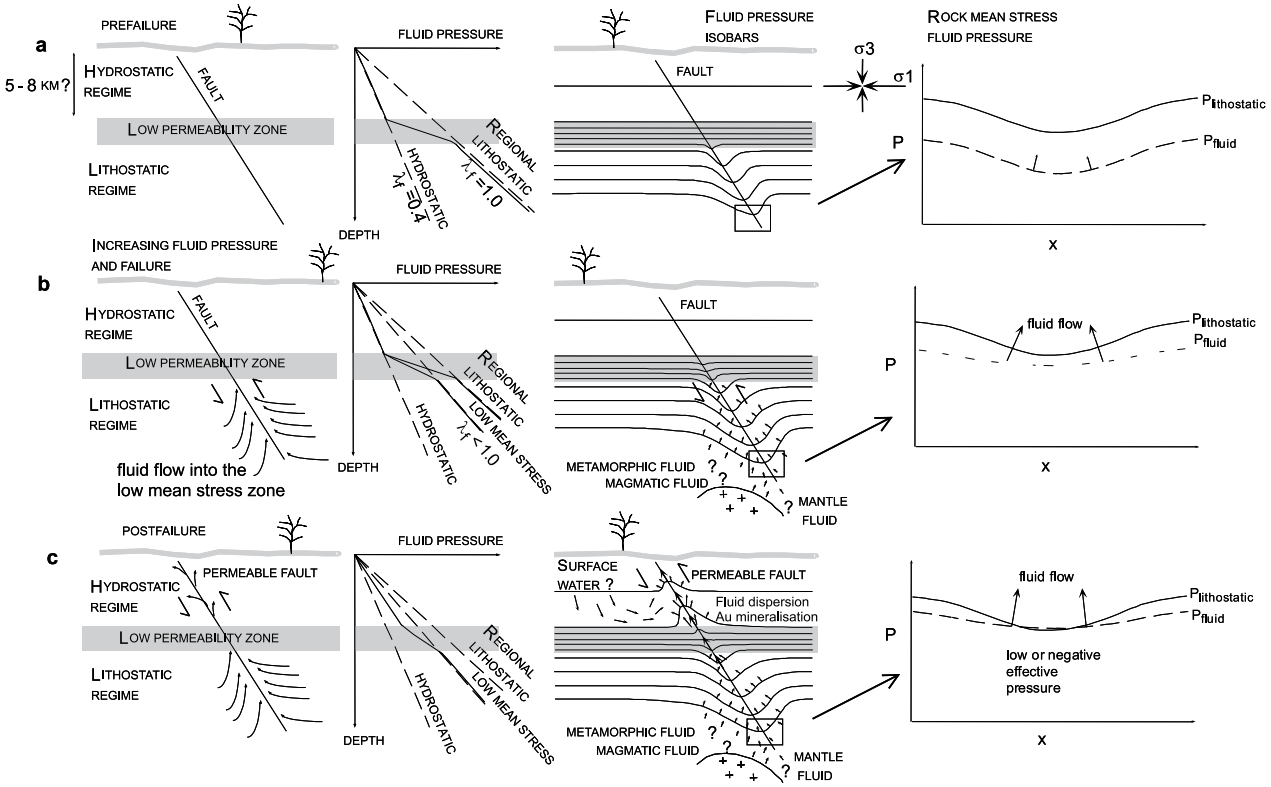

Fig. 1. Schematic cross-sections, fluid-pressure - depth profiles and cross-sections, and rock mean-stress/fluid-pressure profiles at specific depths demonstrating fault-valve behaviour of a reverse fault in a low mean stress zone. Some of the figures are modified from Sibson (1988) and Ridley (1993).
a) A pre-existing fault cuts across an impermeable barrier (greenschist facies boundary; Etheridge et al. 1984). Fluid pressure under the barrier is slightly below lithostatic pressure. Build up of compressional stresses results in variable mean stress along the fault and, consequently, variable fluid pressures. However, fluid is limited because of relatively low permeability and constant fluid content.
b) Fluid pressure below the impermeable barrier increases and results in increased permeability. Fluid flow down a fluid pressure gradient causes increased fluid pressure in the fault and decreased pressure outside of the fault, and results in low or negative effective pressure and further enhances the permeability within the low mean-stress zone. The low or negative effective pressure triggers a failure along the fault which creates extensive fracture permeability.
c) Drainage of geopressured fluid reservoir at depth occurs along the highly permeable fault and its subsidiary structures. Above the impermeable barrier, fluid pressure in the fault exceeds hydrostatic pressure.
Symbols:
pore pressure factor $\lambda_f = P_{fluid}/P_{lithostatic}$
$\lambda_f \sim 1.0$ lithostatic fluid pressure
$\lambda_f \sim 0.4$ hydrostatic fluid pressure
(W.J. Phillips 1972)
σ_1, σ_3 maximum and minimum principal stress
P pressure
x horizontal coordinate axis

by effective pressure, it is increased (Etheridge et al. 1983). As hypothesised by Ridley (1993) fluid flow down a fluid pressure gradient will cause increasing fluid pressures in the low mean-stress zone of initially lower fluid pressure, and the low mean-stress zone will become a zone of relatively low, potentially negative, effective pressure (Fig. 1c). This will further increase permeability and fluid flow into the low mean-stress zone.

With progressively decreasing effective mean-stress, any discontinuity in a favourable orientation is potentially reactivated within the low mean-stress zone. If the discontinuity is continuous through the low permeability barrier, an extensive fracture-permeability zone (Fig. 1c) through the barrier can be created as the failure propagates updip. This highly permeable channelway drains geopressured fluids into the hydrostatic régime, where fluids disperse along the rupture zone and its subsidiary structures. The largest difference between fluid pressure and ambient hydrostatic pressure is just above the impermeable barrier. As the fluid is rapidly migrating, it is likely to be in disequilibrium with wallrocks. In addition, pressure and temperature gradients may enhance mineral deposition. Fluid flow will continue as long as the fluid production exceeds the rate of drainage and keeps the relative fluid pressure high in the fluid focussing area.

Stress fields are dependent dominantly on the geometry of the fault network and rock units and the imposed

regional stress. Therefore, if mineral deposition seals the fault and fluid supply is still large, reactivation of the fault is likely to occur in the same low mean-stress area as long as fault motion does not significantly alter the rock geometry (Ridley 1993). This explains the common occurrence of several stages of veining and mineral deposition in the same area. In addition, it means that time averaged permeability of the fault zone is higher than that of the wall rocks.

It is noted that a pre-existing fault in the low mean-stress zone is not necessary for the initial fluid focussing into that zone in the lithostatic régime. However, if there is no permeable zone through the low permeability zone, fluids will slowly leak through the low permeability zone and disperse near the bottom of the hydrostatic régime. In addition, significant vertical fluid travel may not be required, if the mineralising fluid was derived from crystallising magma (eg. Burrows and Spooner 1987). Low mean stress areas are also preferential sites for intrusions, as the physical controls on magma movement are similar to those of fluid movement and magma will move down pressure gradients towards the sites of low mean stress (Cooper 1990).

In summary, the presented low mean-stress activated-valve model needs excess fluid production compared to the rate of drainage, a low mean-stress zone to collect and focus fluid in the lithostatic fluid-pressure régime, and a conduit from the fluid collection area to the depositional area. Such a model can explain fluid focussing and the observed high fluid pressures in the proximal ore zones in orogenic gold deposits.

Model for local fluid focussing

Hydrothermal ore deposits are characterised by channelised fluid flow and high fluid/rock ratios. In the low to medium-grade metamorphic conditions, fluid pressures are buffered close to lithostatic pressures and fluid flow is generally upward directed (Etheridge *et al*. 1984). Focussing of the upward fluid flow into a discrete channelway, as required to form an ore deposit, is due to lateral variations in hydraulic head. These lateral gradients my be induced structurally by either variations in fracture permeability of active fault zones, or by variations in mean rock stress (eg. Oliver et al. 1990). Mineralized extension veins indicative of supralithostatic fluid pressures are commonly present in orogenic gold systems. These are compatible with fluid focussing into zones of low mean rock stress, where relative fluid pressures are higher compared to the rock pressure but absolute fluid pressures are lower than in surrounding rock (Ridley 1993). Therefore, sites of low mean stress can be simultaneously sites of fluid focussing and of low effective mean-stress.

Ridley (1993) discussed about examples of sites of low mean stress and pointed out the stress heterogeneities which result in layered sequences. He showed that if the imposed stress is such that strain includes a component of extension parallel to layering, then relatively competent layers will have a lower mean stress (Fig. 2) and fluid focussing will be towards more competent layers in the sequence.

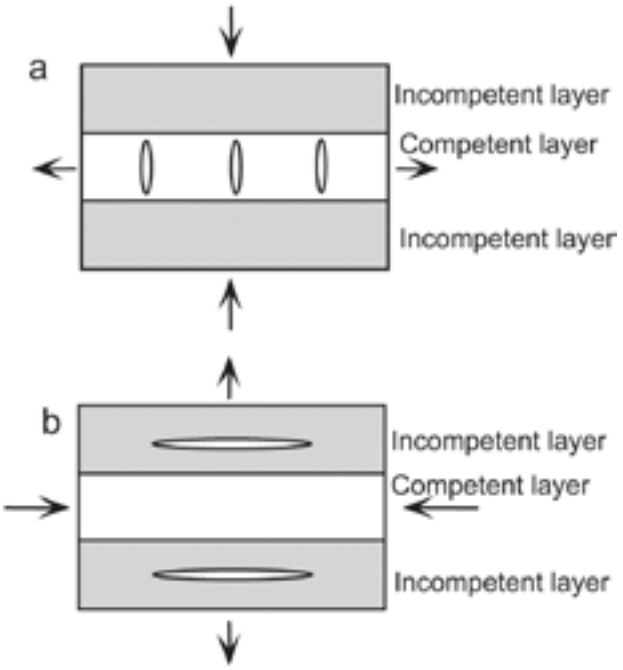

Fig. 2. Dilation in layered sequence. Mean stress will be lower in the competent layer if there is layer-parallel extension and in the incompetent layer if compression is parallel to layering. Modified from (Ridley 1993).

At higher crustal levels ambient fluid pressures are closer to hydrostatic pressures but fluid pressures in fluid channels might be lithostatic and both relative and absolute fluid pressures are higher than in the surrounding rock. Consequently, fluid flow is strongly controlled by permeability. Although high permeability pathways can be lithologically determined, structurally controlled ore deposits are more common in crystalline rocks and, in general, they have formed in reactivated fault systems (eg. Phillips 1972; Sibson *et al*. 1975; Sibson *et al*. 1988, Sibson 1993). A failure of a pre-existing weakness, or intact rock, can be initiated by an increase of differential stress, by an increase in the pore fluid pressure, or by combination of both. In most cases, stress changes lead to decrease of mean stress or, more commonly, decrease of minimum stress.

A model in which fluid focussing in the crust is due to variations in mean stress, or in which failure of pre-existing weaknesses and, therefore, enhanced fracture permeability, is due to lowered mean or minimum stress, allows for the wide variety of structural setting of mineral deposits. Thus, modelling variations in rock stress can provide viable exploration targets.

Stress-fluid pressure relationship at fracture initiation

Three different modes of brittle failure for homogeneous, isotropic, intact rock are shown in relation to loading stress fields on the Mohr diagram in Figure 3 (Sibson 1989). The type of failure depends on the magnitude of the differential stress in relation to the tensile strength of the rock. Depending on the stress state and the shape of the failure envelope, failure may be by:

i) extensional hydrofracture perpendicular to σ_3,
ii) shear failure along conjugate zones about 30° to σ_1, or
iii) extensional shear failure as conjugate zones at, or less than, 30° to σ_1 (Sibson 1989).

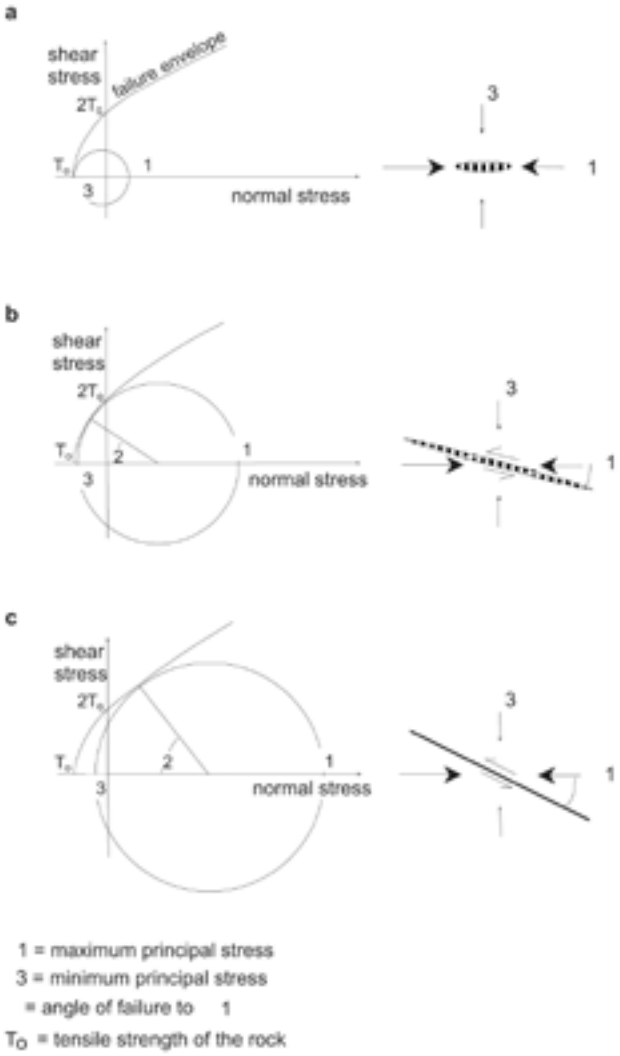

Fig. 3. Modes of failure. Modes of failure in relation to differential stress in homogeneous, isotropic rock. Mohr diagrams illustrate the general failure envelope for intact rock and the stress conditions for the three modes of failure. Modified from (Sibson 1989).
a) Extensional fracturing (hydraulic fracturing)
b) Extensional shear (combination of hydraulic fracturing and shear)
c) Shear fracturing

Figure 4 shows the effect of a plane of weakness on failure using the Mohr-Coulomb failure criterion. The failure envelopes are constructed assuming any orientation of the plane of weakness. Any stress systems for which the Mohr circle overlaps the failure envelope for planes of weakness, but does not touch the envelope for intact rock, may fail preferentially along a plane of weakness. Analysis of the likely mode of failure requires consideration of the orientation of the plane relative to the imposed stress. As for the case of intact rock, failure may be in one of three modes; extension hydrofracturing, shear failure, or extensional shear failure.

Generally, there will be a range of orientations of planes for which failure will occur (Fig. 3) before fracturing or shearing of adjacent intact rock. Pure extensional hydrofracturing only of a plane perpendicular to σ_3 would occur at low differential stress states in which the Mohr circle touches the failure envelope at the normal stress axis (Fig. 3); ie., the fluid pressure exceeds σ_3 plus the tensile strength of the fracture. With increasing fluid pressure or differential stress, the range of orientations of planes which will fail increases. As long as the intersection between the Mohr circle and the failure envelope is in the tensional field, failure will involve hydrofracturing and shearing.

During deformation, failure along the plane or through intact rock can be induced by

i) increasing the fluid pressure, and hence reducing the effective stresses and moving the Mohr circle to the left (Fig. 4a),
ii) increasing σ_1 (Fig. 4b),
iii) increasing the differential stress at constant mean stress ($\delta_m = \sigma_1 + \sigma_{3/2}$) (Fig. 4c), or
iv) decreasing σ_3 (Fig. 4d).

The diagrams in Figure 4 demonstrate that the change of stress state from stable to unstable results in a decrease of mean stress in cases a and d, increase in case b, and constant mean stress in case c. However, the minimum principal stress (σ_3) is constant only in case b and decreases in all other cases. Therefore, it is assumed in the stress modelling that variations in σ_3 give a better indication of proximity to failure, enhanced structural permeability, and fluid flow than the mean stress.

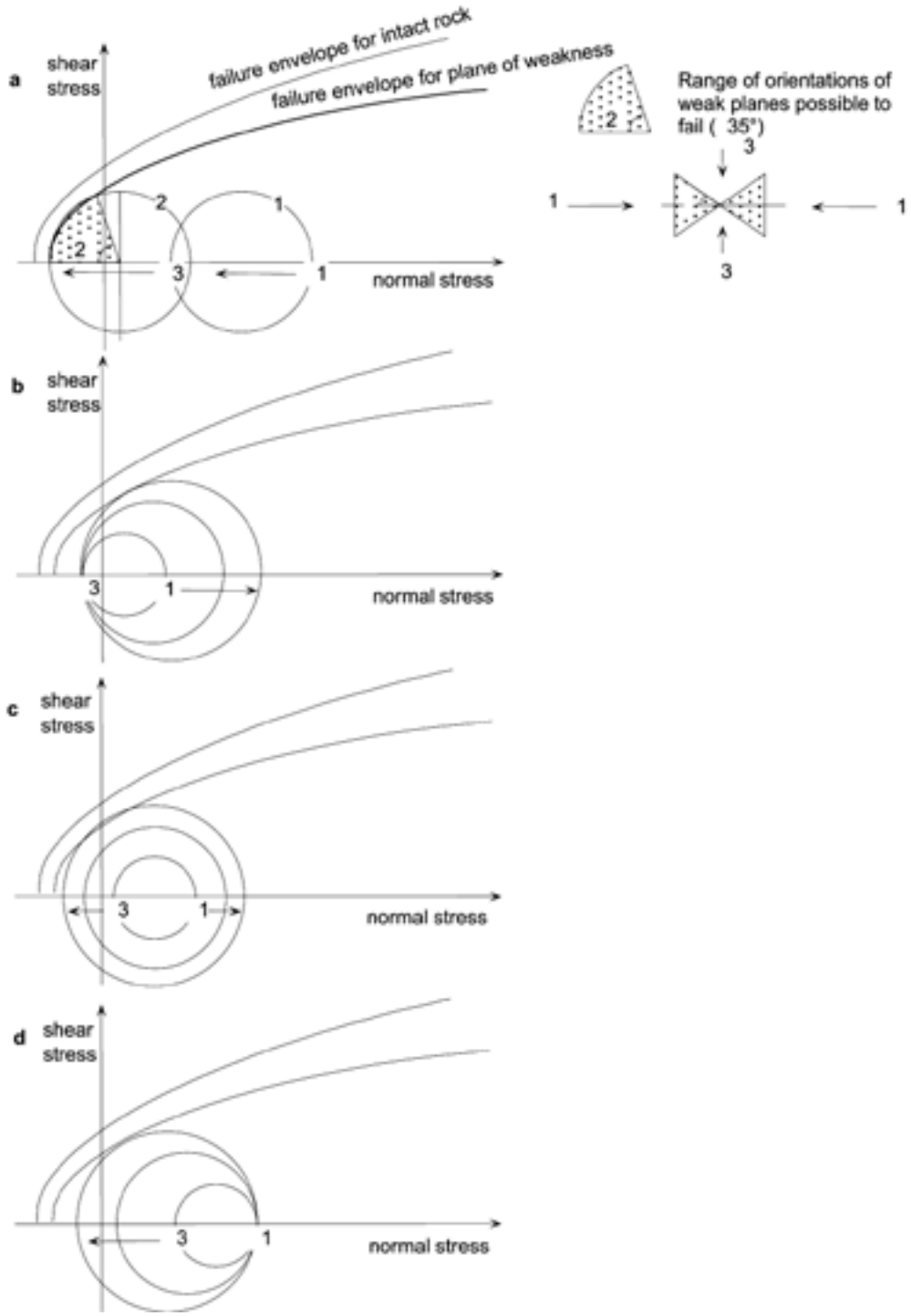

Fig. 4. Stress state changes leading to failure
Schematic Mohr diagrams illustrating possible changes in the stress state which can lead to failure of a plane of weakness.
a) Increasing fluid pressure, for the stress state 2, tensile failure will occur along fractures perpendicular to σ_3, and shear failure along a wide range of orientations of pre-existing planes of weakness.
b) Increasing σ_1 leads to increasing differential stress and shear failure will occur when Mohr circle touches the failure envelope.
c) Increasing differential stress with constant mean stress leads to shear failure.
d) Decreasing σ_3 leads to increasing differential stress and shear failure.

LIMITATIONS OF DEFORMATION SIMULATIONS

In some calculations, especially in those involving discontinuous material, the results can be extremely sensitive to very small changes in initial conditions or trivial changes in the loading sequence. This situation may seem unsatisfactory and may be taken as a reason to mistrust the computer simulations. However, the sensitivity exists in the physical system being modelled and there appear to be at least two sources for the seemingly erratic behaviour.

i. There are certain geometric patterns of discontinuities that force the system to choose, apparently at random, between two alternative outcomes and the subsequent evolution depends on which choice is made. For example in Figure 5, if block A is forced to move down to relative to B, it can either go to the left or to the right of B. In the natural rocks the choice will depend on microscopic irregularities in the grain boundary geometry, anisotropic rock properties, or kinetic energy of the conjugate faults.
ii. There are processes in the system that can be described as softening or more generally as cases of positive feedback. In a fairly uniform stress field, small perturbations are magnified in the subsequent evolution because a region that has more strain softens more and thereby attracts more strain.

Both phenomena give rise to behaviour that is chaotic. Studies of chaotic systems reveals that the detailed evolution of a system is not predictable even in principle. The observed sensitivity of the computer model to small changes in initial conditions or numerical factors is simply a reflection of a similar sensitivity in the real world to small irregularities.

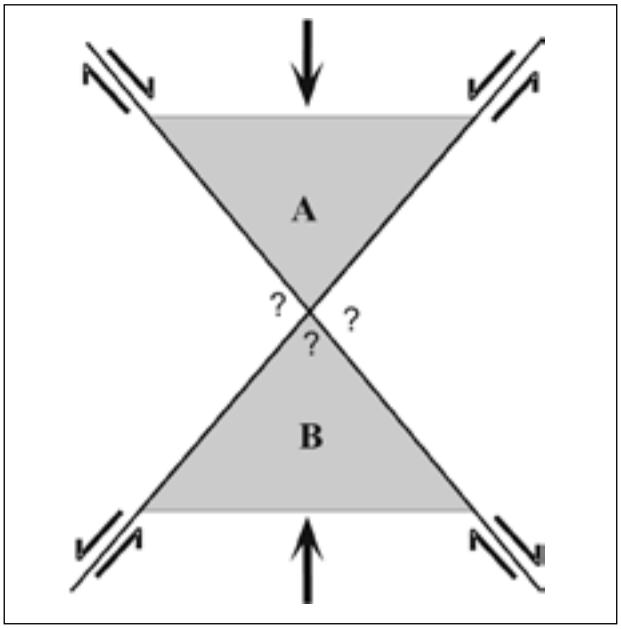

Fig. 5. Conjugate fault problem. Schematic conjugate fault intersection demonstrating the computational problem of symmetric fault intersections (relative to the stress field).

Geometry

Typically, the geological map interpretation is the largest source of uncertainty for the deformation simulation used for structural targeting. The other severe limiting assumption of two-dimensional stress modelling is that the plane of a map does not accurately reflect the stress pattern in an area with complex three-dimensional geometry. In many terrains, like the Central Lapland Greenstone Belt, this may not be a critical restriction, since the vast majority of the observed structures are upright and the majority of gold deposits are hosted in steep structures, although significant exceptions do occur. In addition, in most areas, dip data is not available and a two-dimensional geological model is the only possibility at this scale. The accuracy of the three-dimensional geological interpretation becomes more important in deposit scale modelling where the extent of interest of the vertical dimension is similar to horizontal dimensions.

Far-field stress orientations

Determination of palaeo stress directions is closely related to the understanding the geological history of the area, quality of geological maps and reconstruction of the geometry during the mineralization (Angelier 1979, Ramsay and Huber 1987, Reches 1978, 1983). In many cases, this is not difficult as in linear greenstone belts and fold belts main principal stress direction and tectonic transport is typically perpendicular to the general structural grain. Furthermore, geomechanical modelling is not very sensitive for small differences in stress directions. In addition, several stress directions can be simulated and the result combined. Väisänen (2002) and Hölttä et al (2006, this volume) suggest several tectonic transport directions and block rotations

during the late structural evolution (D_3 and later) in the Central Lapland Greenstone Belt. At this stage the earlier structures were also reactivated. Consequently, it was decided to model all four main compression directions (N-S-, E-W, NE-SW, NW-SE) with some variations in fault classifications.

Material properties

The selection of material properties of rocks is a difficult element in the generation of the palaeo stress model because of high uncertainty in the property database. It should be considered when performing an analysis, that the problem involves a data-limited system and the field data will never be known completely. However, as with the geometry, with the appropriate selection of properties important insight to the physical problem can still be achieved. Furthermore, the relative scale of the rock properties is reasonably well known. The rock properties (Table 1.) for the simulations were estimated from the published data (Clarke 1966) to approximate rock properties at the estimated temperature-pressure conditions (70–100 MPa, 300±50°C) during mineralization. Although the rock properties are not very well known for the pressure-temperature conditions during mineralization, it is likely that the relative scale of rock properties was similar to that indicated by geomechanical tests. Rocks were modelled as Mohr-Coulomb material and the modelling considers only elastic and elasto-plastic stresses and strains, and, therefore, deformation dilatency due to viscous strains is not considered.

Table 1. Material properties used for the UDEC modelling
a) Rock rheologies

Property	Fine grained sedimentary rocks	Mica schist	Quartzite	Ultramafic rock	Mafic rock	Mafic intrusive rock	Granitoid	Unit
Density	2750	2700	2700	3300	2800	3000	2660	kg/m3
Bulk modulus	$8x10^9$	$15x10^9$	$35x10^9$	$15x10^9$	$48x10^9$	$70x10^9$	$55x10^9$	Pa
Shear modulus	$7x10^9$	$10x10^9$	$21x10^9$	$10x10^9$	$24x10^9$	$40x10^9$	$35x10^9$	Pa
Cohesion	$30x10^6$	$50x10^6$	$100x10^6$	$40x10^6$	$60x10^6$	$100x10^6$	$80x10^6$	Pa
Normal stiffness	$1x10^{14}$	$2x10^{14}$	$1x10^{14}$	$2x10^{14}$	$1x10^{14}$	$11x10^{14}$	$1x10^{14}$	Pa/m
Shear stiffness	$1x10^{14}$	$2x10^{14}$	$1x10^{14}$	$2x10^{14}$	$1x10^{14}$	$11x10^{14}$	$1x10^{14}$	Pa/m
Friction angle	10	15	20	15	20	25	20	degree

b) Fault rheologies

Discontinuity property	1st order fault	2nd order fault	Thrust	Granitoid contact	Greenstone contact	Unit
Cohesion	$15x10^6$	$15x10^6$	$15x10^6$	$80x10^6$	$60x10^6$	Pa
Joint normal stiffness	$0.5x10^9$	$0.5x10^{10}$	$0.5x10^{11}$	$1x10^{13}$	$1x10^{13}$	Pa/m
Joint shear stiffness	$0.4x10^9$	$0.4x10^{10}$	$0.4x10^{11}$	$1x10^{13}$	$1x10^{13}$	Pa/m
Friction angle	6	7	8	20	17	degree

NUMERICAL FORMULATION

Stress modelling examines the variation in strain and stress through an inhomogeneous terrain on imposition of a regional stress field. When stressed, an inhomogeneous material develops an inhomogeneous stress field whose components vary with rheological properties and geometry. The modelling is consider-

ing only elastic and elasto-plastic stresses and strains, and, for instance, deformation dilatancy due to viscous strains is not considered.

A number of numerical techniques are available to treat the equations relating variations in stress distribution to the resulting strain pattern. This study utilised the distinct element method (UDEC program, Itasca Consulting Group, Starfield and Cundall 1988), which is a recognised discontinuum modelling approach for simulating the behaviour of jointed rock masses. In the distinct element method, a rock mass is represented as an assembly of discrete blocks. Faults and contacts are viewed as interfaces between distinct bodies. The contact forces and displacements between the stressed assembly of blocks are found through a series of calculations which trace the movements of the blocks. Movements result from the propagation of disturbances, which were caused by applied loads, through the block system.

The algorithm includes:

1. A motion law, which specifies motion of each block due to unbalanced forces acting on it.
2. Force displacement laws which specify forces between blocks
3. Block deformability.

Boundary conditions

Geomechnical model requires estimation of the following three groups of variables:

i) Far-field horizontal stresses
- magnitudes
- orientations

ii) Rock deformation properties
- strength
- moduli

iii) Fault deformation properties
- friction angle
- stiffness

It also requires accurate information on the location and geometry of the polygonal blocks and the faults and shears and this data is contributed through solid geology interpretations.

Preparation of a solid geology map

Geomechanical interpretation was done at 1:250 000 scale (Fig. 6 and 7). Fault and rock geometries were interpreted from 1:100 000 and 1:200 000 scale geological (eg. Lehtonen et al. 1998) and geophysical (processed low altitude aeromagnetic and EM, Airo 2005) maps. In UDEC models, the fault geometry is predetermined and development of new structures cannot be modelled. Discontinuities were divided to faults and contacts. Faults were further divided into first and second order faults, and thrusts using their length, continuity and timing as the main division, and rock contacts to greenstone and granitoid contacts with increasing shear stiffness (Figs. 6 and 7). The E-W trending first order shear clearly related with a lineament of magnetic highs. NW-SE trending is placed to model a deeper basement lineament, which has a more subtle signature in magnetics. Dominating rock type between the discontinuities was used to define material properties for the rock blocks. Since the model is two dimensional, all faults and contacts are treated as vertical.

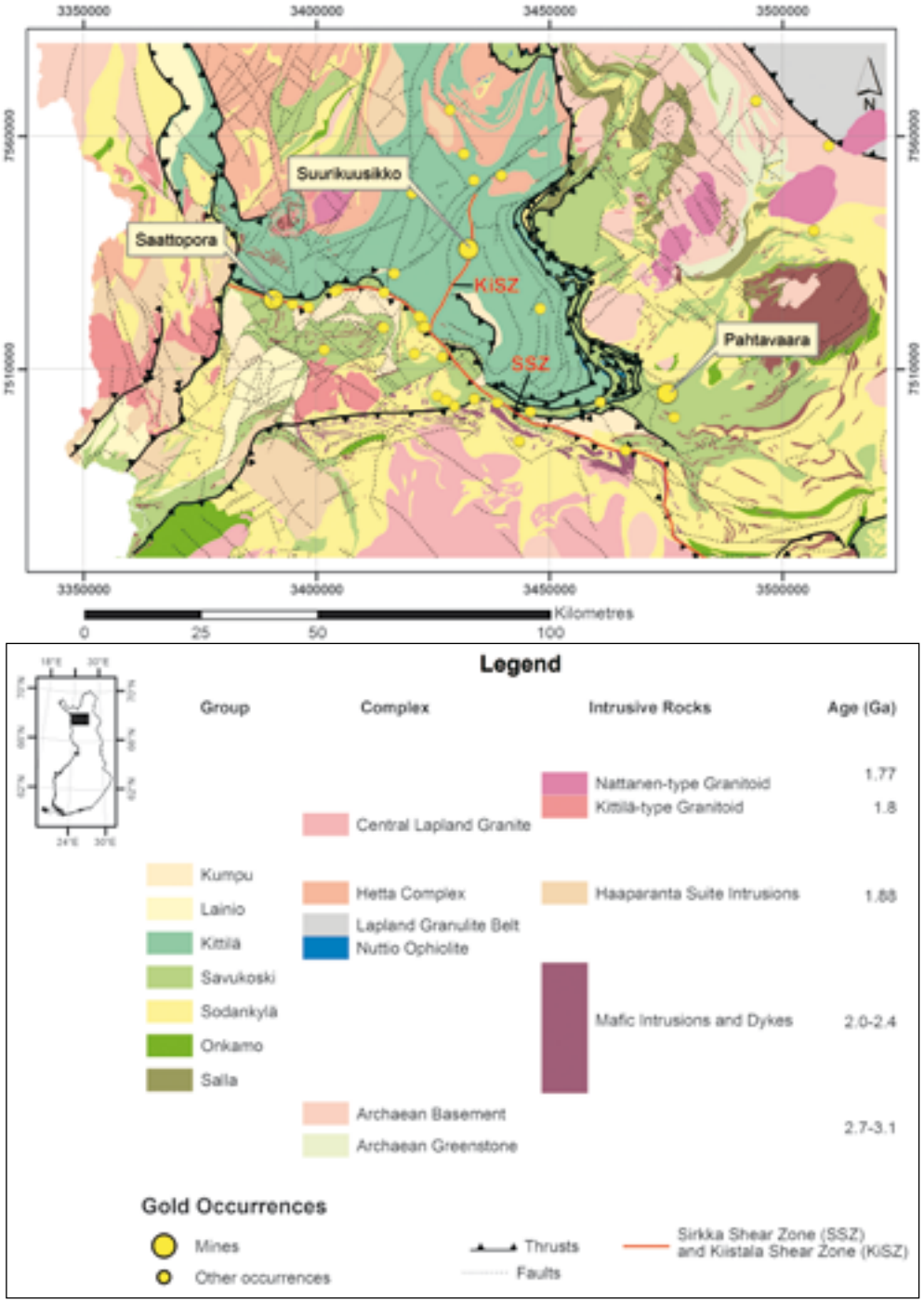

Fig. 6. Geological map of the Central Lapland greenstone belt and locations of the known gold deposits and occurrences (Eilu 1999, http://en.gtk.fi/ExplorationFinland/Commodities/Gold/gtk_gold_map.html).

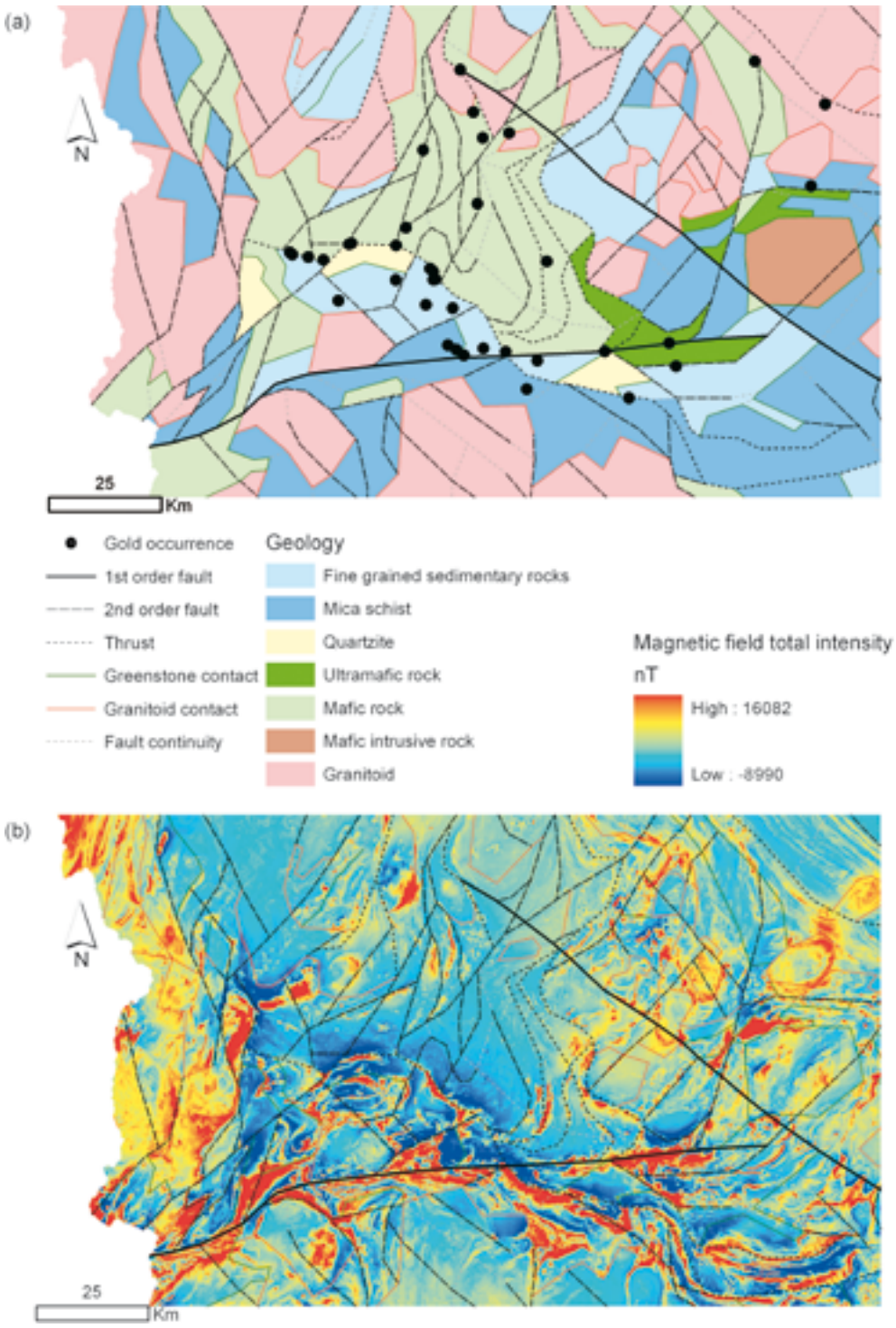

Fig. 7. a) A digitized geomechanical interpretation of the Central Lapland greenstone belt. The geology is simplified to facilitate modelling. The known gold occurrences are shown for reference. b) An aeromagnetic map of the model area overlain with the modelled discontinuity network.

Rheology of rock units and faults

In this study modelling brittle-ductile rheological values (Table 1) were used as the metamorphic grade of the rocks is greenschist to low amphibolite facies, and the Au mineralization was interpreted to be late (D_2 to D_4) in the structural history and to be spatially related to brittle and brittle-ductile faults (Eilu et al 2003, 2006 this volume).

Values of input parameters

The rheology of the granitoid-greenstone area was approximated from the published geomechanical database (Clark 1966). External variables which affect rheology such as confining pressure, temperature, deviatoric stress, pore fluid pressure and strain rate were estimated using typical values of depth to surface of hydrothermal systems, fluid inclusions, failure modes in known deposits, lithostatic pressure, and typical strain rates (10–14 s^{-1}) (Fyfe *et al*. 1978), respectively.

Rheology of the faults was estimated from both laboratory experiments on fracture behaviour, and large-scale studies on slip behaviour on large faults in the western USA (Sleep and Blandpied 1992). First order faults were assigned lower stiffness than second order faults due to their being smoother and more continuous and hence having a smaller roughness component in frictional resistance.

Far field stresses

Structural interpretations by Ward et al. (1989), Väisänen (2002) and Hölttä et al. (2006 this volume) suggest that the maximum principal stress (σ_1) orientation was probably E-W but it may have varied from E-W (D_3) and N-S (D_4) during the gold mineralization. Small (±20°) changes in far field stress orientations do not significantly change the results and, therefore, modelling of N-S, E-W, NW-SE and NE-SW σ_1 orientations was considered a reasonable approximation. The magnitude of the maximum principal stress (100 MPa) corresponds to a depth of about 4–8 km (Engelder 1993). The magnitude of minimum principal stress was 70 MPa confining a deviatoric stress that is large enough to cause some change in the internal stress pattern of the model.

Model variations

Because the structural interpretations of the far field stress orientations are equivocal, and fault classifications in the different geological maps vary, four different far field stress orientations and three different discontinuity classifications were modelled. This results in 12 different models (Table 2). In the model Class I, all discontinuities have been classified from first and second order faults and thrusts to greenstone and granitoid contacts with increasing shear and normal stiffness (Table 1). The normal and shear stiffness of contacts is two magnitudes higher than faults. In the model Class II all discontinuities have the same properties, ie contacts are also modelled as faults. In the model Class III, all faults have the same properties but the contacts are modelled having significantly higher normal and shear stiffness than faults. In all models, fault continuities have the same properties as the host rock block and, consequently, there is no displacement along them.

Table 2. Palaeo stress model variations in Figures 8-11. Stress field refers to the main principal stress (σ_1) direction. Class refers to the variations of discontinuity properties. In the Class I models all fault classes and contacts have different parameters (Table 1), in the Class II models all discontinuities have same properties (2^{nd} order fault properties), and in the Class III models all faults have the same properties (2^{nd} order faults) but the contacts are assigned be stronger than faults.

Model No	Layer	Figure	Stress field	Class
1	kl011	8a	E-W	I
2	kl010	8b	E-W	II
3	kl011b	8c	E-W	III
4	kl013	9a	N-S	I
5	kl012	9b	N-S	II
6	kl013b	9c	N-S	III
7	kl021	10a	NW-SE	I
8	kl020	10b	NW-SE	II
9	kl021b	10c	NW-SE	III
10	kl023	11a	NE-SW	I
11	kl022	11b	NE-SW	II
12	kl023b	11c	NE-SW	III

MODELLING RESULTS

The solid geology model was digitised and the parameter values described above were given to the rock blocks, faults, and lithological contacts. The far field stresses were then applied to the model boundaries and the computation of the resulting deformation begun in UDEC. After sufficient cycles of calculations were completed (typically 500 cycles), the model reached steady state, and the resulting stress pattern was calculated. The results of 12 model variations were exported from UDEC as an ASCII files which were imported into the ArcGIS and the minimum principal stress (σ_3) values were converted into ArcGIS grids. The spatial resolution of the grid is about two kilometres at 1:250 000 scale. The simulated σ_3 distributions are shown in Figures 8–11. As the discontinuities cause the stress variations in UDEC models, most of the σ_3 anomalies are along the faults and are related to fault bends and intersections. The σ_3 distribution in the

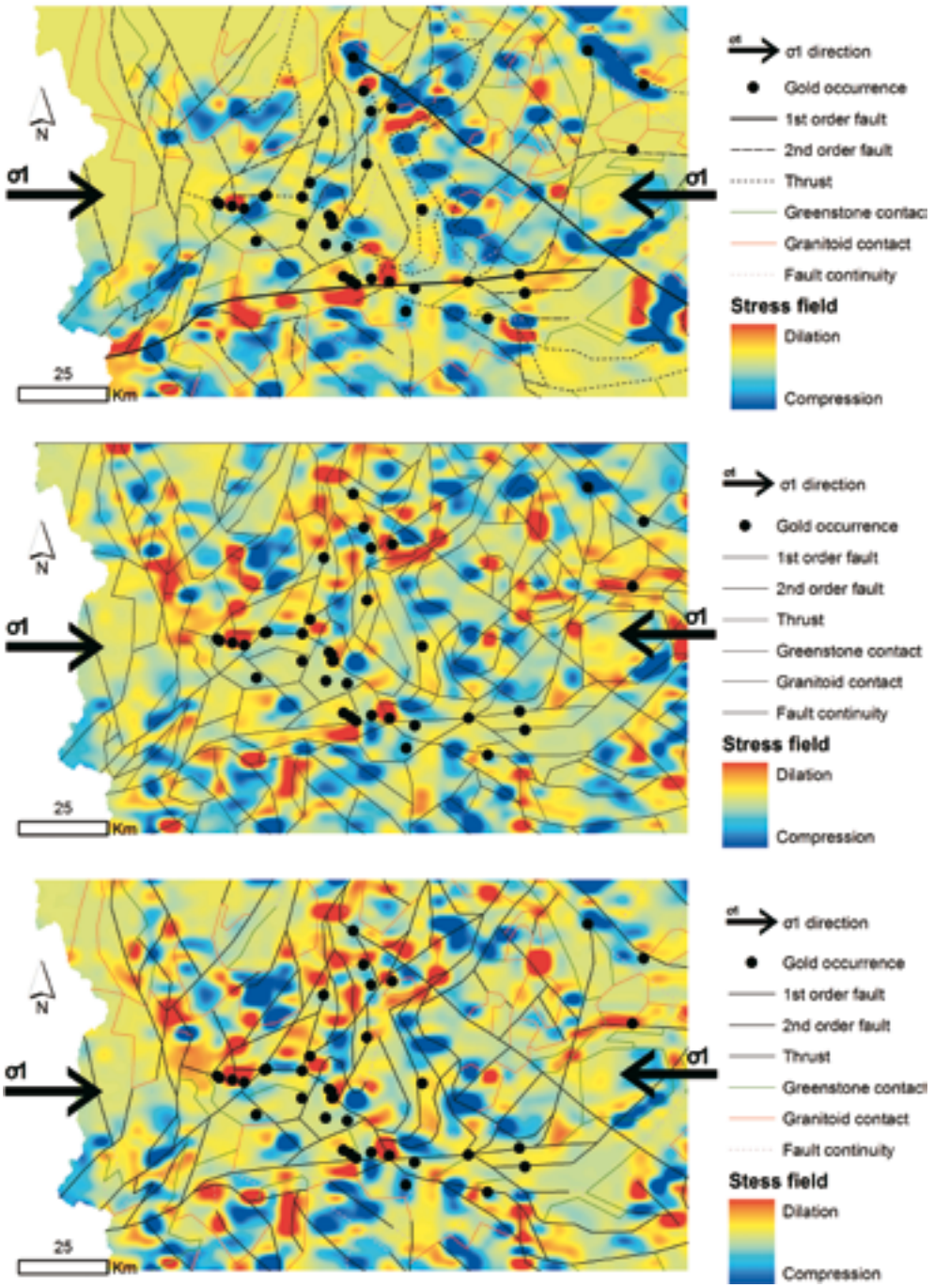

Fig. 8. E–W compression simulations showing minimum principal stress (σ_3) distributions, warm colours indicate low σ_3 and dilation. a) All fault classes and contacts have different parameters (Table 1), b) all discontinuities have the same properties, c) all faults have the same properties but the contacts are assigned to be stronger than faults. Discontinuity network and known gold occurrences are shown to assist correlation between Fig. 6 and Fig. 7.

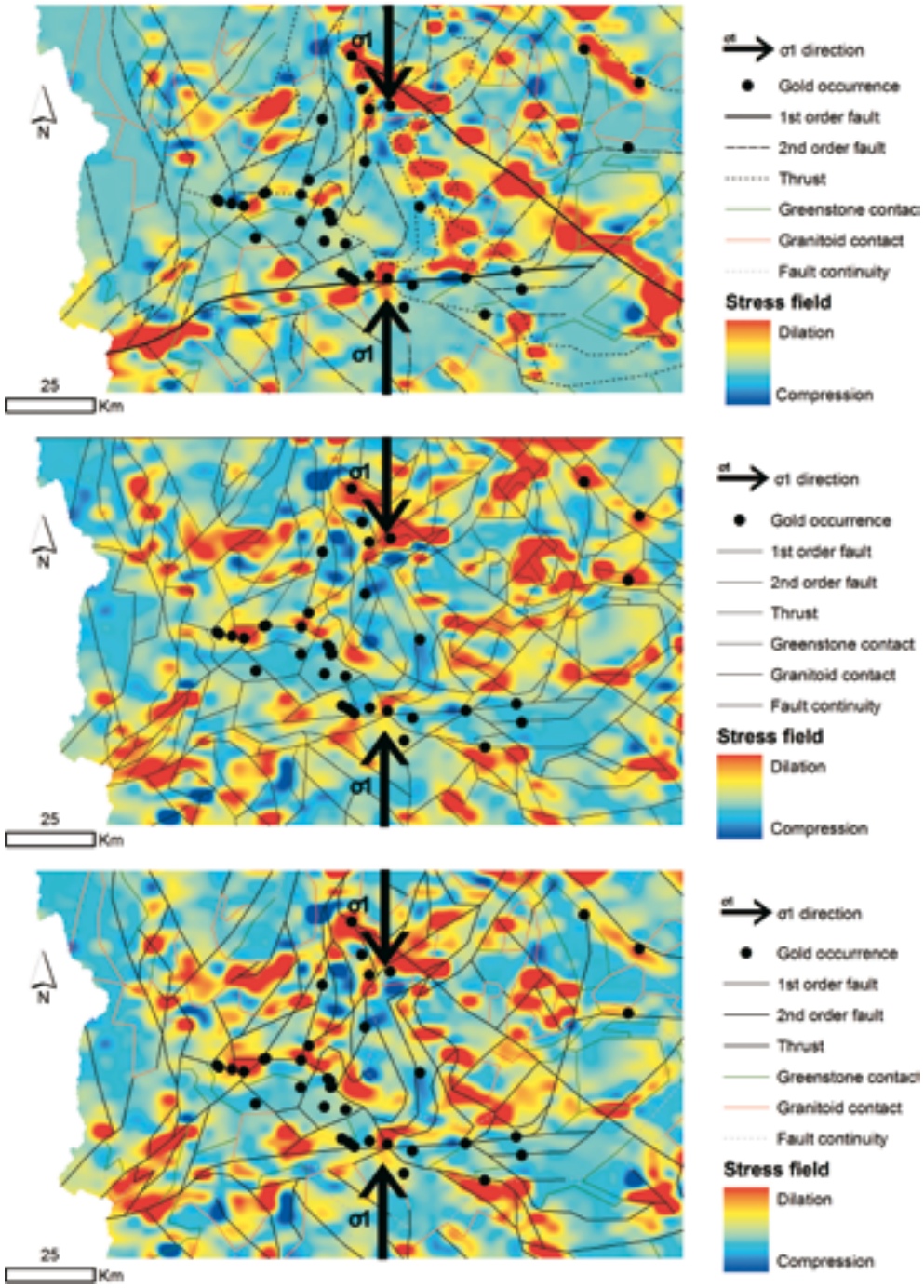

Fig. 9. N-S compression simulations showing minimum principal stress (σ_3) distributions, warm colours indicate low σ_3 and dilation. a) All fault classes and contacts have different parameters (Table 1), b) all discontinuities have the same properties, c) all faults have the same properties but the contacts are assigned to be stronger than faults. Discontinuity network and known gold occurrences are shown to assist correlation between Fig. 6 and Fig. 7.

Class I models (Fig 8a–11a) indicate concentration of deformation along two first class faults and depending on the far field stress these faults are mainly dilating or compressing. In the Class II and III models, σ_3 distribution indicates more evenly distributed strain. In many cases, an opposite far field stress orientation changes a stress anomaly from dilation to compression. Variable number of known gold occurrences is near or within anomalous stress zones but visually it is difficult to define in which model the spatial correlation between σ_3 and gold occurrences it the most significant. In addition, some of the gold occurrences not sited within stress anomalies do not have significant faults nearby and it is probable that these structures

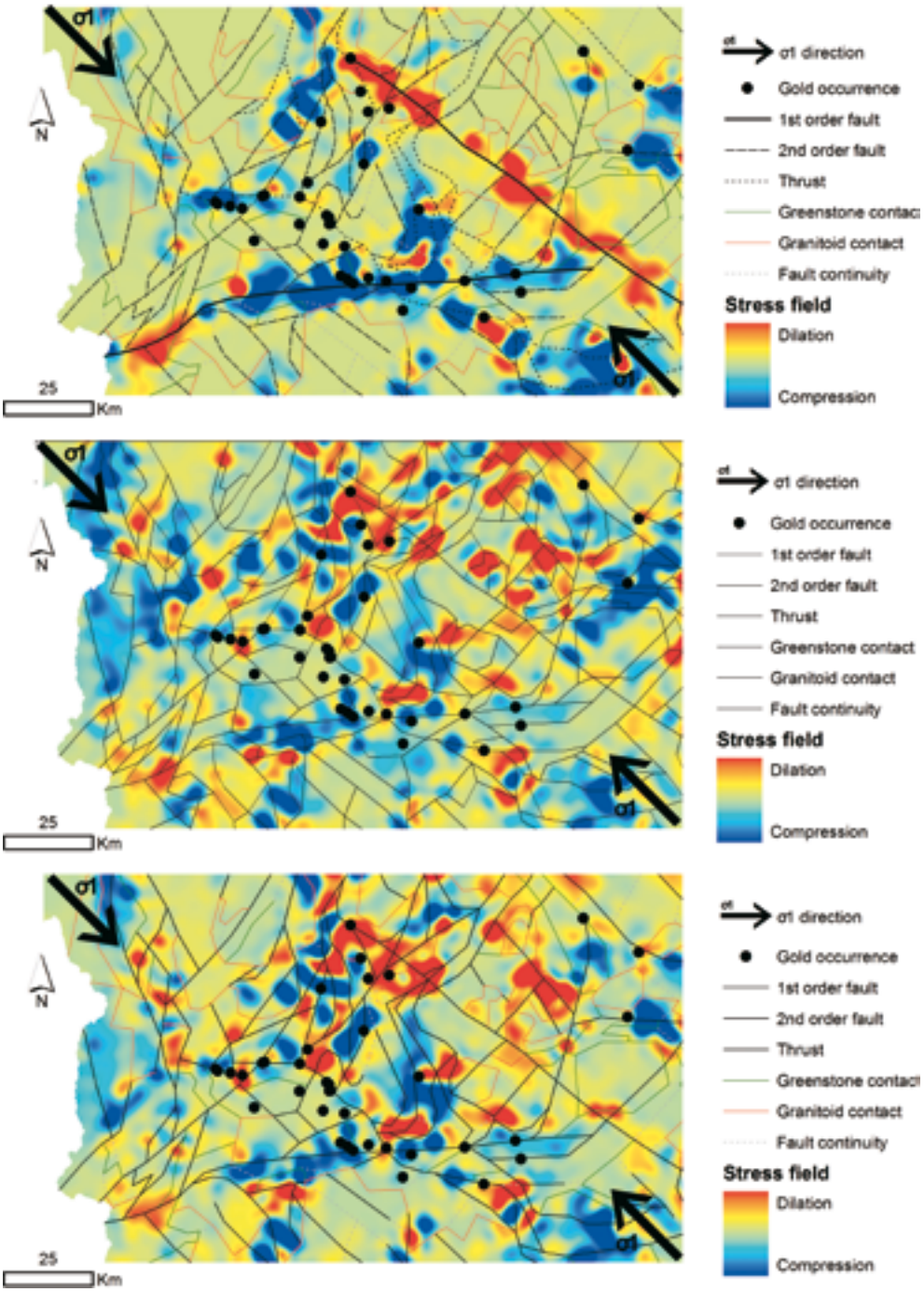

Fig. 10. NW-SE compression simulations showing minimum principal stress (σ_3) distributions, warm colours indicate low σ_3 and dilation. a) All fault classes and contacts have different parameters (Table 1), b) all discontinuities have the same properties, c) all faults have the same properties but the contacts are assigned to be stronger than faults. Discontinuity network and known gold occurrences are shown to assist correlation between Fig. 6 and Fig. 7.

were simply not shown or obvious on the geological and geophysical maps, which were used as an input for the geomechanical interpretation.

To quantity the spatial association between the modelled σ_3 distribution and the orogenic gold occurrences within the CLGB the mean values and the standard cumulative descending weights were calculated following the weights-of-evidence methodology (Bonham-Carter 1994; Raines et al. 2000; Raines and Bonham-Carter 2006). The modelled σ_3 values were reclassified into 12–13 classes using standard deviation method of GIS software. This classification method shows how much a feature's attribute value varies from the mean. The GIS software calculates the mean values and the standard deviations from the mean and the class breaks are then created using these values.

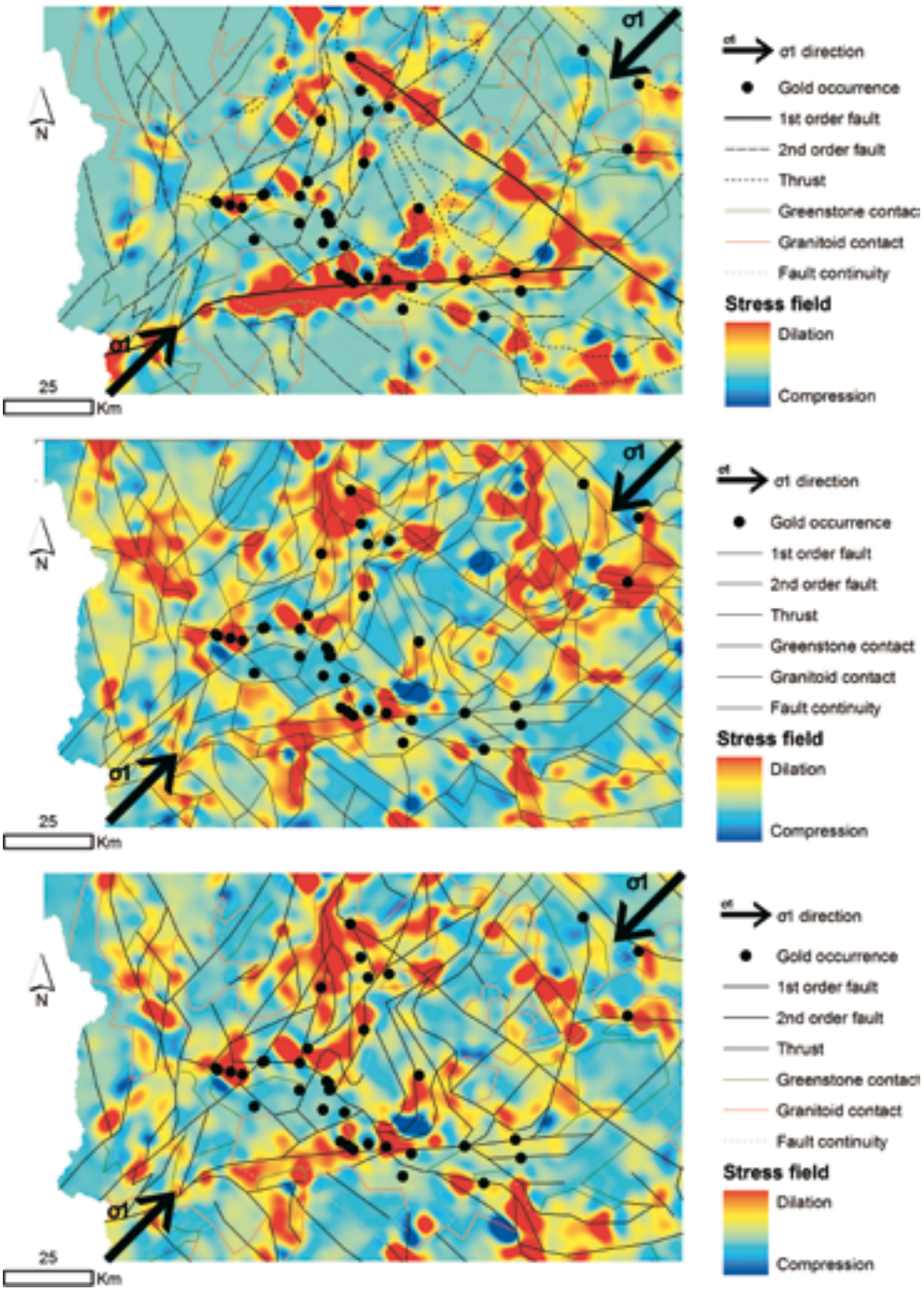

Fig. 11. NE-SW compression simulations showing minimum principal stress (σ_3) distributions, warm colours indicate low σ_3 and dilation. a) All fault classes and contacts have different parameters (Table 1), b) all discontinuities have the same properties, c) all faults have the same properties but the contacts are assigned to be stronger than faults. Discontinuity network and known gold occurrences are shown to assist correlation between Fig. 6 and Fig. 7.

A pair of weights was calculated for each map class of the input σ_3 values. A positive weight (W+) was calculated for presence of each class at the training site, and a negative weight (W-) for absence of that class. The weights are a function of the number of the training sites within a map class and the area of the corresponding map class. The magnitude of the weights depends on this measured spatial association between the map class and the training sites. A weight of zero indicates no spatial association between the training sites and a particular map class. The layers were reclassified into binary patterns by using the maximum contrast value (Table 3, Figs 12–15), which is the arithmetic difference between the weights in the cumulative weights calculation. The σ_3 values in the stress models with the main principal stress (σ_1)

Table 3. Weights (W^+ and W^-), contrast and confidence for the minimum principal stress (σ_3) data layers. The numbers (Model No) refer to Table 1. Weights were calculated by cumulative descending method (from the highest value to the lowest value) and the weights for each data layer at the maximum contrast are reported here ordered by the contrast value. No of training sites=37: total area=18 642 km^2: prior probability=0.0009: contrast=W^+-W^-: Confidence=Contrast/Std (Contrast).

Model No	Layer	Stress field	Class	Area km²	Area %	Points	Points %	W^+	W^-	Contrast	Std (Contrast)	Confidence
3	kl011b	E-W	III	235	1.26	4	10.8	2.1576	–0.1018	2.2595	0.5315	4.2512
2	kl010	E-W	II	817	4.38	7	18.9	1.4648	–0.165	1.6298	0.4205	3.8758
10	kl023	NE-SW	I	743	3.98	6	16.2	1.4045	–0.1363	1.5408	0.4468	3.4485
1	kl011	E-W	I	227	1.22	2	5.4	1.4929	–0.0433	1.5362	0.7286	2.1085
12	kl023b	NE-SW	III	10852	58.22	31	83.8	0.362	–0.9436	1.3056	0.4461	2.9264
11	kl022	NE-SW	II	621	3.33	4	10.8	1.1777	–0.0805	1.2582	0.5302	2.373
5	kl012	N-S	II	1691	9.07	8	21.6	0.869	–0.1486	1.0175	0.3998	2.5454
6	kl013b	N-S	III	1027	5.51	5	13.5	0.90	–0.0885	0.9857	0.4814	2.0476
9	kl021b	NW-SE	III	601	3.22	2	5.4	0.5157	–0.0228	0.5385	0.7276	0.7401
8	kl020	NW-SE	II	603	3.24	2	5.4	0.5116	–0.0226	0.5342	0.7276	0.7342
4	kl013	N-S	I	9036	48.47	22	59.5	0.20	–0.239	0.4425	0.335	1.3209
7	kl021	NW-SE	I	366	1.97	1	2.7	0.316	–0.0075	0.3235	1.0145	0.3189

in E-W and NE-SW direction have stronger spatial association with gold occurrences than those with σ_1 in N-S or NW-SE direction. The area of maximum spatial association pattern for E-W and NE-SW stress models is in most cases very small (<5% of the total study area) except for the model 12 (NE-SW σ_1, Class III).

The models were ranked based on the maximum contrast value, which quantifies the spatial association between the gold occurrences and the map classes. The confidence of the weights calculation was estimated by calculating the studentised contrast (Contrast/Standard deviation of the contrast), which is the measure of the certainty that the contrast is not zero (Bonham-Carter 1994). Confidence values above 1.96 (Table 3), which is about a 97.5% confidence level, were considered acceptable (Raines 1999). All E-W and NE-SW models are above these levels, and only one N-S model (model 4, Class III) and none of the NW-SE stress models bypass this rule. This indicates that the correlations of the E-W and NE-SW models with the known gold occurrences are more reliable than the correlations of the NW-SE and N-S models with the gold occurrences. Consequently, E-W and NE-SW models could be considered as the best predictors for structurally controlled gold mineralization.

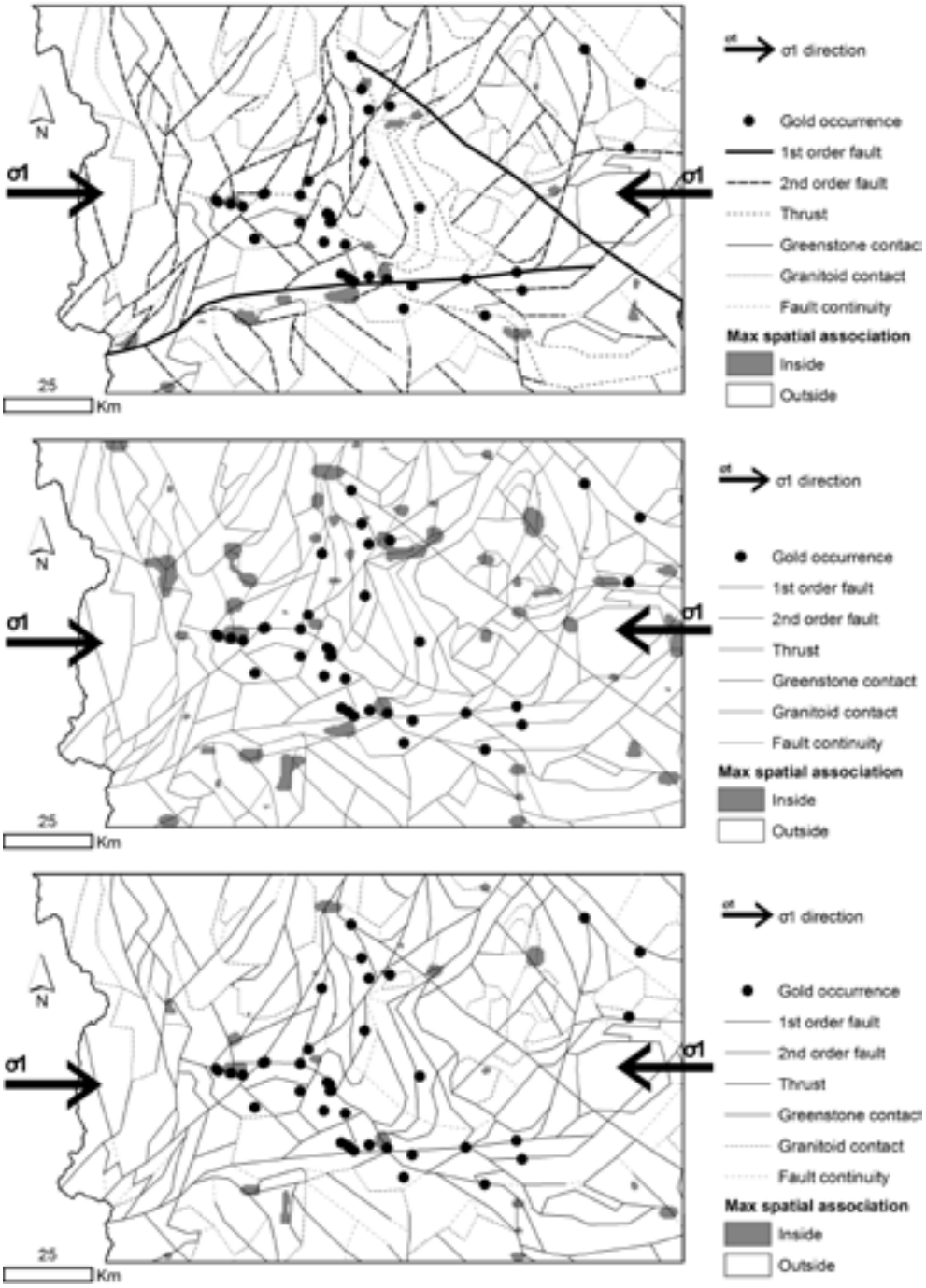

Fig. 12. E–W compression simulations. Maximum spatial association pattern between σ_3 and gold occurrences. a) All fault classes and contacts have different parameters (Table 1), b) all discontinuities have the same properties, c) all faults have the same properties but the contacts are assigned to be stronger than faults.

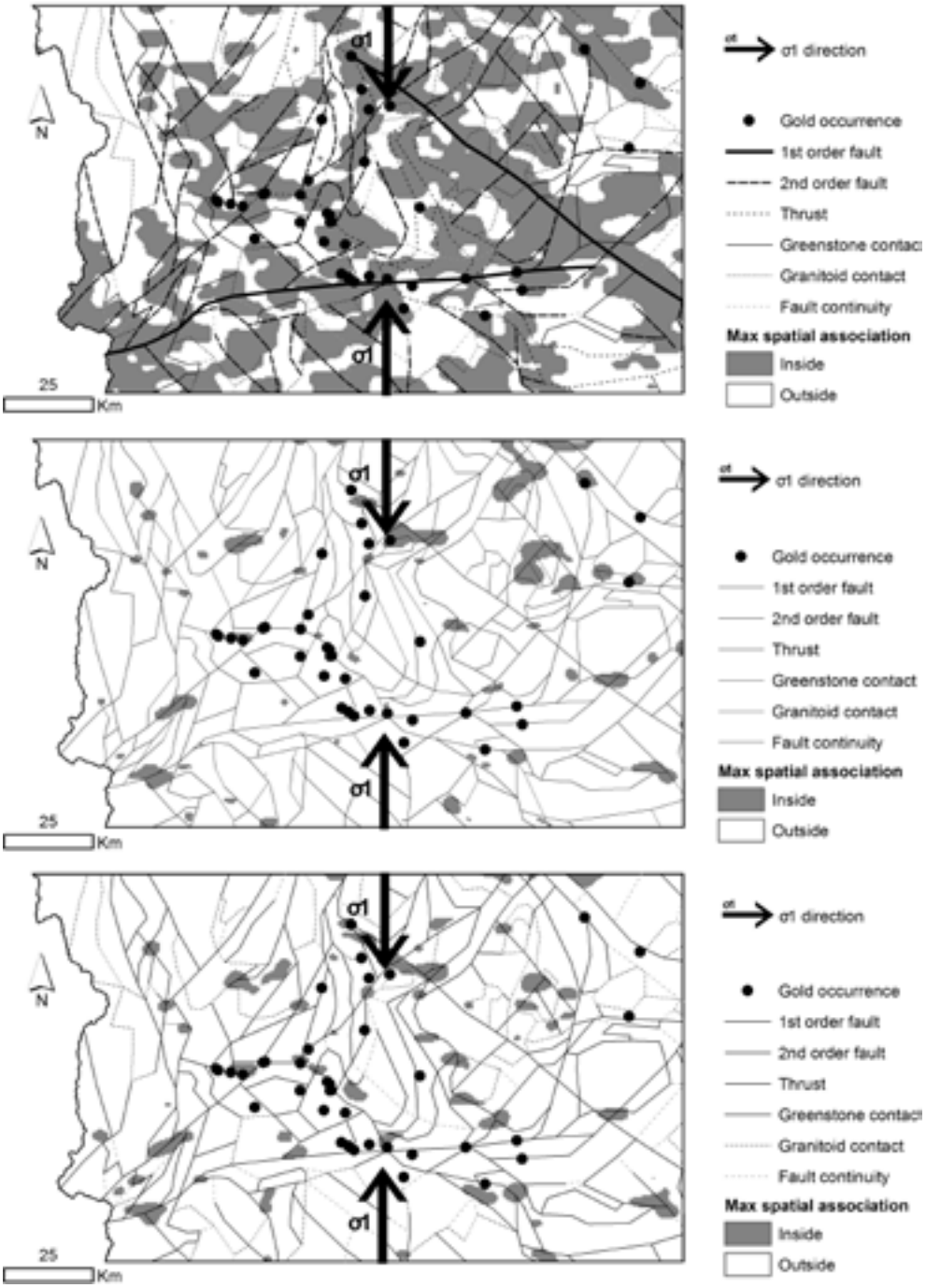

Fig. 13. N-S compression simulations. Maximum spatial association pattern between σ_3 and gold occurrences. a) All fault classes and contacts have different parameters (Table 1), b) all discontinuities have the same properties, c) all faults have the same properties but the contacts are assigned to be stronger than faults.

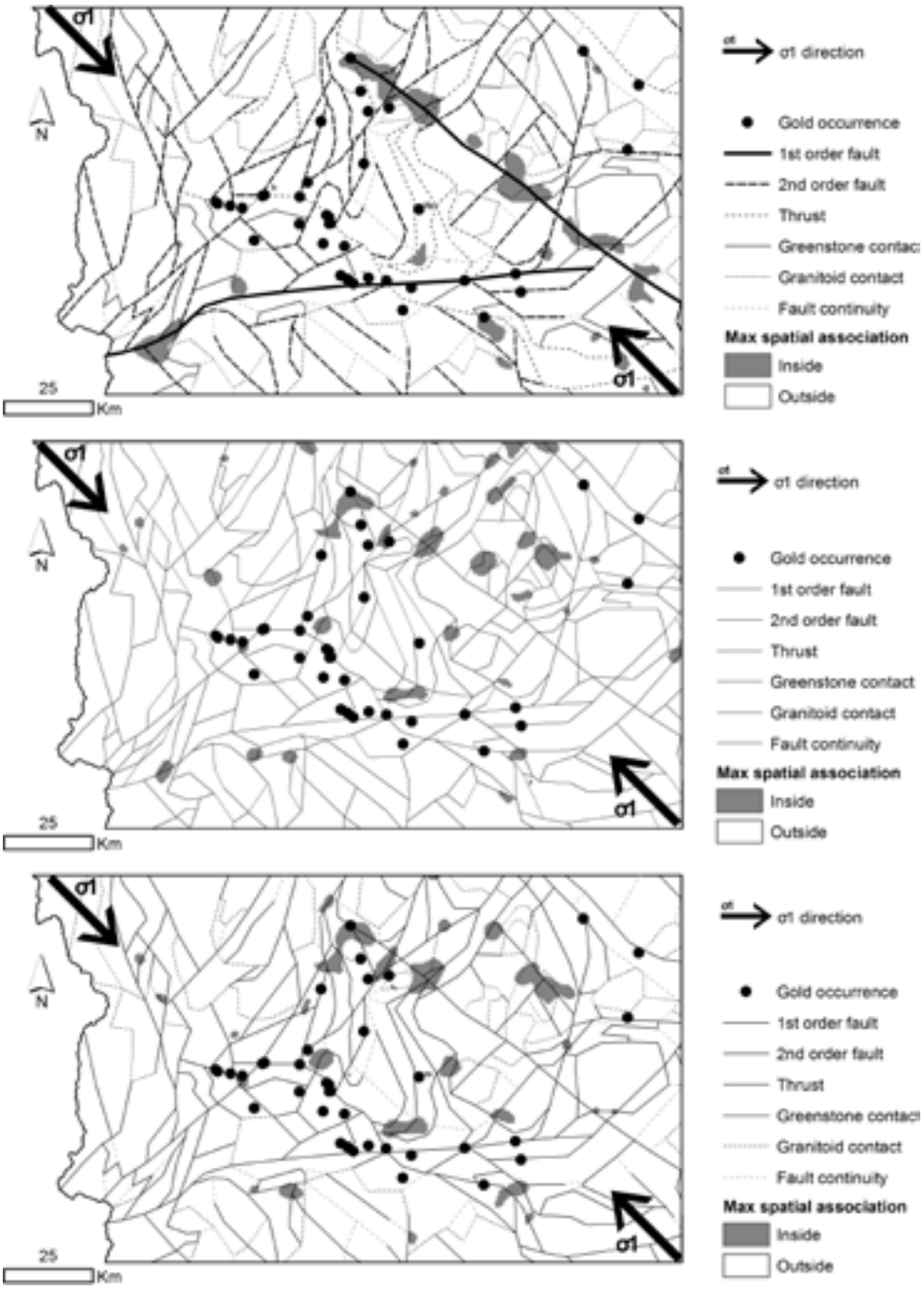

Fig. 14. NW-SE compression simulations. Maximum spatial association pattern between σ_3 and gold occurrences. a) All fault classes and contacts have different parameters (Table 1), b) all discontinuities have the same properties, c) all faults have the same properties but the contacts are assigned to be stronger than faults.

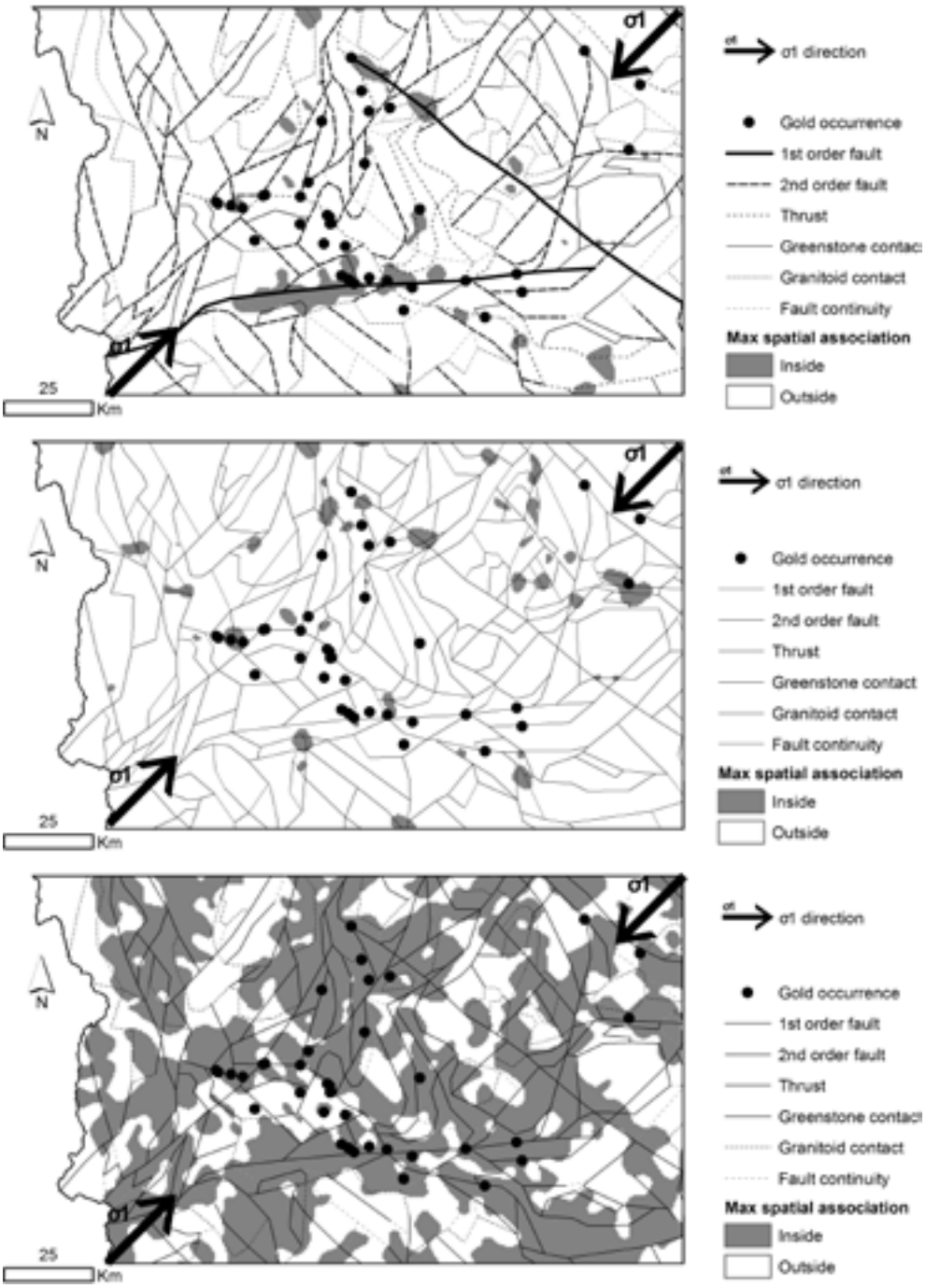

Fig. 15. NE-SW compression simulations. Maximum spatial association pattern between σ_3 and gold occurrences. a) All fault classes and contacts have different parameters (Table 1), b) all discontinuities have the same properties, c) all faults have the same properties but the contacts are assigned to be stronger than faults.

DISCUSSION AND CONCLUSIONS

It is futile to expect a numerical deformation simulation to provide exact results when there is a massive uncertainty in the input data, especially in the geology and interpreted geometry. However, a numerical model is still useful in providing a picture of the mechanisms that may or probably occur in particular physical systems. Models are helpful by providing a series of cause-and-effect examples. The models can be simple, with assumed data that are consistent with known field data at the scale of interest. A very large and complicated model may be just as difficult to understand as the real case and one should try to simplify the geological model as much as reasonably possible.

What should the modelling strategy be in the face of a chaotic system? It appears that the best we can expect

from deformation simulation is a finite spectrum of expected behaviour. Models that contain distributions of initial variations can be constructed. A model can be run several times, with different parameters (sensitivity analysis). Under these conditions, we may expect the fluctuations in behaviour to be triggered by imposed irregularities, rather that by artefacts of the numerical solution scheme. For a geologist, a deformation simulation is an objective way to complete a structural interpretation from a geological map or just to test a structural model to aid exploration.

The two-dimensional palaeo-stress modelling with UDEC code was to define minimum principal stress anomalies (dilation zones), which are interpreted to represent structurally favourable locations for fluid flow and mineralization in the modelled geometry and rheology at 1:250 000 scale in the Central Lapland Greenstone Belt. In different models, which simulate different far field stress orientations and fault stiffness, the spatial correlation of stress anomalies with known Au occurrences vary. The spatial association of stress patterns was quantified with a GIS analysis and the models, which have the strongest spatial correlation with the known gold occurrences, simulated the E-W, NE-SW and N-S compression directions. This is in a good agreement with previous studies, which suggest that the stress field rotated from the N-S to E-W compression during the late stages of the deformation history (eg. Sorjonen-Ward et al. 2003). In addition, the results suggest that the geometry not been significantly changed since the gold mineralization and supports late timing for the mineralization, which is typical for the orogenic gold mineralization (eg. Groves et al. 2000). Important exploration implication is that the area of maximum spatial association pattern of the E-W and NE-SW models, which could be considered as the best predictors for structurally favourable sites for orogenic gold mineralization, is very small. The maximum spatial association pattern area of the E-W model with highest confidence is only 1.3% of the total study area and contains 11% of the known deposits. Previous stress modelling studies have visually estimated the correlation with known mineral occurrences (eg. Holyland and Ojala 1997, Groves et al. 2000). This study shows that GIS techniques are powerful tool to quantify the spatial correlation; anomaly limits, and further reduces the areas of highest prospectivity.

In conclusion, modelling suggests that:

a) the modelled geometry has a control on gold mineralization,
b) the modelled geometry is reasonably accurate,
c) modelling scale is reasonably representative,
d) fault and material properties are representative,
e) modelled geology has not significantly changed since mineralization,
f) stress field during the mineralization was probably E-W or NE-SW as suggested by previous studies,
g) modelled stress anomalies are viable exploration targets

Individual models, which simulate different far field orientations, can be used as prospectivity maps for the orogenic gold mineralization as within the modelled area the exact timing of mineralization relative to the stress field rotation might vary. Furthermore, there are some minimum principal stress anomalies, which occur broadly at the same locations with several modelled far field stress orientations (eg. Saattopora, Fig. 6). This suggests that in the modelled geometry there are locations, which are dilational in several compression directions and may represent the best structural targets. The regional stress modelling is capable of defining anomalies at the scale of gold camps. Once these potentially mineralized areas have been defined, the next stage is to carry out a more detailed modelling (e.g., at 1:25,000 to 1:50,000 scale) to define more specific targets within the defined regional targets.

REFERENCES

Agterberg, F.P. 1974. Automatic contouring of geological maps to detect target areas for mineral exploration. Mathematical Geology 6, 373–395.

An P., Moon W.M. & Rencz, A. 1991. Application of fuzzy set theory to integrated mineral exploration. Canadian Journal of Exploration Geophysics 27, 1–11.

Angelier, J. 1979. Determination of the mean principal direction of stresses for a given fault population. Tectonophysics 56, 17–26.

Bonham-Carter, G.F. 1994. Geographic Information Systems for Geoscientists – Modelling with GIS. Computer Methods in the Geosciences 13. Pergamon Press, New York, 398 p.

Burrows, E. R. & Spooner, E. T. C. 1987. Generation of a magmatic H2O-CO2 fluid enriched in Mo, Au and W within an Archean sodic granodiorite stock, Mink Lake, Northwestern Ontario. Economic Geology 82, 1931–1957.

Carranza, E.J.M. & Hale M. 2001a. Logistic regression for geologically constrained mapping of gold potential, Baguio district, Philippines. Exploration and Mining Geology 10, 165–175.

Carranza, E.J.M. & Hale M. 2001b. Geologically constrained fuzzy mapping of gold mineralization potential, Bauio District, Philippines. Natural Resources Research 10, 125–136.

Chung, C.F. & Agterberg, F.P. 1980. Regression models for estimating mineral resources from geological map data. Mathematical Geology 12, 472–488.

Clark, S. P. 1966. Handbook of Physical Constants. Memoir 97, The Geological Society of America Incorporated, New York, 600 p.

Colvine, A. C., Andrews, A. J., Cherry, M. E., Durocher, M. E., Fyon, A. J., Lavigne, M. J., MacDonald, A. J., Marmont, S., Poulsen, K. H., Springer, J. S. & Troop, D. G. 1984. An integrated model for the origin of Archean lode gold deposits. Ontario Geological Survey, Open File Report, 5524, 98 p.

Colvine, A. C., Fyon, J. A., Heather, K. B., Marmont, S., Smith, P. M. & Troop, D. G. 1988. Archean lode gold deposits in Ontario. Ontario Geological Survey, Miscellaneous Paper 139, 136 p.

Cooper, R. F. 1990. Differential stress-induced melt migration: an experimental approach. Journal of Geophysical Research 95, 6979–6992.

Cox, S. F., Wall, V. J., Etheridge, M. A. & Potter, T. F. 1991. Deformational and metamorphic processes in the formation of mesothermal vein-hosted gold deposits – examples from the Lachlan fold belt in central Victoria, Australia. Ore Geology Reviews 6, 391–423.

D'ercole, C., Groves D.I. & Knox-Robinson C.M. 2000. Using fuzzy logic in a Geographic Information System environment to enhance conceptually based prospectivity analysis of Mississippi Valley -type mineralization. Australian Journal of Earth Sciences 47, 913–927.

Eilu, Pasi 1999. FINGOLD – a public database on gold deposits in Finland. *Geological Survey of Finland, Report of Investigation* 146, p. 224

Eisenlohr, B. N., Groves, D. I. & Partington, G. A. 1989. Crustal-scale shear zones and their significance to Archaean mineralization in Western Australia. Mineralium Deposita 24, 1–8.

Engelder, T. 1993. Stress Regimes in the Lithosphere. Princeton University Press, Princeton, 457 p.

Etheridge, M. A. 1983. Differential stress magnitudes during regional deformation and metamorphism: Upper bound imposed by tensile fracturing. Geology 11, 231–234.

Etheridge, M. A., Wall, V. & Cox, S. F. 1984. High fluid pressures during regional metamorphism and deformation: Implications for mass transport and deformation mechanisms. Journal of Geophysical Research 89, 4344–4358.

Etheridge, M. A., Wall, V. & Vernon, R. H. 1983. The role of the fluid phase during regional metamorphism and deformation. Journal of Metamorphic Geology 1, 205–226.

Fare, R. J., Groves, D. I. & McNaughton, N. J. 1991. A synmetamorphic, lower-granulite facies, lode-gold deposit at Griffin's Find, Western Australia: implications for sources of Archaean auriferous fluids. Geological Association of Canada Special Publication 39, 155–157.

Foster, R. P. 1989. Archaean gold mineralization in Zimbabwe: implications for metallogenesis and exploration. In: Keays, R.R., Ramsay, W.R.H. & Groves, D.I. (ed.), The Geology of Gold Deposits: the Perspective in 1988. Economic Geology Monograph 6, 54–70.

Fyfe, W. S. & Henley, R. W. 1973. Some thoughts on chemical transport processes, with particular reference to gold. Minerals Science and Engineering 5, 295–303.

Fyon, J. A., Schwartz, H. P. & Crocket, J. P. 1984. Carbonatization and gold mineralization in the Timmins area, Abitibi greenstone belt; genetic links with Archaean mantle CO2 degassing and lower crustal granulitization. Geological Association of Canada, Program with Abstracts 9, 65.

Fyon, J. A., Troop, D. G., Marmont, S. & Macdonald, A. J. 1989. Introduction of gold into Archean crust, Superior Province, Ontario-coupling between mantle-initiated magmatism and lower crustal thermal maturation. In: Keays, R.R., Ramsay, W.R.H., Groves, D.I. (ed.), The Geology of Gold Deposits: the Perspective in 1988. Economic Geology Monograph 6, 479–490.

Goldfarb, R.J., Groves, D.I. & Gardoll, S. 2001. Orogenic gold and geologic time: a global synthesis. Ore Geology Reviews 18, 1–75.

Grambling, J. A. 1981. Pressures and temperatures in Precambrian rocks. Earth and Planetary Science Letters 53, 63–68.

Groves, D. I. 1993. The crustal continuum model for the late-Archaean lode-gold deposits of the Yilgarn Block, Western Australia. Mineralium Deposita 28, 366–374.

Groves, D. I., Barley, M. E. & Ho, S. E. 1989. Nature, genesis and tectonic setting of mesothermal gold mineralization in the Yilgarn Block, Western Australia. In: Keays, R.R., Ramsay, W.R.H., Groves, D.I. (ed.), The Geology of Gold Deposits: the Perspective in 1988. Economic Geology Monograph 6, 71–85.

Groves, D. I. & Foster, R. P. 1991. Archaean lode gold deposits. In: Foster, R.P. (ed.) Gold Metallogeny and Exploration. Blackie, Glasgow, 63–103.

Groves, D. I., E., H. S., McNaughton, N. S., Mueller, A. G., Perring, C. S., Rock, N. M. S. & Swarnecki, M. S. 1988a. Genetic models for Archaean lode-gold deposits in Western Australia. In: Ho, S.E. & Groves, D.I. (ed.) Advances in understanding Precambrian gold deposits. Geology Department (Key Centre) & University Extension, The University of Western Australia Publication 12, Nedlands, 1–22.

Groves, D. I., Golding, S. D., Rock, N. M. S., Barley, M. E. & MacNaughton, N. J. 1988b. Archaean carbon reservoirs and their significance to the fluid source for gold deposits. Nature 331, 254–257.

Groves, D. I., Knox-Robinson, C. M., Ho, S. E. & Rock, N. M. S. 1990. An overview of Archaean lode-gold deposits. In: S.E., Ho, D.I., Groves, J.M., Bennet (ed.) Gold Deposits of the Archaean Yilgarn Block, Western Australia: nature, genesis and exploration guides. Geology Department (Key Centre) & University Extension, The University of Western Australia Publication 20, Nedlands, 2–18.

Groves, D.I., Goldfarb, R.J., Knox-Robinson, C.M., Ojala, V.J. Gardoll, S. Yun, G. & Holyland, P.W. 2000. Late-kinematic timing of orogenic gold deposits and significance for computer-based exploration techniques with emphasis on the Yilgarn Block, Western Australia. Ore Geology Reviews. 17, 1–38.

Harris, D. & Pan G. 1999. Mineral favorability mapping; a comparison of artificial neural networks, logistic regression, and discriminant analysis. Natural Resources Research 8, 93–109.

Hodgson, C. J. 1989. The structure of shear-related, vein-type gold deposits: a review. Ore Geology Reviews 4, 231–273.

Holyland, P. W. 1990a. The nature of the lithosphere: cracks and blocks? Terra Sancta Newsletter. (unpaginated).

Holyland, P. W. 1990b. Simulation of the dynamics of Archaean deformation in the Yilgarn Block, Western Australia. In: Glover, J.E., Ho, S.E. (ed.) Third International Archaean Symposium, Perth, Geoconferences W.A. Inc., 347–349.

Holyland, P. W. 1990c. Stress mapping in the Mt. Isa region. Mount Isa Inlier geology conference, Monash University, 76.

Holyland, P. W. 1990d. Targeting of epithermal ore deposits using stress mapping techniques. Pacific Rim 90 Congress, Melbourne, The Australasian Institute of Mining and Metallurgy, III, 337–341.

Holyland, P. W. & Ojala, V. J. 1997. Computer-aided structural targeting in mineral exploration: two- and three-dimensional stress mapping. Australian Journal of Earth Sciences 44, 421–432.

Holyland, P., Ridley, J. R. & Vearncombe, J. R. 1993. Stress mapping technology (STMTM). Geofluids '93: Contributions to an International Conference on Fluid Evolution, Migration and Interaction in Rocks, 272–275.

Hronsky, J. M. A., Cassidy, K. F., Grigson, M. W., Groves, D. I., Hagemann, S. G., Mueller, A. G., Ridley, J. R., Skwarnecki,

M. S. & Vearncombe, J. R. 1990. Deposit- and mine-scale structure. In: S.E., Ho & D.I., Groves, J.M., Bennet (ed.) Gold Deposits of the Archaean Yilgarn Block, Western Australia: nature, genesis and exploration guides. Geology Department (Key Centre) & University Extension, The University of Western Australia, Nedlands, Publication 20, 38–54.

Hölttä, P., Väisänen, M. Väänänen, J, Manninen, T. 2007. Paleoproterozoic metamorphism and deformation in Central Finnish Lapland. In: Gold in the Central Lapland Greenstone Belt, Geological Survey of Finland, Special Paper 44, 7–56.

Jaeger, J. C., Cook, N. G. W. 1979. Fundamentals of Rock Mechanics. John Wiley & Sons, New York, 593 p.

Kerrich, R. 1987. The stable isotope geochemistry of Au-Ag vein deposits in metamorphic rocks. In: Kyser, T.K. (ed.) Stable Isotope Geochemistry of Low Temperature Fluids. 13, Mineralogical Association of Canada, Saskatoon, 287–336.

Kerrich, R. 1989. Shear zone hosted mesothermal gold deposits: a review of geochemical evidence on the sources of fluids and solutes. In: Bursnall, J.T. (ed.) Mineralization and Shear Zones. Short Course Notes 6, Geological Association of Canada, 129–197.

Kerrich, R. 1994. Dating of Archean auriferous quartz vein deposits in the Abitibi greenstone belt, Canada: Ar evidence for a 70- to 100-Ma-time gap between plutonism-metamorphism and mineralization – A discussion. Economic Geology 89, 679–687.

Kerrich, R., Allison, I. 1978. Vein geometry and hydrostatics during Yellowknife mineralization. Canadian Journal of Earth Sciecnes 15, 1653–1660.

Kerrich, R., Cassidy, K. F. 1994. Temporal relationships of lode gold mineralization to accretion, magmatism, metamorphism and deformation – Archean to present: a review. Ore Geology Reviews 9, 263–310.

Knox-Robinson, C. M., Robinson, D. C. & Groves, D. I. 1995. Use of a geographic information system (GIS) to quantify gold prospectivity for a portion of the Southern Cross Province, Western Australia. Southern Cross Greenstone Belt Geology and Gold Mines, Geoconferences (WA) Inc., 127–128.

Lehtonen, M., Airo, M.-L., Eilu, P., Hanski, E., Kortelainen, V., Lanne, E., Manninen, T., Rastas, P., Räsänen, J. & Virransalo, P. 1998. Kittilän vihreäkivialueen geologia: Lapin vulkaniittiprojektin raportti. Summary: The stratigraphy, petrology and geochemistry of the Kittilä greenstone area, northern Finland: a report of the Lapland Volcanite Project. Geologian tutkimuskeskus. Tutkimusraportti 140, 144 p.

Luo, X. & Dimitrirakopoulos, R., 2003. Data-driven fuzzy analysis in quantitative mineral resource assessment. Computers and Geosciences 29, 3–13.

Mair, J.L., Ojala, V.J., Salier, B.P., Groves, D.I. & Brown, S.M., 2000. Application of stress mapping in cross-section to understanding ore geometry, predicting ore zones and development of drilling strategies. Australian Journal of Earth Sciences 47, 895–912.

McNaughton, N. J., Groves, D. I. & Witt, W. K. 1993. The source of lead in Archaean lode gold deposits of the Menzies-Kalgoorlie-Kambalda region, Yilgarn Block, Western Australia. Mineralium Deposita 28, 495–501.

Nesbitt, B. E. 1988. Gold deposit continuum: A genetic model for lode Au mineralization in the continental crust. Geology 16, 1044–1048.

Nesbitt, B. E., Murowchich, J. B. & Muehlenbachs, K. 1986. Dual origins of lode gold deposits in the Canadian Cordillera. Geology 14, 501–509.

Nurmi, P. A., Sorjonen-Ward, P. & Damstén, M. 1993. Geological setting, characteristics and exploration history of mesothermal gold occurrences in the late Archean Hattu schist belt, Ilomantsi, eastern Finland. Geological Survey of Finland, Special Paper 17, 193–231.

Nurmi, P. A. & Ward, P. 1989. Geology and gold mineralization in the Hattu schist belt, Ilomantsi, eastern Finland. Geological Survey of Finland Special Paper 10, 45–48.

Nykänen, V., Salmirinne, H., Hyvönen, E., Hulkki H. & Airo M. 2005. Fuzzy logic spatial modelling as targeting tool for orogenic gold mineralization in the Central Lapland greenstone belt, Northern Fennoscandian Shield, using high-resolution multi-element airborne geophysical data. In: Rhoden H.N., Steininger R.C. & Vikre P.G. eds. Symposium 2005. Window to the World. Symposium Proceedings Volume II, 1159–1167. Geological Society of Nevada, Reno.

Ojala V. J. 1995. Structural and depositional controls on gold mineralization at the Granny Smith Mine, Laverton, Western Australia. PhD thesis, University of Western Australia, Perth (unpubl.).

Ojala, V. J., Ridley, J. R., Groves, D. I. & Hall, G. C. 1993. The Granny Smith gold deposit: the role of heterogeneous stress distribution at an irregular granitoid contact in a greenschist facies terrane. In: Kerrich, R. (ed.) Western Australian gold deposits. Mineralium Deposita 28, 409–419

Oliver, N. H. S., Valenta, R. K. & Wall, V. J. 1990. The effect of heterogeneous stress and strain on metamorphic fluid flow, Mary Kathleen, Australia, and a model for large-scale fluid circulation. Journal of Metamorphic Geology 8, 311–331.

Phillips, W. J. 1972. Hydraulic fracturing and mineralization. Journal of the Geological Society of London 128, 337–359.

Phillips, G. N. 1985. Interpretation of Big Bell/Hemlo-type gold deposits: precursors, metamorphism, melting and genetic constraints. Transactions of the Geological Society of South Africa 88, 159–173.

Porwal, A., Carranza, E.J.M. & Hale, M. 2003. Knowledge-driven and data-driven fuzzy models for predictive mineral potential mapping. Natural Resources Research 12, 1–25.

Raines G.L. 1999. Evaluation of weights of evidence to predict epithermal-gold deposits in the Great Basin of the Western United States. Natural Resources Research 8, 257–276.

Raines G.L. & Bonham-Carter G.F. 2006. Exploratory spatial modelling: demonstration for Carlin-type deposits, central Nevada, USA, using Arc-SDM. In: Harris J.R. (Ed.) GIS for the Earth Sciences. Geological Association of Canada. Special Publication 44, 23–52.

Raines G.L., Bonham-Carter G.F. & Kemp L.D. 2000. Predictive probabilistic modelling using Arview GIS. ArcUser 3, 45–48.

Ramsay, J. G. & Huber, M. I. 1987. The Technique of Modern Structural Geology. Vol. 2 Folds and Fractures. Academic Press, London, 700 p.

Reches, Z. 1978. Analysis of faulting in three-dimensional strain field. Tectonophysics 47, 109–129.

Reches, Z. 1983. Faulting of rocks in three-dimensional strain fields II. Theoretical analysis. Tectonophysics 95, 133–156.

Reddy, R.K.T., Agterberg, F.P. & Bonham-Carter G.F. 1990. Application of GIS-based logistic models to base-metal potential mapping in Snow Lake area, Manitoba. Proceedings, Canadian Conference on GIS, 607–618.

Ridley, J. R. 1993. The relationship between mean rock stress and fluid flow in the crust: With reference to vein- and lode-style gold deposits. Ore Geology Reviews 8, 23–37.

Robert, F. & Kelly, W. C. 1987. Ore-forming fluids in Archaean gold-bearing quartz veins at the Sigma Mine, Abitibi Greenstone Belt, Quebec, Canada. Economic Geology 82, 1464–1482.

Robinson, G.R., Kapo, K.E. & Raines, G.L. 2004. A GIS analysis to evaluate areas suitable for crushed stone aggregate quarries in New England, USA. Natural Resources Research 13, 143–159.

Rogge, D.M., Halden N.M. & Beaumont,-Smith, C. 2006. Application of Data Integration for Shear-Hosted Au mineralization Potential Modelling: Lynn Lake Greenstone Belt,

Northwestern Manitoba, Canada. In: Harris J.R. (Ed.) GIS for the Earth Sciences. Geological Association of Canada. Special Publication 44, 191–210.

Sahoo, N.R. & Pandalai, H.S. 1999. Integration of sparse geologic information in gold targeting using logistic regression analysis in the Hutti-Maski schist belt, Raichur, Karnataka, India – a case study. Natural Resources Research 8, 233–250.

Sibson, R. H. 1987. Earthquake rupturing as a mineralizing agent in hydrothermal systems. Geology 15, 701–704.

Sibson, R. H. 1989. Structure and Mechanics of Fault Zones in Relation to Fault-Hosted Mineralization. The Australian Mineral Foundation, Glenside, 66 p.

Sibson, R. H. 1993. Load-strengthening versus load-weakening faulting. Journal of Structural Geology 15, 123–128.

Sibson, R. H., Moore, R. M. & Rankin, A. H. 1975. Seismic pumping – a hydrothermal fluid transport mechanism. Journal of the Geological Society of London 131, 653–659.

Sibson, R. H., Robert, F. & Poulsen, K. H. 1988. High angle reverse faults, fluid-pressure cycling, and mesothermal gold-quartz deposits. Geology 16, 551–555.

Sleep, N.H. & Blanpied, M.L. 1992. Creep, compaction and the weak rheology of major faults. Nature 359, 687–692.

Sorjonen-Ward, P, Nurmi, P. A., Härkönen, I. & Pankka, H. S. 1992. Epigenetic gold mineralization and tectonic evolution of a lower Proterozoic greenstone terrane in the northern Fennoscandian (Baltic) Shield. In: Sarkar, S. C. (ed.) Metallogeny related to tectonics of the Proterozoic mobile belts. New Delhi: Oxford: IBH Publishing, 37–52.

Sorjonen-Ward, P., Ojala, V. J. & Airo, M.-L. 2003. Structural modelling and magnetic expression of hydrothermal alteration in the Paleoproterozoic Lapland greenstone belt, northern Fennoscandian Shield. In: Eliopoulos, D. G. ... [et al.] (eds.) Mineral exploration and sustainable development: proceedings of the Seventh Biennial SGA Meeting, Athens, Greece, 24–28 August 2003. Vol. 2. Rotterdam: Millpress, 1107–1110.

Starfield, A. M. & Cundall, P. A. 1988. Towards a methodology for rock mechanics modelling. International Journal of Rock Mechanics and Mining Sciences and Geomechanics, Abstracts 25, 99–106.

Strömgård, K. E. 1973. Stress distribution during deformation of boudinage and pressure shadows. Tectonophysics 16, 215–248.

Tangestani, M.H. & Moore, F. 2003. Mapping porphyry copper potential with fuzzy model, northern Shahr-e-Babak, Iran. Australian Journal of Earth Sciences 50, 311–317.

UDEC 1996. Universal Distinct Element Code. User's Manual. Itasca Consulting Group, Inc. Minneapolis, Minnesota. (http://www.itascacg.com/udec.html).

Ward, P., Härkönen, I., Nurmi, P. A. & Pankka, H. S. 1989. Structural studies in the Lapland greenstone belt, northern Finland and their application to gold mineralization. In: Autio, S. (ed.) Geological Survey of Finland. Current Research 1988. Geological Survey of Finland, Special Paper 10, 71–77.

Väisänen, M. 2002. Structural features in the central Lapland greenstone belt, northern Finland. 20 p.

Zadeh, L.A. 1965. Fuzzy sets. Institute of Electric and Electronic Engeneering, Information and Control 8, 338–353.

Gold in the Central Lapland Greenstone Belt, Finland
V. Juhani Ojala (ed.)
Geological Survey of Finland, Special Paper 44, 251–269, 2007.

PROSPECTIVITY ANALYSIS OF GOLD USING REGIONAL GEOPHYSICAL AND GEOCHEMICAL DATA FROM THE CENTRAL LAPLAND GREENSTONE BELT, FINLAND

by
Vesa Nykänen and Heikki Salmirinne

Nykänen,V. &Salmirinne, H 2007. Prospectivity analysis of gold using regional geophysical and geochemical data from the Central Lapland Greenstone Belt, Finland *Geological Survey of Finland, Special Paper 44*, 251–269, 9 figures and 8 tables.

Two spatial modeling techniques, empirical weights of evidence and conceptual fuzzy logic, were used to predict the most prospective areas for gold exploration within the Paleoproterozoic Central Lapland Greenstone Belt in Northern Finland. The study area covers almost 20 000 km^2 in a terrain with excellent infrastructure and easy access in spite of situating in a region some 100 km north from the Arctic Circle.

For the empirical model the spatial association between the known mineral occurrences and selected evidential geoscientific datasets were quantified and used to generalize the original datasets into binary predictor patterns indicating favorable areas. The conceptual model, on the other hand, was created by using expert opinions on the significance of the anomalies within the evidential datasets.

The data used were high-resolution airborne geophysics, regional gravity, and regional scale multi-element till geochemistry. Both methods, empirical and conceptual, give comparable results, which were geologically validated and verified to be meaningful. The models used predicted well the known deposits and highlighted also areas with past and future exploration interest. Both empirical and conceptual approaches proved to be suitable for the purpose and the regional geochemical, geophysical and geological data appeared to be appropriate for regional or reconnaissance scale first stage exploration. According to the evidential data used and the models produced, the Central Lapland Greenstone Belt has regions with high potential for new greenstone hosted orogenic type of gold occurrences to be found.

Key words (Georef Thesaurus, AGI): mineral exploration, gold ores, Central Lapland Greenstone Belt, geophysical methods, geochemical methods, weights of evidence, fuzzy logic, models, geographic information systems, Paleoproterozoic, Kittilä, Sodankylä, Lapland Province, Finland.

Geological Survey of Finland, P.O. Box 77, FI-96101, Rovaniemi, Finland.

*E-mail: vesa.nykanen@gtk.fi, **heikki.salmirinne@gtk.fi***

INTRODUCTION

The geological information collected from the Central Lapland Greenstone Belt (CLGB) is composed of multiple layers of spatial data at several scales and with variable coverage over the area of interest. The total study area used in this project is 18 790 km^2 (Fig. 1), covering the essential parts of the CLGB.

The data available includes airborne high-resolution multi-element geophysical surveys, regional and local scale geochemical surveys and geological mapping in variable scales. There is a need for tools to efficiently and properly manage, manipulate, visualize and integrate this large amount of data. Having the data in digital format gives one an excellent opportunity to utilize Geographic Information Systems (GIS) to be used for quantitative analysis of spatial association between the known mineral occurrences and the variable geological features. The aim of this paper was to make a prospectivity analysis for gold within the CLGB and also to illustrate the possibilities to conduct this task by using the geo-scientific data sets from Northern Finland and certain selected methods as examples of spatial modeling tools. Furthermore, the goal was to use the data sets to make estimations on the most prospective areas for gold by using these spatial analytical techniques. The strengths of the GIS tools used is this ability to integrate and combine multiple geoscientific information into a single prospectivity map, i.e. to condense and generalize from a complex

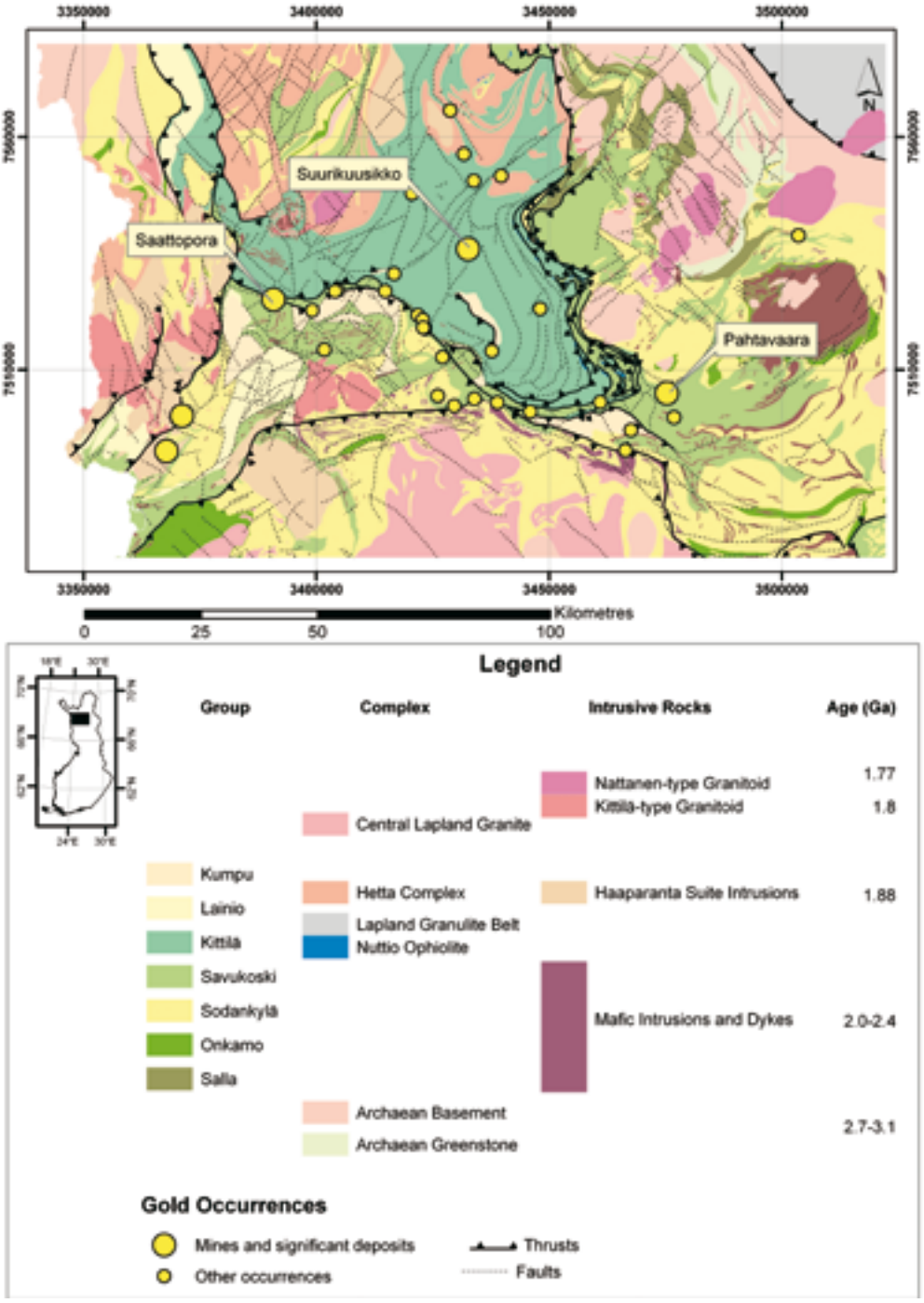

Fig. 1. Location of the study area in Lapland. The known gold occurrences and deposits marked with yellow dots. The most significant deposits are labeled.

Table 1. Empirical and conceptual methods for mineral prospectivity mapping (Bonham-Carter, 1994, Harris et al. 2001).

Type	Method	Model parameters	Criteria from combining input data
Empirical *(data driven)*	Weights of evidence	Calculated from training data (i.e. existing mineral deposits)	Spatial relationship between the known occurrences and input data (use of Bayesian probabilities)
	Logistic regression Neural networks	Calculated from training data (i.e. existing mineral deposits)	Use of training areas around each deposit to gather statistics from each of the input layers; Used to predict the presence or absence of a mineral deposit
Conceptual *(knowledge driven)*	Boolean logic	Estimated by an expert	Summing of binary maps
	Index overlay	Estimated by an expert	Summing of weighted binary maps
	Dempster-Shafer belief theory	Estimated by an expert	A generalization of the Bayesian theory of subjective probability.
	Fuzzy logic	Estimated by an expert	Each input predictor map assigned a fuzzy weight ranging from 0 to 1; all predictor maps then combined using fuzzy operators

mass of information into a substantially simpler form suitable for exploration or land use decisions.

Several tools for statistical and geo-statistical operations may be used to conduct mineral prospectivity mapping. These methods can be divided into two main categories (Table 1), based on the approach: (I) empirical (data driven) and (II) conceptual (knowledge driven) methods (Bonham-Carter, 1994). In the empirical approach, the known mineral deposits are used as 'training points' for examining spatial relationships between the known deposits and particular geological, geochemical and geophysical features. The identified relationships between the input data and the training points are quantified and used to establish the importance of each evidence map and finally integrated into a single mineral prospectivity map. Examples of the empirical methods used are weights of evidence, logistic regression and neural networks. The other major branch is the conceptual (knowledge driven) approach, where we use re-formulation of knowledge about deposit formation into mappable criteria (i.e. threshold values in geochemistry and geophysics etc., certain structures or formations in the geological maps). The areas that fulfill the majority of these criteria are highlighted as being the most prospective. These methods are dependent on the geologist's input and exploration models being thus fairly subjective in nature. By selecting a conceptual method one can benefit from the expertise of the geologists during the modeling process exceeding the capabilities of pure statistics. The methods belonging into this branch include Boolean logic, index overlay (binary or multi-class maps), the Dempster-Shafer belief theory, and fuzzy logic overlay. Especially the latter has been recently widely implemented for the data integration and mineral prospectivity mapping purposes (Chung and Moon, 1990; An et al., 1991, D'Ercole et al., 2000; Knox-Robinson, 2000, Luo and Dimitrakopoulos, 2003).

Direct comparison between these two different approaches (empirical vs. conceptual) is difficult since the methods do not use identical datasets (Singer and Kouda, 1999; Harris et al., 2001). The selection of the preferable method is thus often made based on the available datasets and the goals of the modeling. Harris et al. (2001) give an excellent summary of the different methods. Different methods bring their own characteristics into modelling and allow one also to use them to cross-validate results from one method to another.

METHODS

For this study the multivariate empirical method called weights of evidence (Bonham-Carter et al., 1988; Agterberg et al., 1990) and a conceptual fuzzy logic overlay method were selected for the data integration and analysis. The weights-of-evidence method is based on a log-linear form of Bayes' rule including an assumption that the evidential explanatory categorical (geological maps etc.) or ordered (geochemical and geophysical) variables are conditionally independent with respect to the deposits and occurrences used as training points. The GIS software used in this study is ArcView™ with Spatial Analyst™ (ESRI products).

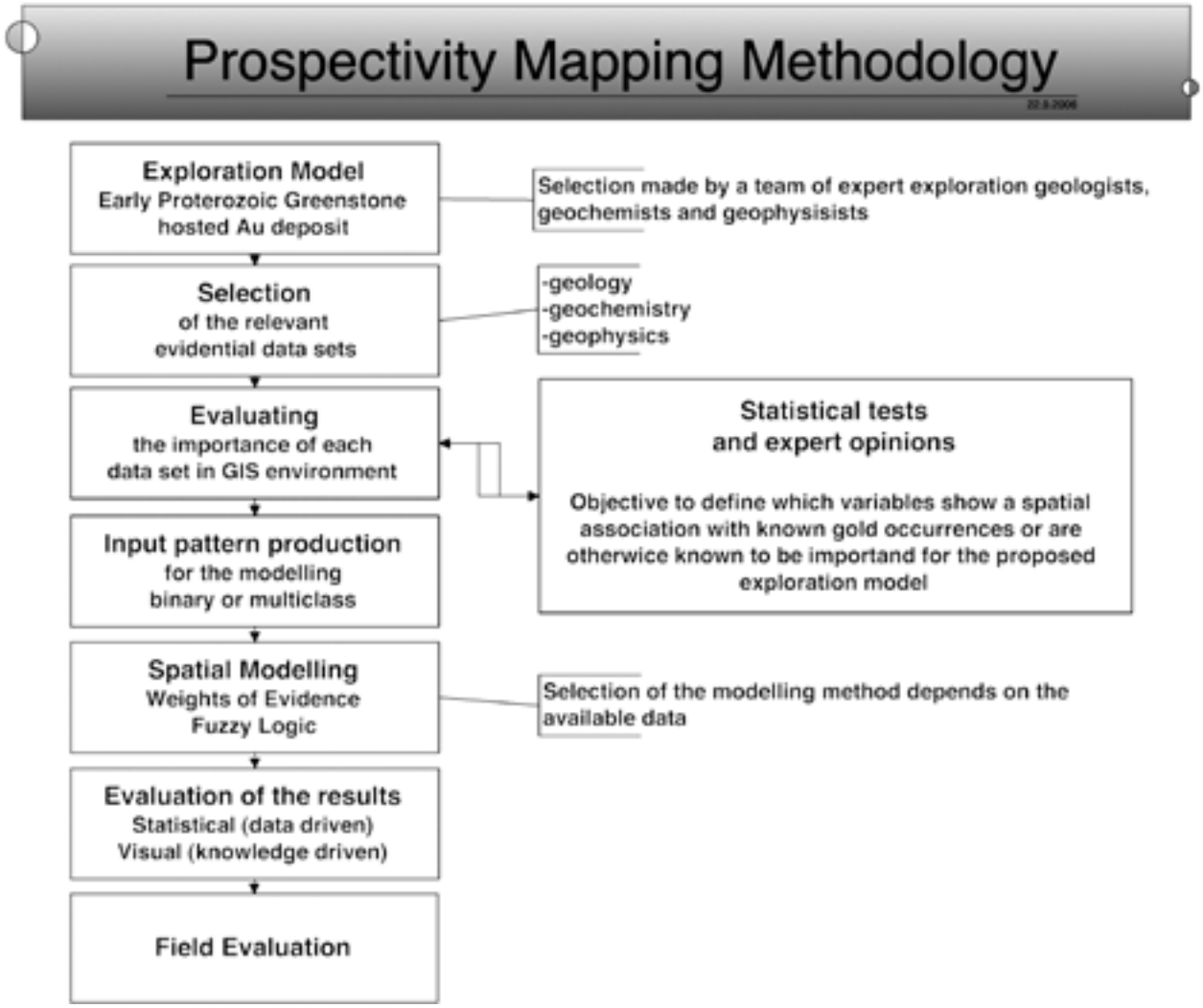

Fig. 2. Flow chart of the methodology used to produce prospectivity maps.

The weights-of-evidence and fuzzy-logic modeling were carried out by using an ArcView add-on called ArcSDM, which is a tool developed by the Geological Survey of Canada and the U.S. Geological Survey (Kemp et al., 2001).

Figure 2 shows how prospectivity mapping methodology can be divided into independent modules. The key issue is the exploration model, which is based on the expertise of the exploration team of geologists, geochemists and geophysicists.

Weights-of-evidence method

The weights-of-evidence method is based on the application of Bayes' Rule of Probability with an assumption of conditional independence (Bonham-Carter, 1994). When this assumption is violated, one can run logistic regression to calculate the posterior probabilities. The essence of the Bayesian approach is to provide a mathematical rule explaining how you should change your existing beliefs in the light of new evidence. In other words, it allows scientists to combine new data with their existing knowledge or expertise. In the weights of evidence modelling this is expressed in terms of prior and posterior probabilities, which are derived in the context of mineral exploration by calculating the spatial association of the known mineral occurrences or deposits (training sites) and the selected series of evidential maps. If the number of training sites falls mostly within a predictor pattern, it is evident that the probability of a training site occurring inside the pattern is higher than the prior probability. Respectively, the probability of having a training site outside the pattern is lower than the prior probability.

Table 2. Terminology used in weights of evidence modeling.

Term	Description
Training site or point	The known locations of which is being predicted. In this study the training sites are known Au deposits and occurrences within the study area
Study area/ analysis extend	The area to be studied and used as the analysis mask.
Evidential theme/ evidence	Maps used for prediction of point objects (mineral occurrences). These can be either in vector or raster format and either binary or multi-class.
Unit cell area/ response theme	The area, which the training sites are assumed to occupy. This is used in order to calculate the probability of the point occurrences. The output of the modeling is a map (response theme) showing the probability that a unit area contains a point i.e. an Au deposit in this study.
Pattern	A map area having consistent, recognizable characteristics.
Weight, W^+, W^-	The value assigned to a pattern as a predictor of the training sites. The weight for inside pattern is denoted as W+ and outside pattern is W-. The weights for areas of missing data are given a value of zero.
Contrast, C	Difference between W+ and W- indicating how well a pattern predicts the training sites. A positive contrast that is significant based on its studentized contrast suggests that a pattern is a useful predictor. The relative values of contrast of the various patterns used in a model indicate the relative degree of importance of each patterns as a predictor.
Confidence (studentized contrast, Stud(C))	The ratio of the contrast and the standard deviation of the contrast. This is used in similar manner to a Student t-test of significance of the contrast. A useful measure of significance of the contrast due to the uncertainties of the weights and missing data.
Prior probability	The probability of a training site occurring per study area (the density of training sites in the study area) before consideration of the evidence.
Posterior probability	The prior probability modified by consideration of the evidence from one or more patterns. The posterior probability is calculated by adding a weight for each pattern to the logit of the prior probability and converting the sums from logits to probability. These calculations assume that the patterns added are conditionally independent.

Bonham-Carter (1994), Raines (1999), Singer and Kouda (1999), Carranza and Hale (2000) provide the detailed formulation of the weights of evidence model, which is only briefly described here. The main terminology used in the spatial modelling is described in the Table 2 (chiefly after Bonham-Carter, 1994; Raines, 1999).

By quantifying the degree of overlap between the training sites and the patterns of the evidential data one can calculate a pair of weights (W^+ and W^-) for each piece of evidence. If more points occur within a pattern than would be due to chance then W^+ is positive and W^- is negative. On the other hand, when W^+ is negative and W^- is positive then there are fewer points within the pattern that would be expected by chance. A positive W^+ value indicates thus a positive association between the training points and the evidence map, whereas a positive W^- value indicates a negative association respectively. By calculating the difference or contrast ($C = W^+ - W^-$) between these two weights for each of the evidential maps, one can get a measure of the association between training sites and these evidence maps (Bonham-Carter et al., 1988). A stronger association shows as higher contrast value. The studentized value of the contrast, the ratio of contrast to its standard deviation, C/s(C), is calculated to test the significance of the contrast values (referred to in ArcSDM as the 'confidence' value). The confidence value gives an estimate of the uncertainty included in the weights calculation. The contrast values are used to generalize the evidential themes from multi-class maps into binary pattern maps indicating areas within each of the maps to be either "favourable" or "non-favourable". The maximum contrast value can be used to point out the threshold to identify an anomaly in the data. The generalization of the multi-class themes is beneficial since the small number of the rare mineral deposits can lead to noisy and unreliable estimates of weights.

By using the presence of a predictor pattern we can then calculate the posterior probability, which is the prior probability multiplied by a factor which depends on the frequency with which training points occur on an evidential map. Posterior probability is larger than prior probability in the areas where the sum of the weights is positive.

Fuzzy Logic method

The conceptual approach is using the expertise of the exploration geologists, geochemists, and geophysicists to define the threshold values for the evidential datasets. For this study, the fuzzy-logic spatial modeling was also produced by using ArcSDM software (Kemp et al., 2001). In classical set theory, the membership of a set is defined as true or false (1 or 0) whereas membership of a fuzzy set is expressed on a continuous scale from 1 to 0 (e.g. somewhere between 'anomalous' vs. 'not anomalous') as shown in Figure 3. The values of fuzzy membership can be chosen based on subjective judgment of an expert. In this study, the fuzzy membership function for each evidential element was defined by experts by taking in account the statistics of each element and the geological background values within each area of interest. Membership reflects degree of truth of some proposition or hypothesis, which is often a linguistic statement such as high magnetic values are anomalous for gold deposits. To define the membership function one needs to define the thresholds for 'not anomalous' and 'anomalous' values and then a function describing the 'maybe – probably' values in between these two thresholds. In this work, a linear function between the thresholds was assumed appropriate, but the shape of the actual function varies due to classification prior giving fuzzy membership values for the classes of the maps (Fig. 3). The fuzzy membership values reflect the relative importance of the each class of the maps used. The closer the fuzzy membership value is to one the more significant is the anomaly. The hypothesis derived from the exploration model was 'is there a gold deposit' and the fuzzy sub sets or intermediate hypotheses were like 'data showing an alteration zone' and 'data showing signs of sulphides'.

After defining the fuzzy membership functions for each evidential map, a variety of operators can be used to combine the membership values together. In this paper, we have used the operators listed in Table 3 (chiefly after Bonham-Carter, 1994).

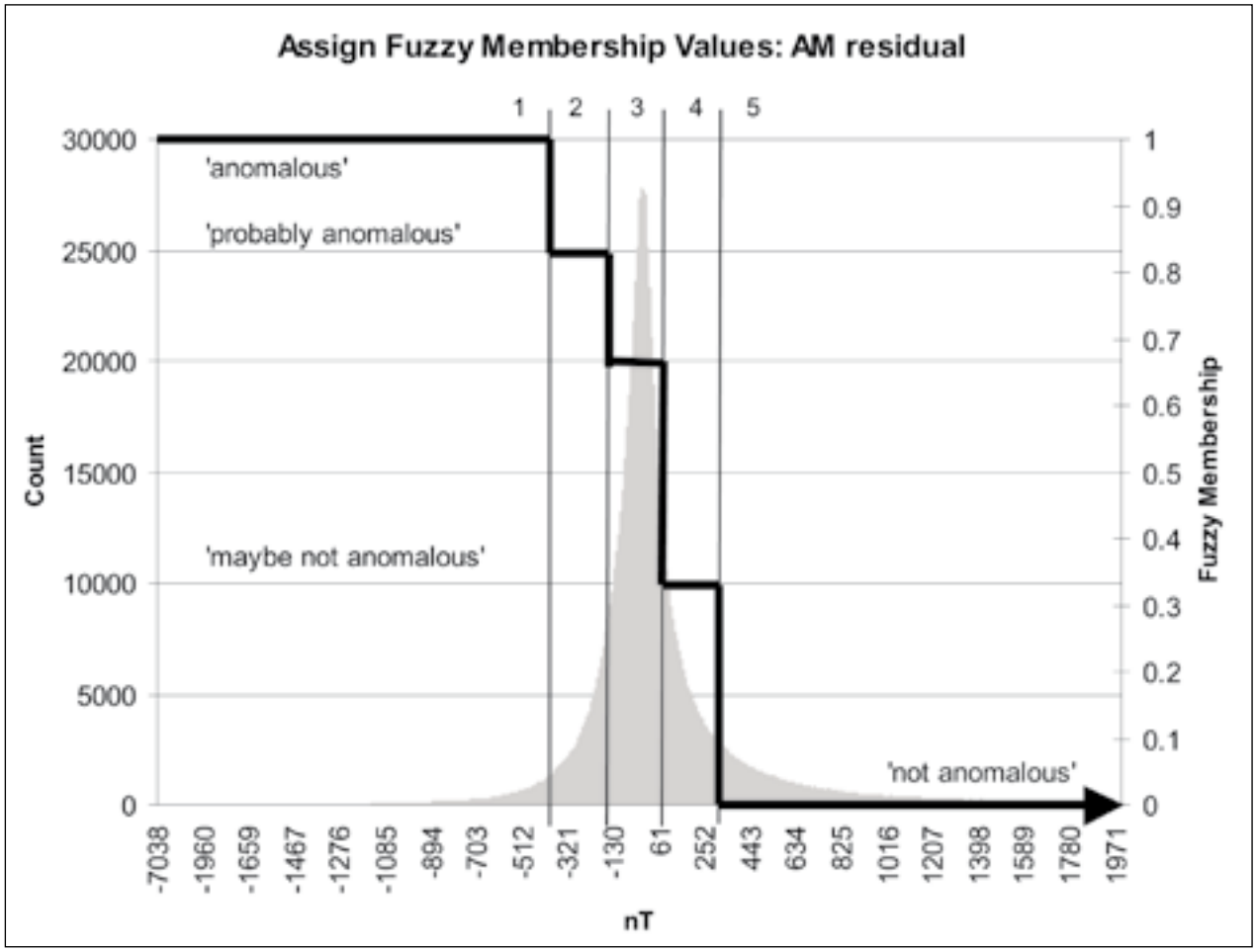

Fig. 3. An example of assigning fuzzy membership values (thick black line). Fuzzy membership value of 1 is 'anomalous' and 0 is 'non-anomalous'. Values between 1 and 0 represent statements 'probably anomalous', 'maybe not anomalous' etc. The original data values were broken into a small number of meaningful classes by using the histogram and then the experts assigned fuzzy-membership values to the classes.

Table 3. Fuzzy operators (Bonham-Carter, 1994).

Operator	Boolean equivalent	Desrciption
Fuzzy AND	AND (logical intersection)	This could also be called as Min-operator as it creates an output, which is controlled by the smallest fuzzy membership values at each location. It results in a conservative estimate of set membership, with tendency to produce small values and minimum areas. Useful to find the areas where all the evidence used need to be present for the hypothesis to be true.
Fuzzy OR	OR (logical union)	This could be called as Max-operator as it creates an output, whose membership values are controlled by the maximum values of any of the input maps. By using this operator any positive evidence may be sufficient to suggest favourability.
Fuzzy Algebraic Product		The combined fuzzy membership values tend to be very small due to the effect of multiplying several numbers less than 1. The output is always smaller than, or equal to, the smallest contributing membership value.
Fuzzy Algebraic Sum		The result is always larger (or equal to) the largest contributing membership value.
Fuzzy Gamma		This is defined in terms of the fuzzy algebraic product and the fuzzy algebraic sum, being a combination of these two operations.

DESCRIPTION OF THE DATASETS

The data used for this study are multi-element low-altitude airborne geophysics, regional gravity, and multi-element till geochemistry. All the basic data are standard data sets produced by the GTK and available on request. The locations of the known Au deposits were taken and slightly modified from the FinGOLD database (Eilu, 1999). For certain larger deposits a few more points were added and some locations were relocated more precisely. The total amount of available training points is 40 representing the Early Proterozoic greenstone hosted gold deposits and occurrences within the study area. For the modeling, we used 35 training points excluding those that were closely clustered together.

High resolution airborne geophysics

The whole study area has been covered by high resolution, systematic, low altitude airborne geophysics. The oldest flights date from 1974 and the most recent were completed during the summer 2002. The mapped properties are magnetic total field intensity, two electromagnetic field components and four gamma radiation components. In this work, aeromagnetic and apparent resistivity of conductive half space calculated from airborne electromagnetic measurements has been used. The flight altitude used is about 30 to 40 meters and line spacing 200 meters. The profile direction has been either N-S or E-W according to the dominant strike of the bedrock. As the flying speed is around 50 m/s, and the recordings has been done two to ten times per second in magnetic and two or four times per second in electromagnetic measurements, the data point separation depending on method is five to 25 meters. The cell size of interpolated grids is 50 m x 50 m.

Known gold occurrences and deposits of CLGB have a strong lithological and structural control, and host rocks are affected by strong multi-stage alteration (Airo and Mertanen, 2001). Large crustal-scale structures, faults, shear, and in many places alteration zones produce observable aeromagnetic lows. To enhance these magnetic lows a median filter was applied by subtracting from the original aeromagnetic data the median value of a four km circular radius neighborhood around each of the cells within the grid. The residual of the aeromagnetic grid was then used in the modeling instead of the original grid. In CLGB, most known gold occurrences are associated with sulphide alteration and sulphides can produce conductivity anomalies. However, conductive graphite bearing volcanic-metasedimentary rocks make the situation more complex. Filtering the resistivity data did not improve the results. Thus, the original resistivity grid was used in the model. Although alteration zones can in some cases be mapped using radiation data, the use of gamma radiation is hampered as, radiation attenuates to zero within the first 30 cm from the source. In this study, the aeroradiometric data has not been used due to large differences in soil cover, large bog areas,

lakes and rivers, which unevenly mask the radiation. Aerogeophysical applications for gold exploration in CLGB has been reviewed by Airo (2006).

Regional gravity

Gravity reflects large crustal-scale structures, lithological units, faults, and shear zones, which can be associated with gold occurrences. Bouguer anomaly data were interpolated to grid cell size of 500 m x 500 m and the horizontal gradient was calculated for the analysis.

The CLGB regional gravimetric survey has been done with a point density of one point/km^2 on the average by GTK and partly also by the Finnish Geodetic Institute (Kääriäinen and Mäkinen, 1997). Regional gravity data measured in CLGB have been described by Salmirinne and Turunen (2007). The gravity survey covers about 62% of the whole study area. In the weights-of-evidence method, training sites in areas of no data were not used for calculation of weights for the gravity theme and these no data areas are treated as "missing data" for which the weights are set to zero. In the fuzzy-logic method these areas of missing data are assigned area-weighted mean of the fuzzy membership of known data. So, in spite of low data density and "missing data" areas, it has been possible to use gravity data, which proved to be meaningful for the analysis.

Regional till geochemistry

The sampling density for the regional till geochemistry is one sample per four km^2. The sampling was conducted in the 1980's (Salminen, 1995). In general, the samples were collected as a composite of three to five sub-samples from an average depth of 1.5 meters taken with a portable percussion drill equipped with a through flow bit. In certain areas, the samples were combined from five to ten line samples, which has caused some artifacts shown as level differences between the map sheets with single samples. The sampled material was chemically unaltered parent till. The samples were dried and the <0.06 mm fraction was sieved for analysis. Hot aqua regia digest was used and Al, Ba, Ca, Co, Cr, Cu, Fe, K, La, Li, Mg, Mn, Mo, Ni, P, Pb, Sc, Sr, Th, Ti, V, Y, Zn and Zr were determined with ICP-AES. In addition, Au, Te and Pd were analyzed with AAS. The original point data were interpolated to grid cell size of 200 m x 200 m.

Geology

Geological mapping has been conducted over the study area mostly at 1:50 000 scale, which are compiled into 1:100 000 scale printed maps and a generalized 1:200 000 scale digitized stratigraphical map of the Kittilä Greenstone Area (Lehtonen et al., 1998). The geological outline of CLGB is given by Hölttä et al. (2007).

Outcrop conditions are generally poor and these areas have been subject only to the first stage exploration, which has typically involved only till sampling and airborne geophysics in addition to geological mapping.

The geological map is based on field mapping guided by interpretation of the airborne geophysics. Thus, there is quite clear correlation between for example the magnetic data and the geological map. In this study, we have avoided the use of the interpreted geological map together with the airborne geophysics. The scale of the geological map currently available also limits its use for spatial modeling together with the high-resolution airborne geophysics. The 1:100 000 geological maps would provide more details and variability to lithological units compared to generalized 1:200 000. We expect to be able to improve the models when the larger scale geological maps of the entire study area are available.

WEIGHTS-OF-EVIDENCE MODELING

To accomplish weights-of-evidence modeling, the original multi-class evidential datasets were generalized into binary predictor patterns. The evidence used were: (1) selected pathfinder elements in till geochemistry and (2) favorable geophysical anomalies. The geological map was not used as evidence, even though it might provide relevant information. The final results of the modeling are, however, compared with and validated by using the geological map.

After calculating the weights for each evidential data, one can use the variation of the weights and the calculated contrasts (i.e. difference between the weights) to select the classes where the spatial association between the training sites and the evidential data sets is optimal i.e. at the maximum contrast value. The evidential data is then divided into two classes (e.g. 'favorable' and 'non-favorable'), which will be used as an input in the data integration.

Figure 4 shows the results of the generalization of the geophysical and combined geochemical data sets. Table 4 is an example of the weights analysis used for generalization. These binary prediction patterns

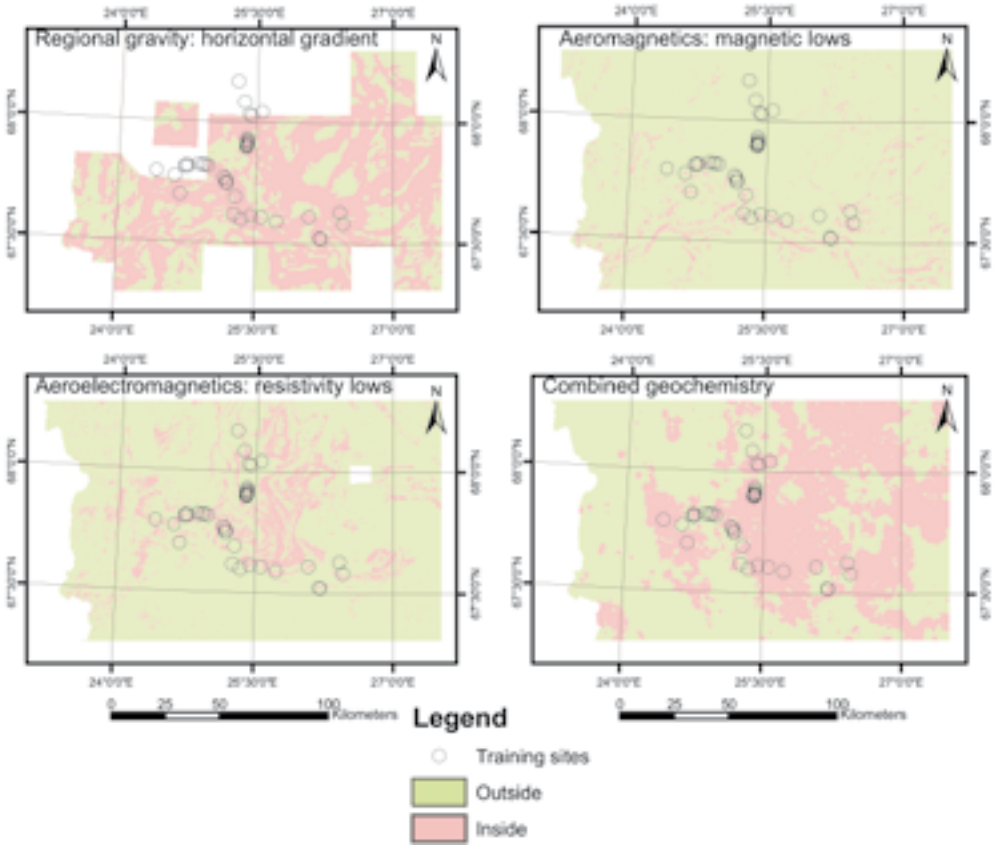

Fig. 4. Binary patterns derived from the generalization of the geophysical and combined geochemical evidential data sets. Green areas are classified as ‘‘non-favorable pattern and red areas as ‘favorable’ pattern. The open circles are the known Au –occurrences and deposits used as training sites. Combination of geochemistry is done by fuzzy logic overlay in three steps. First Fe, As, Te and Ni fuzzy membership values are combined together by using Fuzzy OR operator resulting a combination, which is integrated together with Cu fuzzy membership values by using a Fuzzy AND operator. Finally Au fuzzy membership values are combined with this combination by using a Fuzzy Gamma operator.

Table 4. Weights for airborne magnetics as an example of the weights analyses used for generalizing the magnetic evidence. Class 1 (bold font) was considered as favorable predictor pattern (maximum contrast) and the rest as non-favourable, respectively. The $s(W^+)$, the $s(W^-)$ and the s(C) stand for the standard deviations of the corresponding factors. Stud(C) is the studentized contrast value of C/s(C). #Points = cumulative number of training sites.

Class	Class range (nT)	Area (Sq. km)	#Points	W+	s(W+)	W-	s(W-)	Contrast	S(C)	Stud(C)
1	–7040 – –270	1303.3	9	1.3113	0.3339	–0.2254	0.1962	1.5368	0.3873	**3.9681**
2	–270 – –170	2571.6	12	0.9183	0.2890	–0.2727	0.2086	1.1909	0.3564	3.3413
3	–170 – –110	4053.4	12	0.4624	0.2889	–0.1766	0.2086	0.6390	0.3563	1.7933
4	–110 – –80	5143.0	13	0.3041	0.2775	–0.1441	0.2133	0.4482	0.3500	1.2805
5	–80 – –50	6589.1	14	0.1303	0.2674	–0.0783	0.2183	0.2085	0.3452	0.6041
6	–50 – –30	7802.3	15	0.0302	0.2583	–0.0220	0.2237	0.0522	0.3417	0.1527
7	–30 – –10	9174.3	17	–0.0067	0.2426	0.0064	0.2358	–0.0131	0.3384	–0.0387
8	–10 – 10	10402.3	19	–0.0211	0.2295	0.0257	0.2501	–0.0468	0.3395	–0.1378
9	10 – 30	11463.6	23	0.0729	0.2086	–0.1264	0.2888	0.1993	0.3563	0.5593
10	30 – 60	12647.4	25	0.0580	0.2001	–0.1317	0.3164	0.1897	0.3743	0.5068
11	70 – 110	13954.3	29	0.1081	0.1858	–0.4023	0.4084	0.5104	0.4487	1.1377
12	110 – 190	15219.5	31	0.0880	0.1797	–0.5024	0.5001	0.5904	0.5314	1.1110
13	190 – 320	16363.7	31	0.0154	0.1797	–0.1121	0.5002	0.1276	0.5315	0.2400
14	320 – 630	17572.2	31	–0.0559	0.1797	0.5897	0.5004	–0.6456	0.5317	–1.2141
15	630 – 13820	18762.1	35							

were then pair wise tested for conditional independence to assure that the following modeling would not give over or underestimated results due to conditional dependencies between two or more data sets.

Conditional independence

One assumption with the weight-of-evidence approach is the conditional independence (CI) of evidential maps with regards to the training sites. A pair-wise chi-squared test can be applied and a chi-squared (χ^2) test value calculated for testing CI between binary maps (Bonham-Carter, 1994). Geophysical maps used in this study (aeromagnetic, airborne electromagnetic and horizontal gradient of regional gravity) turned out to be conditionally independent in sufficient level but dependence between till geochemical maps proved to be more complex. The elements of interest (Cu, Fe, As, Te, Ni and Au) were tested against each other. To avoid violation of CI, geochemical anomaly maps of these elements were combined together into one evidence map using the fuzzy logic combination of them as described later in the fuzzy logic section of this paper (Figure 9.).

Table 5 summarizes the pair-wise test of the binary pattern used in final model. With one degree of freedom and probability level of 95%, the test χ^2 value is 3.8 for rejection of the assumption of conditional independence (Bonham-Carter, 1994). Values in Table 5 shows that hypothesis of conditional independence is not rejected at this probability level. Number of occurrences used for χ^2 calculations was 35, which can be too few and cause uncertainty for calculation. Nevertheless, the chi-squared values seem to be insignificant.

The other method for testing CI is the overall test. In the overall test, the total number of occurrences predicted by the model is determined by summation of the product of the area in counts of unit cells times the posterior probability for all cells on the model (Bonham-Carter, 1994). Predicted number of occurrences is usually larger than the observed number. If the predicted number is 10–15% larger than observed, conditional independence between evidential maps may be violated (Bonham-Carter, 1994). In this study, the determined number of predicted occurrences in final model is 42.3, which is 17.3 % larger than the observed number 35. This may indicate some problem with CI, but because χ^2 values does not show any distinct problem between binary pattern of evidential maps and the small number of training points (35) can cause some instability also for overall test, the model was accepted for presentation. A new test for CI (Agterberg and Cheng, 2002) suggests that the conditional independence hypothesis for the current model can be accepted with a probability of slightly less than 90%. The assumption of conditional independence is not required for the logistic-regression method to calculate the posterior probability map. Thus, the logistic-regression method (Agterberg et al., 1993) using the binary generalizations from the weights-of-evidence weights analysis was also calculated to evaluate the possible CI problem. The resulting posterior probability map patterns are similar to the patterns of the weights-of-evidence map. The posterior probability value of the logistic-regression model is on average only 19% lower than the posterior-probability value calculated by the weights-of-evidence method reported here indicating also a minor disturbance in CI.

Table 5. Calculated χ^2 values for testing conditional independence between binary evidence with respect to gold occurrences (35) used in weights of evidence modeling. None of these test statistics are sufficiently high to reject the assumption of conditional independence.

Evidence	Geochemistry	Gravity	Aeromagnetic
Airborne EM	1.64	0.96	1.12
Geochemistry		0.1	0.04
Gravity			0.31

Results and interpretation

Table 6 shows the weights, contrasts and confidences calculated for the model. Confidence values (i.e. the studentized contrast) higher than 2 are considered as 'acceptable' (Bonham-Carter, 1994). All evidence used here exceeds this level. Evidential maps can be ranked by contrast for the degree of correlation with the training sites. Horizontal gradient of regional gravity map has the largest contrast value (2.528) indicating that it is the best predictor. The aeromagnetic map is the weakest predictor, but at a contrast of 1.5 is still quite high. The gravity map does not cover the whole study area and there are quite large areas of missing data affecting uncertainty to calculation of posterior probabilities. Twenty-one gold training sites of 35 fall into the pattern from the gravity data. Note that the airborne EM and aeromagnetic maps are the only evidence with W+ significantly larger than the absolute value of W-. The gravity and geochemistry favour the negative side; so they are defining well the areas of poor prospectivity for gold. Whereas the airborne EM and aeromagnetics favour the positive side; so they are defining well the areas of high prospectivity. Thus all the evidence is contributing, but in different ways. The

Table 6. Weights for the binary evidence used for modeling. The total number of training points is 35. Confidence values >2 are considered as 'acceptable'. Prior probability is 0.0009. The unit cell was 0.5 km2.

Evidence	Area [km²]	#Training sites	W–	W+	Contrast	Confidence
Gravity	7928	21	–2.1217	0.4063	2.528	2.4722
Airborne EM	2732	20	–0.6899	1.3671	2.0571	6.0169
Geochemistry	8227	27	–1.0335	0.6028	1.6362	3.8709
Aeromagnetic	1303	9	–0.2254	1.3113	1.5368	3.9681

spatial variation of uncertainty of the posterior probability and its magnitude are shown in Figure 5.

The resulting prospectivity map (Figure 6) highlights the areas being most favorable for greenstone hosted Au –deposits according to the exploration model used. The sensitivity of the model to specific deposits for the modeling was tested by calculating 23 successive models and leaving out one of the deposits in turn. This is a type of jack-knife test. The posterior probability value of each of the model was associated with the deposit point left out from the model and plotted against the posterior probability of the model including all the training sites resulting the scatter plot in Figure 7. The plot suggest that excluding any other deposit from the model, except Kutuvuoma, would not give significant deviation from the model including all the training sites. The reason for different behavior of Kutuvuoma is due to an artifact driven by the generalized gravity pattern including all the other training sites except Kutuvuoma. This leads into an abnormal high negative weight for the gravity pattern when the Kutuvuoma site is excluded because there are then no training sites in the non-favourable gravity pattern. The ArcSDM software arbitrarily assigns a fractional training site when this situation occurs which causes an anomalous low W-. Those training sites plotting below the prior probability (see the close-up in Fig. 7) are all within 600 m from an area with posterior probability higher than prior probability. Another test of the validity of the model can be made by associating the training sites with the modeled posterior probability. Thus, one can estimate how well the model predicts

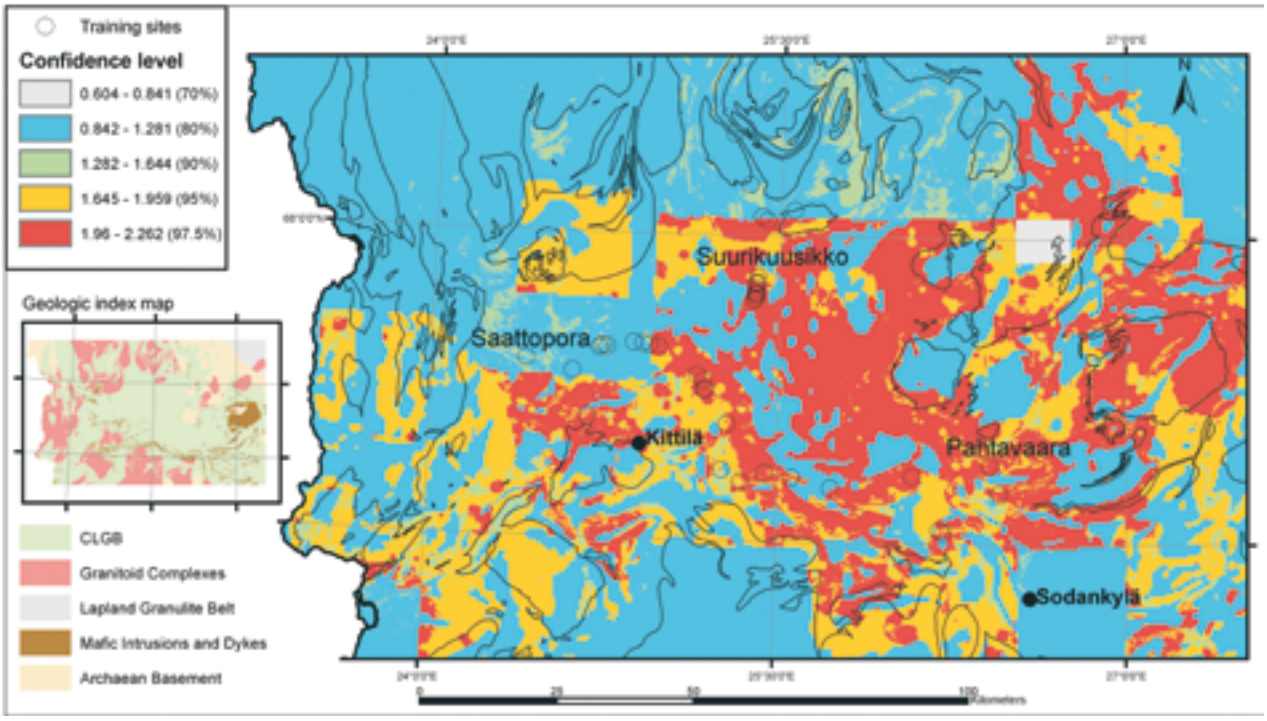

Fig. 5. Map of posterior probability/total uncertainty indicating the spatial variation of confidence that the reported posterior probability is not zero. All the training sites are within the areas that exceed the 80% confidence level. The boundaries of the main lithological units of the geologic index map are shown as black lines in the map, demonstrating that the model excludes most of the non-greenstone rocks as zero posterior probability.

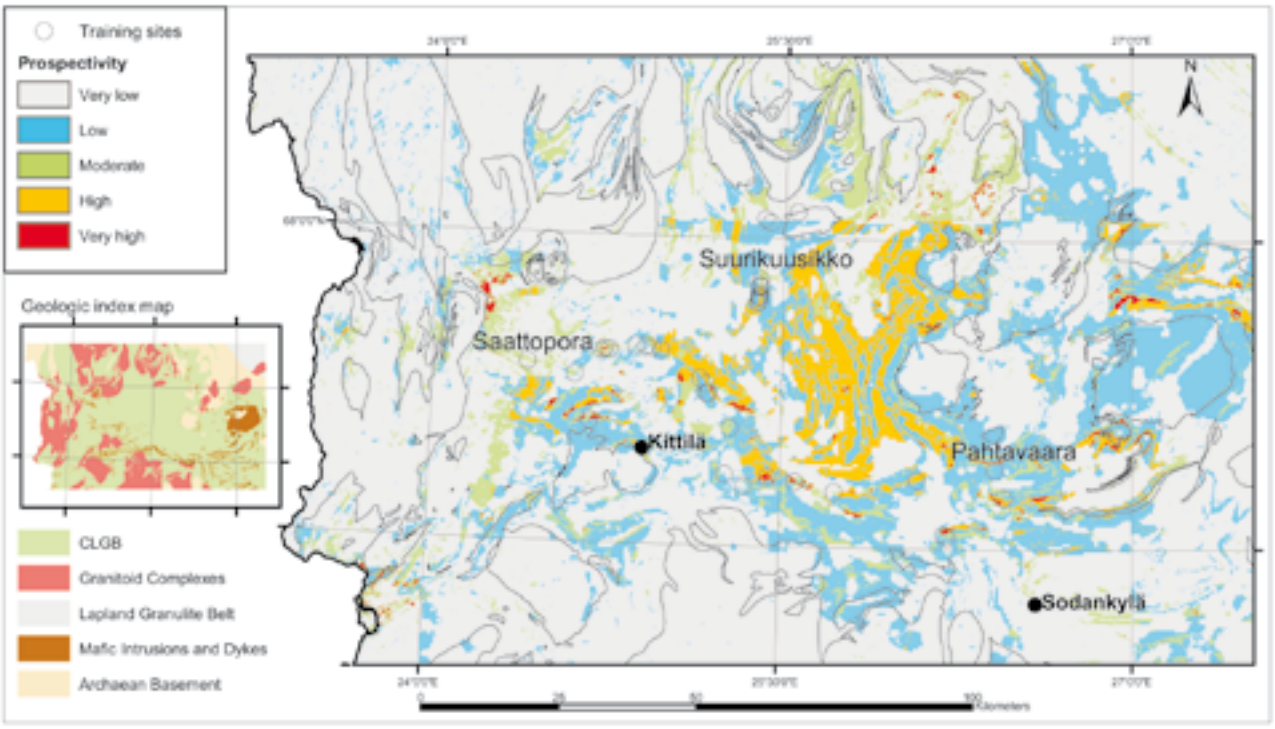

Fig. 6. Weights-of-evidence gold prospectivity map. Posterior-probability model using airborne geophysics, regional gravity and till geochemistry. The lowest class shown in grey represents areas with posterior probability lower than prior probability, which are assumed to not be permissive for greenstone gold deposits. The areas from 'Low' to 'Very high' prospectivity are all above the 80% confidence level as shown in Figure 5. The boundaries of the main lithological units of the geologic index map are shown as black lines in the map. Note that the moderate or higher areas occur only on greenstone rocks.

the training sites. From the total of 35 training sites, 31 are within the classes with posterior probabilities higher than prior probability. If a deposit is considered to occupy an area of 0.5 km^2, which is the unit area used in modeling, the total number of deposits intersecting the classes with posterior probabilities higher than prior probabilities is 35 (i.e. all the training sites) giving perhaps more realistic results. Thus, the model seems to map the training sites reasonably well and one should especially note, that the training sites related to the most significant deposit within the study area found so far, the Suurikuusikko property, also have posterior probability values higher than prior probability falling into the 'high' class in the posterior probability map (Fig. 6).

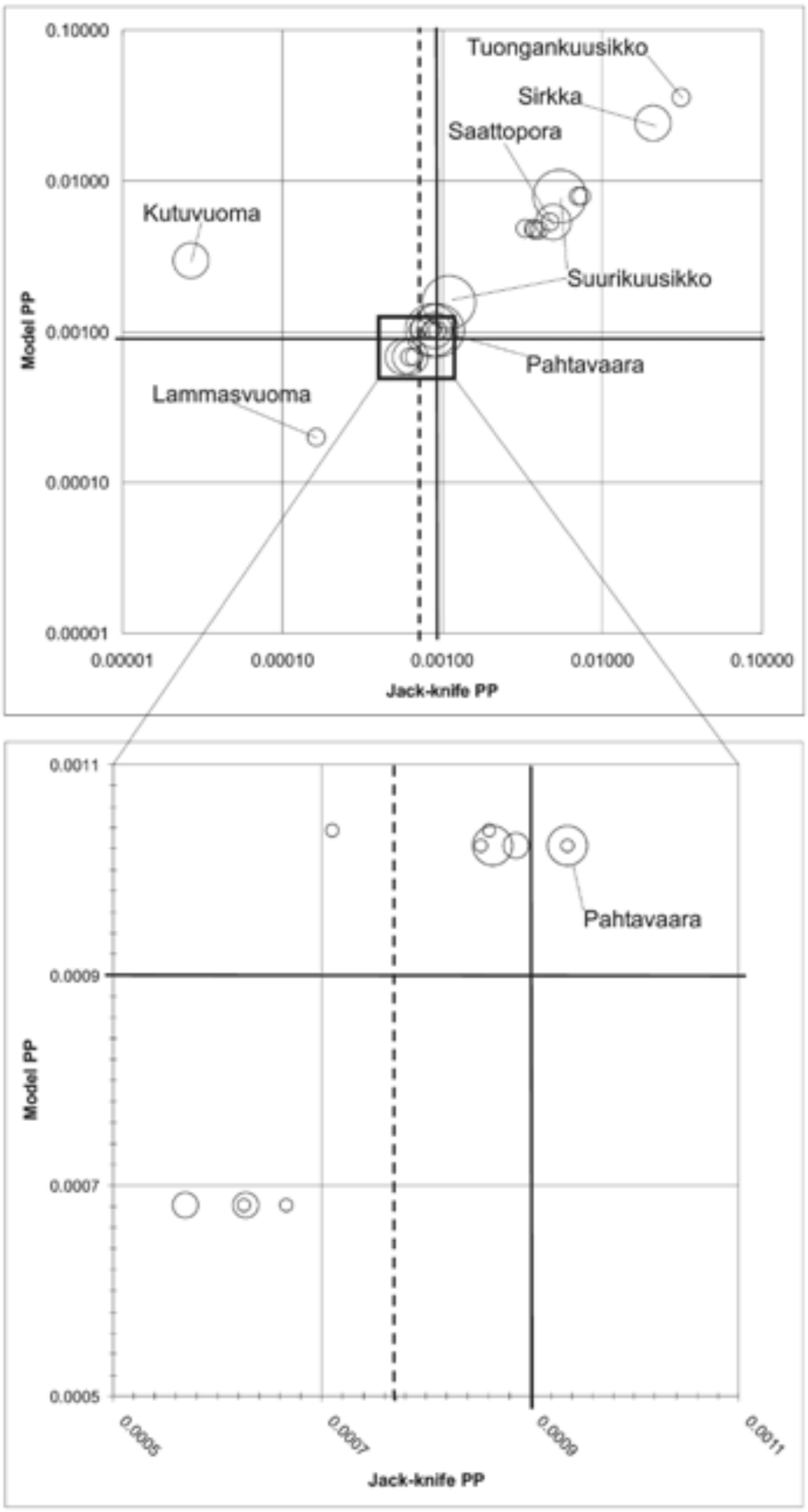

Fig. 7. Results of the jack-knife validation test as a plot of posterior probabilities in the final model and the test models associated with the training sites. The number of training sites used was 35 and prior probabilities varied from 0.0007 (dashed line) to 0.0009 (thick solid line) among the 23 weights of evidence models calculated. The training sites were treated as points in this calculation. The scale in upper plot is logarithmic. The close-up shows posterior probability values from 0.0005 to 0.0017. All the major deposits plot above the prior probability (0.0009).

FUZZY-LOGIC MODELING

First step in fuzzy logic modeling after selecting the appropriate evidential data is to define the relative importance of each of the selected evidential data and assign the fuzzy memberships for the classes of these data. The knowledge of the exploration experts was used to accomplish this task. The assigned fuzzy memberships for each of the evidential data sets are given in Table 7.

The fuzzy membership values were defined after reclassifying the original data by using standard deviation method in ArcView GIS. When reclassifying data using the standard deviations method, ArcView finds the mean value and then places class breaks above and below the mean at intervals of either 1/4, 1/2, or 1 standard deviations until all the data values are contained within the classes. ArcView will aggregate any values that are beyond three standard deviations from the mean into two classes, greater than and less than three standard deviations above and below the mean. In some cases an expert modified the classes manually. The resulting classes were then divided by an expert to be either "anomalous" (fuzzy membership = 1) or "non anomalous" (fuzzy membership = 0) and classes between these two were assigned a linear function between 0 to 1 (Fig. 3). Thus the classification of the data using standard deviation or any other method has a major influence on the final fuzzy membership values. Great care needs to be taken while classifying the data to find the thresholds. Selection of threshold for "anomalous" and "non anomalous" is, however, flexible and is defined by an expert. In Figure 8 all the evidential datasets are displayed according to the fuzzy membership values, red color indicating the significance of the anomaly concerned in each map.

After defining the fuzzy membership values, the evidential data were integrated in several steps according to the exploration model (Figure 8). First the magnetic and resistivity data were combined using a 'Fuzzy AND' operator to define possible conductive alteration zones. Till geochemical evidence was combined in two steps by first integrating metals Fe, As, Te and Ni by 'Fuzzy OR' operator and the resulting map with Cu by using 'Fuzzy AND' operator in order to highlight the anomalies indicating possible sulphide sources. These two intermediate response maps (geophysical and geochemical) were then combined together with regional gravity and Au in till by using 'Fuzzy GAMMA' operator with $\gamma = 0.9$. Since Au tends to have its own characteristics in till, it was used as a single evidence in the final combination as well as the horizontal gradient of the regional gravity, which reflects large crustal structures.

Results and interpretation

The final results are shown as a prospectivity map in Figure 9 classifying the study area based on the relative importance of the integrated datasets. Twenty training sites of 35 fall into fuzzy membership values 0.5 and above, when the training sites are taken as points. Whereas if a training site is surrounded by 600 m buffer representing an area of a site the number is 31 (i.e. 89 %). A significant result is, however, that Suurikuusikko deposit is within the fuzzy membership values 0.7–0.9 suggesting that the current model predicts well Suurikuusikko type of deposit. In addition to good prediction of the known exploration targets, this model also predicts areas with high exploration potential.

Table 7. Thresholds for Fuzzy membership values for the evidential datasets. Classes between these thresholds were linearly transformed to fuzzy membership values between 0 and 1. Each evidence map was reclassified to define classes by the standard-deviation method before the fuzzy membership was calculated. See Figure 3 to understand this process.

Evidence	Not anomalous (0)	Anomalous (1)
Airborne magnetic data (residual nT)	>630	<–270
Airborne EM (Ωm)	>2000	<20
Regional Gravity, horizontal gradient (mgal/500 m)	<1.5	>3.2
Au in till (ppb)	<0.1	>5
As in till (ppm)	<15	>49
Cu in till (ppm)	<48	>116
Fe in till (ppm)	>27610	>57300
Ni in till (ppm)	<62	>129
Te in till (ppm)	<23	>55

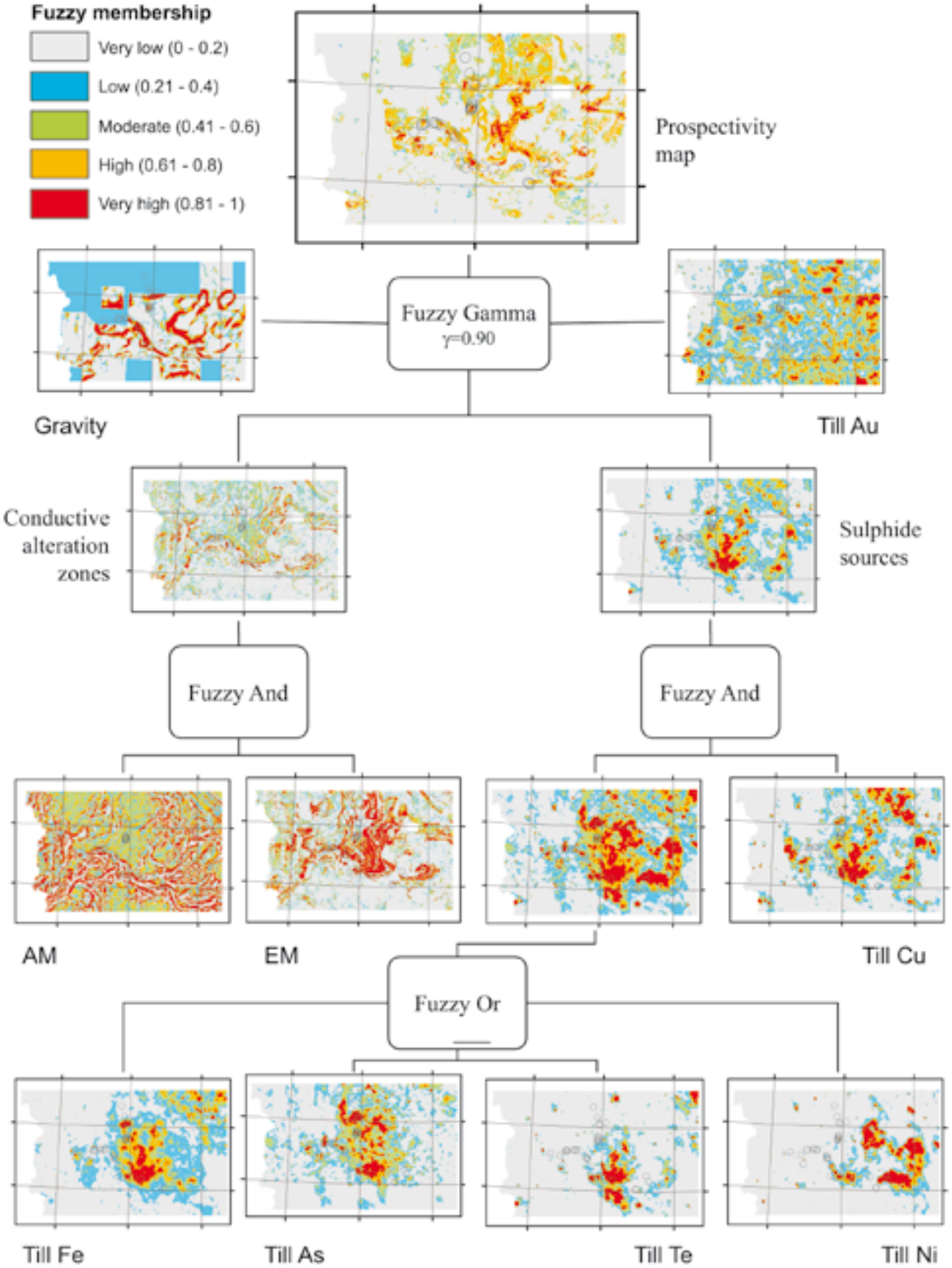

Fig. 8. The inference network of the fuzzy logic model for greenstone-hosted gold deposits. The rounded boxes are the operators (see Table 3 for explanation) and the rectangles represent the evidential data sets and the results.

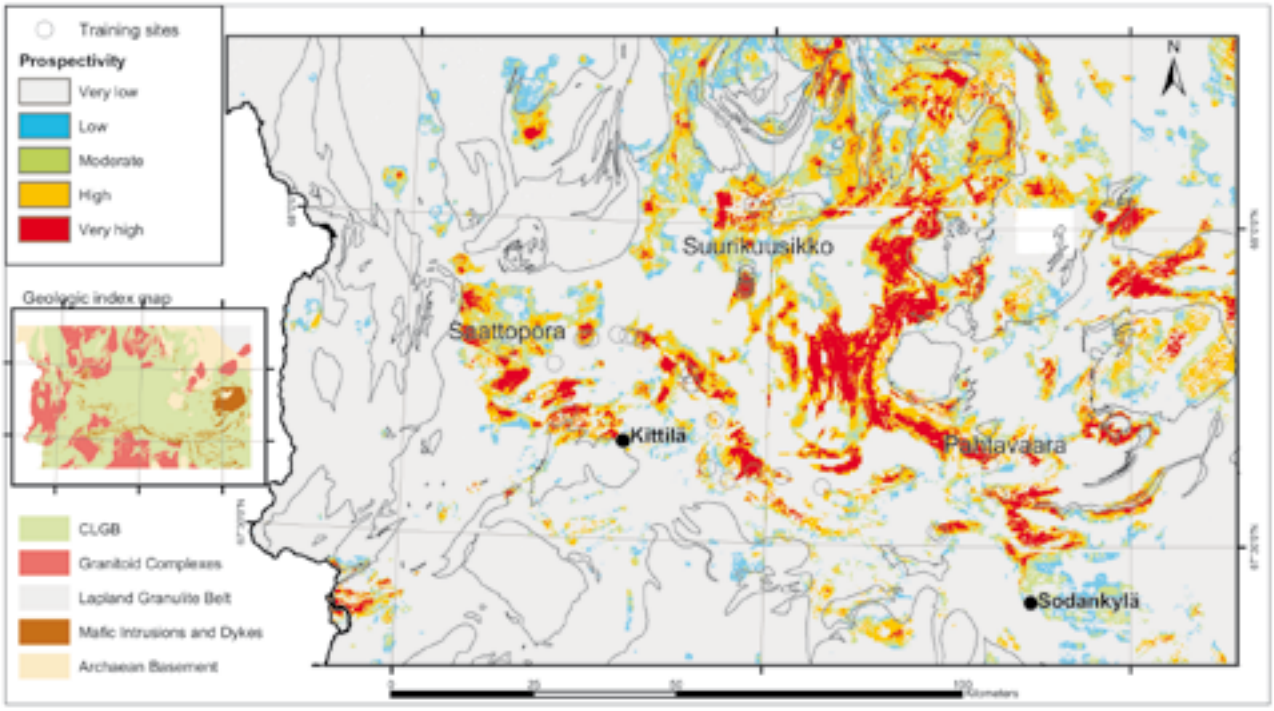

Fig. 9. Fuzzy-logic gold prospectivity map. Fuzzy membership model using airborne geophysics, regional gravity and till geochemistry. The boundaries of the main lithological units of the geologic index map are shown as black lines in the map. Note that most of the non-grey areas are in the greenstone rocks.

DISCUSSION

The aim of the current paper was to make a prospectivity analysis for gold and to test how well the regional datasets of GTK can predict the locations of known deposits. Also the aim was to test the empirical and conceptual approaches. The high-resolution airborne geophysical data would give a chance to interpret spatial models even in greater detail at larger scale than was done in this paper. This would require other evidence as well at the same data resolution and more focused study areas. Comparable data would be local scale geochemical surveys, which would, however, cover only limited areas but would be appropriate data for detailed exploration. For a local scale, a conceptual modeling would perhaps be more suitable since there are seldom statistically enough training points in small areas. The best evidence in the current models was, however, the horizontal gradient derived from the regional gravity data. The large crustal-scale structures seem to have a major control on spatial distribution of Au-deposit within the CLGB. Till geochemistry, which is a widely used exploration tool, is generally a very good data for modeling, but might improve significantly after more elaborate preprocessing than was done here.

In the current weights-of-evidence modeling, all the used training sites were treated as equal or at least being part of the same type common to the greenstone-hosted gold deposits. Each of the occurrences has many unique characteristics, which suggest that they might not be treated as a single deposit style but rather being grouped into several styles resulting in relatively a small number of training sites for each group. As the statistical tests in this paper show, there really is a significant spatial association between the training sites occupying an area of 0.5 km^2 and the specific map patterns used as evidence indicating that all the greenstone-hosted type of Au deposits can be treated as a single group at this scale.

As pointed out by Harris et al. (2001) one should use geostatistical methods to study the spatial behavior of geochemical data before interpolation. This was not done in this study, which might be one reason for a slightly poor predictive capability of the till geochemistry. In addition, the use of geological barriers during the interpolation process might be considered if they are known. Geochemical data is normally found to be a positive type of evidence, not the negative weighting seen here in the weights analyses. This suggests that some other ways of preprocessing the geochemical data should produce better evidence with W+ larger than or at least equal to the absolute value of W- and an increase in the contrast. Similarly, the airborne EM

and magnetics are the only evidence with W+ larger than the absolute value of W-. This result for the magnetics was highly enhanced by using the residual from the median filter. Better filtering of the magnetics and useful filtering of the EM should improve definition of the anomalies from these data and increased contrast. Most of the evidential data used here were as far as possible not interpreted data to be able to avoid biased results. However, one might want to use other highly interpreted evidence as well, together with the geophysical and geochemical data, to exploit the results from structural or any other geological modeling providing spatially referenced datasets with sufficient coverage over the area of interest. Example of this kind of data could be paleostress modeling studies (Holyland and Ojala, 1997; Mair et al., 2000, Ojala and Nykänen, 2007), geological shape analysis (Gardoll et al., 2000) or lithodiversity (Mihalasky and Bonham-Carter, 2001). The resolution and coverage of GTK's airborne geophysics and the contrasts found shows that this data is a strong exploration tool. By integrating this high-resolution data together with other less detailed data in GIS environment, as has been done in this paper, one can extract information that would otherwise be difficult to achieve, and laborious and less effective to accomplish.

The calculated weights of evidence and fuzzy logic models (Figs. 6 and 9) visually correlate with each other, which is obviously the result of the more or less identical evidential data used for the models. The agreement between two nominal-scale maps can be estimated by calculating the coefficient of agreement and kappa (Table 8). The overall kappa value for these two models is moderately low (0.22), but the conditional kappa value for the highest class of the two prospectivity maps is 0.66 and 0.48 for the lowest class suggesting that the two models do correlate at both higher and lower probability levels. The moderate levels do not correlate well due to the experts focusing on the thresholds and not assigning the mid point of fuzzy memberships for the evidential data. The moderate values were not considered important in either model, because the ultimate objective was to define the best targets. The area weighted Spearman's correlation coefficient is 0.80 due to the strong correlation between the lowest classes covering a large area in both of the models. Poor correlation between the moderate classes might be overcome with these models by combining the moderate classes. A noticeable point is that the predicted areas are almost entirely within the greenstone belt and in certain formations, even though geological map was not used as input data. Almost all of the predicted areas are within Savukoski and Kittilä groups, which have been suggested to be

Table 8. Matrix of observed proportions (A) and expected proportions (B) of weights-of-evidence (WofE) and fuzzy-logic (Fuzzy) prospectivity models. The values in the matrix are percent of area. Shaded values in principal diagonal represent areas of agreement. Agreement of observed proportions between these models is 60%. and overall kappa value is 0.22. The conditional kappa values for the classes from 1 to 5 are 0.48, 0.01, 0.08, 0.20 and 0.66, respectively. Spearman's area weighted correlation coefficient is 0.80 Calculation procedures after Bonham-Carter (1994). These tables give a measure of the nature of the agreement or correlation between the two models.

A)

	Fuzzy	**Very low**	**Low**	**Moderate**	**High**	**Very High**	
WofE	**Class**	**0–0.2**	**0.2–0.46**	**0.46–0.59**	**0.59–0.71**	**0.71–0.98**	**Total**
Very Low	**<0.0009**	59.46	2.95	3.81	2.29	0.41	68.93
Low	**0.0009–0.00120**	10.51	1.09	2.74	3.52	1.47	19.32
Moderate	**0.00120–0.00748**	2.42	0.26	0.96	1.72	1.00	6.36
High	**0.00748–0.01**	1.07	0.07	0.42	1.29	2.10	4.94
Very High	**0.01–0.03**	0.05	0.00	0.00	0.09	0.31	0.45
	Total	73.51	4.36	7.93	8.91	5.28	100.00

B)

	Fuzzy	**Very low**	**Low**	**Moderate**	**High**	**Very High**	
WofE	**Class**	**0–0.2**	**0.2–0.46**	**0.46–0.59**	**0.59–0.71**	**0.71–0.98**	**Total**
Very Low	**<0.0009**	50.67	3.01	5.47	6.14	3.64	68.93
Low	**0.0009–0.00120**	14.20	0.84	1.53	1.72	1.02	19.32
Moderate	**0.00120–0.00748**	4.68	0.28	0.50	0.57	0.34	6.36
High	**0.00748–0.01**	3.63	0.22	0.39	0.44	0.26	4.94
Very High	**0.01–0.03**	0.33	0.02	0.04	0.04	0.02	0.45
	Total	73.51	4.36	7.93	8.91	5.28	100.00

most favorable for Au within the CLGB area (Eilu et al. 2007). Thus, it seems that both models would pass a rough geological validation. As already mentioned in the Fuzzy-logic section it is promising that the location of the largest known gold deposit, Suurikuusikko, can be predicted by both models. In addition to the already known targets, the models generate new target areas. The region between Suurikuusikko and Pahtavaara seems to give high response in both of the models and is suggested for more detailed and focused modeling. The areas about 50 km to NE from Pahtavaara mine also appear to be highly prospective as well as the area some 25 km NW from Saattopora.

CONCLUSIONS

The spatial modeling techniques tested here proved to give an efficient tool for exploration geologists to integrate data from several geoscientific sources. Conceptual fuzzy-logic method gives a flexible tool to test exploration models on large datasets in an easily understood manner. The uncertainties of the fuzzy-logic modeling can be difficult to estimate, but an expert validation process would in many cases be appropriate and lead to reliable results. Empirical weights-of-evidence method instead includes comprehensive statistical validation process, which makes it laborious but more reliable. Weights-of-evidence method includes better control for uncertainty, but restricts the amount of evidential data to be used due to the requirement for conditionally independence. On the other hand, the weights calculation provides a convenient way to estimate and quantify spatial association between geographical locations like mineral deposits, rock formations etc. and any spatially referenced geoscientific or other relevant data. The agreement between these two models used in this study seems to be good at the low and high prospectivity areas. For future fuzzy-logic models, it seems that expert control of the middle fuzzy membership is also an important consideration, if these mid-range areas of important to the objectives of the modeling. However, the current paper suggests that the fuzzy-logic model produced here could be applied also to a study area without training sites to accomplish a prospectivity analysis within a reasonable confidence level.

ACKNOWLEDGEMENTS

The authors are grateful to Nils Gustavsson and Graeme Bonham-Carter for reviewing and commenting the early versions of the manuscript. Gary Raines is greatly acknowledged for reviewing the later versions and especially for his numerous and long discussions with the first author concerning the methodology and the rules in modeling. We also thank our colleagues at GTK contributing their expert opinions for the fuzzy logic part of the study.

REFERENCES

Agterberg, F.P., Bonham-Carter, G.F., Cheng, Q. and Wright, D.F., 1993. Weights of Evidence modeling and weighted logistic regression for mineral potential mapping. In: Davis, J.C. and Herzfeld, U.C. (eds.), 1993. Computers in Geology, 25 Years of Progress, Oxford University Press, Oxford, 13–32.

Agterberg, F. P., Bonham-Carter, G. F. and Wright, D. F., 1990. Statistical pattern integration for mineral exploration. In: Gaal, G. and Merriam, D., (eds.) 1990. Computer applications in resource estimation. Prediction and assessment for metals and petroleum. Pergamon Press, Oxford. 1–21.

Agterberg, F.P. and Cheng, Q., 2002. Conditional Independence Test for Weights-of-Evidence Modeling. Natural Resources Research, Vol. 11, No 4. 249–255.

Airo, M.-L., (ed.) 2005. Aerogeophysics in Finland 1972–2004. Methods, system characteristics and applicatoins. Geological Survey of Finland, Special Paper 39, 197 p.

Airo, M.-L. and Mertanen, S., 2001. Magnetic signatures related to Precambrian greenstone-hosted Au mineralizations, northern Fennoscandia. In: Vietnam 2001: IAGA-IASPEI joint scientific assembly, 19–31 August 2001, Hanoi, Vietnam: abstracts. **Hanoi:** IAGA: IASPEI, 263 p.

An, P., Moon, W.M. & Rencz, A.N., 1991. Application of fuzzy theory for integration of geological, geophysical and remotely sensed data. Canadian Journal of Exploration Geophysics, v. 27, no. 1, 1–11.

Bonham-Carter, G.F., 1994. Geographic Information Systems for geoscientists – modelling with GIS. Pergamon, New York, 398 p.

Bonham-Carter, G.F., Agterberg, F.P. & Wright, D.F. 1988. Integration of geological datasets for gold exploratoin in Nova Scotia. Photogrammetric Engineering and Remote Sensing, v. 54, no. 77. 1585–1592.

Carranza, E.J.M. & Hale, M., 2000. Geologically Constrained Probabilistic Mapping of Gold Potential, Bauio District, Philippines. Natural Resources Research, Vol. 9, No. 3, 237–253.

Chung, C.F. & Moon, W.M., 1990. Combination rules of spatial

geoscience data for mineral exploration. Geoinformatics, v.2, no. 2, 159–169.

D'Ercole, C., Groves, D.I. & Knox-Robinson, C.M., 2000. Using fuzzy logic in a Geographic Information System environment to enhance conceptually based prospectivity analysis of Mississippi Valley-type mineralization. Australian Journal of Earth Scinences, v. 47, 913–927.

Eilu, P., 1999. FINGOLD –a public database on gold deposits in Finland. Geological Survey of Finland, Report of Investigation 146. 224 p, 1 figure, 1 table and 2 appendices.

Eilu, P., Pankka, H., Keinänen, V., Kortelainen, V., Niiranen, T. & Pulkkinen, E. 2007. Characteristics of gold mineralization in the greenstone belts of northern Finland. In: Ojala, V.J. (ed.) Gold in the Central Lapland Greenstone Belt, Finland. Geological Survey of Finland, Special Paper 44, 57–106.

Fotheringham, A. S., Brunsdon, C. & Charlton, M. 2000. Quantitative geography: perspectives on spatial data analysis. London. SAGE Publications, 2000. 270 p.

Gardoll, S.J., Groves, D.I., Knox-Robinson, C.M., Yun, G.Y. & Elliot, N., 2000. Developing the tools for geological shape analysis, with regional- to local scale examples from the Kalgoorlie Terrane of Western Australia. Australian Journal of Earth Sciences. Vol. 47, 943–953.

Harris, J.R., Wilkinson, L., Heather, K., Fumerton, S., Bernier, M.A., Ayer, J. & Dahn, R., 2001. Application of GIS Processing Techniques for Producing Mineral Prospectivity Maps – A Case Study: Mesothermal Au in the Swayze Greenstone Belt, Ontario, Canada. Natural Resources Research, Vol. 10, No. 2, 91–124.

Holyland, P.W. & Ojala V.J. 1997. Computer aided structural targeting: two and three-dimensional stress mapping. Australian Journal of Earth Sciences 44, 421–432.

Hölttä, P., Väisänen, M. Väänänen, J. & Manninen, T. 2007. Paleoproterozoic metamorphism and deformation in Central Finnish Lapland. In: Ojala, V.J. (ed.) Gold in the Central Lapland Greenstone Belt, Finland. Geological Survey of Finland, Special Paper 44, 9–44.

Kemp, L.D., Bonham-Carter, G.F., Raines, G.L. & Looney, C.G., 2001. Arc-SDM: Arcview extension for spatial data modelling using weights of evidence, logistic regression, fuzzy logic and neural network analysis. http://ntserv.gis.nrcan.gc.ca/sdm/.

Knox-Robinson, C.M., 2000. Vectorical fuzzy logic: a novel technique for enhanced mineral prospectivity mapping, with reference to the orogenic gold mineralization potential of the Kalgoorlie Terrane, Western Australia. Australian Journal of Earth Scinences, v. 47, 913–927.

Kääriäinen, J. & Mäkinen, J., 1997. The 1979–1996 gravity survey and results of the gravity survey of Finland 1945–1996. Publications of the Finnish Geodetic Institute. N:o 125. 24 p. + 1 app. map.

Lehtonen, M., Airo, M-L., Eilu, P., Hanski, E., Kortelainen, V., Lanne, E., Manninen, T., Rastas, P., Räsänen, J. & Virransalo, P., 1998. The stratigraphy, petrology and geochemistry of the Kittilä greenstone area, northern Finland. A report of the Lapland Volcanite Project. In Finnish with summary in English. Geological Survey of Finland, Report of Investigation 140, 144 p.

Luo, X., Dimitrakopoulos, R., 2003. Data-driven fuzzy analysis in quantitative mineral resource assessment. Computers and Geosciences. Vol. 29, 3–13.

Mair, J.L., Ojala, V.J., Salier, B.P., Groves, D.I. & Brown, S.M., 2000. Application of stress mapping in cross-section to understanding ore geometry, predicting ore zones and development of drilling strategies. Australian Journal of Earth Sciences. Vol. 47, 895–912.

Mihalasky, M.J. & Bonham-Carter, G.F., 2001. Lithodiversity and Its Spatial Association with Metallic Mineral Sites, Great Basin of Nevada. Natural Resources Research, Vol. 10, No. 3.

Ojala, V.J. Nykänen, V. 2007. Paleostress modelling of the Central Lapland Greenstone Belt. In: Ojala, V.J. (ed.) Gold in the Central Lapland Greenstone Belt, Finland. Geological Survey of Finland, Special Paper 44, 209–234.

Raines, G.L., 1999. Evaluation of Weights of Evidence to Predict Epithermal-Gold Deposits in the Great Basin of the Western United States. Natural Resources Research, Vol. 8, No. 4, 257–276.

Salminen, R. (ed.) 1995. Geochemical Mapping in Finland in 1982–1994. In Finnish with summary in English. Geological Survey of Finland, Report of Investigation 130. 47 p. + 24 apps.

Salmirinne, H. & Turunen P. 2007. Ground geophysical characteristics of gold targets in the Central Lapland Greenstone Belt. In: Ojala, V.J. (ed.) Gold in the Central Lapland Greenstone Belt, Finland. Geological Survey of Finland, Special Paper 44, 193–207.

Singer, D.A. & Kouda, R., 1999. A comparison of the weights-of-evidence method and probabilistic neural networks. Natural Resources Research, v. 8, no. 4, 287–298.

www.gtk.fi
info@gtk.fi

Gold in Central Lapland Greenstone belt

Contents

Ojala, V. J.
Editor's Preface 5

Hölttä, P., Väisänen, M., Väänänen, J., Manninen, T.
Paleoproterozoic metamorphism and deformation in Central Finnish Lapland 7

Eilu, P., Pankka, H., Keinänen, V., Kortelainen, V., Niiranen, T., Pulkkinen, E.
Characteristics of gold mineralization in the greenstone belts of northern Finland 57

Patison, N.
Structural controls on gold mineralisation in the Central Lapland Greenstone Belt 107

Patison, N., Salamis, G., Kortelainen, V.
The Suurikuusikko gold deposit: project development summary of northern Europe's largest gold resource 125

Hulkki, H., Keinänen, V.
The alteration and fluid inclusion characteristics of the Hirvilavanmaa gold deposit, Central Lapland Greenstone Belt, Finland 137

Hulkki, H., Pulkkinen, E.
Exploration history of the Kaaresselkä gold-copper occurrence, Central Lapland 155

Holma, M., Keinänen V.
The Levijärvi-Loukinen gold occurrence: An example of orogenic gold mineralisation with atypical metal association 165

Airo, M-L.
Application of aerogeophysical data for gold exploration: implications for the Central Lapland Greenstone Belt. 187

Salmirinne, H., Turunen, P.
Ground geophysical characteristics of gold targets in the Central Lapland Greenstone Belt 209

Ojala, V. J:, Nykänen, V.
Paleostress modelling of the Central Lapland Greenstone Belt: Implications for gold exploration 225

Nykänen, V., Salmirinne, H.
Prospectivity analysis of gold using regional geophysical and geochemical data from the Central Lapland Greenstone Belt, Finland 251

ISBN 978-952-217-020-0 (PDF)
ISBN 978-951-690-980-9 (paperback)
ISSN 0782-8535